Mechanisms of Molecular Brush Inhibition of Protein Adsorption onto Stainless Steel Surface

A thesis submitted in fulfillment of the requirement for the degree of
Doctor Philosophy in Chemical and Process Engineering

By
Norzita Ngadi

Department of Chemical and Process Engineering
University of Canterbury

2009

ACKNOWLEDGEMENT

I would like to express my sincere gratitude to my supervisor, Dr John Abrahamson for his encouragement, guidance and brilliant suggestion throughout this study. My deepest appreciation to my co-supervisor, Prof Conan Fee and Dr Ken Morison for spending their precious time to discuss and clarify issues which greatly help me in taking the research project in the right direction.

I would like to express my gratitude to Professor Richard Haverkamp (School of Engineering and Advanced Technology, Massey University, New Zealand) for his help on the AFM characterization.

I would also like to thank all my friends. Knowing you has made my life here more cheerful and enjoyable.

I would like to acknowledge the Malaysian government for the financial support during my study.

Finally and most importantly, I would like to dedicate this thesis to my mom and dad for their encouragement and support. If not for love and encouragement of my family, this work would never have been successfully completed.

ABSTRACT

Protein-resistant ("non-fouling") surfaces are particularly important in many fields such as medical engineering, dentistry, pharmaceutical processes, bioprocessing, dairy and food manufacturing. Poly(ethylene glycol) (PEG) immobilized onto surfaces has been shown to confer high resistance to protein adsorption. The reasons for variable performance and optimal protein repellency of PEG layers have been the subject of much discussion; however there remains no general consensus on the molecular mechanisms underlying the protein resistance achieved with PEG coatings.

The main objective of this study was to inhibit protein adsorption onto a stainless steel surface. This objective requires an exploration of the mechanisms of protein adsorption on a stainless steel surface and how these mechanisms are modified when a surface inhibits the adsorption of proteins. The stainless steel surface has been chosen as a substrate as it is a commonly used material in many relevant applications such as in the dairy industry, in food processing and in clinical uses.

In order to elucidate the mechanisms of protein-PEG interactions the adsorption of lysozyme, β-casein, apo α-lactalbumin, holo α-lactalbumin and β-lactoglobulin onto various PEG-grafted surfaces was explored. The adsorption was conducted at room temperature and at 40 °C. The modification of bare SS surfaces and adsorption kinetics of proteins on unmodified and modified surfaces (i.e. bare stainless steel and PEG surfaces) has been done in-situ and studied by means of a quartz crystal microbalance with dissipation sensing (QCM-D). The merit of the modification methods studied, compared to those of most published methods is that the process of modification is simple and easy, being done simply by passing a solution over the surface. The methods also do not involve any harmful or hazardous chemicals and thus are safe to be used even in food processing plants.

The PEG coated surfaces prepared in this study were able to inhibit adsorption of β-casein, α-lactalbumin (calcium enriched) and lysozyme proteins especially; the

lowest adsorption of these achieved as a percentage of that on bare stainless steel, β-casein, 45 %, holo α-lactalbumin, 11 % and lysozyme, 1 %. By contrast, and unexpectedly, PEG molecules *enhanced* the adsorption of apo α-lactalbumin (the form without calcium). It is suggested that the PEG to apo α- lactalbumin hydrophobic interaction plays a dominant role which leads to protein aggregation at the surface, for this latter observation. The results have shown that protein stability (i.e. whether it is a soft or a hard protein) greatly influenced the inhibition performance of PEG surfaces. It is apparently more difficult to prevent the adsorption of soft proteins than hard proteins. This appears to be because soft proteins tend to denature regardless of the surface properties (i.e. hydrophilic or hydrophobic) and attach more effectively in their unfolded state. The results also indicated that higher PEG grafting density is not necessarily reflected in better protein inhibition.

At the end of the project, a novel method of surface modification was developed. In this method, stainless steel surfaces were modified by coating the surface with a protein layer (as a base) then followed by the attachment of PEG molecules. Interestingly, the method developed showed an excellent potential for preventing further protein adsorption at room and body temperatures. The adsorption of β-casein, lysozyme, holo α-lactalbumin and β-lactoglobulin on the SS-lysozyme-PEG surfaces was down to about 3, 1, 4 and 0.4 %, respectively compared to that on the bare surface. More interestingly and surprisingly also, there was almost zero adsorption on those surfaces of mixed protein and single protein solutions at the concentration found in milk. The method is believed to have the potential to be applied in the pharmaceutical industry, in the biosensor field and in artificial medical implants with some modifications perhaps to suit the application.

The modelling results demonstrated negative free energy changes on adsorption, consistent with the studied proteins being thermodynamically favoured to adsorb on bare SS. The adsorption of proteins was an endothermic process. The proteins also showed large positive entropy changes on adsorption, indicating adsorption-induced denaturation mechanisms (especially apo α-lactalbumin protein). At high temperatures and concentrations, the adsorption was governed first by diffusion and later by surface kinetics, whereas under lower temperature (i.e. room

temperature) and low concentration conditions (i.e. 0.1 g / L) the adsorption was able to be described solely by surface-reactions.

TABLE OF CONTENTS

CHAPTER THREE: LITERATURE REVIEW OF CHARACTERIZATION

CHAPTER FOUR: LITERATURE REVIEW OF KINETICS THEORY AND INTERPRETATION OF DATA

CHAPTER FIVE: METHODOLOGY

LIST OF FIGURES

LIST OF TABLES

CHAPTER ONE

INTRODUCTION

1.1 Scope of fouling problems

Adsorption of proteins onto a solid surface is believed to be the first step towards formation of a biofilm [Belmarbeiny and Fryer, 1993, Visser and M.Jeurnink, 1997, Wei et al., 2003, Fukai et al., 2004, Bansal and Chen, 2006]. Formation of a biofilm or biofouling is a ubiquitous phenomenon and occurs on many surface materials that have contact with fluid. A biofilm may cause serious microbial contamination problems, for example, in medical engineering, dentistry, pharmaceutical processes, bioprocessing, and food manufacturing. In food manufacturing, for example, adsorption of proteins with other food components leads to fouling of the surfaces of processing equipment. In the dairy industry, fouling deposits cause problems because they not only reduce the processing performance of the equipment but also increase the likelihood of contamination of the products. Instruments for clinical uses also suffer from fouling with proteins upon contact with living tissues and biological fluids. Proteins adsorbed on the surface can prompt the adhesion of viable bacteria and hence spoil the sanitary state of the surface. Fouling not only contaminates the products but it also reduces the efficiency of the process equipment and causes significant increases in capital and operating costs. Obstruction of piping from fouling can also lead to a shutdown of plants and hence economic losses. It has been reported that total costs due to fouling were approximated at 0.25 % of the gross national product (GNP) for the industrialized world, and 0.15 % of the GNP for less industrialized countries such as New Zealand (Zhao and Liu, 2004, Bansal and Chen, 2005). Hence, it is obvious that something needs to be done to prevent or minimize fouling.

1.2 First step protein adsorption

The conventional method to temporarily solve the problem of fouling in the processing equipment is by cleaning either using a mechanical, chemical or disinfection technique. Unfortunately, most of these techniques give problems, for example, frequent cleaning is costly and using chemical additives may cause undesired product contamination or have adverse effects on the environment. Therefore, preventing formation of the initial steps of fouling (that is, protein adsorption) would be a better way of finding a solution and indeed a very important task.

Adsorption of proteins onto a solid surface can be considered a complex phenomenon. This complexity comes from the structural features of protein molecules themselves as they contain hydrophobic and hydrophilic amino acid residues and carry negative and/or positive electric charges. The adsorption of the proteins to the surface was driven by hydrophobic, electrostatic, hydrogen bonding and Van Der Waals interactions. Hydrophobic and electrostatic interactions appeared to be the main driving forces for the adsorption of proteins [Denes, 2004, Pasche et al., 2005, Lamotte et al., 2008]. Electrostatic interaction is important when surfaces are charged in aqueous solution. The detail information of protein adsorption on a surface is in Chapter 2. It is rarely a problem to know how to achieve the adsorption of proteins, but rather to know how to prevent it.

1.3 Prevention and molecular brushes

Various techniques of surface modification have been investigated and applied to transform an actively adsorbing surface into a protein-inert surface. A key to eliminate protein adsorption is to suppress all attractive forces between proteins and the surface. A common approach for blocking the adsorption of proteins is to attach polymer chains by one end to a surface to form well-solvated ‘brushes’ [Schroen et al., 1995, Du et al., 1997, Yang et al., 1999]. In fact, such ‘molecular brushes’ have been extensively studied in recent years due to their high capability to prevent protein adsorption [Yoshikawa et al., 2006, Zhou et al., 2007, Halperin, 2007]. Ranges of methods have been employed for the immobilization of PEG

molecules onto surfaces and these can be broadly classified as either physisorptive or chemisorptive. Another promising technique of surface modification is by altering the surface free energy [Santos et al., 2004, Rosmaninho et al., 2007]. Generally, nonfouling surfaces should be electrically neutral, hydrophilic and possess hydrogen bond acceptors but not hydrogen bond donors [Nath et al., 2004, Zheng et al., 2005, Pasche et al., 2005, Latour, 2006]. The ideal mechanism is hypothesized to be the elimination of electrostatic attractive forces and the hydrophobic interactions between solid surfaces and proteins in solutions. A large number of hydrogen bonds of the surface with water molecules produce large repulsive forces on the protein, leading to a better protein resistance. It is more difficult for the proteins to squeeze out tightly bound water molecules from the interfacial layer to the bulk. Thus, those water molecules form a barrier to prevent direct contact between the proteins and the surface.

1.4 Objective of study

The main objective of this study is to inhibit protein adsorption onto a stainless steel surface (that is, minimizing or delaying fouling to a practical surface much used in the food industry, particularly in the dairy industry). This objective requires an exploration of the mechanisms of protein adsorption on a stainless steel surface and how these mechanisms are modified when a surface inhibits the adsorption of proteins.

The stainless steel surface has been chosen as a substrate as it is a commonly used material in many relevant applications such as in the dairy industry, in food processing and in clinical uses. Furthermore, little experimental study had been done so far on stainless steel surfaces.

1.5 Proteins explored

Three main types of proteins were used in this study; α-lactalbumin, β-casein and lysozyme. α-lactalbumin and β-casein have been chosen to represent proteins in dairy products while lysozyme was chosen as it was widely used in many studies and was well characterized. The proteins used differed in their physical and chemistry

properties. α-lactalbumin, for example, is a compact globular protein with a molecular weight of 14,200 Da and is an acidic protein with an isoelectric point (pI) value of 4.3. Its denaturation temperature is about 64 °C. β-casein meanwhile has a molecular weight of 23,000 Da with a pI value about 5.2. It has a disordered structure with a great flexibility. Its denaturation temperature is about 78 °C. Lysozyme is a more stable protein (that is, a 'hard' protein) than the others. Its denaturation temperature is 74 °C. It has an ellipsoidal shape (3 nm x 3 nm x 4.5 nm) with a molecular weight of 14,600 Da. It is a basic protein with a pI value of 11.1. The difference in physical and chemistry properties among these proteins will be explained further in Chapters 5 and 11. At the end of the study, β-lactoglobulin and native α-lactalbumin proteins were used. β-lactoglobulin was used in order to represent the real situation in the dairy industry. β-lactoglobulin is the most abundant protein in whey and is believed to be the first layer formed at a heat exchanger surface in the dairy industry [Visser and Jeurnink, 1997]. Native α-lactalbumin, which is calcium enriched, meanwhile was used as a comparison with the former α-lactalbumin (that is, calcium depleted). The main difference between these two proteins is the absence/presence of calcium ions.

1.6 Adsorption measurements

In this study, adsorption of protein was performed on an AT-cut quartz crystal diaphragm coated with gold and then a stainless steel layer. The detail of the AT-cut is in Chapter 5. The crystal had a fundamental resonant frequency of 5 MHz and a diameter of 14 mm as shown in Figure 1 (a). The size of this surface was small compared with that of a typical plate heat exchanger used in the dairy industry (Figure 1 (b)) and the uniformity of the surface was higher (see Chapter 9).

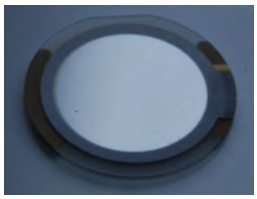

(a) AT-cut gold quartz crystal coated with a stainless steel surface (14 mm diameter) used in this study (area, 1.54×10^{-4} m^2)

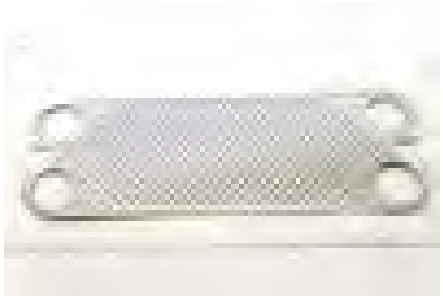

(b) Plate commonly used in a plate heat exchanger (area, 0.38×0.86 m^2). In the plate heat exchanger, it consists of varying number of plates. The image was taken from http://www.alibaba.com/product-free/101604526/heat-exchanger-plate.html

Figure 1.1: Comparison between our substrate and the real plate used in processing equipment used in industry.

1.7 Surface modifications to reduce adsorption

Choices of techniques to modify the surfaces were restricted to those which could be practically used in process equipment. Coating the surface with poly(ethylene glycol) (PEG) was our preference to inhibit protein adsorption. Prior to attachment of PEG molecules, the surface was coated with either a poly(ethylimine)(PEI) or a silicate layer. The modification of the surface was based on the physisorption method. The protein repelling performance of a blend of short and long chains of PEG molecules has also been investigated. It is believed that the proposed method is able to reduce the frequency of cleaning and hence cost of the operating. No one has yet applied these techniques to a surface area large enough for engineering use. If one could do this, significant economic benefits would be found in the prevention of fouling in a number of situations ranging from food processing industries to medical devices.

At the end of the project, a novel method of surface modification was developed. The surface was coated with a layer of protein instead of PEI or silicate

prior to attachment of PEG molecules. Interestingly, the new method showed an excellent potential for preventing further protein adsorption at room and body temperatures.

The merit of this study is that the surface modification introduced was very easy and simple yet promising. From the results obtained, it is most likely that the proposed method is sufficiently practical to be applied in some situations in the industry.

CHAPTER TWO

LITERATURE REVIEW OF BIOFILM, PROTEIN ADSORPTION AND INHIBITION

2.0 INTRODUCTION

This chapter provides a general description of biofilm formation, the mechanism of protein adsorption on a solid surface and how to inhibit the protein adsorption.

2.1 BIOFILM FORMATION OVERVIEW

A biofilm is a complex aggregation of microorganisms growing on a solid surface. Biofilms are common in nature, as bacteria commonly have mechanisms by which they can adhere to surfaces and to each other. Dental plaque is a biofilm. In industrial environment, biofilms can develop on the interiors of pipes and lead to clogging and corrosion. In medicine, biofilms spreading along implanted tubes or wires can lead to harmful infections in patients. The development of biofilm can occur on almost any surface in any environment in which viable microorganisms are present. The steps of the formation of biofilm have been proposed as follows [Kumar and Anand, 1998, Poulsen, 1999]:

1) Conditioning of surface

Organic and inorganic molecules such as ***protein*** can be adsorbed to a solid surface forming a conditioning film. This stage could occur within even less than a minute after a clean surface is exposed to the fluid film [Santos et al., 2006].

2) Adhesion of microbial cells

There are two types of attachment; reversible and irreversible attachment. A reversible attachment involves long range forces (weak interaction) such as Van der Waals, electrostatic forces, and hydrophobic interactions. At this stage, bacteria cells can be easily removed if mild shear force is applied. An irreversible attachment happens after the reversible attachment. It involves short range forces such as dipole-dipole interaction, hydrogen, ionic and covalent bonding, and hydrophobic interactions. The removal of bacteria cells becomes harder and needs stronger forces such as scrubbing or scraping.

3) Microcolony formation

The irreversibly attached bacteria cells will divide and grow. They also produce extracellular polymeric substance (EPS) which act as‘*glue*’, that helps in the anchorage of the cells to the surface and shields the colony from the harsh environment.

4) Biofilm formation

The continuous attachment of the bacterial cells to the already attached bacteria on the surface and its subsequent growth along with associated EPS production forms a biofilm.

5) Detachment of biofilm

As the biofilm ages, the attached bacteria cell must be able to detach and disperse from the biofilm in order to survive and colonize new niches.

2.2 PROTEIN OVERVIEW

2.2.1 Definition of protein

Proteins are complex biopolymer substances made of amino acid residues combined in definite sequences by peptide bonds (also known as a primary structure of protein). Each unit of amino acid contains an acidic carboxyl group (carboxy terminus) and basic amine group (amino-terminus) (refer to Figure 2.1).

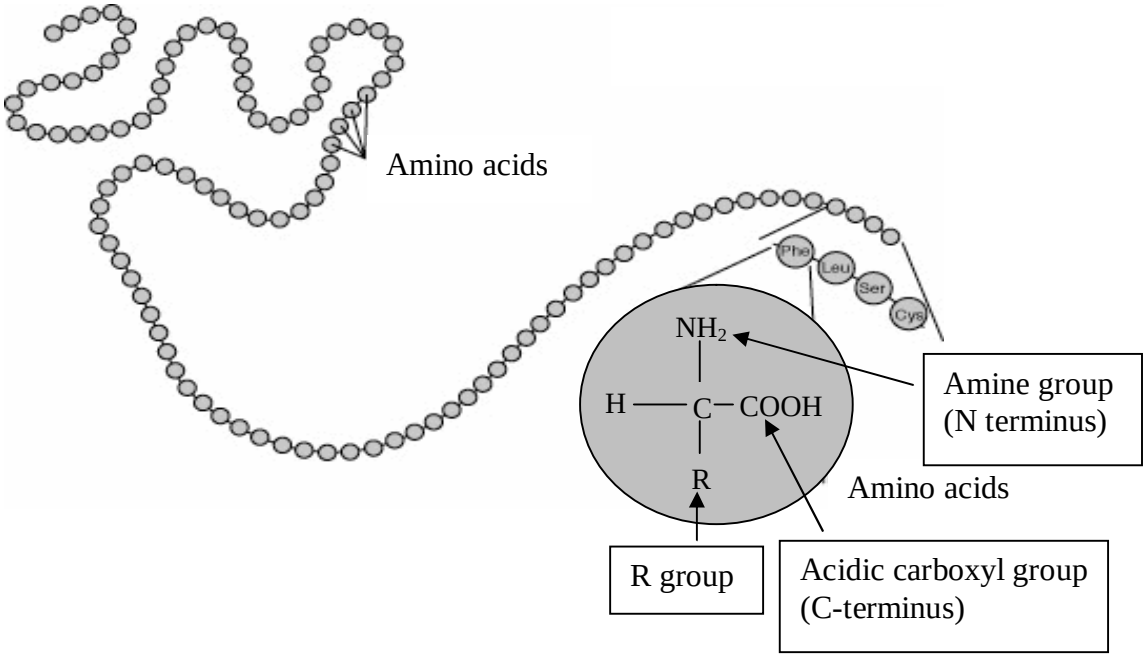

Figure 2.1: Primary protein structure (sequence of a chain of amino acids).

Proteins are also typically known as amphiphilic molecules which contain hydrophobic or hydrophilic, polar or non-polar and charged (both positive and negative) regions. However, the distribution of both positive charges and negative charges is not uniform and usually contains more non-polar patches than polar patches. The non-polar patches make hydrophobic interactions to a surface more important. There are four levels of protein structure; primary, secondary, tertiary and quaternary as shown in Figure 2.2.

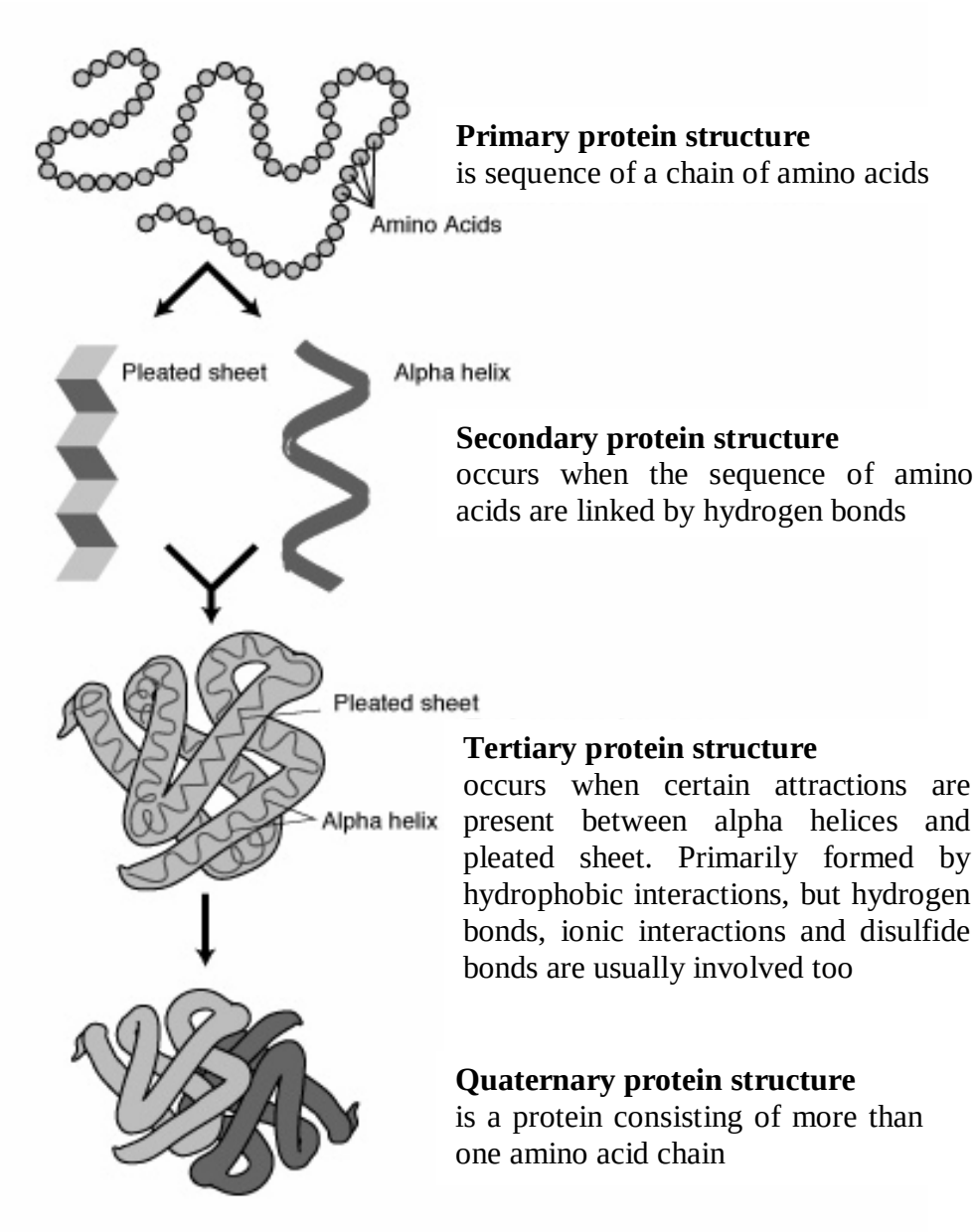

Figure 2.2: Protein structure [http://en.wikipedia.org].

The shape into which a protein naturally folds is known as a native state, which is determined by its sequence of amino acids. Proteins are most stable at their isoelectric point (i.e. pH = pI). Proteins denaturation involves a change in the protein structure (generally an unfolding) with the loss of its activity**.** In many cases, denaturation is irreversible. However, in some cases, denaturation is reversible, and proteins may refold to a native state. An increase in temperature, pressure and a change in pH or the addition of solvent can easily provoke denaturation of the protein. Protein stability can also be disrupted by the introduction of a foreign surface or an interface into the system.

Protein can be divided into two classes; 'soft' and 'hard' proteins. The 'soft' proteins are able to display large conformational changes upon adsorption. Examples of 'soft' protein are bovine serum albumin (BSA), human serum albumin (HSA), immunoglobin (IgG), α-lactalbumin, β-casein and hemoglobin. On the other hand, 'hard' proteins are proteins with a high internal cohesion which undergo limited or no structural rearrangements during adsorption. Examples of 'hard' proteins are α-chymotrypsin, ribonuclease (RNase), cytochrome c, subtilisin, lysozyme and β-lactoglobulin.

2.3 PROTEIN ADSORPTION ON SURFACES OVERVIEW

Protein adsorption plays a central role in many biological processes and it is a very challenging fundamental problem. Proteins have colloidal type of interactions due to their large size. Furthermore, they have additional complexity due to the fact that they are largely inhomogeneous in size, shape and interaction. They can be charged and they can change their conformations upon adsorption.

Adsorption of protein is spontaneous if $\Delta G_{adsorption} = \Delta H_{adsorption} - T\Delta S_{adsorption} < 0$ where G, H, S and T are the Gibbs free energy, the enthalpy, the entropy, and the absolute temperature, respectively. $\Delta_{adsorption}$ represents the change of the thermodynamic function.

In many previous studies [Van Tassel et al., 1998, Ravichandran and Talbot, 2000, Lee et al., 2004,], it was assumed that proteins behave as rigid bodies, such that no conformational changes occur during adsorption (RSA model). However, this assumption is not always true. In fact, conformational changes in the protein can greatly contribute to the driving force for adsorption. Proteins are highly ordered structures. Partial or complete unfolding of the protein on the surface leads to an increase in conformational entropy, which can be the driving force for protein adsorption. To assess the tendency of proteins to unfold on surfaces, it is important to have a clear picture of protein stability.

2.3.1 Protein adsorption driving forces

2.3.1.1 Hydrophobic interaction

Hydrophobic interaction is a strong attraction between nonpolar (hydrophobic) molecules and surfaces in water. For proteins, the dehydration of nonpolar parts of the polypeptide in water is favorable because it leads to a decrease of the Gibbs energy of the system. This hydrophobic dehydration is considered to be the primary driving force for protein adsorption. The hydrophobic interactions between proteins and surfaces typically lead to an extensive unfolding of the proteins, due to an attraction between the hydrophobic parts inside the protein and the surface.

Most studies [Denes, 2004, Voros, 2004, Jonsson et al., 2004, Roach, et al., 2005] have shown that protein adsorption is more favorable towards hydrophobic surfaces rather than hydrophilic surfaces. Indeed, denaturation of proteins [Lamotte et al., 2008] appeared more dominant on hydrophobic surfaces than hydrophilic surfaces.

2.3.1.2 Electrostatic interaction

Electrostatic interaction between proteins and surfaces is another important force that drives protein adsorption. When the surfaces are charged (positively or negatively depending on the type of material), electrostatic interaction **[**Pasche et al., 2005] plays an important role in adsorption because proteins are also charged (depending on the solution pH). If the pH of the solution is below its isoelectric point (pI), the protein will carry net positive charge and vice versa. Pasche et al. [2005] found that on hydrophilic surfaces, structurally stable proteins ('hard' proteins) adsorb only if the electrostatic interaction is favourable (they do adsorb if they have opposite net charge). However, on hydrophobic surfaces they are hardly adsorbed on charged surfaces that carry the same net charge. Less stable proteins ('soft' proteins), [Fukuzaki et al., 1995, Nath et al., 2004 and Pasche et al., 2005] adsorb on both hydrophilic and hydrophobic surfaces even with the same charges (see Figure 2.3 as an example). Figure 2.3 shows the mass surface density of lysozyme (a 'hard protein'), myoglobin (a 'soft' protein) and α-lactalbumin (a 'soft' protein) onto five surfaces with various surface charges. The pH of the solution was 7.4. Thus lysozyme carried net positive charges while both myoglobin and α-lactalbumin carried net negative charges. As can be seen, lysozyme adsorbed only if electrostatic interactions were favourable. Nevertheless, for myoglobin and α-lactalbumin, they adsorbed on the surfaces even if they had the same charge as the surface. When the surface was uncharged (neutral), almost no adsorption occurred, indicating the importance of electrostatic interactions on the protein adsorption. Less stable proteins ('soft' proteins) adsorb on both hydrophilic and hydrophobic surfaces even with the same charge.

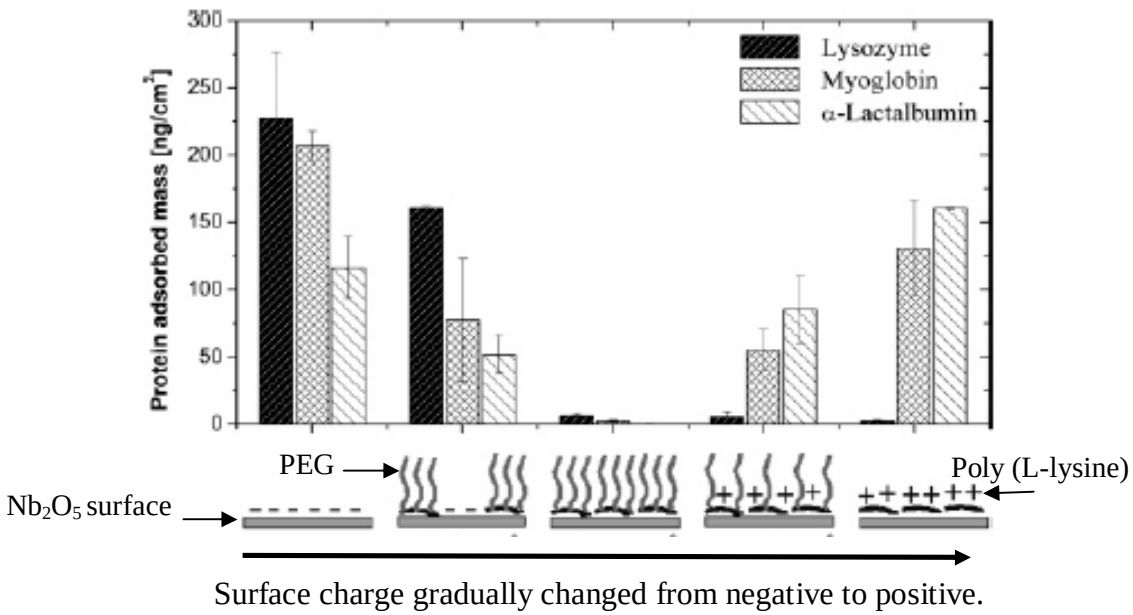

Figure 2.3: Protein adsorbed mass of lysozyme, myoglobin and α-lactalbumin measured in HEPES buffer (pH 7.4) by optical wave light spectroscopy (OWLS), on five surfaces (Nb_2O_2 surfaces modified with poly (L-lysine)-PEG) with various surface charges. From left to right the surface charge gradually changes from negative to positive. Data was taken from Pasche et al. [2005].

2.3.1.3 Van der Waals interaction

Van der Waals (VdW) forces are mostly due to interactions between permanent and induced rotating dipoles interactions and are always present at short distances (1-2 nm). The Van der Waals interaction energy, *VdW*, between a flat surface and a large sphere (>> 2nm) at small separation can be approximated as;

$$vdW = -\frac{AR}{6D} \qquad (2.1)$$

where *A* is the Hamaker constant (J), *R* is the radius of the sphere and D is the closest distance between the sphere and the surface.

Meanwhile, for two spheres of radius *R*, vdW interaction is;

$$vdW = -\frac{AR}{12D} \tag{2.2}$$

For two flat surfaces, the Van der Waals interaction energy per surface area is;

$$vdW_A = -\frac{A}{12\pi D^2} \tag{2.3}$$

2.3.1.4 Hydrogen bonds

Most of the H-bonds in proteins are between amide and carbonyl groups of the polypeptide backbone. The H-bonds are short ranged (<0.1 nm). Formation of H-bonds appears not to be the main driving force for protein adsorption.

2.3.2. Kinetics of protein adsorption on a solid surface

Protein adsorption generally occurs in four steps as shown below:

1) Transport of protein from the bulk towards the interfacial region

   This step normally is driven by Brownian motion and a gradient diffusion. This step is very dependent on the experimental conditions such as temperature, concentration and flow rate.

2) Attachment of protein on a surface (initial protein-surface interaction)

   To adsorb onto a surface, a protein molecule must interact with the surface for a sufficient time to allow binding. For example, the time for fibrinogen molecules to bind strongly with silica surfaces (determined using AFM force mode) was 50 to 200 ms [Hemmerle et al., 1999]. The interaction strength between the protein and the surface will determine the residence time of the initial attachment. There are several possibilities of interaction between the protein and the solid surfaces upon adsorption, such as a random site interaction (unordered binding), an ordered adsorption and an island or a cluster formation. The random site

interaction [Masel, 1996, Kim et al., 2002] usually occurs at low coverage, while at moderate coverage, usually the ordered structure or the islands were formed. In case of a mixture of proteins [Fang et al., 2001], the protein with the highest concentration will dominate the initial adsorption and gradually will be exchanged by the higher affinity species. Normally, concentrations being similar, the initial adsorption is lead by the smaller protein and later is replaced by the larger protein (a large protein has a higher affinity toward a surface compared to a small protein). This sequence of adsorption is known as the *Vroman Effect.*

3) Conformational changes

During the adsorption, some of the adsorbed proteins may experience conformation change or be denatured. This might change the interaction energy with the surface, resulting in an increased residence time and a stronger binding since the denatured protein spread more as compared to its native state [Snopok et al., 2006]. The denaturation [Kim et al., 2002] is more severe on a hydrophobic surface than a hydrophilic surface due to protein-surface interactions that allow hydrophobic residues of protein to contact with the surface. The structural properties of the protein [Nanth et al., 2004] also influence their adsorption and conformational integrity on surfaces. For example, fibrinogen, which has a rod-like shape can reorient from a ‘side on’ to ‘end on’ formation to increase the surface mass density adsorbed. Meanwhile, albumin which is globular in shape, resulted in almost the same surface area coverage in any orientation (see Figure 2.4)[Roach et al., 2005]. Moreover, ‘hard’ proteins tend to adsorb readily on a hydrophobic surface with minimal structural change whereas ‘soft’ proteins adsorb to all the surfaces (hydrophilic and hydrophobic surfaces) with significant conformational changes.

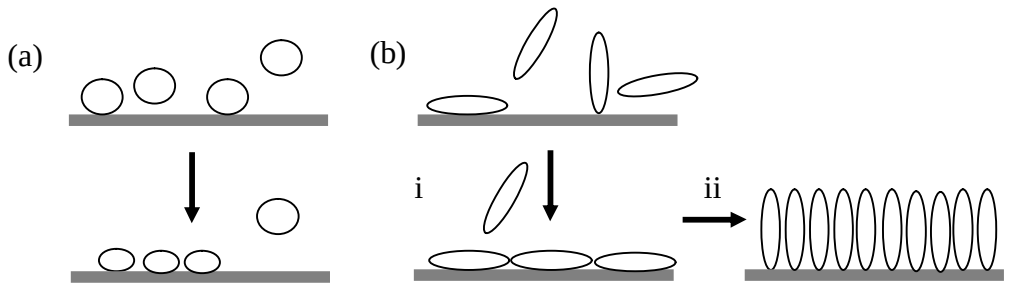

Figure 2.4: A schematic diagram to show (a) a globular protein (for example, bovine serum albumin (BSA)) whose conformation may become distorted on interaction with the surface and (b) a rod-like protein that undergoes a multistage adsorption process where (i) initially the protein adsorbs with its long axis parallel to the surface and then (ii) rearrangement occurs to increase a protein-protein interaction and a surface concentration of protein. Taken from Roach et al. [2005].

4) Detachment of a protein from the surface

If the binding between proteins and surfaces is not too strong (physical adsorption) then the proteins may easily be desorbed. Protein adsorption is usually only partially reversible because proteins undergo structural changes due to adsorption and they are attached with many segments to the surface. Changing the pH or increasing the ionic strength can promote desorption of proteins.

5) Transport away from the surface

This step is just the reverse of step one. It could be that the desorbed protein has an altered structure compared to the native state. In many cases, the desorbed proteins can be readsorbed.

2.3.3 Effects of operating condition on protein adsorption

Protein adsorption is a complex process mostly due to the diverse nature of proteins (for example, size, shape, structure, stability, composition, isoelectric point and flexibility) and the surface properties (such as chemical property, density and architecture). Multiple compounding factors are interrelated and it is difficult to single out the effect of any one on protein adsorption. Below are some examples of operating conditions that could affect protein adsorption.

2.3.3.1 Temperature

Temperature can be considered as the most important factor in protein adsorption. It has been widely reported [Jackler at al., 2002, Desroches and Omanovic, 2008, McColl et al., 2008] that protein adsorption is usually higher at high temperature than at room temperature. Figure 2.5 shows the example of adsorption of lysozyme on the silica-water interface as a function of temperature [Jackler at al., 2002]. As can be seen, the degree of lysozyme adsorption on a silica surface increased strongly with the rise of temperature. Figure 2.6 illustrates the corresponding possible structure of lysozyme adsorption with the respect of temperature.

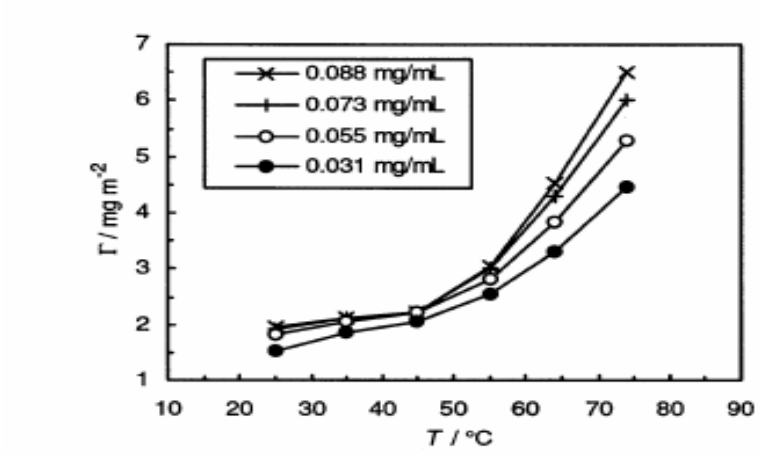

Figure 2.5: Adsorbed mass per surface area of lysozyme (dry basis) as a function of temperature on a silica surface (at a saturation state). The data have been measured using optical reflectometry at different solution concentrations, which are given in the inset. Taken from Jackler et al. [2002].

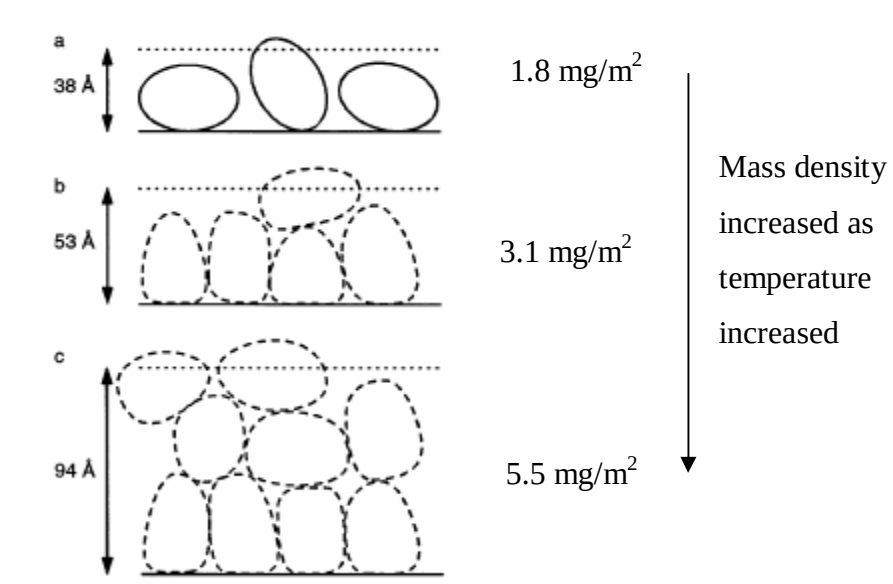

Figure 2.6: Schematic drawings of the proposed structures of lysozyme at (a) 23 °C (b) 63 °C (c), and 80 °C. The dashed lines indicate mainly unfolded lysozyme conformations (measured by reflectrometry without H_2O). Taken from Jackler et al. [2002].

However, in some cases, the adsorption decreases with temperature. For example, Fuzuzaki et al. [1995] reported that gelatin adsorption decreased from 3 to 2 mg/m^2 at temperature ranged from 40 to 80 °C.

2.3.3.2 pH and ionic strength

pH as well as ionic strength are the main contributors to determine the electrostatic attraction or repulsion in protein adsorption. For the effect of pH, refer to Section 2.3.1.3 under electrostatic interaction. In general, the adsorption is minimum if both protein and the surface are neutral [Nath et al., 2004, Pasche et al., 2005]. Cabilio et al. [2000] found a contradictory result of adsorption with respect to pH. They found that α-lactalbumin (pI ≅ 4.3) expressed the highest adsorption at pH 2 and the lowest at pH 11 on platinum surfaces. At pH 11, the protein has a large negative net charge whereas the surface is positively charged. In contrast, at pH 2, the protein has a large positive charge and the surface is positively charged but yet

adsorbed mostly at low bulk concentrations. They believed that the possible explanation for these contradictions could be as follows; at pH 2, the carboxyl groups in α-lactalbumin were protonated and the interaction between (solvated) carboxyl groups and water molecules was rather weak (a dipole-dipole type of interaction). On the other hand, at pH 11, carboxyl groups are depronotonated and negatively charged. Their interaction with water molecules was much stronger (ion-dipole interaction) than that at pH 2. Consequently, dehydration of carboxylate groups at pH 11 and their attachment to the platinum surface required more energy and resulted in a small adsorption on the surface.

Meanwhile, an ionic strength is associated with the thickness of the diffuse ion layer. The charge of the surface [Pasche et al., 2005] will show its effect only within a certain distance to the surface charge. Nath et al. [2004] claimed that adsorption of protein scales inversely with the ionic strength, since an increase in the solution ionic strength shields the charges on the protein and the surface more efficiently, hence reduces protein adsorption. It was reported that at pH far from their pI, the effect of ionic strength disappeared gradually and protein adsorption was no longer dependent on pH when the ionic strength was too high [Hook et al., 1998]. This may explain the otherwise puzzling results of Cabilio et al. [2000] above.

Figure 2.7 shows the effect of ionic strength (1 mM HEPES buffer (H0) to 10 mM HEPES buffer with 150 mM NaCl (H2), on adsorption of lysozyme (pI ≅ 11), myoglobin (pI ≅ 7.0) and α-lactalbumin (pI ≅ 4.3). 1 mM HEPES buffer (H0) to 10 mM HEPES buffer with 150 mM NaCl (H2), lowering the calculated Debye length from about 10 nm down to <1 nm. The adsorption of positively charged lysozyme onto Nb_2O_5 surfaces showed a dependence on the ionic strength, with protein adsorbed mass decreasing as the ionic strength increases. Myoglobin and α-lactalbumin adsorbed in lesser amounts onto Nb_2O_5, and the adsorbed mass was independent of the ionic strength of the solution. This indicates that other mechanisms than electrostatic forces were responsible for the observed adsorption of these proteins, possibly accompanied by a partial unfolding of the proteins at the interface.

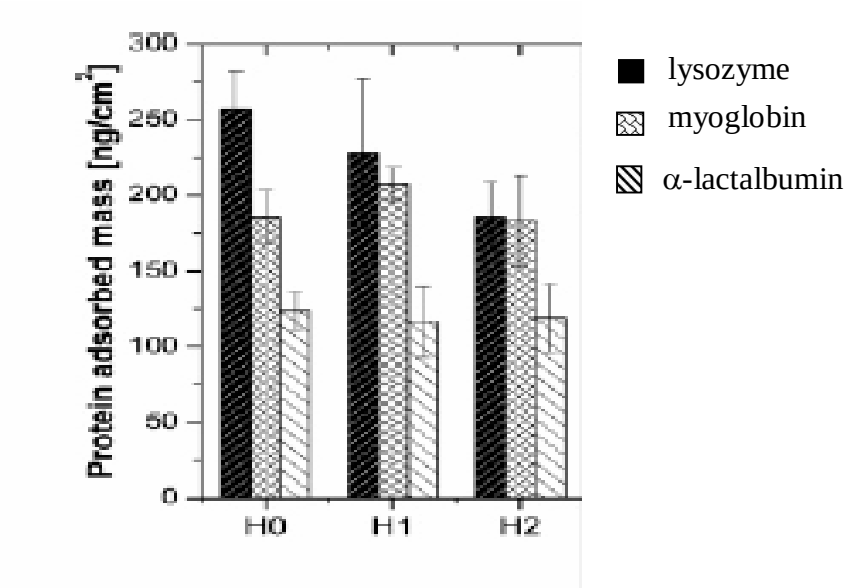

Figure 2.7: Adsorption of lysozyme, myoglobin and α-lactalbumin as a function of ionic strength on a niobium oxide surface (Nb_2O_5). H0, H1 and H2 are the ionic strength of 1 mM HEPES buffer, 10 mM HEPES buffer and 10 mM HEPES buffer + 150 mM NaCl, respectively. The experiments were performed at pH 7.4. Taken from Pasche et al. [2005].

2.3.3.3 Concentration and size of protein

It is well accepted that higher protein concentration results in more adsorption on surfaces and a saturated monolayer is reached faster than for lower concentration [Voros, 2004, Roach et al., 2005, Santos et al., 2006 and Lamotte et al., 2008]. Figure 2.8 shows an example of the effect of concentration on mass density adsorbed.

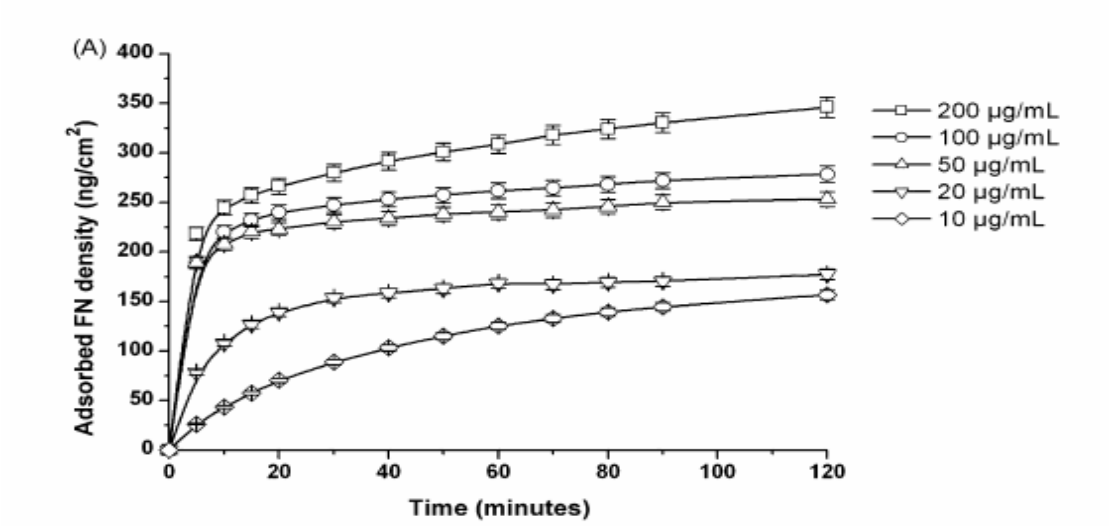

Figure 2.8: Adsorption kinetics of fibrinogen on a bare silica surface during 2 hours at five different concentrations. Taken from Lamotte et al. [2008].

Once the initial protein monolayer is established, additional protein molecules tend to adsorb onto the first layer and form a multilayer. If this happens**,** it is expected that any modification of the surface is no longer effective. It is because the surface modification gives a pronounced effect on only the first monolayer whilst the second and the rest of the layers are more influenced by the interaction between proteins [Addesso et al., 1997]. These protein-protein interactions are via hydrophobic, hydrophilic and ionic interactions or by covalent bonding such as thiol (S-H) group interactions. Figure 2.9 shows an illustration of a monolayer protein (A) and multilayer protein (B).

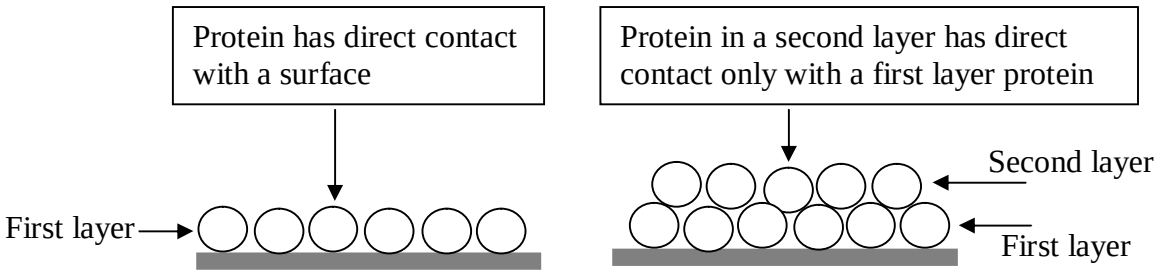

Figure 2.9: Illustration of protein-surface interaction in monolayer (A) and multilayer (B).

The concentration of a protein solution appears to influence the denaturation state of a protein. At low concentration, a protein can maximize interactions with the surface both by its orientations as well as by unfolding (spreading) that leads to denaturation and irreversible adsorption of the protein at the surface. As the protein concentration increases [Veen et al., 2005] the supply rate to the surface increase and the surface will be filled in a shorter time span. Hence, the time available for spreading will be shorter and consequently this suppresses the spreading of protein molecule (most proteins retain the stable conformation). Therefore, the surface mass density adsorbed becomes larger as the adsorbed protein achieves a smaller footprint at the surface (refer to Figure 2.10). The footprint is the surface area that a protein occupies on adsorbing. Note that this is a kinetic rather than an equilibrium thermodynamic argument.

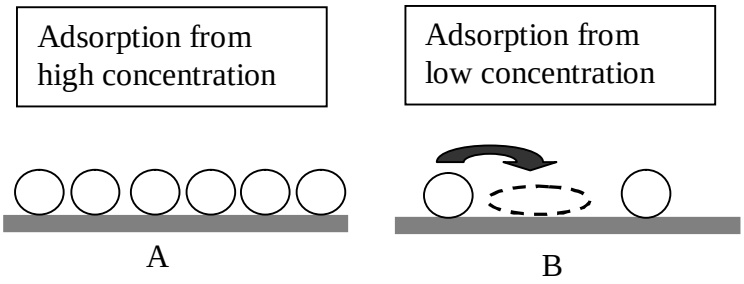

Figure 2.10: Illustration of adsorption from high concentration (A) and from low concentration (B) onto the surface with the same area.

From the protein size point of view, a protein with a smaller size [Voros et al., 2004, Micheal, 2005] generally adsorbs much more and is more compact with a higher mass surface density than a larger protein.

2.4 POLY(ETYLENE GLYCOL) (PEG) OVERVIEW

2.4.1 Poly(ethylene glycol) (PEG)

Poly(ethylene glycol) (PEG) is a synthetic non-toxic polymer and has been approved by the FDA for internal consumption (i.e. makes it suitable for applications in the filed of biomedical devices). The structure of PEG is OH-(-CH_2-CH_2-O-)$_n$-H, usually terminated on each end by an –OH group. Other terminations are possible, such as –OCH_3 (in this case, the polymer is referred to as poly (ethylene oxide) (PEO)) [Alessi et al., 2005], -OCH_2, -NHS, and –COOH. It is linear or branched and is available with a range of molecular weights. It is neutral and possesses no acidic sites (excluding the hydroxyl end-group which acts as a weak hydrogen-bond acid) and has only weakly basic ether linkages.

PEG is highly water soluble and has a good structural fit with water molecules, which assures a strong hydrogen bonding between the ether oxygen atoms of PEG and hydrogen atoms of the water molecules. Figure 2.11 illustrates two water molecules are bonded to each PEG ether group (i.e. 2 water molecules / EG monomer). Large numbers of hydrogen bonds with water molecules produce large repulsive forces with proteins, promoting protein resistance (i.e. associated with high PEG MW). This behaviour is also known as that of excluded volume. However, a hydration layer decreases as PEG grafting density increases [Unsworths et al., 2008].

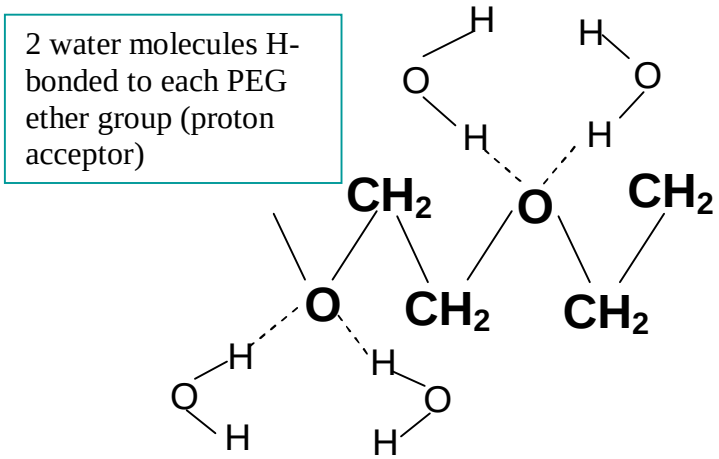

Figure 2.11: Water molecules H-bonded to PEG ether group.

Ethylene oxide segments can adopt multiple configurations and different conformers interact differently with water molecules. The conformers can be divided into a large group of trans and a small group of helical conformers. Trans conformers had non polar characters and were favored at high temperature, whereas the helical conformers had polar characters [Bjorling et al., 1991]. The helical structure of PEG is the characteristic for the crystalline state of the polymer, and it is locally retained when the polymer is dissolved in water. In the helical structure of PEG the bonds of the backbone are arranged in a trans–gauche–trans (*tgt*) order, -OCH_2, C-C and –OCH_2 respectively [Kreuzer et al., 1999, Allessi et al., 2005]. Such a helical conformation contains seven structural units of CH_2-CH_2-O with two helical turns (7/2 helix) with the length of 19.3 Å (for comparison, the length for seven units of the all-trans conformation is 23.9 Å) [Rundqvist et al., 2005]. In a stretch planar 'all trans' form (*ttt*), the chain is fully extended (can be obtained by mechanically stretching the polymer). Hence, with increasing contour length of the polymer chain, the conformation will change from an amorphous via a helical to a planar 'all-trans' structure [Kreuzer et al., 1999].

2.4.2 PEG grafting techniques onto surface

A range of techniques have been employed for the immobilization of PEG onto surfaces and these can be broadly classified as either physisorptive or chemisorptive. Physisorption relies on relatively weak Van der Waals and hydrophobic forces to tether polymers to a surface. Consequently, the polymers are not irreversibly bound [Zhang et al., 2001, Kingshott et al., 2003] to the surface and proteins may be exchanged with the polymer on the surface. One merit with physisorption method is that they are easy and simple.

Chemisorptive methods on the other hand are the most effective way [Zhang et al., 2001, Wei et al., 2003, Zdyrko et al., 2003, Kingshott et al., 2003, Sharma et al., 2004] of creating permanent PEG surfaces. These methods require functional groups to be introduced either onto the substrate surface or onto the PEG hydroxyl group (for example, thiol on a gold surface and silane on a silica surface). However,

exposure to the aqueous environment for prolonged periods can desorb even these covalently attached PEG molecules [Sharma et al., 2004]. Besides that, preparing for chemisorption often requires time consuming, complex processes or multiple steps and use of large amounts of environmentally harmful chemicals. The coupling methods also require relatively complex and often specific substrate-polymer combinations [Zhang et al., 2001, Wei et al., 2003, Zdyrko et al., 2003, Kingshott et al., 2003].

Two basic strategies in chemisorption are either 'grafting to' or 'grafting from' methods as shown in Figure 2.12. Figure 2.12 shows a comparison between 'grafting to' and 'grafting from' techniques; (A) 'grafting to' method, adsorption to surfaces of pre-synthesized polymer chains end-functionalized with an anchoring group, (B) 'grafting from' method, polymer is grown in situ from the surface via a surface-adsorbed initiation group. The 'grafting to' methods can have the advantage that the PEG molecular weight and orientation may be well controlled. However, achieving a high surface coverage is rather difficult because the immobilized polymer chains sterically hinder further diffusion of polymer molecules from solution to the reactive sites at the surface. Meanwhile, the 'grafting from' method has been shown to be very flexible in synthesizing PEG-containing layers with varied thickness, and thus very efficient surface coverage of the base material. However, the control of the PEG layer architecture on a molecular level is limited.

PEG pre-reacted with the reactive group

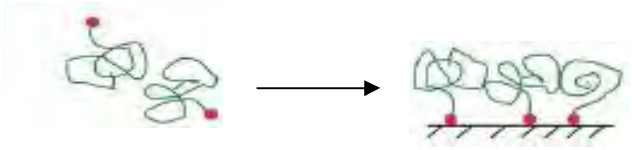

(A) grafting to

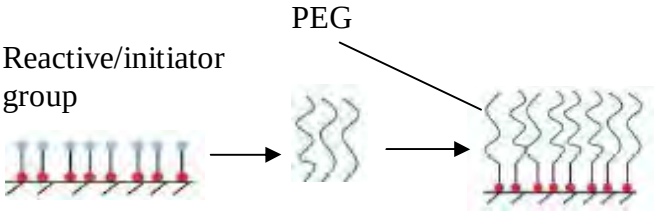

(B) grafting from

Figure 2.12: Technique of grafting (A) 'grafting to' method, adsorption to surfaces of pre-synthesized polymer chains end-functionalized with an anchoring group (B) 'grafting from' method, polymer is grown in situ from the surface via a surface-adsorbed initiation group. Taken from Dalsin and Messersmith [2005].

Grafting at or near a cloud point of PEG as well as conducting grafting from a melt [Wei et al., 2003, Kingshott et al., 2003] rather than in solution can promote formation of a denser polymer layer. The advantage of using a polymer melt is that the polymer chains are not required to diffuse through a solvent to the surface and therefore can overcome the potential barrier present from the already adsorbed chain (i.e. excluded volume). The polymer molecules need to reorient themselves [Zdyrko et al., 2003] within the first monolayer to expose the terminal groups to the surface functionalities - leading to more efficient chain anchoring. Figure 2.13 illustrates the PEG conformation grating below (A) and above cloud point temperature (B). At the cloud point temperature, the polymer loses its solubility and flexibility and thus has less exclusion from already adsorbed molecules (see Section 2.5.1 for the dehydration effect).

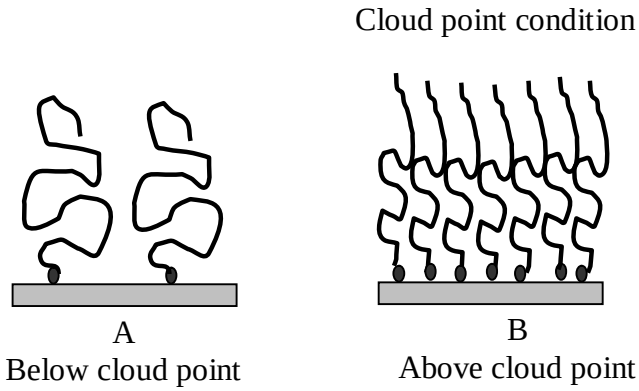

Figure 2.13: The illustrations of the PEG conformation at below (A) and above the cloud point temperature (B).

Other approaches include grafting of PEG using a cold plasma technique [Denes et al., 2001], also known as a dry chemistry method. The plasma deposition process involves monomer fragmentation, rearrangement, cross-linking and polymerization. The technique [Dong et al., 2005] does not involve the usage of bulk toxic reagent, and can be applied to a large variety of substrates. Furthermore it can performed under low pressure (under vacuum, 10^{-2}-10^{-3}mbar) and near room temperature. Thus, gives an advantage for the industry applications. Besides that, [Bremmell et al., 2005] the method is effective and easy to generate a PEG-like structure. It is a one step process since during deposition, two processes can occur simultaneously: the ionization of gaseous species (inducing the plasma creation) and the fragmentation then recombination of monomers (polymerization) (i.e. 'grafting from' technique). These two processes have a strong influence on the properties of the deposited film and can be controlled by tuning the deposition parameters [Bre´tagnol et al., 2006]. In another study [Zhang et al., 2001], UV has been used after argon plasma treatment. UV was used to induce a PEG graft polymerization.

Another approach, which is simple and cost-effective approach for producing surfaces with dense arrays of PEG brushes, relies on the spontaneous assembly of PEG-grafted copolymers onto the surface. Self assembled monolayers (SAMs) can be

prepared simply by adding a solution of the desired molecule onto the substrate surface and washing off the excess (i.e. 'grafting to' technique) [Rundqvist et al., 2005, Menz et al., 2005]. Figure 2.14 shows an example of SAMs of oligoethylene glycol terminated alkanethiols on a gold surface.

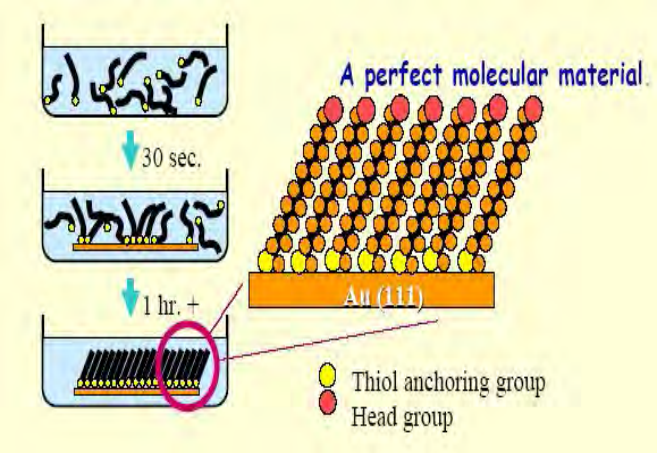

Figure 2.14: Ethylene glycol $(EG)_n$-SH Self-Assembly on Gold (111).

The thiol (S-H) head group will stick to the gold surface with the oligoethylene glycol terminated alkane tail pointing away from the substrate. Sulfur has a particular affinity for gold and binds chemically with a gold surface. Amphiphilic block copolymers consisting of PEG and Polylactide (PLA) can also assemble spontaneously into micelles in an aqueous system [Otsuka et al., 2001]. Ostuni et al. [2003] produced mixed SAMs of two alkanethiolates with different terminal end groups in their work. Nath et al. [2004] discussed the stability of SAMs. They revealed that SAMs are also fragile owing to their molecular scale thickness and tendency of the chemisorbed thiolate to oxidize. This method is widely used on gold and silica surfaces.

Similarly, cationic polyelectrolytes, such as poly(ethylene imine) (PEI) or poly(L-lysine) (PLL) grafted with PEG side chains, have been shown [Pasche et al., 2005, Thierry et al., 2008] to spontaneously adsorb from aqueous solutions onto negatively charged surfaces as shown in Figure 2.15.

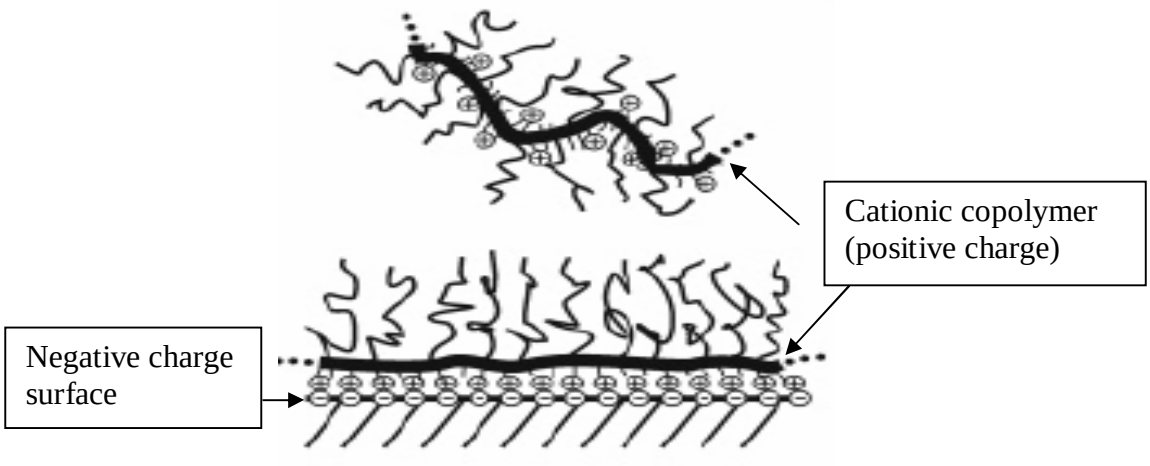

Figure 2.15: Electrostatic interaction between cationic copolymers and negative charge surfaces, for example PEI as the cationic copolymer.

This interaction can be stably immobilized provided that the electrostatic interaction between the surface and polymer backbone is strong. For this surface modification procedure, [Nnebe et al., 2004, Micheal, 2005, Pasche et al., 2005] the PEG can either be prereacted with the PEI and the graft copolymer physically adsorbed to the surface or alternatively the PEG can be grafted onto a preadsorbed PEI layer. However, despite the strength of the electrostatic interactions that control PEI adsorption, PEI coatings are somewhat unstable. A crosslinking modifier such as glutaraldehyde has been used to prevent desorption of PEI from surfaces [Nnebe et al., 2004]. Since this method of immobilization is based on electrostatic interactions, pH is obviously an important parameter for such systems.

An atom transfer radical polymerization (ATRP) is another robust method to graft a high density of PEG onto surfaces. ATRP is a controlled or "living" polymerization based on the use of radical polymerization to convert monomer to polymer [Matyjaszewski et al., 2001, Pyun et al., 2003]. When the ATRP is applied to gold or silica surfaces modified with a thiol or a silane as an initiator, respectively, the polymerization leads to the growth of polymer brushes [Zhao et al., 2005, Brown et al., 2005, Moya et al., 2005, Menz et al., 2005]. This reaction can be carried out in

a controlled way such that it allows precise control over thickness, composition and density of the polymer layer [Tugulu et al., 2005]. The control of the polymerization afforded by the ATRP is a result of the formation of radicals that can grow, but are reversibly deactivated to form dormant species. Reactivation of the dormant species allows the polymer chains to grow again, only to be deactivated later. Such a process results in a polymer chain that slowly, but steadily, grows and has a well-defined end group.

2.4.3 PEG conformation

The conformation of the grafted PEG chain and the thickness of the layer are dependent on the grafting density or spacing between the chains (d) and on the length of the chain, which is related to the Flory radius (R_F) in solution. R_F is the average distance of the atoms of a monomer from the polymer's centre of mass. The Flory radius (R_F) can be estimated using the Equation 2.4

$$R_F = aN^{v} \qquad (2.4)$$

where a is the characteristic monomer dimension (taken as 2.78 Å for the ethylene oxide repeat), N is the degree of polymerization and v may be taken as 0.6 for high-solubility conditions [Unsworth et al., 2005].

Meanwhile,

$$d = \sigma^{-0.5} \qquad (2.5)$$

where σ is the PEG grafting density (chains/area).

At low surface coverage ($d >> 2R_F$), the polymer molecules form either a ‘pancake’ or a ‘mushroom’ structure, depending on whether the interaction between the polymer segments and the surface is attractive or repulsive, respectively. At $d \sim 2R_F$, the ‘mushrooms’ start to interact with each other until the brush transition ($d < 2R_F$), where the polymer chains stretch away from the surface resulting in a ‘brush’

conformation. The illustration of pancake, mushroom and brush is shown in Figure 2.16. The 'mushroom' and in particular 'brush' polymers are more extended and the 'pancake' type is collapsed onto the surface. The polymer tends to collapse on the surface if there is an attractive interaction between the surface and the polymer [Jonsson et al., 2004].

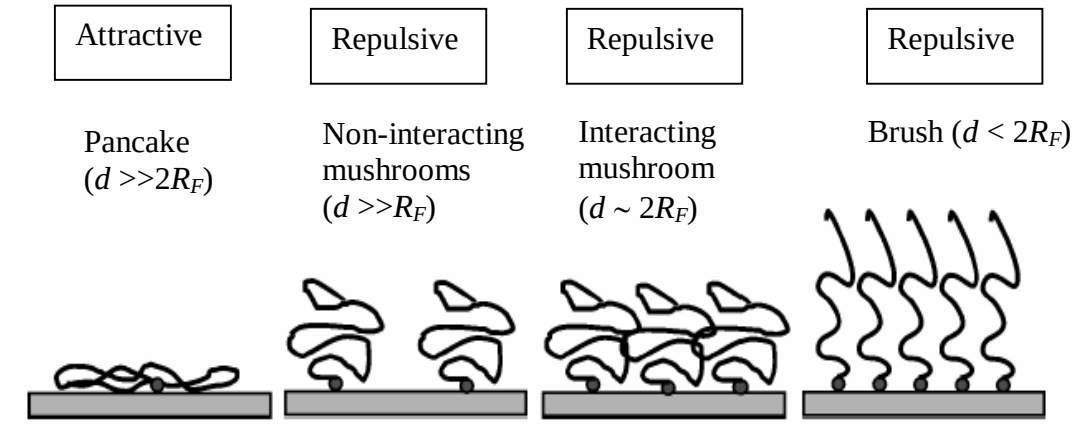

Figure 2.16: Schematic representation of the conformation of end-grafted PEG chains at the interface, depending on whether the chain is attracted to the surface or repelled.

Solvent can influence the form of PEG on a surface dramatically. They can form a 'brush' when PEG molecules were exposed to 'good solvent' (attractive), and when exposed to 'bad solvent' (non-attractive), they do not form a brush (see Figure 2.17).

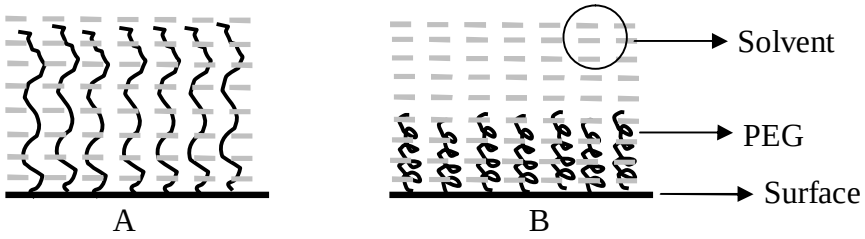

Figure 2.17: Effect of solvent to the PEG conformation (A) PEG chains are exposed to ‘good solvent’ (attractive), the chains will orient into a dense, brush-like structure, (B) Replacement with ‘bad solvent’ (non attractive) causes the PEG brush to rearrange to a more random, coil-like conformation. Taken from Muller et al. [2005].

2.5 PROTEIN-PEG INTERACTION OVERVIEW

2.5.1 Mechanism of protein resistance by PEG

Halperin [1999] in his study has proposed three modes of protein adsorption (see Figure 2.18):

- *Primary adsorption* at the substrate surface due to proteins diffusing through the pores between PEG layers to the underlying substrate (that is, adsorption due to surface-protein attraction), and relevant for small protein molecules that can penetrate through the grafted chain interface (that is, a protein size is smaller than the separation distance between the PEG chains).
- *Secondary adsorption* at the outer edge of the brush due to protein brush-interaction via van der Waals and/or electrical double-layer attraction and relevant for larger proteins (that is, a protein size that is larger than the separation distance between the PEG chains). This adsorption decreases with increasing chain length and may be important for a long cylindrical chain.
- *Tertiary adsorption* occurring from compression of protein molecules into a PEG layer. This is a variation of primary adsorption for very large proteins.

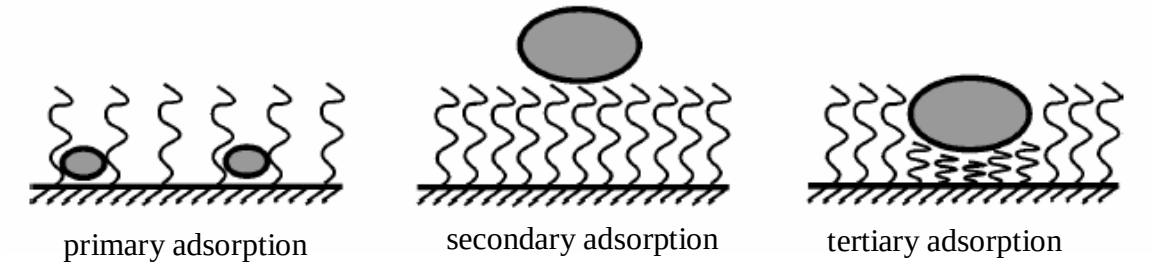

Figure 2.18: Schematic illustration of mode of adsorption; primary, secondary and ternary adsorption [Helparin, 1999].

Thus, to prevent the adsorption of proteins, those three modes of adsorption all have to be eliminated (refer to Figure 2.19):

- *Primary adsorption*

  Dense PEG layers are required (i.e. the spacing between PEG chains should less than the diameter of protein, $d_{PEG} < D_{protein}$) to prevent proteins from diffusing through the PEG layer and adsorbing onto the underlying substrate.

- *Secondary adsorption*

  Adsorption at the top of the PEG layer is avoided when the PEG layer is sufficiently thick to hide the diffuse ion layer; thereby, the minimum thickness required depends on the ionic strength of the protein solution.

- *Tertiary adsorption*

  The mobility of the chains acts as an entropic factor making compression of the chains by proteins unfavorable. PEG's hydrophilicity and ability to accommodate water eliminates hydrophobic interactions, as well as eliminates protein denaturation that would result in an entropic conformational gain for the protein.

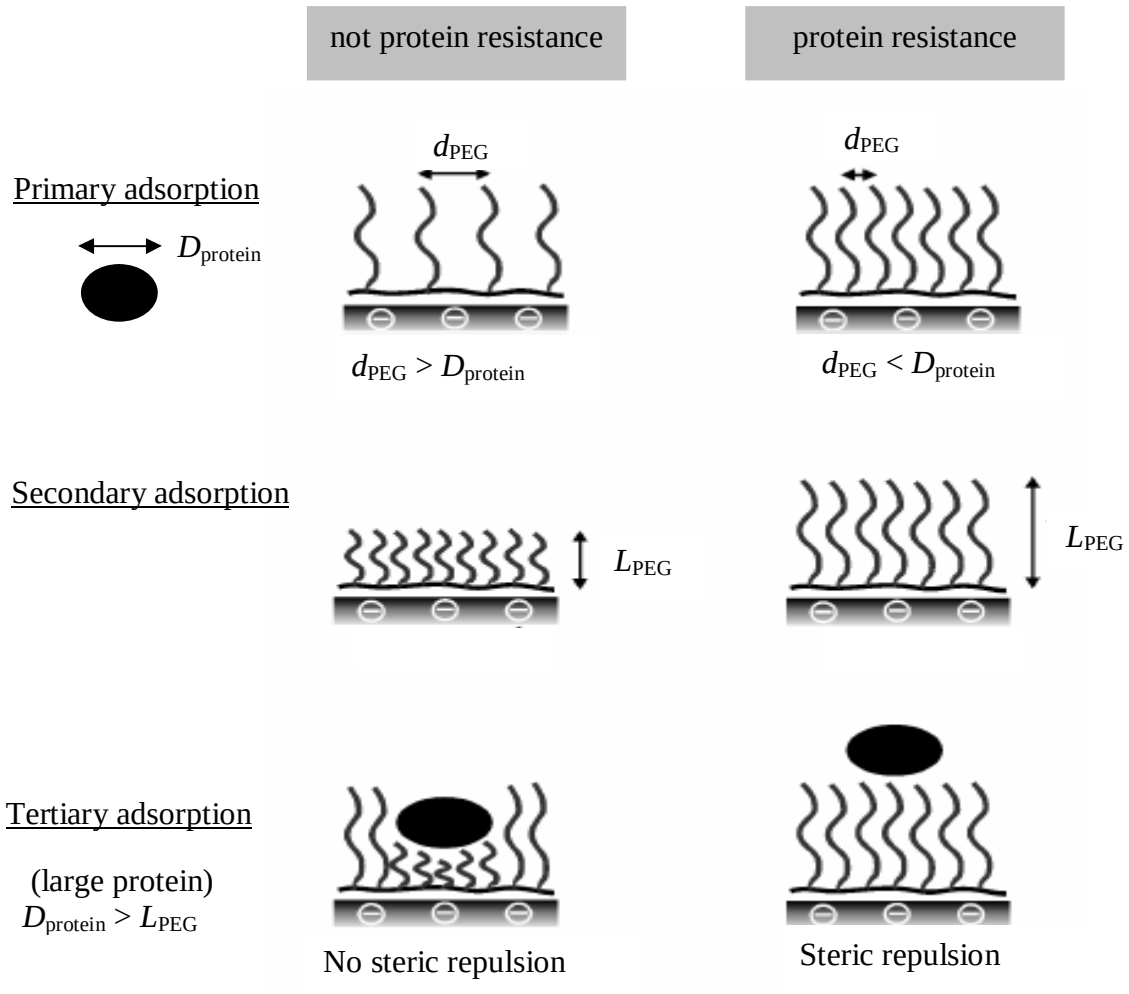

Figure 2.19: Illustration of the different aspects to achieve protein resistance with PEG coatings.

However, Currie et al. [2003] have made some modifications to the tertiary adsorption scheme (see Figure 2.20). They associated the *tertiary adsorption* to small proteins instead of large proteins as proposed by Helparin [1999].

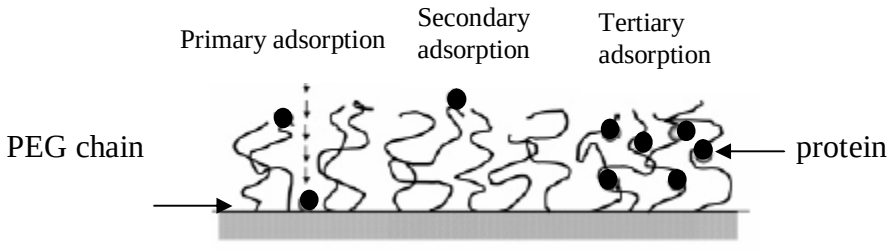

Figure 2.20: Schematic illustration of a possible interaction of probe molecules with a polymer brush. Taken from Currie et al. [2003].

In this mode, the proteins diffusing through the layer are attracted to the PEG chains and do not reach the substrate (that is, interaction between protein and polymer segments within the brush layer occurs). For relatively small proteins, the primary and tertiary adsorption would be particularly important, but they should become less important with increasing protein size and increasing graft density. A larger protein would find it more difficult to diffuse in if the grafting density is high. Heparin et al. [2007] in their recent work also came out with the same description for the tertiary adsorption as Currie et al. [2003] and suggested that the adsorption of small proteins does not significantly perturb the brush structure whereas large proteins can enter the brush only by inducing local compression.

Meanwhile, the protein resistance of PEG coatings is widely reported [Zdyrko, 2003, Archambault et al., 2004, Zheng et al., 2005, Menz et al., 2005] associated with two main mechanisms; (i) steric repulsion and (ii) water barrier:

(i) **Steric repulsion** is attributed to chain compression of the PEG (conformational entropy loss) as the protein approaches the surface of the PEG layer and deforms the chain. The elasticity of the chain then repulses the protein. This hypothesis is often used to explain the action of PEG polymers with a long chain length. Figure 2.21 shows a schematic diagram of the steric repulsion.

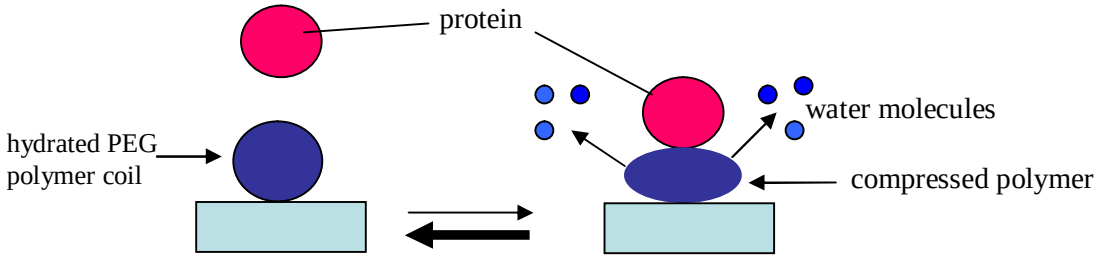

Figure 2.21: Schematic diagram of a steric repulsion.

(ii) **Water barrier** is based on the idea that the binding of water to PEG is sufficiently tight that an approaching protein cannot interact with the surface (see Figure 2.22). Unlike steric repulsion, this theory is in accord with the observation that very short PEG grafts of two or three monomers can give protein resistant surfaces.

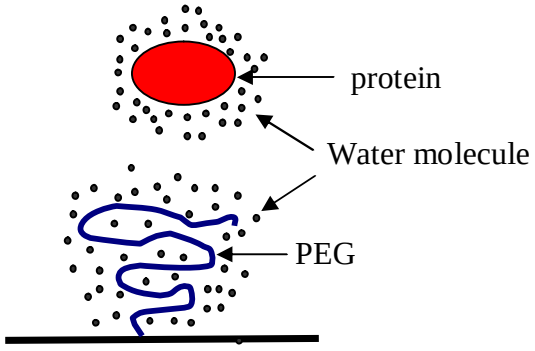

Figure 2.22: Water molecule as a barrier.

2.5.2 Factors affecting the protein resistance by PEG

2.5.2.1 PEG chain length (MW) and grafting density

Theoretically [Szleifer 1997, Satulovsky et al., 2000, Carignano et al., 2000] and experimentally [Prime and Whiteside, 1993, Wei et al., 2003, Archambault et al., 2004, Brash, 2004, Jonsson et al., 2004, Fukai et al., 2004, Liu et al., 2007, Unsworth etal., 2005, Uchida et al., 2005, Yoshikawa et al., 2006, Satomi et al., 2007, Unsworth et al., 2008] approaches have demonstrated the importance of chain length and grafting density of PEG for imparting protein resistance to surfaces. The general trend for protein resistance is that it generally improves as: (i) PEG grafting density is high (a brush regime) [Uchida et al., 2005, Yoshikawa et al., 2006, Satomi et al., 2007a, Satomi et al., 2007b]] and (ii) the length of the PEG chains increases. Higher grafting density is argued to result in more difficulty for proteins to diffuse to the underlying substrate (i.e. equilibrium argument) whereas higher chain lengths results in larger excluded volumes and more pronounced steric repulsion (i.e. kinetic argument). Moreover, a thicker PEG layer implies a larger separation, L, between the surface and the incoming proteins and hence a stronger attenuation of the long range Van der Waals interaction [Archambault et al., 2004, Roosjen et al., 2004]. Therefore, the *secondary adsorption* can be minimized. However, it is difficult to achieve high PEG grafting density and high chain length at the same time. This is because immobilization of longer PEG chains results in a decrease in chain density due to its larger exclusion volume effect during the grafting process. However, a longer PEG chain always results in a larger L [Helparin, 1999, Wei et al., 2004, Archambault et al., 2004, Roosjen et al., 2004, Unsworth et al., 2005]. Conversely, immobilization of shorter PEG chains results in a higher density due to its smaller exclusion volume effect. Although it has a smaller L, higher PEG density may eliminate primary adsorption (i.e. if $d_{PEG} > D_{protein}$).

Prime and Whiteside [1993] reported that the adsorption of fibrinogen, lysozyme, pyruvate kinase and RNAse proteins on self-assembled monolayers (SAMs) on a gold surface reduced with increasing length of the oligo (ethylene oxide) (EO) chains. However, short EO containing chains ($N \geq 1$) can also effectively

resist the adsorption of proteins. They concluded that the principal criterion for protein resistance in their systems was a complete coverage of the surface by an EO film of any thickness. We expect this observation is due to a *water barrier* mechanism. Currie et al. [1999] also used short PEO grafted chains (N = 148) finding that the adsorption of bovine serum albumin (BSA) decreased continuously with the increase of PEO grafting density. For long PEO chains (N = 445 and 7000) however, the adsorption of BSA increased with grafting density at low grafting densities then decreased at high grafting densities. The maximum of adsorption seemed to increase with increasing N (refer to Figure 2.23). They suggested that this observation was due to long chains that easily trap the proteins than short chains.

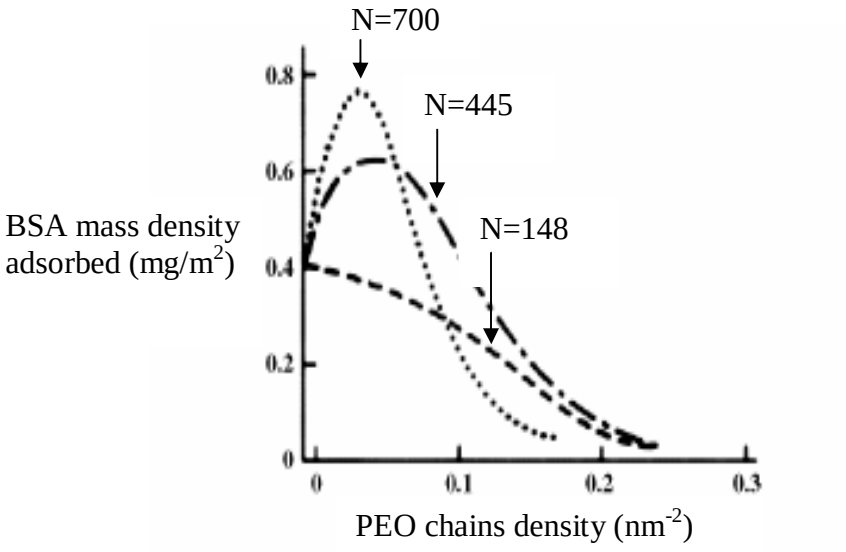

Figure 2.23: BSA adsorption on a hydrophobic polystyrene surface grafted with PEO brushes with different chain length; N =700, 445 and 148. Taken from Currie et al. [1999].

Experimental work done by Wu et al. [2000] also showed that a surface covered with a monomer containing as few as two ethylene glycol (EG) units was able to reduce BSA and human fibrinogen adsorption. They concluded that long

chain polyethylene oxide (PEO) units were not a necessary requirement for non-fouling properties of PEO modified surfaces.

Zhu et al. [2001] have compared the relative protein resistance of short and long ethylene oxide chains, SAMs of PEG 5000, PEG 2000, Oligo(ethylene glycol) O-EG_3 (120 Da) and O-EG_6 (240 Da) on gold surfaces. They used serum protein and a low protein (1 % albumin) culture medium as the protein to adsorb. They found that the protein resistance of O-EG_6 and both PEG SAMs were similar to that measured with the O-EG_3 film. The sample-to-sample variation was less than 1 %. Fibrinogen adsorption was not significantly different [Usworth et al., 2005] for surfaces prepared with PEO of molecular weight 750 (N = 17) and 2000 Da (N = 45) when the chain density was the same (0.5 chains/nm^2). In the study done by Yoshikawa et al. [2006], the grafting density of 0.7 chains / nm^2 showed excellent protein resistance for aprotinin, myoglobulin, bovine serum albumin (BSA) and immunoglobulin (IgG) proteins (the diameter of the proteins ranged from 2 to 13 nm) regardless of chain length (i.e almost zero adsorption). By contrast, at grafting density of 0.007 chains / nm^2, the surface showed a poor resistance against protein adsorption, especially for a small protein, aprotinin (i.e. diameter of about 2 nm) (refer to Figure 2.24). They ascribed this to *tertiary adsorption*. Meanwhile, at intermediate density, 0.06 chains / nm^2, the surface effectively suppressed the adsorption only of larger proteins and not small proteins. Their study shows a good correlation between the protein size and the threshold grafting density beyond which the protein does not adsorb. The adsorption was performed at room temperature.

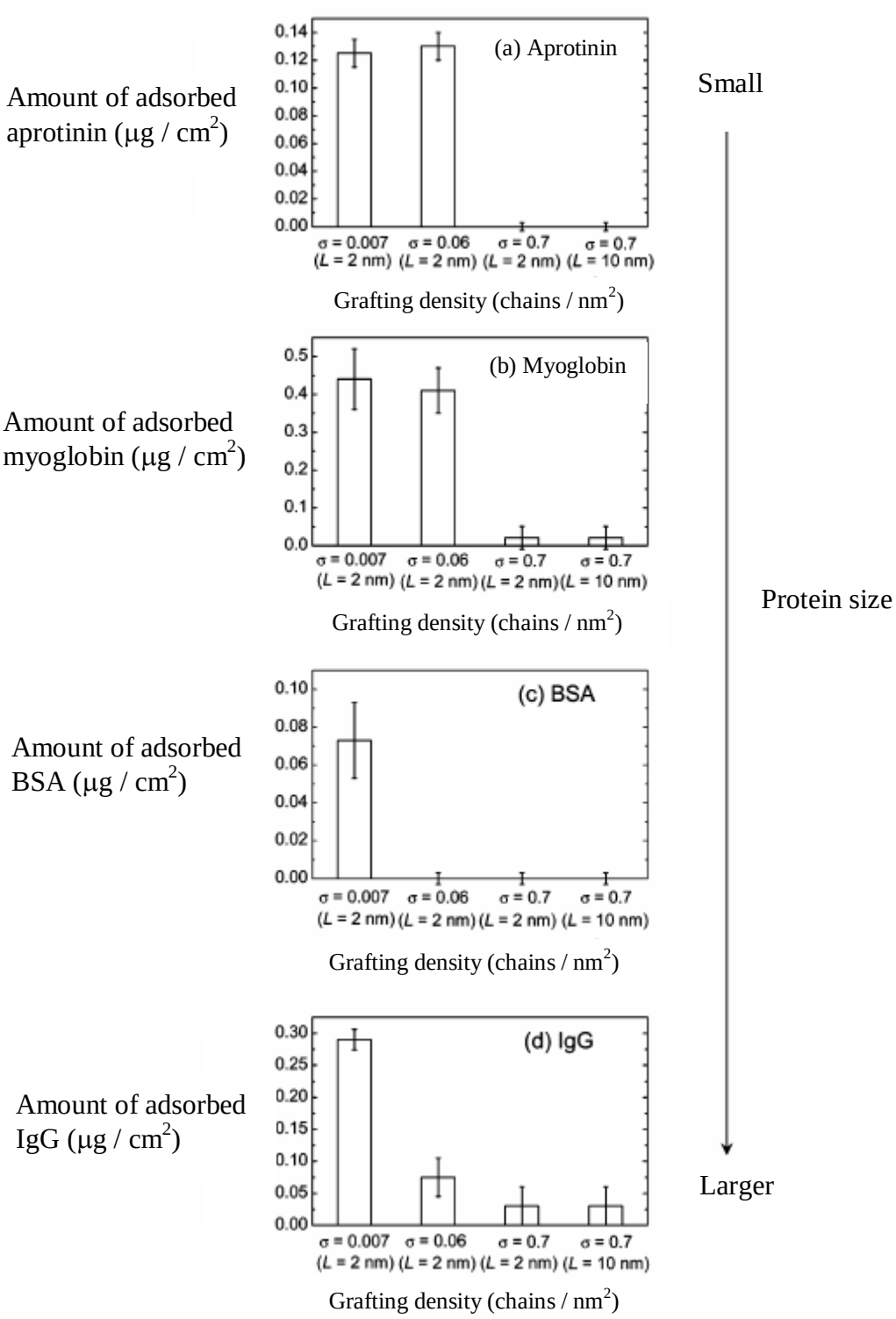

Figure 2.24.: Amounts of adsorbed proteins onto poly (2-hydroyethyl methacrylate) (PHEMA)PHEMA brush surfaces at room temperature. : (a) Aprotinin, (b) Myoglobin, (c) BSA, and (d) IgG. The protein concentration was 1 g / L in all cases. Taken from Yoshikawa et al. [2006].

To study the effect of PEG chain length (MW) against protein adsorption, Satulovsky et al. [2000] have done a simulation study and predicted that the amount of protein adsorbed decreased with the chain length of the grafted polymers, N, up to 25 (close to PEO1000). Same as PEO2000, the amount of protein adsorbed was expected to be almost identical to that of PEO1000. Szleifer [1997] also predicted that protein adsorption is no longer dependent on polymer chain length once it excesses more than 50 ethylene glycol units or about 2000 Da. Simulation study done by Satulovsky et al. [2000] and Carignano et al. [2000] predicted that grafting density has pronounced effect compared to chain length.

Experimental work done by Archambault et al. [2004] demonstrated that the adsorption of proteins decreased with increasing MW of PEO, sharply low MW but more gradually at higher MW (refer to Figure 2.25). The decrease in protein adsorption reached a limit at a molecular weight of 2000 Da with adsorption in the range 30 to 40 % that of the bare surface. In addition, the PEO2000 (N = 45) and PEO5000 (N = 114) surfaces adsorbed similar amounts.

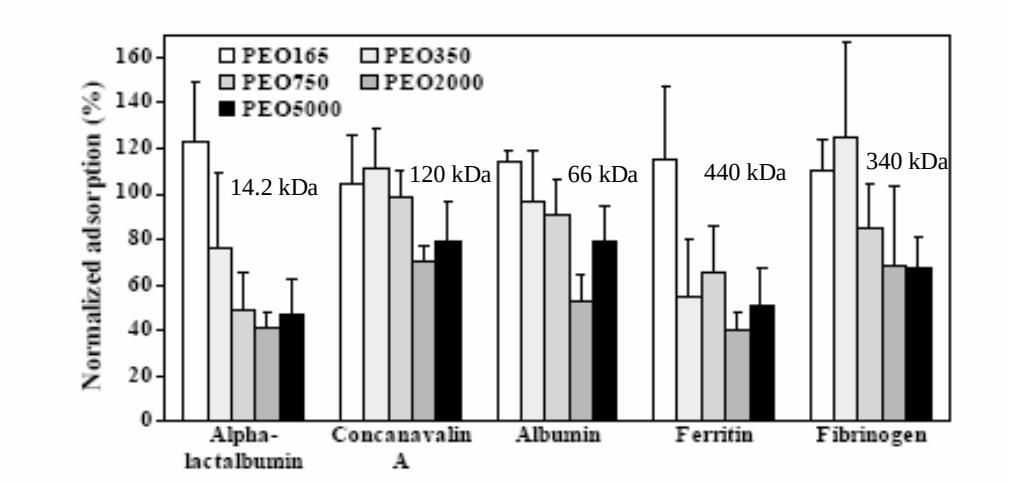

Figure 2.25: Effect of PEO molecular weight (chain length) towards adsorption of various proteins. Taken from Archambault et al. [2004].

Similarly, adsorption of albumin and fibrinogen onto PEO surfaces has been found [Gombotz et al., 2004] to decrease with increasing PEO molecular weight up to 3500 Da (N = 79). A further increase in molecular weight (chain length) resulted only in a slight decrease in protein adsorption. Benhabbour et al. [2008] also studied the relationship between the protein resistance and the PEG MW. They adsorbed lysozyme and fibrinogen on PEG750, 2000 and 5000 Da grafted on a gold surface. They found that the adsorption of both lysozyme and fibrinogen decreased with increasing PEG MW up to 2000 Da. When the PEG MW was further increase to 5000 Da, protein repulsion did not improve. They could not provide a definite explanation for this latter result.

Those findings show that once the grafting number density is enough to shield the surface, the effectiveness of the surface is no longer PEG chain length dependent. The sufficient level to do this may sound arbitrarily, but most of the publications did not report PEG grafting number density quantitatively.

The findings also apparently imply that PEG grafting number density is more important than PEG chain length in inhibition of protein adsorption. Most of studies done [Mcpherson et al., 1998, Archamabult and Brash, 2003, Fukai et al., 2004] supported the conclusion that grafting number density was also more dominant for inhibiting protein adsorption than chain length.

However, if the number density is too high (dense brush regime), the graft itself may become an adsorbent for protein and hence increase the adsorption of protein. Chains that are too dense [Zdyrko et al., 2003, Unsworth et al., 2005] will also dehydrate and lose the flexibility to sweep away the incoming proteins. Theoretical work by Carignano and Szleifer [2000] revealed that a very high surface coverage will modify the chemistry of the surface and may result in an attractive surface to proteins. This indicates that there is a critical value of chain density to effectively suppress the adsorption of protein.

Vaderah et al. [2008] also found that the adsorption of bovine serum albumin (BSA) was 0.04 times lower on surfaces with EO surface coverage of 60 % than of 85 %. They suggested that a near complete inhibition of adsorption of BSA by the lower

grafting number density was caused by the underlying substrate being fully screened by conformationally mobile, surface-bound molecules.

Herrwerth et al. [2003] suggested that the grafted chains must be sufficiently spaced to enable water to penetrate the layer, especially for a PEG layer with methoxy-terminated surfaces. They argued that the protein resistance required both internal and external hydrophilicity. Hydration of the PEG layer decreases as PEG grafting increases.

Unsworth et al. [2005] showed that the adsorption of fibrinogen decreased as the number chain density of PEO2000 Da increased and was minimum at a density of about 0.5 chains / nm^2 (15 % adsorption of that on the bare surface). Refer to Figure 2.26 as an example. Note that this plot the reduction in adsorption. As the PEO2000 Da chain density increased beyond 0.5 chains / nm^2, the adsorption of fibrinogen increased. The optimal chain density of PEO750 for the minimum fibrinogen adsorption was almost the same, at 0.5 chains / nm^2. At this point, the adsorption was also 15 % of that on the bare surface and also started to increase as the chain density increased. However, for PEO5000 Da, the optimal chain density was 0.3 chains / nm^2. At this point, the adsorption of fibrinogen was about 35 % than of the bare surface. In addition, they found the same optimal grafting density for minimum lysozyme adsorption but at a different percentage of adsorption. For example, the minimum adsorption of lysozyme on a PEO750 surface was about 35 % whereas on PEO2000 and PEO5000 surfaces were about 20 and 70 %, respectively. Table 2.1 tabulates a summary of their findings.

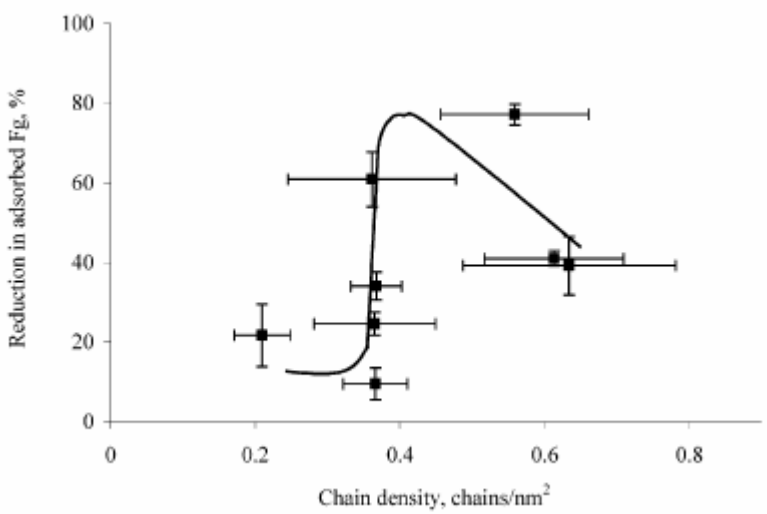

Figure 2.26: Reduction in fibrinogen adsorption onto gold surfaces modified with PEO2000 Da as a function of surface chain density. The reduction of adsorption increased as the PEO grafting density increased up to about 0.5 chains/ nm^2. Beyond this point, reduction decreased. The trend line is provided as a guide for the profile. Taken from Unsworth et al. [2005].

Table 2.1: The percentage of minimum adsorption of lysozyme and fibrinogen on PEO surfaces relative to a bare surface [Unsworth et al., 2005].

Surface	Optimal grafting density (chains / nm^2)	Lysozyme (%)	Fibrinogen (%)
PEO750	0.5	35	15
PEO2000	0.5	20	15
PEO5000	0.3	70	35

In a later study, Unsworth et al. [2008] studied the effect of the PEG hydration layer and moiety groups (-OH and O-CH_3) against protein adsorption. Table 2.2 shows the example of relationship between PEO grafting density and PEO hydration from their work. As can be seen, as the PEO grafting density increased, the degree of PEO hydration decreased. Figure 2.27 shows the adsorption of lysozyme on that

PEO-modified surfaces as a function of chain density. As can be seen, the adsorption of lysozyme decreased with the increasing chain density up to a critical value of 0.5 chains / nm^2; after this point, the adsorption of the proteins on the surface with methoxy-terminated (2000-OCH_3) increased while for hydroxy-terminated (600-OH), the adsorption remained constant. They suggested that the properties related to chain density (conformational freedom, hydration) were the main determinants of resistance at chain densities up to a critical value of about 0.5 chain / nm^2 and the moieties come into play at chain densities greater than the critical value. Moreover, their results showed that relatively dense arrays of methoxy groups promote an increase in lysozyme adsorption, whereas the hydroxyl groups provide a nonfouling effect. They stated that high densities of terminal methoxy groups result in increased interchain association and/or adsorption-induced protein denaturation.

Table 2.2: Relationship between PEO grafting density and PEO hydration. Taken from Unsworth et al. [2008].

PEO	PEO density (chains / nm^2)	PEO hydration, $\frac{M_{H_2O}}{\xi_{PEO}}$
600-OH	0.6 ± 0.1	11 ± 3
	0.7 ± 0.2	9 ± 4
	1.5 ± 0.2	4 ± 1
	2.9 ± 0.2	1 ± 0.5
750- OCH_3	0.2 ± 0.1	28 ± 15
	0.5 ± 0.1	13 ± 4
	1.8 ± 0.2	3 ± 1
	2.3 ± 0.1	2 ± 0.4
2000-OCH_3	0.18 ± 0.01	30 ± 2
	0.35 ± 0.04	18 ± 3
	0.44 ± 0.09	15 ± 4
	0.98 ± 0.05	7 ± 1

PEO hydration in the third column (Table 2.2) represents an estimation of the number of water molecules (M_{H2O}) per PEO monomer and was calculated from Equation

$$\frac{M_{H_2O}}{\xi_{PEO}} = \frac{SA_{PEO}L - V_{PEO}\xi_{PEO}}{V_{H_2O} * \xi_{PEO}} \quad and \quad L = \xi_{PEO}\frac{a^{5/3}}{\sigma^{2/3}}$$

where, SA_{PEO} is the surface area occupied by a single PEO chain (inverse chain density), V_{PEO} is the volume of a PEO monomer residue (65Å^3), V_{H2O} is the volume of a water molecule (14.6Å^3), L is the brush length, ξ_{PEO} is the number of monomers per chain, a is the PEO monomer size (3.5 Å) and σ is the distance between graft points for neighboring chains.

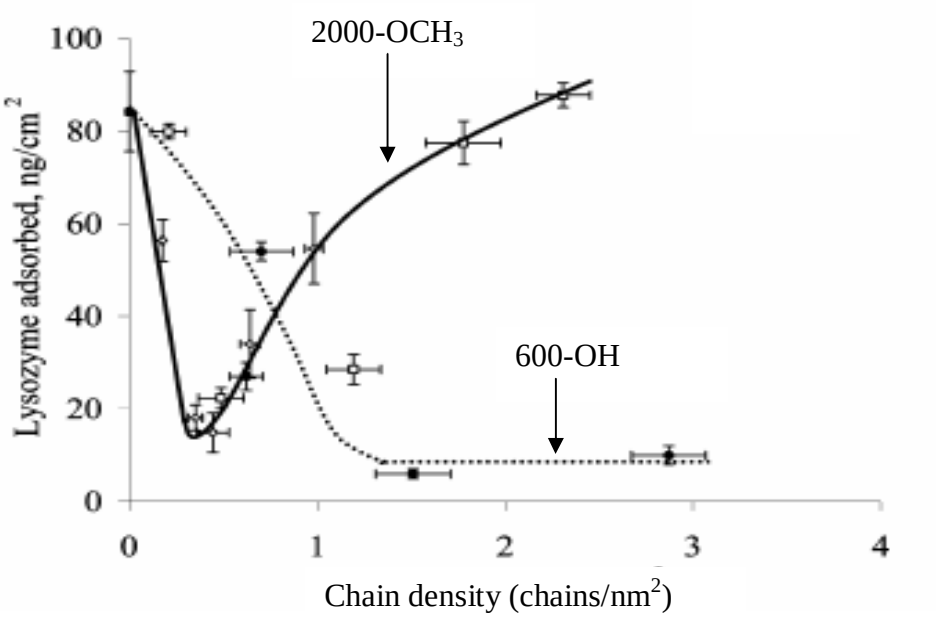

Figure 2.27: Adsorption of lysozyme on PEO-modified surfaces as a function of chain density. Taken from Unsworth et al. [2008].

Thus, while protein resistance requires high chain length and high grafting density to suppress the *primary*, *secondary* and *tertiary* adsorption, there exists a critical value (i.e optimum value) for each of those two factors to give a maximum adsorption resistance. We expect those optima to be determined by water barrier and steric mechanisms. Beyond the critical condition, either a water barrier (hydration) or a steric repulsion mechanism is believed to lose its function.

Yet there is evidence (experimentally and theoretically), which indicates that in some cases PEG does bind to proteins [Abbott et al., 1992, Wang et al., 1997, Harder et al., 1998, Sheth et al., 1997]. For example, Abbott et al. [1992] revealed the existence of subtle attractions between PEO coils and BSA in an aqueous two-phase system. A quantitative simulation model of the solution structure indicated that an attractive interaction energy of about $0.05kT$ per EO unit (where k is the Boltzmann constant and T is the absolute temperature) was sufficient to describe the interactions between BSA and PEO coils.

Studies done by Wang et al. [1997] and Harder et al. [1998] on self-assembled monolayers (SAMs) of ethylene oxide (EO)-terminated alkane thiolates supports the findings of Unsworth et al. [2008]. They revealed that when the EO moieties were in the crystalline helical or amorphous conformation, the SAMs were protein repellent. When the EOs in the SAM were in the all-*trans* form, proteins adsorbed at the SAMs. The protein resistance were explained by the structure of the water layer at the SAMs: water adsorbs much more strongly onto the helical or amorphous EO conformation than onto the all-*trans* EO conformation. They claimed that this stable water film prevents proteins from adsorbing at the SAMs in the helical or amorphous conformation; the less stable water film at the all-*trans* EOs results in protein adsorption.

Currie et al. [1999] revealed the attraction between BSA and *grafted* PEO chains. The dynamic light-scattering experiment done by them showed no attraction between BSA and PEO in bulk solution but grafted chains appeared to bind BSA. They suggested two possibilities: (i) there was no attractive interactions between PEO and BSA but the proteins diffuse into the grafted layer and are “trapped” there (refer to Figure 2.28) and (ii) the surface of BSA consists of hydrophobic and hydrophilic

(charged) areas, similar to that of a micelle. They suggested that the attractive interaction resulted from (weak) attractive hydrophobic interactions between PEO and the micellar surface (refer to Figure 2.28). They argued that, if the proteins were really trapped within the layer, then the adsorbed amount, whilst washing with pure solvent, should decrease in time. However, after adsorbing the BSA at a grafting near the maximum and washing with water for several hours, the adsorbed amount of BSA remained constant. Thus indicated that the interaction between grafted PEO and BSA were attractive in nature and that proteins were not merely trapped within the PEO brush.

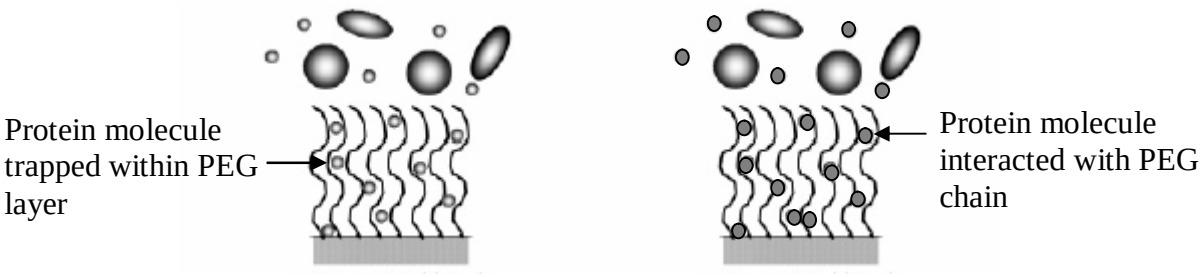

Figure 2.28: Illustration of PEG molecules trapped within a PEG layer (A) and interacted with PEG chains (B).

Bosker et al. [2005] also revealed a similar observation to Currie et al. [1999]. There was an interaction between bovine serum albumin (BSA) and PEO brushes. They ascribed the maximum in BSA adsorption at low grafting density to tertiary adsorption, implying an attraction between BSA and long PEO chain (N=770).

Research done by Sheth et al. [1997] using surface force measurements by an AFM between protein streptavidin and a PEO brush bound to a mica surface, also provided evidence of subtle attraction between protein streptavidin and PEO. They explained the attraction between PEO and streptavidin with a change in conformation of the PEO and not due to structural changes in steptavidin (the measurements were conducted at forces much too low to denature streptavidin). As mentioned earlier, ethylene oxide segments can adopt multiple configurations and different conformers

interact differently with water molecules. The structures and interfacial properties of PEG chains suggested that the interconversion between protein-attractive and protein-resistance PEG was due to segment rearrangements in the polymer chains with non polar segments concentrated near the surface and polar segments at the outer edge. The change from polar to apolar conformation may be induced by compressing the PEO layer. Increasing the temperature or altering the polymer molecular weight [Efremova et al., 2001] could also induce an attractive state. This suggests that along with the surface coverage (grafting density), the conformation of the chains (trans vs helical) also contributes to protein resistance.

Overall, surface coverage (grafting density), chain length, chain flexibility (with hydration) and chain conformation are the major factors that contribute to the protein resistance and most importantly, act inherently together.

2.6 Bimodal PEG

A mixture of long and short chains has been shown [Carignano et al., 2000, Fukai et al., 2004, Uchida et al., 2005, Satomi et al., 2007] theoretically and experimentally to enhance the protein resistance of PEG coating compared to single chains. The effectiveness of the combination chains is attributed to the high mobility of long chains to sweep the incoming protein molecules and the role of the short chains to fill the space close to the surface, reducing the amount of available sites for the adsorbing proteins (see Figure 2.29). For example, Uchida et al. [2005] in their work found that adsorption of bovine serum albumin (BSA) on mixed PEG (5000+2000) grafted on gold surfaces at 25°C was down to 5 % of that on single PEG5000 surfaces. In the following work, Uchida et al. [2007] adsorbed several proteins and peptides with different MW and pI on mixed PEG (5000+2000) surfaces. They found that mixed PEG (5000+2000) surfaces showed almost complete inhibition of non-specific adsorption regardless of the sign of a charge on the protein molecule. This applied not only to high molecular weight proteins but also to low molecular weight peptides.

The main merit for bimodal PEG chains over single PEG chains is that both high grafting density and high chain length can be achieved at the same time.

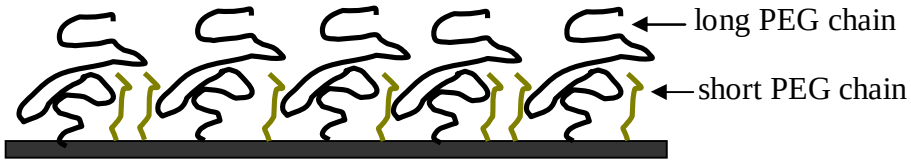

Figure 2.29: Schematic diagram of combination between short and long PEG chains.

CHAPTER THREE

LITERATURE REVIEW OF CHARACTERIZATION

3.0 Introduction

The central part of this thesis work is the application of the quartz crystal microbalance- with-dissipation (QCM-D) technique to monitor protein adsorption in the aqueous phase. Today, a wide range of techniques have been used to study the protein adsorption on solid interfaces (besides QCM-D) such as scanning tip methods, for example, atomic force microscopy (AFM) and optical techniques such as, ellipsometry, optical waveguide lightmode spectroscopy (OWLS) and surface plasmon resonance (SPR). Since the QCM-D has by far been the principal technique used in this study, it is described in most detail. The other techniques meanwhile are described briefly.

3.1 Quartz crystal microbalance with dissipation (QCM-D)

Quartz crystal microbalance with dissipation (QCM-D) is a mass sensing device with the ability to measure very small mass changes as small as a fraction of a monolayer or a single layer of atoms on a quartz crystal resonator in real-time. Traditionally, the QCM was used in vacuum and in gaseous environments. After Nomura and Okuhara [1982] showed that a crystal completely immersed in liquid can also be driven to oscillate in a stable manner, it became a starting point for the development of a new class of bioanalytical tools. QCM-D is a fast tool to study protein adsorption kinetics in aqueous solution [Shen et al., 2001, Kim et al., 2002, Stengel et al., 2005, Paul et al., 2008]. The possibility to monitor the kinetics of adsorption allows an opportunity to model the adsorption and desorption with rate equations. This technique can also describe the conformation of PEG chains either in

a pancake form, in a mushroom form or in a brush regime [Liu et al., 2005]. Mass adsorbed measured with the QCM-D should always be referred to as a '*wet*' mass as QCM-D measurement senses total mass of the film including water coupled to and trapped within the adsorbed film [Stalgren et al., 2002, Hook et al., 2002].

The QCM-D sensor consists of a thin plate of piezoelectric quartz crystal, sandwiched between a pair of metal electrodes, which are used to establish an electric field across the diameter crystal. Also shown is an example of protein molecules adsorbed on one side of the gold coated stainless steel crystal surface.

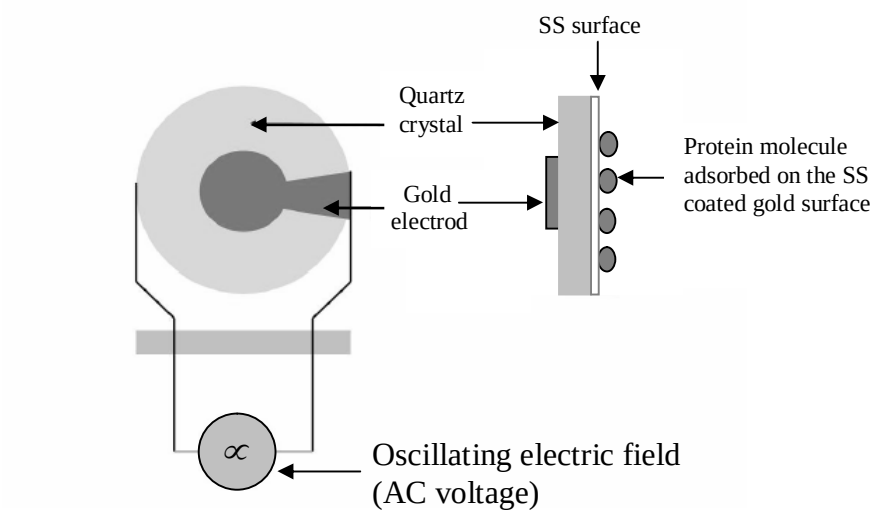

Figure 3.1: Schematic picture of a quartz resonator used in the quartz microbalance.

When an AC voltage is applied over the electrodes, the crystal can be made to oscillate at its fundamental resonant frequency (f_0). Resonance is excited when a sufficient AC voltage is applied with a frequency close to the fundamental resonant frequency (f_0) of the particular crystal. The resonant can be detected at the maximum amplitude. f is measured then D is obtained by suddenly disconnecting the driving field (energy dissipation is measured on the basis of the principle that when the driving power to a piezoelectric oscillator is switched off, the voltage of the crystal decays exponentially and a damped oscillating signal is recorded). The shift in dissipation measured by the QCMD system is due to the change in the damping of the

QCM-D crystal during measurements, which occurs if the viscoelastic properties of the attached layer changes. The dissipation factor (ΔD) is defined by Equation 3.1 below:

$$\Delta D = \frac{E_{dissipated}}{2\pi E_{stored}} \tag{3.1}$$

where $E_{dissipated}$ is the energy dissipated during one oscillation and E_{stored} is the energy stored in the oscillating system.

Therefore, by switching the driving voltage on and off periodically, we can simultaneously obtain a series of the changes of the resonant frequency and the dissipation factor.

The QCM thus measures simultaneously changes in resonance frequency, *f*, and dissipation, *D* (the frictional and viscoelastic energy losses in the system) due to adsorption on a crystal surface; changes in frequency approximately correspond to the mass adsorbed while changes in dissipation factor relate to the viscoelastic properties (shear, viscosity, density) of the layer adsorbed.

3.1.1 Equivalent circuits

Figure 3.2 shows the common electrical equivalent circuit (Butterworth-van-Dyke) of a quartz crystal resonator near resonance [Martin et al., 1991]. The circuit elements can be related to the physical properties of quartz, the perturbing mass layer on one side of the crystal and the contacting liquid. The motional (oscillation) capacitance, C_1, can be seen as a representation of the compliance of the quartz, the motional inductance, L_1, represents the total oscillating mass (quartz plate + electrodes + overlayer) and the motional resistance, R_1, characterizes the sum of the losses due to the motion of the quartz, including such as internal friction in the quartz, losses in the liquid and mounting losses [Martin et al., 1991].

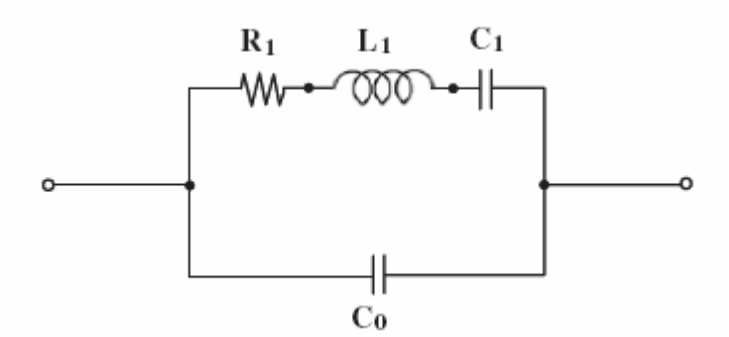

Figure 3.2: Butterworth-van-Dyke-equivalent circuit for the unperturbed quartz crystal.

3.1.2 Data interpretation

The QCM-D data can be analyzed either using the Sauerbrey model or the Kelvin-Voigt viscoelastic model (the Voigt model). The detail of the methods is shown in the next section.

3.1.2.1 Sauerbrey model

The model which predicts a linear relationship between the deposited mass per unit area (Δm) and the measured frequency changes (Δf) was pioneered by Sauerbrey [1951]. The model is based on the assumptions: (i) the adsorbed mass is distributed evenly over the crystal (homogeneous layer) (ii) Δ*m* is much smaller than the mass of the crystal itself (<1 %), and (iii) the adsorbed mass is rigidly attached, with no slip in the added mass due to the oscillatory motion. The relationship is shown in Equation 3.2.

$$\Delta m = -\frac{\rho_q v_q}{2 f_0^{\,2}} \frac{\Delta f}{n} = -\frac{\rho_q t_q}{f_0} \frac{\Delta f}{n} - C \frac{\Delta f}{n} \qquad (3.2)$$

where f_0 is the fundamental frequency when the surface is clean (also when n = 1), ρ_q, v_q and t_q are the specific density, the shear wave velocity and the thickness of the quartz crystal, respectively and n is the number of the overtone (n = 1, 3, 5, 7, 9 ….).

For a 5 MHz quartz crystal, the constant C value is 17.7 ng/cm^2. Hz [Malmstrom et al., 2007, Hemmersam, et al., 2008]. The assumptions of the model result in changes in resonant frequency, Δf, being proportional to the mass accumulated Δm, with no change in dissipation energy. Hence, an adsorbed layer which is rigidly attached gives no change in a dissipation while a loose layer gives a dissipation increase.

Figure 3.3 illustrates the comparison of the induced shifts in f and D due to an adsorbed viscoelastic film when the QCM is oscillating either in a vacuum or in water. As can be seen, the f shift was almost the same in the water and the vacuum. However, the dissipation was increased in the water. Therefore, oscillating the QCM in a liquid medium always relates to a dissipation increment.

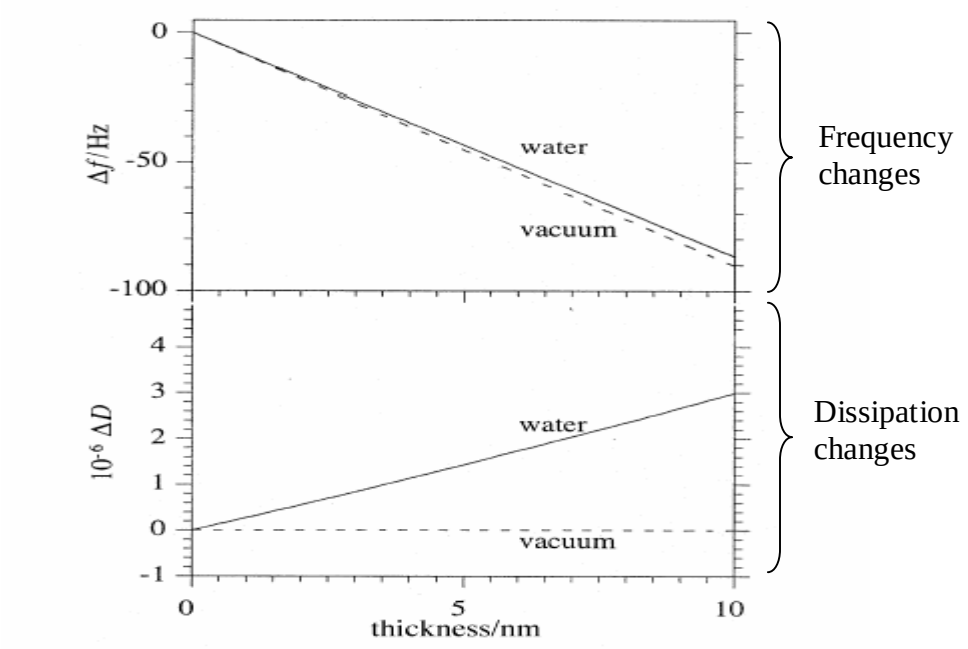

Figure 3.3: Comparison of the induced shifts in f and D due to a viscoelastic film of varying thickness when the QCM is oscillating in a vacuum (------) and water (——).

Nevertheless, the applicability of the Sauerbrey model can be checked by normalizing the Δf at different overtones (n). Irwin et al. [2005] state that if the Δf values at different overtones are similar when they are normalized (for example, $\Delta f_3 / 3 \cong \Delta f_5 / 5 \ldots \cong \Delta f_n / n \cong 5$ Hz (fundamental frequency, f_0)) then the Sauerbrey equation is able to give a valid relationship between a frequency shift and an adsorbed mass.

Plotting ΔD versus Δf is another approach to determine the rigidity of the adsorbed film. One merit for this plot is that one is able to see directly the influence of the protein adsorption on the viscoelastic properties of the adsorbed layer. By comparing the $\Delta D/\Delta f$ values (slope of the ΔD-Δf plot) between proteins one is able to relatively indicate the characteristic of the layer formed, either a rigidly attached layer or a 'soft' (water-rich) layer. A small value of $\Delta D/\Delta f$ indicate a rigidly attached layer whereas a high value indicates a soft and water-rich layer [Hook et al., 1998, Hemmersam et al., 2008, Paul et al., 2008]. Figure 3.4 shows ΔD-Δf plots for lysozyme, bovine serum albumin (BSA) and immunoglobulin (IgG) proteins adsorbed on the phthalocyanine ($CuPcR_8$) surface [Paul et al., 2009]. As can be seen, lysozyme has only one $\Delta D/\Delta f$ slope, whereas BSA and IgG have two $\Delta D/\Delta f$ slopes. Paul and co-workers [2009] state that more than one slope indicates a direct adhesion and orientation change associated with hydrodynamically coupled water. Comparing the $\Delta D/\Delta f$ values between the proteins in Figure 3.4, lysozyme adsorption apparently formed a rigid layer whereas BSA and IgG relatively formed water-rich layers.

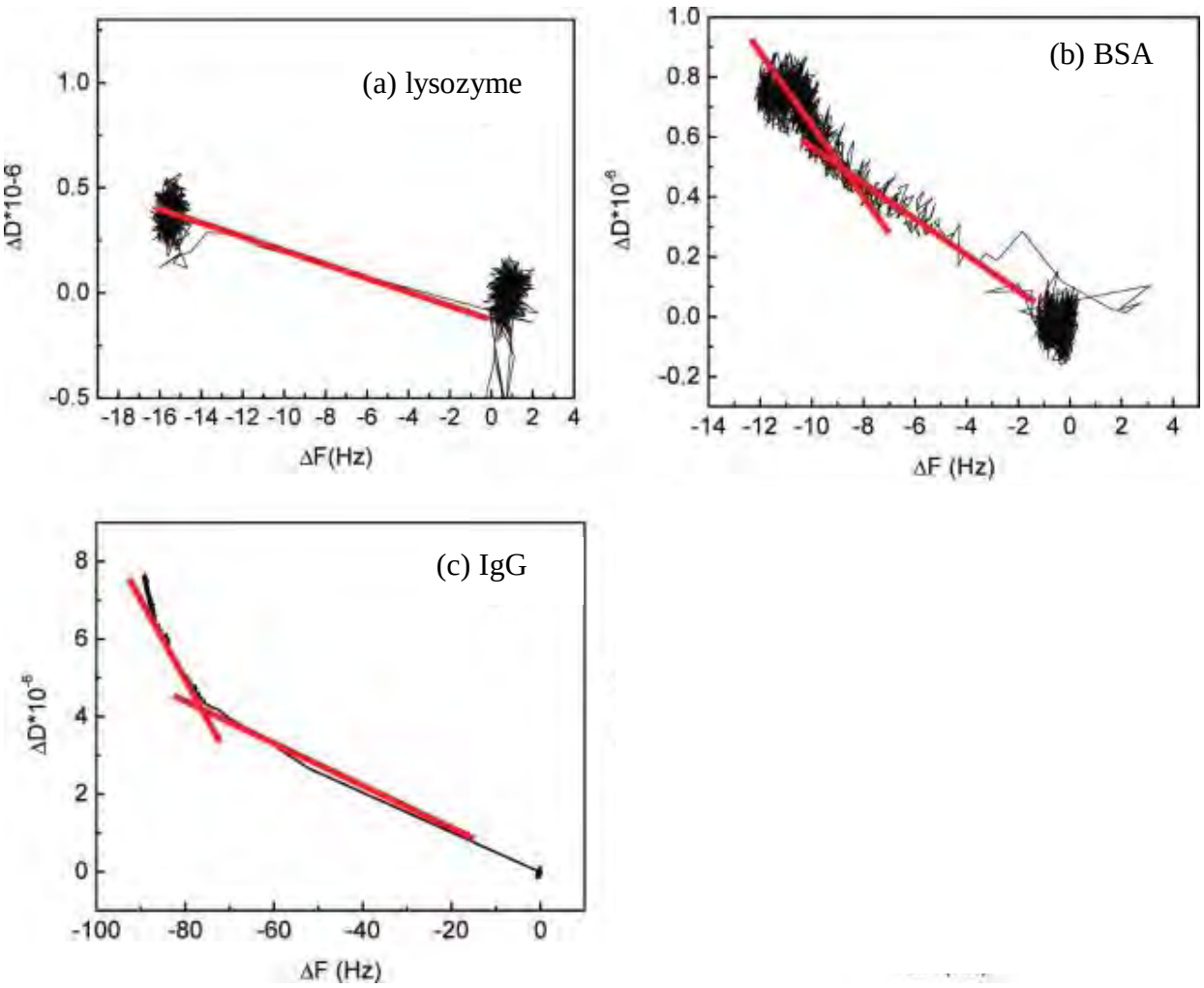

Figure 3.4: Δ*D*-Δ*F* plots for (a) lysozyme at 0.015 mM, (b) BSA at 0.015 mM, and (c) IgG at 0.01 mM adsorbed on the $CuPcR_8$ surface are shown. Lines on the figures are drawn only as a guide. Taken from [Paul et al., 2009].

3.1.2.2 Kelvin-Voigt viscoelastic model (Voigt model)

In many situations, the adsorbed film does not form a rigid layer (for example, hydrated films) and therefore the Sauerbrey model becomes invalid. A film that is '*soft*' will not fully couple to the oscillation of the crystal hence the Sauerbrey model will *underestimate* the mass at the surface. In such conditions, the QCM-D data (*Δf* and *ΔD*) are better interpreted using the Kelvin-Voigt viscoelastic model [Stengel et

al., 2005, Irwin et al., 2005, Weber et al., 2007, Malmstrom et al., 2007, Paul et al., 2009].

The Voigt viscoelastic model is a mechanical model using a parallel combination of a spring and a dashpot to represent the elastic (storage) and inelastic (damping) part of a material. A frequency-dependent complex shear modulus, G^* of the adsorbed film is then represented as Equation 3.3.

$$G^* = G' + iG'' = \mu_f + i2\pi f\eta_f \tag{3.3}$$

where μ_f is the elastic shear modulus, η_f is the shear viscosity and f is the oscillation frequency.

Based on this approach, Voinova et al. [1999] analytically solved the wave equation describing the shear oscillation of a quartz plate covered by a viscoelastic film (uniform thickness and density) that is in contact with a semi-infinite Newtonian liquid under no-slip conditions (see Figure 3.5) [Voinova et al., 1999]. The general solution of this wave equation is referred to as the β-function. The change in resonance frequency, Δf, and dissipation factor, ΔD, of the single adsorbed film can be obtained from the imaginary and the real part of the β-function (refer Equations 3.4 and 3.5) [Voinova et al., 1999, Hook and Kasemo, 2001].

$$\Delta f = \mathrm{Im}(\beta)/2\pi t_q\rho_q \tag{3.4}$$

$$\Delta D = -\mathrm{Re}(\beta)/\pi f t_q\rho_q \tag{3.5}$$

where

$$\beta = \xi_l \frac{2\pi f\eta_f - i\mu_f}{2\pi f} \frac{1-\alpha \exp\left(2\xi_l d_f\right)}{1+\alpha \exp\left(2\xi_l d_f\right)}$$

$$\alpha = \frac{\frac{\xi_l}{\xi_2}\frac{2\pi f\eta_f - i\mu_f}{2\pi f\eta_l} + 1}{\frac{\xi_1}{\xi_2}\frac{2\pi f\eta_f - i\mu_f}{2\pi f\mu_l} - 1}$$

$$\xi_l = \sqrt{-\frac{(2\pi f)^2 \rho_f}{\mu_f + i2\pi\eta_f}}$$

$$\xi_2 = \sqrt{i\frac{2\pi f\rho_l}{\eta_l}}$$

and ρ_l and η_l are the bulk-liquid density and viscosity, respectively while δ_f is the film thickness.

In summary, the Voigt-based viscoelastic model contains four unknown parameters; effective film density (ρ_f), film shear viscosity (η_f), film shear elastic modulus (μ_f), and the film thickness (δ_f) (see Figure 3.5). Since the viscous layers (films) give rise to different penetration depths of the harmonic acoustic frequencies, multiple frequencies can be simultaneously fitted to calculate the values of ρ_f, η_f, μ_f and δ_f (refer to Chapter 5 for the method).

Although the no-slip condition is prevailing in classical hydrodynamics, one aspect of the QCM-D response that has become a contentious issue is the possible role of the slippage phenomenon at the device-liquid interface. A number of theoretical and experimental studies in support of the slippage phenomenon have been summarized in the recent reviews [Ellis et al., 2004, McHale and Newton, 2004, Zhuang et al., 2008]. In order to quantify the slippage effect, the slip boundary

conditions, either as a stress or a displacement or a velocity mismatch across the interface, has been incorporated into the normal no-slip models of the acoustic wave resonators [Ellis et al., 2004].

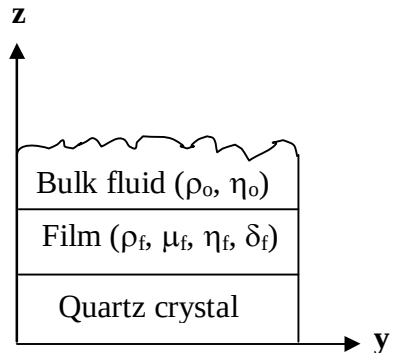

Figure 3.5: Diagram of the system modelled by the Kelvin-Voigt viscoelastic model. The quartz crystal is covered by a thin film that can be described by ρ_f, μ_f, η_f and δ_f under no slip conditions. The film is covered by a semi-infinite Newtonian fluid with ρ_o and η_o properties.

The mass of the layer (M_{voigt}) is obtained after multiplying the fitted value of thickness (δ_{voigt}) with the estimated effective layer density. The Voigt model was solved using a Q-TOOLS software (301 version 2.1, Feb 2006) (refer to Chapter 5 for the details). The effective layer density was assumed as 1200 kg / m^3 (refer to Chapter 11 for the detail). A more detailed discussion of the QCM-D measurement can be found in the review article written by Cooper and Singleton [2007].

3.1.3 Geometry of the cell and fluid mechanics

Figure 3.6 shows the picture of the module cell of the QCM-D, which can be split into top and bottom cells.

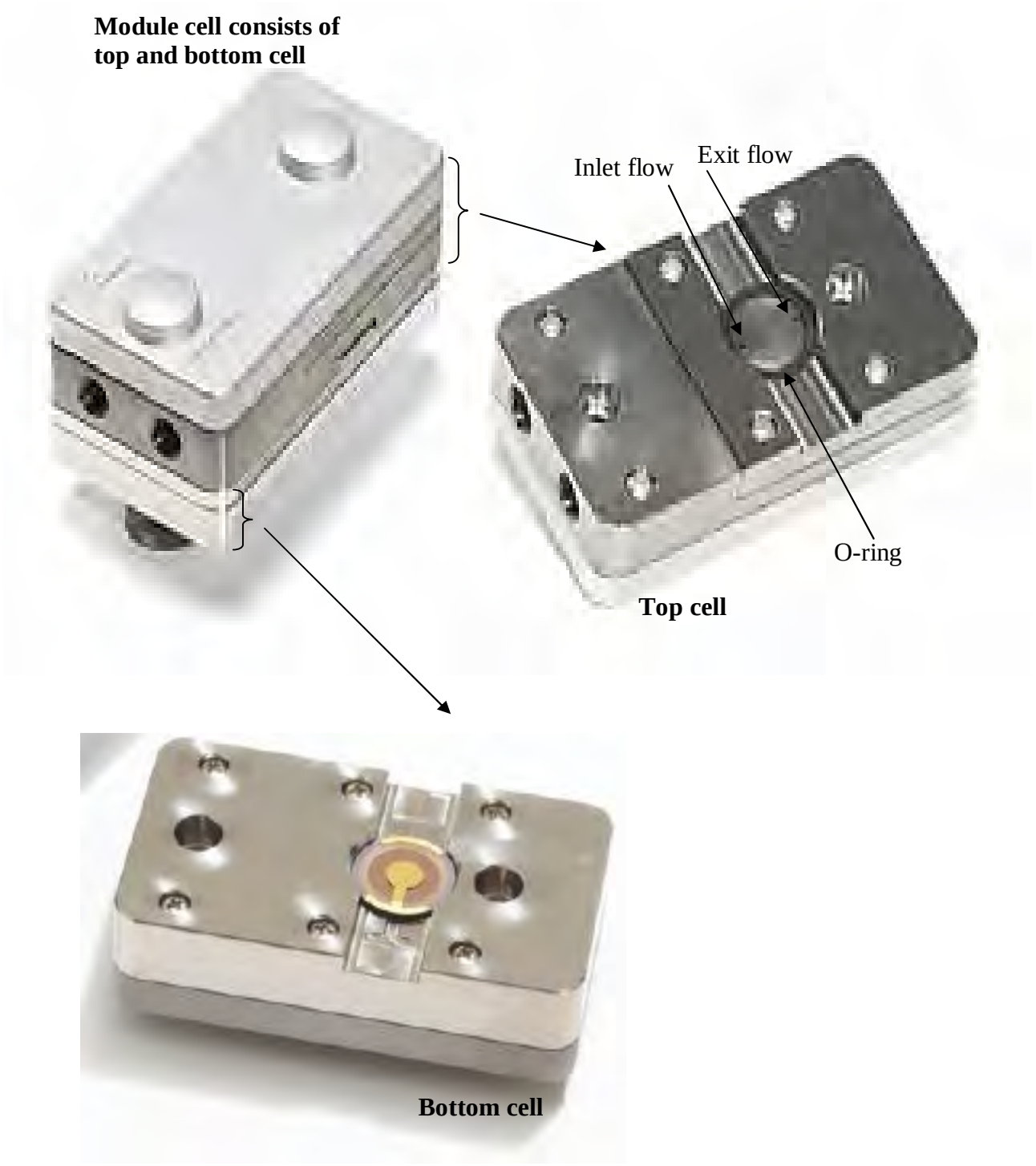

Figure 3.6: Picture of the module cell of the QCM-D.

The illustration of the fluid flow inside the cell is shown in Figures 3.7 (top-view) and 3.8 (front-view). The fluid enters the cell through a small hole and dispersed around the cell and exit through the outlet.

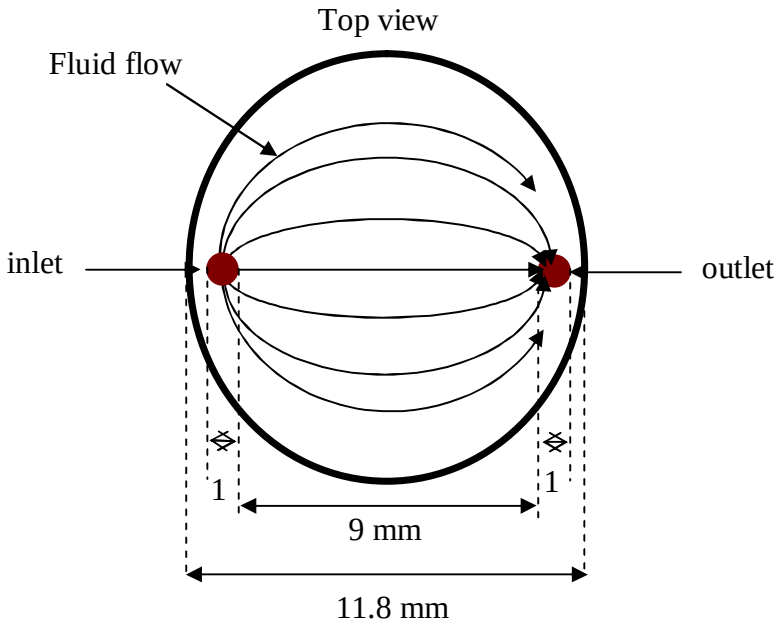

Figure 3.7: Illustration of flow dispersion on the cell. The fluid enters the cell through the inlet and is dispersed around the cell and exits through the outlet (top-overview). All measurements is in mm.

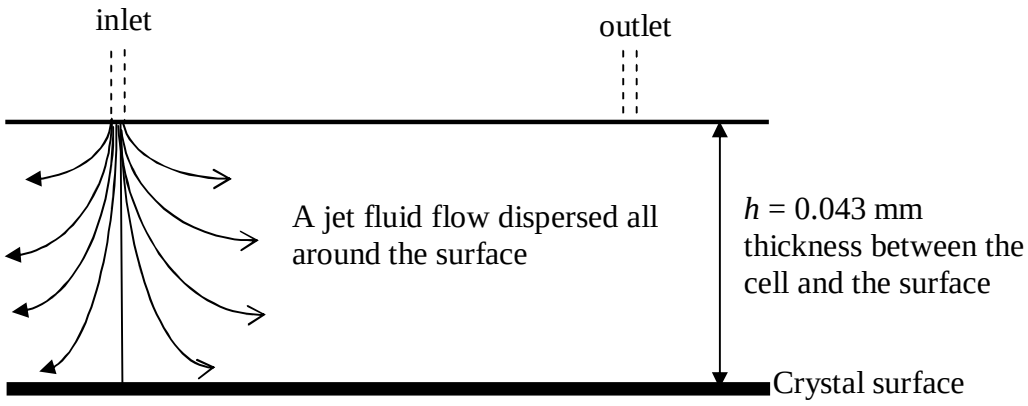

Figure 3.8: Illustration of a jet fluid flow enters the cell and dispersed on the cell (front-overview).

3.2 Atomic force microscopy (AFM)

Atomic Force Microscopy (AFM) is a scanning probe technique and very suitable for analyzing a surface topography. It can be performed in a liquid or an air environment. This technique enables one to observe directly the real-space topography of surfaces on a nanometre scale and in principle may detect the spatial distribution of the adsorbed protein. By imaging in situ, protein adsorption dynamics can be monitored in real time [Kim et al., 2002]. Besides that, the ability of the AFM to measure interfacial forces offers the possibility to study the interfacial factors involved in protein repulsion or adsorption. In particular, force measurements may enable us to understand the interaction forces between protein and protein-resistant PEG layers. This is of crucial interest for a better appreciation of the mechanisms of protein resistance by PEG brushes [Hemmerle et al., 1999].

The means of measurement for the AFM is a sharp tip at the end of a cantilever. Bringing the tip into the vicinity of the surface results in an appreciable interaction between the tip and the surface, and by scanning the tip over the surface, high-resolution images can be obtained.

Three imaging modes can be used to produce topographic images of sample surfaces; contact, tapping and non-contact modes. Contact mode is the original AFM imaging mode and can be implemented in both air and fluid. In this mode, the probe (or tip) is in permanent physical contact with the sample (see Figure 3.9). Topographic images are generated by mapping the distance the tip moves vertically to maintain a constant deflection at every lateral data point. Since in contact mode electrostatic and / or surface tension forces (in air) from the adsorbed layer (either in liquid or air) pull the scanning tip toward the surface, it can damage the samples and distort the image data.

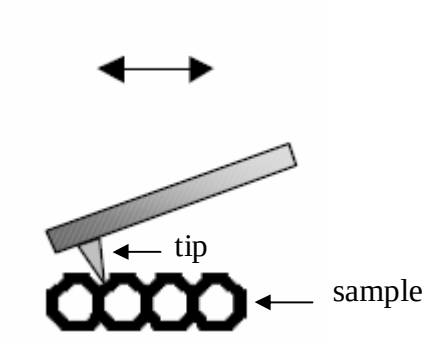

Figure 3.9: AFM contact mode technique. The probe is in permanent contact with the sample surface.

In tapping mode, the probe is oscillated such that the tip contacts the sample surface intermittently (see Figure 3.10). In this mode, the probe-sample interaction force is basically controlled by the changes in the resonance frequency of the cantilever. As the tip approaches the sample, the tip-sample interactions alter the amplitude, resonance frequency, and phase angle of the oscillating cantilever. During scanning, the amplitude of the cantilever oscillation is kept constant, allowing imaging of the topography of delicate samples. The phase shift of the oscillation can be recorded for information on the surface chemistry (particularly damping properties). This method of operation results in lower surface forces, particularly lateral forces, compared to those of the contact mode so less surface damage is inflicted while maintaining higher lateral resolution. Tapping mode AFM tends to be more applicable to general imaging of soft samples, such as biological and polymeric materials, under ambient conditions [Bar et al., 1998, Zhang et al., 1998, Raghavan et al., 2000].

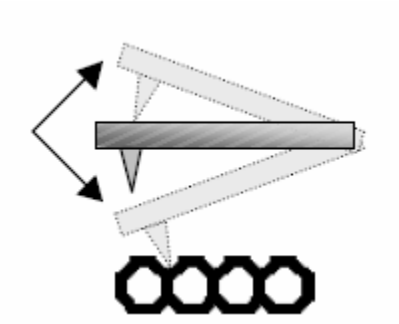

Figure 3.10: AFM tapping mode technique. The probe oscillating at typically constant frequency.

The amount of force applied by the AFM probe to the sample can be reduced further if it is in non-contact mode (Figure 3.11). The cantilever-probe is placed in the attractive force region (that is, where Van der Waals forces and electrostatic potentials influence the tip), and force gradients can be detected. Non-contact mode allows easy, productive imaging of delicate samples in both ambient air and in fluids. The drawback for non-contact mode is the lateral resolution is lower, limited by the tip-sample separation.

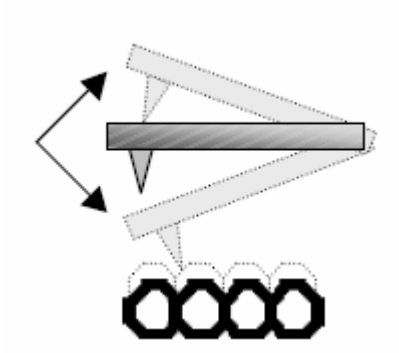

Figure 3.11: AFM non-contact mode technique. The cantilever-probe system is placed at the attractive region and force gradients are detected.

Force mode meanwhile is a non-imaging mode. In this mode, the tip deflection is recorded as a function of the motion of the piezoelectric scanner in the *z*-direction producing a force curve. Force curves can be used to study the molecular attraction and repulsion between the tip and the sample.

3.3 Optical technique

3.3.1 Ellipsometry

Ellipsometry, which is one of the most extensively used techniques for protein adsorption studies measure the thickness, d_f (with 0.1 nm resolution) and reflective index, n_f, of the adsorbed layer [Azzam et al., 1987]. The basic principle of this method is that the polarization state of an incident light beam is changed upon reflection at a planar surface due to changes in the dielectric properties of the interface (i.e. changes occur in both the amplitudes and phases of the oscillating parallel and perpendicular vector components of the electric field) . When proteins are adsorbed on such a surface, the dielectric properties of the interfacial region changes and consequently will change the polarization of the light beam. The change in state of polarization is described by the ellipsometric angles, Ψ and Δ [Azzam et al., 1977]. The electric field can be divided in a component parallel and perpendicular polarized to the plane of incidence. Ψ describes the ratio of reflection coefficients for parallel and perpendicular polarized light (given by the analyzer position) whereas Δ is the difference in phase change between parallel and perpendicular polarized light (given by the polarizer position) (see Figure 3.12). The measured change in polarization can then be mathematically related to the reflective index, n_f and thickness, d_f, of the adsorbed protein layer. The surface mass density adsorbed, Γ, (mass per unit area) then can be calculated using Feijter's formula (Equation 3.6) [Feijter et al., 1978].

$$\Gamma = d_f \frac{n_f - n_0}{d_n / d_c} \tag{3.6}$$

where d_n/d_c is the refractive index change per unit protein concentration (which is protein specific and must be known or assumed) while n_0 is the reflective index measured in bulk.

It should be noted that neither d_f nor n_f can be directly calculated from the change in polarization. Either d_f or n_f has to be known or guessed, after which a mathematical fit relates them to the measured parameters. Consequently, this will

cause an uncertainty in d_f and n_f and hence in Γ. It has been reported that the refractive index of adsorbed protein films was always close to n = 1 [Hook et al., 2002].

Ellipsometry characterization is useful especially to study biological specimens as it is nondestructive, allows measuring under physiological conditions, and offers the possibility to follow and quantify adsorption and desorption processes in real time. One merit with ellipsometry compared to most other techniques, is that the layer thickness (each layer) and consequently the orientation of adsorbed non-symmetric shaped proteins can be derived [Arwin, 2000]. In comparison with the QCM-D technique, the QCM-D does not require reflective surfaces. QCM-D measurement can be performed on any material surfaces as long as the layer can be adsorbed. However, since ellipsometry measurements are performed in reflection mode, the gold surface of the QCM-D could be used as a substrate, which would allow simultaneous QCM-D and ellipsometry measurements. Such combined measurements may answer how the dissipation shift is related to structural alterations detected via the refractive index.

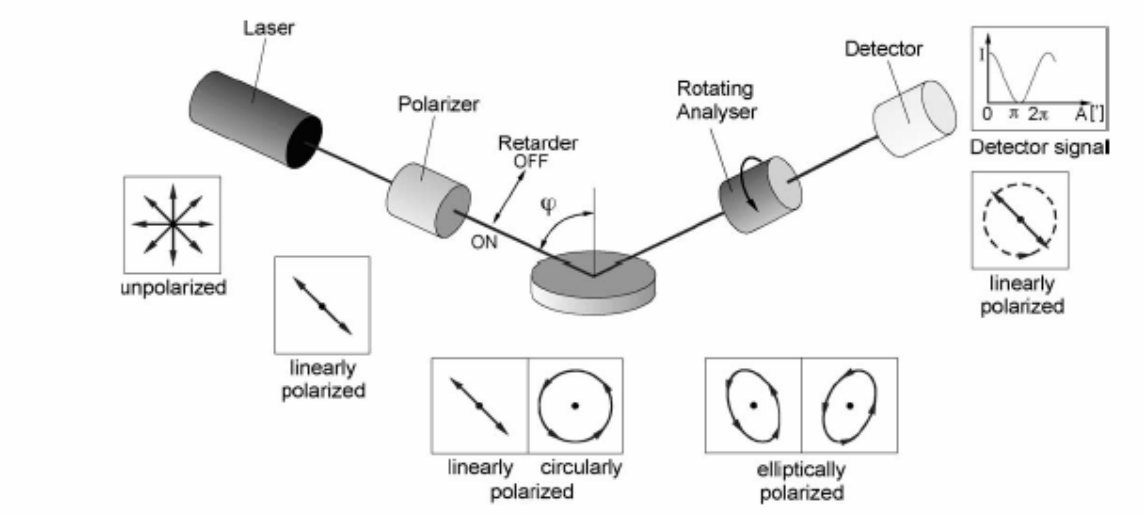

Figure 3.12: Principle of ellipsometry. Taken from [Seitz et al., 2005].

3.3.2 Optical waveguide lightmode spectroscopy (OWLS)

The optical waveguide lightmode spectroscopy (OWLS) technique uses the evanescent field of a He-Ne laser which is coupled into a planar waveguide via an optical grating [Tiefenthaler and Lukosz, 1989]. By varying the angle of the incident light beam, different guided transverse electric (TE) and transverse magnetic (TM) modes can be excited. This incoupled light intensity is measured with a photodetector placed at the end of the waveguide. Continuously measuring the shift of these incoupling angles allows the direct online monitoring of the adsorption of macromolecules above the grating. The schematic of the OWLS working principle can be seen in Figure 3.13.

The optical thickness (d_f) and the refractive index (n_f) of thin (< 50 nm) and homogeneous adsorbed layers can be determined from the phase shifts between TE and TM [Tiefenthaler and Lukosz, 1989]. The surface mass density adsorbed can again be calculated using Feijter's formula (refer to Equation 3.7).

One merit with the OWLS compared to the ellisometry technique is that the light beam does not have to pass through the solution to interact with the surface. Therefore, the changes in the optical properties of the solution do not significantly affect the measurement (changes in solution optical properties will change the polarization light and thus n_f and d_f). However, the main disadvantage is the fact that only highly transparent surfaces can be investigated. Furthermore, since OWLS requires very thin transparent layer, simultaneous measurements with the QCM-D technique are not easily performed. However, the surface of the QCM-D is easily modified and can be prepared so that it is identical with the surface of the optical wave guides.

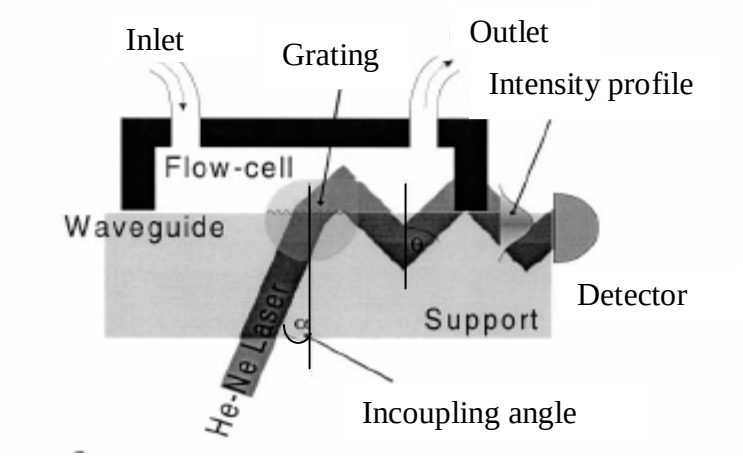

Figure 3.13: Schematic drawing of the grating coupler device in OWLS with the waveguide, the incident laser beam, the incoupling at the grating, the guidance of the light in the waveguiding layer, and the recording of the light intensity at the photodiode. The incoupling conditions are changed by varying the angle α.

3.3.3 Surface Plasmon Resonance (SPR)

Surface plasmon resonance (SPR) spectroscopy is an optical technique that is sensitive to changes in the refractive index of thin films assembled on a noble-metal surface [Englebienne et al., 2003]. Principally, SPR utilizes surface plasmon polariton exitations, which consists of charge-density waves propagating along the interface between a metal and a dielectric material (prism), to sense the local refractive index in the liquid close to the gold surface. The SPR phenomenon occurs when an incident beam of p-polarized light of a given wavelength strikes the surface at a given angle through a prism. In such conditions, photon–plasmon surface electromagnetic waves (surface plasmon polaritons) are created at the metal-dielectric interface. These waves propagate parallel to the metal dielectric interface and the associated optical electric field decays exponentially away from the surface with a typical decay length of 200 nm. This results in a reduced intensity of the reflected light at this angle (i.e. the SPR angle is detected when the intensity of the reflected light is minimum). The detector continuously records the position of the reduced light intensity and calculates the SPR angle of the reflected light (see Figure 3.14).

The SPR angle change is reported as resonance units (RU). As adsorption occurs on top of a surface, the angle of SPR is changed. The changes in SPR angle is proportional to the mass adsorbed at the surface according to Equation 3.7.

$$\Delta m_{SPR} = \frac{C_{SPR}\Delta RU}{\beta} \tag{3.7}$$

where Δm_{SPR} is the surface mass density adsorbed, C_{SPR} is a factor that contains an instrument constant, ΔRU is the measured change in response units, and β is a factor that compensates for the decrease in the SPR signal with distance from the gold substrate. For a plain and gold surface, β is equal to 1 [Stenberg et al., 1991]. ΔRU is a dimensionless quantity and 1RU corresponds to a change of 0.0001° degree which is produced for most proteins by the binding on the sensing layer of approximately 1 ng/mm^2 [Bagha and Holmberg, 2008]. A more detailed discussion of SPR applications can be found in the review article written by Karlsson [2004].

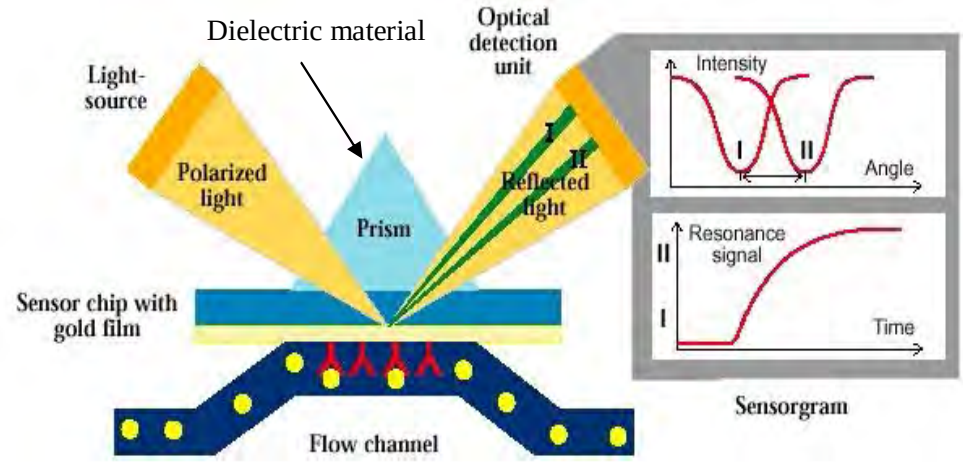

Figure 3.14: Principle work of a surface plasmon resonance (SPR).

As a summary, while being different in technical implementation common to all the optical methods discussed above, is the sensitivity to unknown values of two key parameters is common to all the optical methods discussed above; the effective refractive index and the effective thickness of a biomolecular layer at or close to the solid surface. The surface density of the dry basis adsorbed layers can usually be derived by conversion of measured quantities via the refractive index. The main advantage of optical methods is that the proteins under investigation require no chemical treatments with markers before use (labeling-free). Also, the measurement procedure is quite fast (on the order of a few seconds) and the measured mass is a '*dry*' mass (only mass of protein without contribution of solvent). The disadvantages with the method include the requirement of reflecting surfaces and the rather complex analysis when systems with unknown optical properties are investigated.

3.4 Comparison of QCM-D with optical techniques

In comparison with the optical techniques, one advantage of the QCM-D technique is that the surface material can be freely chosen without having to consider special properties such as optical transparency or reflectivity, as long as the preferred surface material can be deposited as a thin film onto the sensor crystals. An apparent complication in the QCM-D technique is that the method measures coupled water in the film thus giving *overestimation* of the mass of solute adsorbed. However, this can actually constitute an advantage, especially when combined with optical techniques. For example, optical measurements generally provide an accurate estimation of the solute mass surface density adsorbed, while QCM-D measurements, on the other hand, measure the solvent-included mass in combination with the viscoelastic properties of thin films with the latter being directly related to structural properties of the adsorbed film. Hence, by combining both techniques it is possible to resolve the bound solute mass and the coupled solvent in the film [Hook et al., 2001, Hook et al., 2002]. The effective layer thickness and percentage of water bound can be calculated using Equations 3.8 and 3.9 [Hook et al., 2002].

$$d_{eff} = \frac{\Gamma_{QCM}}{\left(\rho_{protein} \times \frac{\Gamma_{optical}}{\Gamma_{QCM-D}}\right) + \rho_{water} \times \left(1 - \frac{\Gamma_{optical}}{\Gamma_{QCM-D}}\right)} \qquad (3.8)$$

$$\%\ water = \frac{\Gamma_{QCM-D} - \Gamma_{optical}}{\Gamma_{QCM-D}} \times 100 \qquad (3.9)$$

where ρ, Γ and d is a density, areal layer mass density and layer thickness, respectively.

Works involving combination of those techniques (QCM-D and optical techniques) have been started about a decade ago when Hook and co-workers have used combinations of QCM-D, ellipsometry and SPR techniques to study the variations in coupled water, viscoelastic properties and film thickness of a *Mytilus edulis* foot protein (mefp-1) during adsorption and cross-linking [Hook et al., 2001]. Stalgren et al. [2001] meanwhile used QCM-D and ellipsometry techniques to study the adsorption of a surfactant (hexaethylene glycol mono-n-tetradecyl ether) on different model surfaces. They revealed that overestimation of mass adsorbed measured by the QCM-D was attributed to two different effects; water that is coupled to the adsorbed layer due to hydration of the polar region of the surfactant and secondly water that is trapped within the adsorbed layer. In the following year, Hook et al. [2002] studied the adsorption of human serum albumin (HSA), fibrinogen (FIB) and hemoglobin and their antibodies respectively, A-HSA, A-FIB and A-Hemoglobin onto titanium oxide surfaces by using combinations of QCM-D, ellipsometry and OWLS techniques. The results obtained proved that the optical techniques of ellipsometry and OWLS gave in most cases constant and comparable results on the adsorbed protein molar '*dry*' mass whereas the QCM-D measurement, as expected overestimated the mass adsorbed. For the two relatively small and globular proteins,

hemoglobin (64.5 kDa) and albumin (65kDa) the measured mass of adsorbed protein was a factor of about 1.75 larger than that measured by optical techniques while it was about 2 to 3.2 times larger for the other proteins (fibrinogen (MW340kDa) and antibodies) (see Figure 3.15).

It has been reported that, the typical QCM-D mass-uptake estimations are between a factor of 1.5 to 4 times larger than the molar 'dry' mass [Caruso et al., 1997, Fawcett et al., 1998]. In another study, the mass density of β-casein adsorbed on a gold surface monitored using QCM-D was greater by a factor of 3 to 5 compared with the optical devices [Lee et al., 2004]. Meanwhile, the mass density of DNA on the gold surface measured with QCM-D was up to 7 times larger compared with the SPR measurement [Su et al., 2005]. The difference between QCM-D and optical techniques appears to depend on the nature and conformation of the adsorbed molecules and the liquid medium used.

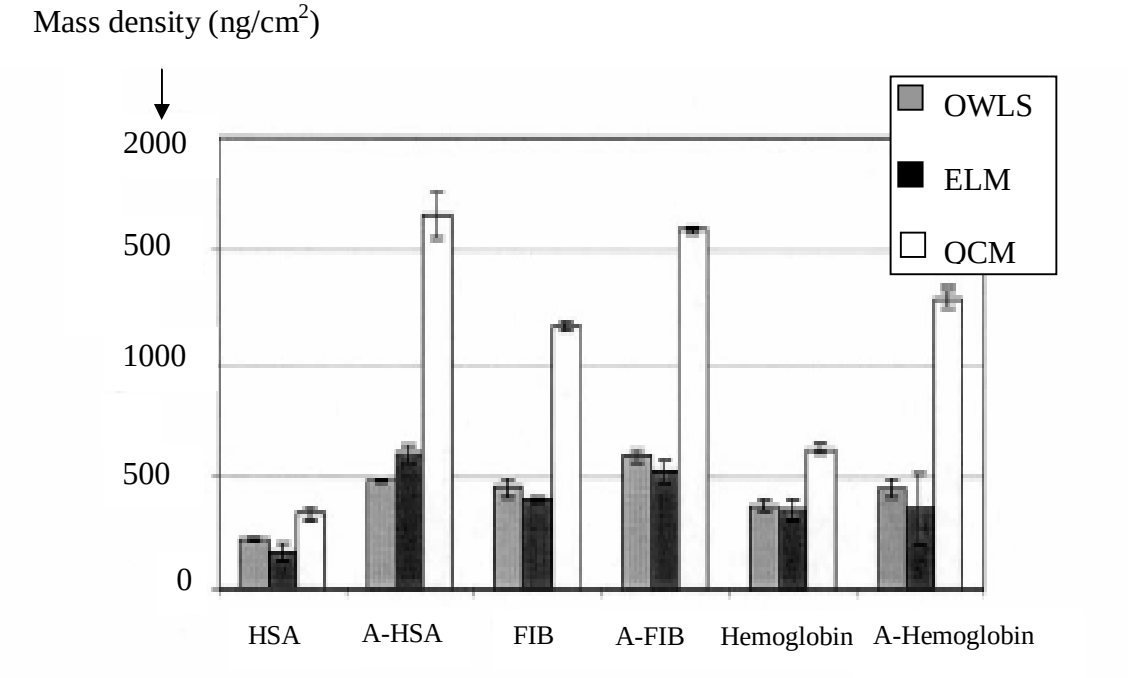

Figure 3.15: Graphic illustration of the experimental protein and antibody adsorption mass surface density results using ellipsometry (ELM), optical waveguide light spectroscopy (OWLS) and quartz crystal microbalance (QCM) techniques. Taken from [Hook et al., 2002].

Other studies done related to this field have also found similar findings, that a combination between the QCM-D and optical techniques gave more accurate determination of the thickness and effective density of the protein layer as well as the adsorbed mass and viscoelastic properties [Reimhult et al., 2004, Zhou et al., 2004, Malmstroom et al., 2007]. Recently Zong et al. [2008] in their study integrated a surface plasmon grating coupler (G-SPR) into a QCM-D for studying a layer-by-layer polyelectrolyte multilayer assembly. This integration was able to eliminate a SPR detection system and using only a QCM detection module to gain the full features of SPR and QCM, including the detection of the optical thickness, the acoustic thickness as well as the adsorption kinetics. The acquired optical and acoustic signals from the same adsorption process allow for a precise comparison of the optical and the acoustic thicknesses of the adsorbed films, from which the packing information of the films (structural transformations) can be extracted.

CHAPTER FOUR

LITERATURE REVIEW OF KINETICS THEORY AND INTERPRETATION OF DATA

4.0 Introduction

Modelling of the adsorption in a single protein system is of considerable interest and includes many different theoretical approaches. Modelling the experimental protein adsorption data with an appropriate model or approach hopefully leads to a clear mechanism of the process itself. The adsorption of a protein generally involves two sequential regimes; first a transport or diffusion limited regime and then a reaction limited regime. In this chapter, several models of protein adsorption are reviewed. The reviewed models include fully reversible adsorption (where equilibrium can be reached, where rate of adsorption = rate of desorption), fully irreversible adsorption (with zero desorption), partially reversible adsorption (some of the adsorbed proteins do not desorb) and adsorption with conformational change (the adsorbed protein tends to unfold). Most of these models include only a reaction limited regime. A model which includes a possible diffusion limited step is also reviewed.

4.1 Langmuir Model

The Langmuir model [Langmuir, 1916] is one of the simplest models and is frequently used for describing the adsorption rate [Brusatori et al., 1999, Gettens et al., 2004, Cosman et al., 2005, Ozkaya, 2006]. Figure 4.1 illustrates the schematic diagram of protein adsorption for the Langmuir model.

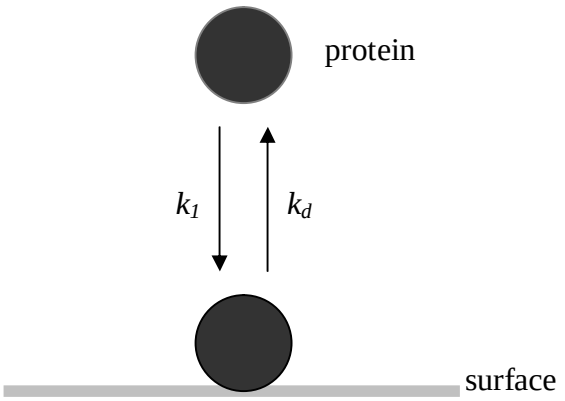

Figure 4.1: Schematic diagram of the Langmuir model.

In this model, the key assumptions are: (i) adsorption onto a surface cannot exceed a monolayer (ii) the adsorbing surface is composed of discrete, identical and non-interacting sites (iii) the ability of a molecule to adsorb to a given site on the surface is independent of the occupation of neighboring sites (that is, no interaction with the neighbours) and (iv) adsorption is reversible.

The kinetic equation for the Langmuir model written in surface concentration, ρ, is shown in Equation 4.1 below.

$$\frac{d\rho}{dt} = k_1 C_0 \left(1 - \frac{\rho}{\rho_{monolayer}}\right) - k_d \rho \qquad (4.1)$$

where $\rho_{\text{monolayer}}$ is the surface concentration of protein corresponding to a complete coverage (mg/m^2), ρ is the amount of protein adsorbed onto the surface (mg/m^2) at time t, C_0 is the bulk concentration of adsorbing protein at the surface (g/L), t is time and k_1 and k_d are the first order adsorption and desorption rate constants, respectively. The units of the concentration can be mass/area, no. of moles/area, area/area or mass/volume. The units of k_1 change accordingly while the units of k_d are s^{-1} if t is in s.

As time approaches infinity ($d\rho/dt \rightarrow 0$), an equilibrium amount of protein adsorbed (ρ_e) at a specific bulk protein solution concentration can be calculated from the balance of the rates on the RHS of Equation 4.1 giving

$$\rho_e = \rho_{monolayer} \frac{k_1 C_0}{k_1 C_0 + k_d} \tag{4.2}$$

A major limitation of the Langmuir equation for protein systems is that it requires the adsorption to be reversible, whilst many studies on protein adsorption have shown an irreversible character of the adsorption process on realistic time scales.

4.2 Random Sequential Adsorption (RSA)

The simplest "particle level" model (that is, taking account of the size of the molecules) used to study the adsorption of large molecules (such as protein), cluster and colloid particles is a Random Sequential Adsorption (RSA) model [Van Tassel et al., 1998]. In this model, particles adsorb to a surface sequentially, at randomly chosen positions, subject to no overlap with previously placed particles (monolayer). Unlike the Langmuir model, the RSA model is restricted to full irreversibility (zero desorption) (see Figure 4.2).

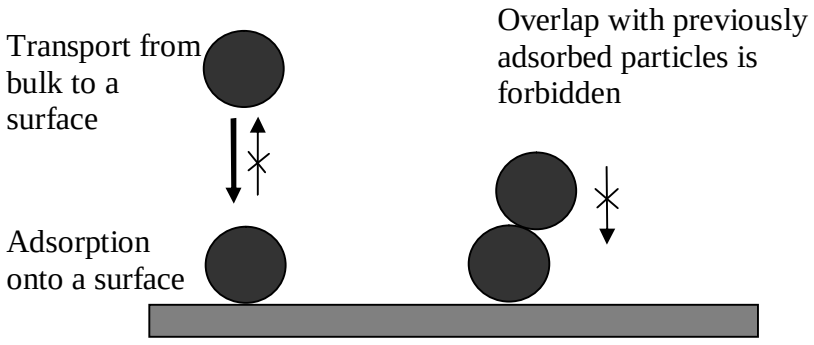

Figure 4.2: A schematic illustration of the simplest Random Sequential Adsorption (RSA) model [Van Tassel et al., 1998].

The kinetic equation for the RSA model is shown in Equation 4.13 below:

$$\frac{d\rho}{dt} = k_1 C_0 \theta(\rho) \tag{4.3}$$

where θ is a fraction of site surface covered with protein molecules (with the property that θ (0) = 0 and θ (ρ_∞) = saturation coverage (the protein packing on the surface will not give 100 % surface coverage). ρ refers to the surface density of protein adsorbed on the surface.

Nevertheless, the standard RSA model is too simple to capture many of the well established features of protein adsorption. Based on the many experiments done, it has been observed that proteins mostly adsorb initially in their native state (folded form) and then can either desorb or undergo a conformational change (unfolded form).

4.3 Spreading Particle RSA Model

An improvement to the RSA model is the Spreading Particle model [Brusatori and Van Tassel, 1999] in which conformation or orientation changes of the surface-adsorbed proteins are incorporated. As indicated in Figure 4.3, the Spreading Particle model depicts protein molecules as particles that adsorb sequentially and randomly onto the surface but without overlap. Once the molecules are adsorbed, two competing events take place; the molecule (spherical) may desorb or may spread symmetrically and instantaneously to a (disk) particle of larger planar or projected diameter. Both of these events occur at given rates. Spreading can occur only if space allows. Spreading usually leads to a larger contact region, thus decreasing the probability that incoming proteins land on a nearby unoccupied surface and also leads to a stronger surface binding, thus decreasing the rate of desorption [Veen et al., 2007].

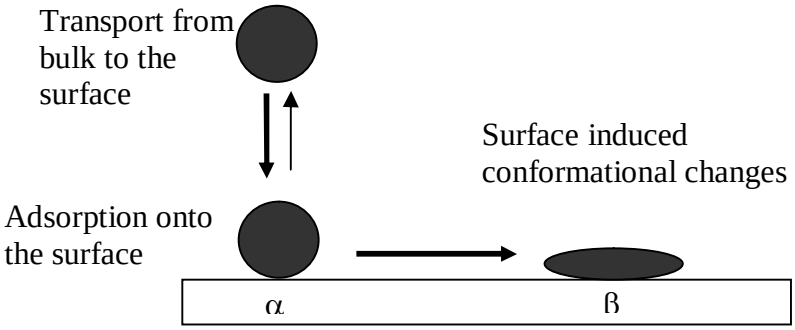

Figure 4.3: A depiction of the events occurring during protein adsorption in the Spreading Particle model. ● Solution state protein (α state). ⬬ Surface altered protein (β state). Note that no surface translation is involved [Brusatori and Van Tassel, 1999].

The key assumptions of this model are: (i) proteins interact laterally through a hard core potential (are rigid particles) (ii) only a single altered state is possible (iii) the surface projections of both spread and unspread states are circular (iv) surface diffusion is negligible.

Equations 4.4 and 4.5 show the kinetic equations for the rate adsorption of proteins in unspread and altered states, respectively.

$$\frac{d\rho_\alpha}{dt} = k_1 C_0 \Phi - k_d \rho_\alpha - k_f \rho_\alpha \Psi \tag{4.4}$$

$$\frac{d\rho_\beta}{dt} = k_f \Gamma_\alpha \Psi \tag{4.5}$$

where ρ_α and ρ_β are the surface densities of proteins in the unspread and altered (spread) states, respectively. The units of ρ depends on the units of C used (the typical units of C are g / L, moles / L and molecules / L). For section 4.4 and the remainder of the thesis, ρ will be in molecules/area. Meanwhile, Φ is the adsorption

probability (the probability that an incoming protein finds space available for adsorption to the surface), ψ is the spreading probability (the probability that already adsorbed molecules have sufficient space to spread), k_f is the spreading rate, k_1 and k_d are the adsorption and desorption constants respectively and C_0 is the bulk concentration at the surface.

Analytical expressions for the adsorption and spreading probabilities (Φ and Ψ) may be derived via the Scaled Particle Theory [Brusatori and Tassel, 1999] (see the next section Part 4.4) with the assumption that the proteins on the surface are at all times in a uniform concentration along the surface and their surface projections are disk shapes.

4.4 Scaled Particle Theory (SPT)

Scaled Particle Theory (SPT) is used to derive analytical expressions for the probability functions in the kinetic equations used in the spreading particle model of Brusatori and Tassel (that is, to estimate the value of Φ and Ψ). The assumptions for this theory are; (i) the proteins on the surface are at all times in a uniform concentration along the surface and (ii) the proteins have disk-shapes (2D) and (iii) the surface projections of both spread and unspread states are circular (proteins are *symmetrically* spread to larger radii.)

The function Φ is defined as the probability of finding a 2D cavity of radius R_α while the function Ψ is defined as the conditional probability of finding a cavity of radius R_β given that a protein diameter, R_α exists in its center.

The final equations of Φ and ψ derived using the SPT are shown in Equations 4.6 and 4.7, respectively. The details of the SPT theory and the adsorption and spreading probabilities (Φ and Ψ) derivation can be found in Brusatori and Van Tassel and Van Tassel papers [Brusatori and Tassel, 1999, Van Tassel, 2003].

$$\Phi = \left(1 - \rho^{*}_{\alpha} - \Sigma^{2}\rho^{*}_{\beta}\right)\exp\left[-\frac{2\left(\rho^{*}_{\alpha} + \Sigma\rho^{*}_{\beta}\right)}{1 - \rho^{*}_{\alpha} - \Sigma^{2}\rho^{*}_{\beta}} - \frac{\rho^{*}_{\alpha} + \rho^{*}_{\beta} + (\Sigma - 1)^{2}\rho^{*}_{\alpha}\rho^{*}_{\beta}}{\left(1 - \rho^{*}_{\alpha} - \Sigma^{2}\rho^{*}_{\beta}\right)^{2}}\right] \quad (4.6)$$

$$\Psi = \exp\left[-\frac{2(\Sigma - 1)\left(\rho^{*}_{\alpha} + \Sigma\rho^{*}_{\beta}\right)}{1 - \rho^{*}_{\alpha} - \Sigma^{2}\rho^{*}_{\beta}} - \frac{(\Sigma^{2} - 1)\left[\rho^{*}_{\alpha} + \rho^{*}_{\beta} + (\Sigma - 1)^{2}\rho^{*}_{\alpha}\rho^{*}_{\beta}\right]}{\left(1 - \rho^{*}_{\alpha} - \Sigma^{2}\rho^{*}_{\beta}\right)^{2}}\right] \quad (4.7)$$

where $\rho^{*}_{\gamma} = \rho_{\gamma}\pi R_{\gamma}^{2}$ ($\gamma = \alpha$ or β) (4.8) and

$$\Sigma = \frac{R_{\beta}}{R_{\alpha}} \quad (4.9)$$

ρ^{*} is a dimensionless surface density (fraction area coverage) while R_{α} and R_{β} are particle radii for the folded ("native") and unfolded forms, respectively. ρ is a surface density of protein adsorbed (see Section 4.3), in molecules/area.

Nevertheless, the limitation for this theory is that, it assumes that the proteins on the surface can always be represented by a projected circle (proteins actually possess a folded three-dimensional structure).

A different group [Shen et al., 2005] proposed a kinetic model that takes into account the adsorption of the unfolded form directly from the bulk. In this model, the protein is assumed to adsorb on the surface in two different states; state 1 and state 2. State 1 can desorb whereas state 2 cannot. The protein in state 2 cannot be washed off by exchange with buffer. In their model, proteins adsorbed in state 1 can also be irreversibly transformed into state 2. The adsorption rate is assumed to be proportional to the protein bulk concentration and the free site surface. A schematic illustration of this model is given in Figure 4.4 and described by Equations 4.10 to 4.13. This model does not use any size of molecule, with point sites for adsorption (each either occupied or vacant), as in the Langmuir model.

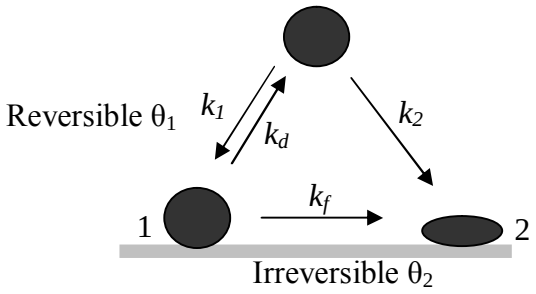

Figure 4.4: Model of protein adsorption kinetics [Shen et al., 2005].

$$\frac{d\theta_1}{dt} = k_1 C_0 (1 - \theta_1 - \theta_2) - (k_d + k_f)\theta_1 \qquad (4.10)$$

$$\frac{d\theta_2}{dt} = k_2 C_0 (1 - \theta_1 - \theta_2) + k_f \theta_1 \qquad (4.11)$$

$$\frac{d\theta}{dt} = \frac{d\theta_1}{dt} + \frac{d\theta_2}{dt} = C_0 (k_1 + k_2)(1 - \theta_1 - \theta_2) - k_d \theta_1 \qquad (4.12)$$

$$\theta = \theta_1 + \theta_2 \text{ and } 0 \le \theta \le 1 \qquad (4.13)$$

where θ_1 and θ_2 denote the fraction of site surface covered with the protein in states 1 (folded proteins) and 2 (unfolded proteins), respectively, k_1 and k_2 are the adsorption rate constants corresponding to states 1 and 2, respectively and k_d and k_f are the desorption and transformation rate constants, respectively.

This model was one of the models used to fit our kinetic data. We called this model an extended Langmuir model. From this model, two modifications have been proposed. The first modification is called the extended Langmuir model with free reversibility while the second modification is called the extended Langmuir model with configurational diffusion. The detail of the proposed models is shown below.

4.4.1 Extended Langmuir model with free reversibility

In this proposed model, a possibility of reversing the surface unfolding was considered. Also the increased area of the unfolded form is taken into account. Thus, a surface back reaction, k_{f2}, and a back reaction from tightly bound to solution, k_{2d}, and a spreading factor, *a* (ratio of unfolded area to folded area for a molecule) were introduced to the original model (the extended Langmuir model). By introducing the *a* term, one is able to define the extent of the denaturation or spreading taking place on the adsorbed protein. If *a* is 1, then the adsorbed protein retains its native form (folded form) and no spreading is taking place. The higher the *a*, the higher the spreading is occurred. The spreading occurs on the surface once the protein is adsorbed, whether via state 1 or directly from solution. The schematic diagram and the respective kinetic equations are shown in Figure 4.5 and Equations 4.14 and 4.15, respectively.

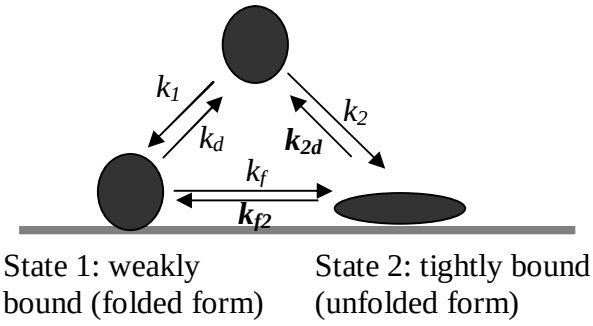

Figure 4.5: Schematic diagram of the proposed kinetic model (extended Langmuir model with free reversibility).

$$\frac{\Delta\theta_1}{\Delta t} = k_1 C_O(1-\theta_1-a\theta_2) - (k_d)\theta_1 - k_f\theta_1(1-\theta_1-a\theta_2)/a + k_{f_2}\theta_2(1-\theta_1-a\theta_2) \quad (4.14)$$

$$\frac{\Delta\theta_2}{\Delta t} = k_2 C_o(1-\theta_1-a\theta_2)/a + k_f\theta_1(1-\theta_1-a\theta_2)/a - k_{f2}\theta_2(1-\theta_1-a\theta_2) - k_{2d}\theta_2 \quad (4.15)$$

4.4.2 Extended Langmuir model with diffusion hindrance through very small pores

In protein adsorption, the incoming protein from the bulk solution faces more difficulty to adsorb on a surface containing more adsorbed protein. The already adsorbed proteins tend to repulse the incoming protein (steric repulsion). Steric repulsion is the dominant protein-protein interaction when the ionic strength of the solution is high and when significant conformational alteration (spreading) is absent [Van Tassel, 2003]. The adsorbed proteins also have more difficulty to transform from a folded form to unfolded form in higher adsorbed concentrations (influence of neighbours) (see Figure 4.6). Therefore, the first modification was further empirically modified by introducing power index '*n*'. The *n* term attempts to allow for the configurational hindrance to diffusion or to electrical charge forces of neighbouring molecules. The *n* term was introduced during adsorption and during transformation from folded to unfolded forms (see Equations 4.16 and 4.17).

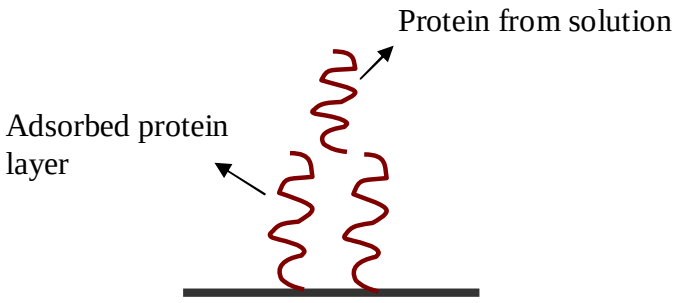

Figure 4.6: Schematic diagram of the proposed kinetic model (an extended Langmuir model with diffusion hindrance through very small pores).

$$\frac{\Delta\theta_1}{\Delta t} = k_1 C_O (1-\theta_1 - a\theta_2)^n - (k_d)\theta_1 - k_f \theta_1 (1-\theta_1 - a\theta_2)^n / a + k_{f2}\theta_2 \qquad (4.16)$$

$$\frac{\Delta\theta_2}{\Delta t} = k_2 C_o (1-\theta_1 - a\theta_2)^n / a + k_f \theta_1 (1-\theta_1 - a\theta_2)^n / a - k_{f2}\theta_2 - k_{2d}\theta_2 \qquad (4.17)$$

4.5 Diffusion-reaction model

All the models reviewed in the previous sections did not account for any mass transport limitation. It has been assumed that concentrations acting at the surface are equal to those in the bulk solution. Adsorption rate data that clearly define kinetic regimes (transport and reaction) are extremely useful in revealing important mechanisms and checking assumptions about the conditions above the surface. In a flow system, a mass transport limiting regime normally does exist at initial stages of adsorption and therefore cannot be ignored [Wittmer and Van Tassel, 2005, Wittmer et al., 2007]. By plotting adsorption rate versus mass density adsorbed, one is able to distinguish between these regimes (see Figure 4.7).

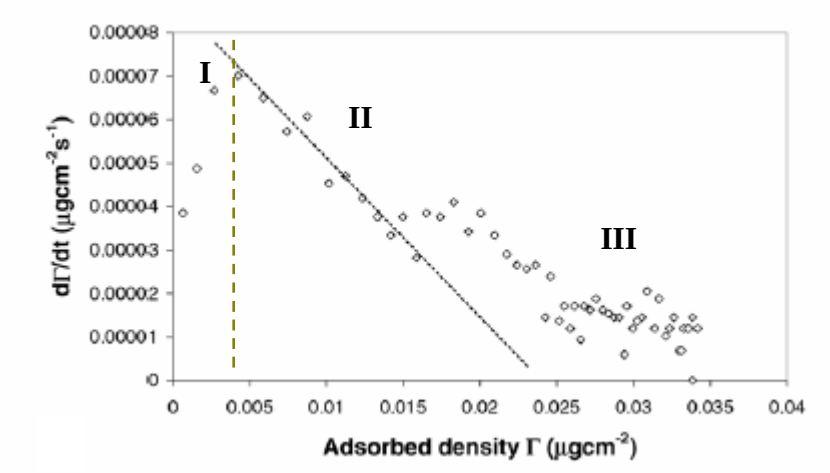

Figure 4.7: An example curve of adsorption rate of fibrinogen versus fibrinogen adsorbed mass, as measured by OWLS. Regimes whose kinetics is limited by transport (I), initial surface effects (II), and asymptotic surface effects (III) are denoted. The asymptotic regime occurs after a maximum rate of adsorption is reached. This regime occurs over longer times compared to other regimes with adsorption to an increasingly blocked surface being the governing mechanism. The line represents a best fit to data in the initial surface limited regime II; the intercept being proportional to the adsorption rate constant k'_1. Taken from [Wittmer and Van Tassel, 2005].

4.6 Diffusion control

Diffusion can be defined as a spontaneous intermingling or mixing of atoms or molecules by a random motion. It gives rise to the motion of the species relative to the motion of the mixture. In the absence of other gradients (such as temperature, electric potential or gravitational potential) molecules of a given species within a single phase will always diffuse from regions of higher concentrations to regions of lower concentrations. This gradient results in a molar flux, J, of the species (for example, for species A), J_A, in the direction of the concentration gradient. The typical units of J_A (moles/area.time) are mol/m^2.s [Fogler, 1992]. The total molar flux, W_A, of species A is the result of two contributions; the molecular diffusion flux, J_A, and the flux B_A resulting from the bulk motion (or convection) of the fluid, B_A (that is, $W_A = J_A + B_A$).

The mathematics that govern the mass transport phenomena of diffusion are based on Fick's laws; Fick's first law (see Equation 4.18) and Fick's second law (see Equation 4.19).

$$J = -D\left(\frac{dc}{dx}\right) \tag{4.18}$$

$$\frac{dc}{dt} = D\left(\frac{d^2c}{dx^2}\right) \tag{4.19}$$

where $\frac{dc}{dx}$ is a concentration gradient and D is a diffusivity (area/time)

The reaction-diffusion system can be described by Fick's law with appropriate boundary conditions to define the surface adsorption process [Hibbert et al., 2002]. If the adsorption rate is limited by diffusion, the adsorption kinetics will depend on the details of the geometry and also on the flow velocity.

Calonder and Van Tassel [2001] in their study modeled the adsorption of human plasma fibronectin on a glass substrate by combining a particle model at the

surface with a boundary layer condition. The transportation of the proteins from a bulk solution to a surface has therefore been considered. They begin their model by considering a thin region of thickness *d* (approximately on the order of a protein diameter) where protein-surface interactions are appreciable. Bear in mind that this thin region is not a concentration boundary layer. The flux through a plane surface in this layer (a distance *z* from the surface) is given by Equation 4.20.

$$J(z) = \left[D\frac{\partial c}{\partial z} + \frac{c(z)}{\xi}\frac{\partial u}{\partial z} \right]\Phi(z) \qquad (4.20)$$

where ξ is a frictional coefficient, expressed as $\xi = kT/D$ (*k* is the Boltzmann constant, *T* is the absolute temperature and *D* is the diffusion coefficient), *u* (*z*) is the translationally averaged potential energy of the protein, and Φ (*z*) is the fractional lateral available area as discussed before (*u* and Φ possess implicit time dependences).

By assuming a steady flux through this thin layer (Equation 4.20) (that is, no concentration gradient in *d* layer) will give an expression for J as shown in Equation 4.21

$$J = \frac{D\left[c(d) - c(0)e^{-u(0)/kT}\right]}{\int_0^d \frac{e^{u(z)/kT}}{\Phi(z)}dz} \qquad (4.21)$$

They also consider a transport from the flowing solution by convective diffusion. The assumptions made are, (i) a linear velocity profile that begins at $z = d$, (ii) negligible diffusion along the flow direction and (iii) a concentration at $z = d$ that remains negligible until the onset of a quasi-steady diffusion-limited regime (that is, *c* ($z = d$) begins to increase very slowly from near zero.

The transport in the space above the *d* layer was modeled as shown in Equation 4.22.

$$\frac{\delta c}{\delta t} + a(z-d)\frac{\delta c}{\delta x} = D\frac{\delta^2 c}{\delta z^2}, \quad t \geq 0,\ x \geq 0,\ z \geq d \tag{4.22}$$

Boundary conditions applied:

$c\ (0, z, t) = c_0$

$c\ (x, d, t) = 0$ (near zero)

$c\ (x, z, 0) = 0$

where x is the distance from the inlet along the direction of the flow (parallel to the surface, z is the vertical distance from the surface (for $z > d$, c also depends on x), a is the shear rate at the surface (a is constant with respect to z and t ($a\ (z, t) = a$)) and c_0 is the bulk concentration.

Figure 4.8 shows an illustration of z, x, d and δ. δ is the concentration boundary layer thickness and defined as the distance from a surface to where the concentration of the diffusing species reaches 99 % of the bulk concentration [Fogler, 1992]. Generally, the thickness of d is on the order of a protein diameter and thus, $d << \delta$.

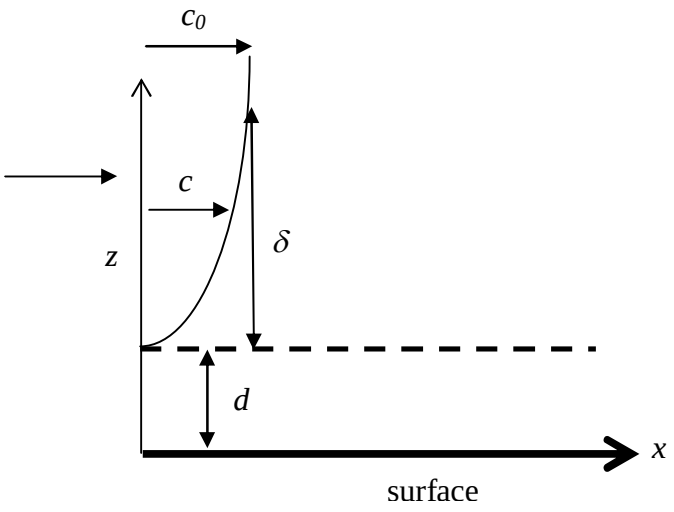

Figure 4.8: Illustration of *z, x, d* and δ.

They considered a boundary concentration layer thickness, δ (*x*, *t*), above which the protein concentration is constant ($z > \delta$) and at which the *z* derivative of the protein concentration vanishes. Therefore, they approximate *c* in terms of δ and *z* as:

$$\frac{c(x,z,t)}{c_0} = \frac{3}{2}\frac{z-d}{\delta(x,t)-d} - \frac{1}{2}\frac{(z-d)^3}{(\delta(x,t)-d)^3} \qquad (4.23)$$

c / c_0 is a dimensionless, therefore δ / d is the characteristic variable and Equation 4.23 can be rewritten to,

$$\frac{c(x,z,t)}{c_0} = \frac{3}{2}\frac{z/d-1}{\delta(x,t)/d-1} - \frac{1}{2}\frac{(z/d-1)^3}{(\delta(x,t)/d-1)^3}$$

Figure 4.9 shows the illustration of z / d versus c / c_0 for different δ / d.

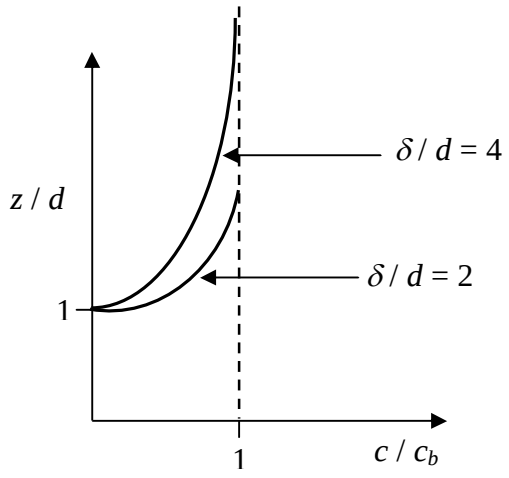

Figure 4.9: Illustration of z / d versus c / c_0 for different δ / d.

Inserting Equation (4.23) into an integrated form of Equation (4.22), a new variable,τ (dimensionless), is defined as shown in Equation 4.24. The solution of dimensionless c / c_0 is expected to be a unique function of τ irrespective of t or x.

$$\tau = \frac{4Dt}{\left(\frac{45Dx}{2a}\right)^{2/3}} \tag{4.24}$$

The definition of $f(\tau)$ is shown in Equation 4.25 and can be solved using Equations 4.26 and 4.27.

$$f(\tau) = \frac{\left(\frac{45Dx}{2a}\right)^{1/3}}{\delta(x,\tau)} \tag{4.25}$$

At $\tau = 0$ and at x = infinity, δ goes to infinity.

$$\frac{df}{d\tau} = \frac{f - f^4}{f - 2\tau} \quad with \quad f(0) = 0 \tag{4.26}$$

Calonder and Van Tassel [2001] state that the analytical solution for Equation 4.26 is as shown in Equation 4.27:

$$\tau(f) = \frac{\left[1 - \left(1 - f^3\right)^{2/3}\right]}{2f^2} \tag{4.27}$$

Figure 4.10 shows the plot of τ versus *f* from Equation 4.27. As can be seen, after a value of $f = 1.2$, τ is a negative value, which is illegal. The maximum value of τ is 0.5. However, the analytical solution for τ (*f*) (Equation 4.27) contradicts the initial condition of *f* (0) = 0 (substituting τ = 0 in Equation 4.27 will give an error value for *f* instead of zero).

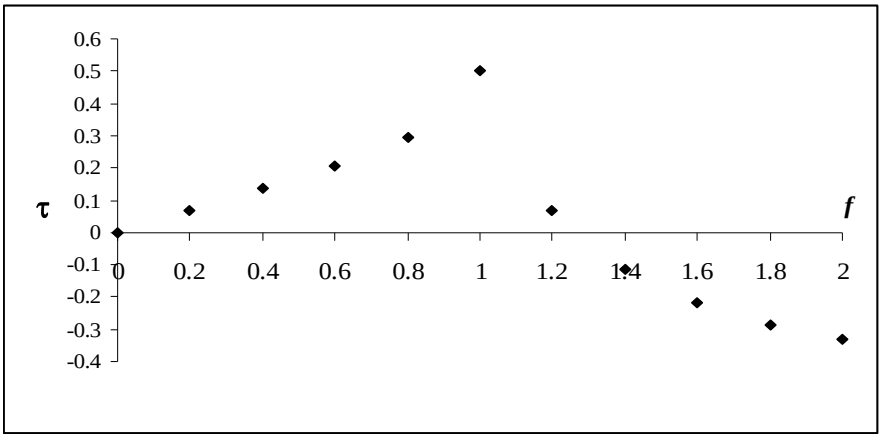

Figure 4.10: Plot of τ versus *f* from Equation 4.27.

They derived the overall rate equations by assuming steady concentrations between *z* = 0 and *z* = *d* (or in other words, no concentration gradient in *d* layer). Therefore, the resulting overall rate equations (written in terms of surface concentration, Γ) are in Equations 4.28 and 4.29. It should be noted that, we have used ρ specifically for

surface concentration when expressed in molecules/area, whereas Coloder and Van Tassel [2001] use Γ for more general units of surface concentration.

$$\frac{\delta\Gamma_\alpha}{\delta t} = \frac{C_0}{\underbrace{\frac{2}{3}\frac{\delta(x,t)}{D}}_{\text{bulk diffusion}} + \underbrace{D^{-1}\int_0^d \frac{e^{u(z)/kT}}{\Phi(z)}dz}_{d\text{ layer}} + \underbrace{\frac{e^{u(0)/kT}}{k_1\Phi(0)}}_{\text{surface}}} - \frac{k_d\Gamma_\alpha}{1+\frac{k_1\Phi(0)}{e^{u(0)/kT}}\left[\frac{2}{3}\frac{\delta(x,t)}{D} + D^{-1}\int_0^d \frac{e^{u(z)/kT}}{\Phi(z)}\right]dz} - k_f\Gamma_\alpha\Psi \tag{4.28}$$

$$\frac{\partial\Gamma_\beta}{\partial t} = k_f\Gamma_\alpha\psi \tag{4.29}$$

The adsorption rate contains three terms in its denominator, that represent 'resistors' in series; accounting for bulk diffusion outside the region of molecular forces, $z > d$, Brownian motion near the surface through the $0 < z < d$ layer and surface reaction, respectively. Distinct kinetic regimes, characterized by a net adsorption rate controlled by one of these mechanisms in each regime are predicted when one of the terms is larger than that of the other two.

Calonder and Van Tassel [2001] have used the above model (Equations 4.28 and 4.29) to model their experimental kinetic data. The fit of the model to their experimental kinetic data is shown in Figure 4.11 (continuous line) for three different bulk protein concentrations. As can be seen, the kinetic data is well-described by the model [Calonder and Tassel, 2001]. In solving the model, the expressions for $k_1 e^{-u(z=0)/kT}$ and $du(z=0)/d\Gamma$ are determined from the intercept of an extrapolated linear region and the slope of the linear region, respectively (from the plot of rate of adsorption versus mass density adsorbed). The potential energy, u, can be determined

by considering an electrostatic and van der Waals contributions between the molecules and the surface [Roth and Lenhoff, 1995]. k_f and σ meanwhile are determined from the fitting. The expression of adsorption probability (Φ) and spreading probability (Ψ), are again estimated using the scaled particle theory (SPT) [Brusatori and Van Tassel, 1999]. Refer to Equations 4.8 and 4.9.

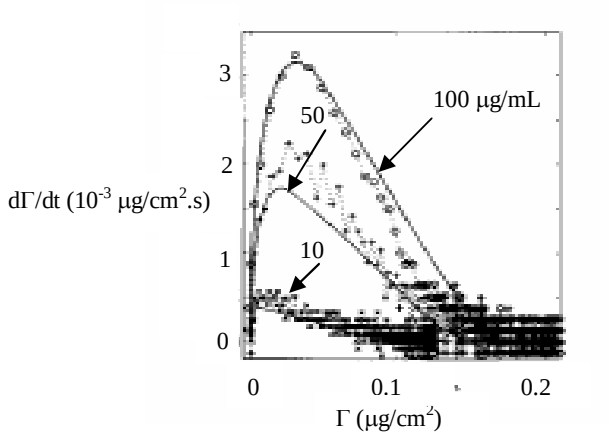

Figure 4.11: Rate of adsorption of human plasma fibronectin to the $SiTiO_2$ surface as a function of adsorbed density as measured using the OWLS. Adsorption data from bulk concentrations of 10, 50 and 100 μg/mL are shown. Also shown are the predictions of the model with a single set of fitted constants (Equations 4.27 and 4.28) (continuous lines). Taken from [Calonder and Van Tassel, 2001].

Van Tassel [2003] also modeled the experimental kinetic data (adsorption of human plasma fibronectin to the $SiTiO_2$ surface) by assuming that the potential energy is not significant and therefore can be ignored (see Equations 4.30 and 4.31). The δ also was assumed to be constant.

$$\frac{d\Gamma_\alpha}{dt} = \frac{C_0}{\frac{\delta}{D} + \frac{1}{k_1\Phi}} - \frac{k_d\Gamma_\alpha}{1 + \frac{k_1\Phi\delta}{D}} - k_f\Gamma_\alpha\Psi \qquad (4.30)$$

$$\frac{d\Gamma_\beta}{dt} = k_f \Gamma_\alpha \Psi \qquad (4.31)$$

The model with δ varying with time (Calonder and Van Tassel, 2001) appeared to more accurately fit the experimental kinetic data than with a constant δ was used [Van Tassel, 2003].

In our study, a model which includes diffusion limitation was also attempted. We proposed some alterations in the diffusion-reaction model from the work of Van Tassel [2003]. The Γ_α and Γ_β, (Equations 4.30 and 4.31) were expressed in terms of fractional site surface coverage, θ_1 and θ_2, respectively (see Equations 4.32 to 4.33). Thus, the equations of 4.30 and 4.31 were multiplied by πR_α^2 and πR_β^2 for both sides, to get an expression for θ_1 and θ_2 respectively (where $\Gamma_\alpha \pi R_\alpha^2 = \theta_1$ and $\Gamma_\beta \pi R_\beta^2 = \theta_2$). Γ are here being expressed in molecules/area, and C_b in Equation 4.32, is in molecules/vol.

$$\frac{d\theta_1}{dt} = \frac{C_0\left(\pi R_\alpha^2\right)}{\frac{\delta}{D} + \frac{1}{k_1\phi}} - \frac{k_d\theta_1}{1 + \frac{k_1\phi\delta}{D}} - k_f\theta_1\psi \qquad (4.32)$$

$$\frac{d\theta_2}{dt} = k_f\theta_1\Psi \qquad (4.33)$$

The expressions for Φ and Ψ (refer Equations 4.8 and 4.9) were also changed. The terms of ρ_α^* (or $\rho_\alpha \pi R_\alpha^2$) and ρ_β^* (or $\rho_\beta \pi R_\beta^2$) from Equations 4.8 and 4.9 were changed to θ_1 and θ_2, respectively as shown in Equations 4.34 and 4.35. Bear in mind that, ρ^* is the dimensionless surface density (fraction of area coverage) while θ is the fraction of site surface coverage. The advantage of θ is that it does not consider the

geometry of the protein used (in most cases, it is hardly to find the exact geometry of the proteins, especially the globular proteins).

$$\Phi = \left(1 - \theta_1 - \Sigma^2\theta_2\right)\exp\left[-\frac{2\left(\theta_1 + \Sigma^2\theta_2\right)}{1 - \theta_1 - \Sigma^2\theta_2} - \frac{\theta_1 + \theta_2 + (\Sigma - 1)^2\theta_1\theta_2}{\left(1 - \theta_1 - \Sigma^2\theta_2\right)^2}\right] \quad (4.34)$$

$$\Psi = \exp\left[-\frac{2(\Sigma - 1)\left(\theta_1 + \Sigma^2\theta_2\right)}{1 - \theta_1 - \Sigma^2\theta_2} - \frac{\left(\Sigma^2 - 1\right)\left[\theta_1 + \theta_2 + (\Sigma - 1)^2\theta_1\theta_2\right]}{\left(1 - \theta_1 - \Sigma^2\theta_2\right)^2}\right] \quad (4.35)$$

The equation of the concentration boundary thickness (δ) from Equation 4.25 was also changed as shown in Equation 4.36. In a QCM cell, the inlet fluid flow behaves as a laminar jet flow. Thus, the maximum velocity of concentration is expected to be at the midpoint z in the cell channel. δ can be measured as a ratio between the bulk concentration to the initial slope of the concentration profile (δ=c_b/initial slope) and therefore δ can be higher than that of the thickness of the cell, h.

$$\delta = K \exp\left(-bt\right) \quad (4.36)$$

where b is dependent on the velocity (v) and the distance from the inlet (x) ($b = v / x$) (δ generally dependent on surface position (which is x) and the fluid velocityn (which is v)). The constant of b should have units of s^{-1} to provide a dimensionless exponent. K meanwhile, refers to the ratio between h to D (see Figure 4.12).

The boundary conditions applied for δ is;

At $t = 0$, $\delta = \infty$

At $t = \infty$, $\delta = 0$

After reach a certain limit, the adsorption is limited by the surface reaction and the diffusion limitation is no longer important. At this condition, c_s

(concentration protein at the surface) = c_0 (concentration of protein in the bulk) and the concentration gradient starts to develop. The rate of adsorption decreases as the mass adsorbed increases and becomes constant after a maximum rate of adsorption is reached (blocked surface being the governing mechanism). Refer to Figure 4.7 for the transition between the regimes in the adsorption process.

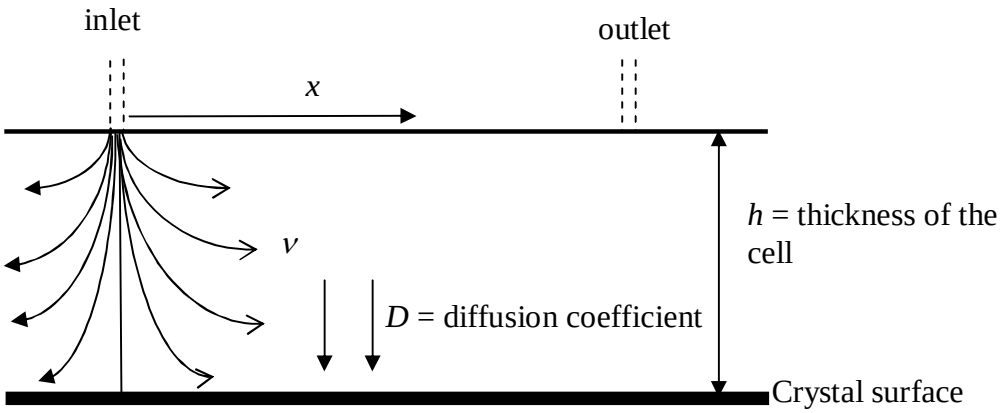

Figure 4.12: An illustration of *z*, *v* and δ in the cell.

The proposed modification of the diffusion-reaction model has shown a good fitting on our kinetic data (see Chapter 10).

4.7 Data interpretation

It should be noted that the adsorption of a protein is spontaneous if $\Delta G_{\text{adsorption}} = \Delta H_{\text{adsorption}} - T\Delta S_{\text{adsorption}} < 0$ as mentioned earlier in Chapter 2. Any proposed mechanism of protein adsorption must be consistent with the relationship between ΔG, ΔH and ΔS. A large negative ΔG value indicates high spontaneous adsorption behaviour (high affinity) towards the surface. The sign of the ΔH value meanwhile indicates whether the process of adsorption is endothermic or exothermic (positive ΔH value relates to an endothermic process and vice versa). The occurrence of denaturation or conformational change during the adsorption is expected to be

correlated to a ΔS value. The larger the value of the (positive) ΔS, the more denaturation (spreading) is indicated [Cabilio et al., 2000]. ΔG, ΔH and ΔS can be calculated using Equations 4.37 and 4.38.

$$\Delta G = -RT(\ln K) \tag{4.37}$$

$$\Delta G = \Delta H - T\Delta S \tag{4.38}$$

R, T and K are a gas constant (8.314 J/K.mol), the absolute temperature (K) in Kelvin unit and an equilibrium constant, respectively. The equilibrium constant, K, is the ratio between the adsorption and desorption constant at equilibrium (k_1 / k_d) (k_1 and k_d must consistent in the units). Plotting ΔG versus T will give a slope and an intercept of ΔS and ΔH, respectively.

Table 4.1 shows a comparison of thermodynamic values for the adsorption of various proteins onto stainless steel surfaces from pH 7 phosphate buffer at 298 K [Cosman et al., 2005]. As can be seen, all the proteins show high spontaneous adsorption behaviour (that is, large negative ΔG_{ADS} values) on the stainless steel surface with BSA showing the greatest affinity. Comparisons of the enthalpy of adsorption, ΔH_{ADS}, show a slightly endothermic process for β-casein (3.6 kJ/mol) and β-lactoglobulin (3.4 kJ/mol) and a larger endothermic value for α-lactalbumin (15.6 kJ/mol). This endothermic process is offset by the large entropy values observed for the three proteins, with the ΔS_{ADS} values of 236, 157 and 192 for α-lactalbumin, β-lactoglobulin and β-casein, respectively. The particularly high entropic value of holo α-lactalbumin (relative to BSA and β-lactoglobulin) suggests that extensive denaturation (unfolded form) of α-lactalbumin occurs during the adsorption process. BSA, in contrast, not only shows the greatest affinity for the surface, (ΔG_{ADS} = -57 kJ/mol) but also by the high value of ΔH_{ADS}, -47.2 kJ/mol. The low entropy for BSA (ΔS_{ADS} = 33 J/K.mol) relative to others proteins, suggests that the molecules remain to a great extent in their native conformation (folded form) during the adsorption process.

Table 4.1: Comparison of thermodynamic values for the adsorption of various proteins onto stainless steel surfaces from pH 7 phosphate buffer at 298 K.

Protein	Surface	$\Delta G_{ADS} \pm 0.8$ kJ/mol	$\Delta H_{ADS} \pm 0.8$ kJ/mol	$\Delta S_{ADS} \pm 1$ J/K.mol
Holo α-lactalbumin	Stainless steel	-54	15.6	236
β-lactoglobulin	Stainless steel	-45	3.4	157
β-casein	Stainless steel	-55	3.6	192
Bovine serum albumin (BSA)	Stainless steel	-57	-47.2	33

The data tabulated in Table 4.1 will be used as a comparison to our kinetics results (refer to Chapter 10 for the kinetics modelling).

CHAPTER FIVE

METHODOLOGY

5.0 Introduction

This chapter describes the details of the experimental work done in this study. There are four main stages of experiment involved in this study. The work was started with the adsorption of proteins namely β-casein, lysozyme and α-lactalbumin on a clean bare stainless steel surface. In this stage, effects of temperature (23, 30, 35 and 40 °C) and concentration (0.1, 0.5 and 1.0 g/L) on the adsorption of proteins onto the stainless steel surface were investigated. The adsorption kinetics data obtained were attempted to model, including a possible diffusion step. These experiments were taken as a control for further experiments.

The experiment was then continued with the modification of the stainless steel surfaces. The modification was done by coating the surfaces with poly(ethylene imine) (PEI) or sodium silicate layers followed by grafting with poly (ethylene) glycol (PEG) molecules. There were two strategies in grafting the PEG onto the anchor layer; first, by using single PEG chains and second, using shorter chains followed with longer chains. The effects of temperature (23 and 40 °C) and PEG end groups (OH or NHS), molecular weights (350, 550, 2000 and 5000 Da) and concentrations (0.1, 1.0 and 5.0 g / L) to PEG conformation ('pancake', 'mushroom' or 'brush') were determined (using Equation 2.1). Nevertheless, 'brush' conformation is our preference.

A simple and easy yet promising technique to inhibit adsorption of protein onto the stainless steel surface is attempted. The selection of PEI as an anchor layer is particularly owing to its rapid and simple electrostatically driven adsorption to negatively charged stainless steel surfaces. It can be done simply at ambient temperature and atmospheric pressure. Silicate layer meanwhile was chosen based on the USPTO Patent Application 20070065591. The patent revealed that coating the stainless steel

surfaces with sodium silicate is able to prevent adsorption of protein. The merits of the proposed modification method compared to the most published methods is that, the process of modification was only done by passing through the solution onto the surfaces and do not involve any hazardous chemical substances. If the approach developed can inhibit adsorption of protein then it will be really a great achievement. Moreover, the modification process was done in situ, enabling for the kinetic measurement.

Once the modification steps were done, protein adsorption was immediately performed on the resulted surfaces. The effectiveness between a single and combination of sizes of PEG chains to repel the adsorption of protein was compared. The adsorption of protein was also done on the PEI and silicate surfaces without the presence of PEG molecules. Thus, the role between anchor layer and PEG molecules to inhibit adsorption of protein can be distinguished.

At the end of the study (not the originally planned), the surfaces were modified by coating with a protein monolayer as an anchor layer instead of a PEI or a silicate layer. The adsorption of the simulated protein in the dairy industry was then performed on the resulted modified surfaces. The adsorption was also performed at high temperature, 80 °C, to mimic realistic conditions for industrial application.

AFM characterization was also carried out on several samples to examine the topography of the surfaces. The general flow of the experiment works is summarized in Figure 5.1.

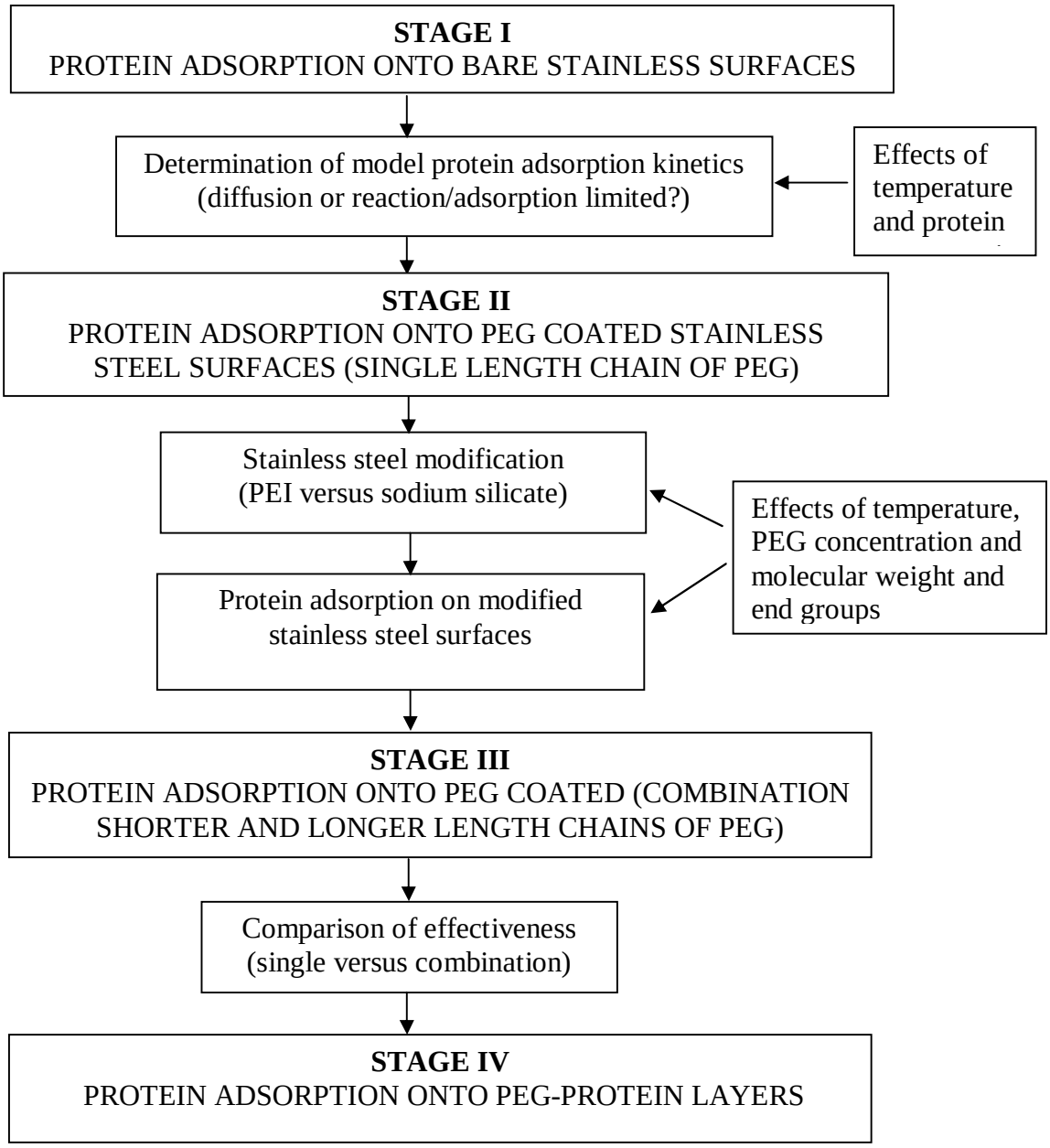

Figure 5.1: Flow of research methodology.

5.1 Materials

5.1.1 Buffer solution

Phosphate buffer solution of 0.1 M (pH 7.2 ± 0.1) was prepared in our laboratory with appropriate proportions of ultra high purity MilliQ water, sodium phosphate dibasic heptahydrate ($Na_2HPO_4.7H_2O$, MW 268.07 gram/mole) and sodium dihydrogen phosphate monohydrate ($NaH_2PO_4.H_20$, MW 137.99 gram/mole). The ratio of MilliQ water to $Na_2HPO_4.7H_2O$ and $NaH_2PO_4.H_20$ used was 0.36 : 0.14 : 050, respectively. $Na_2HPO_4.7H_2O$ and $NaH_2PO_4.H_2O$ were purchased from Sigma–Aldrich and Merck (Steinheim, Germany), respectively. The buffer solutions were degassed with helium prior to use to avoid bubble formation during QCM experiments.

5.1.2 Deionized water (MilliQ water)

Deionized water was used as a PEI and sodium silicate solvent. The MilliQ water was degassed with helium prior to use to avoid bubble formation during QCM experiments.

5.1.3 Protein solution

β-casein, lysozyme, α- lactalbumin with type I (calcium enriched, ≥ 85 %) and III (calcium depleted 85 %) and β-lactoglobulin proteins were purchased from Sigma-Aldrich (St.Louis, Mo,USA) and used without further purification. All the proteins used are from bovine milk except lysozyme, from chicken egg white. Protein solutions were prepared using phosphate buffer solution as a solvent. A stock of protein solutions were kept in a freezer at temperature -4 °C. Protein solutions not used within 48 hours of thawing were discarded. The properties of proteins used are described briefly below:

5.1.3.1 β-casein

Casein is the major protein of bovine milk and consists of α, β and κ types with percentage of 75, 22 and 3 %, respectively. Thus, β-casein protein represents the second most abundant of the caseins in bovine milk. β-casein has a molecular weight of 23,000 Da with an isoelectric point (pI) value about 4.6. It consists of 209 amino acid residues and binds metal cations with high affinity (the binding strength depends strongly on the ion type). β-casein has strong amphiphilic character and is somewhat similar to an anionic detergent with a negatively charged head and an uncharged, essentially hydrophobic tail. This characteristic provides a possibility for β-casein to form micelles in solution. A micelle can be defined as an aggregate of surfactant molecules dispersed in a liquid colloid. A typical micelle in aqueous solution forms an aggregate with the hydrophilic 'head' regions in contact with surrounding solvent, sequestering the hydrophobic tail regions in the micelle centre as shown in Figure 5.2 [www.wikpedia.com]. Besides that, β-casein has a disordered structure with a great flexibility in solution. Thus, it looks more or less like a 'naturally unfolded protein'. The maximum density of monolayer β-casein is approximately 2.3 mg/m^2 [Veen et al., 2007].

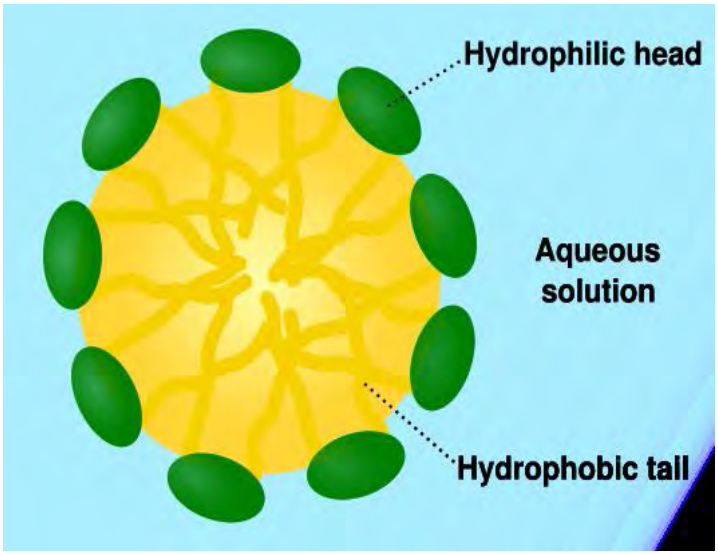

Figure 5.2: Scheme of a **micelle** formed by phospholipids in an aqueous solution.

5.1.3.2 Lysozyme

Lysozyme is an enzyme that is present in egg white, tears, and other secretions. It is responsible for breaking down the polysaccharide walls of many kinds of bacteria. Lysozyme is a globular protein of slightly ellipsoidal shape with the dimensions of 4.5 nm x 3.0 nm x 3.0 nm and molecular weight of 14,600 Da. It is a basic protein with an isoelectric point (pI) value of 11.1. Its denaturation temperature is being 74 °C. The primary structure of lysozyme is a single polypeptide chain of 129 amino acid residues with four disulfide bonds. Lysozyme is known as a 'hard' globular protein in the sense of having a strong internal structure and conformational stability. The maxima adsorption densities of lysozyme are 0.207 and 0.310 mg/m^2 for the hexagonal packing of monolayer molecules adsorbed in side-on and end-on orientations, respectively [Shen et al., 2001, Unsworth et al., 2005].

5.1.3.3 α-lactalbumin

α-lactalbumin is the second most abundant protein in whey with a concentration of 1.2 g/L [Etzel, 2004]. α-lactalbumin is a compact globular protein with a molecular weight of 14, 200 Da and dimension of 3.7 nm x 3.2 nm x 2.5 nm. It is an acidic protein with an isoelectric point (pI) value of 4.3. Its denaturation temperature is about 64 °C. It consists of a single polypeptide chain with a total of 123 amino acid residues and 4 disulfide bonds. It consists of two domains; an α-helical domain and β-sheet domains (see Figure 5.3). α-lactalbumin is known as a 'soft' protein.

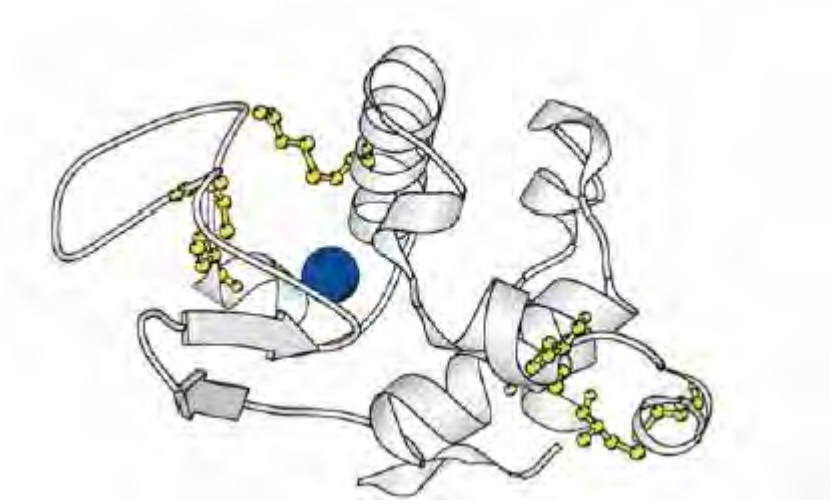

Figure 5.3: Schematic diagram of α-lactalbumin structure in ribbon view. α-lactalbumin contains four disulfide bonds (in yellow), two in the α-domain, one in the β-domain and one cross-linking the two domains. The calcium ion (in blue) is located in the helix-turn-helix motif that spans the interface between α and β-domains.

One of the most interesting features of α-lactalbumin is its ability to bind metal cations such as Ca^{2+} and Zn^{2+}. It binds the calcium ion in a 1:1 ratio at a specific binding site. The binding site for calcium also binds other ions such as Mg^{2+}, Mn^{2+}, Na^{+} and K^{+} but more weakly. The removal of calcium from α-lactalbumin reduced its stability and promotes a conformational change (denatured) [Wehbi et al., 2005]. Apo α-lactalbumin (calcium depleted) which is partially unfolded, is more prone to protein aggregation than the native form (holo α-lactalbumin). It is because, as in the apo form, hydrophobic patches are exposed thus leading to protein aggregation via hydrophobic interactions [Kronman, 1989].

Besides that, removal of Ca^{2+} ions leads to apo α-lactalbumin in a molten globule (MG) state. Molten globule state occurred in conditions of extreme pH, at high temperature, in the presence of mild denaturants and upon removal of calcium ions. The formation of the molten globule is evidenced by a substantial loss of the near-ultraviolet circular dichroism (CD) signal and a significant reduction in NMR

chemical shift dispersion, indicating that the side-chains are substantially disordered. The structure of the α-lactalbumin molten globule is highly heterogeneous, having a largely ordered α-helical domain and a more distorted β-sheet domain than the native protein [Kuwajima, 1996]. Molten globule is a single molecule which has high tendency to aggregate [Regan, 2003].

5.1.3.4 β-lactoglobulin

β-lactoglobulin is the major protein of bovine whey with a concentration of 3.2 g/L [Etzel, 2004]. β-lactoglobulin is a globular protein and has well established primary, secondary, tertiary and quaternary structures. It consists of 162 amino acid residues. β-lactoglobulin is an acidic protein with an isoelectric point (pI) value of 5.2. At neutral pH and room temperature, native β-lactoglobulin exists as a dimer of two globular units, each with a molecular weight of 18,000 Da and a diameter of 3.6 nm. Its unfolding temperature is 75 °C [Santos et al., 2005]. When elevating beyond room temperature and below about pH 3, it dissociates to a monomer.

5.1.4 Poly(ethylene glycol) solution

Poly(ethylene glycol) monomethyl ether (CH_3-PEG-OH) (MW 350, 550, 2000 and 5000 Da) and poly(ethylene glycol) succinimidyl ester (CH_3-PEG-NHS) (MW 2000 and 5000 Da) were purchased from Fluka, Danmstadt, Germany and used as received without further purification. Poly(ethylene) glycol (PEG) solutions were prepared using phosphate buffer solution as a solvent. In this thesis, to elucidate between CH_3-PEG-OH and CH_3-PEG-NHS, CH_3-PEG-OH was referred to as PEG and CH_3-PEG-NHS as PEG-NHS.

5.1.5 Reactive solution

Branched poly(ethylene imine) (PEI) with MW 25,000 and sodium silicate solutions, reagent grade (contains ≅ 14 % NaOH, 27 % SiO_2) with MW 180 Da was purchased from Sigma-Aldrich, St. Louis, Mo. USA. PEI and sodium silicate were

used to coat the stainless steel surface prior to attachment of PEG molecules. The PEI and sodium silicate solutions were prepared using MilliQ water as a solvent at concentration of 30 g/L and 5 %w/v, respectively.

5.1.5.1 Poly(ethylene imine) (PEI)

PEI is a highly branched polymer with about 25 % primary amine groups. The remaining amine groups are secondary (50 %) and tertiary (25 %). Only a small fraction of the groups react with the surface; thus a high concentration of free amino groups is available for PEG grafting. PEI is a cationic copolymer. Figures 5.4 and 5.5 show the schematic diagram of PEI and proposed reaction scheme for the surface modification of stainless steel (SS), respectively.

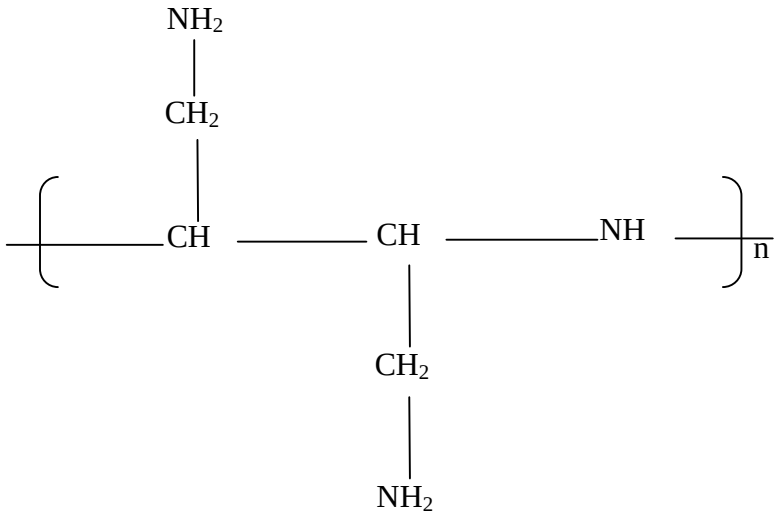

Figure 5.4: Schematic diagram of PEI structure.

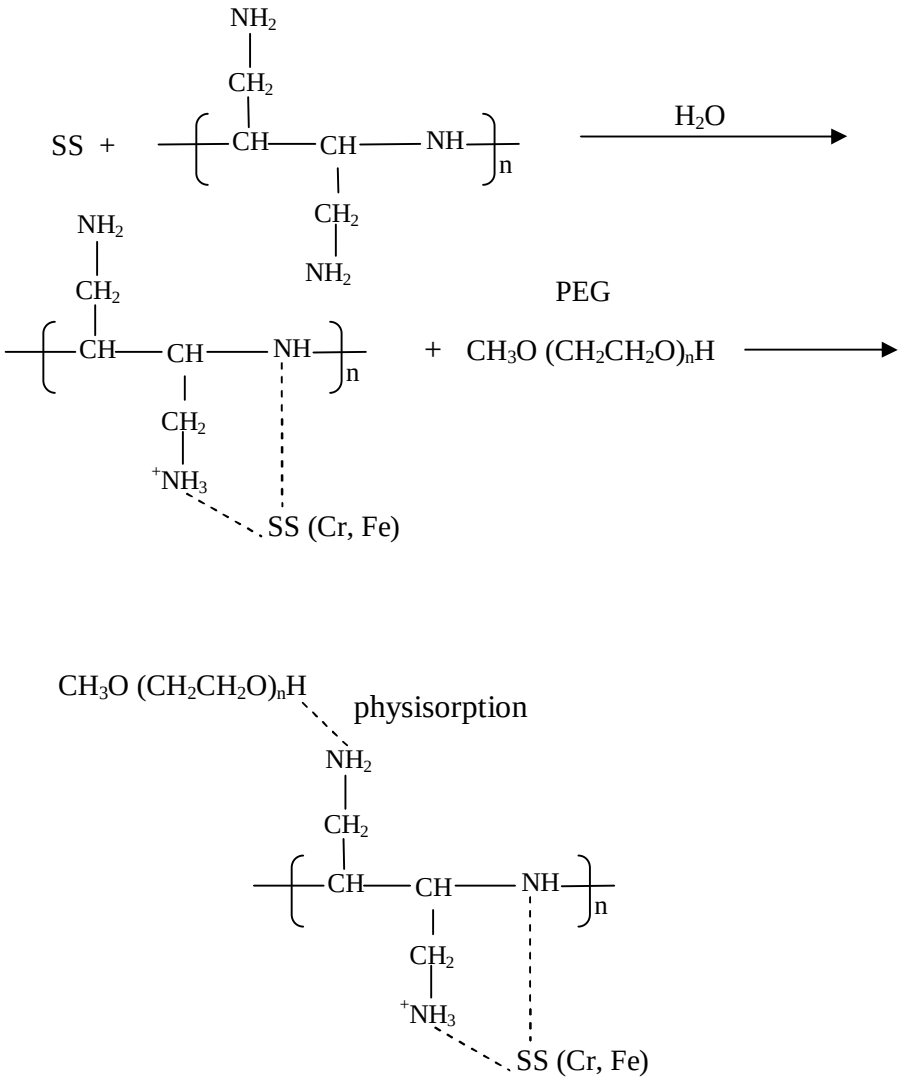

Figure 5.5: Reaction scheme for the surface modification of stainless steel (SS) [Wei et al., 2003]. The first step is the adsorption of PEI onto the SS surface, followed by the grafting of PEG on the SS-PEI surface.

5.1.5.2 Sodium silicate

Figure 5.6 illustrates the proposed reaction scheme for the surface modification of stainless steel (SS) with sodium silicate followed by the grafting of PEG on the SS-silicate surface.

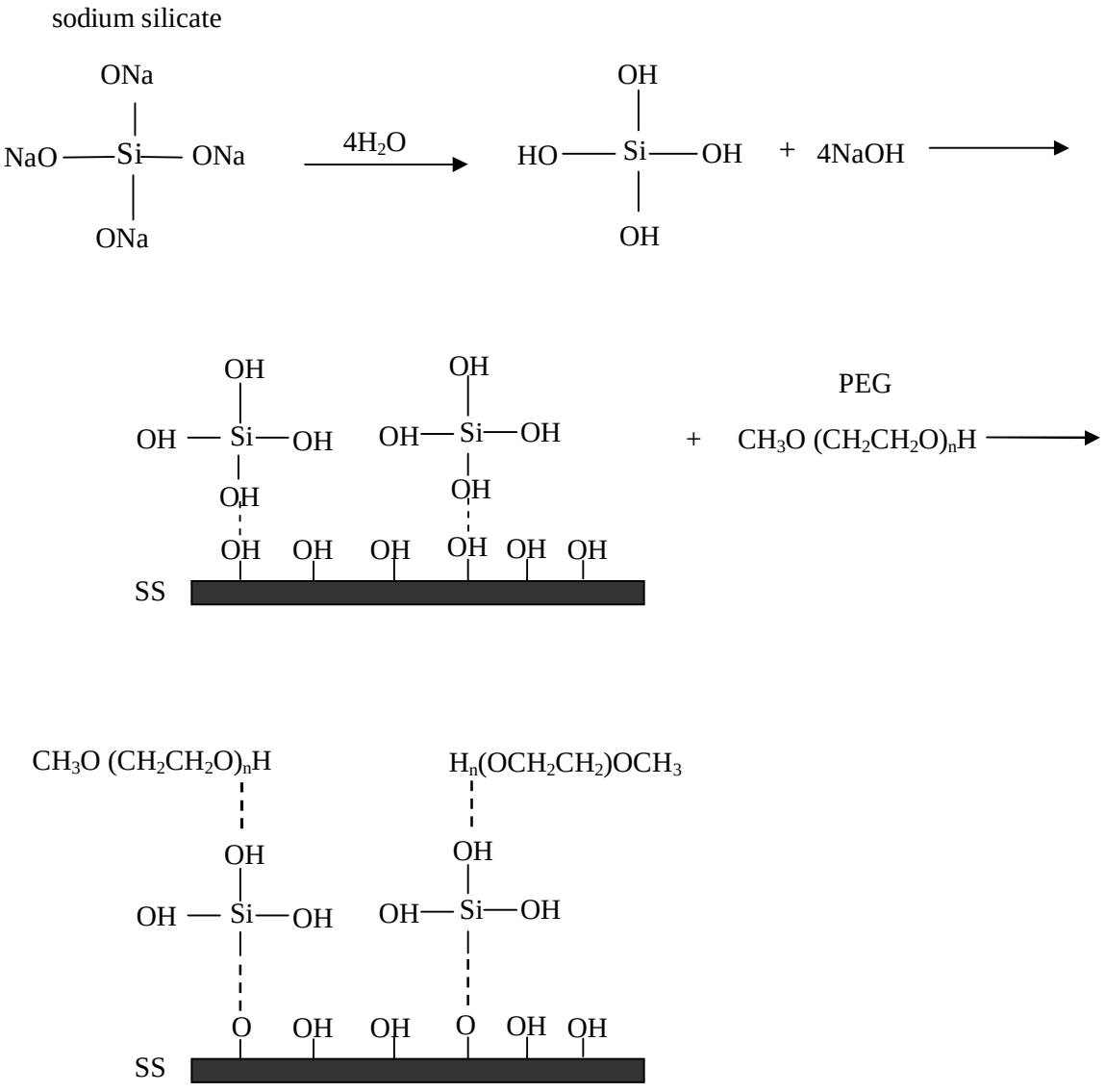

Figure 5.6: Proposed reaction scheme for the surface modification of stainless steel (SS) with sodium silicate, followed by the grafting of PEG on the SS-silicate surface [Zhang et al., 2001].

5.2 Quartz crystal microbalance with dissipation (QCM-D)

A Q-Sense E4 model was purchased from Q-Sense, Goteborg, Sweden. E4 model is the latest generation system from Q-Sense. The Q-Sense E4 system consists of:

(i) Sensor crystal

Sensor crystal is the sensing element itself. Gold coated quartz crystals further coated with stainless steel purchased from Q-Sense Goteborg, Sweden were used as a substrate. The composition of the stainless steel (SS2343) to be sputtered on was carbon (0.03 %), chromium (16.5-18.5 %), nickel (11-14.5 %), molybdenum (2.5-3 %) and iron (64-70 %). The specification of the crystals is shown in Table 5.1 below:

Table 5.1: Quartz crystal Specification.

Specification	Value
Fundamental frequency	5.0 MHz
Cut	AT (see note below)
Diameter	14 mm
Thickness	0.3 mm
Electrode layer	Au, 100 nm
Top layer	SS2343, 50 nm
Finishing	Optically polished (Au layer), surface roughness of electrodes was less than 3 nm (RMS)
Active area of sensor crystal	$\cong 0.2\ cm^2$

Note:

Cut is the term applied to the orientation (rotation) of the quartz wafer or blank in relation to one or more of the three crystallographic atomic axis of the quartz material. Depending on the way the quartz crystal is cut, different modes can be excited (oscillated). The AT cut crystal, which is the most commonly used for QCM applications, is fabricated by slicing through a quartz rod with a cut angle 35°10' with

respect to the optical axis, as shown in Figure 5.7. An AT-cut crystal oscillates in a thickness shear mode. The advantage with the AT-cut quartz crystal is that it has nearly zero frequency drift (small frequency change) in a wide temperature range.

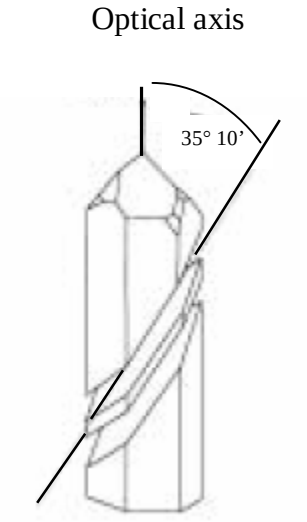

Figure 5.7: AT-cut of a quartz crystal. A quartz plate is cut at an angle of 35°10' with respect to the optical axis.

(ii) Flow module (4 cells in parallel)

There are 4 flow modules in parallel (see Figure 5.8 (a)). Each flow module holds one sensor crystal. The flow module is part of the temperature control environment allowing the measurement liquid to stabilize at the desired temperature before reaching the sensor surface. The module is easily be separated from the chamber platform and disassembled (for example, for cleaning). The module is made of from Titanium, grade 2 and the O-rings and sealing are made of viton. The dimension of the flow module is, 37 mm height x 35 mm width x 63 mm depth (see Figure 5.8 (b)). The maximum volume above each sensor is about 19 μL**.** The tubing that connects the flow module between sample and waste is made of from PTFE. The tubing dimension is 1.56 mm outside diameter (OD) x 0.58 mm inside diameter (ID). The measurement can be done either on flow or stagnant liquid.

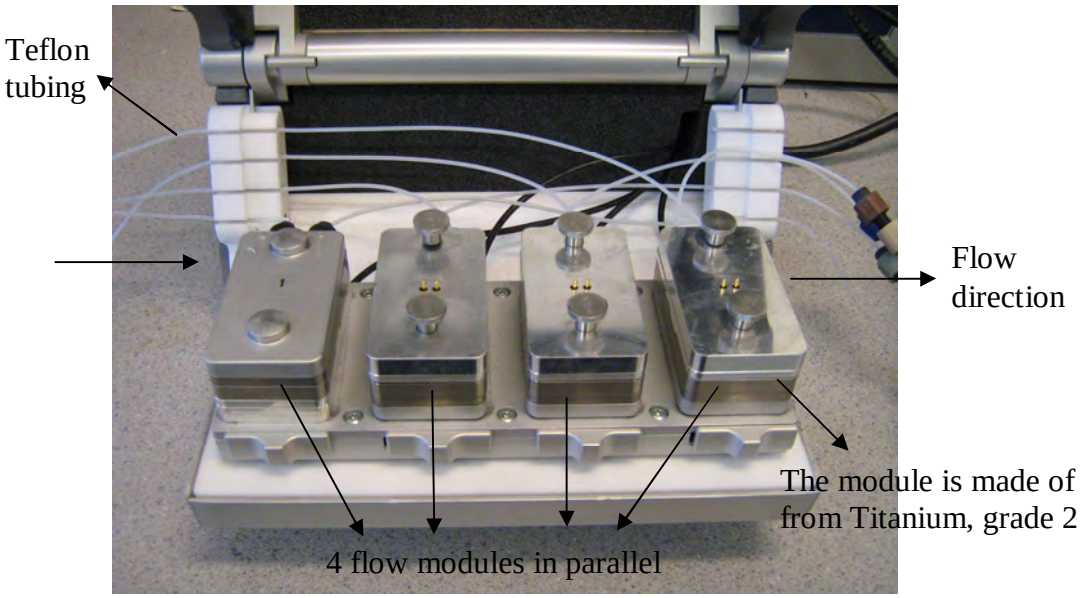

Figure 5.8 (a): Picture of 4 flow modules in parallel.

Figure 5.8 (b): Picture of flow module with a crystal, dimension of a flow module and O-ring position.

(iii) Chamber platform

The chamber platform is the base for the measurement set-up (see Figure 5.9). The platform holds four flow modules. With the window lid closed, the chamber constitutes a controlled temperature environment, with a heating and cooling thermoelectric device beneath the flow module row. The dimension of the chamber platform is 120 mm (height) x 230 mm (width) x 340 mm (depth).

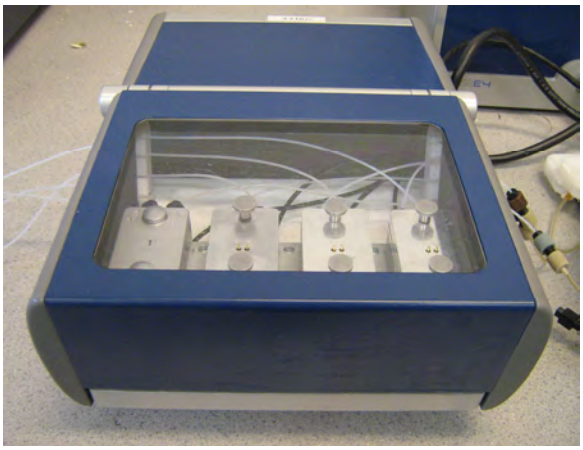

Figure 5.9: Picture of chamber platform with the window lid closed.

(iv) Electronic unit

The electronic unit is a part where the signals are generated and data is collected before being sent to a computer (see Figure 5.10). Also it holds the set temperature in the chamber to be nearly constant.

Figure 5.10: Picture of electronic unit.

(iv) External pump

A 4 channels digital peristaltic pump (Ismatec IPC-N 4) is used as a sample feeder (see Figure 5.11). The motor type used is a DC motor. The maximum flow rate is 120 µL/min. The dimension of the unit is 180 mm (depth) x 140.5 mm (width) x 130 mm (height). The maximum power consumption is 30 Watt.

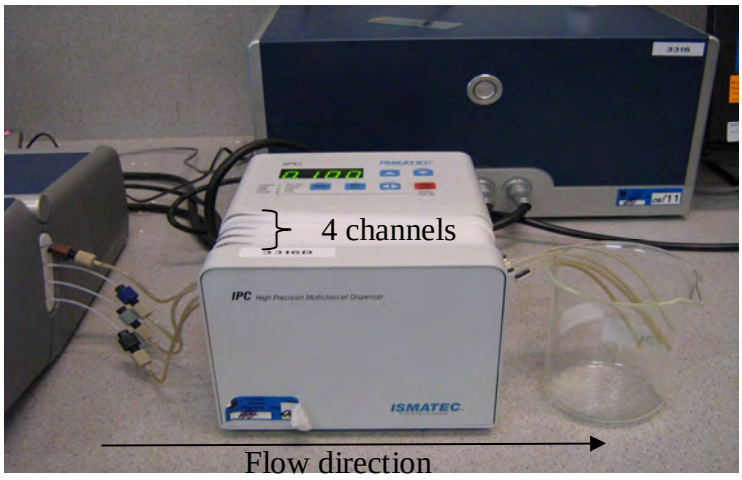

Figure 5.11: Picture of 4 channels digital peristaltic pump.

Figure 5.12 shows a picture of the equipment complete set up used in this study. The details of the Q-Sense E4 model can be found at www. q-sense.com.

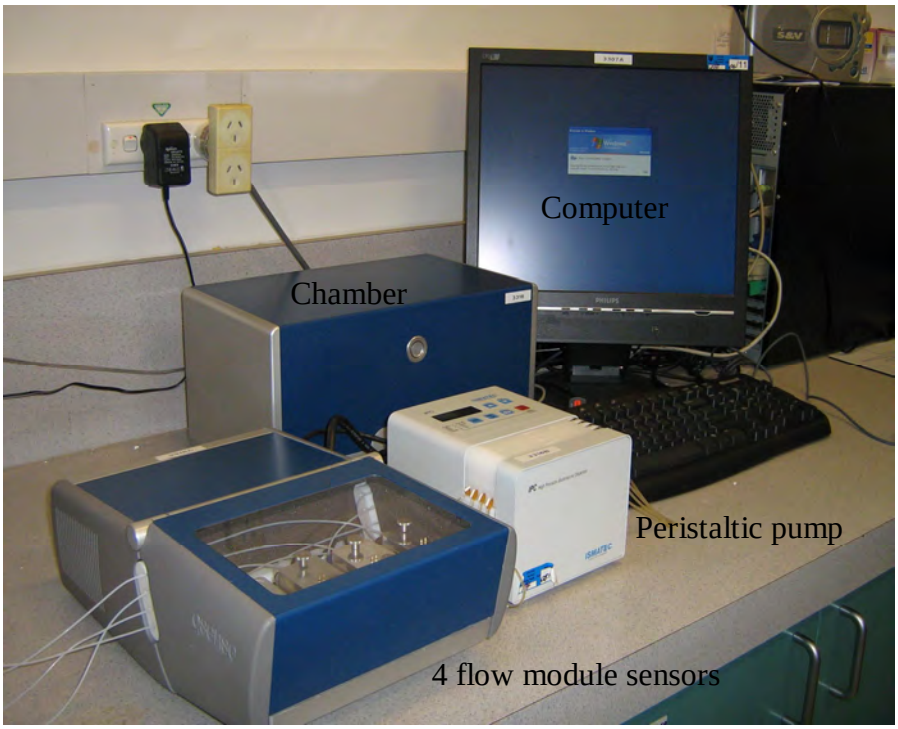

Figure 5.12: Complete set-up of the QCM-D equipment. The set up consists of (i) 4 flow module sensors, (ii) chamber, (iii) peristaltic pump and (iv) computer.

5.3 QCM-D experiment

In this study, the QCM-D experimental works were divided into 6 major stages as shown below.

Experiment A: Adsorption of protein onto a bare stainless steel surface (control experiment)

A quartz crystal was mounted in a flow cell with the stainless steel surface exposed to the solution. Then, β-casein, lysozyme and α-lactalbumin solutions (0.1, 0.5 and 1 g / L) were pumped separately through the QCM flow cell by its peristaltic pump at a flow rate of 100 μL/min. Prior to adsorption of protein, stabilization of frequency and dissipation was achieved by introducing protein free-buffer solution into the cell (to provide a baseline). After protein adsorption had reached steady state, pure buffer solution was immediately re-introduced to remove all unbound protein molecules. Measuring the final frequency change in the presence of pure buffer (referred to the previous baseline in buffer) means that protein adsorption is found without involving changes in the liquid density and viscosity which influence the frequency even without adsorption. The sequence step of protein adsorption onto a bare stainless steel surface is shown Figure 5.13.

Buffer solution → protein solution → buffer solution → NaOH solution → MilliQ water

Figure 5.13: Sequence steps of the adsorption of protein onto a bare stainless steel surface.

The kinetics of sample adsorption and desorption were followed by changes in the resonant frequency of the crystal and dissipation of the crystal vibrations. The frequency and dissipation changes were recorded simultaneously at different overtones (n = 3 (15 MHz), 5 (25 MHz), 7 (35 MHz), 9 (45 MHz) and 11 (45 MHz)). Upon completion of an experiment, NaOH (0.1 M) and milliQ water were introduced to the cell for 30 minutes each for cleaning. The experiments were conducted with the

system temperature stabilized at 23.0, 30.0, 35.0 and 40.0 ± 0.5 °C. Most of these experiments were performed at least three times.

The adsorption of calcium-enriched α-lactalbumin (known as holo α-lactalbumin) was also done. The α-lactalbumin used most often was a calcium depleted type (that is, apo α-lactalbumin). This experiment using the Ca-enriched molecule was performed after finding that PEG coated surfaces *enhanced* the adsorption of apo α-lactalbumin (Chapter 6, part C). The experiment however, was conducted only at concentration of 0.1 g / L under temperature 23.0 and 40.0 ± 0.5 °C.

At the end of the study, β-lactoglobulin protein was used to present the real situation in the dairy industry. Like holo α-lactalbumin, the experiment on a bare stainless steel surface was conducted at concentration of 0.1 g / L under temperature 23.0 and 40.0 ± 0.5 °C.

Experiment B: Modification of a stainless steel surface by coating with poly (ethylene glycol) (PEG) layer

Prior to adsorption of PEI or sodium silicate solution, stabilization of frequency and dissipation was achieved by introducing milliQ water into the cell providing a baseline. After adsorption had reached steady state, milliQ water was immediately re-introduced to remove all unbound PEI or silicate molecules. Then buffer solution was re-introduced and when it had stabled, PEG solution was introduced. Again, after the adsorption of PEG had reached steady state, buffer solution was immediately re-introduced to remove all weakly bound PEG molecules. Most of these experiments were performed at least three times. The sequence step in surface modification is shown in Figure 5.14.

MilliQ water → PEI or silicate solution → MilliQ water → buffer solution → PEG solution → buffer solution

Figure 5.14: Sequence steps in the modification of stainless steel surfaces.

Parameters that were varied in B experiments are:

- Temperature (23 and 40 ± 0.5 °C)
- CH_3-PEG-OH solution concentration (0.1, 1.0, 5.0 and 10.0 g / L)
- CH_3-PEG-OH molecular weight (350, 550, 2000 and 5000 Da)
- Methods (PEI or silicate coated surfaces)

Parameters that were held constant for all B experiments are:

- Flow rate (100 μL/min)
- Buffer pH (7.2 ± 0.1)
- Polyethylenimine (PEI) solution concentration (30 g / L)
- Sodium silicate solution concentration (50 g / L)

The stainless steel surfaces was also modified using PEG-NHS with molecular weighs of 2000 and 5000 Da at concentration of 0.1, 1.0 and 5.0 g / L.

Experiment C: Adsorption of protein onto a PEG coated stainless steel surface

After the surface modification in Experiment B had finished, protein adsorption on the modified surfaces was immediately performed as in Experiment A. Adsorption of protein was conducted at temperatures 23.0 and 40.0 ± 0.5 °C. The concentration of protein used in Experiment C was 0.1 g / L. Most of these experiments were performed at least three times.

Experiment D: Adsorption of protein onto a PEI and silicate coated surface

The adsorption of protein was also performed on PEI and silicate coated surfaces (without the presence of PEG molecules). The experiment conditions used were the same as in Experiment C. Figure 5.15 show the sequence step of adsorption of protein onto PEI (or silicate) coated stainless steel surfaces.

MilliQ water → PEI or silicate solution → MilliQ water → buffer solution → protein solution → buffer solution

Figure 5.15: Sequence steps of the adsorption of protein onto PEI (or silicate) coated stainless steel surfaces.

Experiment E: Modification of a stainless steel surface by coating with a combination of short and long PEG chains

In this stage, stainless steel surfaces were modified as in Experiment B except that instead of using PEG chains of a single length, chains with two lengths were used. The attachment of PEG chains was done successively; the longer PEG chains were introduced first followed by the shorter chains [Uchida et al., 2005, Bosker et al., 2005, Satomi et al., 2007]. Short PEG chains will more easily fill up between the pre-constructed longer PEG chains and thus high PEG grafting density will achieve.

Parameters that were varied in D experiments are:

- Temperatures (23.0 and 40.0 ± 0.5 °C)
- PEG combinations (5000 + 2000, 5000 + 550, 5000 + 350, 2000 + 550, 2000 + 350 and 550 + 350 Da)
- PEG solution concentrations (0.1, 1.0 and 5.0 g / L)
- Methods (PEI or silicate coated surface)

Parameters that were held constant for all D experiments are:

- Flow rate (100 μL/min)
- Buffer pH (7.2 ± 0.1)
- Polyethylenimine (PEI) solution concentration (30 g / L)
- Sodium silicate solution concentration (50 g / L)

The stainless steel surfaces were also modified using PEG-NHS (5000 + 2000) at a concentration of 1 g / L (the surfaces were referred as SS-PEI (30)-PEGNHS (5k+2k)

(1)). The sequence step in modification of stainless steel surfaces is shown in Figure 5.16.

MilliQ water → PEI solution → MilliQ water → buffer solution → PEG-NHS5000 solution → buffer solution → PEG-NHS2000 solution → buffer solution

Figure 5.16: Sequence steps in the modification of stainless steel surfaces.

Experiment F: Adsorption of protein onto a PEG coated stainless steel surface

After the surface modification in Experiment E had finished, protein adsorption on the modified surfaces was immediately performed as in Experiment A. Adsorption of protein was conducted at temperatures 23.0 and 40.0 ± 0.5 °C. The concentration of protein used in Experiment F was 0.1 g / L. Most of these experiments were performed at least three times.

Experiment G: Adsorption of protein solution onto a protein coated stainless steel surface

In this new method of surface modification, a protein layer was used as a base for PEG attachment instead of PEI or silicate layers. The rest of the steps were then the same as in the previous methods (Experiment B). The procedures can be simplified as shown in Figure 5.17. The experiments were conducted at room temperature (23 °C) unless stated.

Buffer solution → base protein (β-casein or β-lactoglobulin or lysozyme) → buffer solution → PEG → buffer solution → protein → buffer solution

Figure 5.17: Sequence steps of the process of surface modification and adsorption of protein.

3 different base protein layers were used:

(i) β-casein layer from a solution of concentration 0.1 g / L.

(ii) β-lactoglobulin layer from a solution of concentration 0.1 g / L.

(iii) Lysozyme layer from a solution of concentration 4 g / L.

The lists of PEG used are as follows:

(i) CH_3-PEG-OH (referred to as PEG in the text). The molecular weights used were 350, 2000 and 5000 Da. The concentrations used were 1.0 and 5 g / L.

(ii) OH-PEG-OH (referred to as PEG-OH in the text). The molecular weight used was 20,000 with a concentration of 1 g / L.

(iii) CH_3-PEG-NHS (referred to as PEG-NHS in the text). The molecular weights used were 2000, 5000, 20,000 and 40,000 Da with a concentration of 1 g / L each.

The effectiveness of the modified surfaces (that is, PEG-protein coated surfaces) to inhibit adsorption of protein was tested with adsorption of:

(i) β-casein

(ii) β-lactoglobulin

(iii) Lysozyme

(iv) Holo α-lactalbumin

(v) Apo α-lactalbumin

The concentration of the above proteins used was 0.1 g / L.

Adsorption of single and mixed protein solutions at the same concentration as in milk was also performed on the SS-lysozyme (4), SS-lysozyme (4)-PEG5000 (5) and SS-lysozyme (4)-PEGNHS5k (1) surfaces (a value inside a bracket is a concentration in g / L). The adsorption was also performed on the bare stainless steel surface as a control. The composition of mix protein solution consists of β-casein (9.3 g / L), β-lactoglobulin (3.2 g / L) and holo α-lactalbumin (1.2 g / L).

The adsorption of protein mix on the PEG5000 (5)-lysozyme (4) and PEGNHS5k (1) surfaces was further conducted at temperatures 40 and 80 °C. To achieve the adsorption at temperature 80 °C, the cell of the flow module was put in the oven (just used the protein in the cell) at temperature 80 °C for 1 hour (QCM-D used in this study only stabilized the temperature up to 40 °C). After that, the cell was remounted and the fundamental frequency of the surface was determined. The sequence step of the whole process is illustrated in Figure 5.18.

Buffer solution → lysozyme (4) solution → buffer solution → PEG → buffer solution → protein mix → flow was stopped → oven (80 °C for 1 hour) → the cell was put back into the chamber platform and the fundamental frequency was measured

Figure 5.18: Sequence steps of the whole process, from surface modification to protein adsorption.

5.4 Adsorption of milk solution on a commercial 316 stainless steel surface

Adsorption of skimmed milk solution was carried out on a modified commercial 304 stainless steel surface. The purpose of this experiment was to examine the effectiveness of the proposed surface modification to inhibit adsorption of the protein in conditions closer to commercial practice.

5.4.1 Apparatus

A disc 65 mm in diameter and 1.1 mm thick with a central 6 mm diameter hole was cut from a 316 stainless steel sheet. The disc was mounted in a standard 50 mm stainless steel dairy fitting (see Figure 5.19). A 50 mm rubber ring was used to give a clean-edged seal. The diameter of the area available for milk adsorption was 47 mm (the expected area exposed to the adsorption was about 1735 mm^2).

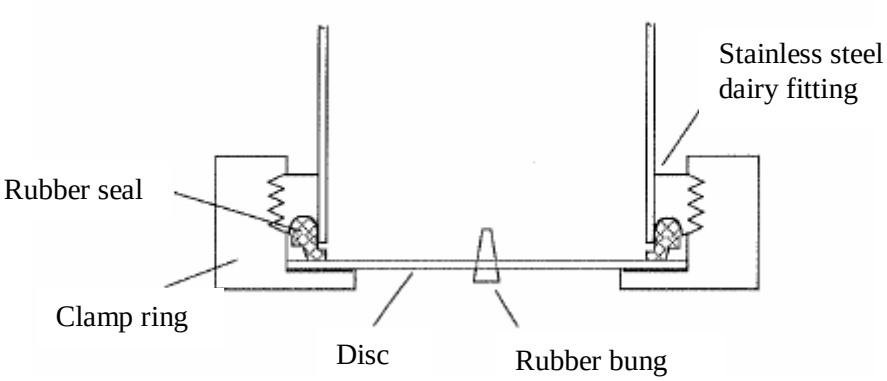

Figure 5.19: Cross section of the chamber.

5.4.2 Disc modification

The disc was modified using a technique developed in Experiment G prior to the adsorption of skimmed milk solution. The disc was immersed in lysozyme (4) solution for 1 hour followed by rinsing with milliQ. Then the disc was immersed in PEG5000 (5) solution for another 1 hour and finally was rinsed with buffer solution.

5.4.3 Milk adsorption

100 mL of pasteurized skimmed milk (4.0 wt% protein, 0.4 wt% fat, 9.8 wt% total solids) were preheated to approximately 60 °C in a microwave oven and poured into the dry chamber that was in the 95 °C waterbath. The milk was agitated at 200 rpm during adsorption with a 30 mm pitched blade impeller located just beneath the top surface of the milk (see Figure 5.20). The chamber was covered with aluminium foil to minimize evaporating moisture loss. During the adsorption period, a 60 mL plastic syringe with U-tube was used to extract any gases that were believed located beneath the disc. The adsorption duration was 1 hour. The details of this experiment can be found in Morison and Thorpe's publication [Morison and Thorpe, 2002].

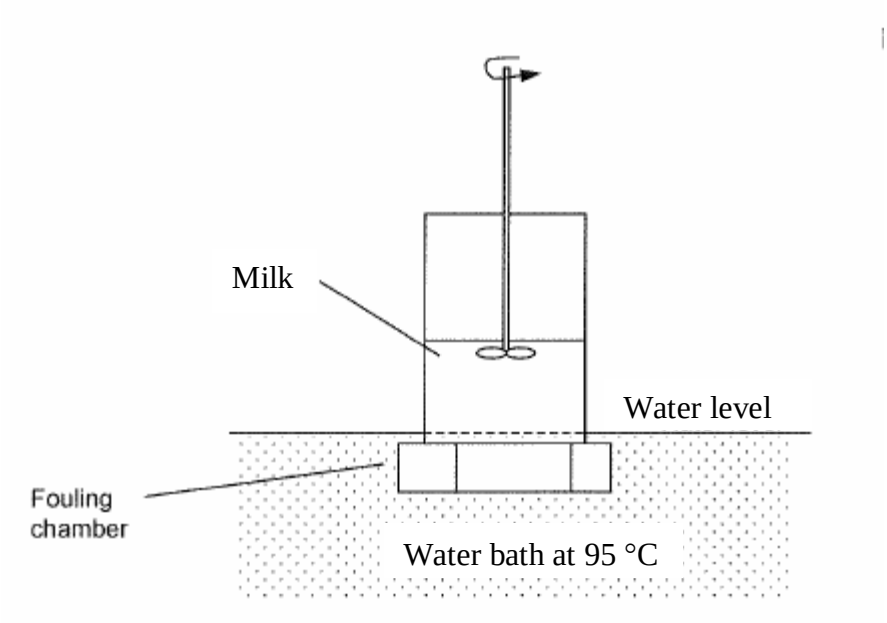

Figure 5.20: Arrangement of adsorption apparatus.

5.5 Crystal cleaning

The crystals were cleaned prior to runs by immersion in a 5:1:1 mixture of milliQ water, ammonia (25 % v/v) and hydrogen peroxide (30 % v/v) ('Piranha' solution) for 5 minutes at 75 °C, followed by thorough rinsing with milliQ water and drying with a moisture-free nitrogen gas stream until completely dry. To finish the cleaning, the crystals were treated with UV light and ozone for 5-10 minutes to remove organic contamination. The UV/ozone treatment was done using a UV Ozone Chamber, Bioforce Nano from Q-Sense Goteborg, Sweden (see Figure 5.21). The crystals can be reused for about 20-25 times.

a

b

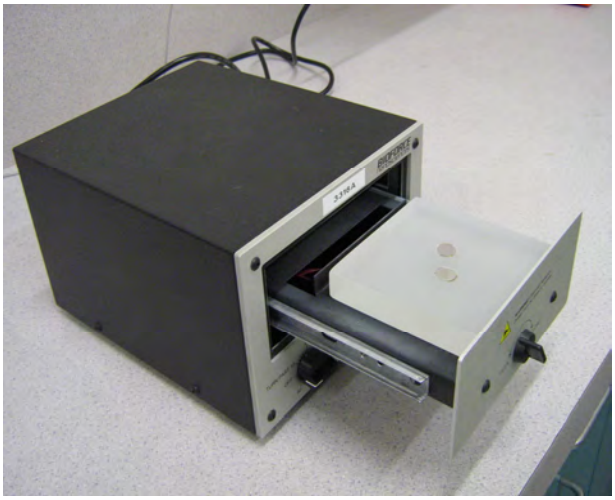

Figure 5.21: (a) ozone chamber (b) ozone chamber from inside view.

5.6 QCM-D analysis

The raw QCM-D results obtained were modeled/calculated using the Voigt model and the Sauerbrey equation from the Sauerbrey model for a comparison. Refer to Chapter 3 for the details of the Sauerbrey model and the Voigt model.

5.6.1 Sauerbrey equation [1951]

$$\Delta m = -C\frac{\Delta f_n}{n} \tag{5.1}$$

5.6.1 Voigt model

Four overtones (fifth, seventh, ninth and eleventh) were used to model the viscoelastic properties of the adsorbed layer using Q-TOOLS software (301 version 2.1, Feb 2006), Q-Sense, Goteborg, Sweden. Parameters assumed fixed were (i) layer density, 1200 kg / m^3, (ii) fluid viscosity, 0.001 kg / m s and (iii) fluid density, 1000 kg / m^3. Parameters fitted were (i) layer viscosity between 0.0001 and 0.05 kg / m s, (ii) layer shear stress between 10^4 and 10^8 Pa, and (iii) layer thickness between 10^{-10} and 10^{-6} m.

The thickness of the layer obtained from the Voigt model, (δ_{voigt}), was then multiplied by the density of the layer to estimate the mass adsorbed per unit surface area, Δm_{voigt}. It was assumed that the effective density of the layer is 1200 kg/m^3. The number density of protein molecules adsorbed was then calculated by dividing the mass adsorbed per unit area by the molecular weight of the protein and multiplying by Avogadro's number (6.023×10^{23} molecules.mol^{-1}).

5.7 Atomic Force Measurement (AFM)

Atomic Force Measurement (AFM) characterization was carried out at Massey University, New Zealand. The AFM model used was MFP-3D from Asylum research [Haverkamp et al., 2007]. It consists of three main compartments; (i) head, (ii) XY scanner and (iii) base (refer to Figure 5.22).

Figure 5.22: MFD-3D AFM equipment.

(i) MFP-3D Head

A "sensored optical lever with diffraction limited optics and a low coherence light source virtually eliminates interference artifacts", according to the manufacturer (Asylum Research). It provides precise measurements of the cantilever position for accurate force and topography measurements.

(ii) MFP-3D XY Scanner

The MFP-3D uses a flexure scanner and patented NPS sensors, which measure the precise position of each axis (X-Y).

(iii)MFP-3D Base

There are three configurations available for illuminating and viewing the sample:

a. Top view for opaque sample.

b. Bottom view for transparent samples.

c. Dual view for both viewing options.

There were 11 samples involved. The characterization was done ex-situ and used the tapping mode in buffer solution. Igor Pro 5 Upgrade software was used to analyze the images.

5.8 Scanning Electron Microscopy (SEM)

Scanning electron microscopy (SEM) characterization was carried out at the Department of Mechanical Engineering, University of Canterbury. The model of SEM used was Jeol JSM7000F. The Jeol JSM7500F is an analytical Field Emission SEM. The JSM7500F offers the highest resolution at the lowest kV of any SEM available, achieving a resolution of 1.4 nm at 1 kV. The JSM7500F provides in-lens performance (1 nm at 15kV) but can handle samples up to 200mm in diameter x 10mm height. The SEM characterization was performed on a new bare quartz crystal (SS2343) and 304 commercial stainless steel surfaces.

5.9 Size Exclusion Chromatography (SEC)

A **s**ize exclusion chromatography **(**SEC) experiment using a Superdex200™ HR 30/10 column (GE Healthcare Technologies) (length 300 mm, diameter 10 mm) attached to an AKTAexplorer™ 10 liquid chromatography system controlled by Unicorn™ software (GE Healthcare Technologies) was performed to determine whether there was an association between α-lactalbumin and PEG molecules in solution.

The underlying principle of SEC is that particles of different sizes will elute (filter) through a stationary phase at different rates. This results in the separation of a solution of particles based on size. Provided that all the particles are loaded simultaneously or near simultaneously, particles of the same size should elute together. This is usually achieved with a column (see Figure 5.23), which consists of a hollow tube tightly packed with extremely small porous polymer beads designed to have pores of different sizes (narrow range of pores).

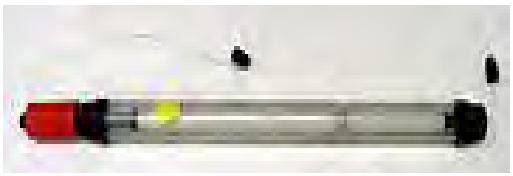

Figure 5.23: A size exclusion column.

Molecules that are smaller than the pore size can enter the particles (polymer beads) and therefore have a longer path and longer transit time than larger molecules that cannot enter the particles. Molecules larger than the pore size can not enter the pores and elute together as the first peak in the chromatogram. Meanwhile, molecules that are smaller than the pore size can enter all pores (as the sizes for pores are closely similar), and have the longest residence time on the column and elute together as the last peak in the chromatogram (see Figure 5.24).

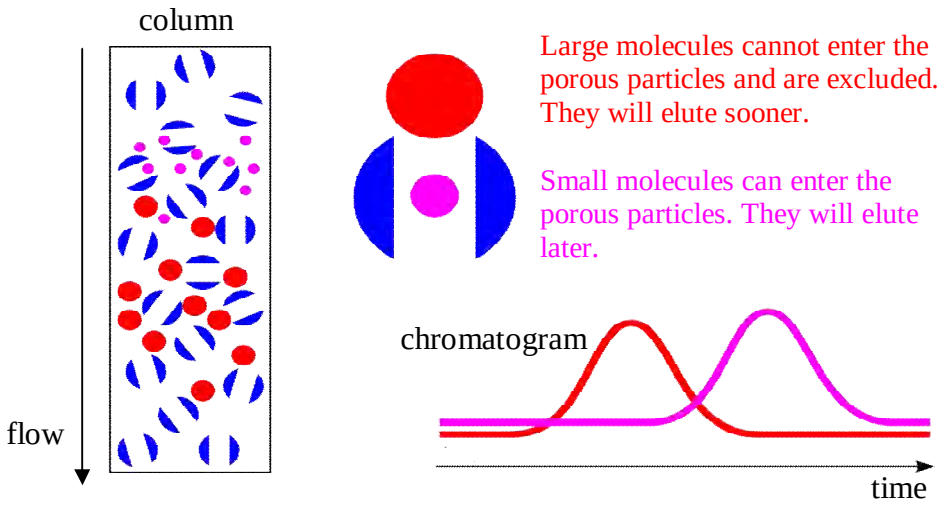

Figure 5.24: A cartoon illustrating the theory behind size exclusion chromatography. Blue, red and purple colours refer to porous bead, large particle and small particle, respectively [http://en.wikipedia.org/wiki/size_exclusion_chromatography].

The SEC experiment was carried out after the experimental results obtained showed that PEG molecules enhanced the adsorption of apo α-lactalbumin. 4 samples were tested:

1. apo α-lactalbumin solution (2 g / L).
2. holo α-lactalbumin solution (2 g / L).
3. mixture of PEG5000 (2 g / L) and apo α-lactalbumin solution (2 g / L).
4. mixture of PEG5000 (2 g / L) and holo α-lactalbumin solution (2 g / L).

The experiments were performed three times.

5.10 Kinetic modelling

The kinetics of adsorption of protein on a bare stainless steel surface was modeled, including a possible diffusion step. The models attempted to fit the experimental data are:

i) Extended Langmuir model (based on work done by Shen et al., 2005).

ii) Extended Langmuir model with free reversibility.

iii) Diffusion – reaction model.

The detail of the kinetic modeling is in Chapter 10.

CHAPTER SIX

QCM-D RESULTS

6.0 Introduction

This chapter presents all the results obtained from the QCM-D experimental work. There are 4 major parts in this chapter; Part A: Adsorption of protein onto a bare stainless steel surface, Part B: Modification of a stainless steel surface, Part C: Adsorption of proteins onto modified surfaces (monomodal PEG surfaces) and Part D: Adsorption of proteins onto modified surfaces (bimodal PEG surfaces).

This chapter begins with Part A. In this part, the adsorption of β-casein, lysozyme and α-lactalbumin are presented successively. This part presents the effects of concentration and temperature on the adsorption of the proteins onto the bare SS surfaces. All the results presented in this chapter are interpreted with the Voigt model.

6.1 PART A: ADSORPTION OF PROTEIN ONTO A BARE STAINLESS STEEL SURFACE

6.1.1 β-casein

6.1.1.1 Adsorption and desorption kinetics of β-casein onto and off a bare stainless steel surface (frequency and dissipation change measurement)

Figure 6.1 shows an example of adsorption and desorption kinetics of β-casein onto and off a stainless steel surface monitored in situ by the QCM-D. Lines with blue and orange based colour refer to frequency change (Δf) and dissipation change (ΔD) at different overtone numbers, *n* (*n* = 3, 5, 7, 9 and 11), respectively. As can be seen, there was a rapid reduction in frequency (interpreted as a mass increase)

upon adsorption from 0.1 g / L β-casein bulk solution onto the surface and the frequency change reached a steady state about 500 seconds later (for example, Δf = -55 Hz at n = 3). Pumping the protein solution into the cell for another 1800 seconds seemed to not change the frequency further. Rinsing the system with protein-free buffer solution increased the frequency change to less than zero (Δf = -30 Hz at n = 3). The result indicated that part of the β-casein molecules were washed off during the flushing with the buffer solution, indicating a *partially reversible* adsorption.

As expected, dissipation change was positive, increasing with adsorption of β-casein protein and leveled off when adsorption reached steady state ($\Delta D = 2.5 \times 10^{-6}$). During desorption, the dissipation change decreased to approximately 1.5×10^{-6} (at n = 3) due to rinsing away weakly-bound protein that was loosely associated with the adsorbed layer. The quantitative kinetics corresponding to this raw data is presented in Chapter 10.

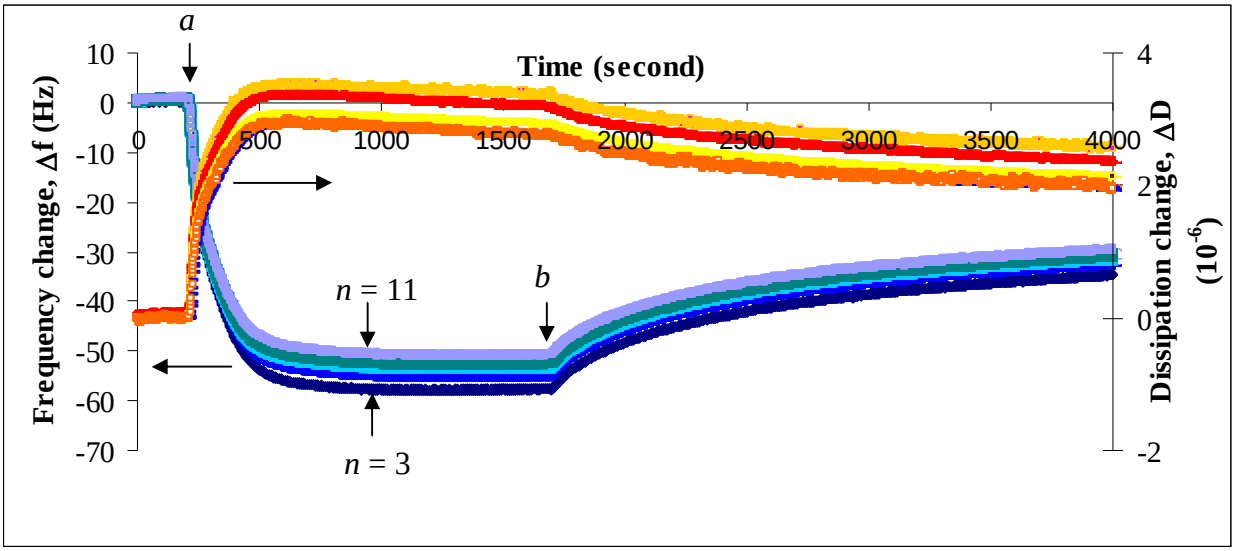

Figure 6.1: Frequency and dissipation factor change of β-casein adsorbing from 0.1 g / L bulk solution onto a bare stainless steel surface at 23 °C. Phosphate buffer solution was replaced with protein solution at point *a* and returned to buffer solution at point *b*.

6.1.1.2 Effects of concentration and temperature on the mass density of β-casein adsorbed on a bare stainless steel surface

Figure 6.2 represents the effects of temperature and solution concentration (0.1, 0.5 and 1 g / L) on the "Voigt mass density" (that calculated using the Voigt layer model) of β-casein adsorbed on a stainless steel surface. The presented data refer to the final steady state *before* and *after* flushing with the buffer solution, shown by bars with a plain and stripe lines, respectively. Also shown is the expected of monolayer β-casein on the SS surface (horizontal dotted line). There was no significant difference in mass density adsorbed from 0.1 to 0.5 g / L solution. However, adsorbing from 1 g / L solution hugely increased the adsorption, by up to 50 % (except at 23°). Rinsing the system with buffer solution removed almost 45 % of the mass adsorbed. Overall, under the experimental conditions, the Voigt mass densities of β-casein remaining after desorption (that is tightly-bound mass) ranged from about 7 to 19 mg/m^2. The corresponding number of molecules adsorbed and mean layer thickness, respectively, was 0.18 to 0.5 molecules / nm^2 and 6 to 16 nm. Refer to Chapter 5 for the detail of the Voigt model and calculation of mass density, number of molecules and mean layer thickness. The maximum surface density of monolayer β-casein is approximately 2.3 mg/m^2 (dry basis) [Veen et al, 2007]. Thus, indicating formation of multilayer β-casein in this study (about 3 to 5 times higher compared to the dry basis). The results obtained almost consistent with the work done by Lee et al. [2004]. They reported that the mass density of β-casein adsorbed on a gold surface monitored using the QCM-D was greater by a factor of 3 to 5 compared with the optical devices (dry basis) [Lee et al., 2004].

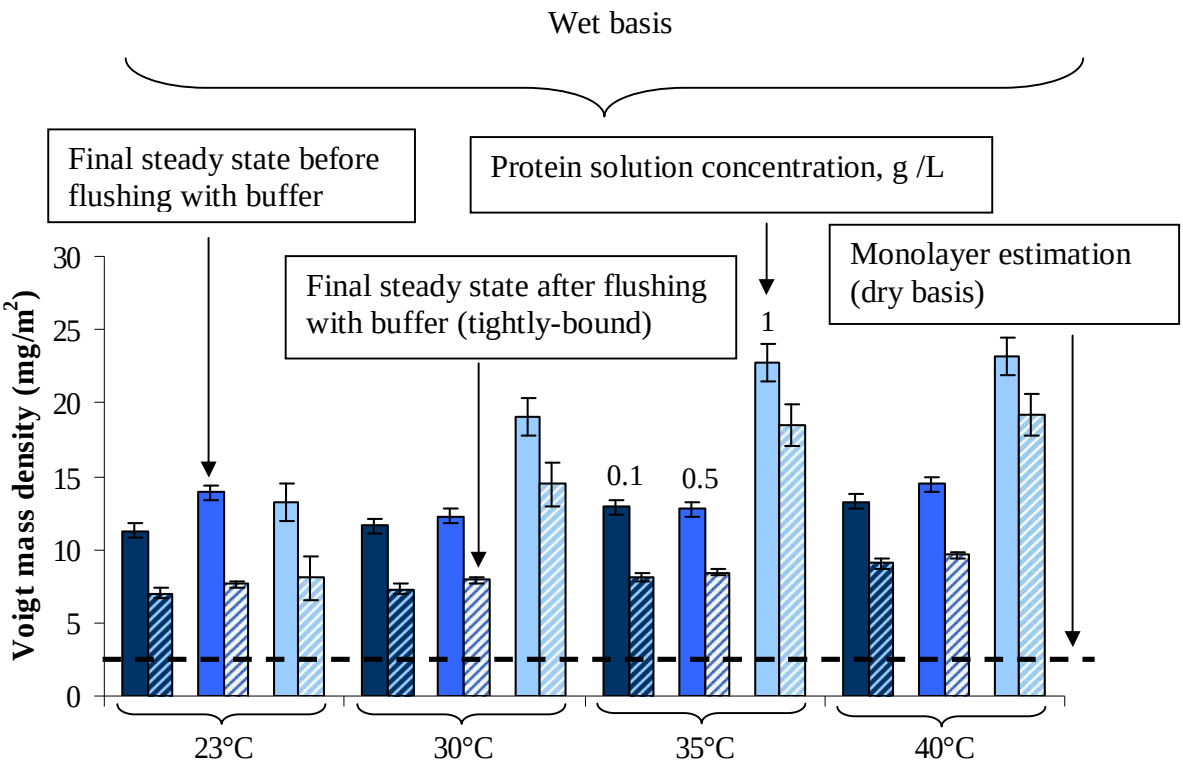

Figure 6.2: The Voigt mass density of β-casein adsorbed at a steady state adsorption and desorption on a bare SS surface as a function of temperature and concentration. Bars with plain and stripe color refer to the mass density adsorbed at a final steady state *before* and *after* rinsing with buffer solution, respectively. Values above bars refer to the protein solution concentration, g / L. The horizontal dotted line refers to the expected monolayer (dry basis).

6.1.2 Lysozyme

6.1.2.1 Adsorption and desorption kinetics of lysozyme onto and off a bare stainless steel surface (frequency and dissipation changes)

Figure 6.3 shows an example of QCM-D data for adsorption of lysozyme from 0.1 g / L solution onto a SS surface conducted at 23 °C. Upon adsorption of protein, the frequency decreased rapidly in the first few seconds followed by a steady, gradual decrease. The system did not completely reach a steady state even after 3 hours of adsorption. The frequency change was almost 5 times lower compared to that of β-casein (Δf = -20 at n = 3). Also can be observed is that the dissipation increased slowly upon adsorption with a low dissipation shift (ΔD = 1 x 10^{-6} at n = 3). Unlike β-casein, rinsing the system with protein-free buffer solution resulted in only small changes in frequency and dissipation, indicating almost *fully irreversible* adsorption.

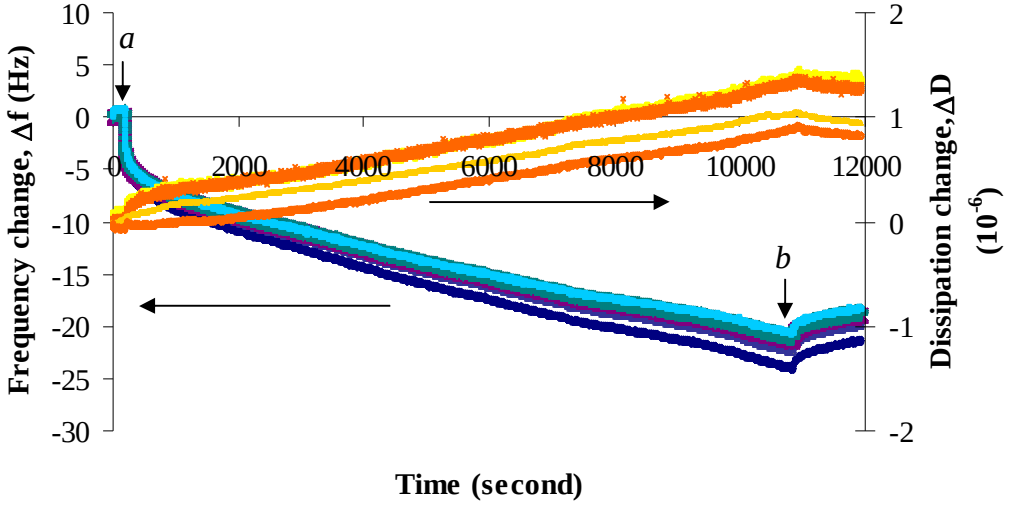

Figure 6.3**:** Frequency and dissipation factor change of lysozyme adsorbing from 0.1 g / L solution onto a bare SS surface at 23 °C. Phosphate buffer solution was replaced with protein solution at point *a* and returned to buffer solution at point *b*.

6.1.2.2 Effects of concentration and temperature on the mass density of lysozyme on a SS surface

Figure 6.4 shows the Voigt mass density of lysozyme adsorbed on a stainless steel surface as a function of temperature and solution concentration (0.1. 0.5 and 1 g / L). There was a gradual increase in mass density adsorbed as concentration and temperature increased. Rinsing the system with buffer solution removed less than 10 % of the mass adsorbed. Overall, under the experimental conditions, the Voigt mass densities of lysozyme remaining after desorption ranged from about 4 to 16 mg / m^2. The corresponding number of molecules adsorbed and mean layer thickness was 0.17 to 0.66 molecules / nm^2 and 3.5 to 13.5 nm, respectively. The maximum surface density of monolayer lysozyme is approximately 3 mg/m^2 (end-on orientation) (dry basis) [Shen et al., 2005]. Thus, indicating a formation of multilayer in this study except on the surface adsorbing from 0.1 g / L solution at 23°.

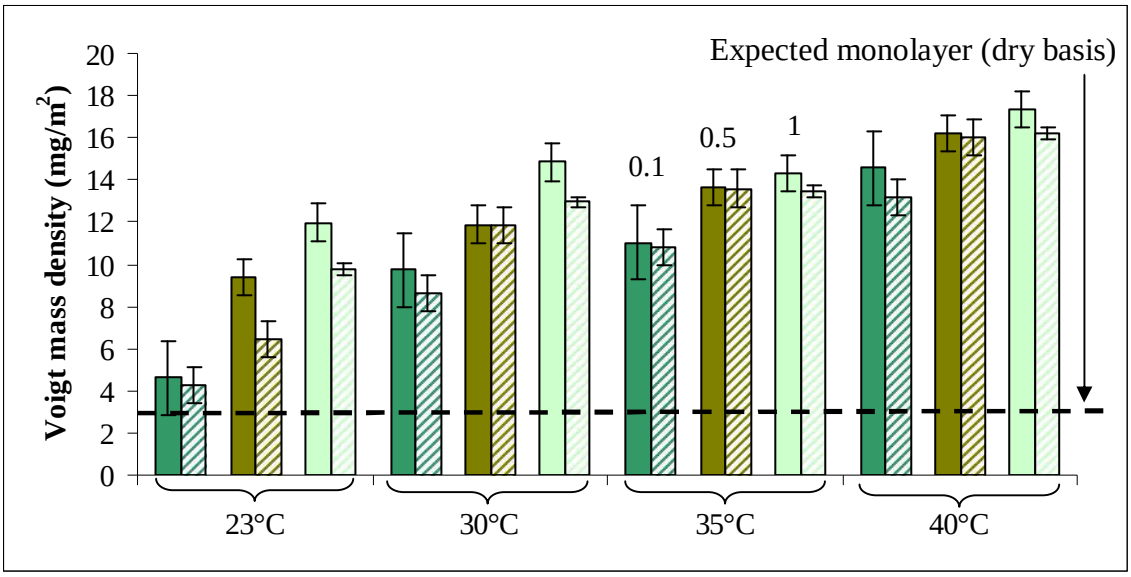

Figure 6.4: Mass density of lysozyme adsorbed at a steady state adsorption and desorption on a bare SS surface as a function of temperature and concentration. Bars with plain and stripe color refer to the mass density adsorbed at a final steady state *before* and *after* rinsing with buffer solution, respectively. Values above bars are protein solution concentration, g / L. The horizontal dotted line refers to the expected monolayer (dry basis).

6.1.3 α-lactalbumin

6.1.3.1 Adsorption and desorption kinetics of α-lactalbumin onto and off a bare SS surface (frequency and dissipation change)

The adsorption kinetic profiles of α-lactalbumin on a stainless steel surface was almost similar to that of β-casein, with a rapid decrease in frequency upon adsorption which quickly tended toward a steady state signal as shown in Figure 6.5. Interesting to note, the steady state adsorption was almost identical to that of β-casein even though the molecular weight of α-lactalbumin (14,200 Da) is almost half of β-casein (23,000 Da). In contrast, the dissipation change at the steady state adsorption was approximately 45 % higher than that of β-casein. Similar to lysozyme, rinsing the system with protein free buffer solution only slightly increased the frequency, indicating almost *fully irreversible* adsorption.

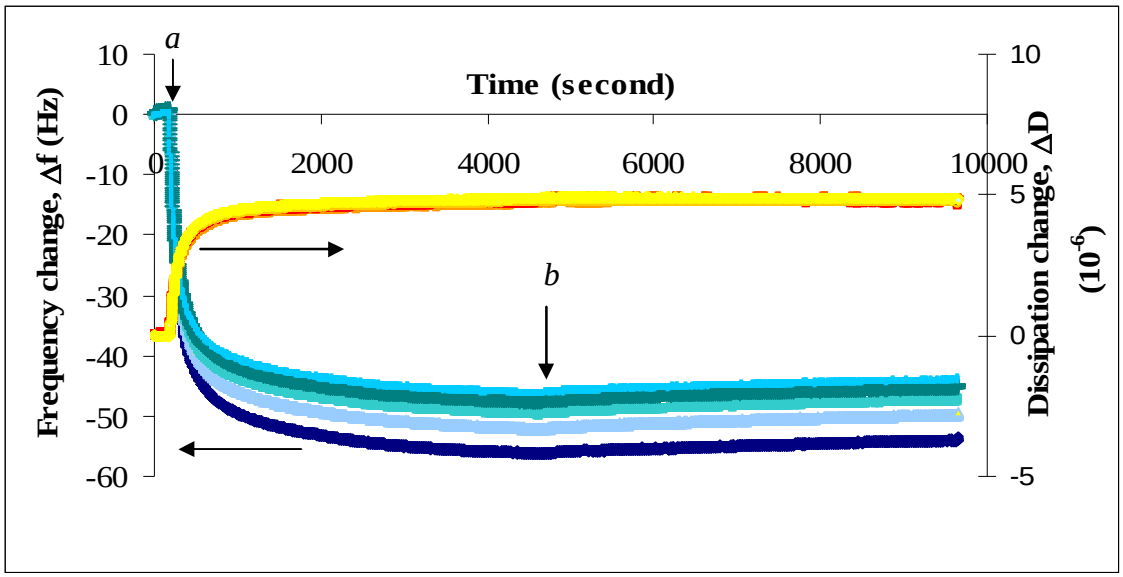

Figure 6.5: Frequency and dissipation factor change of α-lactalbumin adsorbing from 0.1 g / L solution onto a bare SS surface at 23 °C. Phosphate buffer solution was replaced with protein solution at point *a* and returned to buffer solution at point *b*.

6.1.3.2 Effects of concentration and temperature on the mass density of α-lactalbumin on a bare stainless steel surface

Figure 6.6 illustrates the effects of temperature and solution concentration (0.1, 0.5 and 5 g / L) on steady state mass densities of α-lactalbumin before and after rinsing with buffer solution as shown by plain and stripe color bars, respectively. As can be seen, generally, the mass density adsorbed has the same trend regardless of temperature. Rinsing the system with buffer solution, hardly removed the molecules as shown by a low removal percentage (less than 5 %). Overall, under the experimental conditions, the mass density adsorbed (tightly-bound mass) ranged from about 10 to 25 mg / m^2. The maximum surface density of monolayer α-lactalbumin is approximately 2 mg/m^2 (dry basis). The surface mass densities measured using the QCM-D were about 5 to 12 greater than of the dry mass. Thus, indicated the formation of a soft layer (a water-rich layer). This finding was strengthened with the high dissipation energy changes.

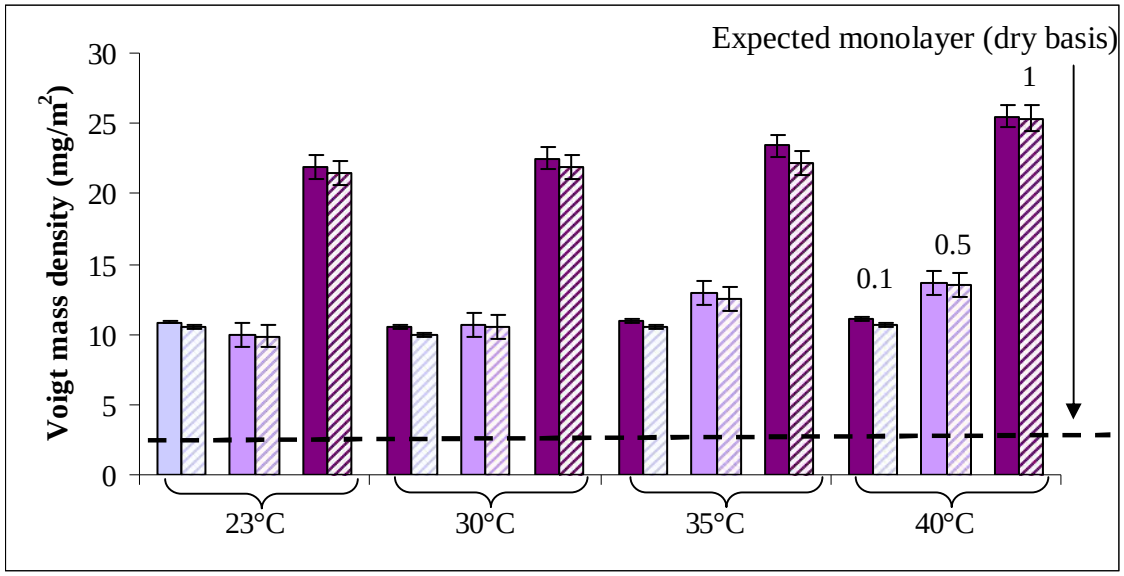

Figure 6.6: The Voigt mass density of α-lactalbumin adsorbed on a bare stainless steel surface as a function of temperature and concentration. Bars with plain and stripe color refer to the mass density adsorbed at a final steady state *before* and *after* rinsing with buffer solution, respectively. Values above bars are protein solution concentration, g / L. The horizontal dotted line refers to the expected monolayer (dry basis).

SUMMARY

From the results obtained in this part, it can be summarized that:

- Adsorption of β-casein, lysozyme and α-lactalbumin proteins increased as concentration and temperature increased.
- β-casein, lysozyme and α-lactalbumin proteins reacted in different ways toward a stainless steel surface. β-casein demonstrated partially reversible adsorption while lysozyme and α-lactalbumin displayed almost fully irreversible adsorption.
- Under the experimental conditions, all proteins formed multilayer on the bare SS surface except on the lysozyme adsorption from 0.1 g / L at 23 °C.

6.2 PART B

MODIFICATION OF STAINLESS STEEL SURFACES BY COATING WITH POLY(ETHYLENE GLYCOL)(PEG) LAYER

This part covers the results obtained on the modification of a stainless steel surface. The stainless steel surface was *coated* with PEI from 30 g / L solution or silicate from 5 g / L solution, then *coated* with PEG from various of molecular weights and concentrations. We represent the prepared surfaces as SS-PEI (30)-PEG surfaces or SS-silicate (50)-PEG surfaces. This part presents the effects of temperature, coating layer (either a PEI layer or a silicate layer), PEG molecular weights and concentrations on PEG grafting density. All the data presented in this part refers to the strongly held adsorption since only those molecules are expected to play a role in inhibition of proteins adsorption (refer to the next part). PEG had been used with either OH or NHS end groups, PEG-OH has been referred to as just PEG whereas PEG-NHS remained the label for the other. At the end of this part all the results have been summarized together.

6.2.1 PEI-PEG on stainless steel

Figure 6.7 shows an example of the modification process done on a stainless steel surface monitored in real time by the QCM-D technique. Lines with blue based color refer to frequency change while orange based color refers to dissipation change. There were six steps involved in the modification; A: Stabilization of a baseline using MilliQ water, B: introduction of PEI solution in water (30 g / L), C: Rinsing of PEI layer with MilliQ water, D: Introduction of buffer solution (providing a baseline for PEG solution), E: Introduction of PEG solution in buffer and F: Rinsing PEG layer with buffer solution.

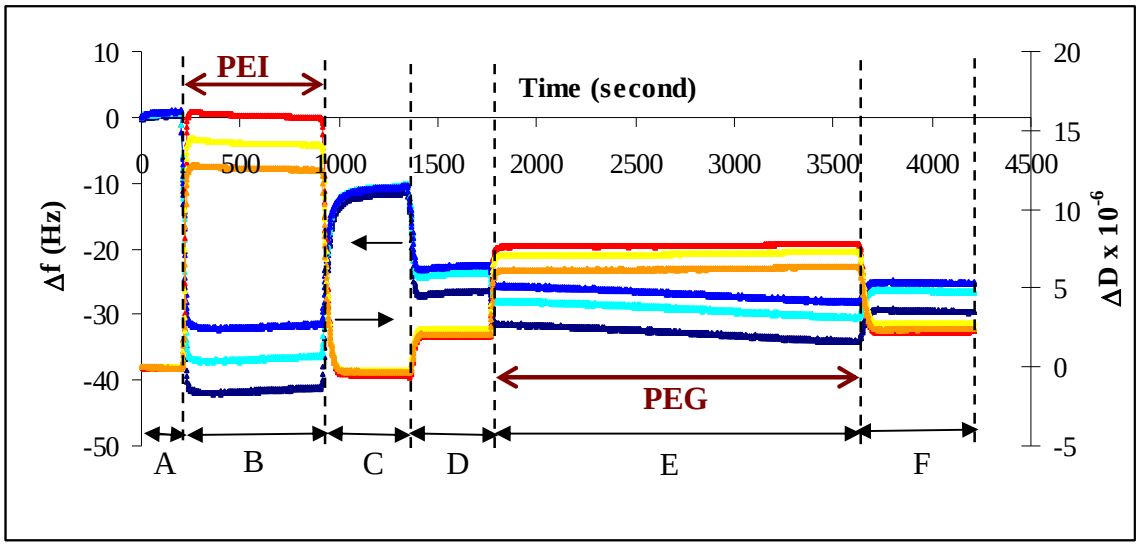

Figure 6.7: Modification of a stainless steel surface monitored in situ by the QCM-D technique. The involved processes were; A: Stabilization of a baseline using MilliQ water; B: Introduction of PEI solution in water (30 g / L); C: Rinsing PEI layer with MilliQ water; D: Introduction of buffer solution (providing a baseline for PEG solution); E: Introduction of PEG solution in buffer; F: Rinsing PEG layer with buffer solution.

6.2.2 PEI on stainless steel

Figure 6.8 shows the adsorption and desorption kinetics of PEI from 30 g / L solution onto and off a stainless steel surface at temperatures of 23 and 40 °C. There was no difference generally between the PEI adsorption and desorption kinetic profiles at the two temperatures. Adsorption of PEI onto the stainless steel surface was fast and reached a steady state in less than 60 seconds. The mass density adsorbed at steady state was about 20 mg / m^2 (≅ 0.5 chains / nm^2) at 40 °C and about 5 % less at 23 °C. When the PEI layers were rinsed with milliQ water, the mass decreased and presumably weakly bound PEI molecules were desorbed. Almost 85 % of the PEI mass was desorbed, leaving approximately 3 mg / m^2 (≅0.07 chains / nm^2) bound on the surfaces at the two temperatures.

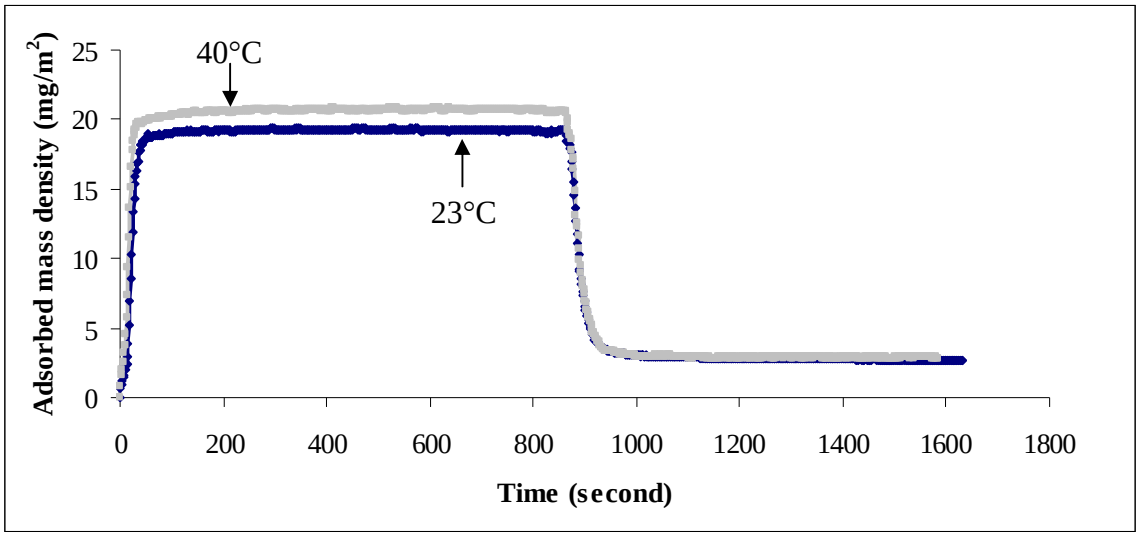

Figure 6.8: The Voigt mass density of PEI adsorbed from 30 g / L solution and desorbed onto and off a stainless steel surface as a function of time. The experiments were conducted at 23 and 40 °C. The data was obtained using the Voigt model.

6.2.3 PEG on PEI on stainless steel

Figure 6.9 shows the tightly-bound PEG molecules on the stainless steel surface coated with a PEI layer at a temperature of 23 °C. We represent a layer of PEI on a SS surface as a SS-PEI (30), where 30 refer to the PEI solution concentration in g / L. As can be seen, the grafting density for PEG350 and 550 Da, remained low from concentration of 0.1 to 1 g / L before increasing by an order of magnitude for PEG concentrations larger than 1 g / L and beginning to level off at concentration of 10 g / L. For PEG2k and 5k Da, the grafting density only doubled over the same concentration range. As the PEG molecular weight increased, the grafting density reduced more than 90 %.

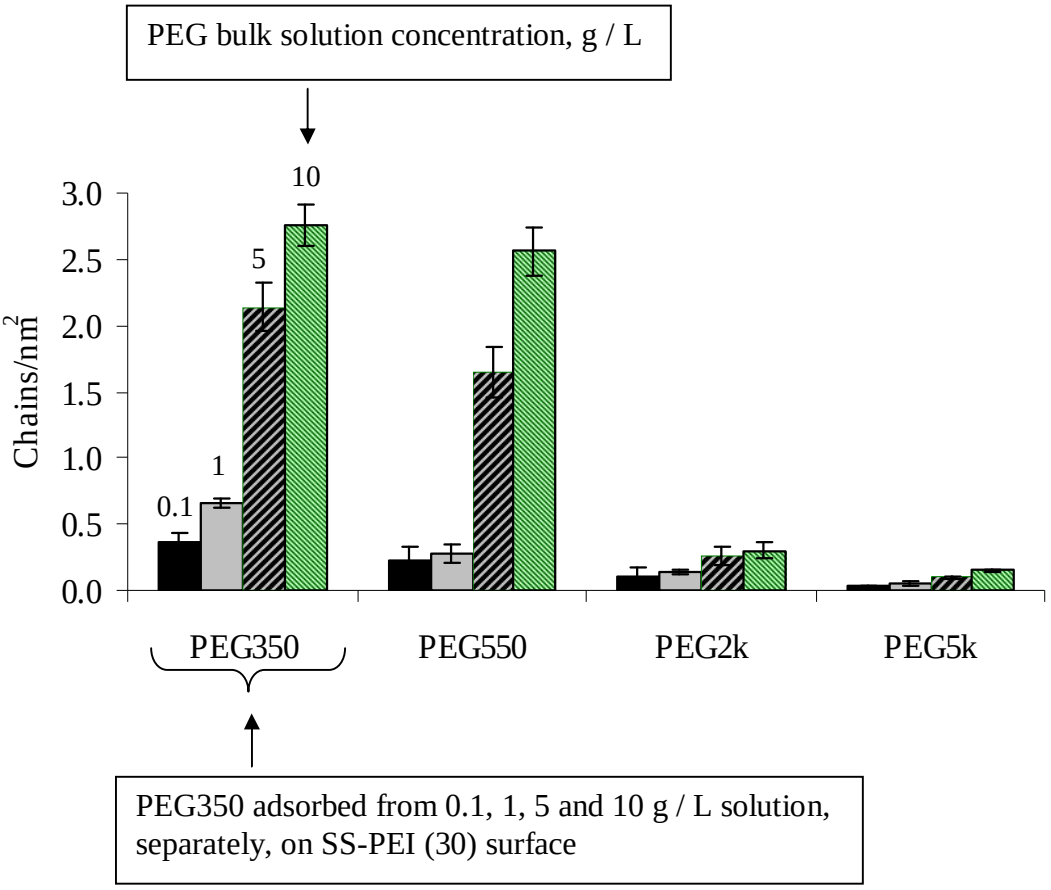

Figure 6.9: Number density of tightly–bound PEG molecules on SS-PEI (30) surfaces as a function of PEG molecular weights and solution concentrations. The experiment was conducted at a temperature of 23 °C. The data was obtained using the Voigt model. Figures above bars are concentration of PEG solution, g / L.

Figure 6.10 shows the Voigt number density of tightly–bound PEG molecules on the SS-PEI (30) surface a temperature of 40 °C. Generally, the PEG number density increased with an increase in concentration and vice versa with PEG molecular weight. It seemed that, the PEG grafting density increased with the temperature only on the surfaces prepared using the lower PEG concentrations of 0.1 and 1 g / L whereas the density decreased at high concentration.

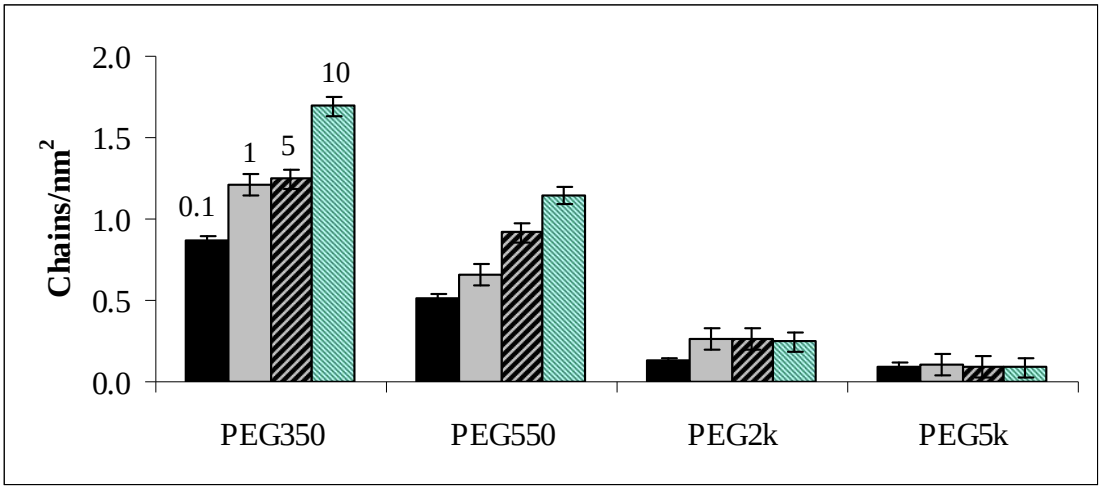

Figure 6.10: Number density of tightly–bound PEG molecules on SS-PEI (30) surfaces as a function of PEG molecular weights and solution concentrations. The experiment was conducted at a temperature of 40 °C. Figures above bars are concentration of PEG solution, g / L.

6.2.4 Silicate-PEG on stainless steel

The QCM-D response on modification of stainless steel surfaces using sodium silicate as a coating is in Appendix A. The processes involved were the same as modification with the PEI (Figure 6.7) except at step B, sodium silicate solutions (50 g / L) were used instead of the PEI solutions. 50g / L solution was used to achieve a faster steady state.

6.2.5 Silicate on stainless steel

Figure 6.11 shows adsorption and desorption kinetics of silicate from 50 g / L solution onto and off a stainless steel surface at temperatures of 23 and 40 °C. There was no significant difference between the silicate adsorption and desorption kinetic profiles at the two temperatures. The adsorption was fast initially followed by a gradual increase before leveling off at time less than 500 seconds. The mass density adsorbed at steady state was about 6.5 mg / m^2, corresponding to 21 molecules / nm^2 at the two temperatures. When the silicate layers were rinsed with phosphate buffer,

the mass decreased and weakly bound silicate molecules were desorbed. Almost 90 % of the silicate mass were desorbed, leaving approximately 0.8 mg / m^2 (≅2.5 chains / nm^2) bound on the surface at the two temperatures.

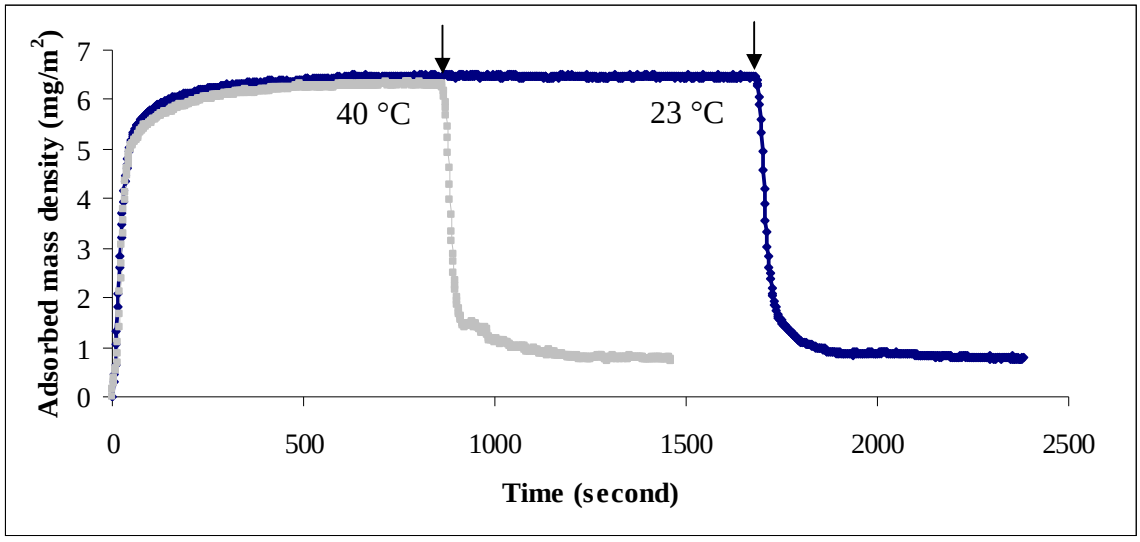

Figure 6.11: The Voigt mass density of silicate adsorbed from 50 g / L solution and desorbed onto and off a stainless steel surface as a function of time. The experiments were conducted at 23 and 40 °C.

6.2.6 PEG on silicate on stainless steel

Figures 6.12 and 6.13 display the tightly-bound PEG molecules on the stainless steel surface coated with a silicate layer at 23 and 40 °C, respectively. We represent a layer of silicate on a SS surface as a SS-silicate (50), where 50 refer to the silicate solution concentration in g /L. At the two temperatures, the trend of the PEG grafting density towards the PEG molecular weight and solution concentration was the same; the PEG grafting density increased as concentration increased and decreased as PEG molecular increased. The PEG grafting density on the SS-silicate (50) surface had shown a similar trend as on the SS-PEI (30) surface with the rise of the temperature; the PEG grafting density increased with the temperature only on the surfaces prepared using PEG concentrations of 0.1 and 1 g / L whereas it decreased at

high concentration. As a comparison, PEG grafting density generally was about 10 to 30 % higher on SS-PEI (30) surfaces than on SS-silicate (5) surfaces.

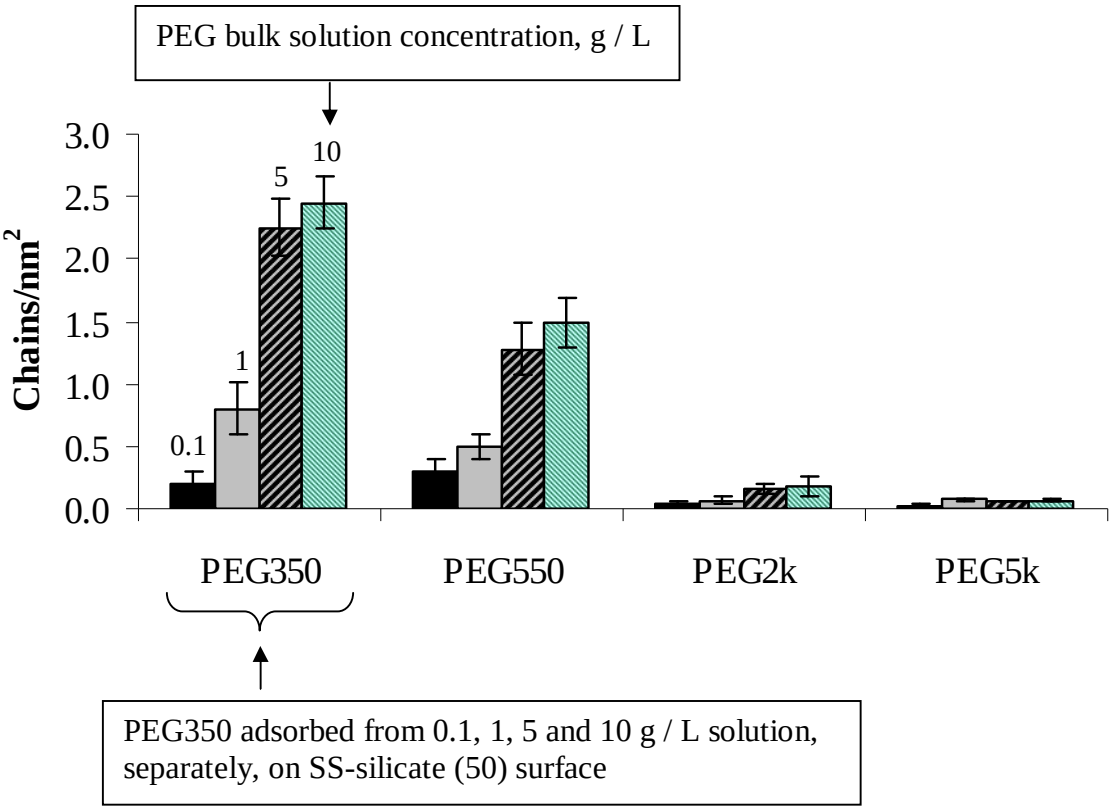

Figure 6.12: Number density of tightly–bound PEG molecules on SS-silicate (50) surfaces as a function of PEG molecular weight and solution concentration. The experiment was conducted at a temperature of 23°C. The data was obtained using the Voigt model. Figures above bars are concentration of PEG solution, g /L.

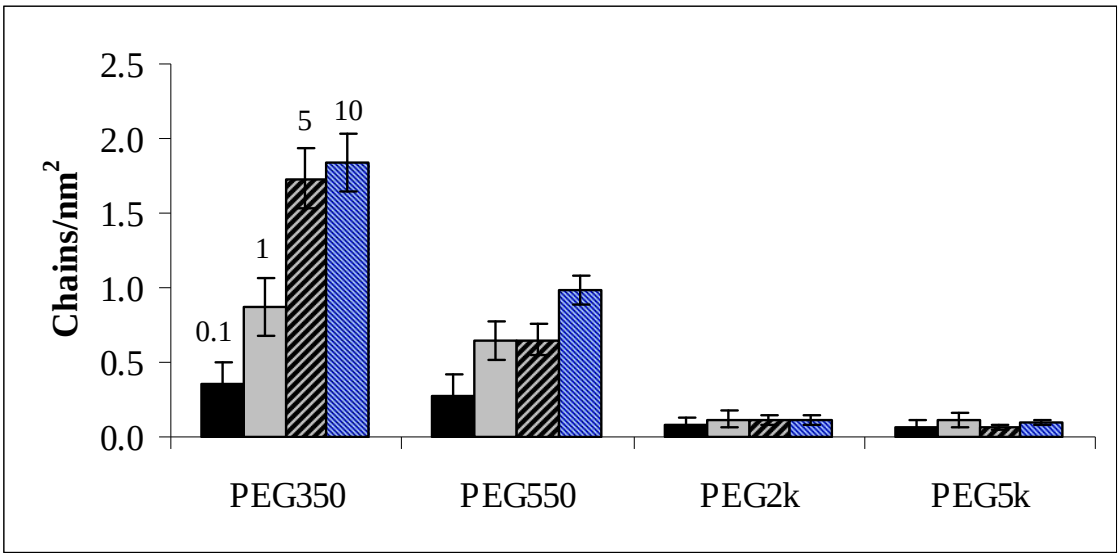

Figure 6.13: Number density of tightly–bound PEG molecules on SS-silicate (50) surfaces as a function of PEG molecular weight and solution concentration. The experiment was conducted at 40 °C. The data was obtained using the Voigt model. Figures above bars are concentration of PEG solution, g / L.

6.2.7 PEG-NHS on PEI on stainless steel

Figure 6.14 shows the tightly-bound PEG-NHS molecules on the SS-PEI (30) surface at 23 °C. Only PEG-NHS of 2k and 5k Da have been used (high PEG MW has shown better protein inhibition than low PEG MW, refer to the next parts). The mass density for PEG-NHS2k increased by up to 90 % as the PEG solution concentration increased from 0.1 to 1 g / L and almost no change with further increase. Meanwhile, for PEG-NHS5k, the grafting density increased about 75 % as PEG concentration increased from 0.1 to 1 g / L before leveling off at a concentration of 5 g / L.

PEGNHS grafting density on the SS-PEI (30) surfaces was generally higher than of PEG-OH grafting density on the same surface; by up to 50 % (refer to Figures 6.9 and 6.14).

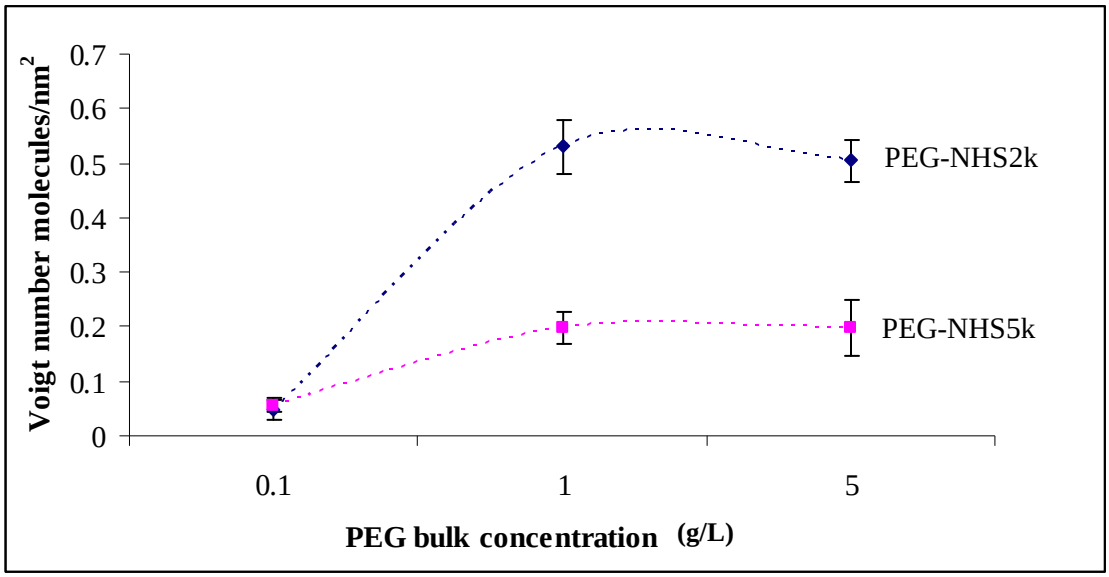

Figure 6.14: Number density of tightly–bound PEG-NHS molecules on SS-PEI (30) surfaces as a function of PEG molecular weight and solution concentration (0.1, 1 and 5 g / L). The experiment was conducted at a temperature of 23 °C. The data was obtained using the Voigt model.

BIMODAL PEG SURFACES

This section presents the result of bimodal PEG grafting density on the SS-PEI (30) and SS-silicate (50) surfaces The bimodal PEG surfaces were prepared using 6 of PEG combinations; PEG (5k+2k), (5k+550), (5k+350), (2k+550), (2k+350) and (550+350) ((refer to Chapter 5 for the bimodal PEG surfaces preparation procedure). The bimodal PEG surfaces were prepared using PEG solution concentration of 0.1, 1 and 5 g / L.

6.2.8 Bimodal PEG on PEI on stainless steel

Figure 6.15 shows the bimodal PEG grafting density adsorbed from 1 g / L of PEG solution on SS-PEI (30) surfaces at 23 and 40 °C. The grafting density of bimodal PEG was the highest with PEG (550 + 350) combination. A surface with PEG (5k+2k) combination meanwhile gave the lowest bimodal PEG density. There was no significant trend on the bimodal PEG grafting density towards the temperature.

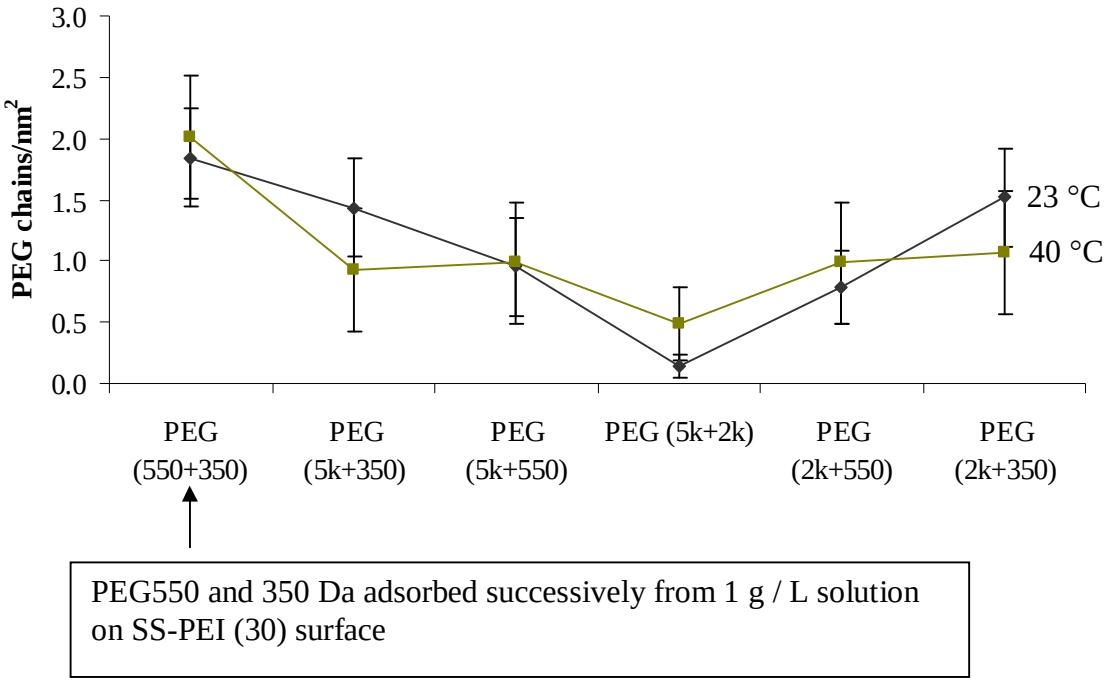

Figure 6.15: Bimodal PEG grafting density adsorbed from 1 g / L of PEG solution on SS-PEI (30) surfaces.

Figure 6.16 shows the grafting density of bimodal PEG on the SS-PEI (30) surface adsorbed from 0.1 and 5 g / L of PEG solution. The experiment was performed at a temperature of 23 °C. The was no significant different in the bimodal PEG grafting density adsorbing from either at 0.1 or at 1 g / L (refer to Figures 6.15 and 6.16). However, adsorbing the PEG from 5 g / L solution enhanced the bimodal PEG grafting density, by up to 50 %.

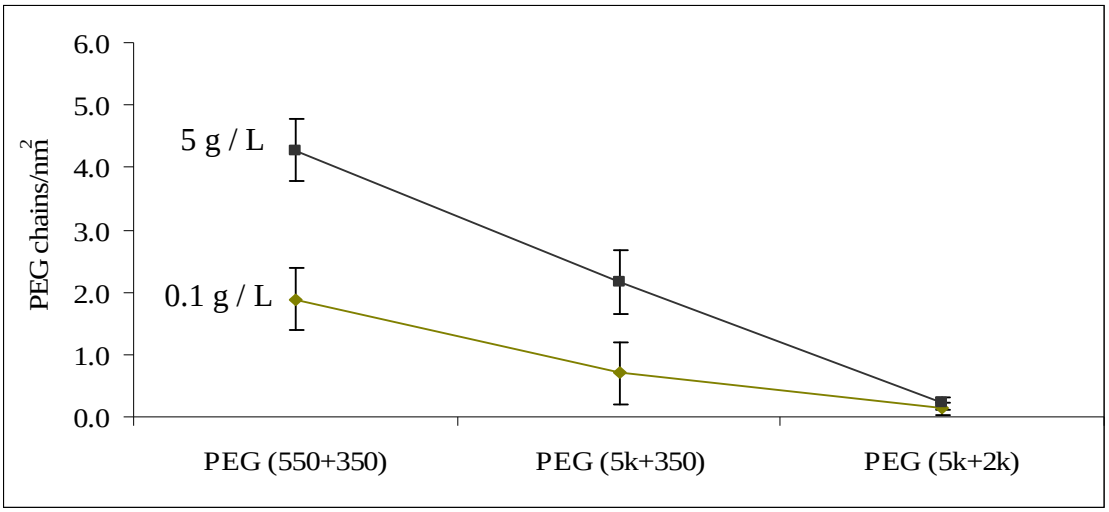

Figure 6.16: Bimodal PEG grafting density on SS-PEI (30) surfaces adsorbed from 0.1 and 5 g / L of PEG solution. The experiment was performed at a temperature of 23 °C.

Increasing the temperature from 23 to 40 °C, also enhanced the bimodal PEG grafting density to almost double especially on the surfaces prepared using the highest PEG solution concentration, 5 g / L (see Figures 6.16 and 6.17).

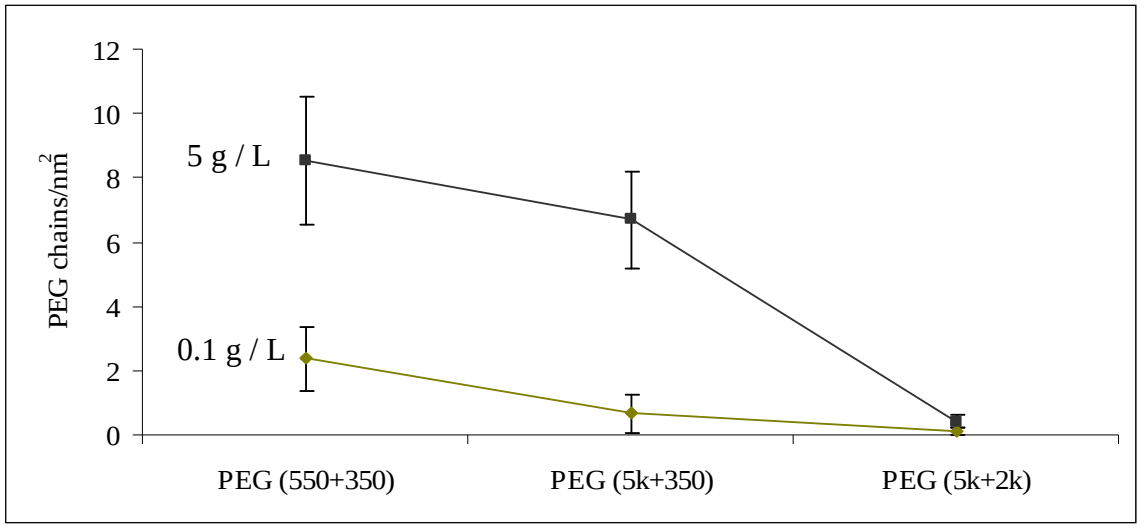

Figure 6.17: Bimodal PEG grafting density on SS-PEI (30) surfaces adsorbed from 0.1 and 5 g / L of PEG solution. The experiment was performed at a temperature of 40 °C.

6.2.9 Bimodal PEG on silicate on stainless steel

Figure 6.18 displays the bimodal PEG grafting density on the SS-silicate (50) surface adsorbed from 1 g / L PEG solution concentration at 23 and 40°C. As can be seen, the bimodal PEG grafting density was higher at a temperature of 23 °C than that at 40 °C, except on the surfaces prepared using combinations of PEG (5k+2k) and PEG (2k+550); the bimodal PEG grafting density was almost the same on those surfaces.

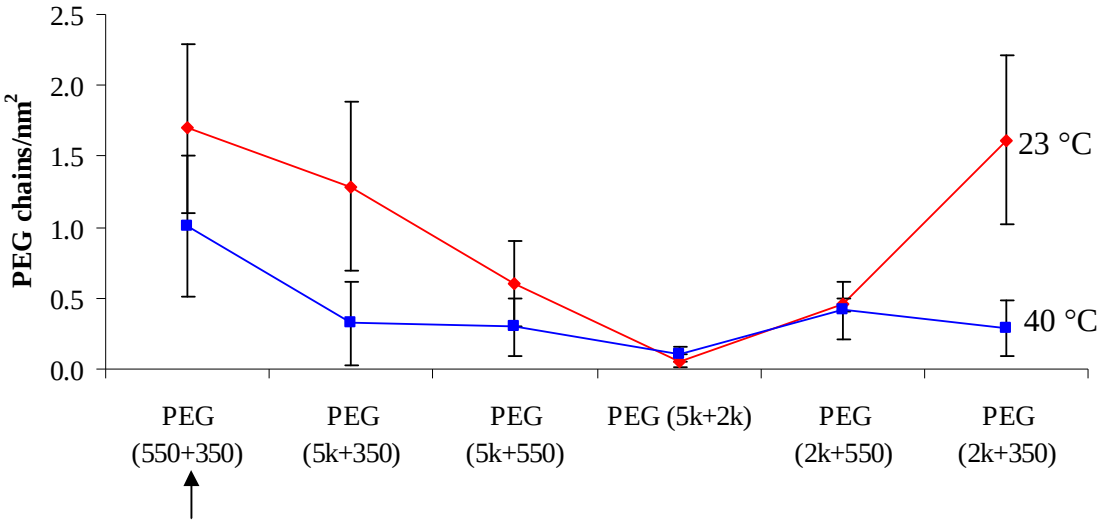

Figure 6.18: Bimodal PEG grafting density on SS-silicate (50) surfaces adsorbed from 1 g / L of PEG solution at 23 and 40 °C.

Increasing either the temperature from 23 to 40 °C or increasing the PEG solution concentration from 0.1 to 5 g / L, resulted in a huge enhancement in the PEG bimodal grafting density, by up more than 50 % (refer to Figures 6.19 and 6.20).

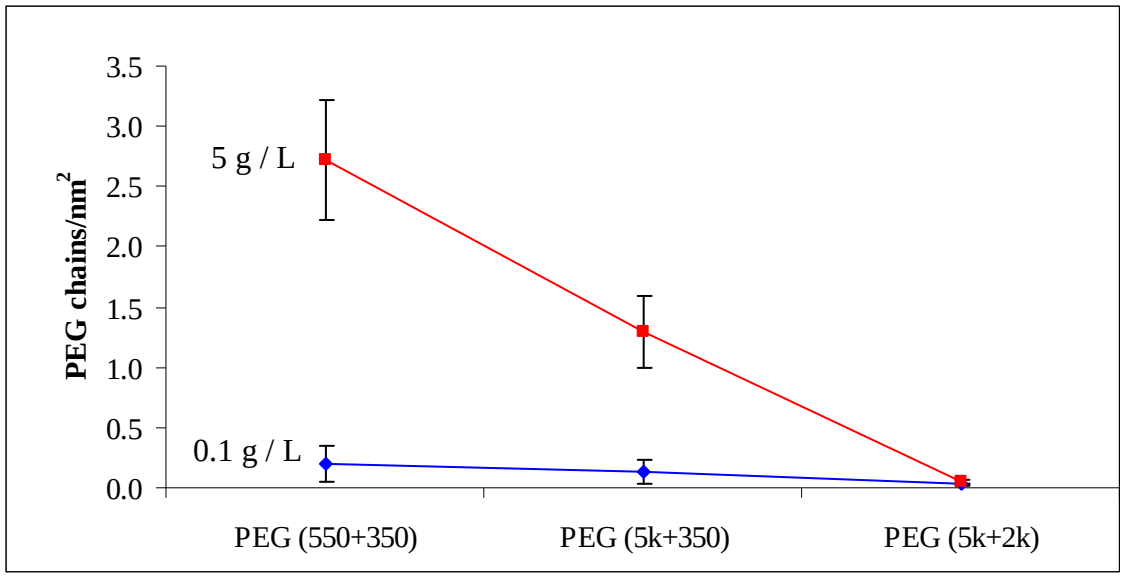

Figure 6.19: Bimodal PEG grafting density on SS-silicate (5) surfaces adsorbed from 0.1 and 5 g / L of PEG solution. The experiment was performed at a temperature of 23 °C.

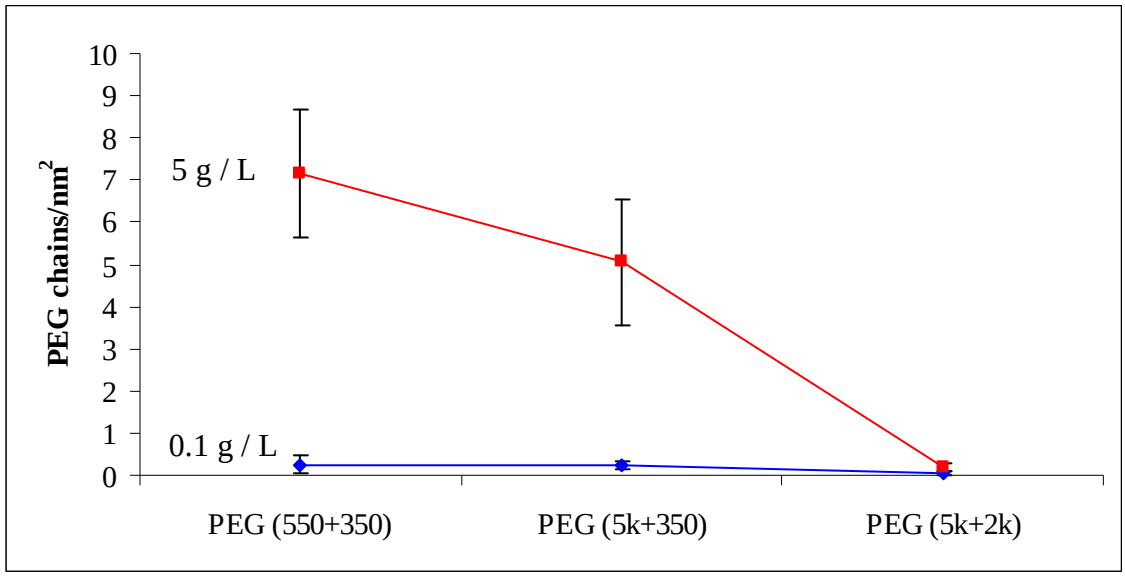

Figure 6.20: Bimodal PEG grafting density on SS-silicate (5) surfaces adsorbed from 0.1 and 5 g / L of PEG solution. The experiment was performed at a temperature of 40 °C.

SUMMARY

From the results obtained in Part B, it can be summarized that:

Monomodal PEG surfaces

- PEG grafting density increased as PEG solution concentration increased and decreased with an increase in PEG molecular weight (chain length).
- PEG grafting density generally was about 10 to 30 % higher on the SS-PEI (30) surfaces than on the SS-silicate (5) surfaces.
- PEG-NHS grafting density on the SS-PEI (30) surface was generally higher than of PEG-OH on the same surface; by up to 50 %.

Bimodal PEG surfaces

- Bimodal PEG grafting density generally increased as PEG concentration and temperature increased.
- Bimodal PEG grafting density was the highest at a combination of PEG (550 + 350) and vice versa at a combination of PEG (5k + 2k).
- Bimodal PEG grafting density generally higher on the SS-PEI (30) surfaces than that on the SS-silicate (50) surfaces.
- Bimodal PEG grafting density was higher than of the monomodal PEG grafting density, by more than 50 %.

6.3 PART C: ADSORPTION OF PROTEINS ON MONOMODAL PEG SURFACES

This part covers the adsorption of β-casein, lysozyme and α-lactalbumin proteins from 0.1 g / L bulk solution on the SS-PEI (30)-PEG and SS-silicate (50)-PEG surfaces (monomodal PEG surfaces) (see part B). This part presents the effectiveness of the monomodal PEG surfaces to inhibit the adsorption of proteins. At the end of this part all the results have been summarized together. The mechanisms of protein adsorption on the monomodal PEG surfaces will be clarified and discussed in Chapter 11.

6.3.1 β-casein

6.3.1.1 Mass density of β-casein on SS-PEI (30)-PEG surfaces: Effects of temperature, PEG solution concentration and molecular weight

Figure 6.21 depicts the final steady state values of the Voigt mass density of β-casein *before* and *after* rinsing with buffer on a bare SS, SS-PEI (30) and SS-PEI (30)-PEG surfaces for PEG of various molecular weights and concentrations at a temperature of 23 °C. Values above bars are percentage of *strong adsorption* compared to that on the bare SS surface. The horizontal dashed line was drawn at the bare SS value to make an easy comparison between modified and unmodified surfaces. As can be seen, the adsorption of β-casein was lower on the SS-PEI (30)-PEG surfaces than that on the bare SS surface. By contrast, more mass were adsorbed on a SS-PEI (30) surface than of the bare SS surface. Increasing the PEG solution concentration generally reduced the β-casein adsorption. The adsorption of β-casein was the lowest on the SS-PEI (30)-PEG2k surface, down to almost 60 %. Flushing the protein layer with buffer solution removed by up to 40 % of the mass density adsorbed.

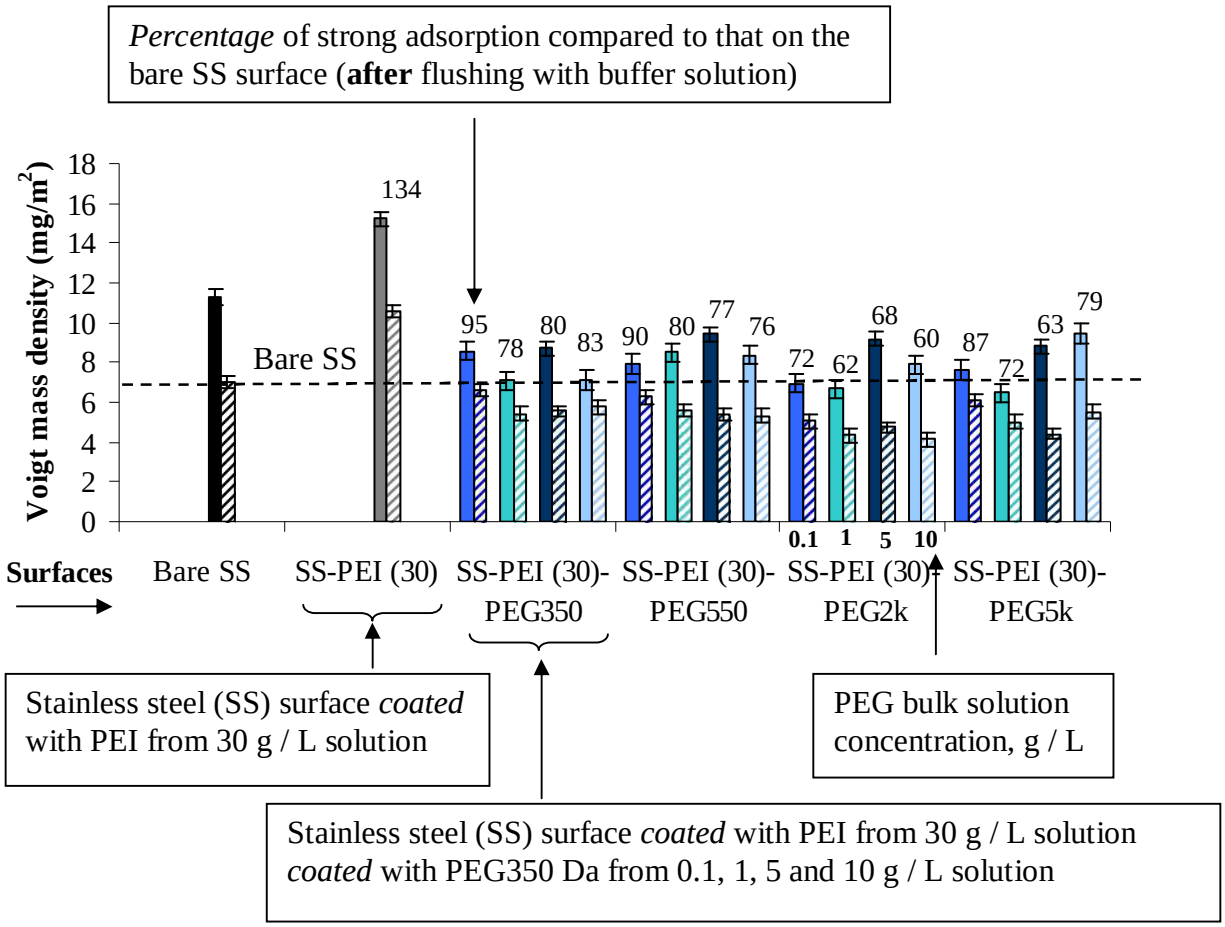

Figure 6.21: The Voigt mass density of β-casein adsorbed on a bare SS, SS-PEI (30) and SS-PEI (30)-PEG surfaces for PEG of various molecular weights and concentrations at a temperature of 23 °C. Bars with plain and stripe color refer to the mass density adsorbed at a final steady state *before* and *after* rinsing with buffer solution, respectively. Values above bars are percentage of *strong adsorption* compared to that on the bare SS surface.

The effectiveness of the SS-PEI (30)-PEG surfaces in preventing adsorption of β-casein at a temperature of 40 °C is shown in Figure 6.22. As can be seen, generally, the adsorption of β-casein on the SS-PEI (30)-PEG surfaces was slightly higher at 40 than of at 23 °C.

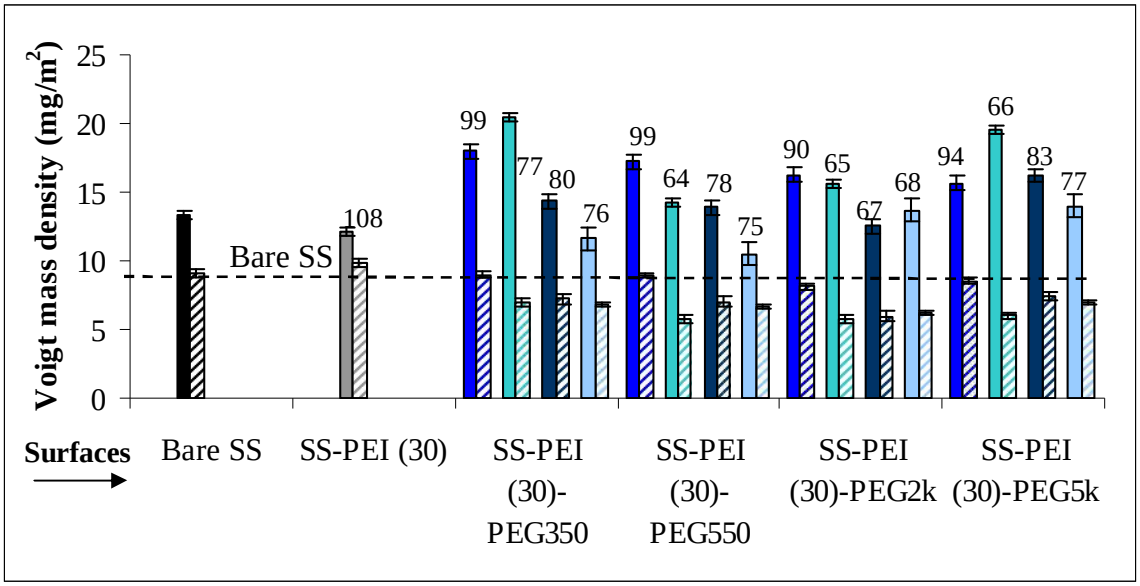

Figure 6.22: The Voigt mass density of β-casein adsorbed on a bare SS, SS-PEI (30) and SS-PEI (30)-PEG surfaces for PEG of various molecular weights and concentrations at 40 °C. Bars with plain and stripe color refer to mass density adsorbed at final steady state *before* and *after* rinsing with buffer solution, respectively. Values above bars are percentage of *strong adsorption* compared to that on the bare SS surface.

6.3.1.2 Mass density of β-casein on SS-PEI (30)-PEGNHS surfaces: Effects of temperature, PEG solution concentration and molecular weight

Figure 6.23 shows the Voigt mass density of tightly-bound β-casein on SS-PEI (30)-PEGNHS2k and SS-PEI (30)-PEGNHS5k surfaces at 23 ad 40 °C. The surfaces were prepared using PEG solution concentration of 0.1, 1 and 5 g / L. Surprisingly, the presence of PEGNHS molecules with a lower concentration seems to have no role in repelling β-casein adsorption. Interestingly, the adsorption of β-casein was lower at 40 than of at 23°C. As a comparison, adsorption of β-casein apparently was lower on the SS-PEI (30)-PEG surfaces compared to that on the SS-PEI (30)-PEGNHS surfaces.

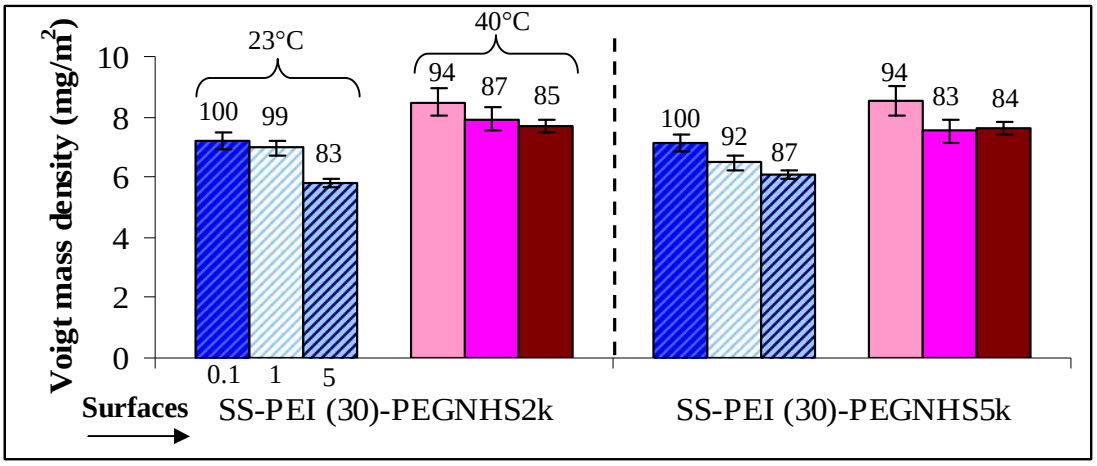

Figure 6.23: The Voigt mass density of tightly-bound β-casein adsorbed on SS-PEI (30)-PEGNHS2k and SS-PEI (30)-PEGNHS5k surfaces at 23 and 40 °C. The surfaces were prepared using PEG solution concentration of 0.1, 1 and 5 g/ L (shown by values below bars). Values above bars are percentage of *strong adsorption* compared to that on the bare SS surface.

6.3.1.3 Mass density of β-casein on SS-silicate (50)-PEG surfaces: Effects of temperature, PEG solution concentration and molecular weight

Figure 6.24 shows the final steady state values of mass density of β-casein *before* and *after* rinsing with buffer on a bare SS, SS-silicate (50) and SS-silicate (50)-PEG surfaces for PEG of various molecular weights and solution concentrations at a temperature of 23 °C. As can be seen, the adsorption was lower on the SS-silicate (50)-PEG surfaces than that on the bare SS surface; the adsorption down to less than 60 %. The adsorption of β-casein was less on the surfaces prepared using high PEG solution concentration (5 and 10 g / L). Nevertheless, the surfaces which were prepared using short PEG chains (PEG350 and 550 Da) and low PEG solution concentration (0.1 and 1 g / L) were still capable to reduce the adsorption of β-casein.

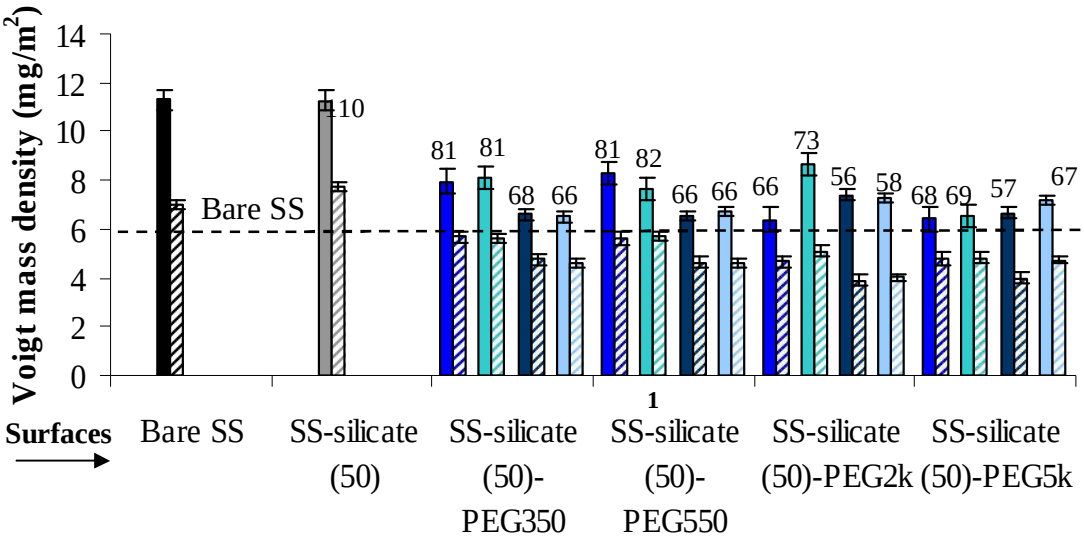

Figure 6.24: The Voigt mass density of β-casein adsorbed on a bare SS, SS-silicate (50) and SS-silicate (50)-PEG surfaces for PEG of various molecular weights and solution concentration at a temperature of 23 °C. Bars with plain and stripe color refer to mass density adsorbed at final steady state *before* and *after* rinsing with buffer solution, respectively. Values above bars are percentage of *strong adsorption* compared to that on the bare SS surface. Values below bars are PEG solution concentration, g / L.

Figure 6.25 shows the Voigt mass density of β-casein adsorbed at a steady state adsorption and desorption on a bare SS, SS-silicate (50) and SS-silicate (50)-PEG surfaces for PEG of various molecular weights and solution concentrations at a temperature of 40 °C. The horizontal dashed line was drawn at the bare SS value to make an easy comparison between modified and unmodified surfaces. It was interesting to note that the adsorption of β-casein on the SS-silicate (50)-PEG surfaces at 40 °C was much lower than that at 23 °C. At glance, the SS-silicate (50)-PEG surfaces prepared using low PEG molecular weight and low PEG solution concentration were still competent to reduce the adsorption of β-casein. Also, interesting to note, a SS-silicate (50) surface (without presence of PEG molecules) was able to reduce the adsorption of β-casein as good as SS-silicate (50)-PEG surfaces. Overall, the percentage of adsorption of β-casein on the modified surfaces was down to less than 50 % than that on the bare SS surface.

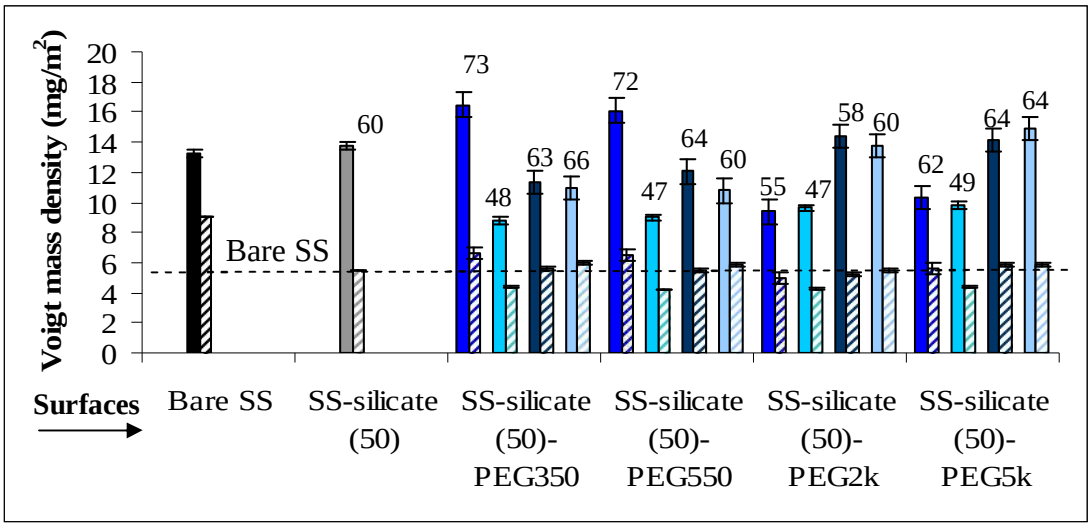

Figure 6.25: The Voigt mass density of β-casein adsorbed on a bare SS, SS-silicate (50) and SS-silicate (50)-PEG surfaces for PEG of various molecular weights and solution concentration at a temperature of 40 °C. Bars with plain and stripe color refer to mass density adsorbed at final steady state *before* and *after* rinsing with buffer solution, respectively. Values above bars are percentage of *strong adsorption* compared to that on the bare SS surface.

6.3.2 Lysozyme

6.3.2.1 Mass density of lysozyme on SS-PEI (30)-PEG surfaces: Effects of temperature, PEG solution concentration and molecular weight

Figure 6.26 shows the Voigt mass density of tightly-bound lysozyme on a bare SS, SS-PEI (30) and SS-PEI (30)-PEG surfaces for PEG of various molecular weights and solution concentrations at 23 °C. As depicted, the presence of PEG molecules reduced the adsorption of lysozyme to less than 12 %. It was more interesting to note that the adsorption of lysozyme was even lower on the SS-PEI (30) surfaces than that on the SS-PEI (30)-PEG surfaces.

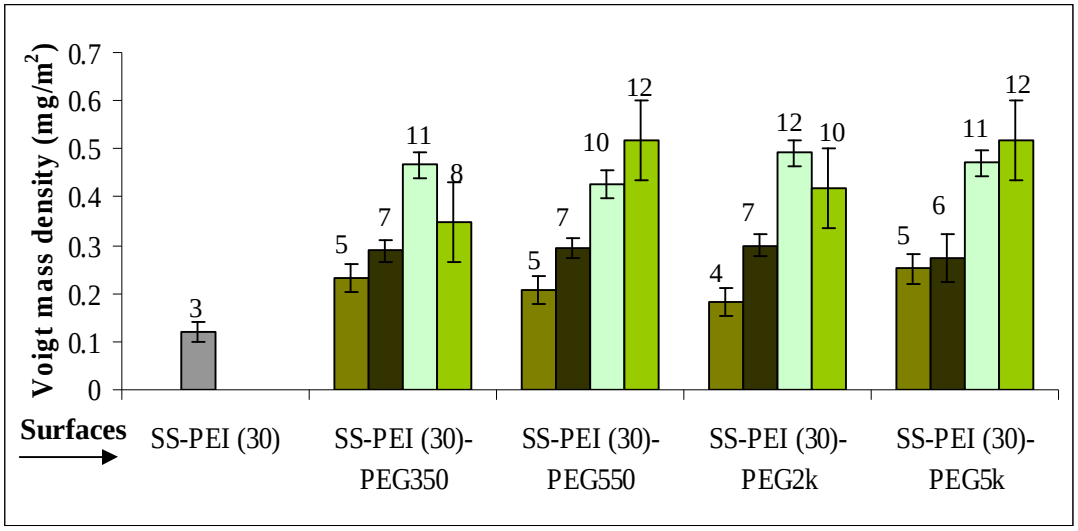

Figure 6.26: The Voigt mass density of tightly-bound lysozyme on SS-PEI (30) and SS-PEI (30)-PEG surfaces for PEG of various molecular weights and solution concentrations at a temperature of 23 °C. Values above bars are percentage of *strong adsorption* compared to that on the bare SS surface.

Figure 6.27 shows the Voigt mass density of tightly-bound lysozyme on SS-PEI (30) and SS-PEI (30)-PEG surfaces for PEG of various molecular weights and concentrations at 40 °C. By comparing Figures 6.26 and 6.27, it can be seen that the adsorption of lysozyme on SS-PEI (30) and SS-PEI (30)-PEG surfaces were about 40 % lower at a temperature of 40 than that at 23 °C. In general, at 40°C, the adsorption

\of lysozyme was down to less than 7 % on the SS-PEI (30)-PEG surfaces. Again, the adsorption of lysozyme was about 50 % lower on the SS-PEI (30) surface than that on the SS-PEI (30)-PEG surfaces. Neither PEG molecular weight nor PEG solution concentrations affect to the adsorption of lysozyme significantly.

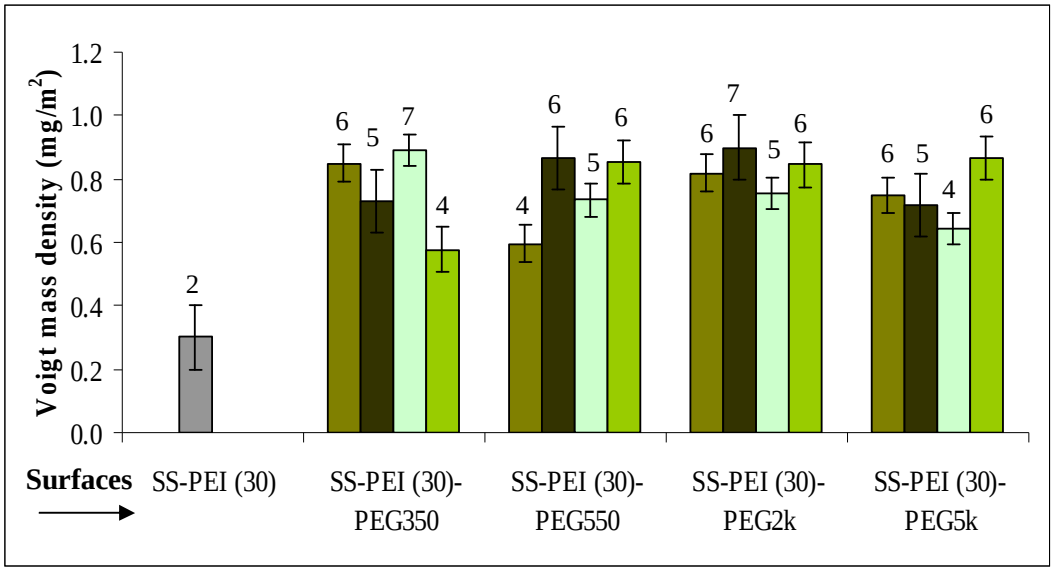

Figure 6.27: The Voigt mass density of tightly-bound lysozyme on SS-PEI (30) and SS-PEI (30)-PEG surfaces for PEG of various molecular weights and solution concentrations at a temperature of 40 °C. Values above bars are percentage of *strong adsorption* compared to that on the bare SS surface.

6.3.2.2 Mass density of lysozyme on SS-silicate (50)-PEG surfaces : Effects of temperature, PEG solution concentration and molecular weight

Figure 6.28 shows the adsorption of lysozyme on SS-silicate (50) and SS-silicate (50)-PEG surfaces at 23 °C. The adsorption of lysozyme down to less than 15 % on the SS-silicate (50)-PEG surfaces than of the bare SS surface. By contrast, the adsorption of lysozyme on the SS-silicate (50) surfaces (without PEG molecules) was about 80 % higher than that on the SS-silicate (50)-PEG surfaces.

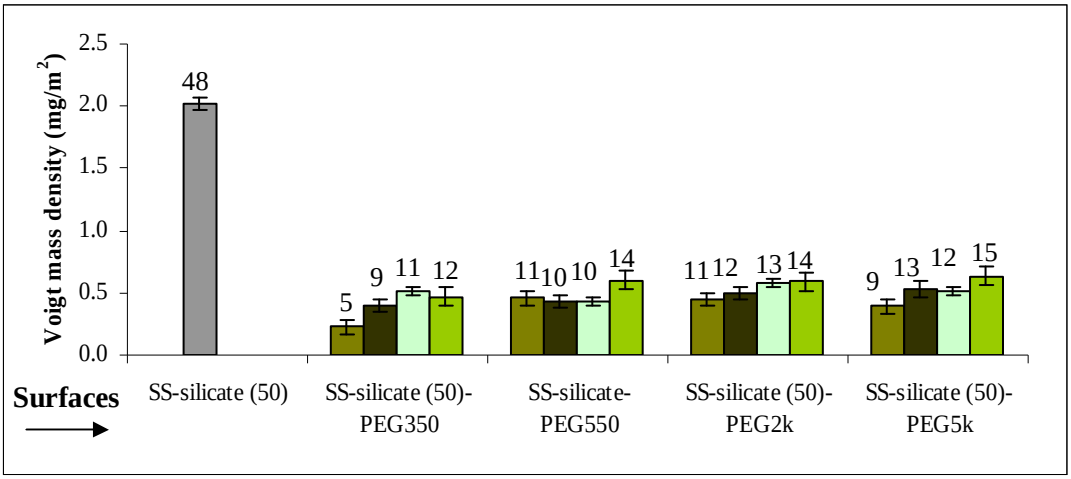

Figure 6.28: The Voigt mass density of tightly-bound lysozyme on SS-silicate (50) and SS-silicate (50)-PEG surfaces for PEG of various molecular weights and solution concentrations at 23 °C. Values above bars are percentage of *strong adsorption* compared to that on the bare SS surface.

Increasing the temperature from 23 to 40 °C decreased the percentage of the adsorption of lysozyme on the SS-silicate (50)-PEG surfaces to almost 50 % (see Figure 6.29). The adsorption on the SS-silicate (50) surfaces (without PEG molecules) was also lower at 40 than at 23 °C, by up to 70 %.

As a comparison, the SS-PEI (30)-PEG surfaces appeared to be better to inhibit adsorption of lysozyme compared to that of the SS-silicate (50)-PEG surfaces.

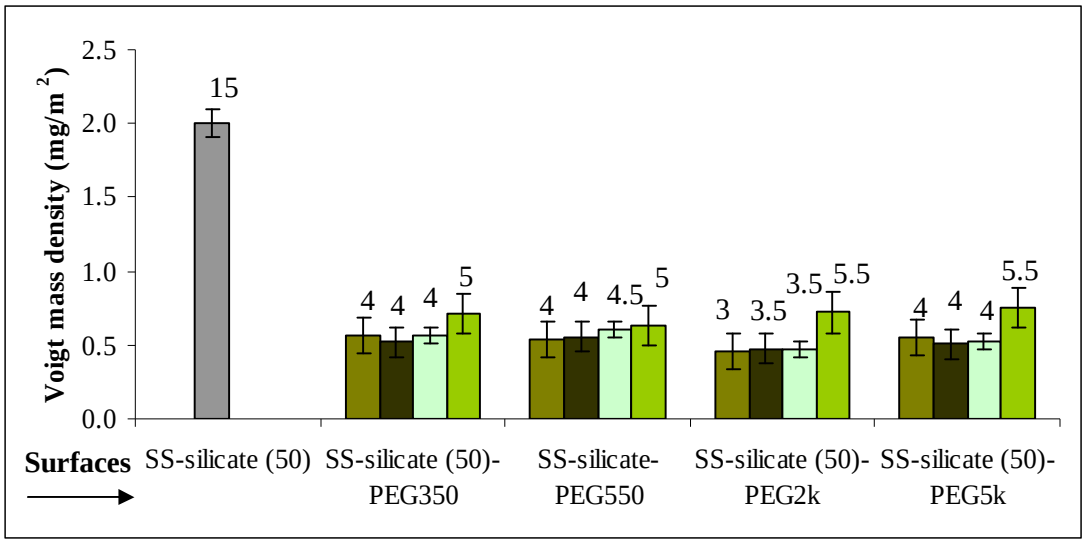

Figure 6.29: The Voigt mass density of tightly bound lysozyme on SS-silicate (50) and SS-silicate (50)-PEG surfaces for PEG of various molecular weights and solution concentrations at a temperature of 40 °C. Values above bars are percentage of *strong adsorption* compared to that on the bare SS surface.

6.3.3 α-lactalbumin

6.3.3.1 Mass density of α-lactalbumin on SS-PEI (30)-PEG surfaces: Effects of temperature, PEG solution concentration and molecular weight

Figure 6.30 presents the Voigt mass density of tightly-bound apo α-lactalbumin on a bare SS, SS-PEI (30) and SS-PEI (30)-PEG surfaces for PEG of various molecular weights and solution concentrations at 23 °C. The horizontal dashed line was drawn at the bare SS value to make an easy comparison between modified and unmodified surfaces. Unexpectedly, the adsorption of apo α-lactalbumin was about 26 % *higher* on the SS-PEI (30) and SS-PEI (30)-PEG surfaces.

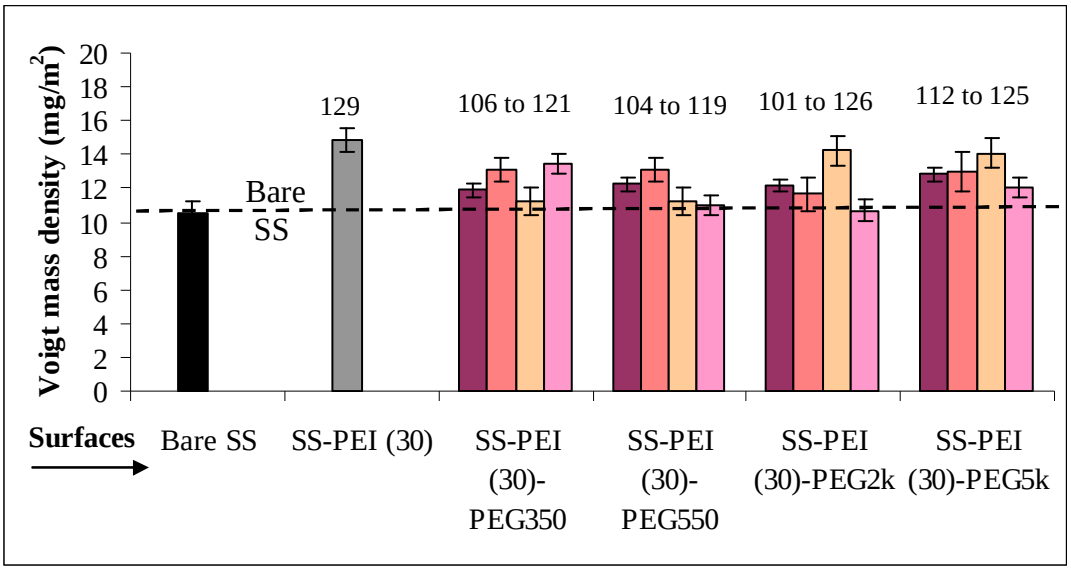

Figure 6.30: The Voigt mass density of tightly bound α-lactalbumin on a bare SS, SS-PEI (30) and SS-PEI (30)-PEG surfaces for PEG of various molecular weights and solution concentrations at 23 °C. Values above bars are range of percentage of *strong adsorption* compared to that on the bare SS surface.

At 40 °C, similarly, the presence of PEG (or PEI) molecules generally *enhanced* the adsorption of apo α-lactalbumin (see Figure 6.31).

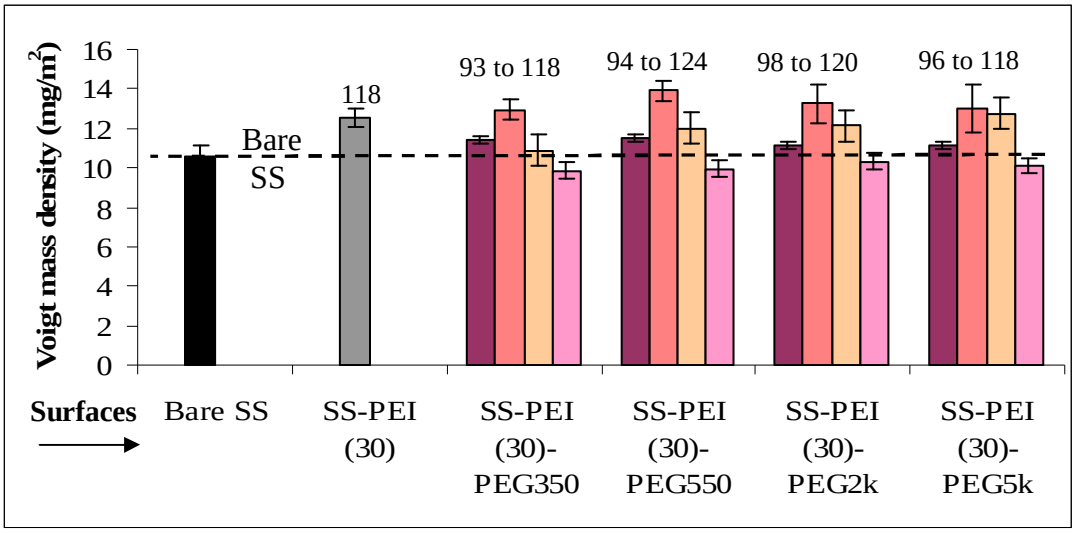

Figure 6.31: The Voigt mass density of tightly-bound α-lactalbumin on a bare SS, SS-PEI (30) and SS-PEI (30)-PEG surfaces for PEG of various molecular weights and solution concentrations at 40 °C. Values above bars are range of percentage of *strong adsorption* compared to that on the bare SS surface.

6.3.3.2 Mass density of α-lactalbumin on SS-silicate (50)-PEG surfaces: Effects of temperature, PEG concentration and molecular weight

Figures 6.32 and 6.33 show the Voigt mass density of tightly-bound apo α-lactalbumin on a bare SS, SS-silicate (50) and SS-silicate (50)-PEG surfaces for PEG of various molecular weights and solution concentrations at 23 and 40°C, respectively. As can be seen, the adsorption of α-lactalbumin was *higher* on the SS-silicate (50) and SS-silicate (50)-PEG surfaces than of the bare SS surface. This indicates that coated the SS surface with either PEI (30)-PEG or silicate (50)-PEG layers, enhanced the adsorption of α-lactalbumin.

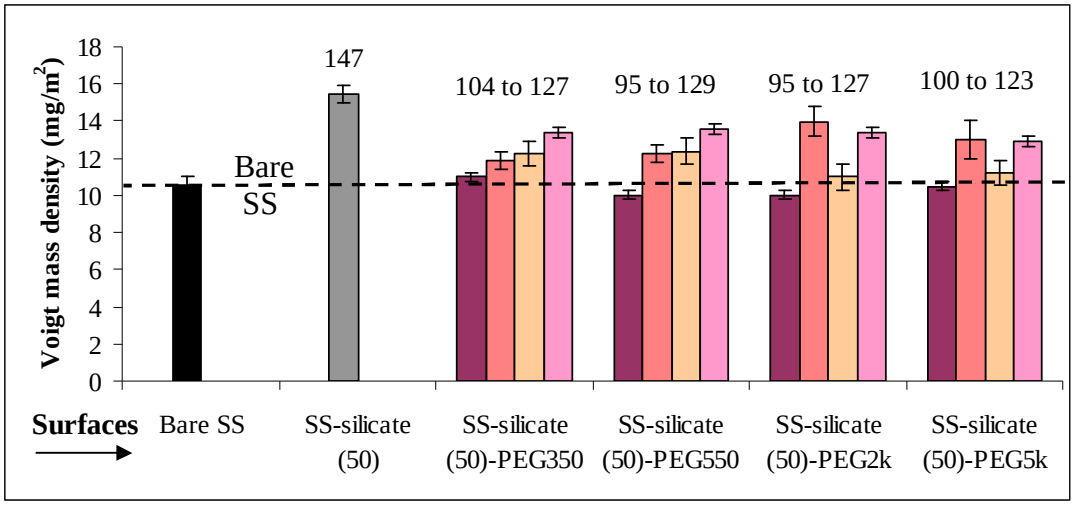

Figure 6.32: The Voigt mass density of tightly-bound α-lactalbumin on a bare SS, SS-silicate (50) and SS-silicate (50)-PEG surfaces for PEG of various molecular weights and solution concentrations at 23°C. Values above bars are range of percentage of *strong adsorption* compared to that on the bare SS surface.

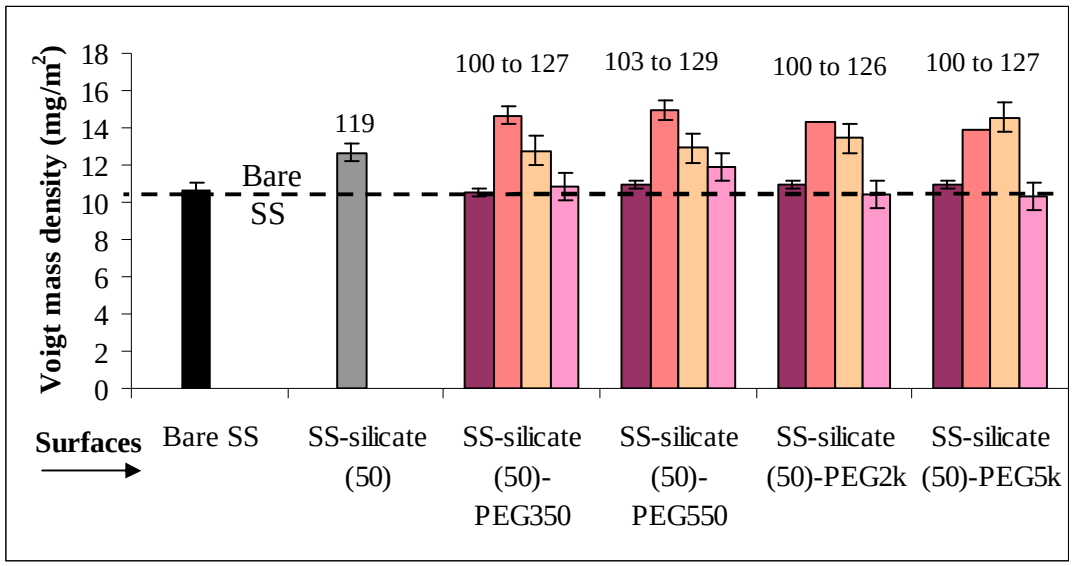

Figure 6.33: The Voigt mass density of tightly-bound α-lactalbumin on a bare SS, SS-silicate (50) and SS-silicate (50)-PEG surfaces for PEG of various molecular weights and solution concentrations at 40 °C. Values above bars are range of percentage *of strong adsorption* compared to that on the bare SS surface.

6.3.3.3 Mass density of α-lactalbumin on SS-PEI (30)-PEGNHS surfaces

Figure 6.34 shows the Voigt mass density of tightly-bound apo α-lactalbumin on a bare SS, SS-PEI (30)-PEGNHS2k and SS-PEI (30)-PEGNHS5k surfaces at 23 °C. The surfaces were prepared using PEG solution concentration of 0.1, 1 and 5 g / L (shown by values above bars). As can be seen, the adsorption of α-lactalbumin was higher on the SS-PEI (30)-PEGNHS surfaces than of the bare SS surface. This indicates that, either using PEG-OH or PEG-NHS resulted in the enhancement of the adsorption of α-lactalbumin.

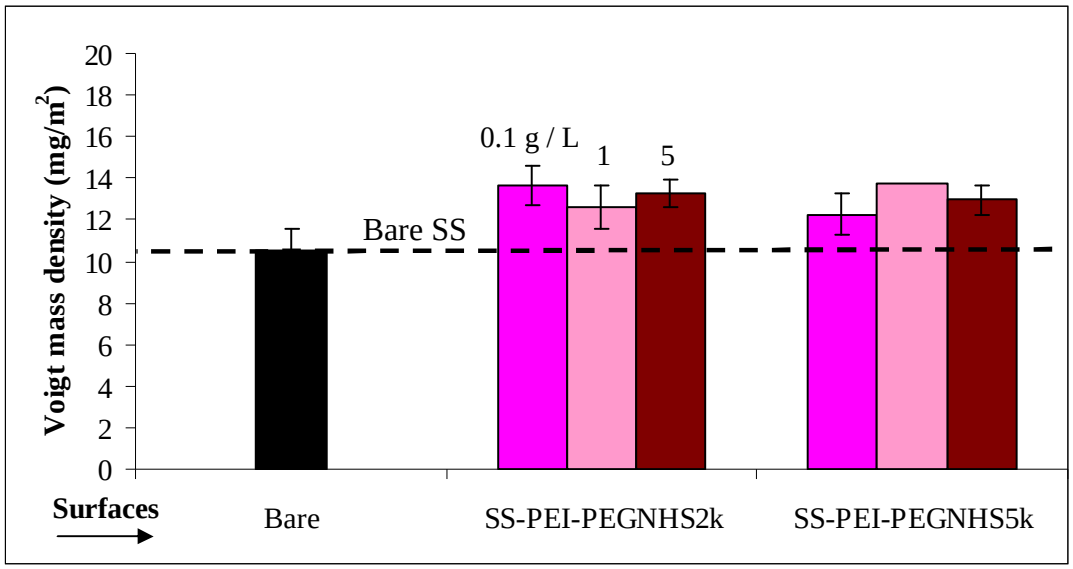

Figure 6.34: The Voigt mass density of tightly-bound α-lactalbumin on a bare SS, SS-PEI (30)-PEGNHS2k and SS-PEI (30)-PEGNHS5k surfaces at 23 °C. Values above bars are the PEG solution concentration, g / L.

6.4 PART D: ADSORPTION OF PROTEINS ON BIMODAL PEG SURFACES

This part covers the adsorption of β-casein, lysozyme and α-lactalbumin proteins from 0.1 g / L bulk solution on the bimodal PEG surface. The data shown in this part refers to the Voigt mass density of *tightly-bound* proteins adsorbed on the surface. The mechanisms of protein adsorption on the bimodal PEG surfaces will be clarified and discussed in Chapter 11.

6.4.1 β-casein

6.4.1.1 Mass density of β-casein on bimodal SS-PEI (30)-PEG surfaces: Effects of temperature, PEG concentration and combination

Figure 6.35 presents the mass density of β-casein tightly-bound on a bare SS and bimodal SS-PEI (30)-PEG surfaces for PEG of various combinations at 23 °C. The surfaces were prepared using PEG solution concentration of 1 g / L. Unexpectedly, the adsorption of β-casein on any bimodal PEG surfaces generally were *higher* than that on the bare SS surface, up to 24 %.

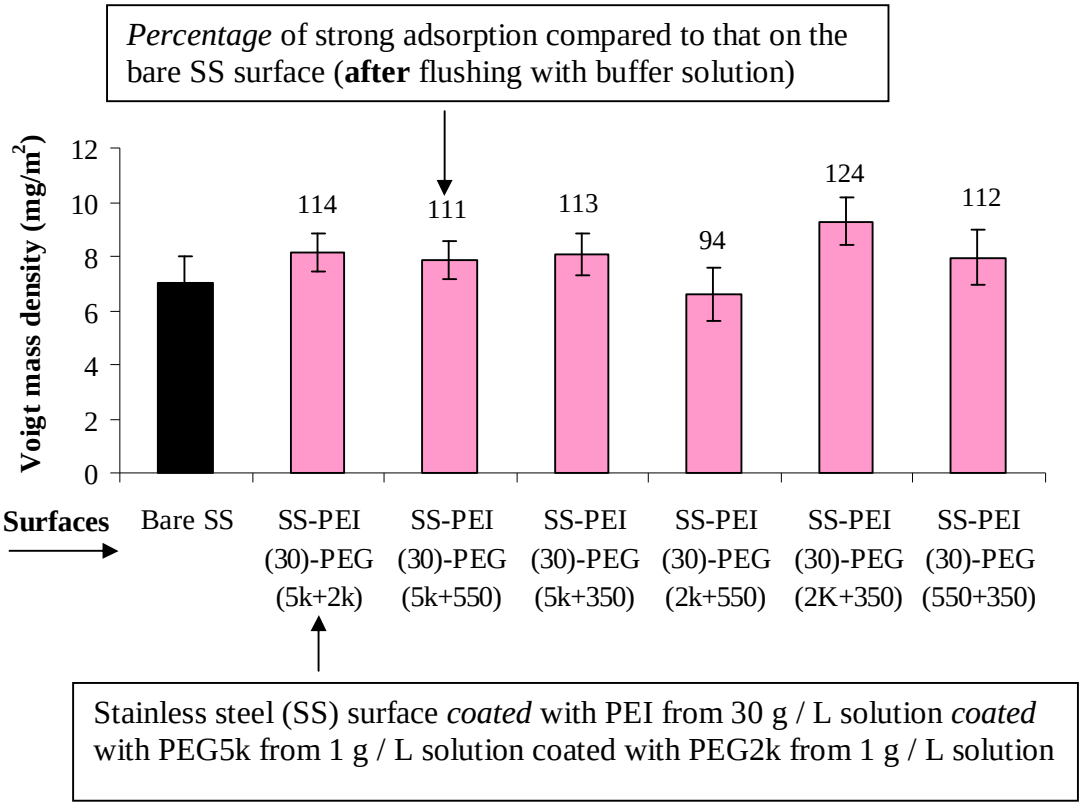

Figure 6.35: The Voigt mass density of tightly-bound β-casein on the bare SS and bimodal SS-PEI (30)-PEG surfaces for PEG of various combinations at 23 °C. The surfaces were prepared using PEG concentration of 1 g / L. Values above bars are percentage of *strong adsorption* compared to that on the bare SS surface.

The adsorption of β-casein also generally was *higher* on the bimodal PEG surfaces prepared using PEG concentration of 0.1 and 5 g / L compared to that on the bare SS surface (see Figure 6.36).

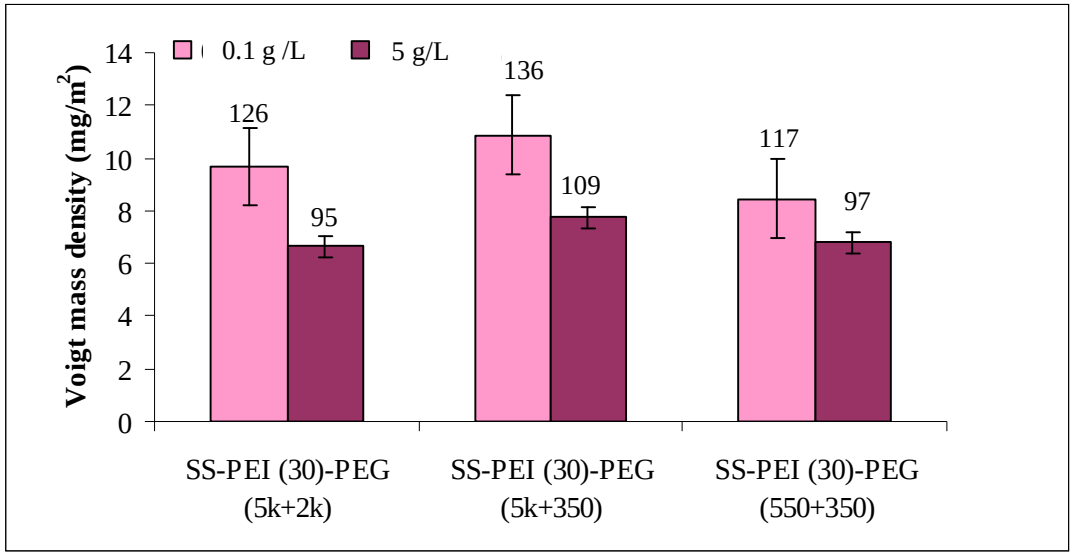

Figure 6.36: The Voigt mass density of tightly-bound β-casein on bimodal SS-PEI (30)-PEG surfaces for PEG of various combinations at 23 °C. The surfaces were prepared using PEG concentration of 0.1 and 5 g / L. Values above bars are percentage of *strong adsorption* compared to that on the bare SS surface.

Interestingly, the adsorption of β-casein on the SS-PEI (30)-PEG surfaces was lower at 40 than at 23°C (see Figures 6.37 and 6.38). The adsorption β-casein was down to almost 50 % on the surfaces prepared using PEG solution concentration of 5 g / L.

As a comparison, monomodal SS-PEI (30)-PEG surfaces generally were better to inhibit adsorption of β-casein than of the bimodal SS-PEI (30)-PEG surfaces.

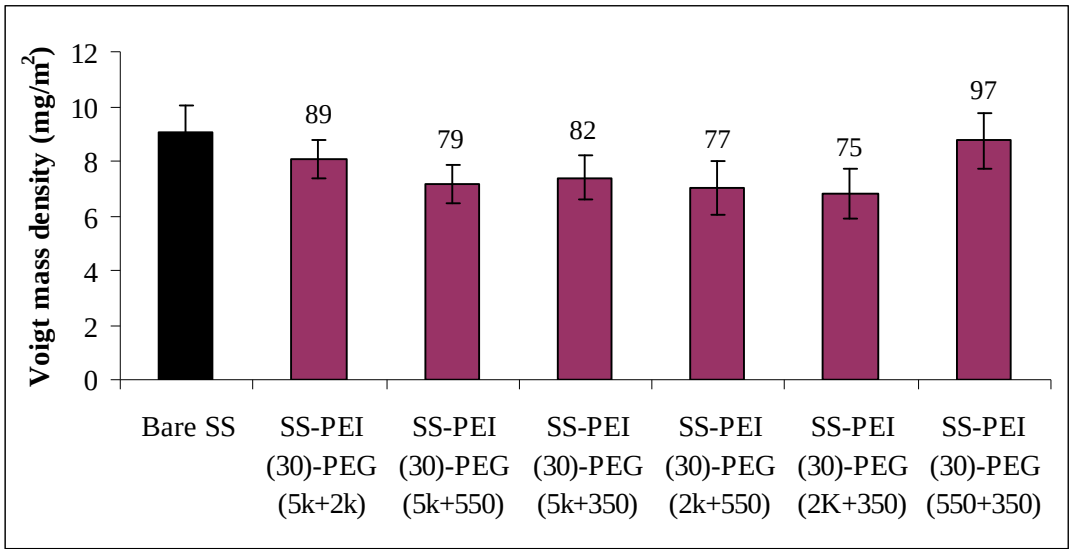

Figure 6.37: The Voigt mass density of tightly-bound β-casein on the bare SS and bimodal SS-PEI (30)-PEG surfaces for PEG of various combinations at 40 °C. The surfaces were prepared using PEG concentration of 1 g / L. Values above bars are percentage of *strong adsorption* compared to that on the bare SS surface.

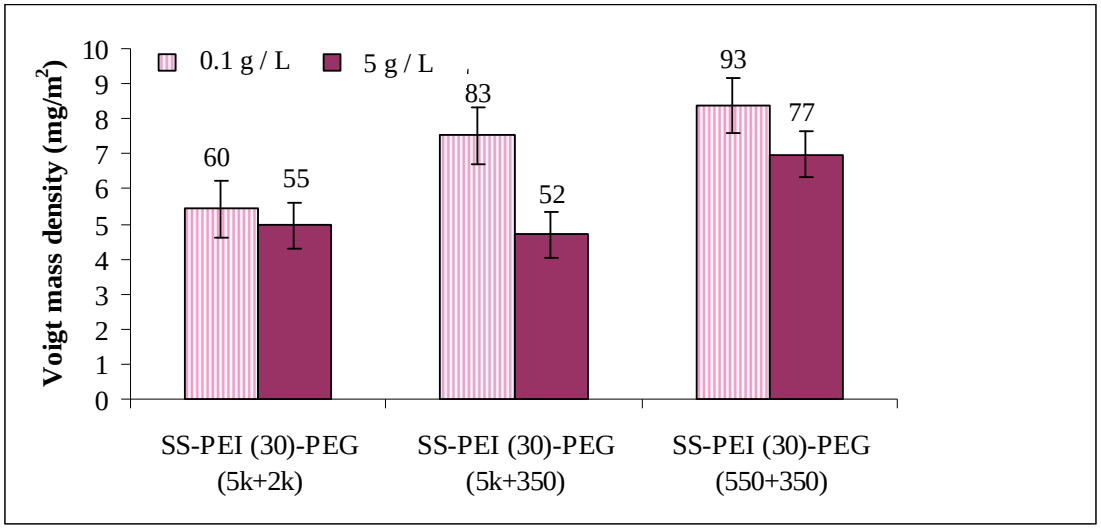

Figure 6.38: The Voigt mass density of tightly-bound β-casein on bimodal SS-PEI (30)-PEG surfaces for PEG of various combinations at 40 °C. The surfaces were prepared using PEG concentration of 0.1 and 5 g / L. Values above bars are percentage of *strong adsorption* compared to that on the bare SS surface.

6.4.1.2 Mass density of β-casein on bimodal SS-silicate (50)-PEG surfaces: Effects of temperature, PEG concentration and combination

Figure 6.39 shows the mass density of β-casein tightly-bound on a bare SS and bimodal SS-silicate (50)-PEG surfaces for PEG of various combinations at 23 °C. The surfaces were prepared using PEG solution concentration of 1 g / L. The adsorption of β-casein on these bimodal PEG surfaces only was down to less than 10 %. Comparing to Figure 6.24, it appeared that bimodal PEG SS-silicate (50)-PEG surfaces were less effective to inhibit adsorption of β-casein than of the monomodal SS-silicate (50)-PEG surfaces. Nevertheless, bimodal SS-silicate (50)-PEG surfaces apparently were better to inhibit adsorption of β-casein than of the bimodal SS-PEI (30)-PEG surfaces.

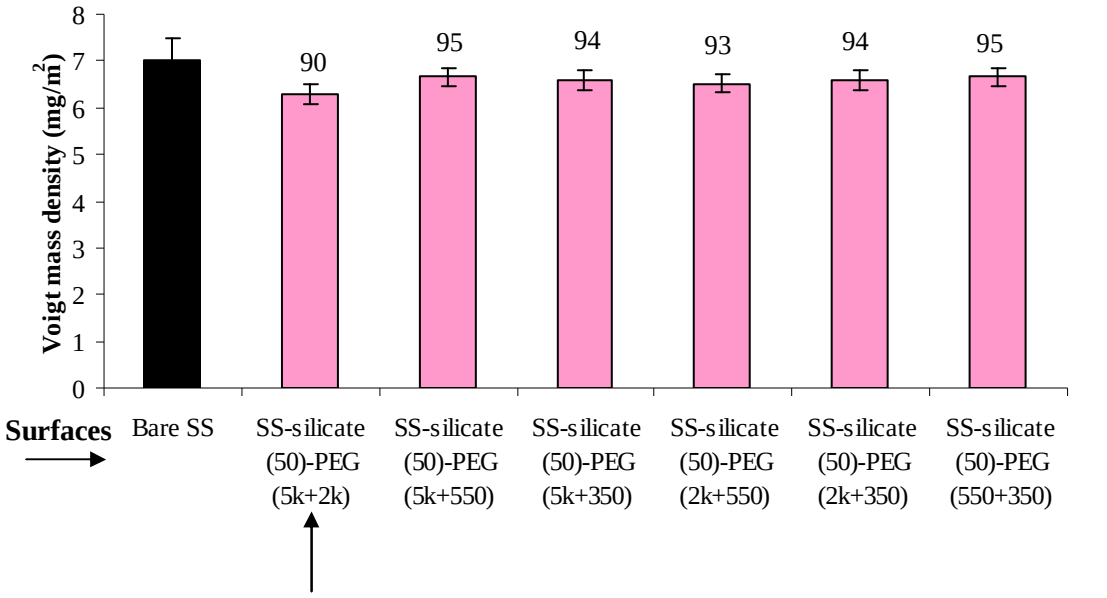

Figure 6.39: The Voigt mass density of tightly-bound β-casein on the bare SS and bimodal SS-silicate (50)-PEG surfaces for PEG of various combinations at 23°C. The surfaces were prepared using PEG solution concentration of 1 g / L. Values above bars are *percentage* of strong adsorption compared to that on the bare SS surface.

The bimodal PEG surfaces which were prepared using 0.1 and 5 g / L concentration of PEG seemed to much better to inhibit adsorption of β-casein than that using concentration of 1 g / L (Figure 6.40).

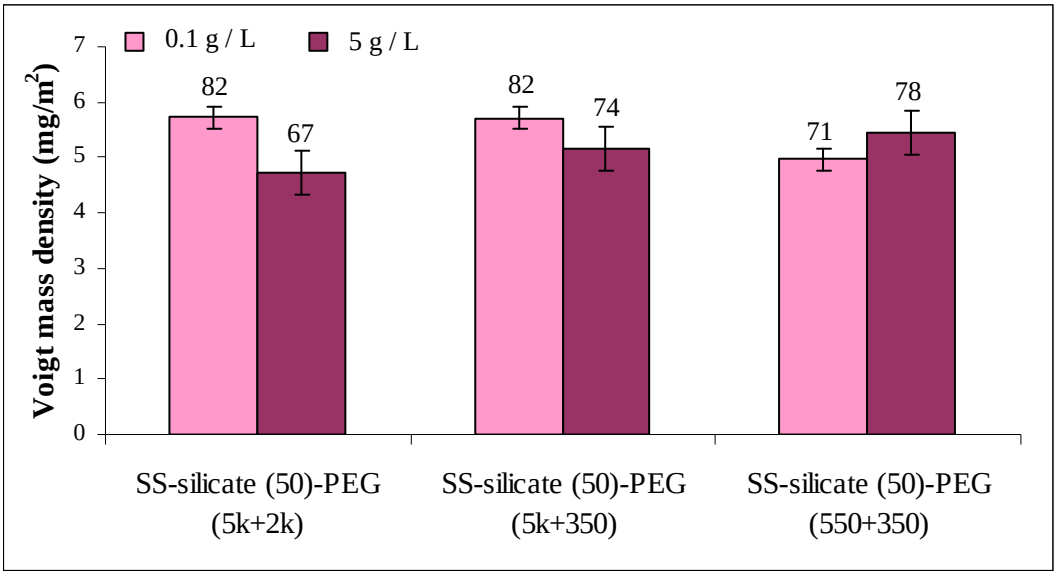

Figure 6.40: The Voigt mass density of tightly-bound β-casein on the bimodal SS-silicate (50)-PEG surfaces for PEG of various combinations at 23°C. The surfaces were prepared using PEG solution concentration of 0.1 and 5 g / L. Values above bars are *percentage* of strong adsorption compared to that on the bare SS surface.

Interestingly, at 40 °C, the adsorption of β-casein reduced to almost 50 %. Nevertheless, the adsorption was almost the same on the surfaces regardless of concentration used (refer Figures 6.41 and 6.42).

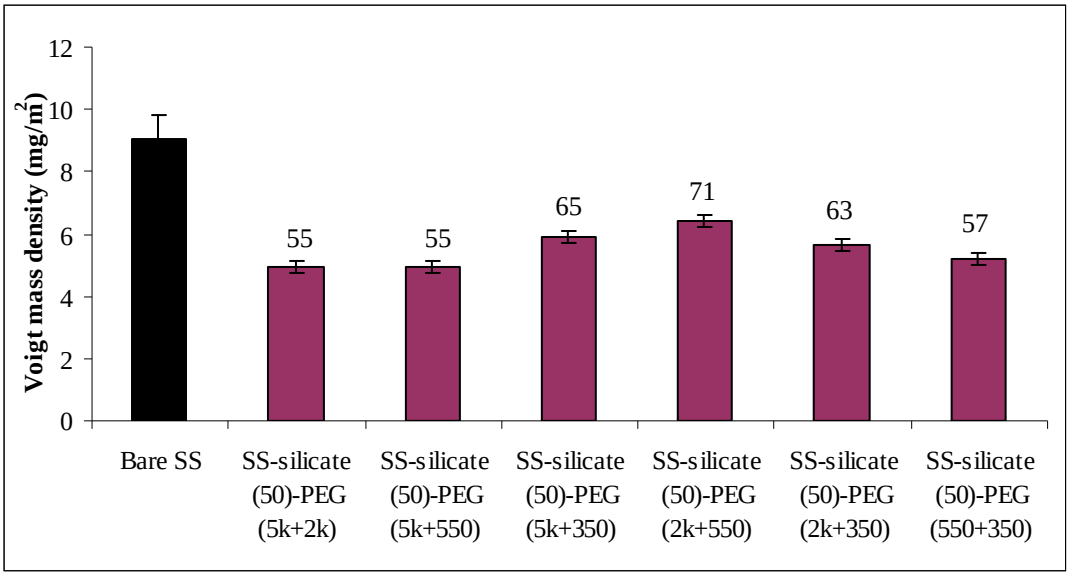

Figure 6.41: The Voigt mass density of tightly-bound β-casein on the bimodal SS-silicate (50)-PEG surfaces for PEG of various combinations at 40°C. The surfaces were prepared using PEG solution concentration of 1 g / L. Values above bars are *percentage* of strong adsorption compared to that on the bare SS surface.

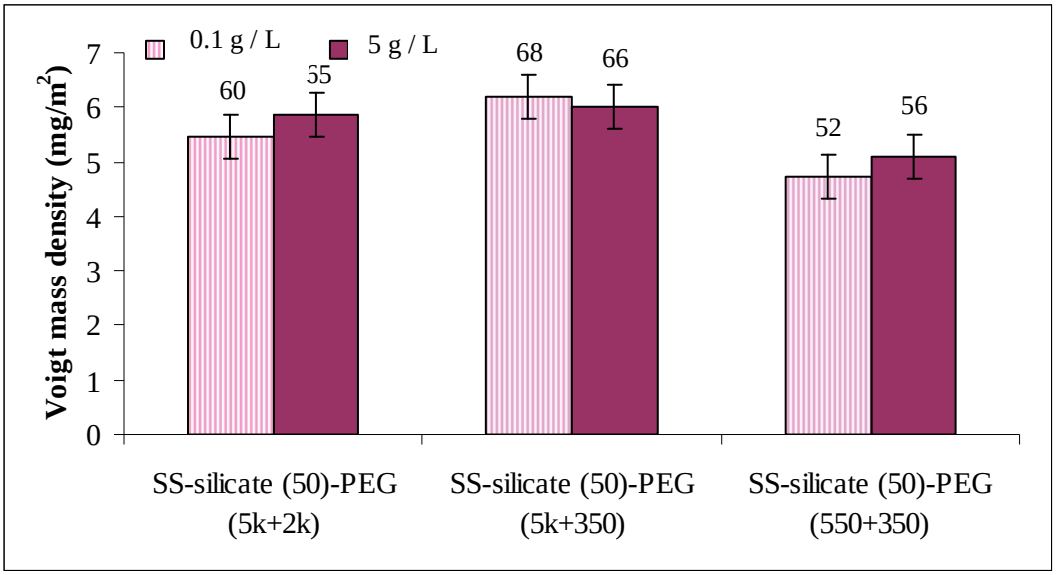

Figure 6.42: The Voigt mass density of tightly-bound β-casein on the bimodal SS-silicate (50)-PEG surfaces for PEG of various combinations at 40°C. The surfaces were prepared using PEG solution concentration of 0.1 and 5 g / L. Values above bars are *percentage* of strong adsorption compared to that on the bare SS surface.

6.4.1.3 Mass density of β-casein on bimodal SS-PEI (30)-PEGNHS surfaces

Figure 6.43 shows the Voigt mass density of tightly-bound β-casein adsorbed on the bimodal SS-PEI (30)-PEGNHS (5k+2k) surfaces at temperatures of 23 and 40 °C. The surfaces were prepared using PEG-NHS of 1 g / L. As can be seen, the mass density of β-casein adsorbed was down to about 50 % at the two temperatures compared to that on the bare SS surface.

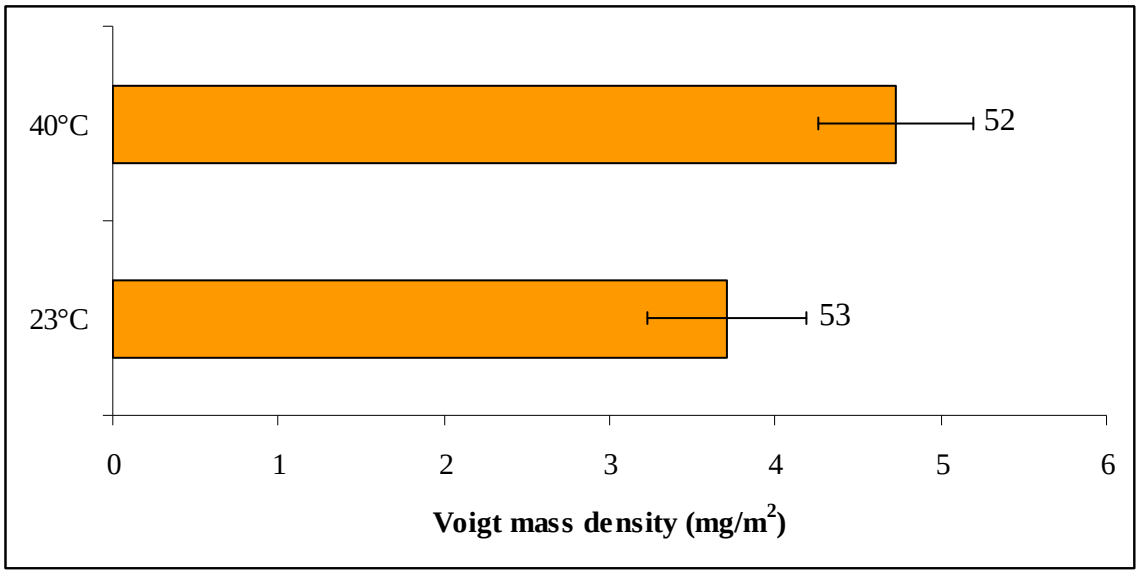

Figure 6.43: The Voigt mass density of tightly-bound β-casein adsorbed on the bimodal-SS-PEI (30)-PEGNHS (5k+2k) surfaces at temperatures of 23 and 40 °C. The surfaces were prepared using PEGNHS of 1 g / L. Values above bars are percentage of *strong adsorption* compared to that on the bare SS surface.

6.4.2 Lysozyme

6.4.2.1 Mass density lysozyme on bimodal SS-PEI (30)-PEG surfaces: Effects of temperature, PEG concentration and combination

Figure 6.44 shows the mass density of tightly-bound lysozyme on bimodal SS-PEI (30)-PEG surfaces for PEG of various combinations at a temperature of 23 °C. The surfaces were prepared using PEG solution concentration of 1 g / L. Unlike β-casein, the adsorption of lysozyme was much lower on the bimodal PEG surfaces that that of the monomodal PEG surfaces especially using combination of PEG5k and 2k Da; the adsorption of lysozyme was down to 1 % on this surface.

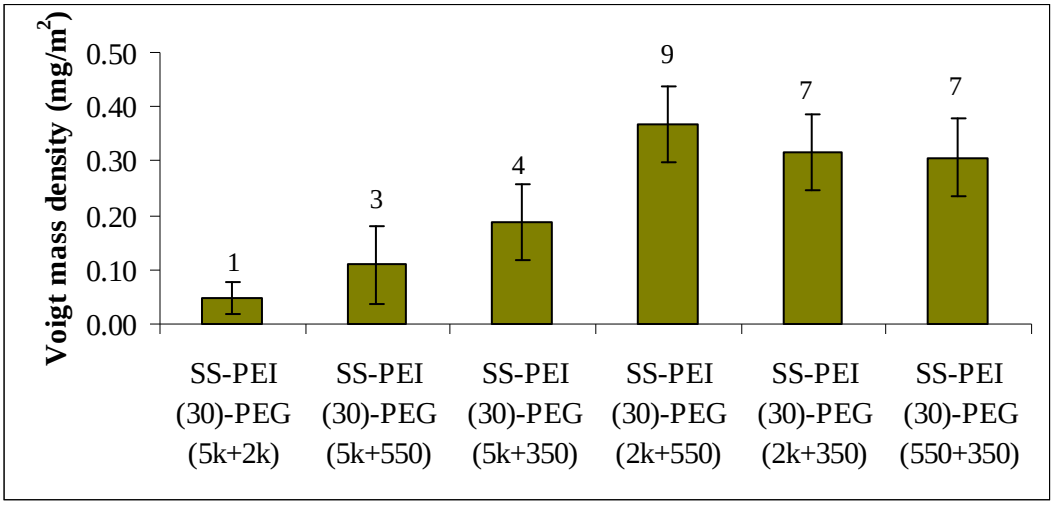

Figure 6.44: The Voigt mass density of tightly-bound lysozyme on bimodal SS-PEI (30)-PEG surfaces for PEG of various combinations at 23 °C. The surfaces were prepared using PEG solution concentration of 1 g / L. Values above bars are *percentage* of strong adsorption compared to that on the bare SS surface.

There was no difference generally on the adsorption of lysozyme either performed at a temperature of 23 or at 40 °C as shown in Figure 6.45.

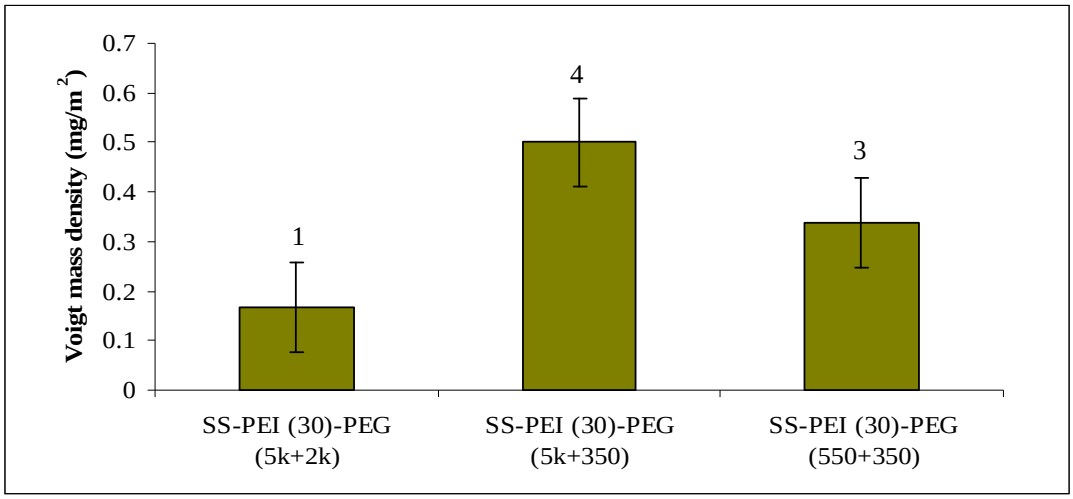

Figure 6.45: The Voigt mass density of tightly-bound lysozyme on bimodal SS-PEI (30)-PEG surfaces for PEG of various combinations at 40 °C. The surfaces were prepared using PEG solution concentration of 1 g / L. Values above bars are percentage of *strong adsorption* compared to that on the bare SS surface.

Nevertheless, the adsorption of lysozyme was higher on the bimodal PEG surfaces prepared using PEG solution concentration of 0.1 and 5 than that of 1 g / L (refer to Figure 6.46).

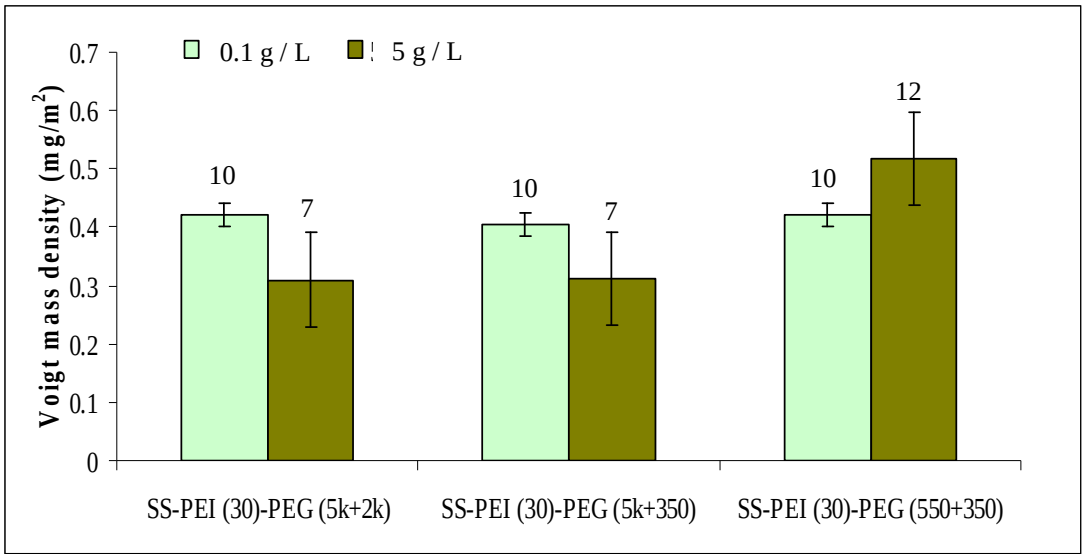

Figure 6.46: The Voigt mass density of tightly-bound lysozyme on bimodal SS-PEI (30)-PEG surfaces for PEG of various combinations at 23 °C. The surfaces were prepared using PEG solution concentration of 0.1 and 5 g / L. Values above bars are percentage of *strong adsorption* compared to that on the bare SS surface.

6.4.2.2 Mass density lysozyme on bimodal SS-silicate (50)-PEG surfaces: Effects of temperature, PEG concentration and combination

Figure 6.47 displays the Voigt mass density of tightly-bound lysozyme on bimodal SS-silicate (50)-PEG surfaces for PEG of various combinations at 23 °C. The surfaces were prepared using PEG concentration of 1 g / L. Comparing Figures 6.44 and 6.47, the bimodal SS-silicate (50)-PEG surfaces appeared to be less competent to inhibit adsorption of lysozyme compared to that of the bimodal SS-PEI (30)-PEG surfaces.

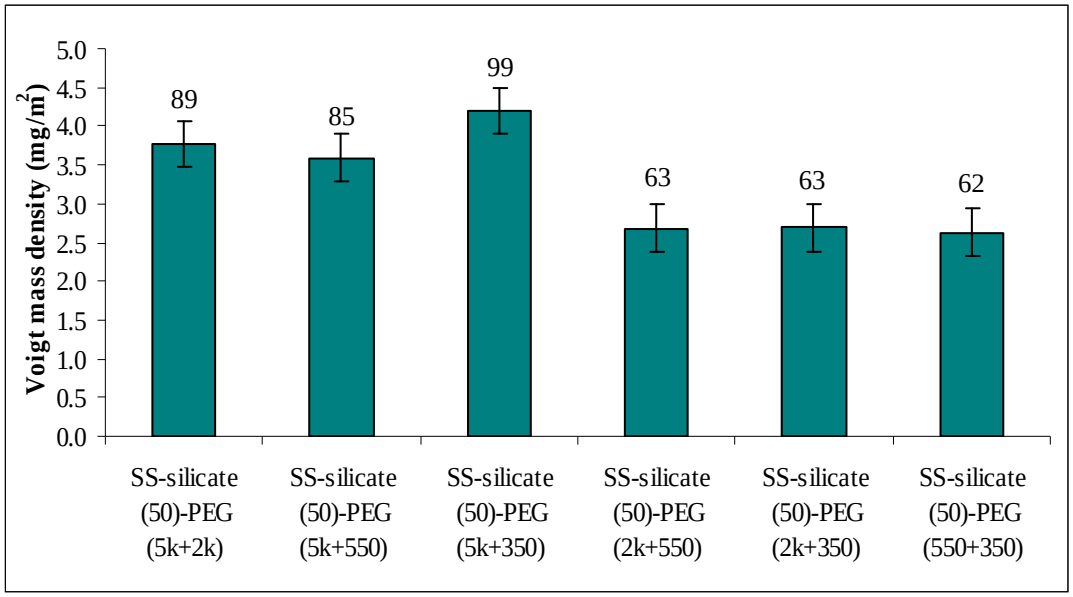

Figure 6.47: The Voigt mass density of tightly-bound lysozyme on bimodal SS-silicate (50)-PEG surfaces for PEG of various combinations at 23 °C. The surfaces were prepared using PEG solution concentration of 1 g / L. Values above bars are percentage of *strong adsorption* compared to that on the bare SS surface.

The adsorption of lysozyme was slightly lower on the surfaces which were prepared using either 0.1 or 5 than of 1 g / L. Yet, the adsorption still was higher on the bimodal SS-silicate (50)-PEG surfaces if compared to that on the bimodal SS-PEI (30)-PEG surfaces.

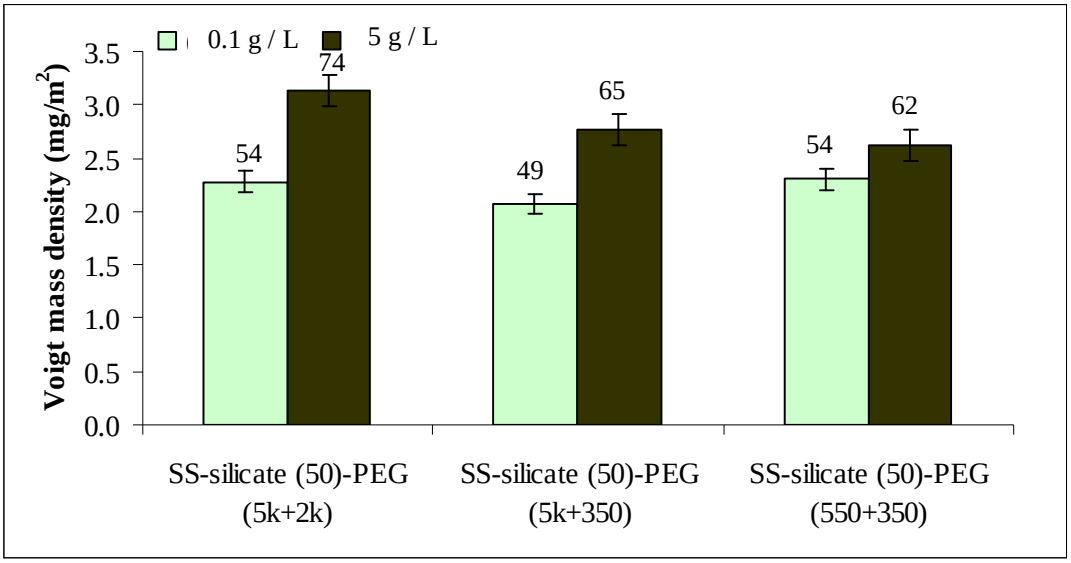

Figure 6.48: The Voigt mass density of tightly-bound lysozyme on bimodal SS-silicate (50)-PEG surfaces of various combinations at a temperature of 23 °C. The surfaces were prepared using PEG concentration of 0.1 and 5 g / L. Values above bars are percentage of *strong adsorption* compared to that on the bare SS surface.

Interestingly, increasing the temperature from 23 to 40 °C greatly reduced the adsorption of lysozyme (see Figure 6.49).

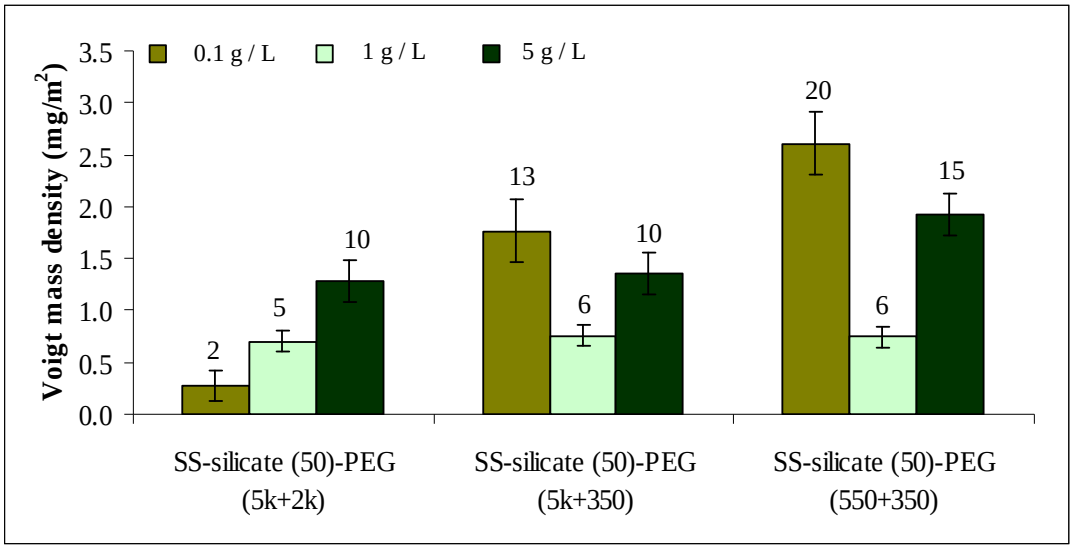

Figure 6.49: The Voigt mass density of tightly-bound lysozyme on bimodal SS-silicate (50)-PEG surfaces for PEG of various combinations at 40 °C. The surfaces were prepared using PEG solution concentration of 0.1, 1 5 g / L. Values above bars are percentage of *strong adsorption* compared to that on the bare SS surface.

6.4.2.3 Mass density of lysozyme on bimodal SS-PEI (30)-PEGNHS surfaces

Figure 6.50 shows the Voigt mass density of tightly-bound lysozyme adsorbed on the bimodal SS-PEI (30)-PEGNHS (5k+2k) surface at temperatures of 23 and 40 °C. Interestingly, the adsorption was down to 1 % at the two temperatures.

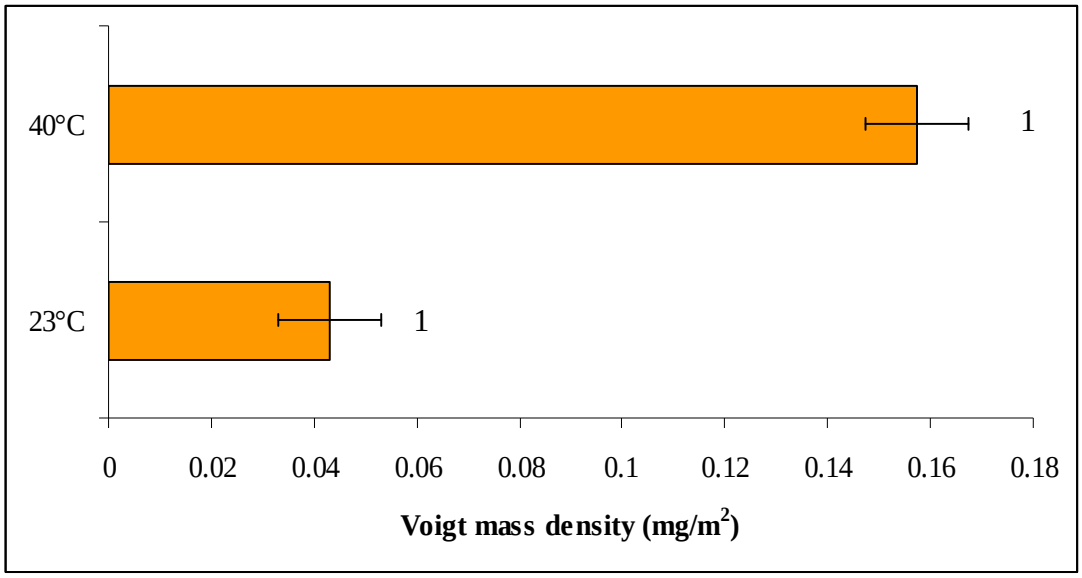

Figure 6.50: The Voigt mass density of lysozyme adsorbed on the bimodal SS-PEI (30)-PEGNHS (5k+2k) surfaces at temperatures of 23 and 40 °C. The surfaces were prepared using PEGNHS solution concentration of 1 g / L. Values above bars are percentage of *strong adsorption* compared to that on the bare SS surface.

6.4.3 α-lactalbumin

6.4.3.1 Mass density of α-lactalbumin on bimodal SS-PEI (30)-PEG surfaces: Effects of temperature, PEG solution concentration and combination

Figure 6.51 shows the mass density of tightly-bound α-lactalbumin on the bimodal SS-PEI (30)-PEG surfaces at 23 °C. The horizontal dashed line was drawn at the bare SS value to make an easy comparison between modified and unmodified surfaces. Similarly to the adsorption on the monomodal SS-PEI (30)-PEG surfaces, the adsorption of α-lactalbumin also was higher on the bimodal SS-PEI (30)-PEG surfaces compared to that on the bare SS.

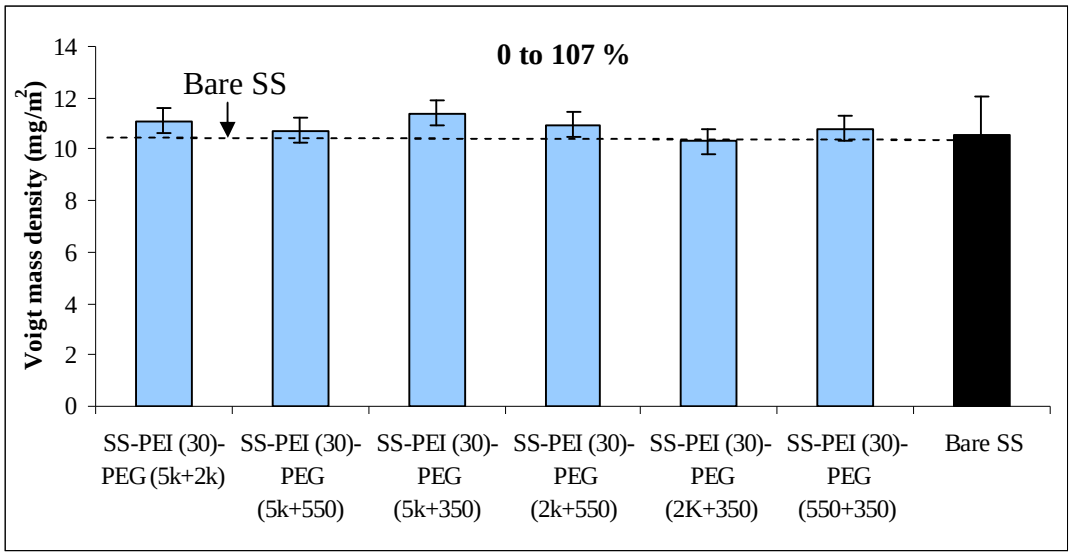

Figure 6.51: The Voigt mass density of tightly-bound α-lactalbumin on a bare SS and bimodal SS-PEI-PEG surfaces for PEG of various combinations at 23 °C. The surfaces were prepared using PEG concentration of 1 g / L. Values above bars are *percentage* of strong adsorption compared to that on the bare SS surface.

Changing either the temperature from 23 to 40 °C or PEG concentration from 1 g / L to either 0.1 or 5 g / L, seemed to not give any changes on the adsorption of α-lactalbumin; the adsorption was *higher* with the presence of PEG molecules (see Figures 6.52 and 6.53).

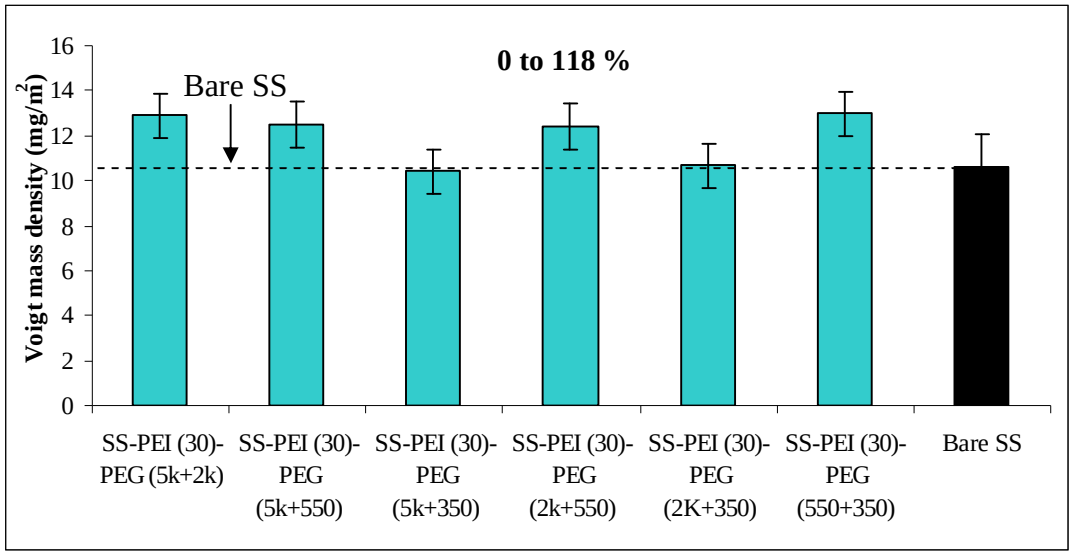

Figure 6.52: The Voigt mass density of tightly-bound α-lactalbumin on a bare SS and bimodal SS-PEI-PEG surfaces for PEG of various combinations at 40 °C. The surfaces were prepared using PEG solution concentration of 1 g / L. Values above bars are *percentage* of strong adsorption compared to that on the bare SS surface.

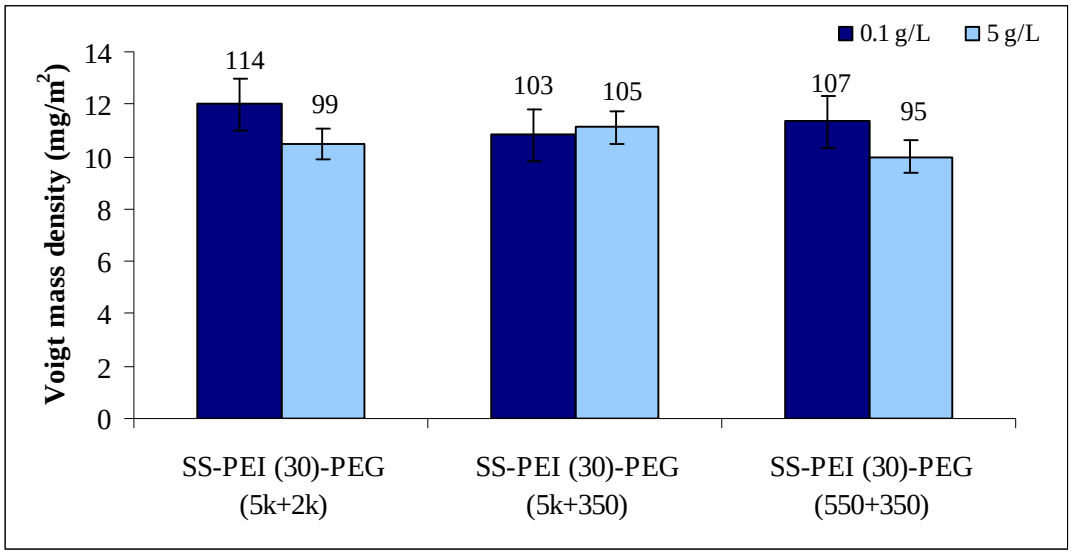

Figure 6.53: The Voigt mass density of tightly-bound α-lactalbumin on bimodal SS-PEI (30)-PEG surfaces for PEG of various combinations at 23 °C. The surfaces were prepared using PEG solution concentration of 0.1 and 5 g / L. Values above bars are percentage of *strong adsorption* compared to that on the bare SS surface.

6.4.3.2 Mass density of α-lactalbumin on SS-silicate (50)-PEG surfaces: Effects of temperature, PEG concentration and combination

There was no difference on the adsorption of α-lactalbumin on the SS-silicate (50)-PEG surfaces either on any PEG combinations, on any PEG solution concentrations, on any PEG moieties (OH or NHS) or on any temperatures; the adsorption was *higher* on the modified surfaces than of the bare SS surface (Figures are not shown).

6.5 Holo α-lactalbumin (calcium enriched)

6.5.1 Adsorption of holo α-lactalbumin onto SS-PEI (30)-PEG and SS-silicate (50)-PEG surfaces

From the results of Parts C and D, it showed that adsorption of apo α-lactalbumin was higher on both of the SS-PEI (30)-PEG and the SS-silicate (50)-PEG surfaces compared to that on the bare SS surface. This section presents the adsorption of holo α-lactalbumin (that is, calcium-enriched) proteins on bare SS, SS-PEI (30), SS-PEI (30)-PEG, SS-silicate (50) and SS-silicate (50)-PEG surfaces as a comparison to that of apo α-lactalbumin (that is, calsium-depleted) adsorption.

Interesting to note, the adsorption of holo α-lactalbumin was down to less than 16 % on the SS-PEI (30)-PEG surfaces. The adsorption on the SS-PEI surface meanwhile was down to about 30 % (see Figure 6.54).

Unexpectedly, the adsorption of holo α-lactalbumin on the SS-silicate (50)-PEG based surfaces was generally *higher* than that on the bare SS surface as can be seen in Figure 6.55. The mechanisms involved will be discussed in Chapter 11.

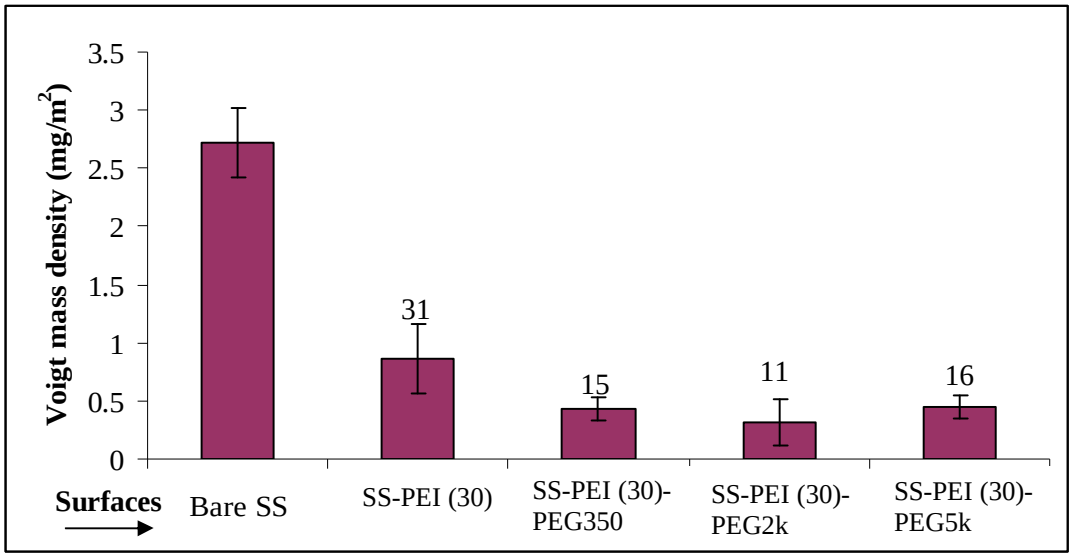

Figure 6.54: The Voigt mass density of tightly-bound holo α-lactalbumin on bare SS, SS-PEI (30) and SS-PEI (30)-PEG surfaces for PEG of various molecular weights at 23°C. The surfaces were prepared using PEG concentration of 1 g / L. Values above bars are percentage of *strong adsorption* compared to that on the bare SS surface.

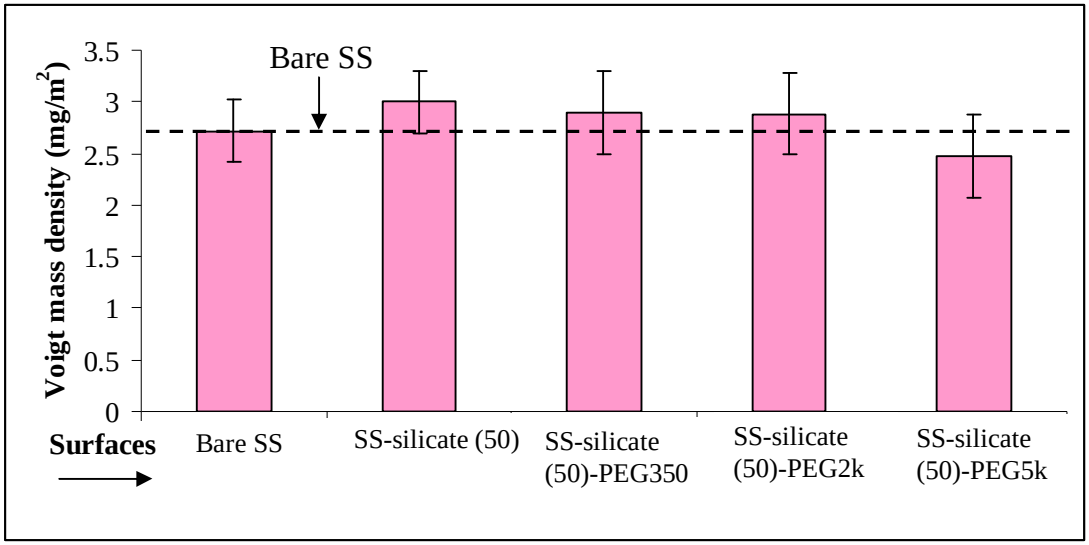

Figure 6.55: The Voigt mass density of tightly-bound holo α-lactalbumin on bare SS, SS-silicate (50) and SS-silicate (50)-PEG surfaces for PEG of various molecular weights at 23°C. The surfaces were prepared using PEG concentration of 1 g / L

SUMMARY

The results obtained in this part, can be summarized by:

Adsorption on monomodal PEG surfaces

a) β-casein

- Adsorption of β-casein was down to 62 % on SS-PEI (30)-PEG surfaces whereas more than 50 % on SS-silicate (50)-PEG surfaces.
- Adsorption of β-casein was slightly higher at 40 than that at 23 °C on SS-PEI (30)-PEG surfaces and vice versa on SS-silicate (50)-PEG surfaces.
- SS-silicate (50)-PEG surfaces were slightly better to inhibit adsorption of β-casein than that of SS-PEI (30)-PEG surfaces.
- Surfaces which were prepared using PEG-NHS were less competent to inhibit adsorption of β-casein compared to that of the surfaces with PEG-OH.
- Generally, PEG with molecular weight of 2k Da more superior to inhibit adsorption of β-casein than the others.

b) Lysozyme

- Adsorption of lysozyme was down to 4 % on the monomodal PEG surfaces.
- Adsorption of lysozyme on both SS-PEI (30)-PEG and SS-silicate (50)-PEG surfaces was lower at 40 °C than that at 23 °C; by up to 40 %.
- At 23 °C, the SS-PEI (30)-PEG surfaces were better to inhibit adsorption of lysozyme than that of the SS-silicate (50)-PEG surfaces. However, at 40 °C, the percentage of lysozyme adsorption was almost the same on both SS-PEI (30)-PEG and SS-silicate (50)-PEG surfaces.
- Neither PEG solution concentration nor PEG molecular weight significantly influenced the adsorption of lysozyme.

c) Apo α-lactalbumin

- The adsorption of apo α-lactalbumin was generally enhanced with the presence of PEG molecules.

Adsorption on bimodal PEG surface

a) β-casein

- Adsorption of β-casein was 50 % higher at 40 than that at 23 °C on both the bimodal SS-PEI (30)-PEG and SS-silicate (50)-PEG surfaces.
- At 23 °C, β-casein adsorption on the bimodal SS-PEI (30)-PEG surfaces generally increased by up to 24 %.
- Surfaces which were prepared using PEG-NHS were able to decrease the adsorption of β-casein to up 50 % at the two temperatures.
- Bimodal SS-silicate (50)-PEG surfaces were slightly better to inhibit adsorption of β-casein than that of the bimodal SS-PEI (30)-PEG surfaces.
- Generally, combination between PEG5k and 2k Da was superior to inhibit adsorption of β-casein than the others combinations.

c) Lysozyme

- The adsorption of lysozyme was down to 1 % on SS-PEI (30)-PEG surfaces.
- Adsorption of lysozyme on SS-PEI (30)-PEG surfaces was not influence much by the ranged of temperature used and vice versa on the SS-silicate (50)-PEG surfaces. The adsorption was almost 90 % higher at 23 than that at 40 °C on the SS-silicate (50)-PEG surfaces.
- SS-PEI (30)-PEG surfaces were generally more capable to inhibit adsorption of lysozyme than SS-silicate (50)-PEG surfaces.
- Surfaces which were prepared using PEG-NHS was able to reduce the adsorption of lysozyme to 1 % at the two temperatures.
- Surfaces which were prepared using combinations of PEG5k and 2k Da were generally better to inhibit adsorption of lysozyme than the other combinations.

c) Apo α-lactalbumin

- The adsorption of apo α-lactalbumin was higher on the bimodal PEG surfaces than that of the bare SS surface.

CHAPTER SEVEN

ADSORPTION OF PROTEINS ONTO PROTEIN-PEG SURFACES

7.0 Introduction

This chapter covers the results obtained on the adsorption of protein onto protein-PEG based surfaces. The stainless steel surfaces (SS) were modified by coating the surface with a protein layer (as a base) then followed by the attachment of PEG molecules. This technique was developed based on the fact that proteins naturally adsorbed spontaneously on any solid surfaces, in any conditions. Three different proteins were used as a base layer for the PEG attachment; (i) β-casein (ii) β-lactoglobulin and (iii) lysozyme. β-casein and β-lactoglobulin were used as these proteins were present in milk in the dairy industry. Lysozyme meanwhile was used because; (i) it is a 'hard' protein, (ii) able to form a compact monolayer (has a small size) and (iii) has higher affinity towards a stainless steel surface (low percentage of desorption, refer to Chapter 6 and Shen et al., 2005**)**. PEG with various end-groups (that is, OH, NHS and CH_3), molecular weights (that is, 350, 2000, 5000, 20,000 and 40,000 Da) and concentrations (that is, 1 and 5 g / L) were used in this part of experiment. The effectiveness of the modified surfaces to inhibit adsorption of proteins at room temperature (23 °C) was tested on β-casein, β-lactoglobulin, lysozyme, apo and holo α-lactalbumin samples. The concentration of the tested proteins used was 0.1 g / L.

Protein was adsorbed from a single protein solution and a mixed protein solution at the concentrations of milk on the modified and unmodified SS surfaces, to represent more closely the real situation in the dairy industry. The adsorption of the mixed protein was conducted at 23, 40 and 80 °C.

Overall, the reduction of protein adsorption on the SS-protein-PEG based surfaces was highly significant. An excellent protein adsorption inhibition at room

temperature and body temperature was a great achievement. The mechanism related to this finding will be clarified and discussed in Chapter 11.

7.1 β-casein (0.1 g / L) as a base layer for PEG attachment

For the first trial, a stainless steel surface was *coated* with β-casein from 0.1 g / L solution, then *coated* with PEG from 1 g / L solution of various molecular weights (also from 5 g / L solution for PEG5k Da). β-casein was then adsorbed on the prepared surfaces (we represent the prepared surface as SS-β casein-PEG in this case). The Voigt mass density of tightly bound β-casein (0.1 g / L) adsorbed on the SS-β casein-PEG surfaces for PEG of various molecular weights is depicted in Figure 7.1. Values above the bars are percentages of strong adsorption compared to that on the bare SS surface.

As can be seen, the reduction of β-casein was the best on the SS-β casein (0.1)-PEG5k (5) surface; the adsorption was down to less than 10 % on this surface. Meanwhile, there was no significant difference in adsorption of β-casein between the rest of the surfaces, about 21 to 24 % of adsorption.

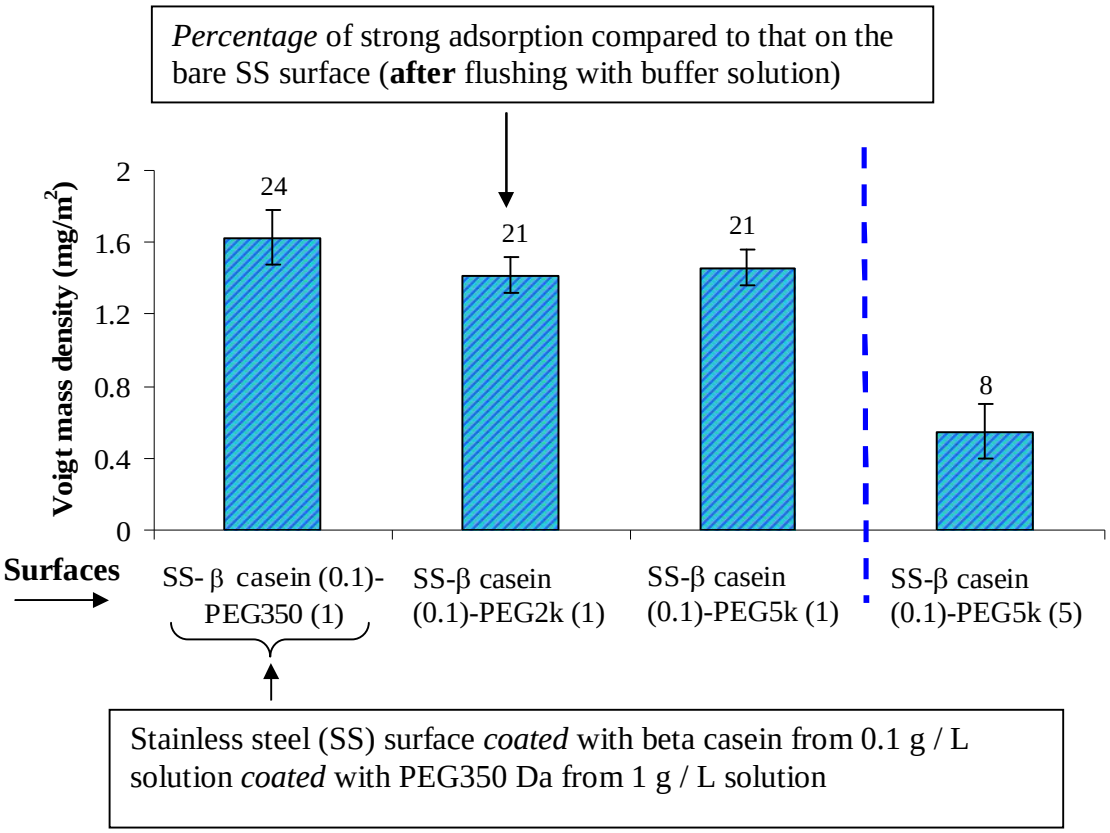

Figure 7.1: The Voigt mass density of tightly-bound β-casein (0.1 g / L) adsorbed on SS-β casein-PEG surfaces for PEG of various molecular weights at a temperature of 23 °C.

In general, the results obtained showed that the SS-β casein-PEG surfaces were able to repel adsorption of β-casein much better than that of the SS-PEI-PEG and SS-silicate-PEG surfaces. The adsorption of β-casein on previous modified surfaces was more than 50 % of that on the bare SS surface (see Chapter 6, part C and D). This is also a significant reduction in adsorption by applying PEG5000 from a stronger solution.

7.2 β-lactoglobulin (0.1 g / L) as a base layer for PEG attachment

For the second trial, a stainless steel surface was *coated* with β-lactoglobulin from 0.1 g / L from solution, *coated* with PEG5k Da from 1 g / L solution to produce a SS-β lactoglobulin (0.1)-PEG5k (1) surface. Then, β-lactoglobulin, β-casein and apo α-lactalbumin were deposited on the modified SS surface separately. The mass density of tightly-bound β-lactoglobulin, β-casein and apo α-lactalbumin adsorbed on the SS-β lactoglobulin (0.1)-PEG5k (1) surfaces at 23 °C is shown Figure 7.2. As can be seen, the adsorptions of the proteins follow the adsorption on the bare SS surface (similar proportions for each). It was interesting to note that, the prepared surface was able to *reduce* the adsorption of apo α-lactalbumin protein (from the previous results reported in Chapter 6, the adsorption of apo α-lactalbumin was *increased* with the presence of PEG molecules). This observation will be discussed in Chapter 11.

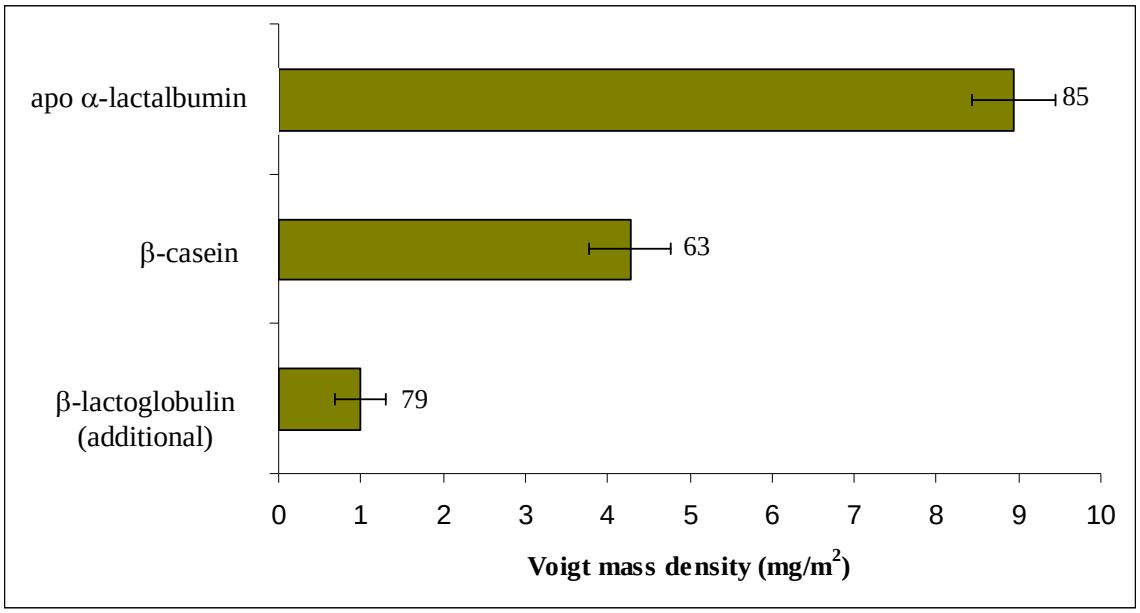

Figure 7.2: The Voigt mass density of *tightly-bound* β-lactoglobulin, β-casein and apo α-lactalbumin adsorbed on SS-β lactoglobulin (0.1)-PEG5k (1) surfaces at a temperature of 23 °C. Values to the right of the bars are strongly held adsorptions as a *percentage* of that on the bare SS surface.

Since β-lactoglobulin has been used for the first time in this work, adsorptions on the SS-PEG-PEI and SS-PEG-silicate based surfaces were also carried out as a comparison. Figure 7.3 shows the adsorption of β-lactoglobulin on bare SS, silicate, silicate-PEG5k (1), PEI and PEI-PEG5k (1) surfaces.

Generally, adsorption of β-lactoglobulin was lower on the modified surfaces than that on the bare SS surface. PEI and PEI-PEG5k (1) surfaces appeared to be slightly better in rejecting adsorption of β-lactoglobulin compared to that on silicate and silicate-PEG surfaces. However, β-lactoglobulin adsorptions on PEI and PEI-PEG surfaces (or silicate and silicate-PEG surfaces) were almost the same, indicating that PEG has no significant role in rejection of β-lactoglobulin adsorption. Comparing Figures 7.3 and 7.2, showed that the use of β-lactoglobulin as an attachment anchor for PEG5k showed little difference in the adsorption of β-lactoglobulin compared with the other treatments shown in Figure 7.3. Thus, indicating that this protein (β-lactoglobulin) is not effective as an anchor.

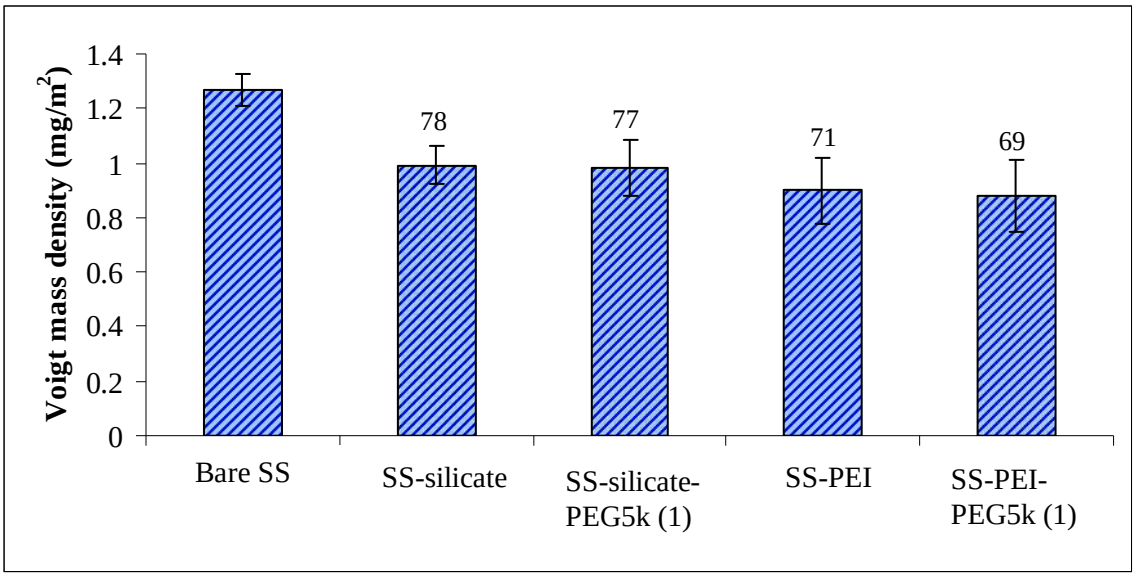

Figure 7.3: The Voigt mass density of *tightly-bound* β-lactoglobulin (0.1 g / L) adsorbed on a bare, silicate and silicate-PEG5k (1), PEI and PEI-PEG5k (1) surfaces at a temperature of 23 °C. Values above bars are *percentage* of strong adsorption compared to that on the bare SS surface.

7.3 Lysozyme (4 g / L) as a base layer for PEG attachment

For the third trial, lysozyme has been chosen as a protein layer for the attachment of PEG molecules. In this screening stage, the PEG molecules with different moieties (NHS, OH and CH_3) and molecular weights (5, 20 and 40 kDa) were attached on a stainless steel surface *coated* with lysozyme from 4 g / L solution (we represent the prepared surface as SS-lysozyme (4) in this case). 4 g / L solution was used to achieve a faster steady state. β-casein (0.1 g / L) adsorption was then performed on the prepared surfaces. β-casein was also adsorbed on a SS-lysozyme (4) surface (without the presence of PEG molecules) as a comparison.

Figure 7.4 shows the chain density of tightly-bound PEG5k (5), PEG-OH (1) PEG-NHS20k (1) and PEG-NHS40k (1) on a SS-lysozyme (4) surface (plotted on a log scale). For clarification, PEG, PEG-OH and PEG-NHS refer to OH-PEG-CH_3, OH-PEG-OH and OH-PEG-NHS, respectively. As observed, the sequence of the chain density from low to high is as follows; PEG-NHS20k (1) > PEG5k (5) > PEG-NHS40k (1) > PEG-OH20k (1).

The Voigt mean layer thickness for those PEGs (from Figure7.4) can be obtained directly from the Voigt analysis (refer to Chapters 5). The spacing between chains, *d*, meanwhile can be calculated using Equation 7.1

$$d = \sigma^{-0.5} \tag{7.1}$$

where σ is a PEG grafting density (chains/area)

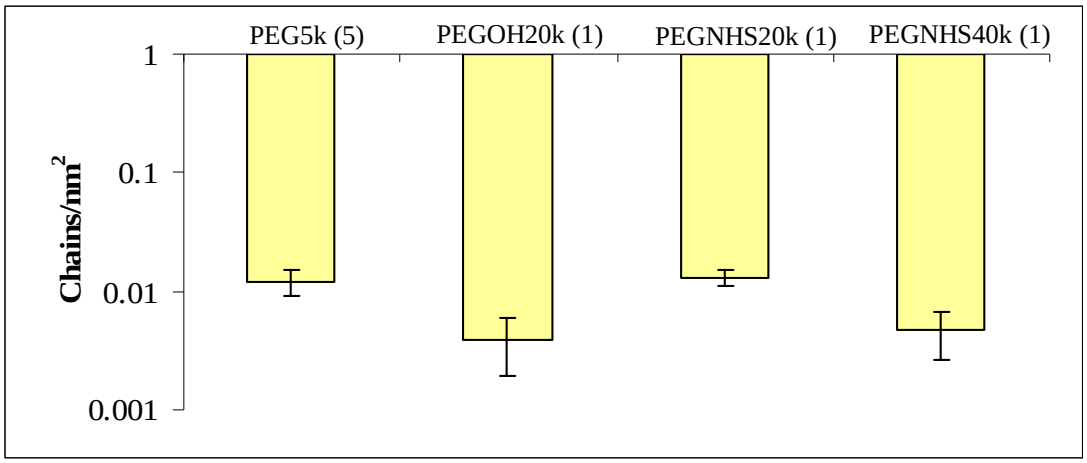

Figure 7.4: Chain density of tightly-bound PEG molecules (different moieties and molecular weights) on a stainless steel surface *coated* with lysozyme from 4 g / L solution (plotted on a log scale).

The mass density of tightly bound β-casein adsorbed on the modified surfaces is depicted in Figure 7.5. As can be seen, the presence of PEG-NHS20k (1), PEG-OH20k (1) and PEG-OH5k (5) molecules greatly reduced the adsorption of β-casein; the adsorption was down to about 5 %, compared to that on the bare SS surface. Unexpectedly, the adsorption of β-casein on the surface prepared using PEG-NHS40k (1) was almost 80 % higher than that on the PEG-OH20k even though the surfaces had almost the same PEG chain density (Figure 7.4).

It was interesting to note that, a SS-lysozyme surface (that is, without the presence of PEG molecules) able to limit the adsorption of β-casein to less than 20 % of that on the bare SS surface. This observation was more interesting since lysozyme and β-casein proteins have different net charges yet repulsion occurred. As a comparison, the SS-lysozyme (4)-PEG based surface appeared to be a better surface to inhibit adsorption of β-casein than SS-β casein-PEG (refer Figure 7.1) or SS-β lactoglobulin-PEG (refer Figure 7.2) based surfaces. Therefore, the SS-lysozyme (4)-PEG5k (5) surface was used for further runs.

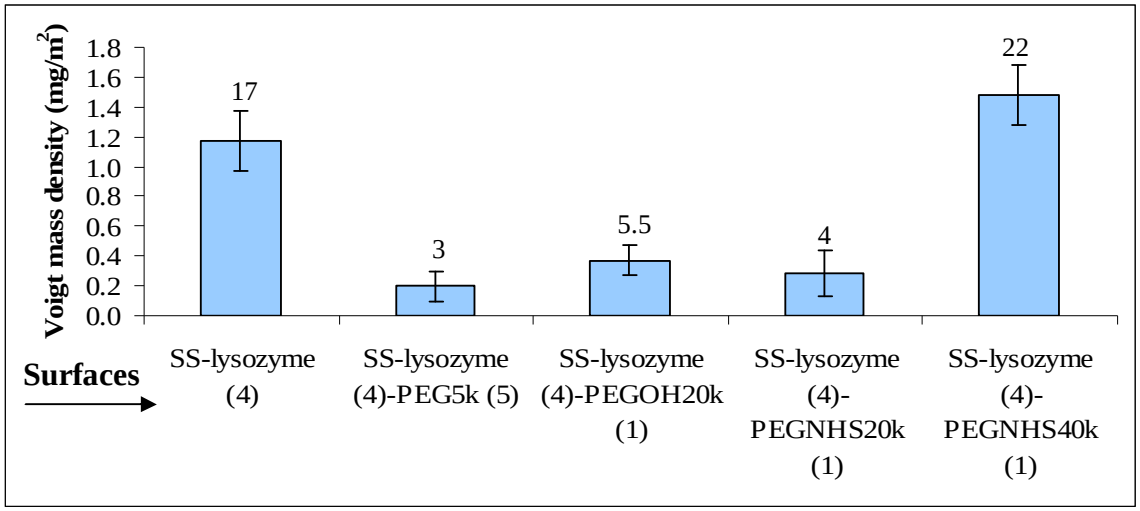

Figure 7.5: The Voigt mass density of tightly-bound β-casein (0.1 g / L) adsorbed on the various surfaces at a temperature of 23 °C. Values above bars are *percentage* of strong adsorption compared to that on the bare SS surface.

Table 7.1 displays the properties of the based protein layer used (that is, lysozyme, β-casein and β-lactoglobulin) for the attachment of PEG molecules. The data shown are those after flushing with buffer solution (strongly held adsorption) and was analyzed using the Voigt model (refer to Chapter 5 for the calculation of number density, and mean spacing between molecules).

Table 7.1: Lysozyme, β-casein and β-lactoglobulin protein layer properties on a bare stainless steel surface at a temperature of 23 °C obtained from the Voigt model (strongly held adsorption).

	Lysozyme (4 g / L)	β-casein (0.1 g / L)	β-lactoglobulin (0.1 g / L)
Surface density (mg/m^2)	8.0 ± 0.4	6.9 ± 0.1	1.26 ± 0.06
Surface number density ($molecules/nm^2$)	0.33 ± 0.01	0.18 ± 0.03	0.042 ± 0.002
Mean layer thickness (nm)	6.75 ± 0.30	5.73 ± 0.08	1.05 ± 0.05
Mean spacing between molecules (nm)	1.75 ± 0.04	2.35 ± 0.02	4.86 ± 0.13
Dimension (nm)	3 x 3 x 4.5	*R = 2.3	*R = 3.6
Estimation of monolayer density (mg/m^2)	3 (end-on adsorption) [Shem et al, 2005)]	2.3 [Veen et al, 2009]	1.47

*R is a molecule radius

7.4 Adsorption of proteins onto SS-lysozyme (4)-PEG5000 (5) surfaces

Figure 7.6 shows the Voigt mass density of β-lactoglobulin, lysozyme, holo α-lactalbumin and β-casein adsorbed on a SS-lysozyme (4)-PEG5k (5) surface. As can be seen, there was almost no adsorption of β-lactoglobulin on the surface. The adsorption of holo α-lactalbumin and β-casein was almost the same. Meanwhile, the use of either lysozyme or β-lactoglobulin (refer to Figure 7.2) as an attachment vehicle for PEG showed almost the same in the adsorption of apo α-lactalbumin (the adsorption of apo α-lactalbumin on the SS-lysozyme (4)-PEG5k (5) surface was 87 % of that on the bare SS surface (a figure is not shown)). The explanation for this observation is in Chapter 11.

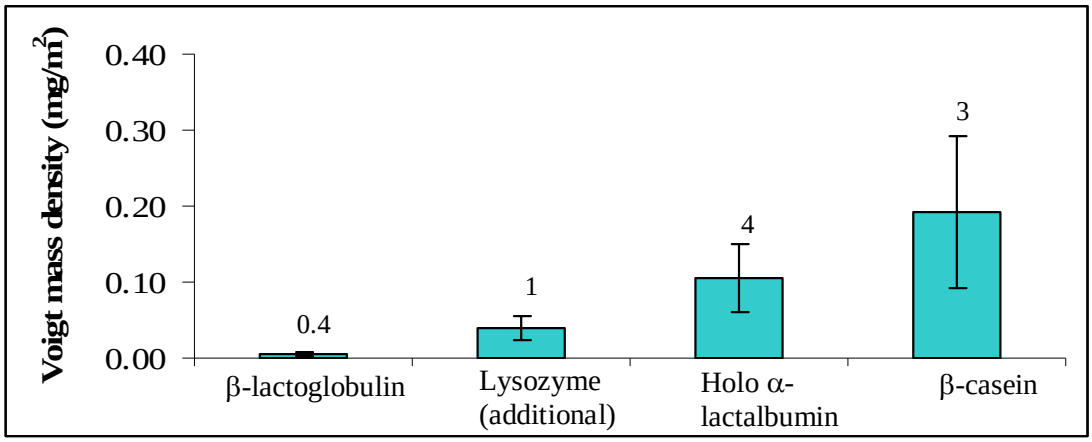

Figure 7.6: The Voigt mass density of tightly-bound β-lactoglobulin, lysozyme, holo α-lactalbumin and β-casein adsorbed on the SS-lysozyme (4)-PEG5k (5) surface at temperature 23 °C. Values above bars are *percentage* of strong adsorption compared to that on the bare SS surface.

7.5 Adsorption of proteins onto SS-lysozyme (4) surfaces

The four proteins (Figures 7.6) were further adsorbed on a SS-lysozyme (4) surface (without the presence of PEG molecules). This was to find the role of PEG5k (5) molecules on inhibition of the protein adsorption. The result obtained is depicted in Figures 7.7 and 7.8. In general, the adsorption of β-casein and β-lactoglobulin were higher on the SS-lysozyme (4) surface than that on the SS-lysozyme (4)-PEG5000 (5) surface.

.

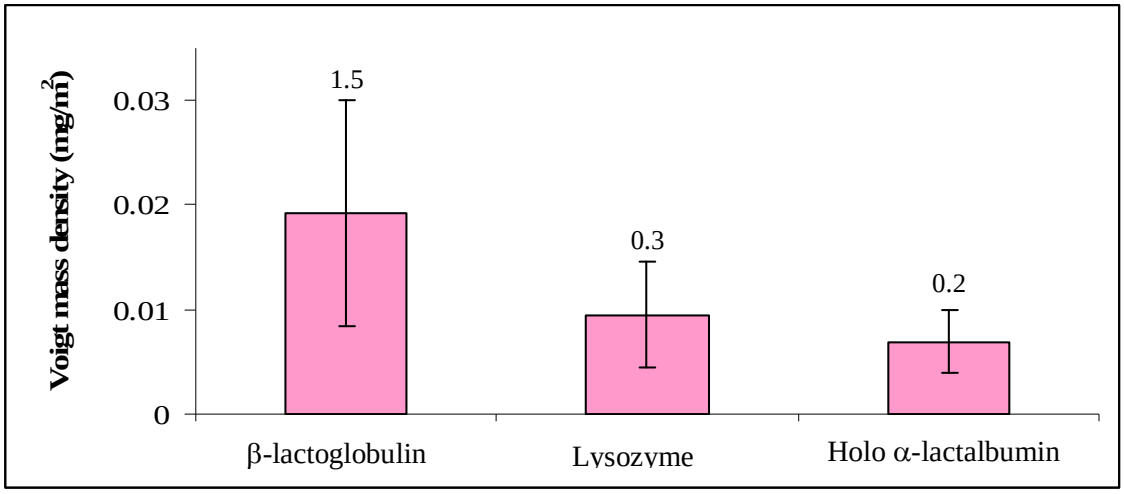

Figure 7.7: The Voigt mass density of *tightly-bound* β-lactoglobulin, lysozyme and holo α-lactalbumin adsorbed on the SS-lysozyme (4) surfaces at a temperature of 23 °C. Values above bars are *percentage* of strong adsorption compared to that on the bare SS surface.

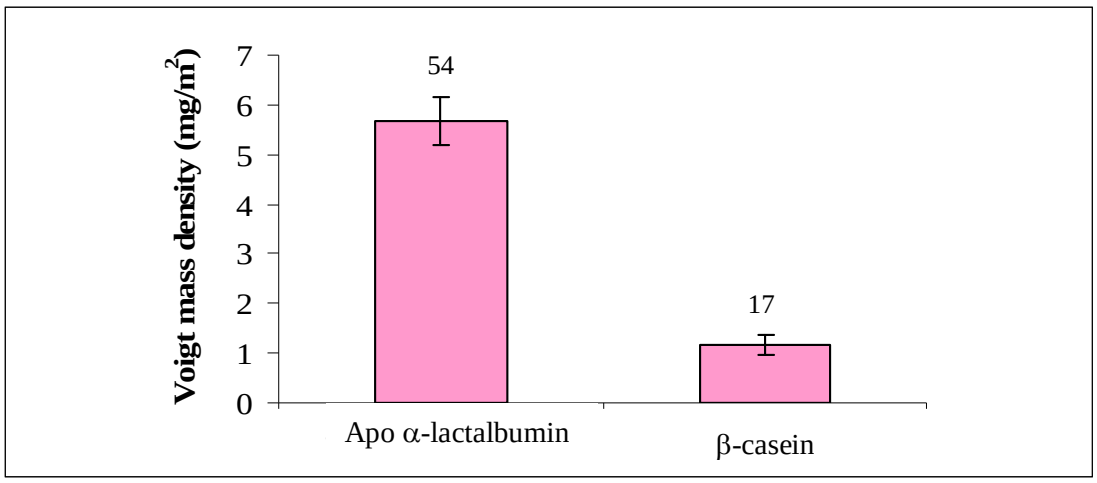

Figure 7.8: The Voigt mass density of *tightly-bound* apo α-lactalbumin and β-casein adsorbed on the SS-lysozyme (4) surfaces at a temperature of 23 °C. Values above bars are *percentage* of strong adsorption compared to that on the bare SS surface.

The role of PEG molecules on the inhibition of the protein adsorption can be seen easily by comparing the adsorption on the SS-lysozyme (4)-PEG5000 (5) surface to that on the SS-lysozyme (4) surface (refer to Table 7.2). As can be seen, the presence of PEG molecules greatly enhanced the adsorption of holo α-lactalbumin, with the ratio about 15. Besides that, there was a slight increase in the additional adsorption of lysozyme with the presence of PEG molecules. Generally, PEG molecules interacted differently with different proteins. This finding will be discussed further in Chapter 11.

Table 7.2: The ratio of protein adsorption on the SS-lysozyme (4)-PEG5k (5) SS surface to that on the lysozyme (4) surface (Voigt analysis).

Protein	Voigt mass density on the SS-lysozyme (4) surface (mg/m^2)	Ratio of adsorption on the SS-lysozyme (4)-PEG5000 (5) surface to that on the SS-lysozyme (4) surface
Holo α-lactalbumin (refer Figures 7.6 and 7.7)	0.007	15.35
Lysozyme (refer Figures 7.6 and 7.7)	0.0095	4.14
β-lactoglobulin (refer Figures 7.6 and 7.7)	0.019	0.26
β-casein (refer Figures 7.6 and 7.8)	1.17	0.16
Apo α-lactalbumin (refer Figures 7.6 and 7.8)	5.67	1.60

7.6 Adsorption of proteins onto SS-lysozyme (4)-PEGNHS surfaces

β-lactoglobulin (0.1 g / L) was further adsorbed on SS-lysozyme (4)-PEGNHS2k (1), SS-lysozyme (4)-PEGNHS5k (1) and SS-lysozyme (4)-PEG-NHS20k (1) surfaces (see Figure 7.9). The adsorption of β-lactoglobulin generally was down to less than 5 % on those surfaces compared to that on the bare SS surface.

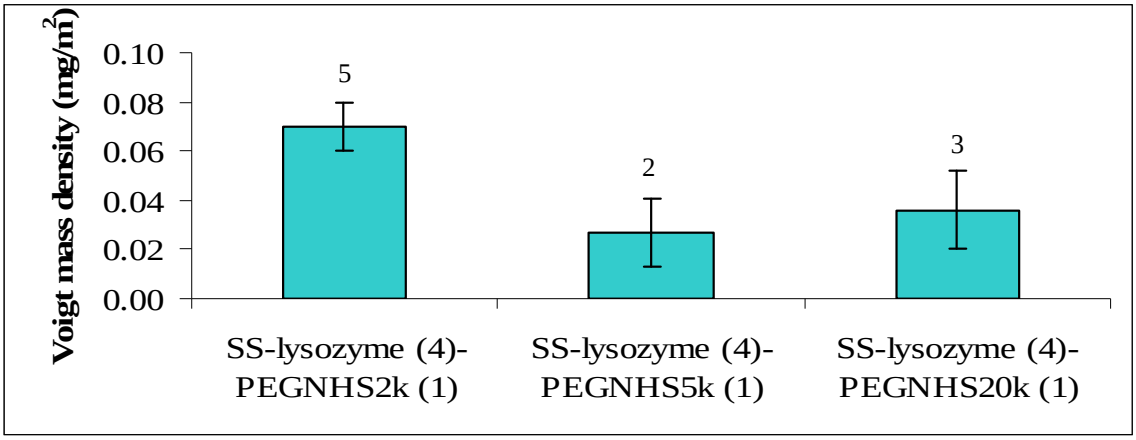

Figure 7.9: The Voigt mass density of *tightly-bound* β-lactoglobulin adsorbed on SS-lysozyme (4)-PEGNHS (1) surfaces for PEGNSH with various molecular weights at a temperature of 23 °C. Values above bars are *percentage* of strong adsorption compared to that on the bare SS surface.

From the results obtained in Figure 7.9, the SS-lysozyme (4)-PEGNHS5k (1) surface appeared to be the promising surface to inhibit adsorption of β-lactoglobulin. The effectiveness of this surface to repel the adsorption of protein was further tested on holo α-lactalbumin and β-casein proteins (see Figure 7.10, plotted in a log scale). As can be seen, there was almost no adsorption of holo α-lactalbumin on the surface. Meanwhile, for β-casein, the adsorption was less than 20 % of that on the bare SS surface.

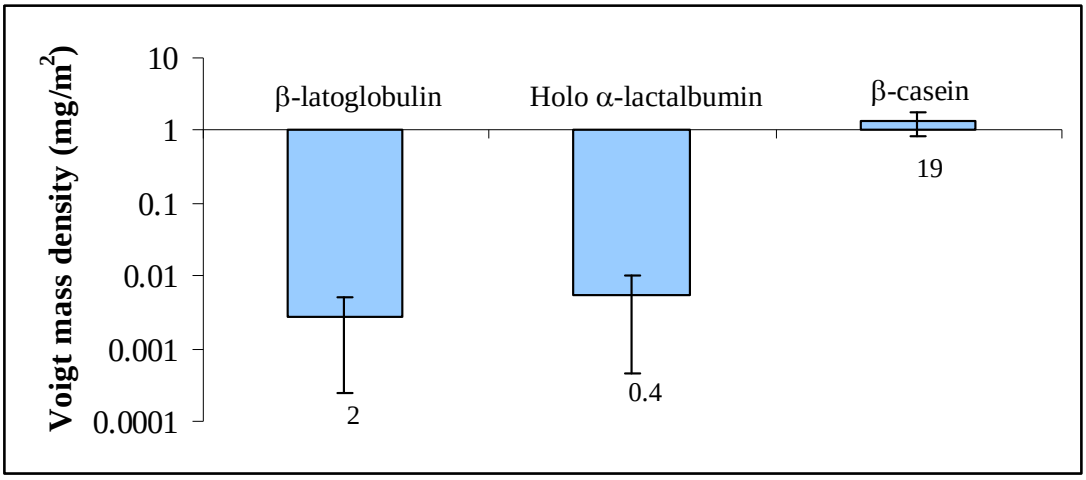

Figure 7.10: Mass density of *tightly-bound* β-lactoglobulin, holo α-lactalbumin and β-casein adsorbed on a SS-lysozyme (4)-PEGNHS5k (1) surface (plotted in a log scale). Values below the bars are *percentage* of strong adsorption compared to that on the bare SS surface.

Figure 7.11 shows the chain density of tightly bound PEG-NHS2k (1), PEG-NHS5k (1) and PEG-NHS20k (1) on a SS-lysozyme (4) surface (plotted in a log scale). The grafting density of PEG-NHS2k was the highest at 0.28 chains / nm^2 followed by PEG-NHS5k and PEG-NHS20k at 0.09 and 0.01 chain / nm^2, each. Refer to section 7.3 for the corresponding Voigt mean layer thickness and spacing between chains calculation.

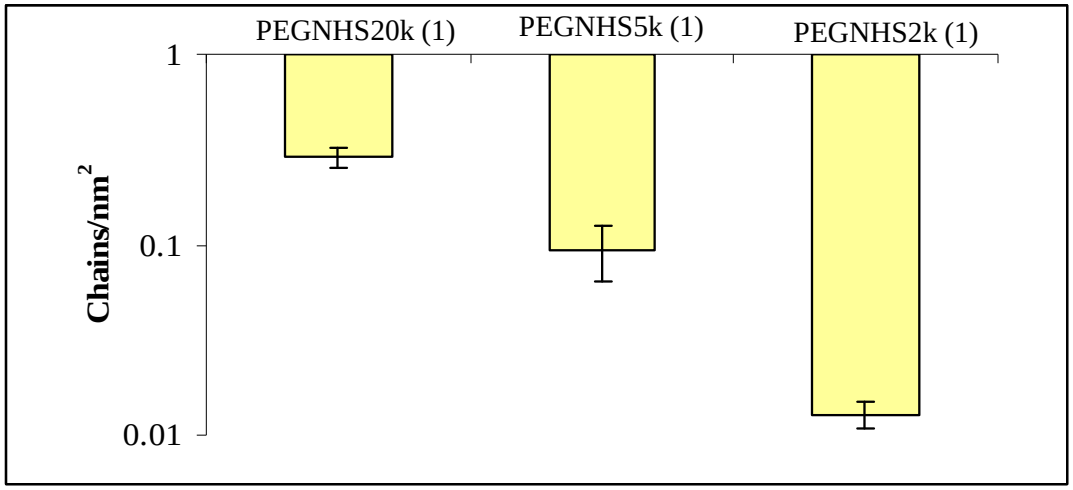

Figure 7.11: Chain density of tightly bound PEG-NHS2k (1), PEG-NHS5k (1) and PEG-NHS20k (1) on a lysozyme (4) layer (plotted in a log scale).

7.7 Adsorption of mixed and single protein solutions at the concentration of milk

The work was continued by adsorbing mixed protein solution onto SS-lysozyme (4), SS-lysozyme (4)-PEG5k (5) and SS-lysozyme (4)-PEGNHS5k (1)-surfaces. The mix protein solution consists of β-casein (9.3 g / L), β-lactoglobulin (3.2 g / L) and holo α-lactalbumin (1.2 g / L). The result of the tightly-bound mass density adsorbed on the surfaces is shown in Figure 7.12. Values above bars are percentage of the strong adsorption compared to that of the mix on the bare SS surface (after flushing with the buffer). Surprisingly, there was almost no adsorption on the SS-lysozyme (4)-PEG5k (5) surface (that is, almost 100 % removal during the flushing), ± 0.008 mg/m^2. Meanwhile, there was no significant difference on the adsorption of the protein mix either on the SS-lysozyme (4) surface or the SS-lysozyme (4)-PEGNHS5k (1) surface.

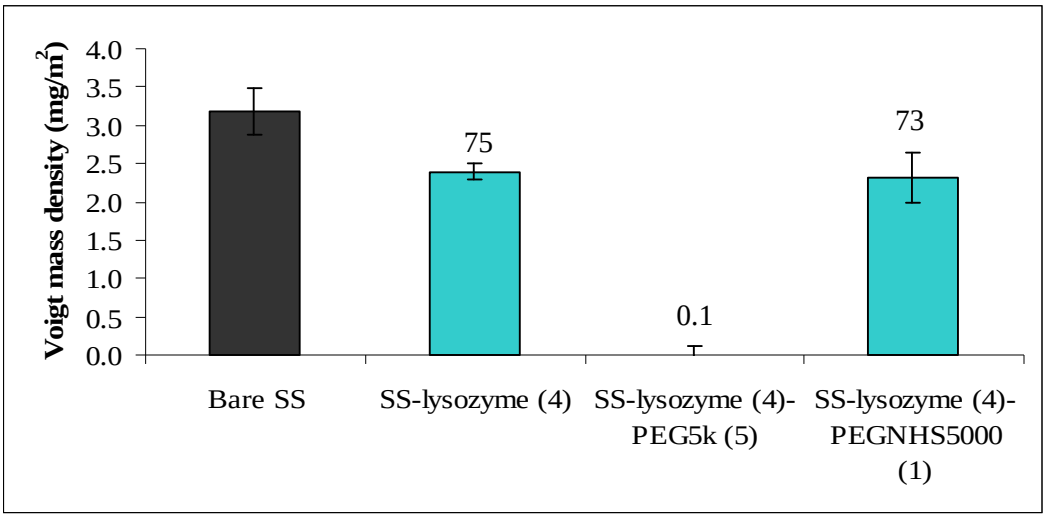

Figure 7.12: The Voigt mass density of *tightly-bound* mix protein adsorbed on the SS-lysozyme (4), SS-lysozyme (4)-PEGk (5) and SS-lysozyme (4)-PEGNHS5k (1) surfaces at temperature of 23 °C. Values above bars are *percentage* of the strong adsorption compared to that of the mix on the bare SS surface.

The experiment was further carried out using single protein solutions; β-lactoglobulin (3.2 g / L), holo α-lactalbumin (1.2 g / L) and β-casein (9.3 g / L). The adsorption of the protein was done separately on a SS-lysozyme (4)-PEG5k (5) surface at 23 °C (see Figure 7.13). The adsorption of mixed protein solution also was plotted for a comparison. The surface has been chosen as it appeared to be the most promising surface to inhibit adsorption of the protein mix (see Figure 7.13). As can be seen, flushing the protein adsorbed with the buffer solution resulted in 100 % removal of β-lactoglobulin, holo α-lactalbumin, β-casein and mixed protein with the error of ± 0.010, ± 0.026, ± 0.020 and ± 0.008 mg/m^2, respectively.

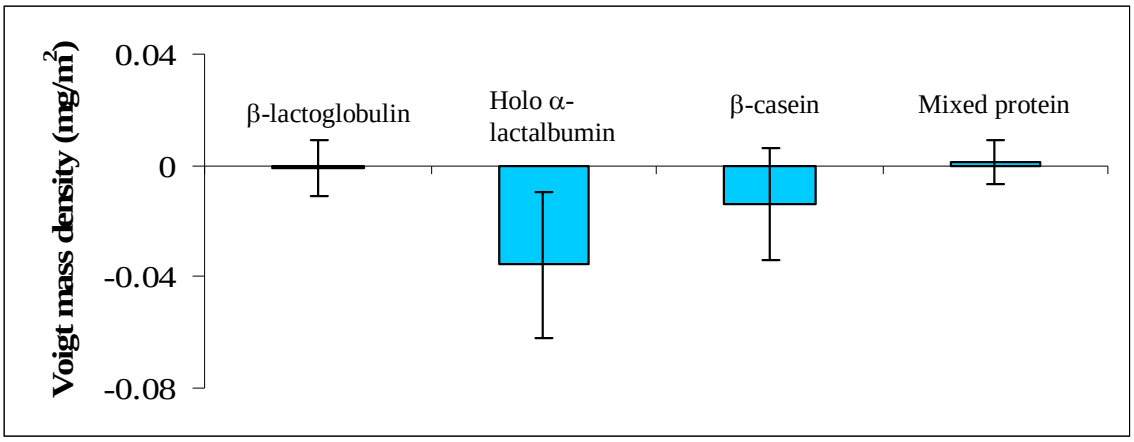

Figure 7.13: Mass density of single and mixed protein solutions at the concentration of milk on SS-lysozyme (4)-PEG5k (5) surfaces after flushing with buffer solution. The data was obtained using the Voigt model.

7.8 Stability test

Figure 7.14 presents the cumulative mass density of the mix protein on a PEG5000 (5)-lysozyme (4) surface after flushing with buffer solution at room temperature (23 °C) (that is, a strong adsorption). The plotted data was obtained using the Voigt model. The stability of the SS-lysome (4)-PEG5k (5) surface to inhibit adsorption of the mix protein was tested for 12 days *continuously*. The adsorption of the protein mix was measured after 1.5 hours, 2 days, 6 days, 9 days and 12 days on the same surface. At each of these times, the protein solution was replaced by buffer until a new steady reading was obtained. This reading was plotted in Figure 7.14. Then, the flow of protein solution was resumed until the next time for measurement. As can be seen, there was no mass adsorbed after 1.5 hrs (that is 100% removal during the flushing). After 2 days, about 2 % of that mass density found on the bare SS was tightly bound on the surface. The accumulated adsorption *decreased* with time after that, so that a layer of 0.025 mg/m^2 formed after around 10 days, perhaps a steady value.

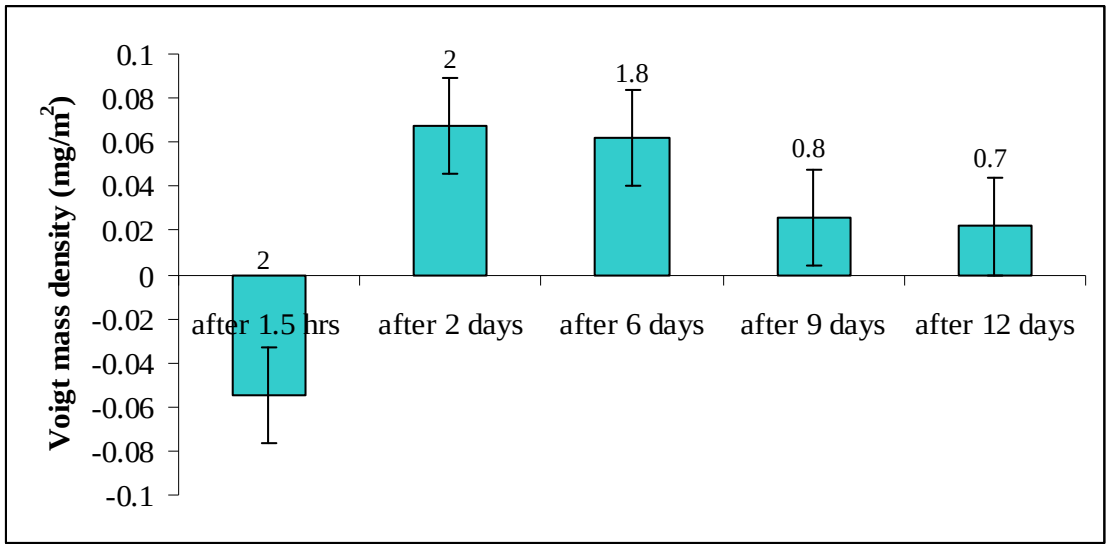

Figure 7.14: The cumulative Voigt mass density of the mixed protein on a SS-lysozyme (4)-PEG5k (5) surface after flushing with buffer solution. Values above bars are percentage of strong adsorption compared to that of the mix on the bare SS surface.

7.9 Effect of non flow condition on adsorption of protein mix on a stainless steel surface

Figure 7.15 shows the effect of a non-flow condition on adsorption of the protein mix on bare stainless steel surfaces at 23 °C. The data was compared with a flow condition (Q = 100μL / min). As can be seen, mass density of the protein mix adsorbed (before or after flushing with buffer solution) on the surfaces was similar for both conditions.

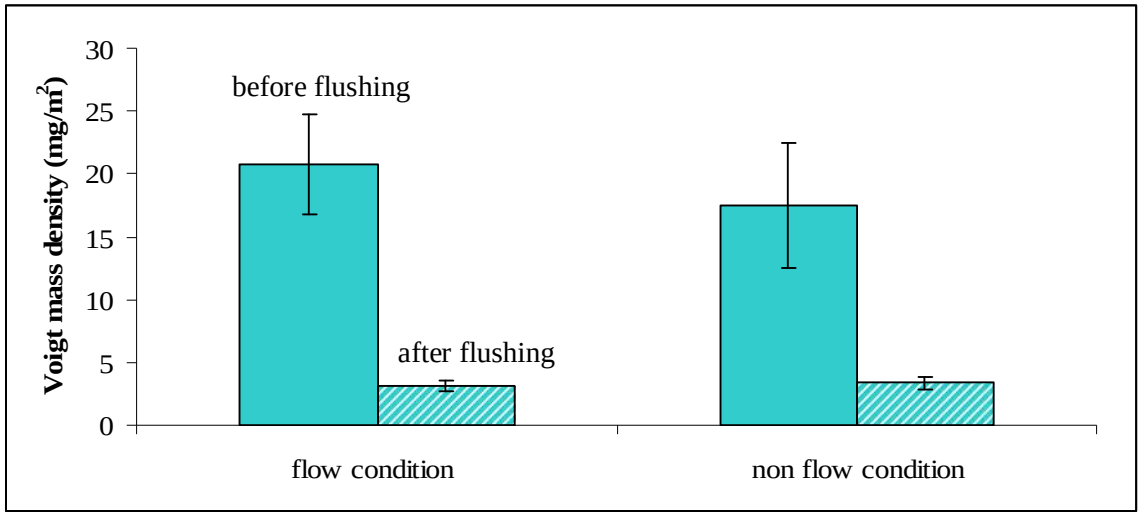

Figure 7.15: The Voigt mass density of a protein mix on bare stainless steel surfaces under a flow and a non-flow condition at 23 °C. Plain and stripe bars are mass density adsorbed on the stainless steel surface before and after flushing with buffer solution, respectively.

7.10 Effect of temperature on the adsorption of the protein mix

The experimental work was continued into a realistic condition for industrial application. In this experiment, the adsorption of the mix protein on SS-lysozyme (4)-PEG5k (5) and SS-lysozyme (4)-PEGNHS5k (1) surfaces was conducted at a temperature of 80 °C (the normal operating temperature for a heat exchanger). The adsorption of the mix protein was also conducted at a temperature of 40 °C for a comparison. The result of the effect of temperature on adsorption of the mix protein is depicted in Figures 7.16 (temperatures of 23 and 40 °C) and 7.17 (temperature of 80 °C). Referring to Figure 7.16, flushing the protein mix adsorbed resulted in 100 % removal (refer to the stripe bars), except on the SS-lysozyme (4)-PEGNHS5k (1) (B), surface (at 23 °C). At this temperature, about 65 % of protein mix were *tightly-bound* on the SS-lysozyme (4)-PEGNHS5k (1) surface compared to that on the bare surface.

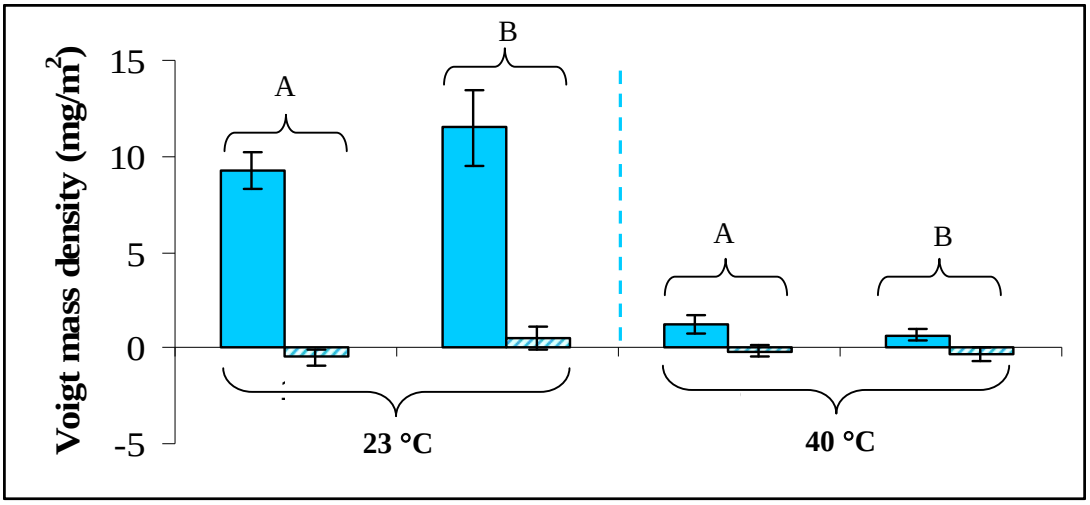

Figure 7.16: The Voigt mass density of a protein mix on the SS-lysozyme (4)-PEG5k (5) (A) surface and the SS-lysozyme (4)-PEGNHS5k (1) (B) surface at 23 and 40 °C. Plain and stripe bars are mass density adsorbed on the surfaces before and after flushing with buffer solution, respectively.

At a temperature of 80 °C meanwhile, the data was compared based on the frequency changes (Δf) at n = 7 *before* flushing with the buffer solution (n is an overtone number) (Figure 7.17). The comparison has been made based on the Δf because the experiment at 80 °C was done only by measuring the fundamental frequency without running the QCM cell (refer to Chapter 5, Experiment G for the method). As can be seen, the adsorption of the mixed protein at 80 °C was higher than that on the bare surface when measured at the same temperature. Nevertheless, bear in mind, the percentage of the adsorption shown in the plot refer to the adsorption *before flushing* with the buffer.

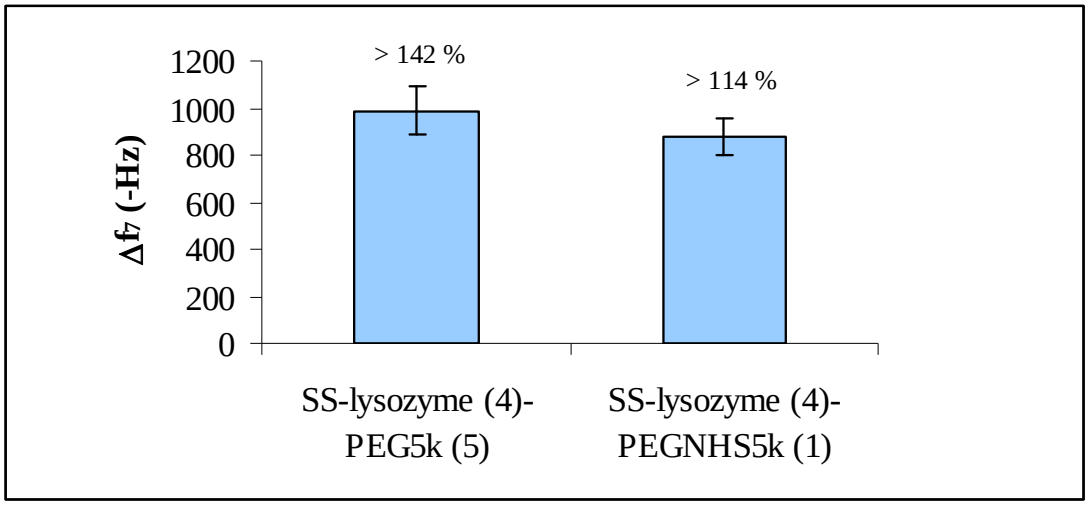

Figure 7.17: Adsorption of the mixed protein on SS-lysozyme (4)-PEG5k (5) and SS-lysozyme (4)-PEGNHS5k (1) surfaces at 80 °C. The data was compared based on the frequency changes at n = 7 (*before flushing* with buffer). Values above bars are percentage of adsorption compared to that on the bare SS surface at the same temperature.

Overall, the reduction of protein adsorption on the SS-protein-PEG based surfaces was highly significant. An excellent protein adsorption inhibition at room temperature and body temperature was a great achievement. The mechanism of this will be clarified in Chapter 11.

CHAPTER EIGHT

AFM RESULTS

8.0 Introduction

This chapter presents the AFM characterization results. The characterization has been carried out in order to see the morphology of the QCM crystals coated with Au, coated with stainless steel (refer to Chapter 5 for the surface detail). The topographic image of the characterized surface was presented in a two-dimensional (2D) image along with the corresponding phase image. The phase image often provides significantly more contrast than the topographic image (height image), thus the existence of molecules can be seen more clearly in phase than in height images. The phase image has also been shown to be sensitive to material surface properties, such as stiffness, viscoelasticity, and chemical composition [Raghavan et al., 2000]. The magnification of all the images is indicated by the scan dimension, which is 5 μm x 5 μm.

The AFM model used was MFP-3D from Asylum research located at School of Engineering and Advanced Technology, Massey University, New Zealand with the help from Professor Richard Haverkamp. The characterization was done ex-situ and using the tapping mode in buffer solution (the prepared surfaces for the characterization were kept in buffer solution for 2 to 3 days before imaging with the AFM). Igor Pro 5 Upgrade software was used to analyze the images.

The AFM characterization was done on the bare SS, SS-protein (0.1), SS-PEI (30), SS-silicate (50), SS-PEI (30)-PEG (5) and SS-PEI (30)-PEG (5)-protein (0.1) surfaces.

The surfaces will be compared to the bare SS surface based on the RMS surface roughness. Surface roughness can be defined as the root mean square value of the vertical deviations from the average surface level over a specified surface

length. The lower the RMS is, the smoother the surface. The roughness of the surface is commonly characterized by the root-mean-square (RMS) value, which is a parameter of deviation of surface pixels from the average surface level as shown in Equation 8.1 [Gan et al., 2007].

$$RMS = \left[\left(\frac{1}{N^2} \right) \sum_{i=1}^{N} \sum_{j=1}^{M} \left(H(i, j) - \overline{H} \right)^2 \right]^{1/2} \qquad (8.1)$$

where H is the surface pixel level, i and j are pixel locations and $\overline{H}$ is the average surface level.

8.1 Bare stainless steel surface

Figures 8.1 and 8.2 show respectively the AFM lateral 2D topography (height) image and phase image of a bare SS surface. From the scale in Figure 8.1, zero refers to the level at the average surface; positive value (above zero) refers to the height of the peak (molecules) above the average surface whereas negative value (below zero) refers to the height of the peak (molecules) below the average surface. From Figure 8.1, the structure of the surface was apparently homogeneous with the highest peak from the average surface around 4 to 5 nm. Also observed, different phases existed on the surfaces with some dark dots distributed randomly on the surface as depicted in Figure 8.2. The RMS roughness of the bare SS surface was calculated by the AFM package to be about 1.25 nm.

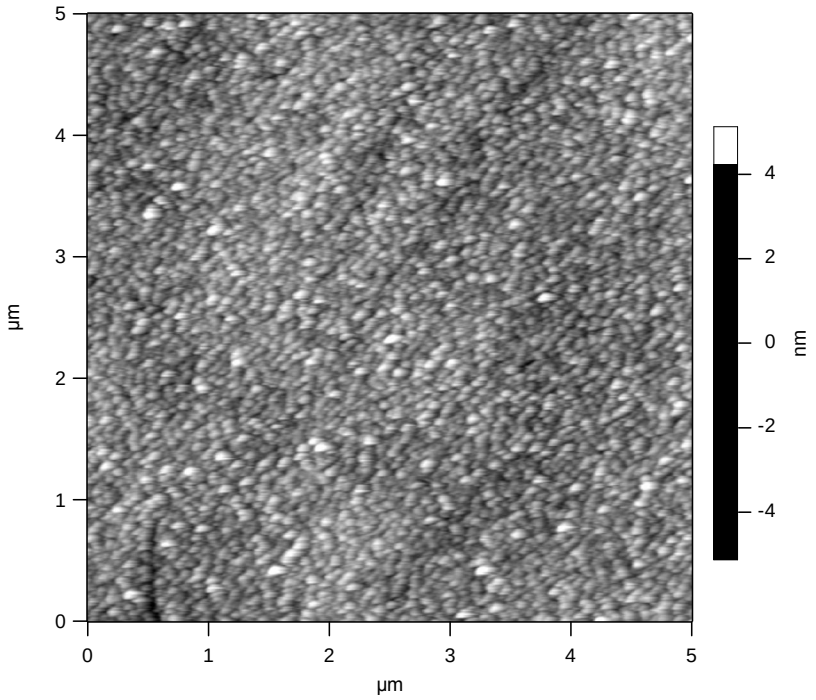

Figure 8.1: 2D AFM height image morphology of a bare SS surface.

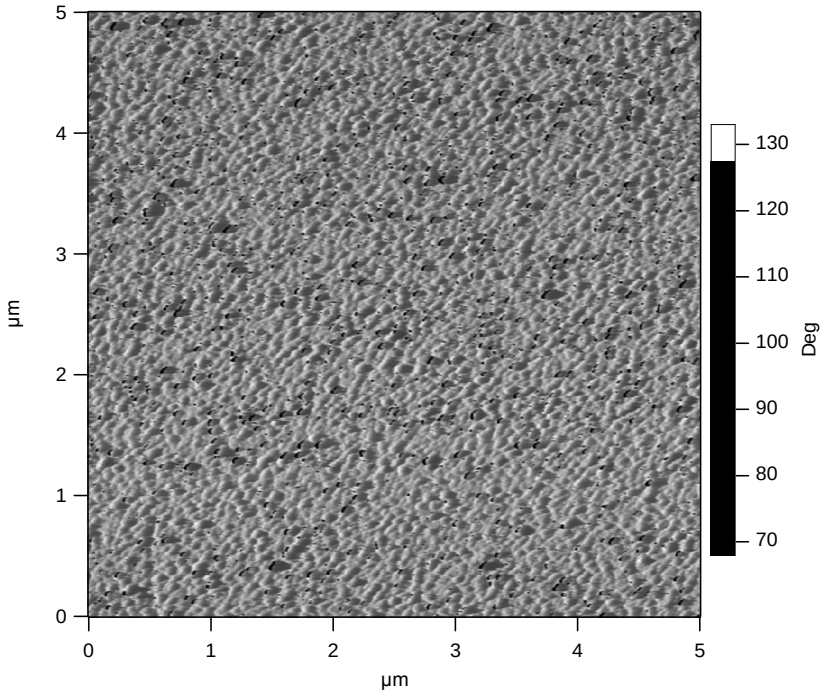

Figure 8.2: 2D AFM phase image morphology of a bare SS surface.

8.2 Protein layer on a bare stainless steel surface

A protein layer surface was prepared by adsorbing the protein (that is, β-casein, lysozyme and apo α-lactalbumin) from 0.1 g / L solution on a bare SS surface at room temperature until a steady state was reached, followed by rinsing with a buffer solution until the frequency leveled off. Thus, the protein layer surface for the characterization refers to the strongly held adsorption. The surface was kept in buffer solution for 2 days before imaging with the AFM.

8.2.1 β-casein on SS surface

Figures 8.3 and 8.4 show respectively the topographic (height) and phase images of a β-casein layer on a bare SS surface (SS-β-casein (0.1)). Deposition of β-casein molecules enabled us to visualize the formation of globules distributed randomly on the surface with some bulky features (islands), with the diameter of approximately 100 to 200 nm. The islands enable us to estimate the mass surface density of proteins deposited on the surface. The estimated fractional surface coverage was about 0.008 (less than 1 % of the total coverage). Figure 8.5 shows a simple model of the average and globules (islands) on the surface where it has been assumed that the surface is flat. The average height has been calculated from the statistical package of the AFM to have a zero average, a calculation including the presence of the islands. *h* refers to the height of the islands from the average surface (for example *h* is about 5 nm for SS-β-casein (0.1) surface, see Figure 8.3). The fractional surface coverage can be estimated by calculating the number of islands (*n*) multiplied by the average area of island, then divided by the total area. Only the obvious islands (shown by white colour on a topographic image) were considered for the calculation. The total height of the islands *b* is the sum of *h* (known) and *d* (unknown). To estimate the contribution of mass due to the islands, we need to know *b*, and hence *d*. The mass adsorbed meanwhile can be estimated by multiplying the number of islands (*n*) by the volume of the island (area x total height, *b*) with the effective density, 1200 kg / m^3. The height of the islands below the average surface (*d*) can be calculated using Equations 8.2 to 8.4.

$$RMS^2{}_{protein} = RMS^2{}_{substrate} + \frac{SS_{island}}{N} \tag{8.2}$$

$$RMS^2{}_{protein} = RMS^2{}_{substrate} + RMS_{island}{}^2 \tag{8.3}$$

where,

$$RMS^2{}_{protein} = \frac{1}{N}\left(SS_{substrate} + SS_{island}\right)$$

$$RMS^2{}_{island} = \frac{SS_{island}}{N}$$

and

$$\frac{SS_{island}}{N} = \frac{f_{island}(h)^2 + (N-f)(d)^2}{N} = a_f h^2 + (1-a_f)d^2 \tag{8.4}$$

Substituted Equation 8.3 into Equation8.2

$$RMS^2{}_{protein} - RMS^2{}_{substrate} = a_f h^2 + \left(1-a_f\right)d^2 \tag{8.5}$$

Then,

$$d = \left[\frac{RMS^2{}_{protein} - RMS^2{}_{substrate}}{a_f h^2}\right]^{1/2} \tag{8.6}$$

a_f is an area coverage of islands, h is a height above the average surface and d is a height below the average surface.

RMS value for the corresponding surface is obtained from the AFM result. The calculation of $\frac{SS_{island}}{N}$ is based on the frequency that the tip scanned the area of islands (this can be obtained by estimating the area of each island on the image, refer to Figure 8.3). Referring to Figure 8.5, the number of frequency over the number of data, N, is equal to the fractional area coverage (total area of the islands divided by

the area of the image, 25μm^2). The fractional area of the substrate then can be obtained by subtracting the island area coverage, (1-a_f). Then *d* can be calculated using Equation 8.6. The example of calculation of *d* is shown below:

$$d = \left[\frac{(1.52)^2 - (1.25)^2 - (0.008) * 5^2}{(0.992)} \right]^{1/2}$$

$$d = 0.74\ nm$$

The *d* value obtained was 0.74 nm, therefore the total height of the island, *b* was about 5.74 nm (5 nm + 0.74 nm). The estimated mass density, Γ, adsorbed on the surface due to the islands was then about 0.055 mg/m^2. The example of calculation of the estimated surface density, Γ, is shown below:

$$\Gamma = \left(\frac{0.008 m^2}{m^2} \right) * \left(5.74 \times 10^{-9}\, m \right) * \left(1200 \frac{kg}{m^3} \times 10^6\, mg \right) = 0.055 \frac{mg}{m^2}$$

This value was about 1 % of the QCM-D measurement indicating the islands consist of a small fraction of the QCM-D deposited. Comparing Figures 8.2 and 8.4 (phase images), it seems that the background of the SS-β-casein (0.1)) surface was smoother than of the bare SS surface. However, the RMS roughness of the SS-β-casein (0.1) surface was calculated by the AFM package to be 1.520 nm.

To see the contribution of the islands on the *roughness* of the surfaces, it was assumed that the *d* = 0 to give a minimum contribution to RMS^2_{island} and thus the max $RMS^2_{protein\ layer}$ can be determined. Also, it has been assumed that the thickness of the protein layer was constant (that is, the RMS of the substrate was equal to the RMS of the top of the layer). Refer to Equation 8.7.

$$(RMS_{protein})^2 = \underbrace{(RMS_{substrate})^2 + (RMS_{layer\ protein})^2}_{(RMS_{coating})^2} + (RMS_{island})^2 \qquad (8.7)$$

Given,

$$\left(RMS_{island}\right)^2 = a_f h^2$$

The proportion of the mean square (MS) of the protein surface explained by the islands, p_{island}, is therefore can be calculated by dividing the MS of the island by the MS of the protein surface. The example for this calculation is shown below:

$$p_{island} = \frac{\left(RMS_{island}\right)^2}{\left(RMS_{protein}\right)^2} = \frac{0.008 * 5^2}{1.52^2} = \frac{0.2}{2.31} = 0.087$$

It shows that the roughness of the SS-β-casein (0.1) surface explained by the islands is only about 9 % of the total roughness.

The ratio of the MS of the coating to that of MS of the substrate, $R_{c/s}$, $\left(\frac{RMS_{coating}^{\ 2}}{RMS_{substrate}^{\ 2}}\right)$ can give us the information of either the protein layer formed uneven layer (MS of coating > MS of substrate) or the protein layer had filled in the surface valleys (MS of coating < MS of substrate). If the thickness of protein layer was constant (i.e. similar variation like the substrate), the ratio will be equal to 1. The example for this calculation is shown below:

$$\left(RMS_{coating}\right)^2 = \left(RMS_{protein}\right)^2 - \left(RMS_{island}\right)^2$$

$$\left(RMS_{coating}\right)^2 = \left(1.52\right)^2 - 0.2 = 2.11$$

$$\left(RMS_{coating}\right) = 1.45\ nm$$

Therefore,

$$R_{c/s} = \frac{\left(RMS_{coating}\right)^2}{\left(RMS_{substrate}\right)^2} = \frac{1.45^2}{1.25^2} = 1.35$$

This indicates that β-casein layer formed uneven layer on the surface. Thus, indicating that mainly the protein layer has contributed to the roughness of the SS-β-casein (0.1) surface.

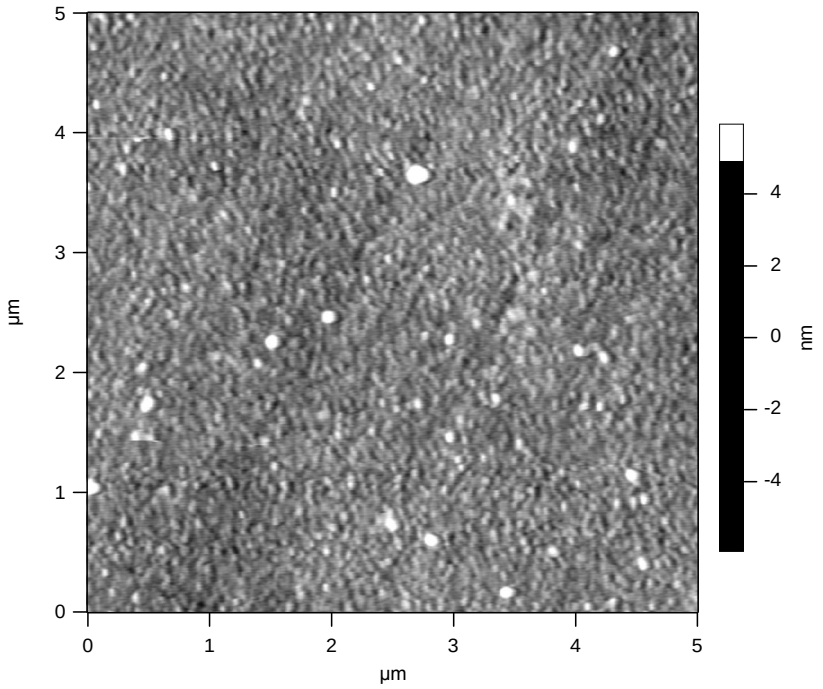

Figure 8.3: 2D AFM height image morphology of SS-β-casein (0.1) surface.

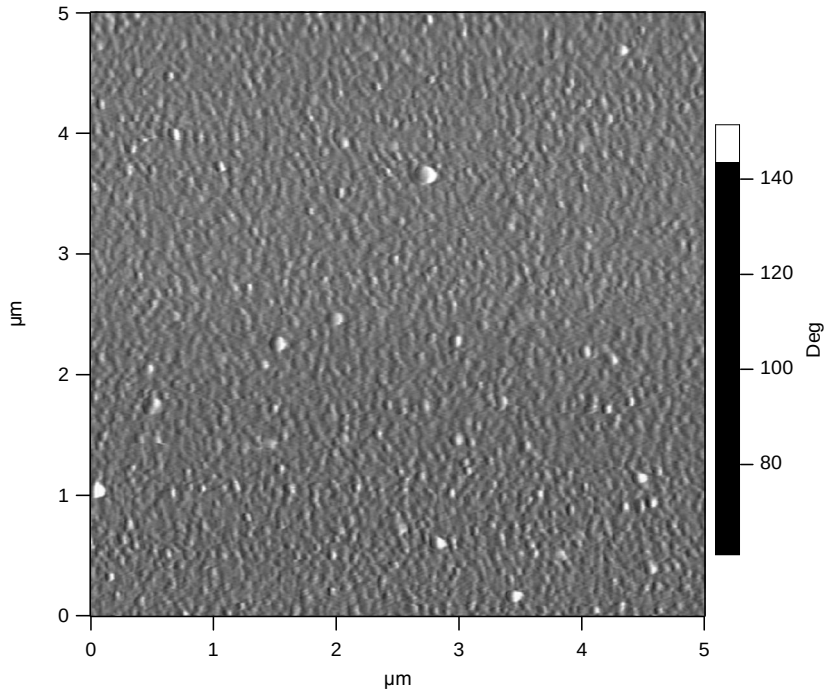

Figure 8.4: 2D AFM phase image morphology of SS-β-casein (0.1) surface.

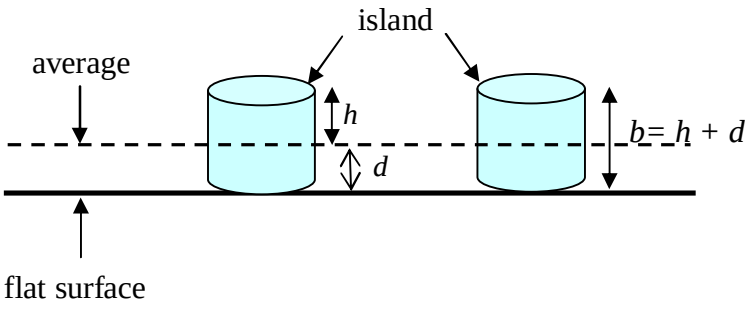

Figure 8.5: Illustration of average surface and island.

8.2.2 Lysozyme on SS surface

Figures 8.6 and 8.7 show respectively the surface topography image and the corresponding phase image of a lysozyme layer on a bare SS surface (SS-lysozyme (0.1)), (the image was not so good with some lines). As can be seen, there were bulky features (which is believed to be lysozyme groups) with different sizes of approximately 200 to 260 nm diameter, distributed randomly on the surface. The estimated fractional surface coverage was about 0.02 (2 % of the total coverage). The maximum height of the island from the average surface, *h*, was about 5 nm. The RMS roughness of the SS-lysozyme (0.1) surface was calculated by the AFM package to be 2.198 nm. From Equation 8.6, the calculated *d* value was 1.68 nm, therefore the total height of the island, *b* was about 6.68 nm (5 + 1.68 = 6.68). The estimated mass density adsorbed due to the islands was then 0.2 mg/m^2. This value was about 5 % of the QCM-D measurement.

Table 8.1 tabulates the proportion of the MS of the protein surface explained by the islands, p_{island}, and the ratio of the MS of the coating to that of MS of the substrate, $R_{c/s}$, of SS-lysozyme (0.1) surface. The data were obtained from the same analysis described for β-casein. Similar to β-casein, the islands of lysozyme provided just a small amount of the variation, about 10 %. This also indicated that the islands contain only a small fraction of the QCM-D deposited. Thus, the high RMS value of the SS-lysozyme (0.1) surfaces was mainly resulted from the large variation of the protein layer as shown by the high value of $R_{c/s}$.

Table 8.1: The proportion of the MS of the protein surface explained by the islands, p_{island}, and the ratio of MS of the coating to that of MS of the substrate, $R_{c/s}$, of SS-lysozyme (0.1) surface.

Parameter	Value
p_{island}	10 %
$R_{c/s}$	2.8

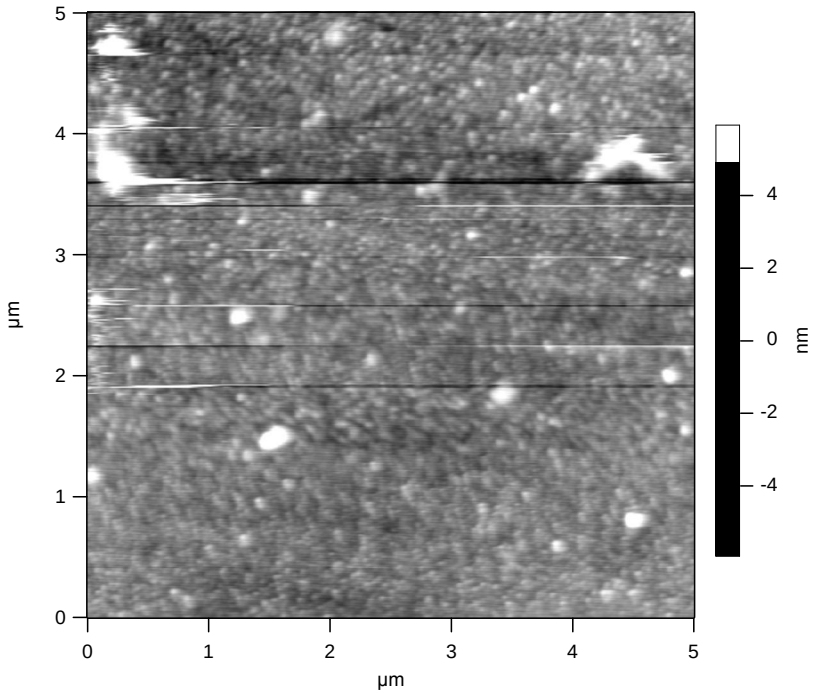

Figure 8.6: 2D AFM height image morphology of SS-lysozyme (0.1) surface.

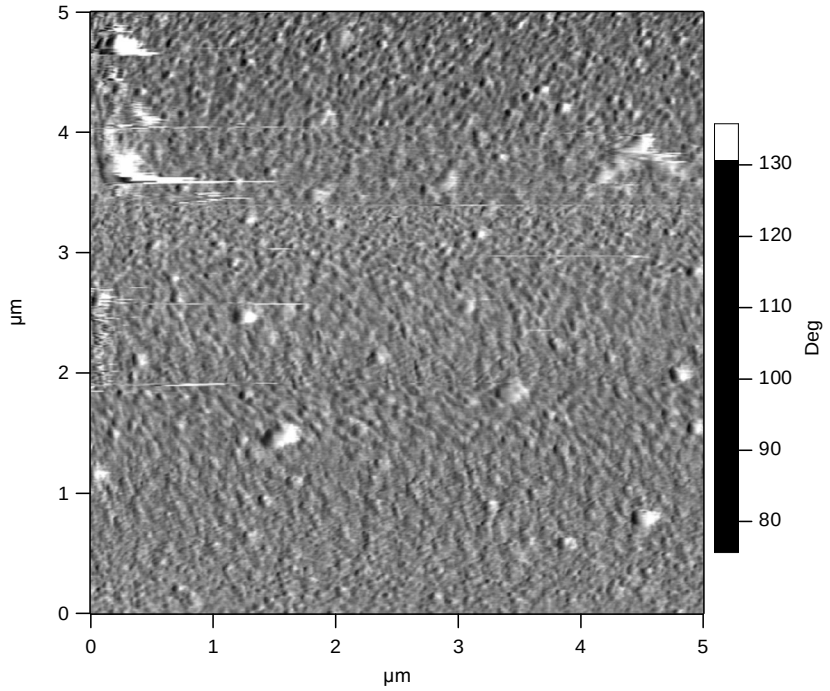

Figure 8.7: 2D AFM phase image morphology of SS-lysozyme (0.1) surface.

8.2.3 Apo α-lactalbumin on SS surface

Figures 8.8 and 8.9 show the surface topography image and the corresponding phase image of an apo α-lactalbumin layer on a bare SS surface (SS-apo α-lactalbumin (0.1)), respectively. As can be seen, there were bulky features (which is believed to be aggregates of apo α-lactalbumin molecules) with different size of approximately 130 to 330 nm diameter, distributed randomly on the surface (see Figure 8.9). The estimated fractional surface coverage was about 0.03 (3 % of the total surface coverage). From Figure 8.8, the maximum height of the islands from the average surface, *h*, was about 10 nm. Meanwhile, the RMS roughness of the SS-apo α-lactalbumin (0.1) surface was calculated by the AFM package to be 3.299 nm. The *d* value obtained from the same analysis described for β-casein was 2.55 nm, therefore the total height of the island, *b* was about 12.55 nm (12 nm + 2.55 nm). The estimated mass density adsorbed due to the islands was then 0.5 mg/m^2. This value was about 2 % of the QCM-D measurement.

Table 8.2 tabulates the proportion of the MS of the protein surface explained by the islands, p_{island}, and the ratio of MS of the coating to that of MS of the substrate, $R_{c/s}$, of SS-apo α-lactalbumin (0.1) surface. The data were obtained from the same analysis described for β-casein. As can be seen, compared to β-casein and lysozyme, the roughness of the SS apo α-lactalbumin (0.1) surface explained by the islands was high, almost 30 %. The layer of protein also formed a very rough surface.

Table 8.2: The proportion of the MS of the protein surface explained by the islands, p_{island}, and the ratio of MS of the coating to that of MS of the substrate, $R_{c/s}$, of SS-apo α-lactalbumin (0.1) surface.

Parameter	Value
p_{island}	28 %
$R_{c/s}$	5.0

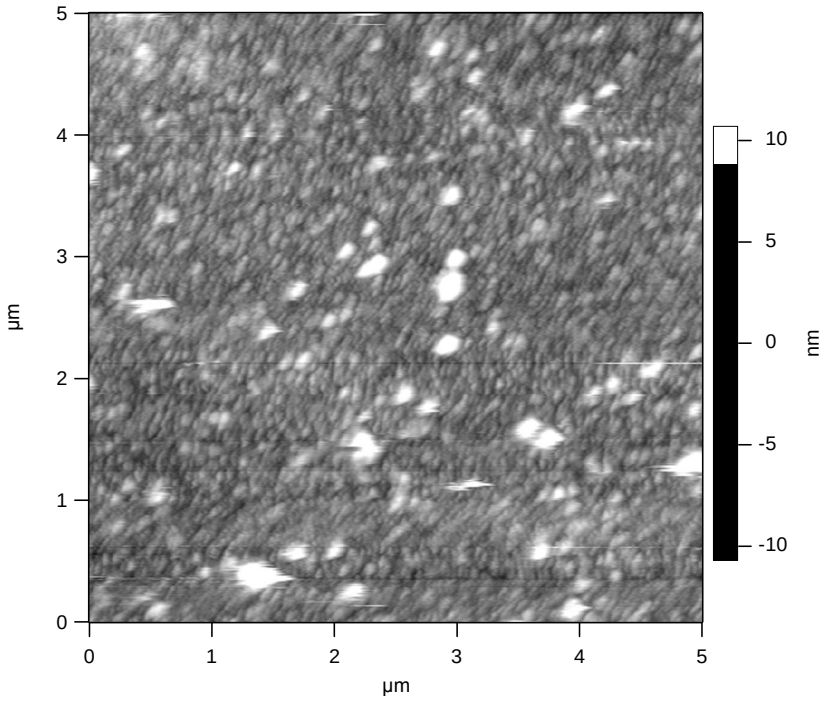

Figure 8.8: 2D AFM height image morphology of SS-apo α-lactalbumin (0.1) surface.

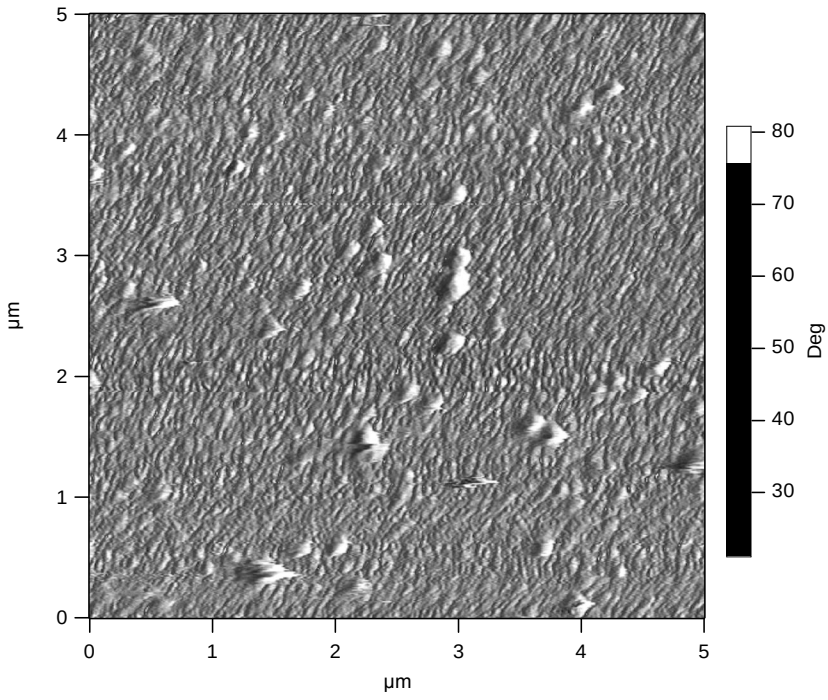

Figure 8.9: 2D AFM phase image morphology of SS-apo α-lactalbumin (0.1) surface.

8.3 Coating layer

A PEI layer surface was prepared by adsorbing PEI from 30 g / L solution on a bare SS surface at room temperature until a steady state was reached, followed by rinsing with a buffer solution until the frequency leveled off. Thus, the PEI layer surface for the characterization refers to the strongly held adsorption.

A silicate surface meanwhile was prepared by adsorbing sodium silicate from a 50 g / L solution on a SS surface at room temperature until a steady state was reached, followed by rinsing with a buffer solution until the frequency leveled off. All the prepared surfaces were kept in buffer solution for two days before imaging with the AFM.

8.3.1 PEI on SS surface

Figures 8.10 and 8.11 show the surface topography image and the corresponding phase image of a PEI layer on a bare SS surface (SS-PEI (30)), respectively. From the phase image (Figure 8.11), we can see that relatively small globules of PEI molecules with the diameter size of approximately 60 to 130 nm were distributed randomly on the surface. The estimated fractional surface coverage was about 0.005 (less than 1 % of the total surface coverage). The maximum height of the islands from the average surface, *h*, was about 7 nm (see Figure 8.10). The RMS roughness of the SS-PEI (30) surface was calculated by the AFM package to be 1.995 nm. The *d* value calculated from Equation 8.6 was 1.48 nm, therefore the total height of the island, *b* was about 8.48 nm (7 nm + 1.48 nm). The estimated mass density adsorbed due to the islands was then 0.06 mg/m^2, which is about 3 % of the QCM-D measurement.

Table 8.3 tabulates the proportion of the MS of the surface explained by the islands, p_{island}, and the ratio of MS of the coating to that of MS of the substrate, $R_{c/s}$, of SS-PEI surface. The data were obtained from the same analysis described for β-casein. As can be seen, the roughness of the surface explained by the islands was 6 %. Also protein layer formed uneven thickness on the surface.

Table 8.3: The proportion of the MS of the surface explained by the islands, p_{island}, and the ratio of MS of the coating to that of MS of the substrate, $R_{c/s}$, of SS-PEI surface.

Parameter	Value
p_{island}	6 %
$R_{c/s}$	2.4

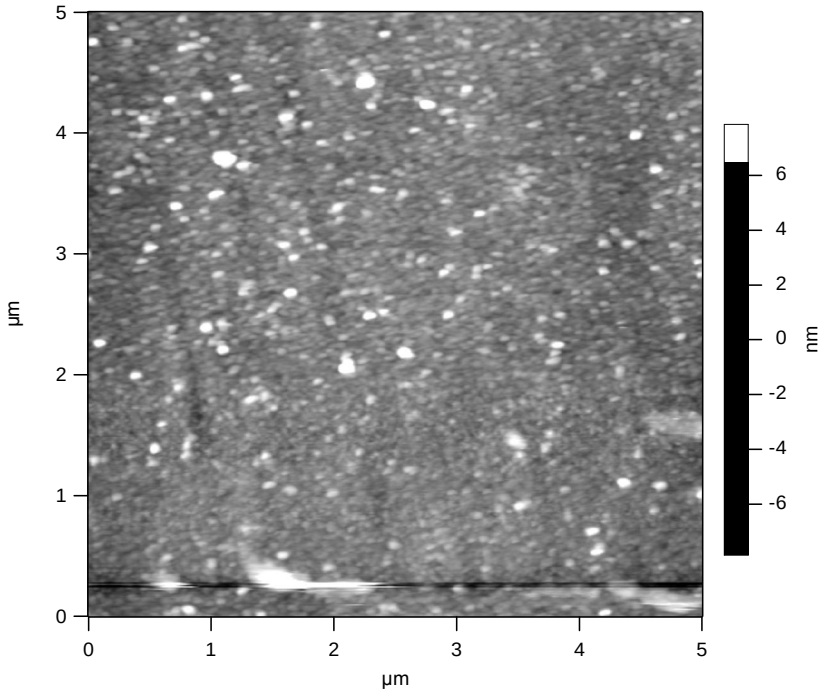

Figure 8.10: 2D AFM height image morphology of SS-PEI (30) surface.

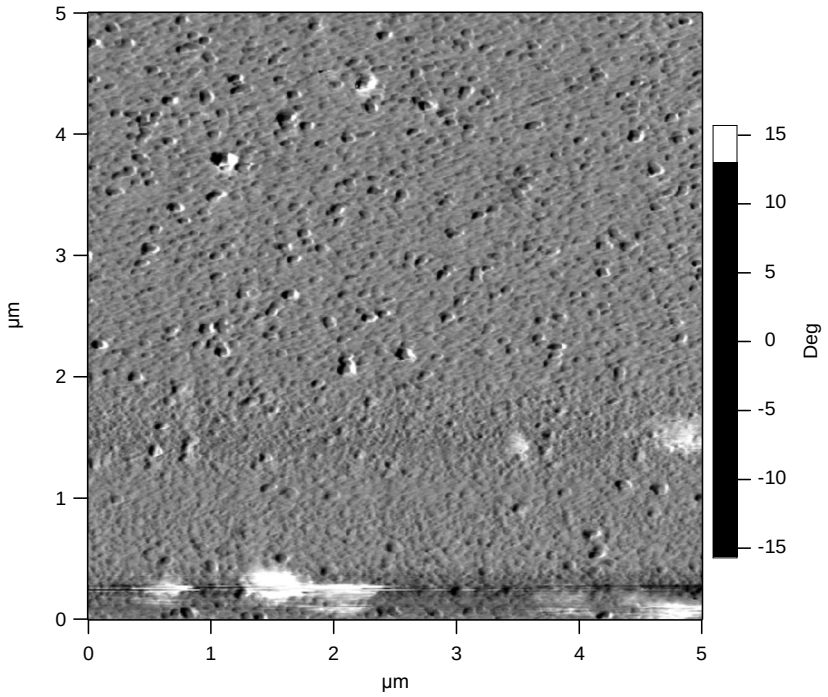

Figure 8.11: 2D AFM phase image morphology of SS-PEI (30) surface.

8.3.2 Silicate on SS surface

Figures 8.12 and 8.13 show the surface topography image and the corresponding phase image of a silicate layer on a bare SS surface (SS-silicate (50)), respectively. As can be seen, the bulky features of silicate molecules with the diameter size of approximately 130 to 200 nm were distributed randomly on the surface (see Figure 8.13). The estimated fractional surface coverage was about 0.008 (less than 1 % of the total surface coverage). The maximum height of the islands from the average surface, *h*, was about 5 nm (see Figure 8.12). The RMS roughness of the SS-silicate (50) surface was calculated by the AFM package to be 1.318 nm. The *d* value calculated from Equation 8.5 was 0.16 nm, therefore the total height of the island, *b* was about 5.16 nm (5 nm + 0.16 nm). The estimated mass density adsorbed due to the islands was then 0.05 mg/m^2, which is about 6 % of the QCM-D measurement.

Table 8.4 tabulates the proportion of the MS of the surface explained by the islands, p_{island}, and the ratio of MS of the coating to that of MS of the substrate, $R_{c/s}$, of SS-silicate surface. The data were obtained from the same analysis described for β-casein. Unlike others, the $R_{c.s}$ was equal to 1. This indicates that the protein layer have similar variation like the substrate.

Table 8.4: The proportion of the MS of the surface explained by the islands, p_{island}, and the ratio of MS of the coating to that of MS of the substrate, $R_{c/s}$, of SS-silicate surface.

Parameter	Value
p_{island}	12 %
$R_{c/s}$	1.0

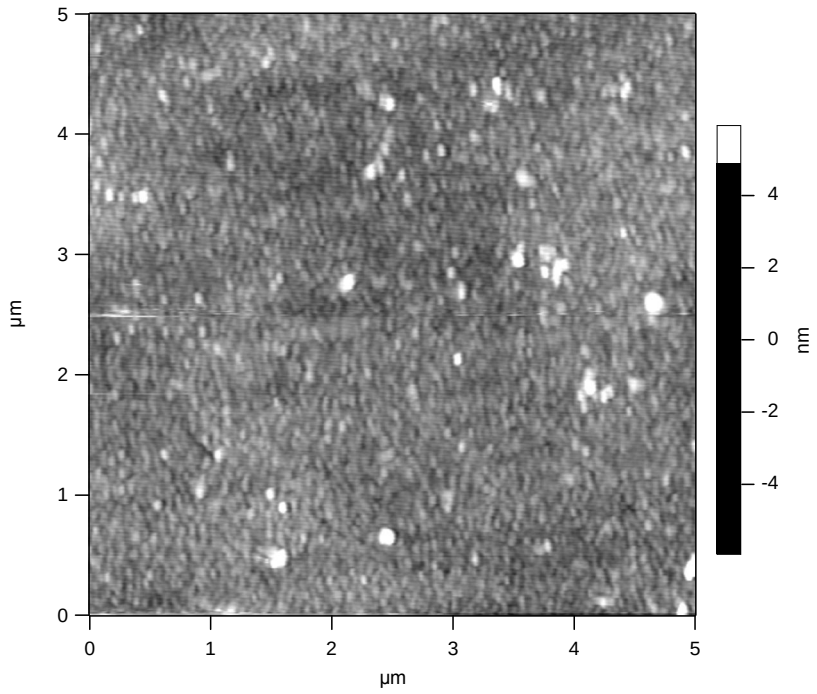

Figure 8.12: 2D AFM height image morphology of SS-silicate (50) surface.

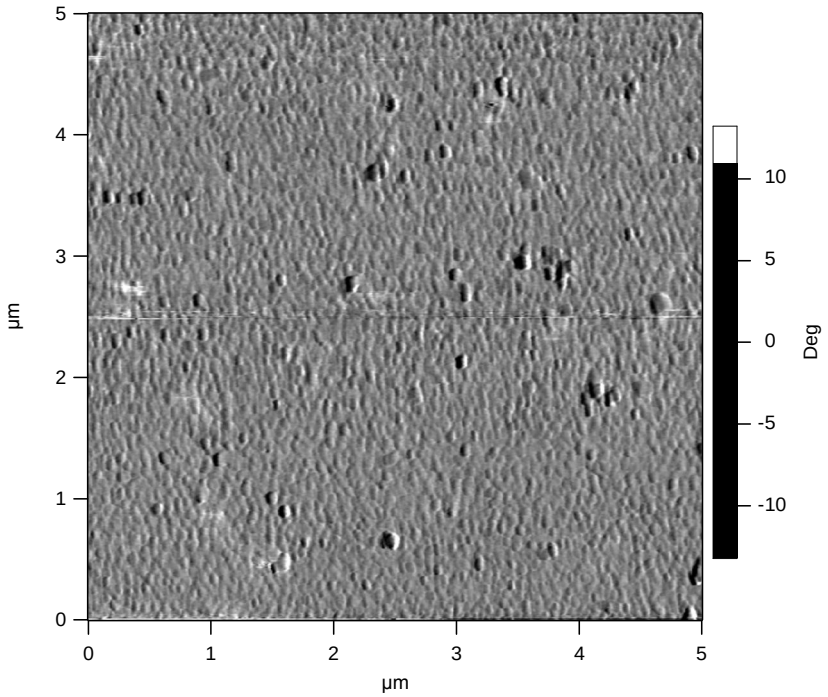

Figure 8.13: 2D AFM phase image morphology of SS-silicate (50) surface.

8.4 PEG on PEI on SS surface

PEI-PEG surfaces were prepared by adsorbing PEG of various MW (350, 2000 and 5000 Da), separately, from 5 g / L solution onto a PEI surface at room temperature, followed by rinsing with buffer solution until the frequency leveled off (Refer to Chapter 5 for the procedure detail). The surfaces for the characterization refer to the strongly held adsorption. All the prepared surfaces were kept in buffer solution for three days before imaging with the AFM.

8.4.1 PEG350 on PEI on SS surface

Figures 8.14 and 8.15 show the respective surface topography image and the phase image of a PEG350 layer on a PEI coated SS surface (SS-PEI (30)-PEG350 (5)). There were irregular and bulky features of PEG350 molecules with the diameter size of approximately 130 to 330 nm distributed randomly on the surface. The

estimated fractional surface coverage was about 0.009 (about 1 % of the total surface coverage). The maximum height of the islands from the average surface, *h*, was about 15 nm (see Figure 8.14). The RMS roughness of the SS-PEI (30)-PEG350 (5) surface was calculated by the AFM package to be 2.639 nm. The *d* value calculated from Equation 8.6 was 0.98 nm. For this calculation, the RMS for the substrate was referred to the RMS of the SS-PEI (30) surface instead of the RMS of the bare SS surface. The example of the calculation is shown below:

$$d = \left[\frac{(2.639)^2 - (1.995)^2 - (0.009) * 15^2}{(0.991)} \right]^{1/2}$$

$$d = 0.98\ nm$$

Therefore the total height of the island, *b* was about 15.98 nm (15 nm + 0.98 nm). The estimated mass density adsorbed due to the islands was then 0.2 mg/m^2. This value was about 16 % of the QCM-D measurement.

Table 8.5 tabulates the proportion of the MS of the surface explained by the islands, p_{island}, and the ratio of MS of the coating to that of MS of the substrate, $R_{c/s}$, of SS-PEG350 surface. The data were obtained from the same analysis described for β-casein except for the calculation of $R_{c/s}$, the MS of the SS-PEI (30) was used instead of the MS of the bare SS. As observed, the $R_{c/s}$ was quite low indicating that protein layer has almost similar variation like the substrate. This indicates that the islands provided a relatively large amount of the variation. The high p_{island} is believed resulted from the largest globules formed, with the diameter around 330 nm (refer to Figures 8.14 and 8.15, marked with the circular dash).

Table 8.5: The proportion of the MS of the surface explained by the islands, p_{island}, and the ratio of MS of the coating to that of MS of the substrate, $R_{c/s}$, of SS-PEG350 surface.

Parameter	Value
p_{island}	29 %
$R_{c/s}$	1.3

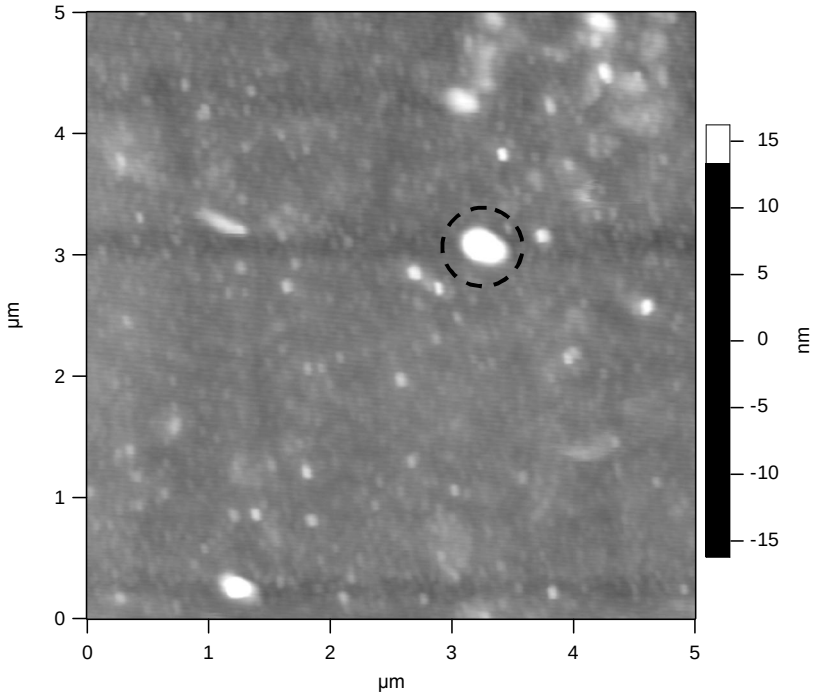

Figure 8.14: 2D AFM height image morphology of SS-PEI (30)-PEG350 (5) surface. The circular dash showed the largest globules, with the diameter around 330 nm.

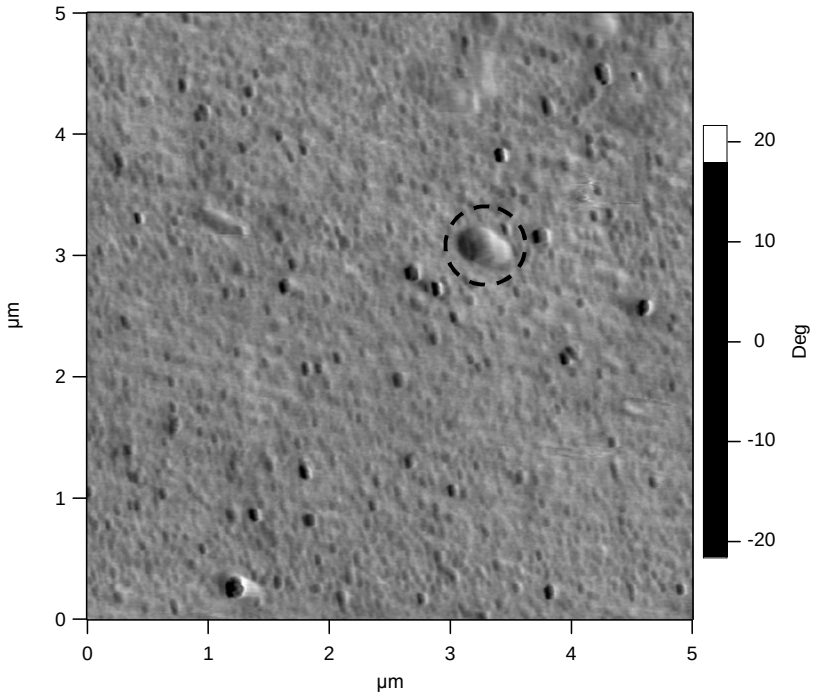

Figure 8.15: 2D AFM phase image morphology of SS-PEI (30)-PEG350 (5) surface. The dash circle showed the largest globules, with the diameter around 330 nm.

8.4.2 PEG2k on PEI on SS surface

Figures 8.16 and 8.17 show the respective surface topography image and the phase image of a PEG2000 layer on a PEI coated SS surface (SS-PEI (30)-PEG2k (5)). The globules distributed randomly on the surface with different bulky features with the size of approximately up to 260 to 400 nm diameter (see Figure 8.17). The estimated fractional surface coverage was about 0.06 (6 % of the total surface coverage. The maximum height of the islands from the average surface, *h*, was about 15 nm (see Figure 8.16). Meanwhile the RMS roughness of the SS-PEI (30)-PEG2k (5) surface was calculated by the AFM package to be 4.065 nm. The *d* value obtained from the same analysis described for PEG350 was 0.02 nm, therefore the total height of the island, *b* was about 15.02 nm (15 nm + 0.02 nm). The estimated mass density adsorbed due to the island was then 0.6 mg/m^2, which is about 70 % of the QCM-D measurement.

Table 8.6 tabulates the proportion of the MS of the surface explained by the islands, p_{island}, and the ratio of MS of the coating to that of MS of the substrate, $R_{c/s}$, of SS-PEG2000 surface. The data were obtained from the same analysis described for β-casein except for the calculation of $R_{c/s}$, the MS of the SS-PEI (30) was used instead of the MS of the bare SS. As can be seen, unlike others, the p_{island} of the PEG 2k was very high. This indicates that the islands provided a large amount of the variation. The $R_{c/s}$, meanwhile was slightly lower than 1, indicating that PEG 2k layer had filled in the surface valleys. This indicates that the large value of the RMS of the SS-PEI (30)-PEG2k (5) surface was mainly resulted from the islands formation.

Table 8.6: The proportion of the MS of the surface explained by the islands, p_{island}, and the ratio of MS of the coating to that of MS of the substrate, $R_{c/s}$, of SS-PEG2000 surface.

Parameter	Value
p_{island}	81 %
$R_{c/s}$	0.8

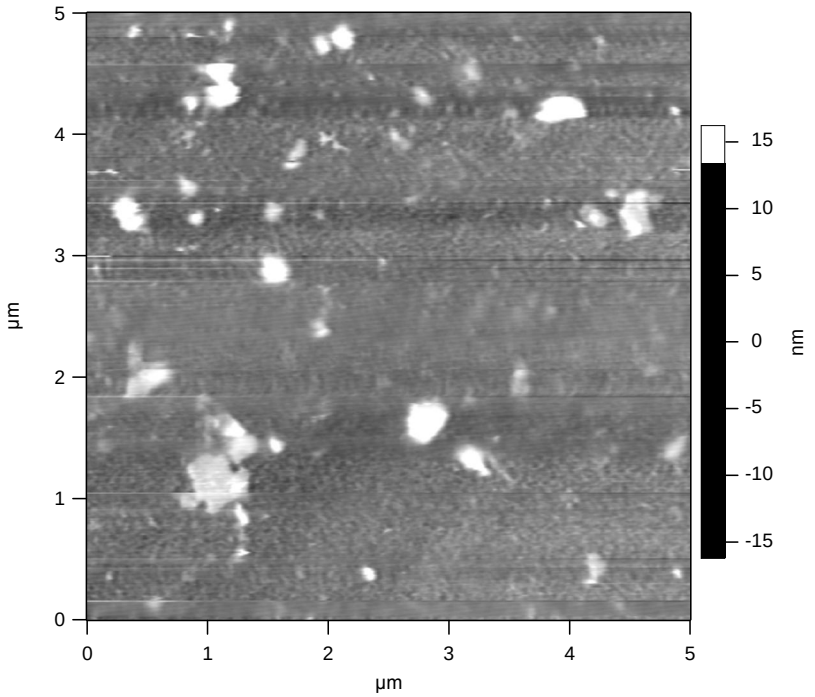

Figure 8.16: 2D AFM height image morphology of SS-PEI (30)-PEG2k (5) surface.

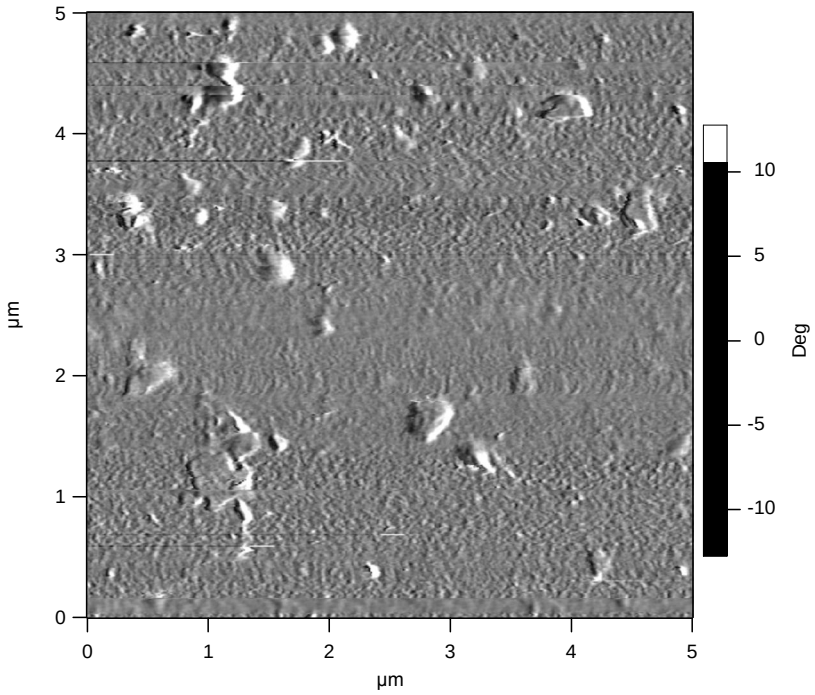

Figure 8.17: 2D AFM phase image morphology of SS-PEI (30)-PEG2k (5) surface.

8.4.3 PEI-PEG5k on SS surface

Figures 8.18 and 8.19 show respectively the surface topography image and the phase image of a PEG5000 layer on a PEI coated SS surface (SS-PEI (30)-PEG5k (5)). It seems that PEG molecules distributed randomly on the surface with different globule size of approximately 100 to 130 nm (see Figure 8.19). The estimated fractional surface coverage was about 0.008 (less than 1 % of the total surface coverage). The maximum height of the islands from the average surface, *h*, was about 10 nm (see Figure 8.18). The RMS roughness of PEG5000 surface was calculated by the AFM package to be 4.008 nm. The *d* value obtained from the same analysis described for PEG350 was 0.02 nm, therefore the total height of the island, *b* was about 10.02 nm (10 nm + 0.02 nm). The estimated mass density adsorbed due to the islands was then 0.1 mg/m^2, which is about 12 % of the QCM-D measurement.

Table 8.7 tabulates the proportion of the MS of the surface explained by the islands, p_{island}, and the ratio of MS of the coating to that of MS of the substrate, $R_{c/s}$, of SS-PEG5000 surface. The data were obtained from the same analysis described for β-casein except for the calculation of $R_{c/s}$, the MS of the SS-PEI (30) was used instead of the MS of the bare SS. Surprisingly, the p_{island} of the PEG 5k was very small compared to either PEG350 or PEG 2k especially. This is probably because, the size of the PEG 5k islands formed were relatively low compared to PEG350 and PEG2k. However, the reason why PEG 5k molecules had smaller globules than that of the PEG2k cannot be explained at this point. The $R_{c/s}$ meanwhile was large, indicating a large amount of variation than of the substrate.

Table 8.7: The proportion of the MS of the surface explained by the islands, p_{island}, and the ratio of MS of the coating to that of MS of the substrate, $R_{c/s}$, of SS-PEG5000 surface.

Parameter	Value
p_{island}	5 %
$R_{c/s}$	4.0

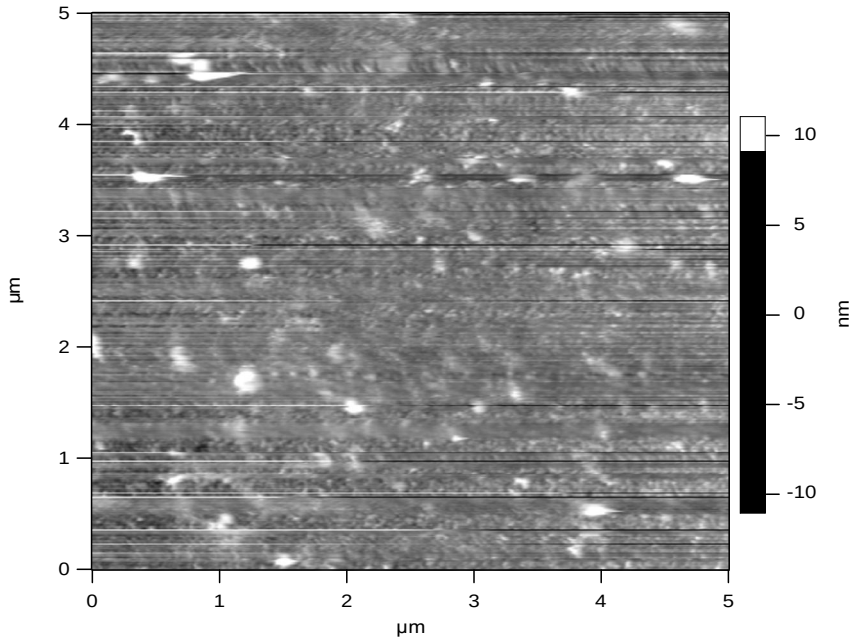

Figure 8.18: 2D AFM height image morphology of SS-PEI (30)-PEG5k (5) surface.

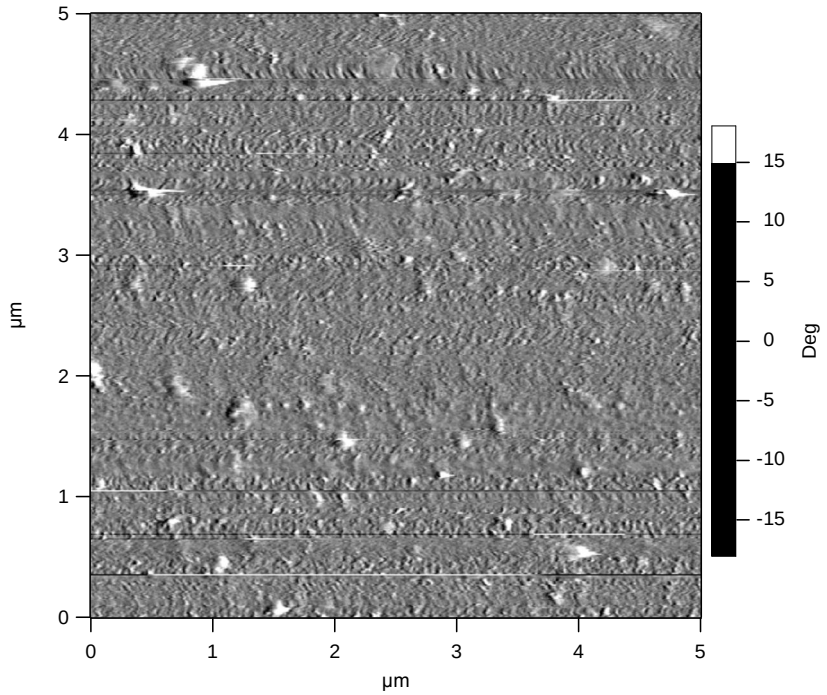

Figure 8.19: 2D AFM phase image morphology of SS-PEI (30)-PEG5k (5) surface.

8.5 α-lactalbumin layer on a SS-PEI (30)-PEG2k (5) surface

A surface was prepared by adsorbing α-lactalbumin from 0.1 g / L solution on a SS-PEI (30)-PEG2k (5) surface at room temperature, followed by rinsing with buffer solution until the frequency leveled off. Two types of α-lactalbumin were used, apo and holo α-lactalbumin (native). The main difference between these two proteins is the absence and presence of calcium ions, corresponding to apo and holo α-lactalbumin, respectively. The characterization has been carried out to see the influence of calcium ions on the structure (morphology) of the surface.

8.5.1 Apo α-lactalbumin layer on SS-PEI (30)-PEG2k (5) surface

Figures 8.20 and 8.21 show the surface topography image and the phase image of apo α-lactalbumin layer on a PEI-PEG2000 coated SS surface (SS-PEI (30)-PEG2k (5)- apo α-lactalbumin (0.1)), respectively. The maximum height of the islands from the average surface, *h*, was about 16 nm (see Figure 8.18). The molecules were distributed randomly on the surface with different bulky features with the apo α-lactalbumin size of approximately up to 260 to 400 nm diameter (see Figure 8.21). The estimated fractional surface coverage was about 0.04 (4 % of the total surface coverage). Meanwhile, the RMS roughness of apo α-lactalbumin layer on the PEI-PEG2000 surface was calculated by the AFM package to be 3.463 nm.

Table 8.8 tabulates the proportion of the MS of the surface explained by the islands, p_{island}, and the ratio of MS of the coating to that of MS of the substrate, $R_{c/s}$, of apo α-lactalbumin layer on SS-PEI (30)-PEG2k (5) surface. The data were obtained from the same analysis described for β-casein except for the calculation of $R_{c/s}$, the MS of the SS-PEI (30)-PEG2k (5) surface was used instead of the MS of the bare SS.

Table 8.8: The proportion of the MS of the surface explained by the islands, p_{island}, and the ratio of MS of the coating to that of MS of the substrate, $R_{c/s}$, of apo α-lactalbumin layer on SS-PEI (30)-PEG2k (5) surface.

Parameter	Value
p_{island}	75 %
$R_{c/s}$	0.2

By contrast to others, the $p_{substrate}$ was very large. A very low $R_{c/s}$ value indicated that the apo α-lactalbumin layer had filled in the valleys of the substrate. Therefore, the high RMS of the SS-PEI (30)-PEG2k (5)-apo α-lactalbumin (0.1) surface was presumably because of the islands formation.

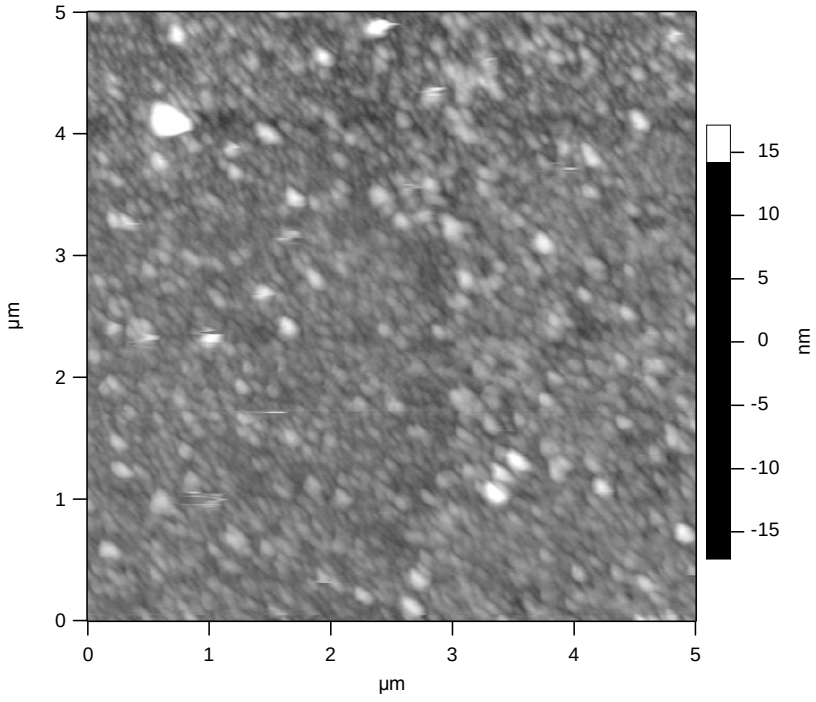

Figure 8.20: 2D AFM height image morphology of SS-PEI (30)-PEG2k (5)-apo α-lactalbumin (0.1) surface.

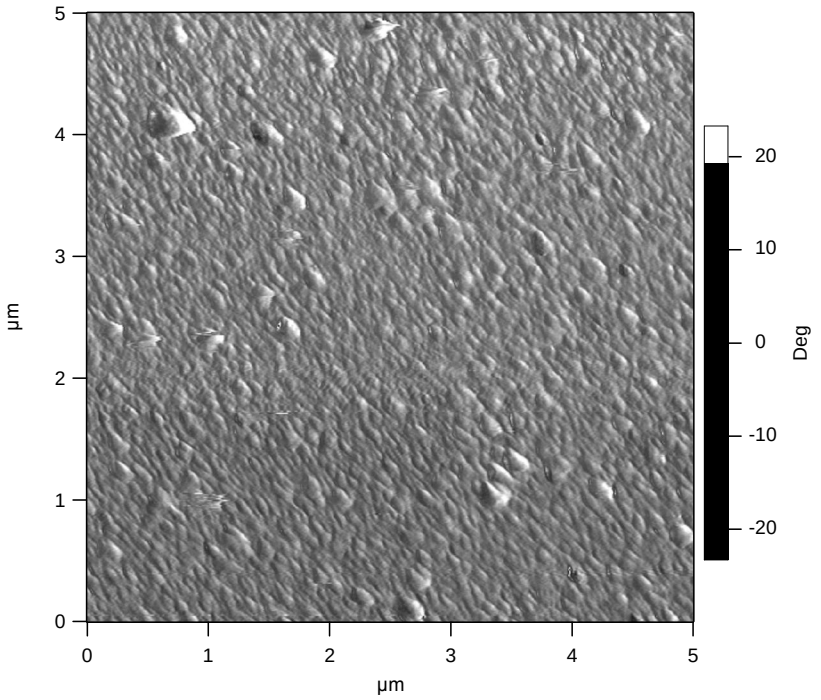

Figure 8.21: 2D AFM phase image morphology of SS-PEI (30)-PEG2k (5)-apo α-lactalbumin (0.1) surface.

8.5.2 Holo α-lactalbumin on SS-PEI (30)-PEG2k (5) surface

Figures 8.22 and 8.23 show respectively the surface topography image and the phase image of a holo α-lactalbumin layer on a PEI-PEG2000 coated SS surface (SS-PEI (30)-PEG2k (5)-holo α-lactalbumin (0.1)). The maximum height of the islands from the average surface, *h*, was about 7 nm. The surface seems smooth with some bulky features (about 200 nm in diameter) which are believed was holo α-lactalbumin groups (see Figure 8.23). The estimated fractional surface coverage was about 0.017 (about 2 % of the total surface coverage).

Table 8.9 tabulates the proportion of the MS of the surface explained by the islands, p_{island}, and the ratio of MS of the coating to that of MS of the substrate, $R_{c/s}$, of holo α-lactalbumin on SS-PEI (30)-PEG2k (5) surface. The data were obtained from the same analysis described for β-casein except for the calculation of $R_{c/s}$, the MS of the SS-PEI (30)-PEG2k (5) surface was used instead of the MS of the bare SS.

Table 8.9: The proportion of the MS of the surface explained by the islands, p_{island}, and the ratio of MS of the coating to that of MS of the substrate, $R_{c/s}$, of holo α-lactalbumin on SS-PEI (30)-PEG2k (5) surface.

Parameter	Value
p_{island}	33 %
$R_{c/s}$	0.1

Similar to observation on the SS-PEI (30)-PEG2k (5)-apo α-lactalbumin (0.1) surface, the $R_{c/s}$ value was very low. This suggests that holo α-lactalbumin layer had filled in most of the valleys of the surface. The low value of $R_{c/s}$ is expected to have a correlation with the black regions observed on the phase image (refer to Figure 8.23). However, the black regions on the phase image (Figure 8.23) are suggested from a huge different in phases existed between holo α-lactalbumin molecules and the surrounding (most probably PEG 2k or / and PEI molecules).

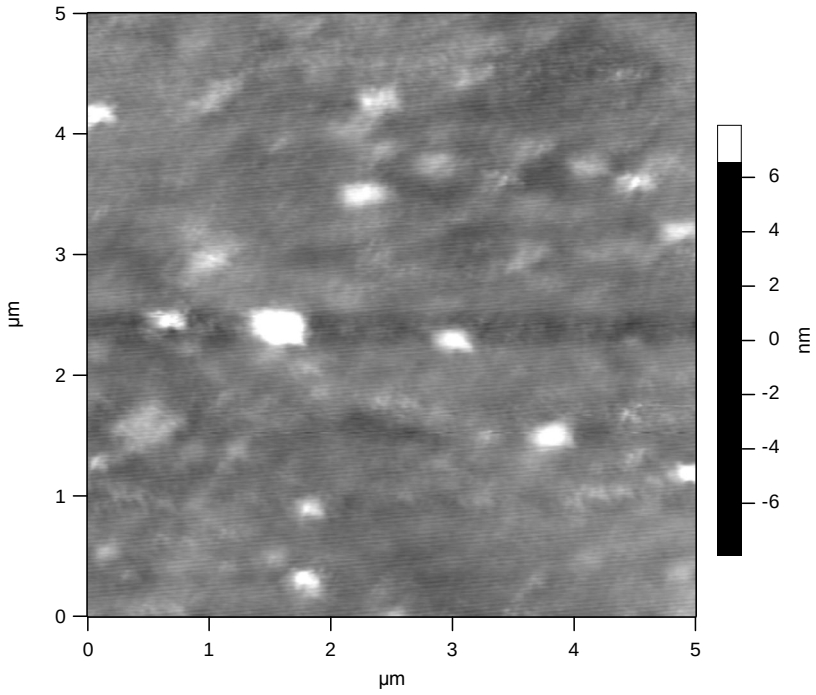

Figure 8.22: 2D AFM height image morphology of SS-PEI (30)-PEG2k (5)-holo α-lactalbumin (0.1) surface.

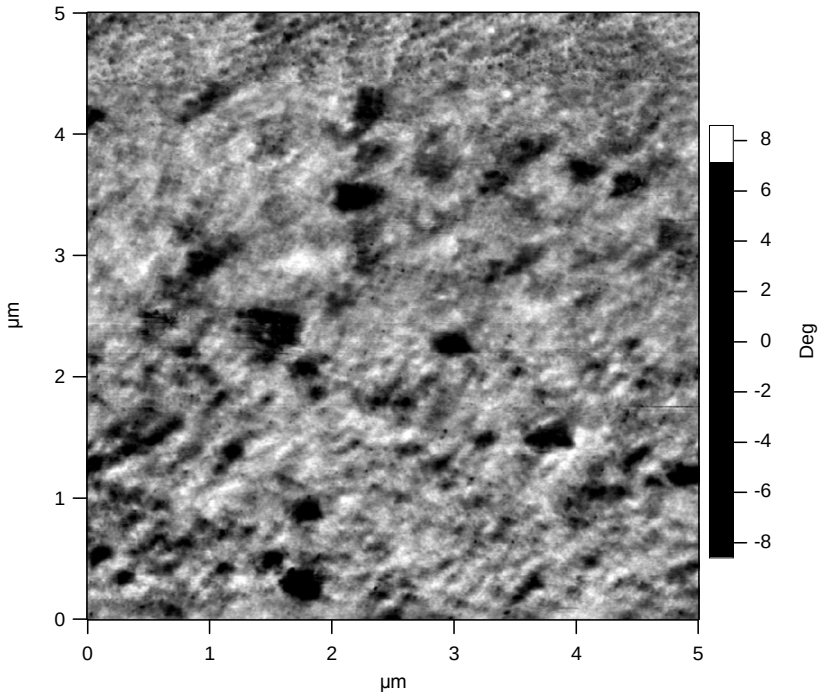

Figure 8.23: 2D AFM phase image morphology of SS-PEI (30)-PEG2k (5)-holo α-lactalbumin (0.1) surface.

8.6 Summary

Table 8.10 shows a summary of the surface roughness, approximate islands height, estimated diameter size of the islands and the proportion of the MS protein layer (or a PEI layer or a silicate layer or a PEG layer) explained by the islands, p_{island}. From the analysis, it has been shown that, generally, the formation of islands did not significantly affect to the surface roughness except of PEG2k and apo α-lactalbumin (this is shown with high p_{island}). The p_{island} of a SS-PEI (30)-PEG2k (5)-apo α-lactalbumin (0.1) surface was about two times higher than that of the SS-PEI (30)-PEG2k (5)-holo α-lactalbumin (0.1) surface, indicating that the proteins behaved differently towards PEG molecules. By comparing images between these two surfaces, we can see that both images have almost similar structure except more islands existed on the SS-PEI (30)-PEG2k (5)-apo α-lactalbumin (0.1) surface which indicated higher mass density adsorbed. This observation was consistent with the

results obtained from the QCM-D measurement, the presence of PEG enhanced the adsorption of apo α-lactalbumin (refer to Chapter 6). It appeared that holo α-lactalbumin and apo α-lactalbumin molecules had filled in the SS-PEI (30)-PEG2k (5) surface valleys. However, it was unexplained why the p_{island} for PEG5k was much lower than of the PEG350 and PEG5k. Besides that, the estimated mass densities adsorbed due to the islands were much lower compared to that on the QCM-D measurement and even less than the expected monolayer density. From the images, it was clearly shown that, the molecules tend to aggregate rather adsorbed individually. However, since the characterization referred to the tightly-bound molecules (after rinsing with buffer solution), we expected that the single adsorbed molecules were desorbed during the rinsing and left the aggregate molecules. The aggregated molecules have a larger surface area to bind with the surface and thus more difficult to desorb. The results obtained will be discussed further in Chapter 11.

Table 8.10: Summary of the surface roughness (RMS), estimated island height, estimated diameter size of the islands and percentage of island proportion.

Surface	Roughness (RMS) (nm)	Estimated island height (nm)	Estimated diameter size of the islands (nm)	Percentage of island proportion, p_{island} (%)
Bare SS	1.25	5	-	0
SS-β-casein (0.1)	1.520	5.74	100 to 200	9
SS-lysozyme (0.1)	2.198	6.68	200 to 260	10
SS-apo α-lactalbumin (0.1)	3.299	12.55	130 to 330	28
SS-PEI (30)	1.995	8.48	60 to 130	6
SS-silicate (50)	1.318	5.16	130 to 200	12
SS-PEI (30)-PEG350 (5)	2.639	15.98	130 to 330	29
SS-PEI (30)-PEG2k (5)	4.071	15.02	260 to 400	81
SS-PEI (30)-PEG5k (5)	4.008	16.02	100 to 130	5
SS-PEI (30)-PEG2k (5)-apo α-lactalbumin (0.1)	3.463	10	260 to 400	75
SS-PEI (30)-PEG2k (5)-holo α-lactalbumin (0.1)	1.584	7	200	33

CHAPTER NINE

STAINLESS STEEL SURFACE CHARACTERIZATION

9.0 Introduction

This chapter describes the result of our stainless steel surface (QSENSE-SS2343) specimen characterization using an atomic force microscopy (AFM) and X-ray photoelectron spectroscopy (XPS) using the scanning electron microscopy (SEM). The surface characterization also was done on commercial stainless steel (SS 304) surfaces as a comparison. The SS 304 surface used was a flat sheet with a thickness of 0.85 mm (from New Zealand steel company).

9.1 X-ray photoelectron spectroscopy (XPS) characterization

Figures 9.1 and 9.2 show a typical XPS spectrum of SS2343 and SS 304 surfaces, respectively. A XPS spectrum is a plot of the number of electrons detected (Y-axis, ordinate) versus the binding energy of the electrons detected (X-axis, abscissa). Each element produces a characteristic set of XPS peaks at characteristic binding energy values that directly identify each element that exists in or on the surface of the material being analyzed. Overall, the components of a stainless steel surface detected by XPS are chromium (Cr), iron, nickel (Ni), silica (Si) and molybdenum (Mo) ions. However molybdenum ions were not detected on a SS2343 surface; at keV around 2.00, the peak of Au was detected instead of the Mo ions peak.

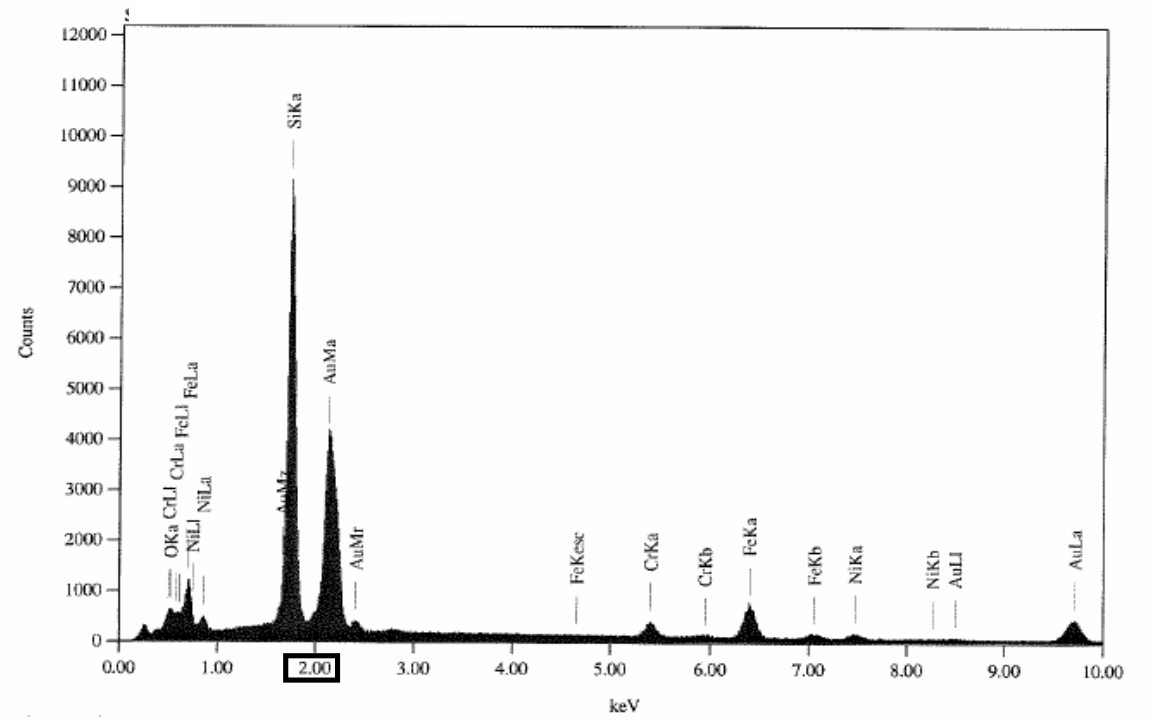

Figure 9.1: XPS spectrum of a SS2343 surface.

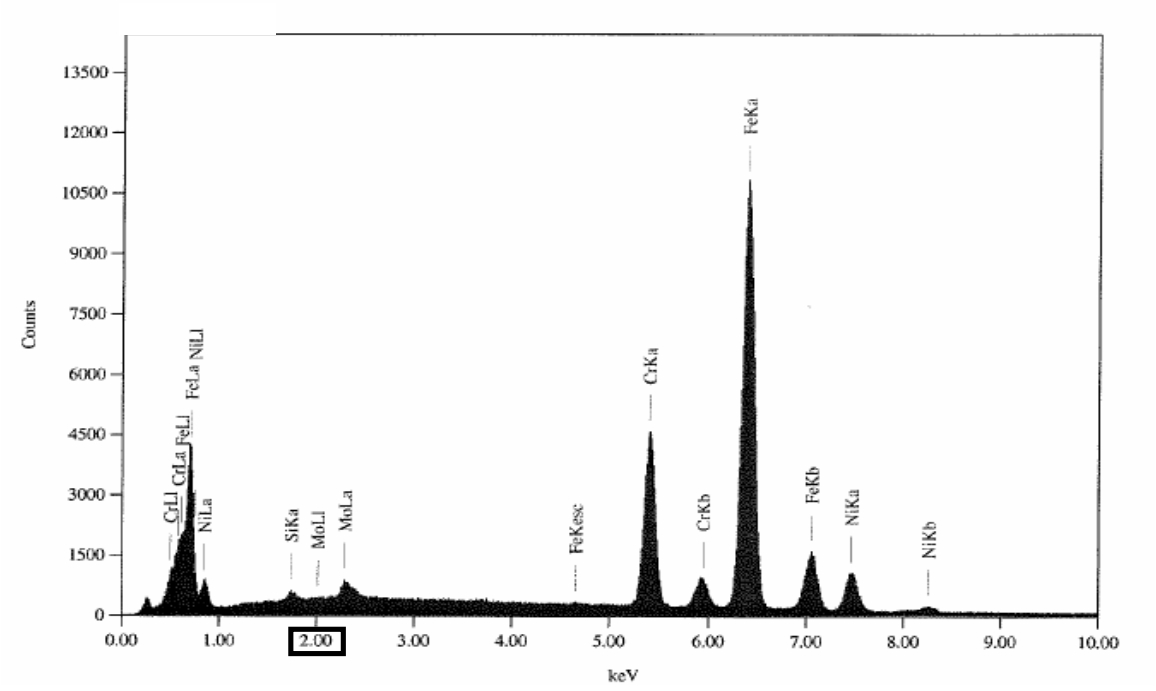

Figure 9.2: XPS spectrum of a SS 304 surface.

A summary of the percentage of the component composition of SS2343 and SS 304 surfaces detected by XPS characterization is presented in Tables 9.1 and 9.2, respectively. The data were taken at four different spots on the same surface. It seems that the components of the materials were distributed evenly on the surface. For the SS2343 surface, Au ions appeared to be the major compositions whereas on the SS 304 surface, was iron ions.

Table 9.1: Percentage of the component composition of a SS2343 surface. The data were taken at four different spots on the same surface.

	I	II	III	IV
Component	Composition (%)	Composition (%)	Composition (%)	Composition (%)
Cr	3.01	2.92	3.11	3.07
Iron	9.87	9.34	9.64	9.47
Ni	1.55	1.96	1.88	2.22
Silica	27.05	27.63	26.98	27.14
Oxide	3.58	3.84	3.92	3.40
Au	54.93	54.31	54.47	54.70
Molybdenum	Not detected	Not detected	Not detected	Not detected

Table 9.2: Percentage of the component composition of a SS 304 surface. The data were taken at four different spots on the same surface.

	I	II	III	IV
Component	Composition (%)	Composition (%)	Composition (%)	Composition (%)
Cr	17.57	17.14	17.22	17.51
Iron	69.85	70.52	69.37	70.24
Ni	10.14	10.14	10.28	10.02
Silica	0.40	0.23	0.54	0.37
Molybdemum	2.03	1.98	2.59	1.87

9.2 Atomic force microscopy (AFM)

Figures 9.3 and 9.4 show respectively the AFM lateral 2D topography (height) image and phase image of a bare SS2343 surface. From the scale in Figure 8.1, zero refers to the level at the average surface; positive value (above zero) refers to height of the peak (molecules) above the average surface whereas negative value (below zero) refers to the height of the peak (molecules) below the average surface. From Figure 9.3, the structure of the surface was apparently homogeneous with the highest peak from the average surface around 4 to 5 nm. Also observed, different phases existed on the surfaces with some dark dots distributed randomly on the surface as depicted in Figure 9.4. The RMS roughness of the SS2343 surface was calculated by the AFM package to be about 1.25 nm.

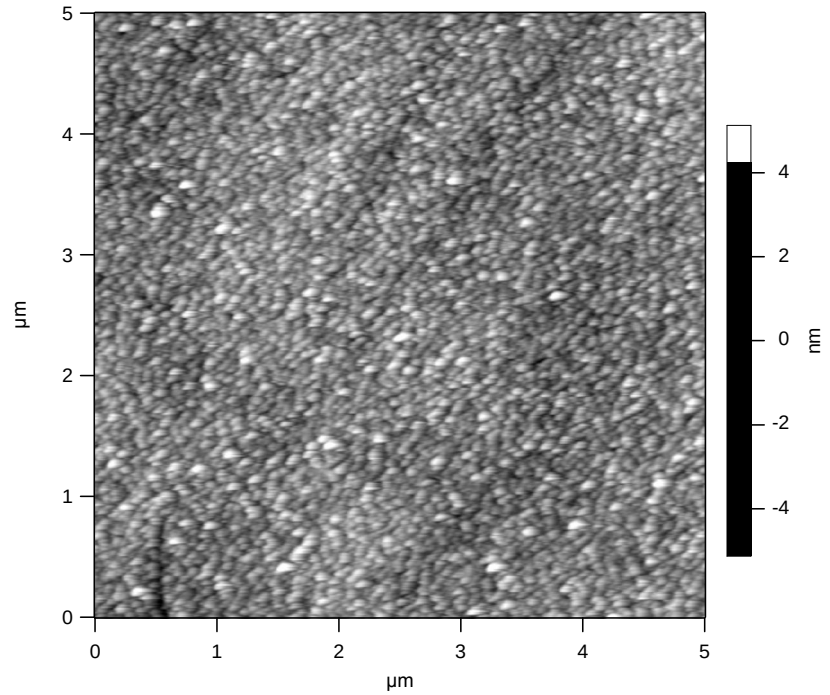

Figure 9.3: 2D AFM height image morphology of a bare SS2343 surface.

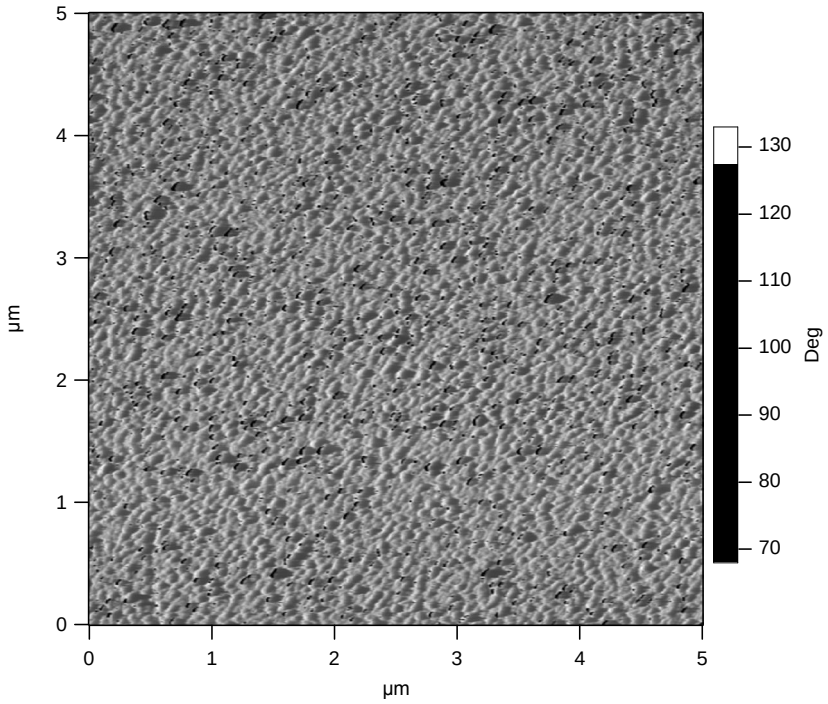

Figure 9.4: 2D AFM phase image morphology of a bare of a bare SS2343 surface.

9.3 Scanning electron microscopy (SEM)

Figures 9.5 and 9.6 illustrate respectively the SEM image of SS2343 and SS 304 surfaces. As can be seen, the SEM image for the SS2343 surface appeared to be more homogenous compared to that of the SS 304 surface. There was apparently like layers on a SS 304 surface.

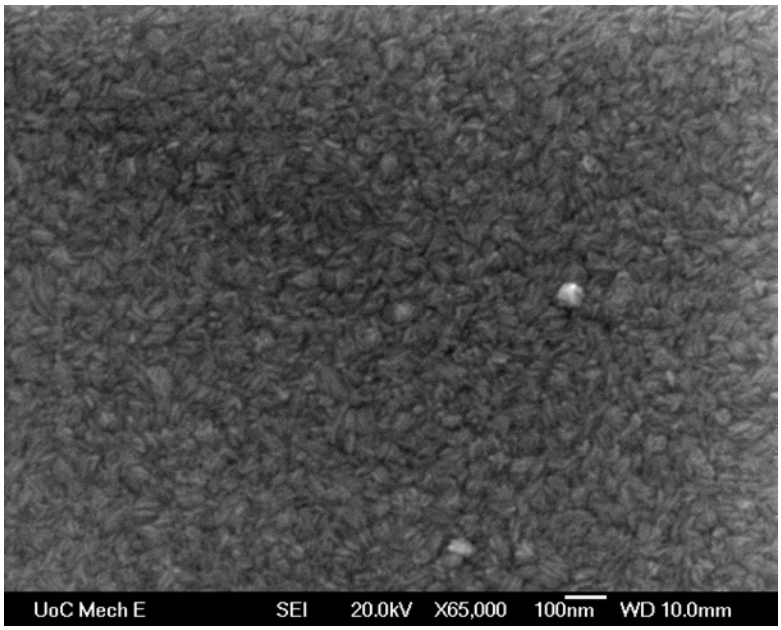

Figure 9.5: SEM image of a SS2343 surface.

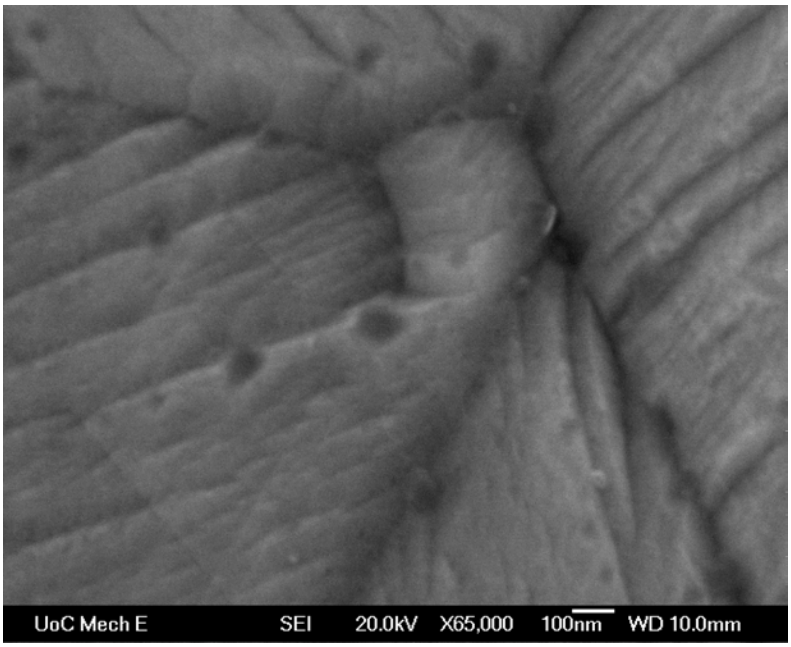

Figure 9.6: SEM image of a SS 304 surface.

CHAPTER TEN

KINETIC MODELLING AND INTERPRETATION OF DATA

10.0 Introduction

The kinetics of adsorption of proteins on a bare stainless steel surface was modeled, including a possible diffusion step. The purpose was to find the best model that can fit our kinetic data allowing the interpretation of the adsorption process. All the models were solved using the Microsoft Excel Solver version 2003, based on a finite divided difference approach. From the results obtained, it appeared that at higher temperatures and concentrations, the kinetic data were much better interpreted using diffusion-reaction models than simple surface reaction models. It appeared that, at high temperatures and concentrations, the adsorption of proteins onto a bare stainless steel surface was governed by a diffusion-reaction mechanism. A surface reaction was apparently appropriate only at room temperature and when adsorbing from the lowest concentration, 0.1 g / L. Only the results of the fitting with a diffusion-reaction model are presented here whereas the fitting with surface reaction models are depicted in Appendix B.

DIFFUSION-REACTION MODEL

10.1 Diffusion-reaction regime

Further insight into the adsorption process may be achieved by a closer analysis of the adsorption rate. Figures 10.1 to 10.4 show examples of rates of adsorption as a function of surface density and time for β-casein at different concentrations and temperatures. As can be seen, it clearly delineates diffusion limiting and reaction limiting regimes. The diffusion limited regime was

characterized by an increasing rate of adsorption while the surface limited regime was characterized by a decreasing rate of adsorption. The former occurred initially with diffusion from flowing solution to the surface being the slow, limiting mechanism (characterized by an increasing rate of adsorption from an initial value of zero). This regime continued until a maximum rate of adsorption was reached. The reaction limited regime occurred over longer times, with adsorption to an increasingly blocked surface being the governing mechanism (characterized by a decreasing rate of adsorption).

Although the presence of kinetic regimes can be inferred from plots of surface density versus time, their identification and quantification are greatly facilitated by a rate of adsorption versus surface density representation as shown in Figures 10.2, 10.4, 10.5, 10.6, 10.7 and 10.8.

From Figures 10.1 and 10.3, the transient diffusion period decreased from about 6 to 3 seconds as concentration and temperature increased from 0.1 g / L (23 °C) to 1 g / L (40 °C). Within this period, about 1 and 8 mg/m^2 of β-casein were adsorbed as shown in Figure 10.2 and 10.4, corresponding to about 10 and 40 % of the final adsorption, respectively. This indicates that as concentration and temperature increased the rate of reaction at a surface increased faster than the rate of diffusion. Further increase in concentration and temperature most probably will result that the whole adsorption is in diffusion limited regime. If this is the case, then the surface modification is no longer important for inhibition of protein adsorption.

The same finding was observed on lysozyme protein. As concentration and temperature increased from 0.1 g / L (23 °C) to 1 g / L (40 °C), the percentage of mass adsorbed within the diffusion regime increased from about 6 to 36 % of the final adsorption (refer to Figures 10.5 and 10.6). For α-lactalbumin protein, the mass adsorbed within the diffusion period from a concentration of 0.1 g / L and a temperature of 23 °C was higher than that of β-casein or lysozyme, which is about 25 % of the final adsorption. Almost half of mass were adsorbed (≅ 45 % of the final adsorption) within the diffusion regime when adsorbing from concentration of 1 g / L at 40 °C (refer to Figures 10.7 and 10.8).

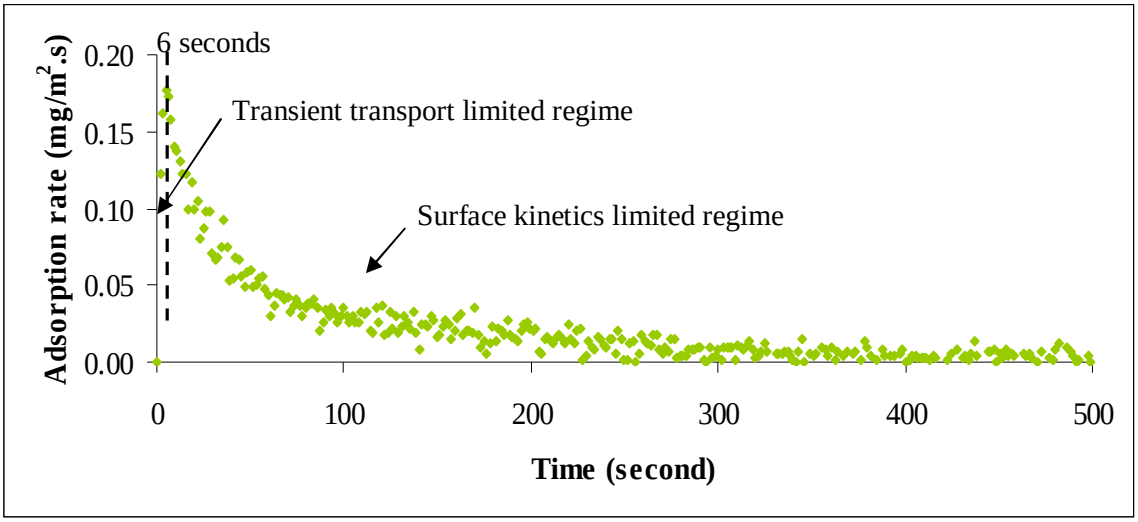

Figure 10.1: Adsorption rate of β-casein from 0.1 g / L solution at 23 °C onto a SS surface as a function of time. Left hand side of vertical line represents the transient transport-limited region while right hand site represents the surface kinetics-limited regime.

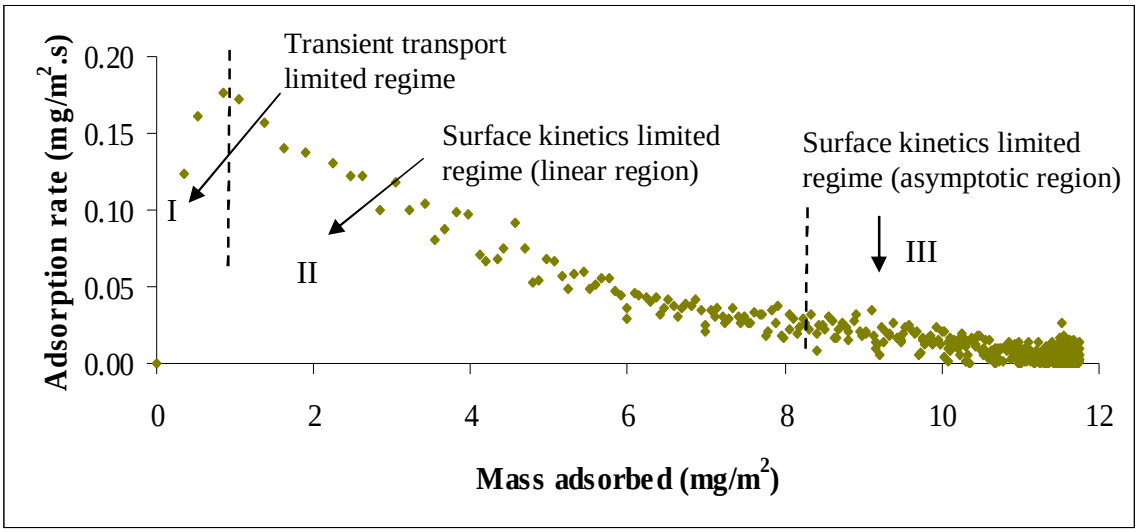

Figure 10.2: Adsorption rate of β-casein from 0.1 g / L solution at 23 °C onto a stainless steel surface as a function of mass adsorbed (mg/m^2). Regime I, II and III refer to transient transport limited regime, surface kinetics limited regime (linear regime) and surface kinetics limited regime (asymptotic region), respectively.

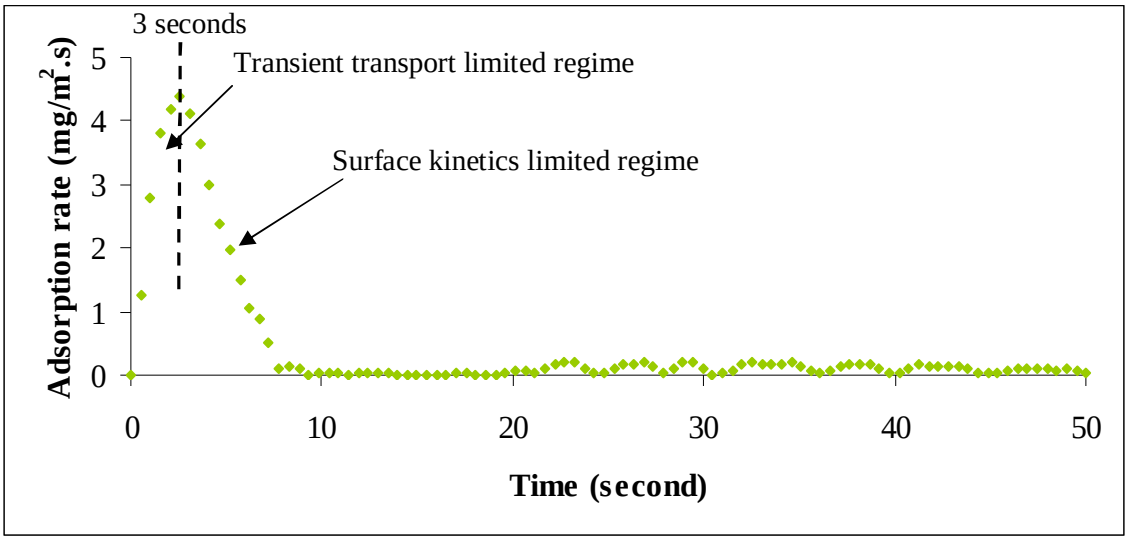

Figure 10.3: Adsorption rate of β-casein from 1 g / L solution at 40 °C onto a SS surface as a function of time. Left hand side of vertical line represents the transient transport-limited region while right hand site represents the surface kinetics-limited regime.

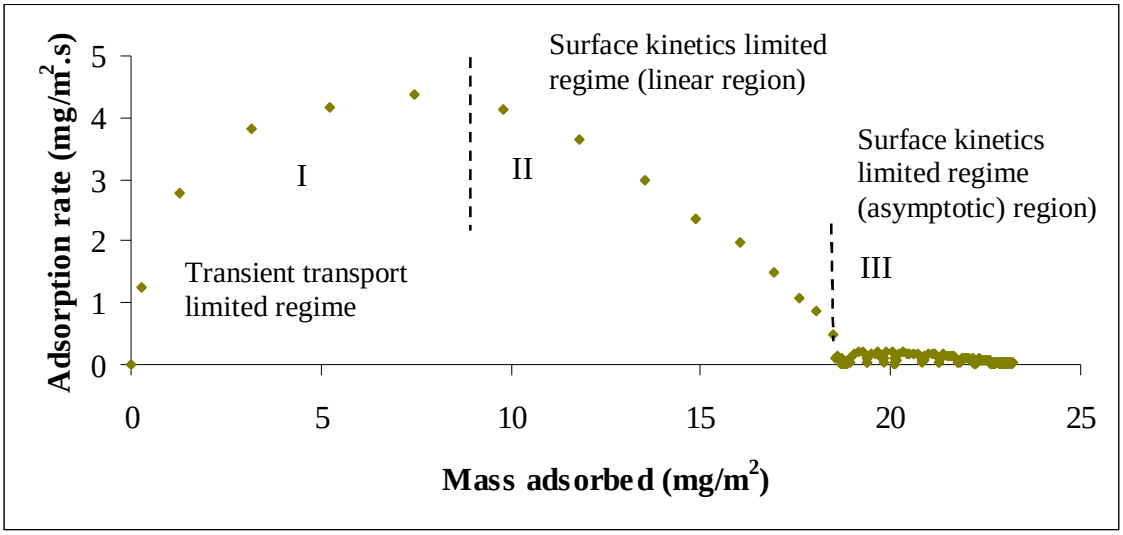

Figure 10.4: Adsorption rate of β-casein from 1 g / L solution at 40 °C onto a SS surface as a function of mass adsorbed (mg/m^2). Regime I, II and III refer to transient transport limited regime, adsorption limited regime (linear regime) and adsorption limited regime (asymptotic region), respectively.

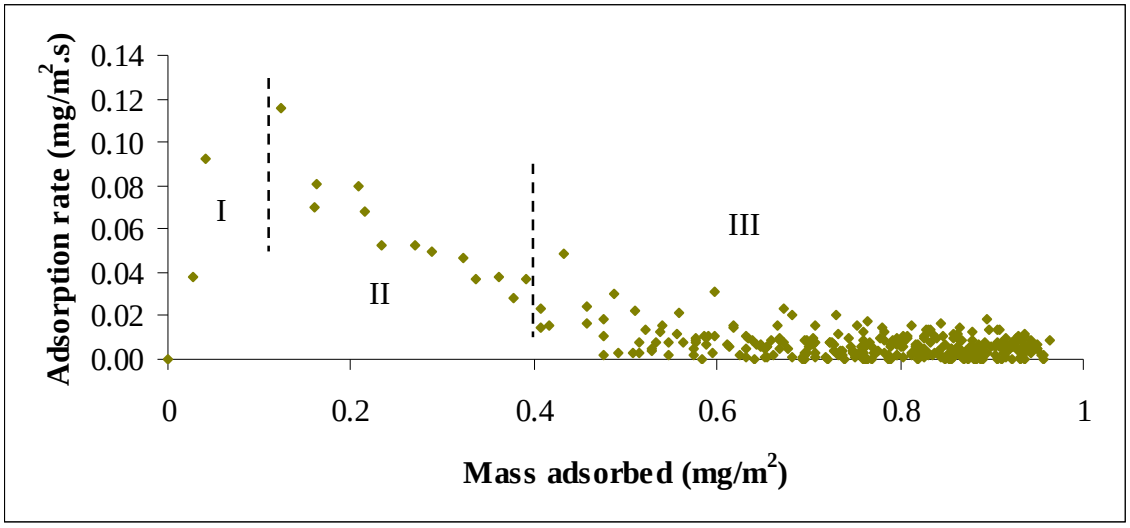

Figure 10.5: Adsorption rate of lysozyme from 0.1 g / L solution at 23 °C onto a SS surface as a function of mass adsorbed (mg/m^2). Regime I, II and III refer to diffusion limited regime, adsorption limited regime (linear regime) and adsorption limited regime (asymptotic region), respectively.

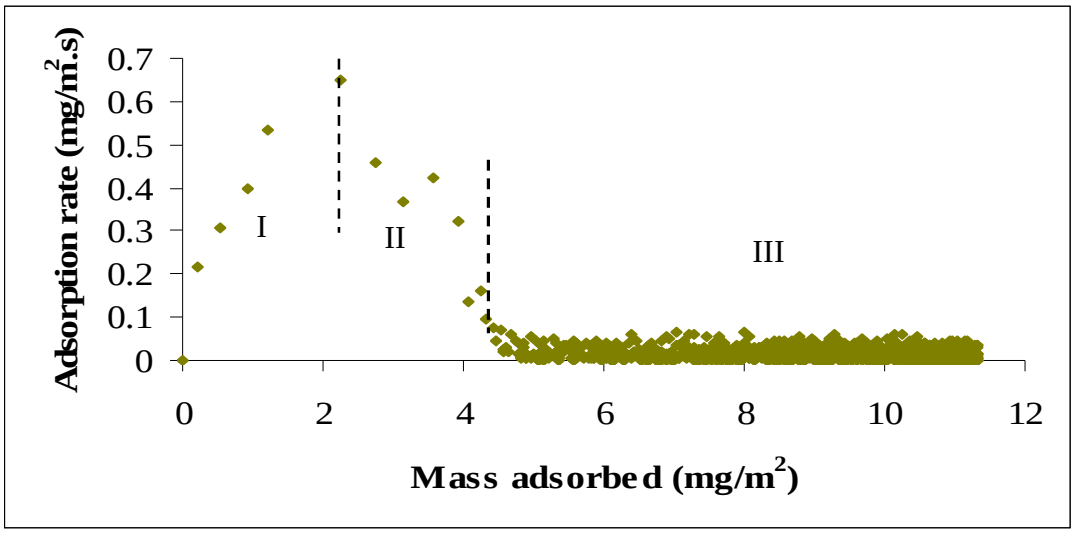

Figure 10.6: Adsorption rate of lysozyme from 1 g / L solution at 40 °C onto a SS surface as a function of mass adsorbed (mg/m^2). Regime I, II and III refer to diffusion limited regime, surface kinetics limited regime (linear regime) and surface kinetics limited regime (asymptotic region), respectively.

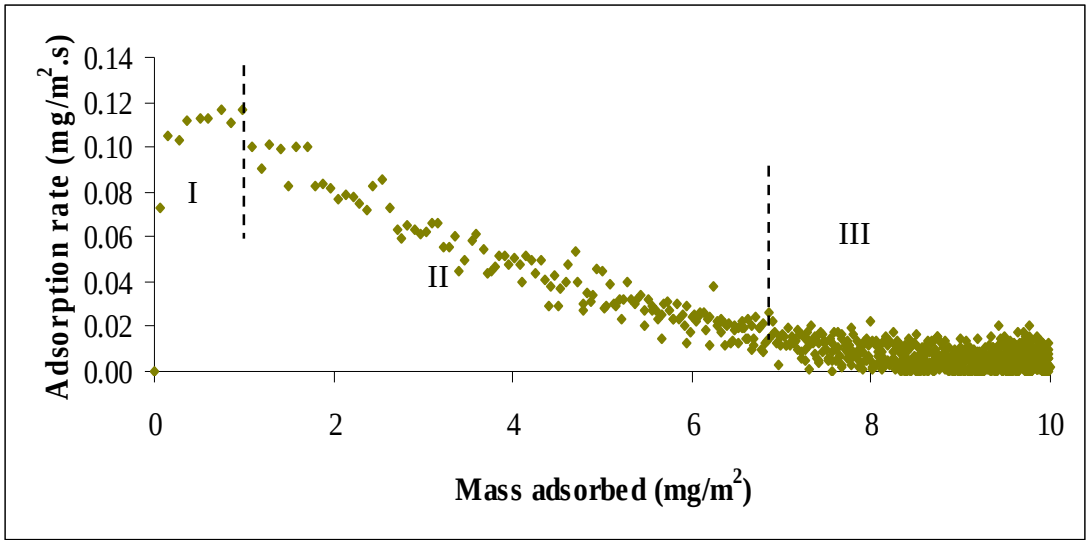

Figure 10.7: Adsorption rate of α-lactalbumin from 0.1 g / L solution at 23 °C onto a SS surface as a function of mass adsorbed (mg/m^2). Regime I, II and III refer to diffusion limited regime, surface kinetics limited regime (linear regime) and surface kinetics limited regime (asymptotic region), respectively.

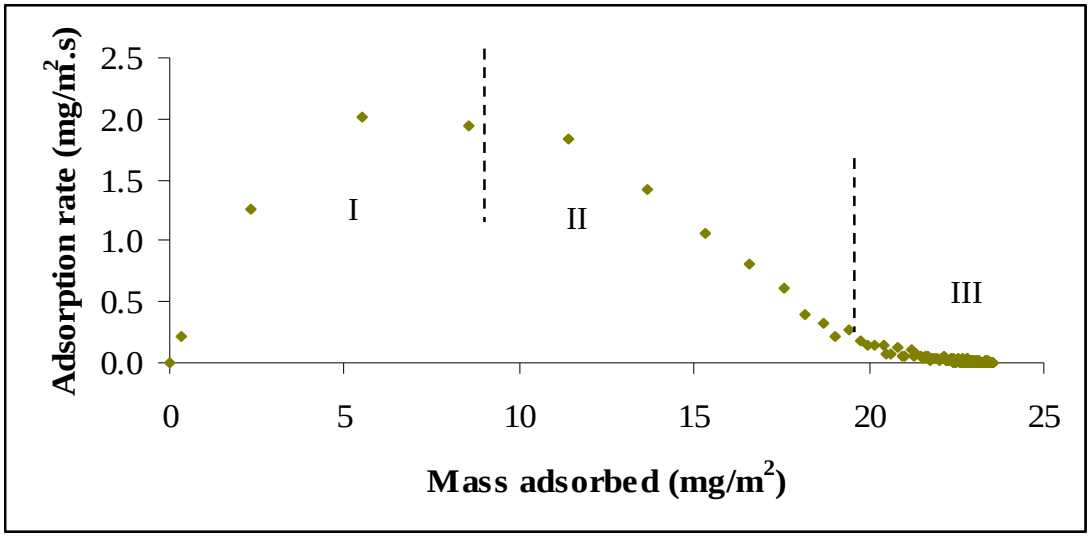

Figure 10.8: Adsorption rate of α-lactalbumin from 1 g / L solution at 40 °C onto a SS surface as a function of mass adsorbed (mg/m^2). Regime I, II and III refer to diffusion limited regime, surface kinetics limited regime (linear regime) and surface kinetics limited regime (asymptotic region), respectively.

It is clearly showed that, the diffusion limited regime becomes more significant at high temperatures and concentrations. Therefore, the diffusion-reaction model was used to fit our kinetic data. The next section shows the result of the fitting using the diffusion-reaction model (refer to Equations 4.32 to 4.36 for the detail of the model). Figure 10.9 illustrates the schematic diagram of the diffusion-reaction model used in this chapter.

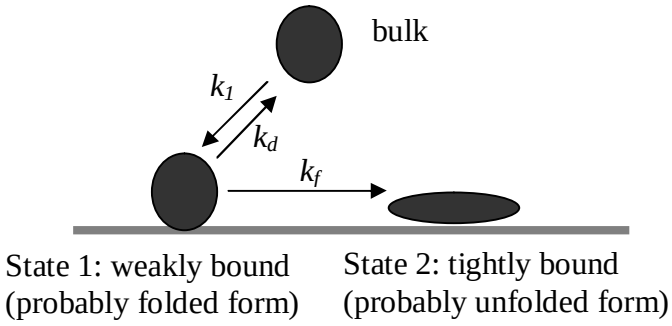

Figure 10.9: Schematic diagram of the diffusion-reaction model.

The adsorption kinetics data has also been modeled using a surface reaction model, that is by neglecting the diffusion term (i.e. using the same equation as the diffusion-reaction model except the diffusion term was neglected). The surface reaction model has been attempted to fit the kinetic data under the lowest (refer to Figure 10.10) and highest (refer to Figure 10.11) experimental operating conditions. As can be seen, the surface reaction model was apparently appropriate only at room temperature and when adsorbing from the lowest concentration, 0.1 g / L (refer to Figure 10.9). At high concentration and temperature (i.e. 1 g / L and 40 °C), the model failed to fit the data well (refer to Figure 10.11). This indicates that the diffusion was important at high temperature and concentration.

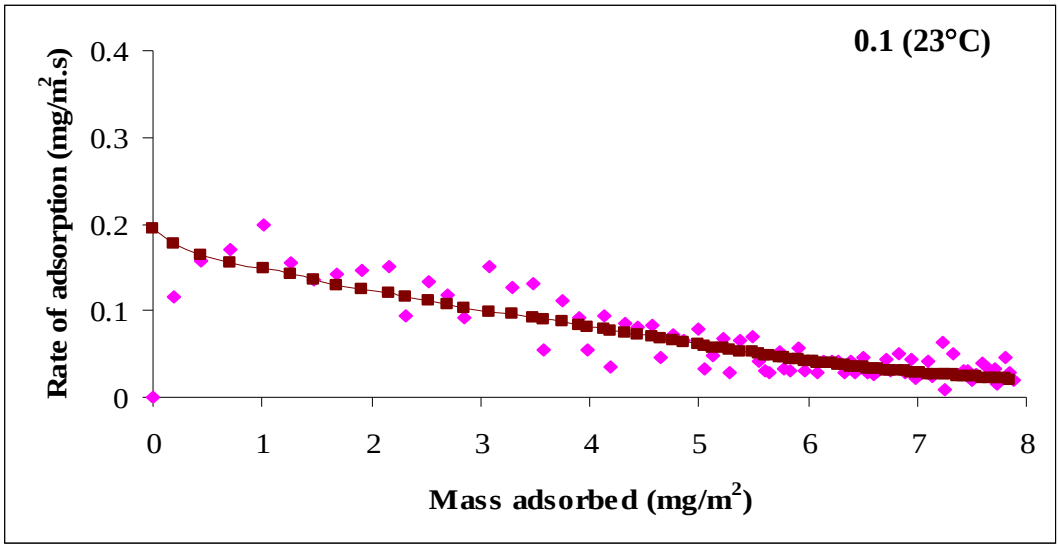

Figure 10.10: Adsorption rate of β-casein (mg/m^2.s) from 0.1 g / L solution onto a bare SS surface as a function of mass adsorbed (mg/m^2) at 23 °C. The data was fitted using a surface reaction model (continuous line).

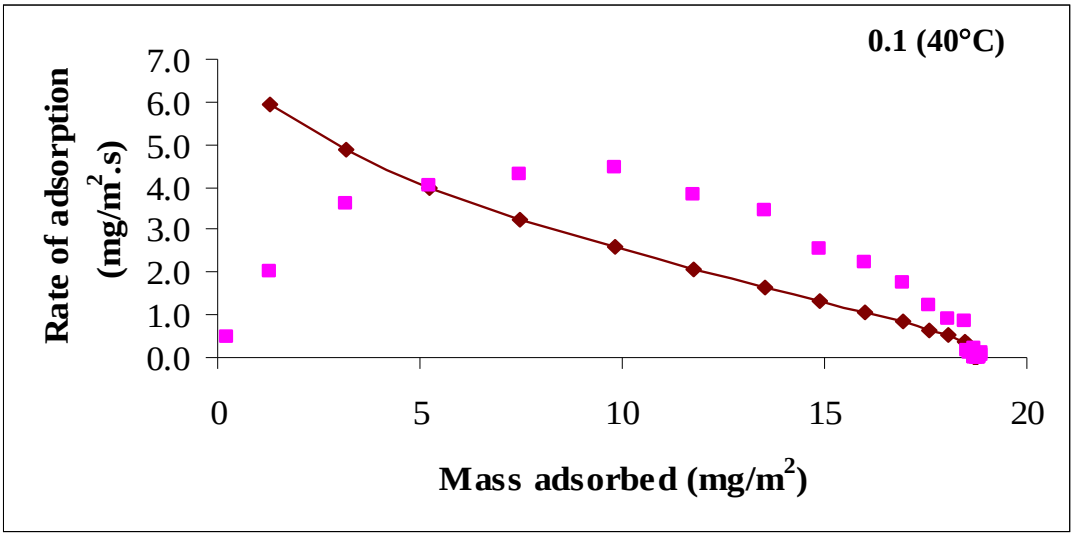

Figure 10.11: Adsorption rate of β-casein (mg/m^2.s) from 1 g / L solution onto a bare SS surface as a function of mass adsorbed (mg/m^2) at 40 °C. The data was fitted using a surface reaction model (continuous line).

10.1.1 β-casein

Figure 10.12 illustrates an example of the experimental mass density of β-casein on a bare SS surface adsorbed from 1 g / L solution at 23 °C fitted using a diffusion-reaction model developed in this study (see Chapter 4, section 4.6). As can be seen, the diffusion-reaction model was able to fit the data reasonably well (refer to Chapter 4 for the detail of diffusion-reaction model).

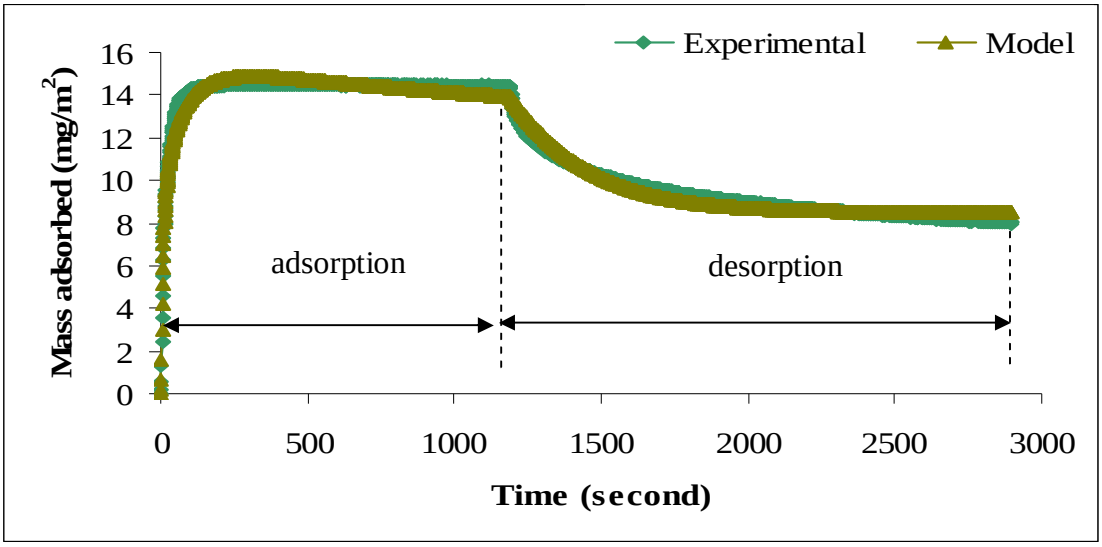

Figure 10.12: Mass density of β-casein on a bare SS surface adsorbed from 1 g / L solution at 23 °C. The data were fitted using a diffusion-reaction model developed in this study.

Figures 10.15 to 10.24 show the rate of β-casein adsorption as a function of mass adsorbed under all the experimental conditions. The data was fitted using a diffusion-reaction model (shown by the continuous line). Also shown in the plot is the region of expected single layer. It was assumed that the expected single layer is 1.5 to 3 times higher than that of theoretical single layer. Then, the expected single layer of β-casein range from 3.5 to 7 mg/ m^2. In general, at low concentration (0.1 g / L), the region of expected single layer was within the surface kinetics limited regime regardless of temperature. At the intermediate concentration (0.5 g / L), the region of

expected single layer meanwhile was between transient transport limited and surface kinetics limited (linear region) regimes regardless of temperature. At high concentration (1 g / L), the region of expected single layer was within the transient transport limited regimes regardless of temperature.

In general, the diffusion-reaction model was able to fit the adsorption kinetics data reasonably well except on the adsorption kinetics conducting under these operating conditions: (i) bulk concentration of 0.5 g / L at 40°C, (ii) bulk concentration of 1 g / L at 30°C and (iii) bulk concentration of 1 g / L at 35°C. Since the trend of rate of adsorption (mg / m^2.s) versus mass adsorbed (mg / m^2) under those conditions is similar, only one example is represented here (see Figure 10.13). Figure 10.13 shows the fitted adsorption rate of β-casein (mg/m^2.s) from 0.5 g / L solution onto a bare SS surface as a function of mass adsorbed (mg/m^2) at 40 °C. As can be seen, the adsorption decreased as shown by the dashed circle (i.e. occurs in the multilayer region). Comparing Figure 10.13 to its kinetic raw data (mass density adsorbed versus time)(refer to Figure 10.14a), one can see that the region of circular dash is located in the region shown by the arrow (Figure 10.14). There are several possibilities that are thought to contribute to this observation (decrement in adsorption):

i) desorption either from weak-weak interactions between the proteins (most probably in multilayers region) or from a shear wall stress (most probably in a single layer region).

ii) error in estimating the total adsorption. The rate of adsorption depicted in Figure 10.13 is obtained by subtracting the mass density at time *t* +1 with the mass density at time *t* and divided with the time difference (from Figure 10.14a) (refer to Equation 10.1).

$$rate\ of\ \ adsorption = \left(\frac{mass\ \ density_{t+1} - mass\ \ density_{t}}{(t+1) - t} \right) \qquad (10.1)$$

Since the QCM-D raw data is measured every second, the fluctuation of mass density obtained is there. Figure 10.14b expanded the time axis illustrated in Figure 10.14a, so that the spikes can be seen clearly. As can be seen in Figure 10.14b, there is a fluctuation in the data from about t = 10 seconds. Thus, it is suggested that this fluctuation contribute to a strange observation in Figure 10.13.

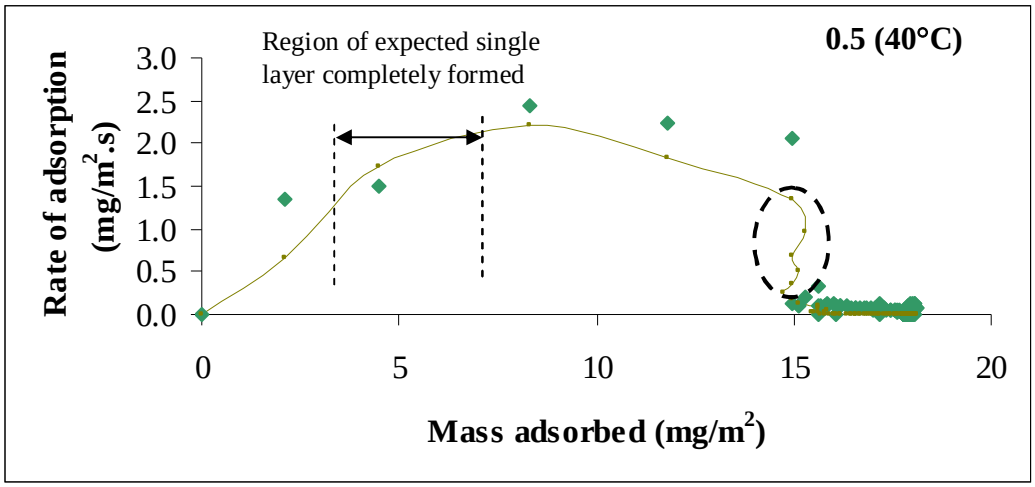

Figure 10.13: Adsorption rate of β-casein ($mg/m^2.s$) from 0.5 g / L solution onto a bare SS surface as a function of mass adsorbed (mg/m^2) at 40 °C. Continuous line refers to the prediction of the model with a single set of fitted constants. Also shown is the region of expected single layer.

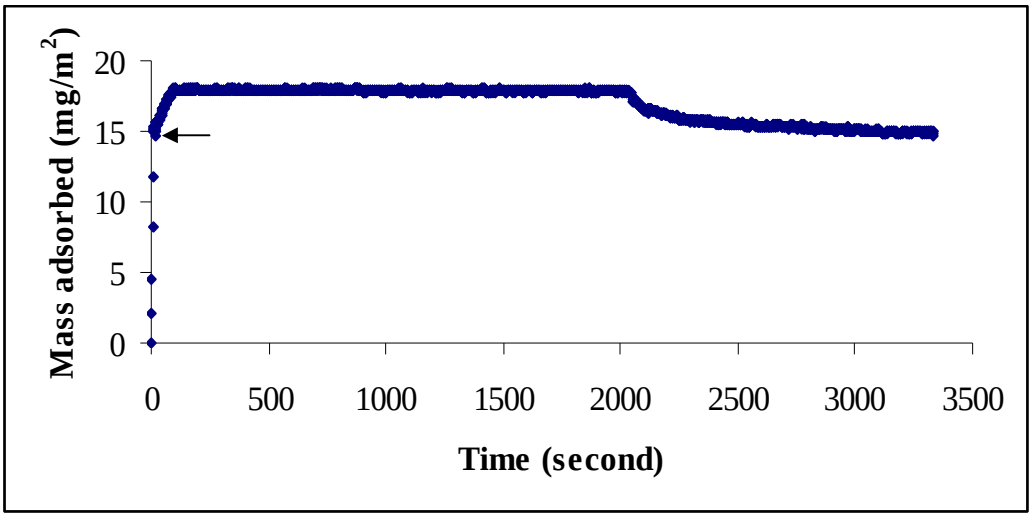

Figure 10.14a: Mass density of β-casein (mg/m^2) on a bare SS adsorbed from 0.5 g / L solution as a function of time at 40 °C.

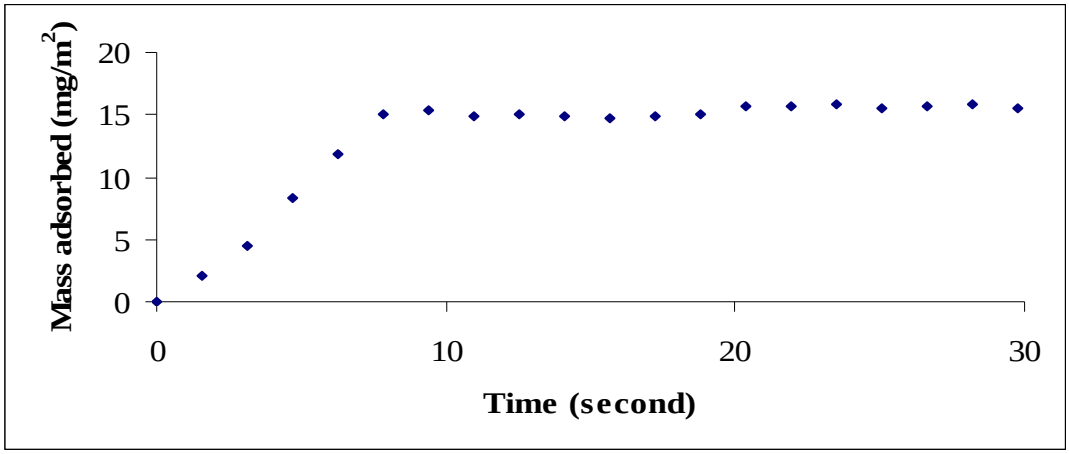

Figure 10.14b: Mass density of β-casein (mg/m^2) on a bare SS adsorbed from 0.5 g / L solution within 30 seconds at 40 °C.

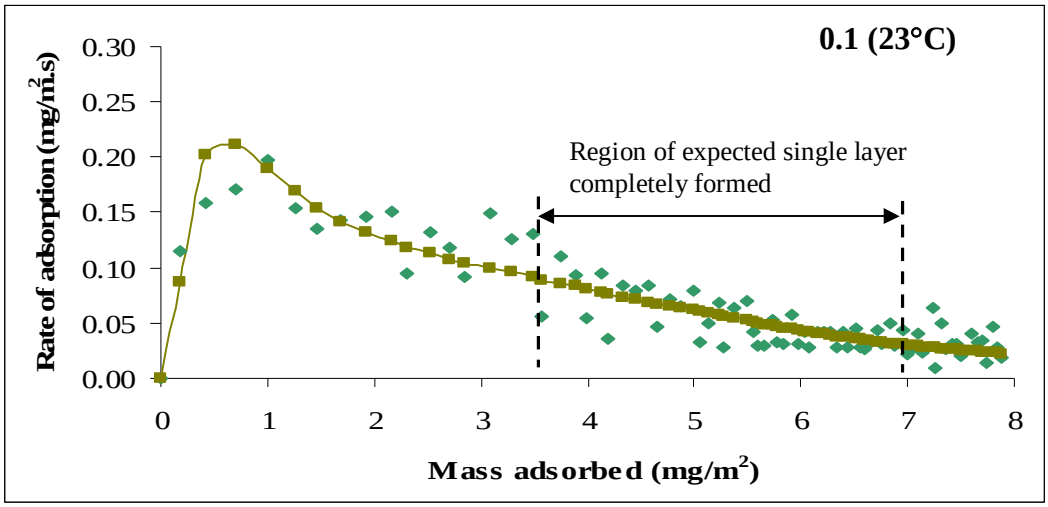

Figure 10.15: Adsorption rate of β-casein (mg/m^2.s) from 0.1 g / L solution onto a bare SS surface as a function of mass adsorbed (mg/m^2) at 23 °C. Continuous line refers to the prediction of the model with a single set of fitted constants. Also shown is the region of expected single layer.

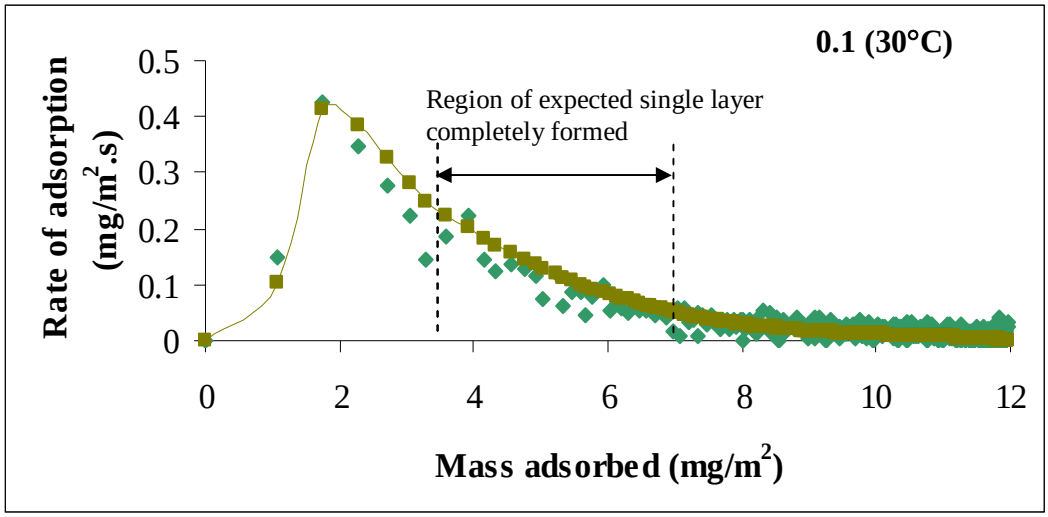

Figure 10.16: Adsorption rate of β-casein (mg/m^2.s) from 0.1 g / L solution onto a bare SS surface as a function of mass adsorbed (mg/m^2) at 30 °C. Continuous line refers to the prediction of the model with a single set of fitted constants. Also shown is the region of expected single layer.

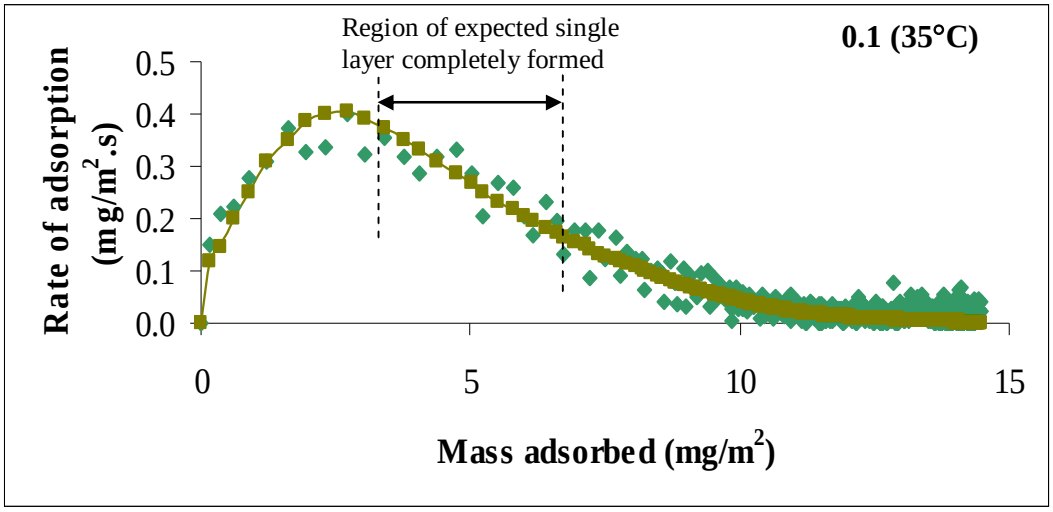

Figure 10.17: Adsorption rate of β-casein (mg/m^2.s) from 0.1 g / L solution onto a bare SS surface as a function of mass adsorbed (mg/m^2) at 35 °C. Continuous line refers to the prediction of the model with a single set of fitted constants. Also shown is the region of expected single layer.

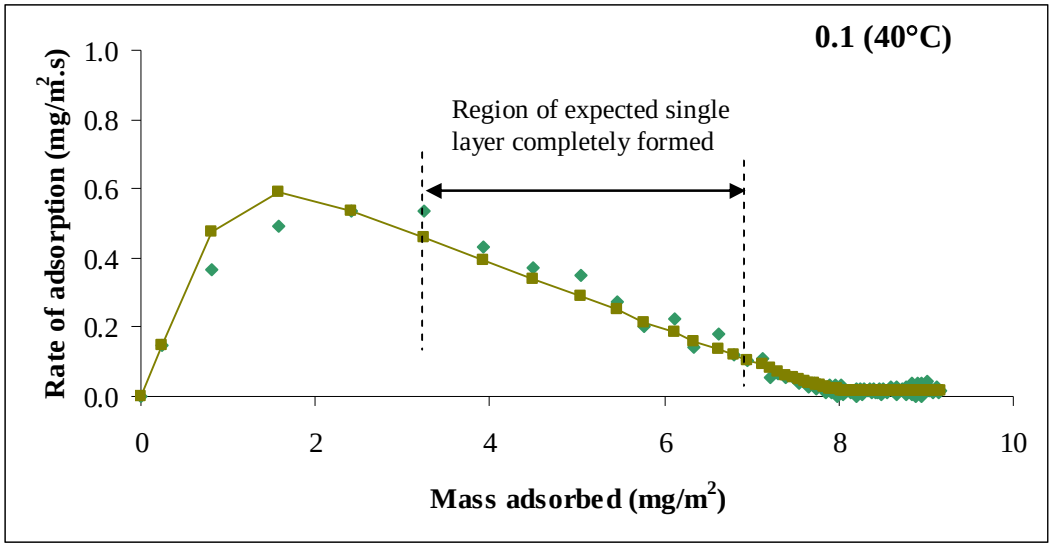

Figure 10.18: Adsorption rate of β-casein (mg/m^2.s) from 0.1 g / L solution onto a bare SS surface as a function of mass adsorbed (mg/m^2) at 40 °C. Continuous line refers to the prediction of the model with a single set of fitted constants. Also shown is the region of expected single layer.

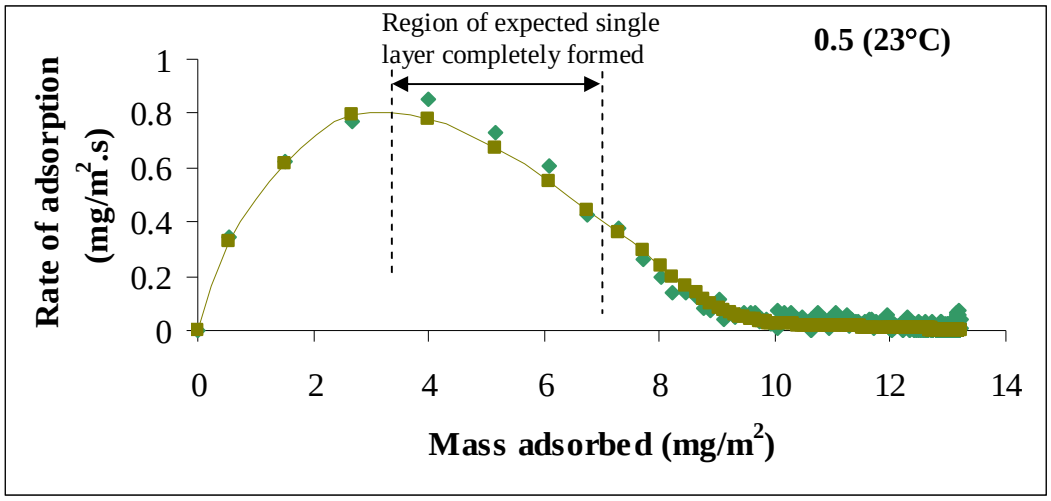

Figure 10.19: Adsorption rate of β-casein (mg/m^2.s) from 0.5 g / L solution onto a bare SS surface as a function of mass adsorbed (mg/m^2) at 23 °C. Continuous line refers to the prediction of the model with a single set of fitted constants. Also shown is the region of expected single layer.

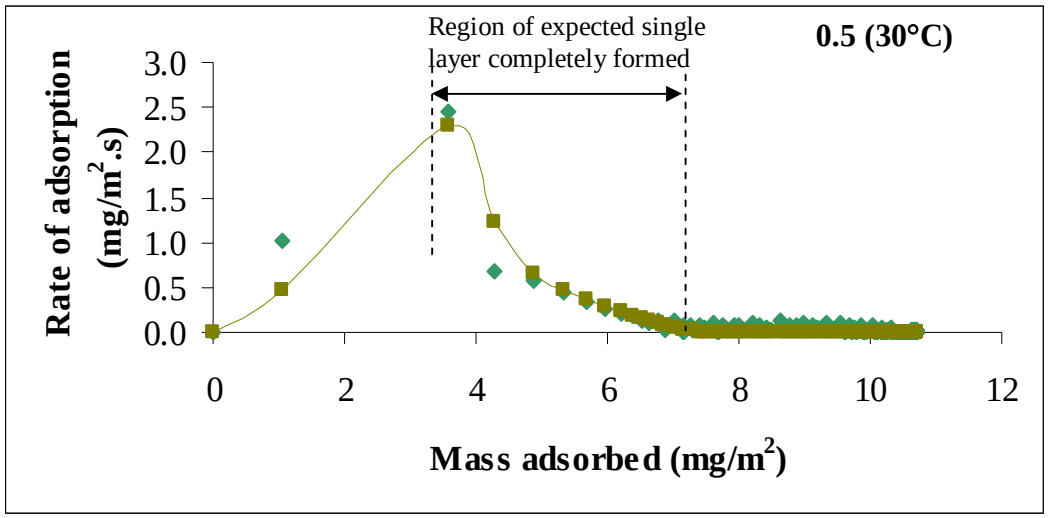

Figure 10.20: Adsorption rate of β-casein (mg/m^2.s) from 0.5 g / L solution onto a bare SS surface as a function of mass adsorbed (mg/m^2) at 30 °C. Continuous line refers to the prediction of the model with a single set of fitted constants. Also shown is the region of expected single layer.

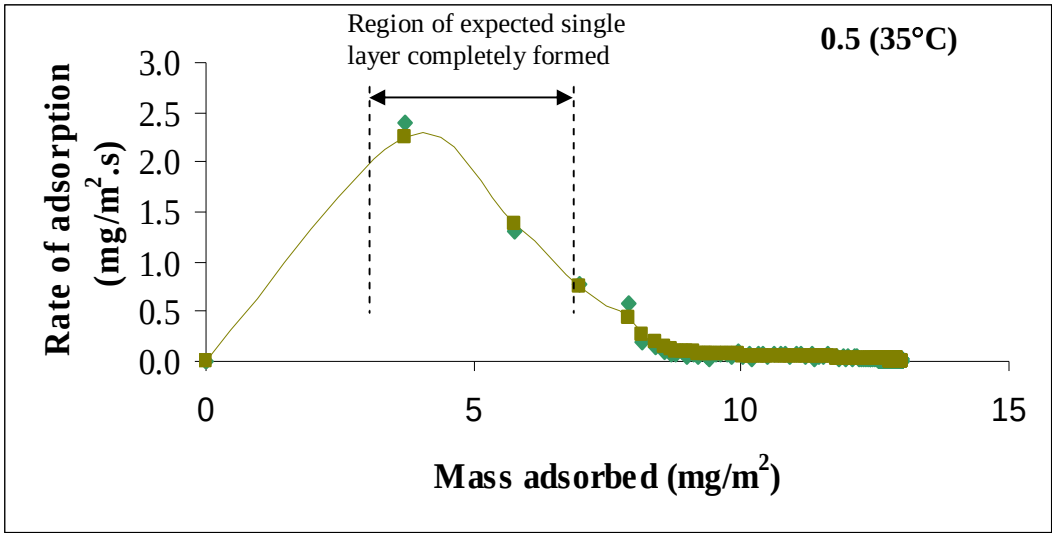

Figure 10.21: Adsorption rate of β-casein (mg/m^2.s) from 0.5 g / L solution onto a bare SS surface as a function of mass adsorbed (mg/m^2) at 35 °C. Continuous line refers to the prediction of the model with a single set of fitted constants. Also shown is the region of expected single layer.

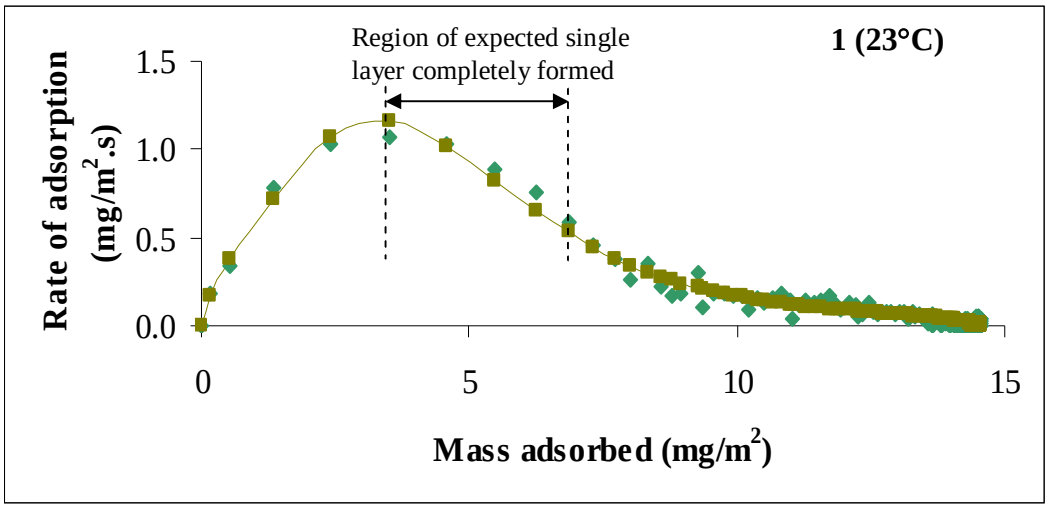

Figure 10.23: Adsorption rate of β-casein (mg/m^2.s) from 1 g / L solution onto a bare SS surface as a function of mass adsorbed (mg/m^2) at 23 °C. Continuous line refers to the prediction of the model with a single set of fitted constants. Also shown is the region of expected single layer.

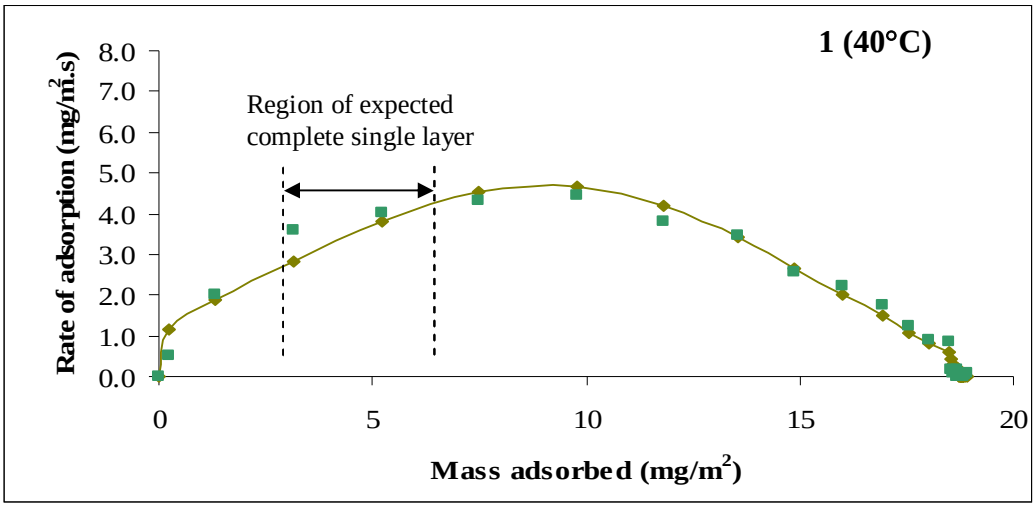

Figure 10.24: Adsorption rate of β-casein (mg/m^2.s) from 1 g / L solution onto a bare SS surface as a function of mass adsorbed (mg/m^2) at 40 °C. Continuous line refers to the prediction of the model with a single set of fitted constants. Also shown is the region of expected single layer.

Figures 10.25 to 10.29 show respectively the fitted parameters of k_1, k_d, k_f, b and a as a function of temperature and concentration modelled using a diffusion-reaction model. Interestingly, the fitted parameters seemed did not affect much by a concentration, especially shown by k_1.

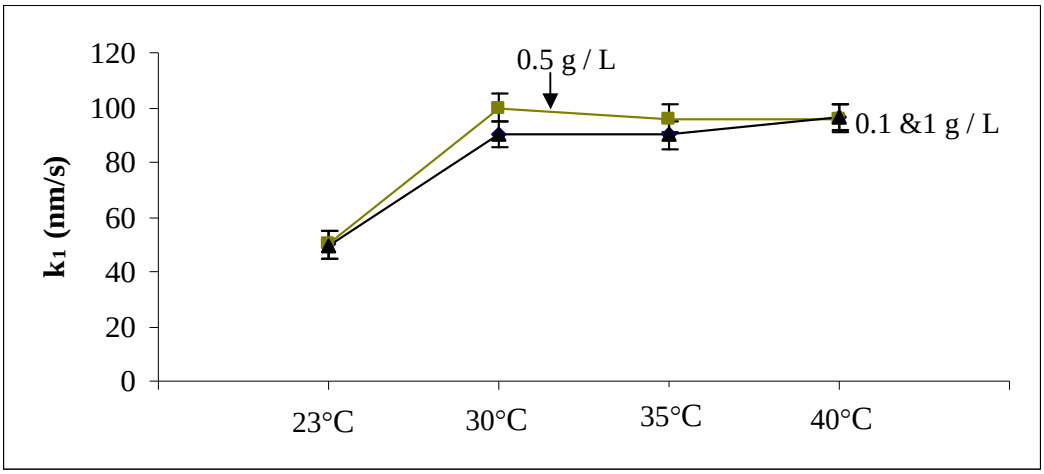

Figure 10.25: Fitted adsorption rate constant, k_1 (nm/s), as a function of temperature and concentration of β-casein in the solution of 0.1, 0.5 and 1 g / L modeled using a diffusion-reaction model.

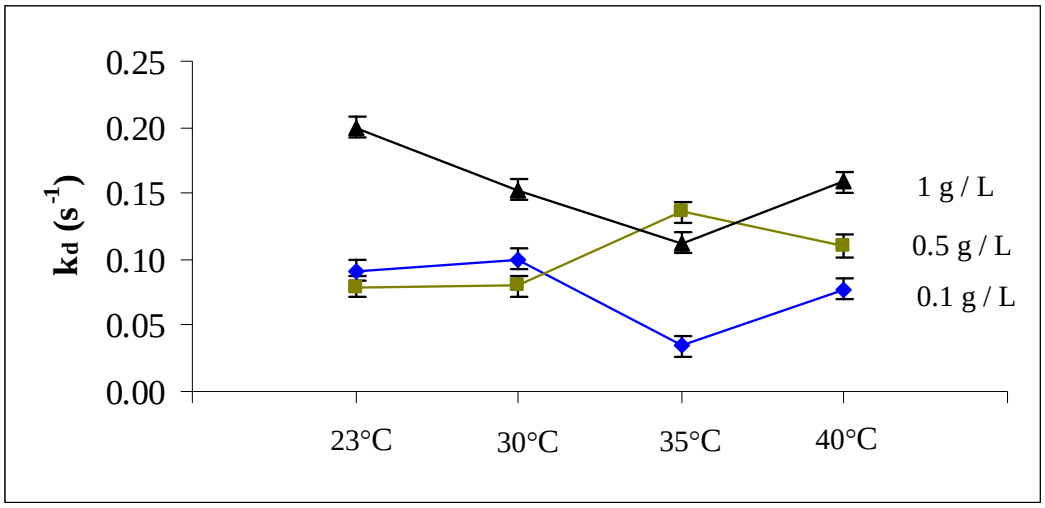

Figure 10.26: Fitted desorption rate constant, k_d (1/s), as a function of temperature and concentration of β-casein in the solution of 0.1, 0.5 and 1 g / L modeled using a diffusion-reaction model.

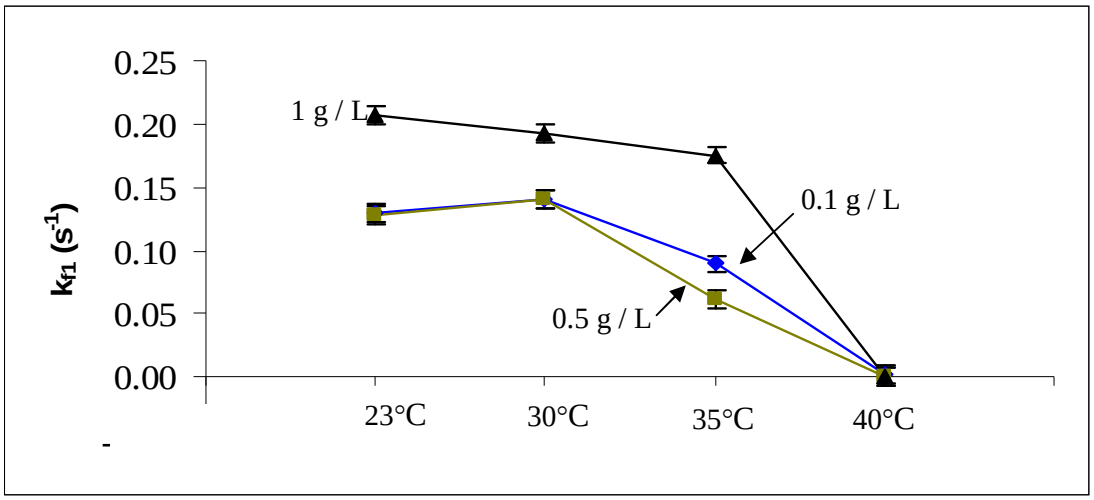

Figure 10.27: Fitted transformation to tightly held rate constant, k_f (1/s), as a function of temperature and concentration of β-casein in the solution of 0.1, 0.5 and 1 g / L modeled using a diffusion-reaction model.

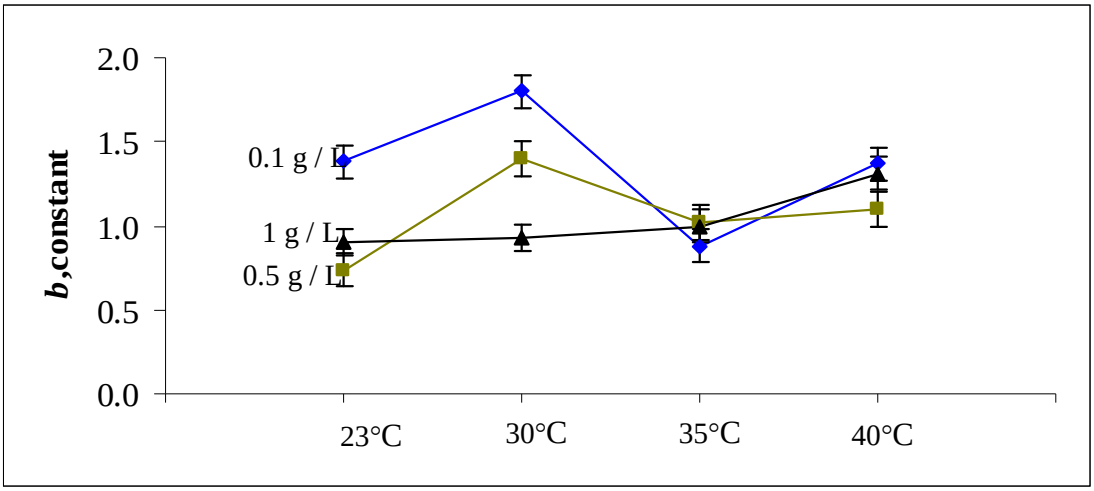

Figure 10.28: Fitted constant axplying factor, *b*, as a function of temperature and concentration of β-casein in the solution of 0.1, 0.5 and 1 g / L modeled using a diffusion-reaction model.

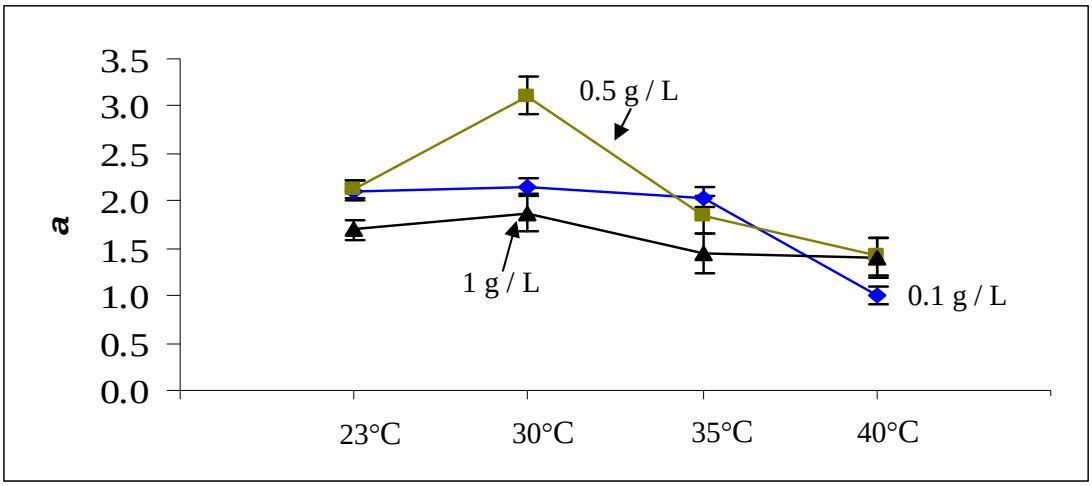

Figure 10.29: Fitted constant spreading factor, *a*, as a function of temperature and concentration of β-casein in the solution of 0.1, 0.5 and 1 g / L modeled using a diffusion-reaction model.

10.1.2 Lysozyme

Figures 10.30 to 10.35 show the results of the fitting using a diffusion-reaction model on some of the lysozyme kinetics data. In general, the diffusion-reaction model was able to fit the data well. Similar to β-casein, the region of expected single layer was incorporated in the plots. The expected single layer of lysozyme ranged from about 4.5 to 9 mg / m^2 (it was assumed that the expected single layer is 1.5 to 3 times that the theoretical single layer).

In general, the region of expected single layer of lysozyme was within the surface kinetics limited regime (asymptotic region) regardless of either temperature or concentration.

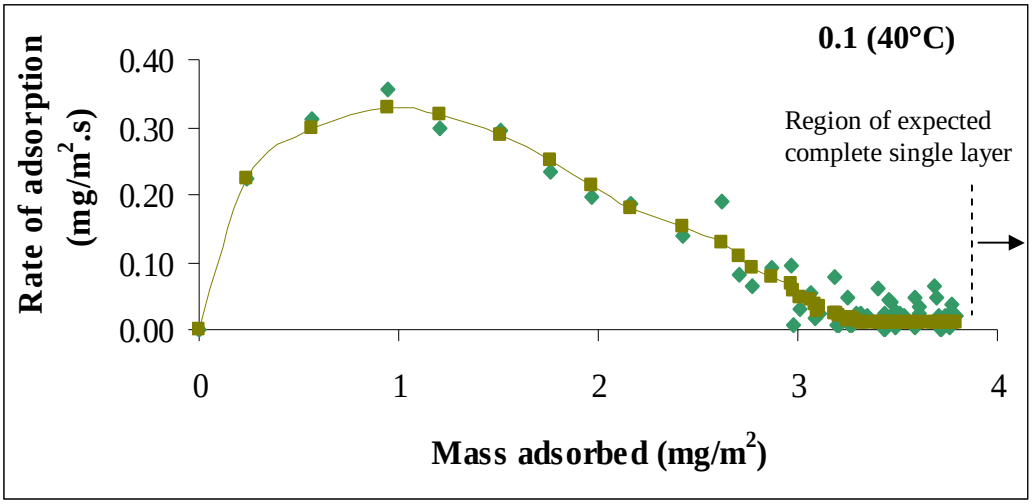

Figure 10.30: Adsorption rate of lysozyme (mg/m^2.s) from 0.1 g / L solution onto a bare SS surface as a function of mass adsorbed (mg/m^2) at 40 °C. Continuous line refers to the prediction of the model with a single set of fitted constants. Also shown is the region of expected single layer.

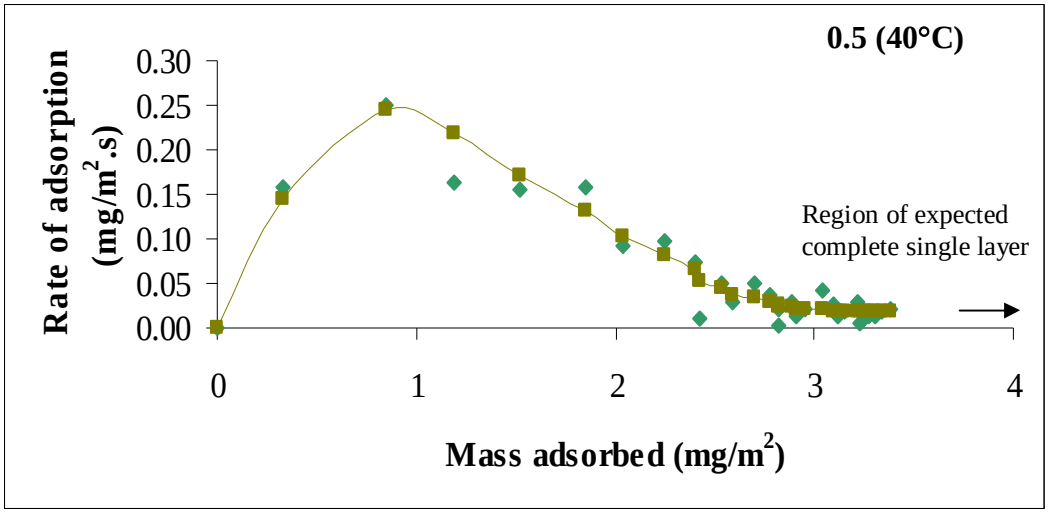

Figure 10.31: Adsorption rate of lysozyme (mg/m^2.s) from 0.5 g / L solution onto a bare SS surface as a function of mass adsorbed (mg/m^2) at 40 °C. Continuous line refers to the prediction of the model with a single set of fitted constants. Also shown is the region of expected single layer.

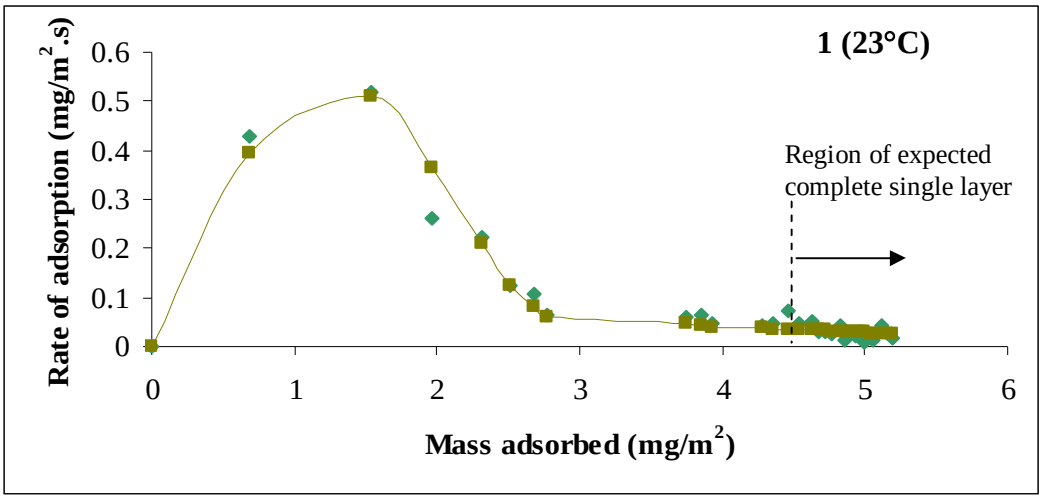

Figure 10.32: Adsorption rate of lysozyme (mg/m^2.s) from 1 g / L solution onto a bare SS surface as a function of mass adsorbed (mg/m^2) at 23 °C. Continuous line refers to the prediction of the model with a single set of fitted constants. Also shown is the region of expected single layer.

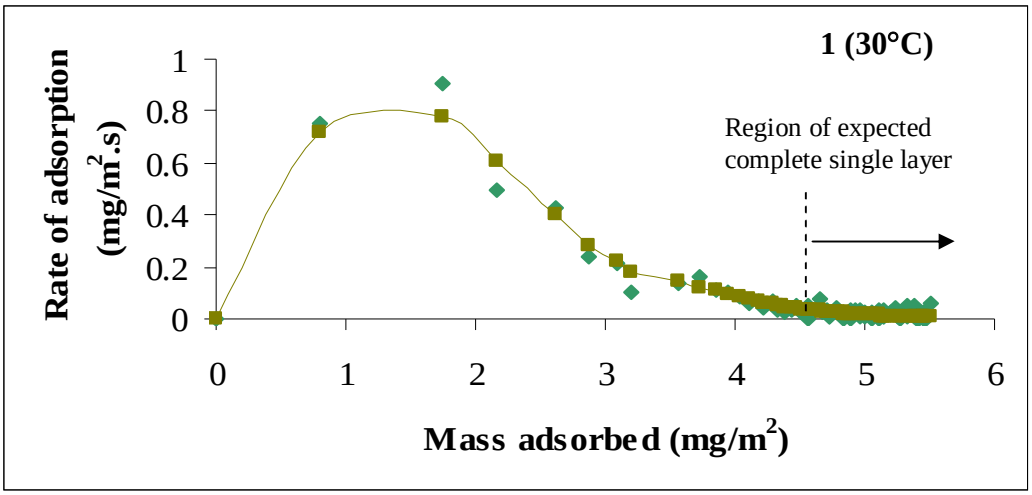

Figure 10.33: Adsorption rate of lysozyme (mg/m^2.s) from 1 g / L solution onto a bare SS surface as a function of mass adsorbed (mg/m^2) at 30 °C. Continuous line refers to the prediction of the model with a single set of fitted constants. Also shown is the region of expected single layer.

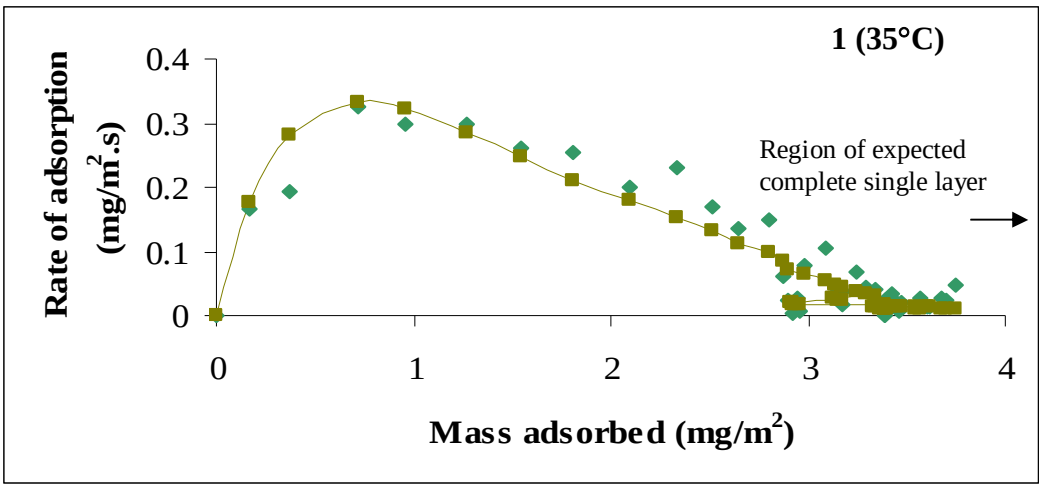

Figure 10.34: Adsorption rate of lysozyme (mg/m^2.s) from 1 g / L solution onto a bare SS surface as a function of mass adsorbed (mg/m^2) at 35 °C. Continuous line refers to the prediction of the model with a single set of fitted constants. Also shown is the region of expected single layer.

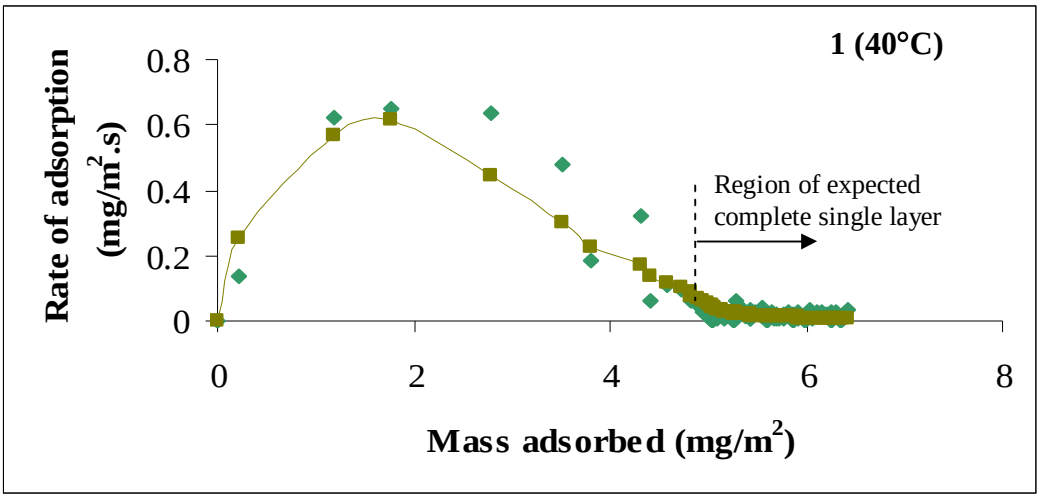

Figure 10.35: Adsorption rate of lysozyme (mg/m^2.s) from 1 g / L solution onto a bare SS surface as a function of mass adsorbed (mg/m^2) at 40 °C. Continuous line refers to the prediction of the model with a single set of fitted constants. Also shown is the region of expected single layer.

Figures 10.36 to 10.40 show respectively the fitted parameters of k_1, k_d, k_f, a and b as a function of temperatures and concentrations modeled using a diffusion-reaction model. As can be seen, the fitted parameters were increased slightly with temperature. Also, the fitted parameters did not deviate much with concentration.

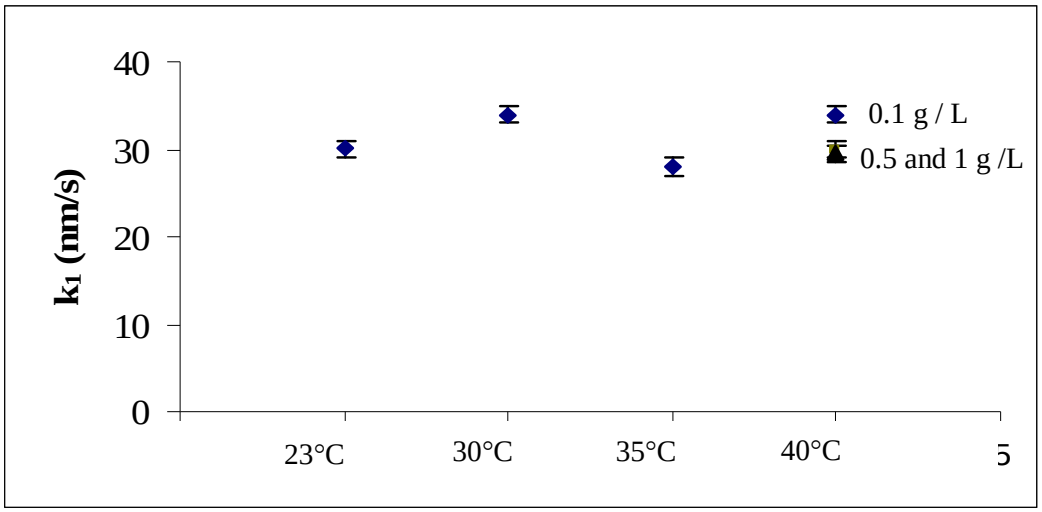

Figure 10.36: Fitted adsorption rate constant, k_1 (nm/s), as a function of temperature and concentration of lysozyme in the solution modeled using a diffusion-reaction model.

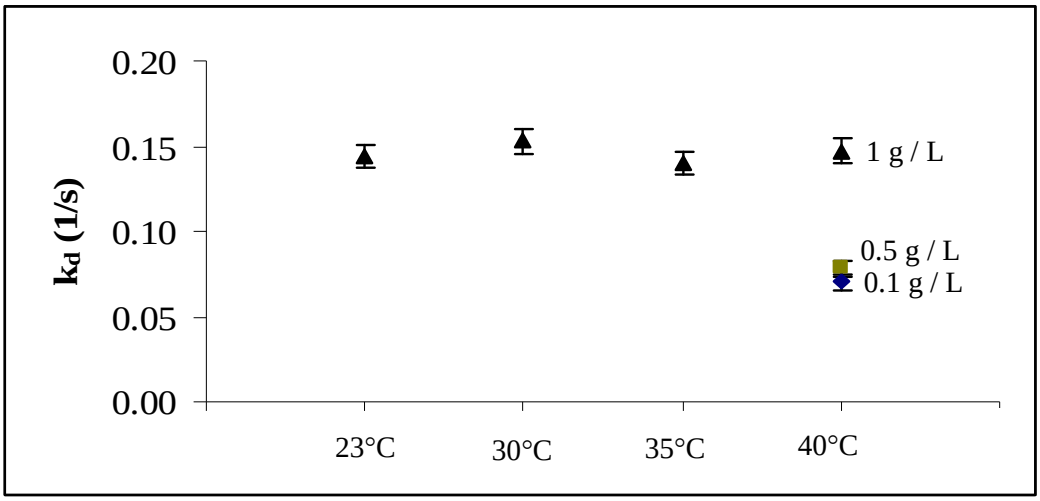

Figure 10.37: Fitted desorption rate constant, k_d (1/s), as a function of temperature and concentration of lysozyme in the solution modeled using a diffusion-reaction model.

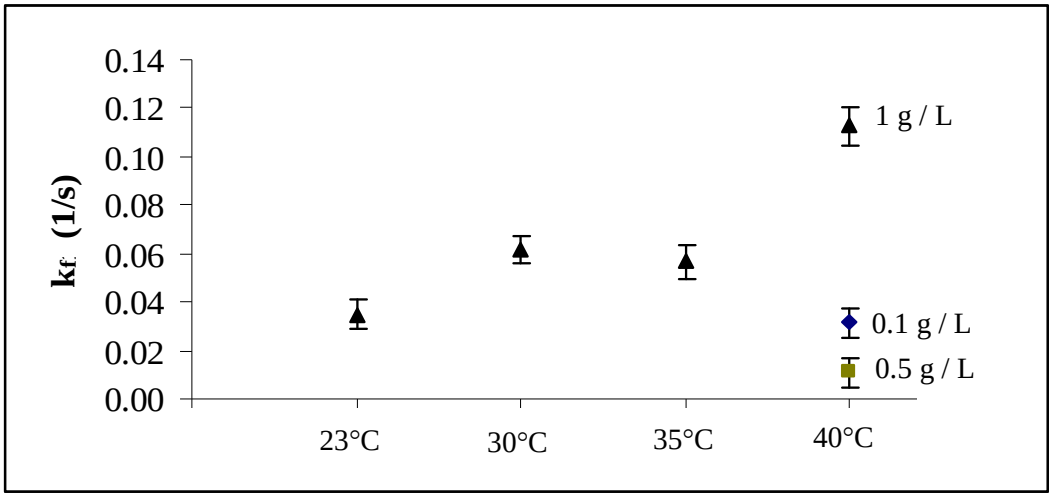

Figure 10.38: Fitted transformation to tightly held rate constant, k_f (1/s), as a function of temperature and concentration of lysozyme in the solution modeled using a diffusion-reaction model.

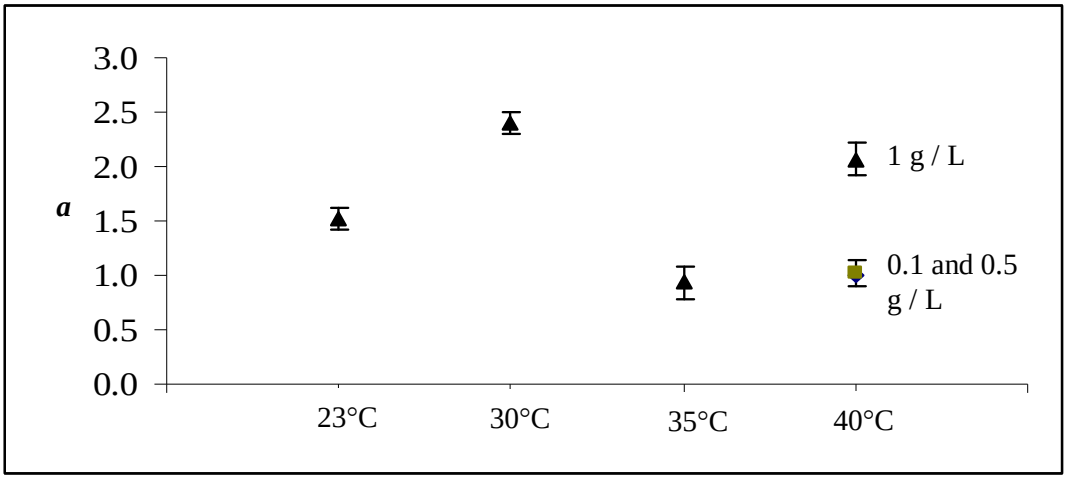

Figure 10.39: Fitted constant spreading factor, *a*, as a function of temperature and concentration of lysozyme in the solution modeled using a diffusion-reaction model.

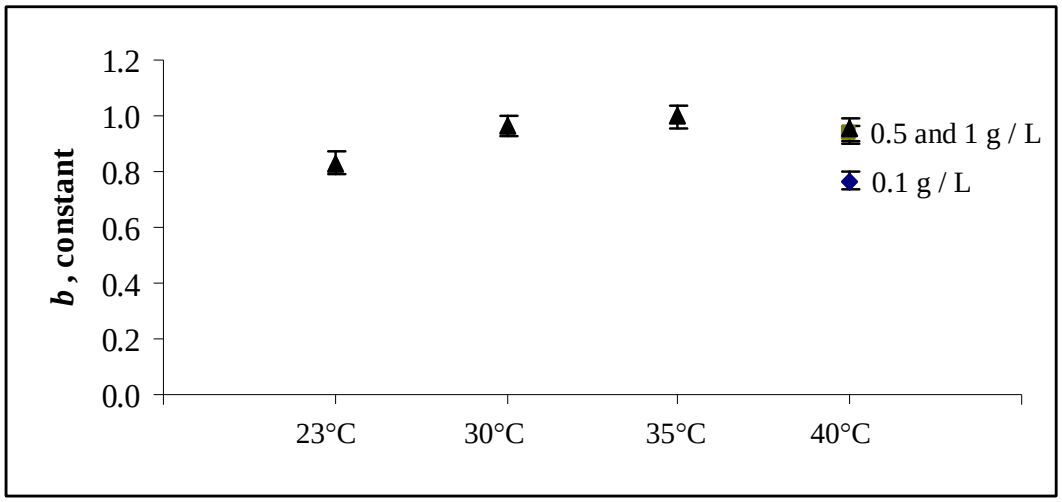

Figure 10.40: Fitted constant axplying factor, *b*, as a function of temperature and concentration of lysozyme in the solution modeled using a diffusion-reaction model.

10.1.3 Apo α-lactalbumin

Figures 10.41 to 10.46 show the fitting results on some of the apo α-lactalbumin kinetics data (modelled using a diffusion-reaction model). Similar to β-casein and lysozyme, the diffusion-reaction model fitted the adsorption kinetics data of apo α-lactalbumin well. The region of expected single layer of apo α-lactalbumin ranged from about 3 to 6 mg / m^2 (it was assumed that the expected single layer is 1.5 to 3 times that the theoretical single layer).

In general, at low concentration, the region of expected single layer formed was within the surface kinetics limited regime (linear region), whereas at high concentration (1 g / L), the region of expected single layer formed was within the transient transport limited regime (regardless of temperature).

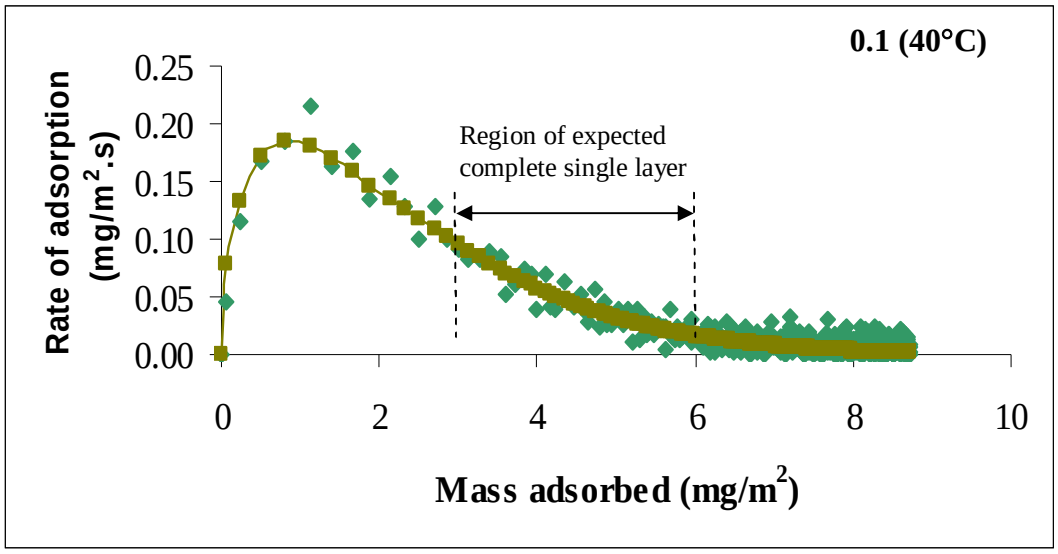

Figure 10.41: Adsorption rate of α-lactalbumin (mg/m^2.s) from 0.1 g / L solution onto a bare SS surface as a function of mass adsorbed (mg/m^2) at 40 °C. Continuous line refers to the prediction of the model with a single set of fitted constants. Also shown is the region of expected single layer.

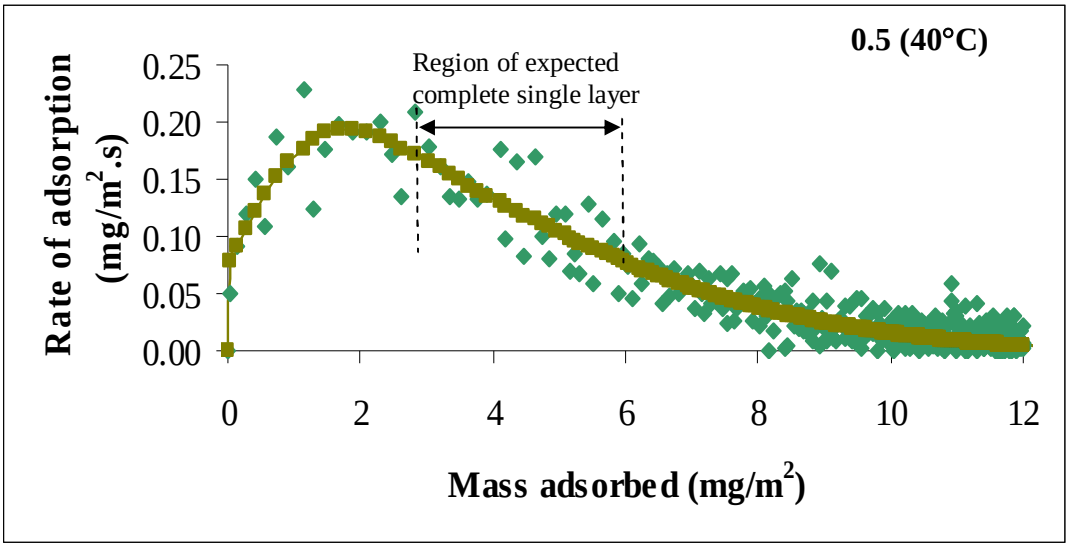

Figure 10.42: Adsorption rate of α-lactalbumin (mg/m^2.s) from 0.5 g / L solution onto a bare SS surface as a function of mass adsorbed (mg/m^2) at 40 °C. Continuous line refers to the prediction of the model with a single set of fitted constants. Also shown is the region of expected single layer.

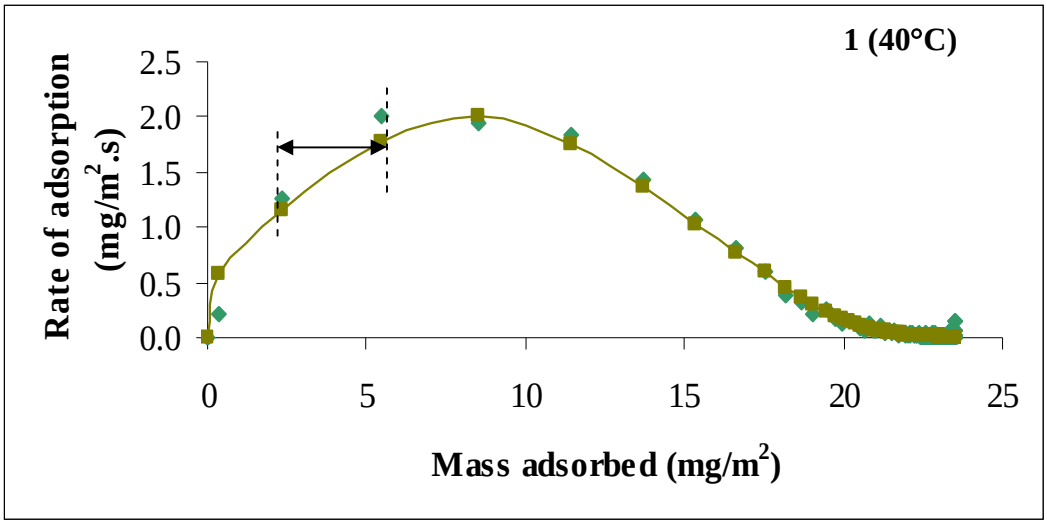

Figure 10.43: Adsorption rate of α-lactalbumin (mg/m^2.s) from 1 g / L solution onto a bare SS surface as a function of mass adsorbed (mg/m^2) at 40 °C. Continuous line refers to the prediction of the model with a single set of fitted constants. Also shown is the region of expected single layer.

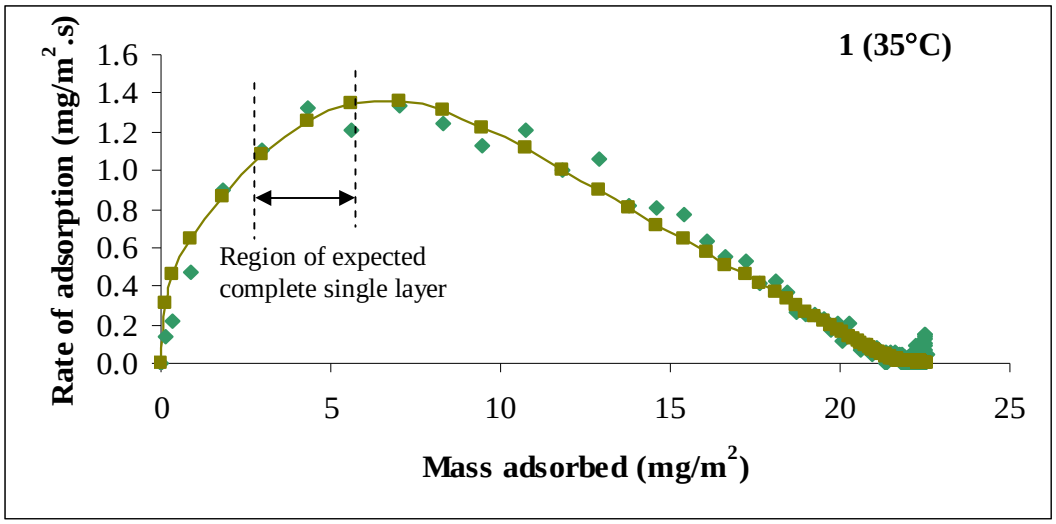

Figure 10.44: Adsorption rate of α-lactalbumin (mg/m^2.s) from 1 g / L solution onto a bare SS surface as a function of mass adsorbed (mg/m^2) at 35 °C. Continuous line refers to the prediction of the model with a single set of fitted constants. Also shown is the region of expected single layer.

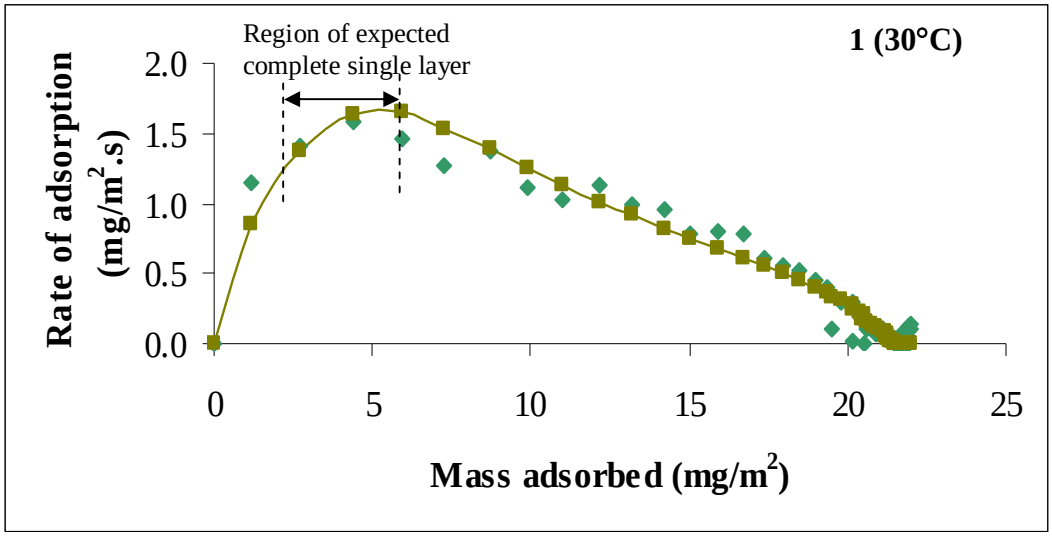

Figure 10.45: Adsorption rate of α-lactalbumin (mg/m^2.s) from 1 g / L solution onto a bare SS surface as a function of mass adsorbed (mg/m^2) at 30°C. Continuous line refers to the prediction of the model with a single set of fitted constants. Also shown is the region of expected single layer.

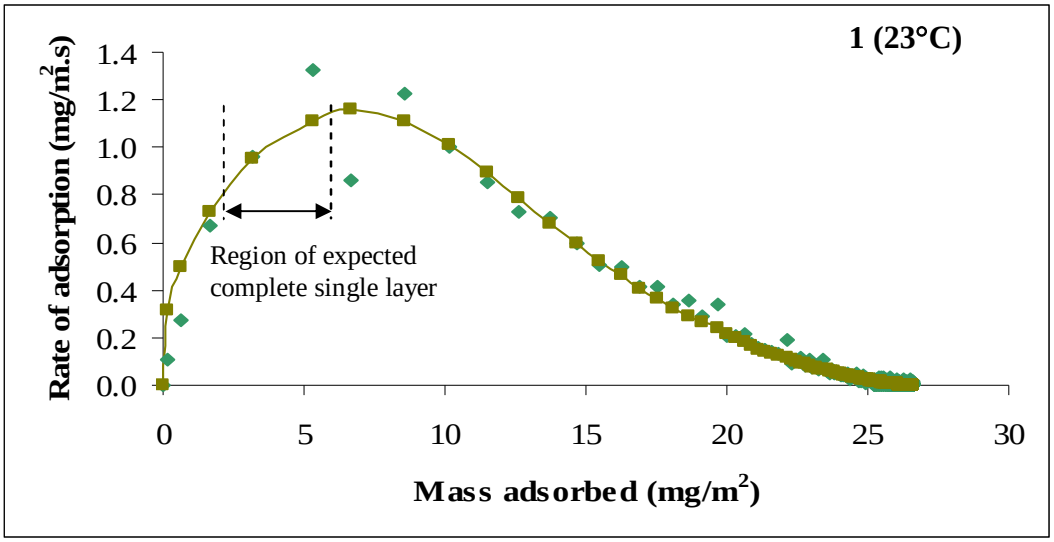

Figure 10.46: Adsorption rate of α-lactalbumin (mg/m^2.s) from 1 g / L solution onto a bare SS surface as a function of mass adsorbed (mg/m^2) at 23°C. Continuous line refers to the prediction of the model with a single set of fitted constants. Also shown is the region of expected single layer.

Figures 10.47 to 10.51 show respectively the fitted parameters of k_1, k_d, k_f, a and b as a function of temperatures and concentrations modelled using a diffusion-reaction model. As can be seen, the fitted parameters were increased as temperature was increased and slightly deviated with concentration.

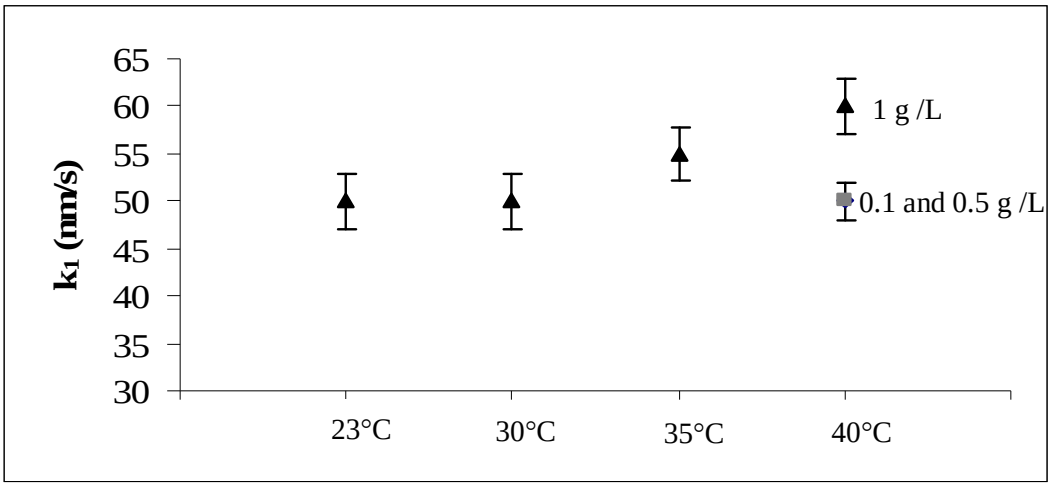

Figure 10.47: Fitted adsorption rate constant, k_1 (nm/s), as a function of temperature and concentration of α-lactalbumin in the solution modeled using a diffusion-reaction model.

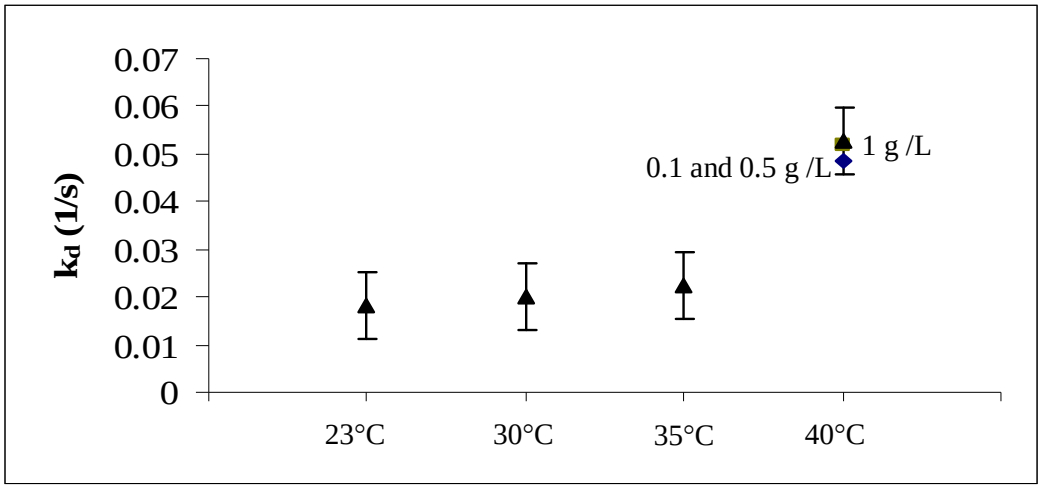

Figure 10.48: Fitted desorption rate constant, k_d (1/s), as a function of temperature and concentration of α-lactalbumin in the solution modeled using a diffusion-reaction model.

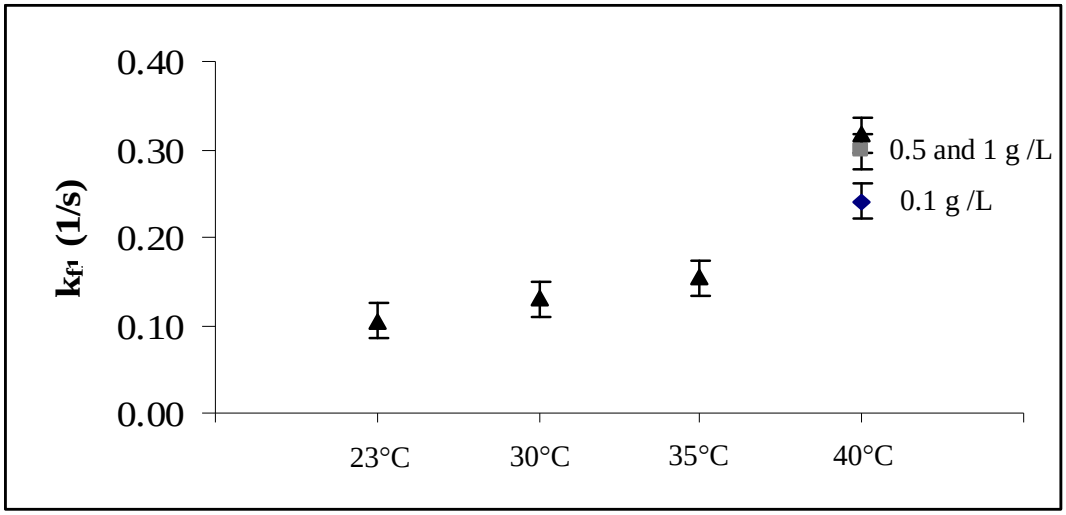

Figure 10.49: Fitted transformation to tightly held rate constant, k_f (1/s), as a function of temperature and concentration of α-lactalbumin in the solution modeled using a diffusion-reaction model.

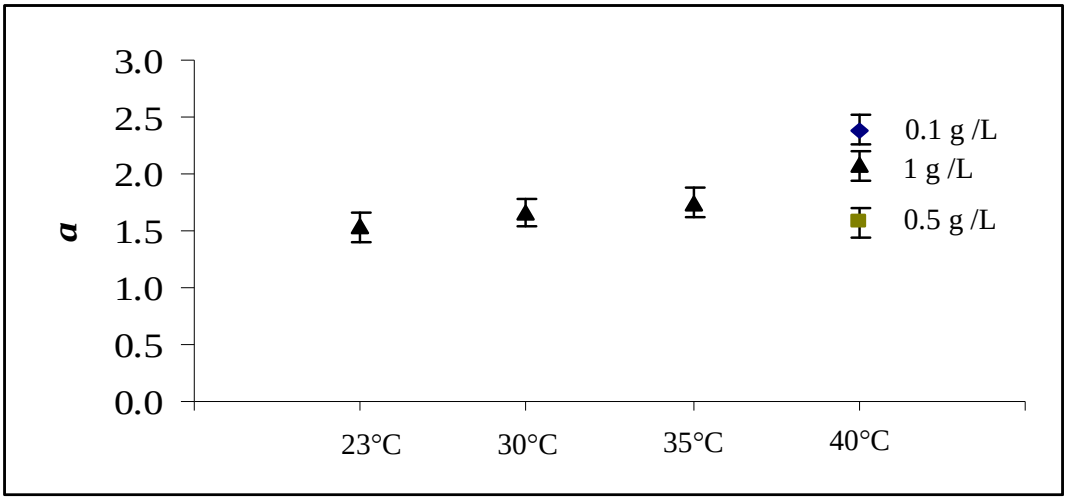

Figure 10.50: Fitted constant spreading factor, *a*, as a function of temperature and concentration of α-lactalbumin in the solution modeled using a diffusion-reaction model.

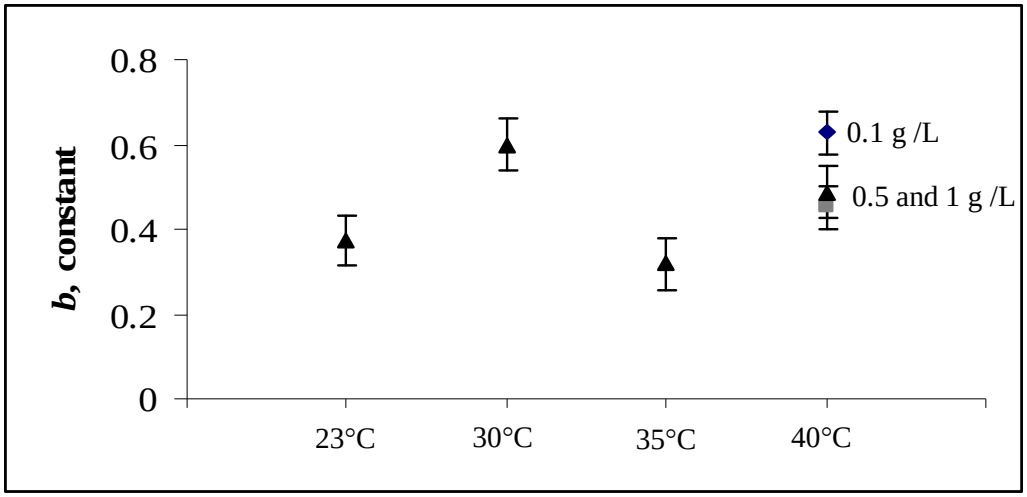

Figure 10.51: Fitted constant axplying factor, *b*, as a function of temperature and concentration of α-lactalbumin in the solution modeled using a diffusion-reaction model.

10.1.4 Gibbs energy of weak adsorption, ΔG_{ads}

Figure 10.52 presents the dependence of the Gibbs energy of adsorption, ΔG_{ads}, (weak adsorption) of β-casein, lysozyme and α-lactalbumin on the temperature (refer to Equations 4.37 and 4.38). As can be seen, as the temperature was increased, the ΔG_{ads} of the proteins was decreased slightly. From the ΔG_{ads}, it showed that α-lactalbumin was the most favorably adsorbed on the bare SS, followed with β-casein and lysozyme.

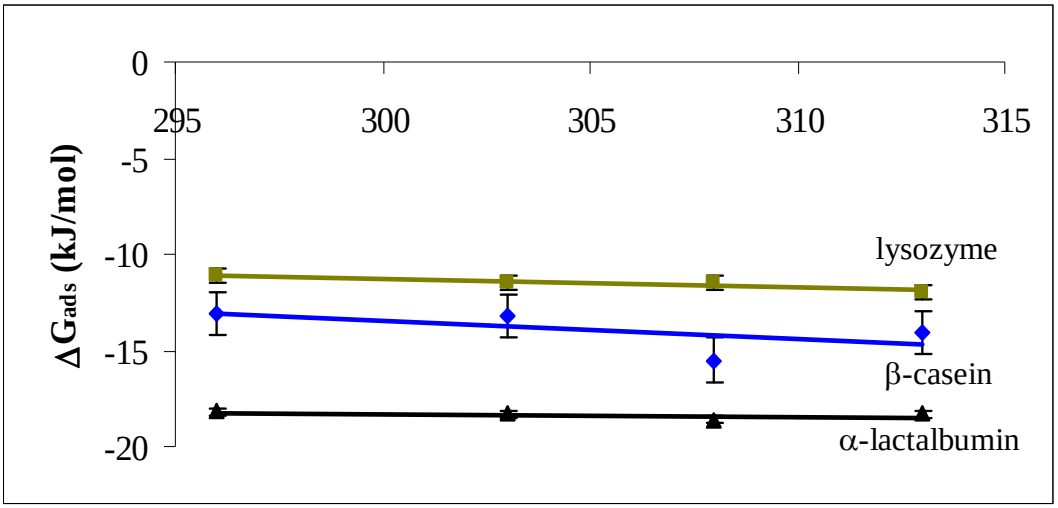

Figure 10.52: Dependence of the Gibbs energy of adsorption, ΔG_{ads}, on the temperature of protein in the solution.

Table 10.1 show the comparison of thermodynamic values for the weak adsorption of β-casein, lysozyme and apo α-lactalbumin onto a stainless steel surface from pH 7.2 phosphate buffer at 296 K obtained from this study. Relatively, apo α-lactalbumin showed the greatest affinity towards a stainless steel surface, followed with β-casein and lysozyme accordingly. Based on the entropy change values, ΔS, it is suggesting that, relatively apo α-lactalbumin has experienced extensive denaturation during the adsorption followed by β-casein and lysozyme. A low value

of ΔS shown by lysozyme relative to apo α-lactalbumin and β-casein is expected to be related to its stability since lysoyzme is a hard protein.

Table 10.1: Comparison of thermodynamic values for the weak adsorption of β-casein, lysozyme and apo α-lactalbumin onto a stainless steel surface from pH 7.2 phosphate buffer at 296 K (the data was modelled using a diffusion-reaction model).

Protein	ΔG_{ADS} (kJ/mol)	ΔH_{ADS} (kJ/mol)	ΔS_{ADS} (J/K.mol)
β-casein	-13 ± 2	15 ± 4	95 ± 5
Lysozyme	-11 ± 1	3 ± 1	47 ± 2
Apo α-lactalbumin	-18 ± 1	-14 ± 1	13.6 ± 2

CHAPTER ELEVEN

DISCUSSION

11.1 Error in measurement

11.1.1 Random errors in surface mass density adsorbed

Most values of Γ (surface mass density) given in the thesis for steady state adsorption values are means of several separate measurements done under the same conditions. Each 'measurement' has resulted from interpretation of frequency and dissipation measurements with a model resulting in possible consistent error (discussed below). Here we confine discussion to random errors.

All the error bars that have been incorporated in the graph of the mass density adsorbed are referred to the standard deviation of the individual measurements error (SD). The SD was calculated based on Equation 11.1

$$SD = \frac{s}{\sqrt{n}} \qquad (11.1)$$

where *s* is the standard deviation of individual measurements in the sample and *n* is the number of data in the sample, which was generally 3 or 4.

By plotting the residual ($y_{ij} - \bar{y}_i$) vs the mean, $\bar{y}_i$, for the whole range of measurements in this study, we can see the variation of the residual over the range of means. Figure 11.1 shows the plot of residuals ($y_{ij} - \bar{y}_i$) as a function of mean $\bar{y}_i$, for 30 sets of measurement under different conditions (see sources of variations below). As can be seen, there are no significant changes in residuals over the range of means. Thus, we can pool the variance (s_P^2) for individual measurement error.

$$s_P^{\,2} = \frac{(n_1-1)s_1^{\,2} + (n_2-1)s_2^{\,2} + \ldots\ldots + (n_k-1)s_k^{\,2}}{(n_1-1)+(n_2-1)+\ldots\ldots+(n_k-1)} = \frac{\sum_i \sum_j (y_{ij} - \bar{y}_i)^2}{\sum_i \Phi_i} \qquad (11.2)$$

where, s_i is the variance of sample i with n_i measurements and ϕ_i number of degrees of freedom.

From those measurement, the sum of all the squared residuals is 0.88 $(mg / m^2)^2$ and the total error degrees of freedom is 58. Thus from Equation 11.2, $s_p^{\,2}$ = 0.015 $(mg / m^2)^2$.

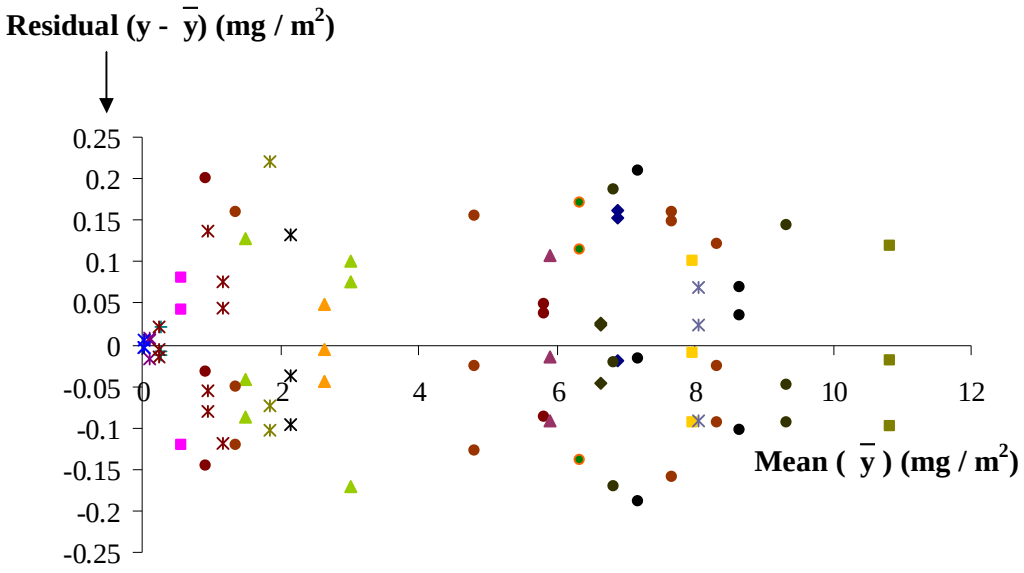

Figure 11.1: Plot of residuals as a function of mean for 30 sets of measurement under different concentrations and temperatures.

Example of calculation of mean limits:

Table 11.1 shows the set of 4 separate measurements of the adsorption of β-casein from 0.1 g / L solution onto a bare SS surface at room temperature. The true value for mass density of β-casein can be calculated as lying in the range $\bar{x} \pm \frac{s}{\sqrt{n}} t_{\alpha}(\phi)$.

The square root of pooled variance, s_p^2 was used to represent s. *t* (*student test*) is a function of confidence probability α, and number of degrees of freedom. The numbers degrees of freedom for this example = 58. If we choose 95 % confidence level (confidence level 2α = 0.1), then $t = t_{0.1}(58) = 1.96$. Then the error in $\bar{x}$ is;

$$\frac{s_p t_{\alpha}}{\sqrt{n}} = \frac{\left(\sqrt{0.015}\right) * 1.96}{\sqrt{4}} = 0.12\ mg / m^2$$

Therefore, the mass density of β-casein value is 6.88 ± 0.12 mg / m^2.

Table 11.1: Set of data of the mass density, Γ, of β-casein adsorbed from 0.1 g / L solution onto a bare SS surface at room temperature.

Run	Final mass density adsorbed (mg/m^2)
I	7.034
II	7.043
III	6.863
IV	6.587
Mean, $\bar{\Gamma}$	6.88

Sources of variations

As mentioned early, the residuals ($y_{ij} - \bar{y}_i$) plotted in Figure 11.1 were taken from 30 sets of measurement under different conditions. The measurements cover the different temperatures (23, 30, 35 and 40 °C), concentrations (0.1, 0.5 and 1 g / L), type of proteins (β-casein, lysozyme and α-lactalbumin) and type of PEG (PEG350, 550, 2000 and 5000 Da) used in this study.

11.1.2 Random errors in fitting the kinetic models

The measurements used for fitting kinetics were listed in a sequence of single measurements. For the kinetic data, the error of the fitted parameters refers to a confidence interval based on the sum of squares of the residuals of the fitting (SS). The percentage error for a confidence probability of 10 % (5 % each side) of fitted parameter A_{fit} can be calculated using Equation 11.3.

$$\%\ error = \frac{A_{\alpha} - A_{fit}}{A_{fit}} x100 \tag{11.3}$$

where A_{fit} is the fitted parameter from one-sided fitting (least squares) and A_{α} is determined by consciously varying the value of A away from A_{fit}, and plotting the calculated sum of squared residuals SS. A_{α} is the value (2 values, one upper and one lower) of A where the sums of squared residuals, SS, rises to a certain multiple of the minimum fitted SS, determined by Equation 11.4 (Box et al., 1978). See Figure 11.2.

$$SS_{\alpha} = SS_{fit}\left(1 + \left(\frac{N}{n-N}\right)F_{\alpha}\left(N, n-N\right)\right) \tag{11.4}$$

where, SS_{α} is the value of SS at α confidence level (see Figure 11.1), SS_{fit} is the SS from least squares fitting (obtained using Microsoft Excel Solver version 2003), N is the number of fitted parameters, n is the number of data and $F_{\alpha}(N, n\text{-}N)$ is the upper 100α % point of the F distribution with N and $n\text{-}N$ degrees of freedom (obtained from the statistical table).

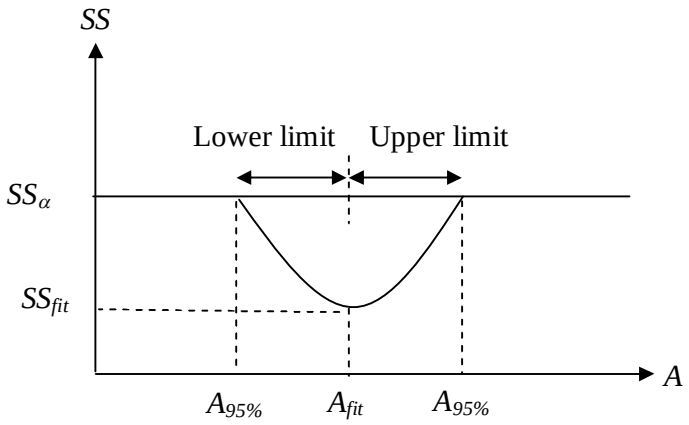

Figure 11.2: Illustration of *SS* versus *A* (Box et al. [1978]).

The SS curve as a function of A (a partial variation) is obtained by keeping other fitted parameters constant and manually changing *A* until reaches a SS value equal to the calculated SS_α. The value of *A* at this point is called A_α. We will choose $\alpha = 0.05$ for all fittings in this thesis.

For all fittings, the mean layer thickness, *h*, obtained from the Voigt model (raw data) was divided by the fitted value of h_{max} to get an expression of fractional surface coverage (θ). Thus, all the kinetic data used for modelling in this thesis was in a fractional surface coverage basis. In this approach, we assume that a protein layer is a single molecules layer.

We can now multiply this fractional surface coverage, θ, by h_{max} and by ρ_{layer} to obtain a mass surface coverage, $\Gamma = \theta\ h_{max}\ \rho_{layer}$ in kg / m^2 * (10^6 mg / kg) to obtain our usual units of Γ in mg / m^2.

Below is an example of the working calculation (i.e. used the data of adsorption kinetics of α-lactalbumin on a bare SS from 1 g / L solution at 40 °C). The data has been modelled using a diffusion-reaction model that includes all the possible reactions that can occur in adsorption process. The model has been solved using the Microsoft Excel Solver version 2003.

Table 11.2: The fitted parameters of α-lactalbumin adsorption on a SS surface from 1 g / L solution at 40 °C. A diffusion-reaction model that includes all the possibilities of reactions has been used to model the data (using the least squares method).

Fitted Parameter	Fitted value (x) (used least squares)
h_{max} (nm)	90.0078
k_1 ($s^{-1}.M^{-1}$)	60.0047
k_d (s^{-1})	0.0727
k_f (s^{-1})	0.0782
k_2 (s^{-1})	30.048
k_{2d} (s^{-1})	0.00309
k_{f2} (s^{-1})	0.00158
SS_{fit} $(mg / m^2)^2$	0.5644

From Table 11.2, N = 7 and n (from the kinetic data (not shown here)) = 207 and SS_{fit} = 0.5644 $(mg / m^2)^2$. The value for $F_{0.05}$ (7, 207) at 95 % confidence level = 1.94 (single sided).

Substituting these values into Equation 11.3,

$$SS_{95\%} = 0.5644\left(1+\left(\frac{7}{200}\right)*1.94\right) = 0.6027\,(mg / m^2)^2$$

giving $SS_{95\%} / SS_{fit}$ = 1.068 and thus $SS_{95\%}$ equal to 0.6027 $(mg / m^2)^2$.

Then, take k_1 as an example parameter and by keeping the other parameters constant, the value of k_1 was changed from 60.0047 until the SS_{fit} value was equal to 0.6027 $(mg / m^2)^2$. This step was done manually. The k_1 for this SS was 60.9462 for the upper limit and was 59.0632 for the lower limit, i.e. a ± 2 % variation. Table 11.3 tabulates the result obtained, together with similar results for the other fitted constants.

Table 11.3: The upper and lower 95 % confidence level values and percentage of error for the fitting parameters.

Fitted Parameter	Fitted value (x) (used least squares)	Upper (U) and lower (L) 95 % confidence level	± % error
h_{max} (nm)	90.0078	89.8950 (L), 90.1207 (U)	0.1
k_1 ($s^{-1}.M^{-1}$)	60.0047	59.0632 (L), 60.9462 (U)	1.5
k_d (s^{-1})	0.0727	0.0715 (L), 0.0740 (U)	2
k_f (s^{-1})	0.0782	0.0704 (L), 0.0860 (U)	9
k_2 (s^{-1})	30.048	29.751 (L), 30.345 (U)	1
k_{2d} (s^{-1})	0.00309	0.00301 (L), 0.00318 (U)	3
k_{f2} (s^{-1})	0.00158	0.00141 (L), 0.00175 (U)	11
SS_{fit} (mg / m^2)^2	0.5644	0.6027	-

The fitting error variance of the QCM-D mass density measurements was

$$s_{fit}^{\ 2} = \frac{SS_{fit}}{n-N} = \frac{(0.5644)}{200} = 0.0028\left(mg/m^2\right)^2$$

$$s_{fit} = (0.0028)^{0.5} = 0.053\, mg/m^2$$

The ratio of variance = $F = \frac{s_{fit}^{\ 2}}{s_{error}} = \frac{0.0028}{0.015} = 1.87$

The ratio of variance is larger than the theoretical critical value, thus we can reject the null hypothesis that the fitting error variance comes from the same source as the general measurement error. A larger value of SS_{fit} indicates some added inaccuracy of the fitting. This is may have resulted from the assumption of a single layer (see discussion later). However, these experimental variances are of the same order of magnitude.

For solving the kinetic models, the Microsoft Excel Solver has been used under the conditions tabulated in Table 11.4. The model has been solved based on a finite divided difference approach. This approach iterated from the initial guess value up to 100 times with the precision of the Solver to fit the parameters set at 0.000001. This approach used a forward derivative estimated by the tangent method. The tolerance of the Solver to solve the model is 5 %.

Table 11.4: Parameters and conditions of the Microsoft Excel Solver used in solving the kinetic models.

Parameter	Condition
Maximum time iteration	100 secs
Iterations	100
Precision	0.000001
Tolerance	5 %
Convergence	0.0001
Estimates	Tangent

11.1.3 Consistent error - water in layers

QCM-D measurement senses total mass of the film including water *coupled* to and *trapped* within the adsorbed film [Stalgren et al., 2002, Hook et al., 2002]. The mass adsorbed from the QCM-D measurement can be referred to as a '*wet*' mass. From QCM-D measurements alone, it has been realised by many workers that the contribution of the solvent to the total mass is not easy to establish. Associated with this is the uncertainty in the assumed layer density of 1200 kg / m^3. The density of the layer should lie between that of a protein layer and that of water. Hook et al. [2002] reported that the density of typical proteins is 1400 kg / m^3 [Hook et al., 2002]. Changing the assumed layer density in the Voigt model from 1000 to 1400 kg / m^3 (40 % increase) gave about 20 to 40 % increase in the estimated mass of the layer. Our assumption of 1200 kg / m^3 should lead to at most a ± 20 % error in total layer mass. It is expected that the 20 % variation not to affect general conclusions regarding the mass density adsorbed.

A combination between the QCM-D and optical techniques such as ellipsometry and optical waveguide lightmode spectroscopy (OWLS) has shown can resolve the bound solute mass and the coupled solvent in the layer (refer to Equations 3.8 and 3.9) [Hook et al., 2002, Muller et al., 2005]. This is because these optical techniques are sensitive to only the 'dry mass' of a substance adsorbed onto the surface. Hook et al. [2002] found that for small and globular proteins such as hemoglobin (64.5 kDa) and albumin (65kDa) the measured mass of adsorbed protein was a factor of about 1.75 times larger than that measured by optical techniques while it was about 2 to 3.2 times larger for large proteins (fibrinogen (MW340kDa) and antibodies). Meanwhile, the mass density of DNA on the gold surface measured with QCM-D was 7 times larger compared with the SPR measurement [Su et al., 2005]. The mass density of β-casein adsorbed on a gold surface monitored using the QCM-D meanwhile was greater by a factor of 3 to 5 compared with that using the common optical devices [Lee et al., 2004]. This may not be accurate since the comparisons to optically-derived masses have been made based on values obtained from a review and not from the same experiment study. However, the ratio of QCM-D and optical techniques can be as high as 10, depending on the nature, the conformation of the adsorbed molecules, and the liquid medium used (Hook et al., 2001, Cho et al., 2004). These studies have

showed convincingly that solvent is also included in the layer measured by a QCM-D.

11.1.4 Consistent error - Voigt model versus Sauerbrey model

The ratio between wet mass to dry mass is dependent on the layer density only if the QCM-D data is analyzed using the Voigt model. For the Sauerbrey model, the calculation of surface mass densities is not requiring the information of a layer density (refer to Chapter 3 for the Sauerbrey equation). As explained in Chapter 3, the applicability of the Sauerbrey model or the Voigt model can be checked by two ways. The first is by normalizing (expressing as a fraction) the Δf at different overtones (n). If the Δf values at different overtones are similar when they are normalized (for example, $\Delta f_3 / 3 \cong \Delta f_5 / 5 \ldots \cong \Delta f_n / n \cong 5$ Hz (fundamental frequency, f_1)) then the Sauerbrey equation is able to give a valid relationship between a frequency shift and an adsorbed mass [Irwin et al., 2005]. The second was to check is by plotting ΔD versus Δf as adsorption increases. One merit of this plot is that one is able to see directly the influence of the protein adsorption on the viscoelastic properties of the adsorbed layer. By comparing the $\Delta D/\Delta f$ values (slope of the ΔD-Δf plot) between proteins one is able to relatively indicate the characteristic of the layer formed; either a dense layer or a 'soft' (water-rich) layer.

Table 11.5 shows approximate slopes of $\Delta D/\Delta f$ from QCM-D measurements for each of the protein layers studied in this thesis under all experimental conditions. The data was taken during a plateau desorption which referred to the remaining protein layer (that is, strongly-bound) on the surface. A low $\Delta D/\Delta f$ value indicates a mass addition without significant dissipation increase during adsorption, which is characteristic of a rigidly attached layer. In contrast, a large $\Delta D/\Delta f$ value corresponds to a soft layer.

Table 11.5: Ratio of dissipation and frequency changes ($\Delta D/\Delta f$) of the remaining layer (tightly-bound) for protein adsorption on stainless steel.

Concentration (g/L)	Temperature (°C)	$\cong(\Delta D/\Delta f)\text{x}10^{-6}$ (β-casein)	$\cong(\Delta D/\Delta f)\ \text{x}10^{-6}$ (lysozyme)	$\cong(\Delta D/\Delta f)\ \text{x}10^{-6}$ (α-lactalbumin)
0.1	23	0.071	0.066	0.111
	30	0.071	0.066	0.111
	35	0.066	0.062	0.111
	40	0.066	0.058	0.125
0.5	23	0.066	0.052	0.111
	30	0.076	0.050	0.167
	35	0.071	0.050	0.167
	40	0.071	0.050	0.125
1.0	23	0.076	0.050	0.083
	30	0.076	0.052	0.070
	35	0.083	0.050	0.070
	40	0.076	0.050	0.080

From Table 11.5, the adsorbed proteins appeared to form a more or less hydrated layer with increasing softness (water-rich) in the order: lysozyme > β-casein > α-lactalbumin. Relatively, α-lactalbumin has apparently the largest water content of the three proteins. Also, the softness of α-lactalbumin (i.e. water content) apparently was decreased as protein solution was increased. However, the softness of lysozyme and β-casein layers were apparently not temperature and concentration dependent (i.e. the $\Delta D/\Delta f$ was almost the same under all the experimental conditions used). We expect that the differences shown by those proteins are associated with their structure conformations during the adsorption. For example, α-lactalbumin is a soft protein and has a high tendency to denature (i.e. unfold) upon adsorption on SS. High water content observed for α-lactalbumin is probably associated with a loosely packed unfolded form (will be discussed in section 5.4)**.** β-casein meanwhile is already in a flexible random coil configuration in the bulk solution and presumably this flexibility will result a loose flexible layer. Lysozyme, which is a relatively small and hard protein,

showed a lower of $\Delta D/\Delta f$ value than the other proteins. Voros et al. [2004] stated that proteins with smaller size have generally a higher adsorption and their adsorption layer is more compact with a higher number density (dense layer). Moreover, most probably, lysozyme was partially unfolded during the adsorption (will be discussed later). The findings obtained in this study indicated that the type of proteins used influenced the softness of the layer.

Table 11.6 shows an example of slopes of $\Delta D/\Delta f$ from QCM-D measurements for PEG350, 550, 2000 and 5000 Da on a silicate layer studied in this thesis under some of the experimental conditions at room temperature.

Table 11.6: Ratio of dissipation and frequency changes ($\Delta D/\Delta f$) of the remaining layer (tightly-bound) for PEG adsorption on a silicate layer at room temperature.

Concentration (g/L)	$\cong(\Delta D/\Delta f)\text{x}10^{-6}$ PEG350	$\cong(\Delta D/\Delta f)\ \text{x}10^{-6}$ PEG550	$\cong(\Delta D/\Delta f)\ \text{x}10^{-6}$ PEG2000	$\cong(\Delta D/\Delta f)\ \text{x}10^{-6}$ PEG5000
0.1	0.32	0.15	1.05	0.70
1	0.26	0.11	0.60	0.48
5	0.35	0.16	0.19	0.21

As can be seen from Tables 11.5 and 11.6, the $\Delta D/\Delta f$ for a PEG layer is larger than a protein layer. This indicates a possibility that more water content consists in a PEG layer. The analysis done in this study showed that the mass densities of protein adsorbed obtained using the Voigt model were about three times higher than those using the Sauerbrey model on the same data. Meanwhile, the PEG adsorption was about 7 times higher in the same direction. This increased discrepancy appears to be correlated with the $\Delta D/\Delta f$ values which are presumably related to the highly solubility of PEG in water. As mentioned in Chapter 2, PEG forms a hydrated layer with two water molecules are H-bonded to each PEG ether group. Heuberger et al. [2004] also demonstrated that the amount of coupled water for PEG layer was more than 80 % of the total mass. Hook et al. [2002] meanwhile reported that the amount of coupled water ranged between 70 to 170 %

for proteins and about 200 % for antibodies. The percentage of coupled water in the layer can be calculated using Equation 11.5.

$$\%\ water = \frac{\Gamma_{QCM-D} - \Gamma_{optical}}{\Gamma_{QCM-D}} \times 100 \qquad (11.5)$$

They claimed that the exact amount of solvent water dependent on the type of protein and the structure of the protein layer formed at the sensor-liquid interface.

Thus, it has been decided here to choose the Voigt model to estimate the mass density adsorbed since for a hydrated layer, it is expected to be more accurate to interpret the data with the Voigt model than with the Sauerbrey model. We need to thus bear in mind that all the mass surface densities obtained from QCM-D measurements presented in this study include the mass proportion of water in the adsorbed layer (i.e. *'wet' mass*).

11.2 Kinetics and diffusion

Modelling the experimental protein adsorption kinetics with an appropriate model hopefully leads to a clear mechanism of the process itself. The adsorption of a protein from a suddenly introduced protein solution generally involves two sequential regimes; first a transport or diffusion limited regime and then a reaction limited regime. In this study, several surface reaction models were used with two also including a diffusion-limiting step. This appears to be the first time a diffusion limited model has been used for QCM kinetic interpretation.

11.2.1 Diffusion-reaction versus surface-reaction model

From the results obtained, it appeared that at higher temperatures and concentrations, the kinetic data were much better interpreted using diffusion-reaction models than simple surface reaction models (refer to Chapter 10). Under these conditions, more than one-third of the total mass density adsorbed was within the diffusion limited regime. Changani et al. [1997] emphasized that while the adsorption is controlled by diffusion (diffusion limited), deposition of protein on a surface will not be a strong function of temperature. Both flow rate of solution and mixing the solution do affect to the diffusion of protein onto the surface. Increasing a flow rate of solution or increasing the mixing of protein will enhance the diffusion of protein. Consequently, the period of diffusion limited regime becomes shorter. If adsorption is controlled by a surface process (reaction limited), deposition of protein will be a function of the surface temperature but not necessarily the bulk temperature.

The diffusion and reaction limited regimes can easily be delineated by plotting a graph of rate of adsorption versus mass density adsorbed (refer to Figure 11.3). Refer to Chapter 4 for details.

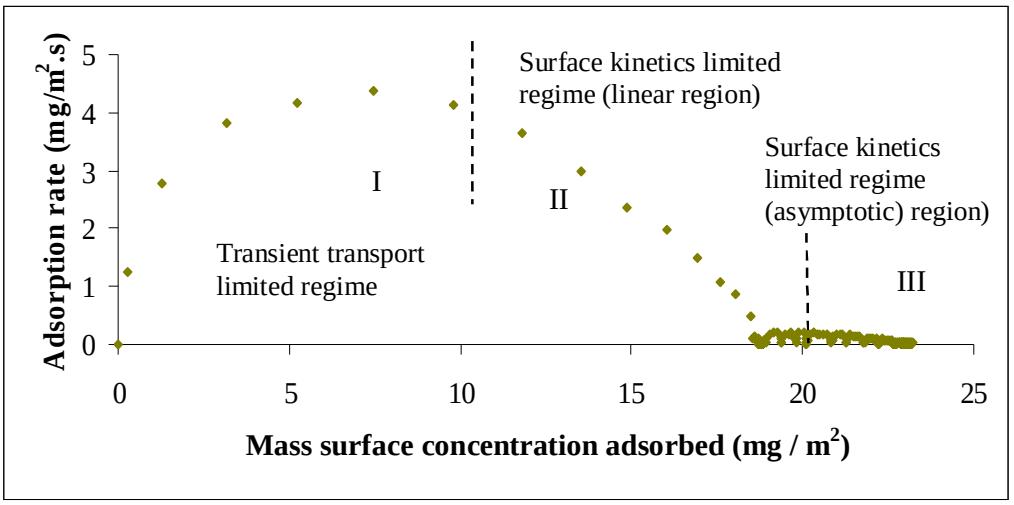

Figure 11.3: Adsorption rate of β-casein onto a SS surface suddenly exposed to a flow of 1 g / L β-casein at 40 °C as a function of mass surface concentration adsorbed (mg/m^2). Regime I refers to a transient transport limited regime and II and III refer to two surface kinetics limited regimes, a linear region and an asymptotic region. Refer to Chapter 4 for the description for each regime.

Based on the modeling results obtained in this study it appeared that the diffusion was important at high temperatures and concentrations. Neglecting diffusion was apparently appropriate only at room temperature and when adsorbing from the lowest concentration, 0.1 g / L (see Figures 11.14 and 11.15 for comparison). Figures 11.14 and 11.15 show respectively, the adsorption of β-casein from 0.1 g / L solution at room temperature and adsorption from 0.5 g / L at 30 °C. The data were modelled using the diffusion-reaction and simple surface reaction models. As can be seen, fitting with the diffusion-reaction model and the simple surface reaction model showed no significant difference at the lower condition. The simple reaction model apparently fitted the data reasonably well (except at the early stage of adsorption). However, at the intermediate condition (adsorbing from 0.5 g / L solution at 35°C) the surface reaction model apparently failed to fit the data well (see Figure 11.15). This indicates that simple surface reaction models are appropriate under low temperature (i.e. room temperature) and concentration conditions (i.e. 0.1 g / L).

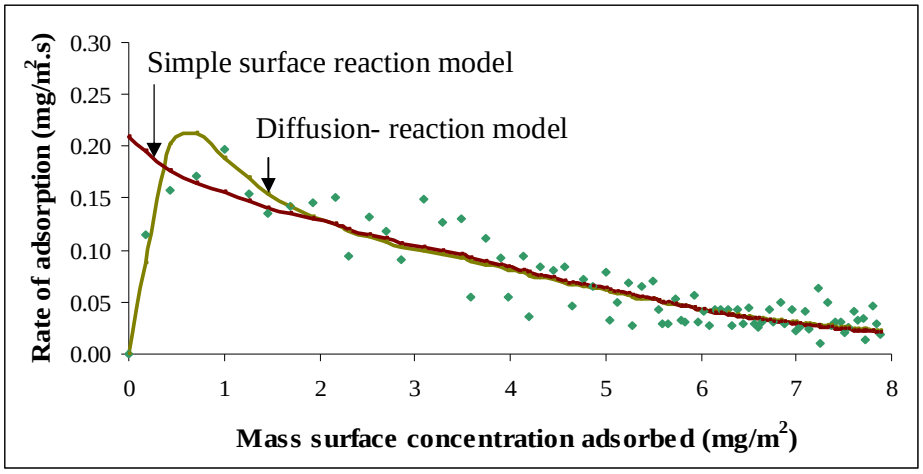

Figure 11.4: Adsorption rate of β-casein onto a SS surface suddenly exposed to a flow of 0.1 g / L β-casein at 23 °C as a function of mass surface concentration adsorbed (mg/m^2). The data were fitted using both a diffusion-reaction and a simple surface reaction model.

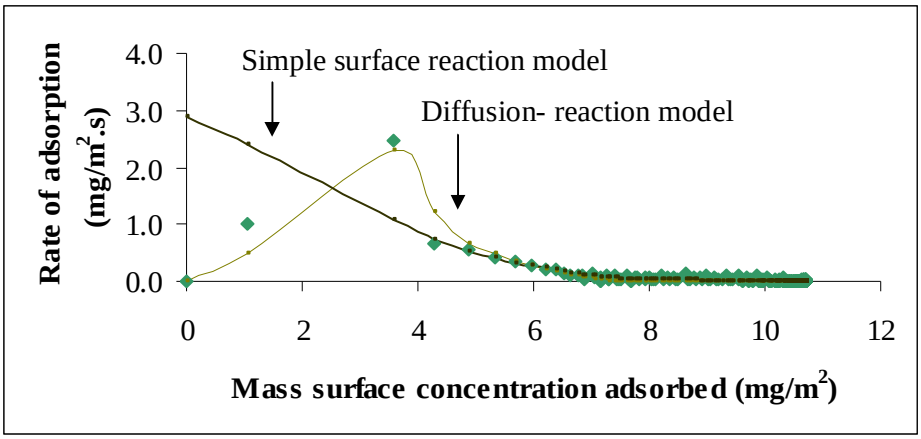

Figure 11.5: Adsorption rate of β-casein onto a SS surface suddenly exposed to a flow of 0.5 g / L β-casein at 30 °C as a function of mass surface concentration adsorbed (mg/m^2). The data were fitted using both a diffusion-reaction and a simple surface reaction model.

11.2.2 Reverse reaction

In this study, we also attempted to model the adsorption considering all possibilities of reactions that can occur in the adsorption process. Figure 11.6 illustrates all these possibilities of reactions that can occur in the adsorption process. In this surface reaction model, the protein is assumed to adsorb on the surface in two different states; state 1 (probably folded form) and state 2 (probably unfolded form). Both state 1 and 2 are reversible and can be desorbed by exchange with buffer. Proteins adsorbed in state 1 can also be reversibility transformed into state 2.

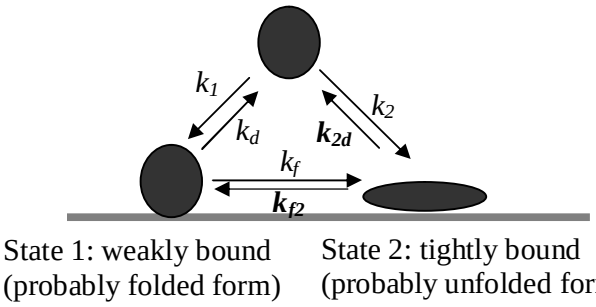

Figure 11.6: Illustration of adsorption of protein considering a surface back reaction (k_{f2}) and a back reaction from tightly bound to solution (k_{f2}).

By considering all the possibilities of reactions, one is able to determine $\Delta G, \Delta H$ and ΔS for each forward reaction. This can give a clear picture of what is happening in the adsorption. For example, if the rate constant of k_f, k_{f2}, k_2, and k_{2d} are relatively very small compared to k_1 and k_d, thus the adsorption follows Langmuir adsorption kinetics. Meanwhile, if k_f is larger than k_{f2}, then the protein has experienced extensive denaturation. $\Delta G, \Delta H$ and ΔS are associated with the respective pairs of rate constants. The sign and the magnitude of those thermodynamic parameters helps in the identification of the reaction; either favourable or unfavourable, endothermic or exothermic or folded or unfolded.

Figure 11.7 shows all the possible reactions of β-casein (refer to Figure 11.5) adsorbing from 0.1 g / L solution at temperature of 23°C as a function of time**.** Those rates were obtained by fitting the kinetic data using a surface reaction

model (refer to Figure 11.6). As can be seen, the rate of adsorption to a weakly bound state (*A*) decreased with time. It is because the rate of adsorption is dependent on the rate constant of adsorption, bulk concentration and available fraction surface coverage. As the adsorption process proceeded, the available area for the adsorption is decreased, thus the rate of adsorption will decrease. Once adsorbed, two competing events take place simultaneously, desorption (*B*) and transformation (*C*) to the strongly held form. These two processes increased rapidly with time. After a period (i.e. 120 secs), the rate of desorption and transformation to the strongly held form start to decrease. More molecules were desorbed than being transformed to the weakly held form in this process. Also, there was a possibility that the probably unfolded β-casein aggregated together and thus limited back transformation to weakly held form (*D*) (i.e.the rate of transformation to the strongly held form was much larger than the rate of transformation to the weakly held form). The adsorption to the tightly bound (*E*) and its reversibility (*F*) apparently were not significant under this experimental condition.

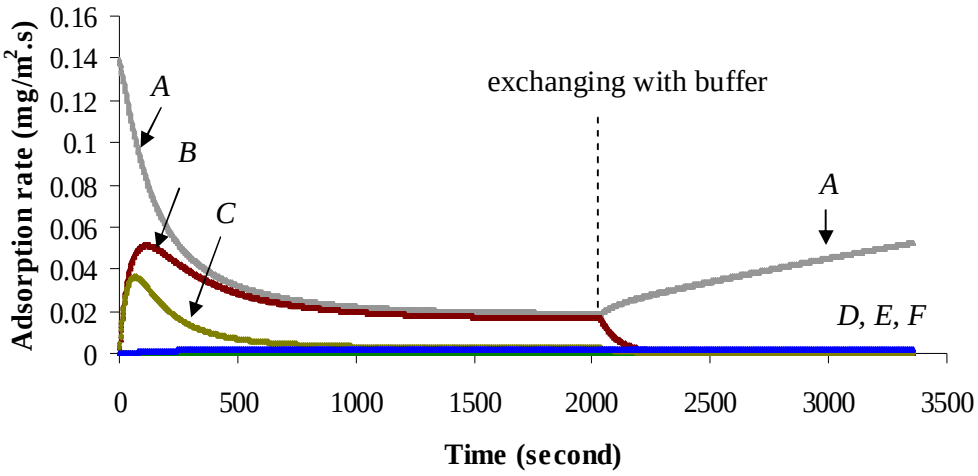

$$\frac{\Delta\Gamma_1}{\Delta t} = \overbrace{k_1 C_O\left(1-\Gamma_1-a\Gamma_2\right)}^{A} - \overbrace{\left(k_d\right)\Gamma_1}^{B} - \overbrace{k_f\Gamma_1\left(1-\Gamma_1-a\Gamma_2\right)/a}^{C} + \overbrace{k_{f_2}\Gamma_2\left(1-\Gamma_1-a\Gamma_2\right)}^{D}$$

$$\frac{\Delta\Gamma_2}{\Delta t} = \overbrace{k_2 C_o\left(1-\Gamma_1-a\Gamma_2\right)/a}^{E} + k_f\Gamma_1\left(1-\Gamma_1-a\Gamma_2\right)/a - k_{f2}\Gamma_2\left(1-\Gamma_1-a\Gamma_2\right) - \overbrace{k_{2d}\Gamma_2}^{F}$$

Figure 11.7: Rates of β-casein adsorbing from 0.1 g / L solution at temperature of 23°C as a function of time. The reaction rates were obtained by fitting the kinetic data used in Figure 11.4 using the surface reaction model depicted in Figure 11.6. *A*, *B*, *C*, *D*, *E* and F refer to respectively, the rate of adsorption to a weakly bound state, rate of desorption, rate of transformation to strongly held, rate of transformation to weakly held, rate of adsorption to the tightly bound and its reversibility.

11.2.3 Diffusion-reaction model

In the first diffusion-reaction model used in this study, only the adsorption to a weakly bound state and its reversibility and the transformation to a tightly bound form are considered (refer to Figure 11.8).

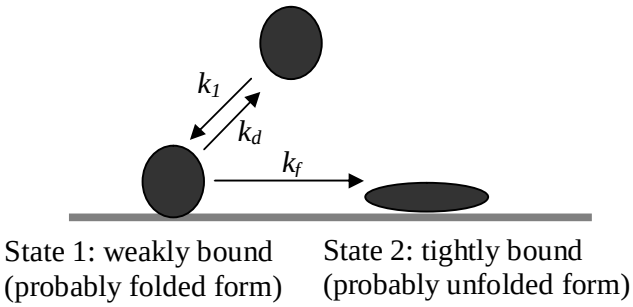

Figure 11.8: Illustration of adsorption of protein modelled using a diffusion-reaction model (this study).

Rate constants of adsorption (k_1), desorption (k_d), and transformation to strongly held adsorption (k_f) were taken as parameters to be fitted. The rate constants carry the units of s^{-1} except of k_1, nm/ s. $\left(\frac{\delta_0}{D}\right)$, h_{max}, a and b also were taken as parameters to be fitted. Bulk concentration and radian of the proteins were taken as fixed parameters.

The analysis done showed that the diffusion-reaction model was able to give an excellent fit of the kinetic data for all the proteins studied in this thesis under all the experimental conditions (refer to Chapter 10). Besides that, in general, the rate of adsorption (before and after a complete formation of expected single layer) showed smooth trends with no apparent discontinuities. This indicates that one set of surface kinetics appears to work for fitting the experimental results. This also showed that our assumption of a monolayer model is too simple. It is suggested that a surface diffusion may occur during adsorption (in this model, it is assumed that all adsorbed molecules stay in the same place). This is because AFM characterization done in this study showed that proteins

formed islands during adsorption. The study done by Kim et al. [2005] supports this suggestion. In their study, adsorption of lysozyme on a mica surface formed clusters after several minutes of adsorption.

Table 11.7 shows the fitted $\left(\frac{\delta_0}{D}\right)$ values for each protein under all the experimental conditions. In general, the type of proteins, varying temperatures and concentrations did not much influence the fitted $\left(\frac{\delta_0}{D}\right)$. The fitted $\left(\frac{\delta_0}{D}\right)$ was slightly higher at high concentrations and temperatures. For example, the fitted $\left(\frac{\delta_0}{D}\right)$ for both β-casein and lysozyme was apparently constant under all the operating conditions used. The fitted $\left(\frac{\delta_0}{D}\right)$ for α-lactalbumin meanwhile was slightly higher at high concentration and temperature compared to others.

Table 11.7: The fitted $\left(\frac{\delta_0}{D}\right)$ for each protein under all the experimental conditions (this study).

Concentration (g/L)	Temperature (°C)	$\left(\frac{\delta_0}{D}\right)$ (β-casein) (s/nm)	$\left(\frac{\delta_0}{D}\right)$ (lysozyme) (s/nm)	$\left(\frac{\delta_0}{D}\right)$ (α-lactalbumin) (s/nm)
0.1	23	0.04		
	30	0.04		
	35	0.04		
	40	0.04	0.04	0.04
0.5	23	0.05		
	30	0.04		
	35	0.04		
	40	0.04	0.04	0.07
1.0	23	0.04	0.04	0.06
	30	0.04	0.04	0.04
	35	0.04	0.06	0.08
	40	0.06	0.06	0.08

It has been reported that, the diffusion coefficient, *D*, for β-casein, lysozyme and α-lactalbumin, respectively, is 2 x 10^{-10} m^2 /s [Miller et al., 2004], 6 x 10^{-10} m^2 / s and 1 x 10^{-10} m^2 / s [Engel et al., 2002].

Table 11.8 shows the calculated δ_0 (concentration boundary thickness) for each protein. The δ_0 is obtained by substituting the assumption of *D* to the $\left(\frac{\delta_0}{D}\right)_{fit}$ in Table 11.7. Also shown is (δ_0 / $D^{1/3}$) (in brackets) (will be discussed later).

Example of calculation: From β-casein data at a concentration of 1 g / L and temperature of 40 °C.

$$\left(\frac{\delta_0}{2x10^{-10}}\right) = 0.06x10^9$$

$$\delta_0 = \left(0.06x10^9\right) * \left(2x10^{-10}\right) = 0.012\,m$$

Table 11.8: Concentration boundary thickness, δ_0, for β-casein, lysozyme and α-lactalbumin under the experimental conditions used in this study. Also shown is (δ_0 / $D^{1/3}$) (in bracket).

Concentration (g / L)	Temperature (°C)	δ_0 (β-casein) (m). Value in bracket is (δ_0 / $D^{1/3}$) (s / m)	δ_0 (lysozyme) (m). Value in bracket is (δ_0 / $D^{1/3}$) (s / m)	δ_0 (α-lactalbumin) (m). Value in bracket is (δ_0 / $D^{1/3}$) (s / m)
0.1	23	0.008 (13.67)		
	30	0.008 (13.67)		
	35	0.008 (13.67)		
	40	0.008 (13.67)	0.024 (28.43)	0.004 (8.60)
0.5	23	0.01 (17.10)		
	30	0.008 (13.67)		
	35	0.008 (13.67)		
	40	0.008 (13.67)	0.024 (28.43)	0.007 (15.0)
1.0	23	0.008 (13.67)	0.024 (28.43)	0.006 (12.92)
	30	0.008 (13.67)	0.024 (28.43)	0.004 (8.60)
	35	0.008 (13.67)	0.036 (42.65)	0.008 (17.22)
	40	0.012 (20.50)	0.036 (42.65)	0.008 (17.22)

From Table 11.8, δ_0 for lysozyme appeared to be the largest compared to other two proteins because of the larger diffusivity. There was apparently no significant difference in δ_0 between β-casein and α-lactalbumin. Also, the values of δ_0 were about 80 to 720 times larger than the height of the cell (the height of the cell is about 0.00005 m).

11.2.4 Mass boundary layer

δ or the concentration boundary layer thickness can be defined as the distance from a surface to where the concentration of the diffusing species reaches 99 % of the bulk concentration (see Figure 11.8) [Fogler, 1992]. Nearly all the resistance to mass transfer is found in this layer. The dashed line in Figure 11.9 (A) represents the concentration profile predicted by the simpler film model, while the solid line gives a more realistic profile) [Fogler, 1992].

There are two length scales in the y direction, the momentum boundary layer thickness, δ_m and the concentration boundary layer thickness δ_c (see Figure 11.9 (B)) [Bird et al., 1962]. Both δ_m and δ_c are important because:

- If $\delta_m << \delta_c$, the velocity profile is essentially uniform as the concentration changes from 0 to c_b. In this condition, the momentum boundary layer lies entirely within the mass boundary layer.
- If $\delta_c << \delta_m$, the velocity profile is linear as the concentration changes from 0 to c_b. In this condition, the mass boundary layer lies entirely within the momentum boundary layer.
- If $\delta_c \sim \delta_m$, the concentration and momentum boundary layers have similar thickness. In this condition, the mass and momentum boundary layers have similar size.

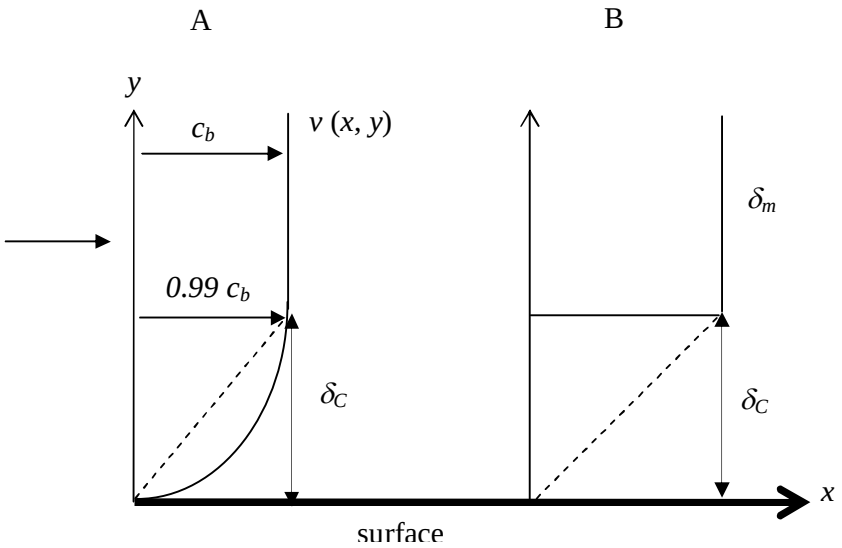

Figure 11.9: Illustration of boundary layer thickness; (A) actual profile (solid line) and predicted simpler line (dashed lines) and (B) momentum boundary layer thickness, δ_m and the concentration boundary layer thickness δ_c.

The Schmidt number, Sc, describes the relative importance of momentum and diffusive transport. $Sc = \frac{\mu}{\rho D}$ where μ is the viscosity, ρ is the density and D is the diffusion coefficient

Bird et al. [1962] in their analysis of diffusion and chemical reaction in laminar flow along a flat plate have introduced Δ that is the ratio between δ_c and δ_m, $\Delta = \frac{\delta_c}{\delta_m}$.

In the absence of chemical reaction or with relatively slow reaction, $\Delta = Sc^{-1/3}$ [Bird et al., 1962]. In this application, to find δ_0 we focus on the early stages of the adsorption ($t \rightarrow 0$) where surface reaction is not controlling, so we can use Bird's relationship.

$\delta_m \alpha \mathrm{Re}^n$, n is usually -1/2 [Edwards et al., 1978], so,

$$\delta_c \alpha \delta_m \left(\frac{\rho D}{\mu}\right)^{1/3} \alpha \left(\frac{\mu}{\rho d}\right)^{1/2} * \left(\frac{\rho D}{\mu}\right)^{1/3} \alpha \left(\frac{\mu}{\rho}\frac{D^2}{d^3}\right)^{1/6}$$

From the above relationship, it was clearly shown that $\delta_0 = \delta_c\,(t = 0)$ is a function of ρ, d, μ, and D.

This indicates that the $\left(\frac{\delta_0}{D^{1/3}}\right)$ will be constant if the cell flow geometry and flow properties of the fluid are constant.

However, the fitted $\left(\frac{\delta_0}{D}\right)$ values were formed to be constant for different proteins, with different expected diffusivities D (see Table 11.7). When the δ_0's were calculated, and hence $\left(\frac{\delta_0}{D^{1/3}}\right)$, the latter values varied appreciably (see Table 11.8).

The differences may resulted from the magnitude of Re (-1/2) and Sc (-1/3) used to derive the δ_0. In our system, the flow is behaved like a jet whereas the magnitude of -1/2 is applied on a flow that parallel to a flat plate.

Nevertheless, it is tempting to use the $\left(\frac{\delta_0}{D}\right)$ value of 0.04 s / nm as at least a first approximation for any future study of kinetics with this QCM model in aqueous solutions, irrespective of the molecule adsorbing onto the crystal surface.

As explained in Chapter 4, the maximum velocity of concentration in this study is expected to be at the midpoint z in the cell channel (see Figure 11.10). Referring to Figure 11.10, δ_0 can be measured as a ratio between the bulk concentration to the initial slope of the concentration profile, $\delta_0 = \frac{c_b}{initial\ slope}$, and δ_0 can be higher than that of the thickness of the cell, h.

The modelling results showed that δ_0 was larger than the thickness of the cell, *h* (refer to Table 11.7) and consistent with our prediction.

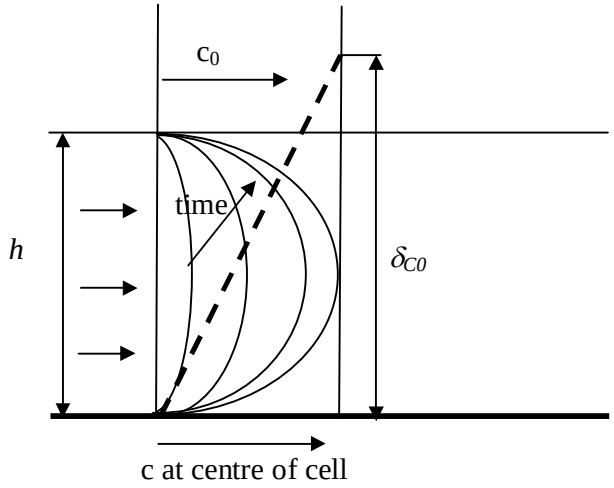

Figure 11.10: Illustration of mass velocity profile inside the cell and determination of δ_0 (this study).

The approximate time required for the protein solution to pass across the crystal surface was about 45 secs. This approximation is taken from the transition between regime C (water) and D (buffer solution) in Figure 6.7. For a QCM-D cell, the crystal surface senses the deposition of mass most sensitively at the centre of the surface. The mean residence time of the protein solution in the cell (i.e. the time taken for the cell to fill the surface, meanwhile was about 12 secs (V/Q = 20μL / 100μL/ min = 0.2 min = 12 secs).

Mixing (turbulence and diffusion) and stratification (at the wall, in the jet) are believed to be the factor for the difference between the two times obtained. The mixing will preserve a zero difference but stratification will encourage a difference. Adsorption time scales have an enormous influence on the dynamics of proteins at interfaces. Protein interactions at an interface, including relaxation, rearrangement, unfolding and denaturation, occur over generally different time scales [Daly et al., 2003, Santos et al., 2006]. Adsorption time scales also strongly influence the degree of desorption. Given enough residence

time at an interface, protein adsorption is always irreversible [Koutsopoulus et al., 2005].

The residence time of the protein solution is dependent on the flow rate; the residence time is increased if the flow rate is decreased.

The concept of the fluid of the flow in the QCM can be related to that in an *aerosol impactor* (round impactor) [Marple and Willeke, 1976]. Figure 11.11 shows streamlines and particle trajectories for a typical impactor. W, T and S refer respectively to a jet width or diameter, a nozzle throat length and a jet-to-plate distance, respectively.

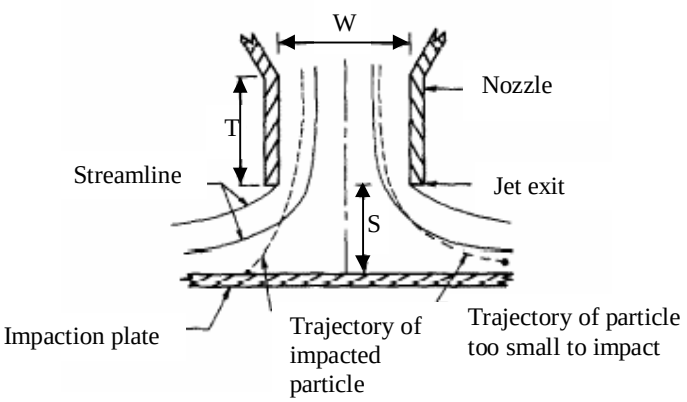

Figure 11.11: Streamlines and particle trajectories for a typical impactor. Taken from [Marple and Willeke, 1976].

For the round impactor, the Re number is calculated using Equation 11.5.

$$\mathrm{Re} = \frac{\rho V_0 W}{\mu} \qquad (11.5)$$

where, ρ, V_0, W and μ are refer respectively to a fluid density, a mean fluid velocity at throat, a jet diameter and a fluid viscosity.

Figure 11.12 meanwhile illustrates the theoretical velocity profiles along the impaction plate for the round impactor for Re numbers = 10, 3000 and 25,000. *Re* number of 10 is our interest since the *Re* number achieved in this study is below 10.

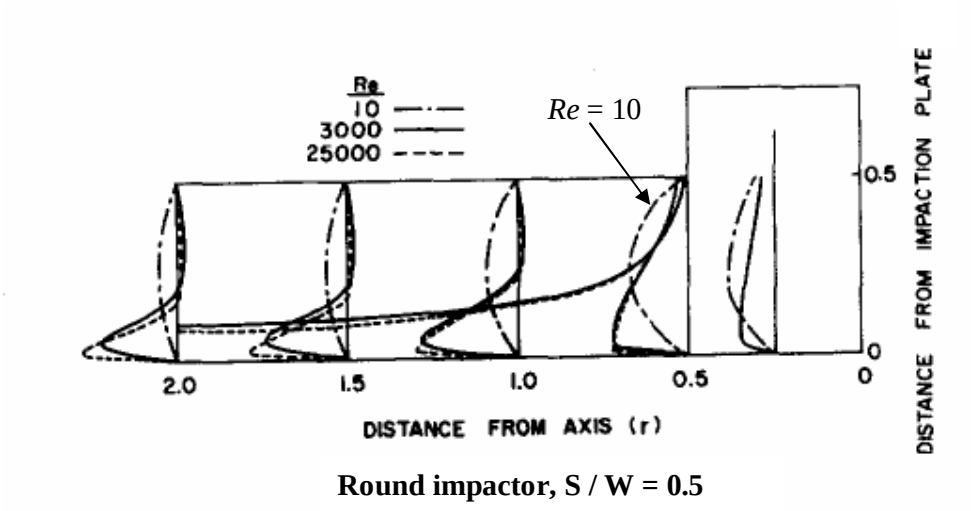

Round impactor, S / W = 0.5

Figure 11.12: Theoretical velocity profiles along the impaction plate for the round impactor for *Re* = 10, 3000 and 25,000. Taken from Marple and Willeke [1974].

As can be seen, the flow is changing continuously over this range of Reynolds numbers. At *Re* = 10 the flow fills the entire channel above the impaction plate. For the two larger Reynolds numbers (i.e. 3000 and 25,000), the free streamline did not reattach. The figure also shows that the boundary layer along the impaction plate becomes thinner as the Reynolds number is increased. Besides that, there is a large change in the velocity profile from *Re* = 10 to *Re* = 3000 and relatively small changes in the profile from *Re* = 3000 to *Re* = 25,000. However, it is of interest to note that the boundary layer thickness remains essentially constant along the impaction plate and is smaller for *Re* = 25,000 than for *Re* = *3000* [Marple et al., 1976].

Effect of shear stress / shear rate on the protein adsorption behaviour

In this study, we did not investigate the effect of shear rate or shear stress on the removal of the adsorbed proteins (i.e. the flow rate was fixed constant at 100 μL / min). Thus, the effect of shear stress or shear rate on the adsorption behaviour is discussed based on the literature. Shear rate can be defined as $\gamma = \frac{\partial u}{\partial y}$ while shear stress can be defined as $\tau = \mu \frac{\partial u}{\partial y}$, where μ is the viscosity of the solution, u is the flow velocity and y is the distance from the surface [Yeh et al., 2007].

Many studies done in a single layer adsorption [Wertz and Santore, 2002, Daly et al., 2003, Santos et al., 2006, Yeh et al., 2007 and Pereira et al., 2008] have found that wall shear stress does affect the protein adsorption behaviour. Santos et al.[2006] had reported that a flow rate and hence shear stress influenced the adsorption behaviour of proteins by affecting the transport of bulk proteins to the surface, by removing the adsorbed proteins from the surface. Wall shear rate induced by the flow is not only able to remove the deposited proteins on the surface but it also affects the orientation rate of the adsorbed proteins [Daly et al., 2003]. Yeh et al. [2007] explained that the theoretical calculations on protein-surface interactions (i.e. Van der Waals, electrostatic and hydrophobic) and shear stress are able to describe the mechanisms for protein desorption from a lead zirconate titanate plate (PZT) surface.

However, they [Yeh et al., 2007] found that a shear stress itself was not sufficient to remove the adsorbed proteins on the surface. The removal of the adsorbed proteins is also dependent on the residence time. The decrease in the protein residence time allowed the adsorbed proteins on the surface to be removed more quickly, a much stronger effect [Santos et al., 2007] than the increase in the flow hydrodynamics (shear rate).

Various shear rate values have been used in experimental studies [Daly et al., 2003, Choi and Foster, 2003, Santos et al., 2006, Yeh et al., 2007, Yang et al., 2008, Pereira et al., 2008]. The value of shear rate can be as high as 4800 s^{-1} [Choi and Foster, 2003]. In a QCM-D cell, a range of wall shear rate typically used is about 0.1 to 6 s^{-1} (i.e. with a range of flow rate, 30 to 100 μL / min) [Yang et al., 2008]. Meanwhile, the typical shear rates used in industrial processing are; stirring, 10^{-1} to $10^{-3}s^{-1}$; pumping, 10^{2} to 10^{3} s^{-1}; spraying,10^{3} to 10^{4} s^{-1} and

rubbing, 10^4 to $10^5 s^{-1}$ [Fox and McSweeney, 2003]. This indicates that the shear rates used in industrial practice are generally much higher than the shear rates used in laboratories.

An increase in the shear stress results in a reduction of boundary layer thickness. If the flow rate is sufficiently high and hence shear rate is high, the transport effects do not dictate the initial adsorption rate [Choi and Foster, 2003]. The Leveque equation (refer to Equation 11.7) (Lok et al., 1983) which includes shear stress in its formula can be used to determine whether the adsorption process is a diffusion limited adsorption or a kinetic limited adsorption.

$$\frac{d\Gamma}{dt} = 0.538D\left(\frac{\gamma}{Dx}\right)^{1/3} C \qquad (11.7)$$

where x is the distance from the flow cell inlet to the point of observation, γ is the wall shear rate, D is the diffusion coefficient of the protein, and C is the bulk concentration of the protein.

The Leveque equation applies only if a steady-state concentration profile is established before the surface coverage becomes large enough that it reduces the adsorption rate [Wertz and Santore, 2002, Daly et al., 2003, Choi and Foster, 2003, Pereira et al., 2008]. Therefore, the Leveque equation applies only when the adsorption rate does not decrease before a characteristic time, (τ), to establish the steady-state concentration profile, is reached (refer to Equation 11.8).

$$\tau = \left(\frac{x^2}{\gamma^2 D}\right)^{1/3} \qquad (11.8)$$

If the steady state concentration profile is established before τ and the experimental adsorption rate is significantly slower than that predicted by the Leveque equation, then the experimental adsorption rate is surface kinetics-limited [Choi and Foster, 2003].

Table 11.9 shows the Leveque initial adsorption rate (mg / m^2.s) and t (s) for each protein studied in this study. The Leveque initial adsorption rate and t are obtained from Equation 11.6 and 11.7, respectively. In this calculation, the shear

rate, γ, is taken as 7 s^{-1} (the approximate shear rate at 100μL / min) and *x* is 7 mm (the most sensitive area of the surface). As a comparison, the experimental initial adsorption rate for each protein studied is also shown in Table 11.10. It can be seen, for β-casein, the experimental adsorption rate is generally higher than that predicted by the Leveque equation (at high temperature; 35 and 40°C) while for lysozyme and α-lactalbumin, the experimental adsorption rate is lower than that predicted by the Leveque equation. According to the criteria mentioned above, it indicates that for β-casein, the adsorption is diffusion-limited at high temperature and surface kinetics-limited at low temperature. Both lysozyme and α-lactalbumin showed surface kinetics-limited adsorption. However, it can be argued that the Leveque equation uses the diffusivity, and also the shear rate and assumes that velocity and concentration profiles are already established, so there is no effect of transients. This fact by itself cannot show that the diffusion is limiting.

Table 11.9: Leveque initial adsorption rate (mg / m^2.s) and *t* (s) for each protein studied in this study. The leveque initial adsorption rate and *t* are obtained from Equations 11.6 and 11.7, respectively.

Protein	**Concentration (g / L)**	***t* (s) (Leveque *t* calculation)**	**Leveque initial adsorption rate (mg / m^2.s)**
β-casein	0.1	17	0.184
	0.5	17	0.920
	1	17	1.840
lysozyme	0.1	12	0.383
	0.5	12	1.913
	1	12	3.827
α-lactalbumin	0.1	21	0.116
	0.5	21	0.579
	1	21	1.160

Table 11.10: Experiment initial initial adsorption rate for each protein studied in this study.

Concentration (g/L)	temperature (°C)	β-casein Experimental initial adsorption rate (mg / m^2.s)	lysozyme Experimental initial adsorption rate (mg / m^2.s)	α-lactalbumin Experimental initial adsorption rate (mg / `m^2.s)
0.1	23	0.176	0.084	0.020
	30	0.281	0.088	0.049
	35	0.331	0.099	0.058
	40	0.378	0.171	0.103
0.5	23	0.507	0.099	0.163
	30	0.630	0.157	0.181
	35	0.930	0.268	0.266
	40	0.971	0.284	0.366
1.0	23	0.704	0.988	0.243
	30	1.830	1.142	0.280
	35	2.478	1.325	0.360
	40	3.082	1.362	0.407

11.3 Energy adsorption

As explained in Chapter 2, the adsorption of a protein is spontaneous if $\Delta G_{adsorption} = \Delta H_{adsorption} - T\Delta S_{adsorption} < 0$. Any proposed mechanism of protein adsorption must be consistent with the relationship between ΔG, ΔH and ΔS. A large negative ΔG value indicates high spontaneous adsorption behaviour (high affinity) towards the surface. The sign of the ΔH value meanwhile indicates whether the process of adsorption is endothermic or exothermic (positive ΔH value relates to an endothermic process and vice versa). The occurrence of denaturation or conformational change during the adsorption is expected to be correlated to a ΔS value. The larger the value of the (positive) ΔS, [Cabilio et al., 2000] the more denaturation (spreading) is indicated.

As mentioned early in the previous section, diffusion-reaction models have been shown to better model our kinetic measurements than the surface reaction models. Thus, for discussing the energy of adsorption, the results obtained only from a diffusion-reaction model are used.

Table 11.11 shows the comparison of thermodynamic values for the adsorption of β-casein, lysozyme and apo α-lactalbumin onto a stainless steel surface in this study from pH 7.2 phosphate buffer at 296 K. All the possibilities of reverse reactions that can occur in the adsorption process are considered (refer to Figure 11.6). This is because the reverse reaction can be used to derive ΔG, ΔH and ΔS. ΔG, ΔH and ΔS values tabulated in Table 11.9 were obtained using Equations 4.37 and 4.38 (refer to Chapter 4).

$$\Delta G = -RT(\ln K) \tag{4.37}$$

$$\Delta G = \Delta H - T\Delta S \tag{4.38}$$

Plotting ΔG versus T then gives a slope and an intercept of ΔS and ΔH, respectively.

Table 11.11: Thermodynamic values for the adsorption to weakly-bound, adsorption to tightly-bound and transformation from weakly-bound to tightly-bound of β-casein, lysozyme and apo α-lactalbumin on a stainless steel surface from pH 7.2 phosphate buffer at 296 K (this study).

Protein		ΔG_{ADS} (kJ/mol)	ΔH_{ADS} (kJ/mol)	ΔS_{ADS} (J/K.mol)
β-casein	Adsorption to weakly-bound (i.e. k_1/k_d)	-11 ± 3	35 ± 10	162 ± 90
	Adsorption to tightly-bound (i.e. k_2/k_{2d})	-21 ± 8	54 ± 25	250 ± 130
	Transformation to strongly held (i.e. k_{f1}/k_{f2})	-4 ± 10	18 ± 25	74 ± 80
Lysozyme	Adsorption to weakly-bound (i.e. k_1/k_d)	-10 ± 4	36 ± 10	154 ± 90
	Adsorption to tightly-bound (i.e. k_2/k_{2d})	-22 ± 8	18 ± 20	131 ±80
	Transformation to strongly held (i.e. k_{f1}/k_{f2})	-3 ± 8	12 ±10	67 ± 50
Apo α-lactalbumin	Adsorption to weakly-bound (i.e. k_1/k_d)	-16 ± 4	47 ± 10	209 ± 70
	Adsorption to tightly-bound (i.e. k_2/k_{2d})	-20 ± 4	16 ± 30	130 ± 50
	Transformation to strongly held (i.e. k_{f1}/k_{f2})	-11 ± 13	30 ± 20	125 ± 80

Based on the ΔG_{ads} for weak and strong adsorption, there was no significant difference between the studied proteins. This indicates that all the studied proteins, either soft proteins or hard proteins have almost the same affinity towards a stainless steel surface.

All the studied proteins in this study are suggested to unfold (denatured) upon adsorption on a stainless steel surface (shown by a positive sign of ΔS). Based on the entropy change values, ΔS, of transformation to strongly held, it showed that apo α-lactalbumin has the highest positive value than the other two proteins. It is suggested that, relatively apo α-lactalbumin has experienced extensive denaturation during the adsorption. Meanwhile, the ΔS value of transformation to strongly held for both lysozyme and β-casein was almost the same. Low value of ΔS (transformation to tightly held form) shown by lysozyme is expected to be related to its stability since lysozyme is a hard protein whereas for β-casein, is probably because it is already in flexible random coil configuration form.

Van't Hoff analysis

The van 't Hoff equation (also known as the van 't Hoff isochore) in chemical thermodynamics relates the change in temperature (T) to the change in the equilibrium constant (K) given the standard enthalpy change (ΔH) for the process [Smith et al., 2001].

$$\frac{d \ln K}{d \frac{1}{T}} = -\frac{\Delta H}{R} \tag{11.9}$$

From Equation (11.9), plotting ln K versus $1/T$ gives a slope of $-\frac{\Delta H}{R}$. Figure 11.13 shows the illustration of graph of ln K versus $1/T$.

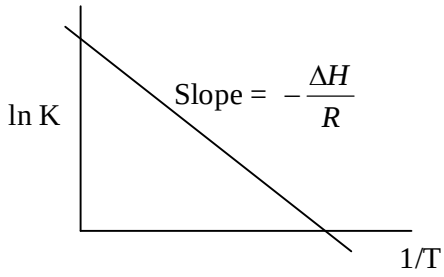

Figure 11.13: Illustration of graph of ln *K* versus 1/*T*.

Generally, the linear van't Hoff equation is utilized to calculate the thermodynamic parameters when the experiments are performed in a narrow temperature range (i.e. with the assumption that heat capacity, enthalpy change and entropy change are supposed to be invariable in this dependence [Chen et al., 2003].

Table 11.12 shows the ΔH values obtained using the Van't Hoff equation. Also shown is the value of ΔG and ΔS. The ΔG and ΔS values, respectively, were determined from $\Delta G = -RT \ln K$ and $\Delta S = (\Delta H - \Delta G)/T$ [Kaplan and Giiner, 2006].

Table 11.12: ΔH of the adsorption to weakly-bound, adsorption to tightly-bound and transformation from weakly-bound to tightly-bound of β-casein, lysozyme and apo α-lactalbumin on a stainless steel surface from pH 7.2 phosphate buffer at 296 K obtained using the Van't Hoff equation (this study). Also shown is the value of ΔG and ΔS, determined from $\Delta G = -RT \ln K$ and $\Delta S = (\Delta H - \Delta G)/T$, respectively.

protein		ΔG_{ADS} (kJ/mol)	ΔH_{ADS} (kJ/mol)	ΔS_{ADS} (J/mol)
β-casein	Adsorption to weakly-bound (i.e. k_1/k_d)	-11 ± 3	0.569 ± 0.050	39
	Adsorption to tightly-bound (i.e. k_2/k_2d)	-21 ± 3	0.790 ± 0.040	73
	Transformation to strongly held (i.e. k_{f1}/k_{f2})	-4 ± 3	0.338 ± 0.035	14
Lysozyme	Adsorption to weakly-bound (i.e. k_1/k_d)	-10 ± 3	0.523 ± 0.285	35
	Adsorption to tightly-bound (i.e. k_2/k_2d)	-22 ± 3	0.196 ± 0.120	75
	Transformation to strongly held (i.e. k_{f1}/k_{f2})	-3 ± 3	0.273 ± 0.190	11
α-lactalbumin	Adsorption to weakly-bound (i.e. k_1/k_d)	-16 ± 3	0.653 ± 0.320	56
	Adsorption to tightly-bound (i.e. k_2/k_2d)	-20 ± 3	0.287 ± 0.226	68
	Transformation to strongly held (i.e. k_{f1}/k_{f2})	-11 ± 13	0.324 ± 0.155	38

As can be seen (refer to tables 11.11 and 11.12), the ΔH_{ads} values obtained from the Van't Hoff equation (Table 11.12) were much lower than the first approach (Table 11.11). By contrast, the values of ΔS tabulated in Table 11.12 were higher compared to those in Table 11.11. In general, the values of ΔG, ΔH and ΔS for both approaches are not consistent. Ideally, the sum of Gibbs free energy, enthalpy and entropy for the cycle of reactions in both the clockwise and the counterclockwise directions should be equal to zero. In practice, however, the sum of experimental data may deviate significantly from zero [Matulis, 2001].

Although van't hoff dependence is a convenient method for thermodynamic analysis, the obtained enthalpy may differ from that observed by microcalorimetric measurements. This phenomenon may occur because of the

heat capacity change varying with temperature for most protein-surface interaction systems. Furthermore, the underlying binding mechanism may differ with temperature, and the heat capacity of the molecules involved may also vary with operating temperature [Chen et al., 2003].

It should be noted that, both ΔG and ΔS are dependent on the reference state or the concentration, which is totally arbitrary [Matulis, 2001]. Thus, for a validity comparison to others work, the reference state of ΔG (or ΔS) should be consistent. There is a number of such standard states used to define Gibbs energies and entropies of aggregation, among which the most popular are molar and mole fraction standard states [Matulis, 2001]. Thermodynamic functions are designated as 'standard' when they refer to changes in which reactants and products are all in their standard and their normal physical state. For example, the standard molar enthalpy of formation of water at 298 K is the enthalpy change for the reaction

$$H_2(g) + \frac{1}{2}O_2(g) \rightarrow H_2O(l) \qquad (11.10)$$

ΔH^0_{298} = -285.83 kJ.mol^{-1}. The superscript 0 is used to denote standard state and the temperature should be indicated.

Another aspect to be highlighted is that the role of solvent, particularly when hydrophobic interactions are invoked, needs to be included in the entropy change analysis; $\Delta S_{total} = \Delta S_{protein} + \Delta S_{water}$ (nonpolar patches of the protein surface are shielded by water molecules arranged in an ordered structure; when two non-polar patches come together, the water molecules are expelled and go to a free, less ordered state, which increases their entropy). However, most of studies done on protein adsorption to surfaces does not properly account for the role of water in the process and, in so doing, fails to distinguish unifying trends in protein adsorption. For example, literature illustrations depict protein and adsorbent surfaces without put together hydration layers, one layer for protein and one for surface, and do not consider how these layers are displaced or coalesced as protein and surface come into close contact. Many modern computational models probing surface–protein interactions regard water as a complicating feature that can be

ignored for the sake of reasonable computational time (Vasquez et al., 1994, Cramer & Truhlar 1999, Head-Gordon & Hura 2002). When water is included in such models, it is usually only those molecules directly adjacent to the protein that comprise the 'bound-water layer', classically measured by δ in grams-water-per-gram-protein (Durchschlag et al., 2001, Garcia de la Torre, 2001, Harding 2001), where δ~0.35 is found to be a representative average value (Durchschlag & Zipper 2001). This protein-bound water layer falls well short of the volume which must be displaced when a protein molecule approaches a hydrated adsorbent surface. That is to say, since two objects cannot occupy the same space at the same time, a volume of interfacial water at least equal to the partial specific volume, v^o, ($0.70 \leq v^o \leq 0.75$ cm^3 g^{-1} protein) of the adsorbing protein have to be moved (Chalikian & Breslauer 1996). If protein adsorbs in multi-layers, then clearly much more water must be displaced. Some of this interfacial water is bound to the adsorbent surface to an extent that varies with surface energy (Vogler 1998, 2001). Consequently, protein adsorption is found to scale with water wettability (Vogler 1992*a*, Vogler et al., 1993), and hence, surface hydration need to be incorporated into protein–adsorption models. Indeed, accounting for water in protein adsorption has become a significant concern of quartz crystal microbalance (QCM) measurement because QCM not only measures adsorbed protein mass but also 'trapped' (Hook & Kasemo, 2001) or 'intra layer' (Hook et al., 1998) or 'hydrodynamically coupled' (Hook et al., 2002) water.

Related to our study was the study done by Cosman et al. [2005]. However, in their study only one reverse reaction was considered (weakly bound to bulk) and no surface rearrangement was included. Refer to Table 11.13 for the thermodynamic values obtained in their study. Both holo α-lactalbumin and β-casein showed high spontaneous adsorption behaviour on a stainless steel surface (i.e. large negative ΔG_{ads}). However, relatively, β-casein showed a slightly endothermic process (ΔH_{ADS} =3.6 kJ/mol) while a larger endothermic process for holo α-lactalbumin (ΔH_{ADS} =15.6 kJ/mol). They suggested that particularly high entropic change value (ΔS_{ADS} =236 J/K.mol) of holo α-lactalbumin was related to the extensive denaturation during the adsorption on the surface, possibly with a

loss of calcium resulting in disruption of its tertiary structure to form the stable molten globular state. Meanwhile, β-casein is already in a flexible random coil configuration, therefore they suggested that the large ΔS_{ADS} value was probably contributed from other aspects of the adsorption process such as changes in the hydrated states of the protein upon adsorption in addition to the protein structural changes.

Table 11.13: Comparison of thermodynamic values for the adsorption of β-casein and holo α-lactalbumin on a stainless steel surface described using the Langmuir isotherm from pH 7 phosphate buffer at 298 K [Cosman et al., 2005].

Protein	ΔG_{ADS} (kJ/mol) ± 0.8	ΔH_{ADS} (kJ/mol) ± 0.8	ΔS_{ADS} (J/K.mol) ± 1
β-casein	-55	3.6	192
Holo α-lactalbumin	-54	15.6	236

Wehbi et al. [2005] studied the adsorption of holo α-lactabumin and apo α-lactabumin on a platinum surface at pH 7 and temperature of 298K (refer to Table 11.14). The adsorption was described using the Langmuir model. They have found that the value of enthalpy change (ΔH_{ADS}) was very low for apo α-lactalbumin, about twelve times lower than of holo α-lactalbumin. They explained that the lower ΔH_{ADS} value obtained for the apo type might come from the fact that apo α-lactalbumin was in a molten globule state (MG) and was already partially unfolded and therefore its ΔH_{ADS} was lower in comparison to the value for the holo type. The same explanation goes to the observation of ΔS_{ADS}. This also indicated that, a larger amount of energy is necessary to activate holo α-lactalbumin to start denature compared with the apo α-lactalbumin. It is because apo α-lactalbumin is already partially unfolded as mentioned above.

Table 11.14: Comparison of ΔH_{ADS} and ΔS_{ADS} for holo α-lactalbumin and apo α-lactalbumin from Wehbi et al. [2005]. The values of ΔH_{ADS} and ΔS_{ADS} were obtained from relationship $\Delta G_{adsorption} = \Delta H_{adsorption} - T\Delta S_{adsorption}$.

Protein	ΔG_{ADS} (kJ/mol)	ΔH_{ADS} (kJ/mol)	ΔS_{ADS} (J/K.mol)
Holo α-lactalbumin	-47	12	197
Apo α-lactalbumin	-50	2	164

Table 11.15 shows a comparison of literature Gibbs energy of adsorption values for β-casein, lysozyme and α-lactalbumin for a variety of surfaces. As can be seen, there was a significant different between their studies and this study. These differences are expected because:

- The model used to describe the adsorption is different.
- The substrate used is different.
- The operating conditions used are different.

Table 11.15: Comparison of literature Gibbs energy of adsorption values for β-casein, lysozyme and α-lactalbumin for a variety of surfaces.

Protein	ΔG_{ADS} (kJ/mol)		
	Stainless steel	Platinum	Sillica
β-casein	-55[a] (at ph=7, T=298) [Cosman et al., 2005]		
Lysozyme			23[d] (ph=7, T=294) [Larsericsdotter et al., 2004]
Apo α-lactalbumin	-40[b] (at ph=6, T=298K) [Adesso et al., 1997]	-50[c] (at ph=7, T=298) [Cabilio et al., 2000]	
Holo α-lactalbumin	-54[a] (at ph=7, T=298) [Cosman et al., 2005]	-47[c] (at ph=7, T=298) [Cabilio et al., 2000]	

[a] Adsorption of β-casein and holo α-lactalbumin to high-purity austenitic low-carbon stainless steel surface from pH 7 phosphatte buffer and 298K described using the Langmuir isotherm. $\Delta G_{adsorption}$ has been calculated using relationship of $\Delta G_{adsorption} = -RT (\ln K)$

[b] Adsorption of apo α-lactalbumin on a 304 stainless steel surface from pH 6 phosphate buffer and 298K described using the Langmuir isotherm

[c] Adsorption of holo and apo α-lactalbumin on a platinum surface from pH 7 phosphate buffer and 298K described using the Langmuir isotherm

[d] Adsorption of lysozyme on a negatively charged silica surface from pH 7 HEPES buffer and 294 K measured using DSC experiment

The thermodynamic values obtained in this study help to clarify the mechanism of the adsorption of β-casein, lysozyme and apo α-lactalbumin on a stainless steel surface. All the proteins are thermodynamically favourable to adsorb on a SS surface. Relatively, apo α-lactalbumin has experienced extensive denaturation once adsorbed followed by β-casein and lysozyme. Less denaturation observed for lysozyme is believed from its stability. It is suggested that the protein stability do strongly influence the adsorption mechanisms.

11.4 Mechanisms in operation during protein adsorption

11.4.1 Protein adsorption overview

As explained in Chapter 2, protein adsorption may be driven by different protein-surface forces, including Van der Waals, hydrophobic and electrostatic forces. Protein adsorption can also be driven by entropy gain from conformational changes in the protein during adsorption (especially for endothermic reactions). The analysis done in this study showed that all the studied proteins were denatured during adsorption on a stainless steel surface. α-lactalbumin, which is a soft protein, experienced an extensive denaturation as shown by the high ΔS value (transformation to tightly held). We expected that lysozyme was only partially unfolded upon adsorption on the SS surface in this study (shown by low value of ΔS of transformation to tightly held). We also expected that once the protein molecules were unfolded during the adsorption they tended to aggregate (will be discussed later).

Important parameters for adsorption are including pH, temperature, the ionic strength, the properties of the protein and the surface and also the nature of the solvent. Refer to Chapter 2, section 2.3.3 for the effects of these parameters on the protein adsorption. Table 11.16 shows the physical properties of the studied proteins in this thesis. Also shown is the expected driving forces of β-casein, lysozyme and α-lactalbumin on a stainless steel surface. Stainless steel surface is a hydrophobic surface [Teixeira et al., 2005, Gulec et al., 2005] and has an isoelectric point (pI) value of 4.3 [Fukuzaki et al., 1995]. Thus, at pH 7.2 (this study), a stainless steel is negatively charged.

Table 11.16: Physical properties, expected driving forces, ΔH and ΔS of β-casein, lysozyme and α-lactalbumin (refer to Chapter 2).

Property	β-casein	Lysozyme	α-lactalbumin
Molar mass ($gmol^{-1}$)	23,000	14,600	14,200
Dimensions (nm)	2.3	4.5 x 3 x 3	3.7 x 3.2 x 2.5
Isoelectric point (pH units)	4.6	11.1	4.3
Net charged at pH 7.2	Negative	Positive	Negative
Type of protein	Soft	Hard	Soft
Acid amino residues	209	129	123
Expected driving forces during adsorption on a bare SS surface	Hydrophobic and conformational entropy gain (repulsive electrostatic)	Hydrophobic and attractive electrostatic (mainly)	Hydrophobic and conformational entropy gain (repulsive electrostatic)

11.4.1.1 β-casein on SS

From the QCM-D results, it has been shown that the adsorption of β-casein on a stainless steel surface was fast (took less than 10 minutes to reach a steady state) and demonstrated a partially reversible adsorption. We expected that a fast adsorption experienced by β-casein resulted from its disordered structure with a great flexibility for the interaction with the surface. Consistent with our finding was the work done by Murray and Cros [1998]. They claimed that the fast adsorption of β-casein on the hydrophobic gold surface was due to its flexibility. Fibrinogen which also has a flexible structure has also shown a fast adsorption [Liu et al., 2007].

Here, it was expected that the adsorption of β-casein onto the stainless steel surface was driven by entropy gain and hydrophobic interaction. The entropy gain arises from the conformational changes of β-casein during the adsorption. Lee et al. [2001] indicated that flexible protein molecules readily undergo conformational change during the adsorption. Therefore the expected electrostatic

repulsion between negatively charged β-casein and the negatively charged oxide ('bare') surfaces was apparently compensated mainly by the entropy gain. This is shown with the high value of entropy change for β-casein in this study. However, there is also possibility that electrostatic attraction between β-casein and surfaces could occur since the distribution of ionic patches on the surface of a protein is not uniform. Wang et al. [2004] reported that the surface hydrophobicity alone may not be the best indicator as to whether proteins will adhere (i.e. hydrophobic interaction). They stated that the chemistry, packing or orientation of surface protein molecules in solution may also be involved.

There was a possibility that β-casein adsorbed as micelles in this study since it was reported that the minimum concentration of protein solution for micelle formation, called the critical micelle concentration (CMC) was about 0.5 g / L [Kul et al., 1997], while in this study, solution concentration up to 1 g / L was used. The micelles undergo structural relaxation on a hydrophobic surface as the outer surface of micelles is hydrophilic. The adsorption after the relaxation of micelles is slightly smaller than the adsorption of the isolated protein molecules but the difference is not significant. Yet, Lee et al. [2004] found that a high ionic strength of solution (such as NaCI > 0.1 M) could diminish the formation of micelles. In this study, the ionic strength of buffer solution used was 90 mM, which is lower than 0.1 M. Thus, the possibility of micelle formation is there. A formation of islands observed from our AFM characterization however most probably was not derived from micelles since the adsorption done was less than the CMC of 0.5 g / L at 0.1 g / L.

Studies done on the adsorption of β-casein on hydrophobic solid surfaces (such as a hydrophobic silica surface) [Tiberg et al., 2001] showed that β-casein formed a monolayer at these surfaces with the hydrophobic segment of the protein sticking to the surface, forming a densely packed layer while highly charged N-terminal portion (hydrophilic) extending into the solution (a loose layer). This behaviour was confirmed with the neutron reflection study of casein adsorption on a hydrophobic silica surface [Tiberg et al., 2001]. In this study, rinsing a β-casein layer with a buffer solution largely reduced the mass adsorbed especially at high temperature and concentration (by up to 40 %). The removal of β-casein molecules [Tiberg et al., 2001] was most likely occurred from the outer self-

associated casein molecules in the adsorbed bilayer. Apart from that, one also has to consider the large steric repulsion within the layer as β-casein is a highly flexible molecule.

11.4.1.2 Lysozyme on SS

By contrast to β-casein, the adsorption of lysozyme on a stainless steel surface was slow (took hours to reach a steady state) and displayed almost fully irreversible adsorption. Consistent with this finding was the work done by Wahlgren et al. [1995]. They found that the adsorption of lysozyme on the hydrophilic silica surface took about 2 hours to reach a steady state. Similar time dependence was also observed by Malmsten [1995] and McGuire et al. [1995] for lysozyme layers adsorbed on a hydrophobic surface. Malmsten [1995] also showed that even after 2 hours period there was still a gradual increase in lysozyme adsorption on the ethylated silica surface. Lysozyme also showed an irreversible adsorption on a mica surface [Kim et al., 2002]. Liu et al. [1998] explained the irreversibility of lysozyme on the hydrophobic surface as resulting from both the hydrophobic attraction of the hydrophobic fragments in lysozyme to the hydrophobic surface and electrostatic repulsion within the adsorbed layer. They [Liu et al., 1998] argued that the hydrophobic surface induced the exposure of hydrophobic fragments from the lysozyme. They suggested that the denatured lysozyme adsorbed in the form of peptide chains with the hydrophobic amino acid side chains attached to the surface with the hydrophilic side chains extending into the bulk solution. Kim et al. [2002] stated that the adsorbed lysozyme undergo conformational changes in the first layer that assisted in a multilayer formation. Besides that, the irreversibility of lysozyme [Veen et al., 2007] might be due to a surface aggregation of the protein. The difference between denaturation and aggregation is that denaturation is normally reversible, but aggregation is not [Changani et al., 1997]. Always protein denatures first then followed with an aggregation. Kim et al. [2002] stated that once protein was adsorbed onto the surface, will undergo conformational change due to protein-surface interaction. This unfolded protein will expose its hydrophobic residues and will interact with other adsorbed proteins, which were also unfolded. Thus, this resulted in a surface aggregation.

From the enthalpy and entropy changes obtained in this study, we expect that the adsorption of lysozyme onto a stainless steel surface was driven from (mainly) electrostatic attraction hydrophobic interactions and entropy gain as well (i.e. hydrophobic interactions induced to conformational change). We expect that the entropy gain be due to a breaking down of a secondary and a tertiary lysozyme structure during the adsorption on the hydrophobic surface. Since lysozyme is a hard protein, we expect, it undergoes partially unfolding during the adsorption.

11.4.1.3 Apo α-lactalbumin

The adsorption of apo α-lactalbumin on a stainless steel surface was very fast (took less than 1 minute to reach a steady state) and displayed almost fully irreversible adsorption. From the analysis done in this study, apo α-lactalbumin showed the highest positive entropy change than β-casein and lysoyme, indicating an extensive denaturation (adsorption-induced denaturation mechanism). Bettoni et al. [2001] had shown that removal of calcium from α-lactalbumin induced a conformational change of the protein in solution (that is a conversion from holo α-lactalbumin to apo α-lactalbumin) and increased its hydrophobicity. To support this, Veen et al. [2007] suggested that the driving force for adsorption of (negative) α-lactalbumin on a negatively charged silica surface was neither electrostatic nor helped by dehydration of the hydrophilic surface. Since α-lactalbumin is a soft protein, they expected that adsorption-induced structural changes in the α-lactalbumin molecules increased the effective protein adsorption affinity and therewith contributed to the irreversibility of the adsorption.

Thus, we expect that the adsorption of apo α-lactalbumin onto the stainless steel surface in this study was driven by hydrophobic interactions and conformational entropy gain.

Experiments done using a native α-lactalbumin (calcium enriched) displayed a different trend upon adsorption onto the SS surface compared to that of apo α-lactalbumin. Adsorption of holo-α-lactalbumin was very slow and had not reached a steady state even after hours. Also, the final area mass density of holo α-lactalbumin was lower than that of apo α-lactalbumin. It was reported that [Cabilio et al., 2000) carboxylate groups were responsible for the interaction with

the surface. The number of carboxylate groups in α-lactalbumin is 21 (20 carboxylate groups from acidic amino acids residues and one from the carboxylate terminus of the protein). However, the Ca^{2+} ion is bound to four carboxyl groups, therefore, the total number of carboxylate groups available for binding of holo α-lactalbumin to the surface is 17. However this discrepancy is small and doubt did not significantly affect to the adsorption. The possible reason is most likely relates to their hydrophobicity. As mentioned early, removal of Ca^{2+} increased the hydrophobicity of α-lactalbumin and is expected will have a stronger hydrophobic interaction with the SS surface.

Nevertheless, similarly to apo α-lactalbumin, holo α-lactalbumin also demonstrated almost fully irreversible adsorption. The adsorption behaviour of holo α-lactalbumin was very similar to that of lysozyme. The most possible reason is that α-lactalbumin and lysozyme are two related proteins of 123 and 129 amino acid residues, respectively and share a similar three-dimensional structure, including four disulfide bonds. The notable differences among these two proteins are: (i) lysozyme has ability to adopt partially folding states in acid solution whereas α-lactalbumin adopts molten globules state [Veen et al., 2000] and (ii) α-lactalbumin resides in its calcium binding properties whereas lysozyme is not.

11.4.2 Multilayer

The possibility of adsorbed multilayers for each of the proteins studied in this thesis especially at high concentration and temperature cannot be ruled out. This is because the steady state mass adsorbed obtained in this work (QCM-D measurement) was higher than the theoretical maximum mass for a single-layer. The transition from monolayer to multilayers for each of the proteins studied in this study (refer to Chapter 10 on graphs of rate of adsorption (mg / m^2.s) versus mass adsorbed (mg / m^2)) showed that generally the rates had smooth trends, with no apparent discontinuities. This indicates that one set of surface kinetics appears to work for fitting the experimental results. However, the kinetics related to are somewhat more ill-defined than monolayer models. It is most likely that a surface diffusion exists (whereas the model developed assumed that all adsorbed

molecules stay in the same place). The existence of surface diffusion is strengthened with the growth of protein islands observed from AFM characterization done in this study.

Pellenc and co-workers [2005] have developed a diffusion-aggregation model that accounts for a surface diffusion of folded proteins only (i.e. the diffusion of unfolded proteins is not allowed), hence, the higher the unfolding probability, the shorter the diffusion length. At low unfolding probability, most of the proteins may diffuse and aggregate to a small number of clusters where unfolding is favoured. The higher the unfolding probability, the higher the number of clusters, so that proteins mostly form dimers and the system finally tends to a random sequential adsorption, where almost no diffusion takes place. Between the two behaviours, the unfolding of isolated proteins is high enough to increase the cluster number and thus favour neighbor-induced unfolding and low enough to allow diffusion and subsequent aggregation. It is therefore possible that a smooth transition between monolayer and multilayers results from slow surface diffusion rather than slow bulk diffusion.

AFM characterization cannot give directly the amount of mass density adsorbed. The amount of mass density adsorbed can be estimated only from the islands which appeared on the surface (refer to Chapter 8). It is suggested here that the height of the islands is useful information for multilayer determination. This is because, it has been reported [Kim et al., 2005] that bilayer formation will start only if a full monolayer was established.

In the model developed (this study), the protein molecules were assumed to adsorb on the bare SS surface randomly and form a monolayer. However, there is a possibility that after some times of adsorption, two surfaces may exist; a bare SS surface (a SS surface without proteins adsorbed) and a protein surface (a SS surface with proteins already adsorbed and expected to be mainly unfolded proteins). Thus, the incoming proteins may adsorb either on a bare SS surface or on a protein surface. They may also adsorb on both surfaces at the same time. This leads to the suggestion that multilayers may exist even though the bare SS surface is not fully covered with proteins. However, this suggestion need to be studied further since it contradicts Kim's statement; that the additional protein molecules adsorb onto the first layer only once the initial protein monolayer is completed [Kim et al., 2005]. Most probably the adsorbed proteins in this study experienced

a slow surface diffusion, as discussed above. Once adsorbed on the SS surface, the proteins (mainly folded proteins) may diffuse to other adsorbed proteins (can be either unfolded or folded proteins) and bind. This leads to a protein aggregation.

Table 11.17 shows the mass densities of β-casein, lysozyme and α-lactalbumin adsorbed on the bare stainless steel surface measured using both QCM-D and AFM (this latter measurement was restricted to the islands which appeared on the surface). Also shown is the theoretical single layer protein mass densities and expected single layer densities allowing for H_2O based on the following assumption. For an expected single layer allowing for H_2O, we assumed it was 1.5 times that the theoretical single layer. As described earlier [Hook et al., 2002], for small and globular proteins such as hemoglobin (64.5 kDa) and albumin (65kDa) the measured QCM-D mass of adsorbed protein is a factor of about 1.75 times higher than that measured by optical techniques while it is about 2 to 3.2 times higher for large proteins (fibrinogen (MW340kDa). Since, proteins studied in this thesis have much lower MW than fibrinogen, therefore, we believed that these assumptions are justified.

As shown in Table 11.17, the QCM-D mass density then indicated multilayers with all three proteins (even if one considers that the single layer allowing for H_2O is 3 times larger than of the theoretical dry single layer). By contrast, the estimated mass density adsorbed due to the islands (from AFM characterization) showed average densities much lower than the QCM-D measurement and even much less than a theoretical single layer.

Table 11.17: Mass density of β-casein, lysozyme and α-lactalbumin adsorbed on the bare stainless steel surface obtained from QCM-D and AFM in this study. Also shown is the theoretical single layer mass density and expected single layer allowing for H_2O.

Protein	Theoretical single layer (dry basis) (mg/m^2)	[a]Single layer allowing for H_2O (wet basis) (mg/m^2)	QCM-D experiment in this study (wet basis) (mg/m^2)	AFM, islands (wet basis) (mg/m^2)
β-casein	2.3	3.45	7 to 19	0.055
Lysozyme	2 (side-on), 3 (end- on)	3 (side-on), 4.5 (end-on)	4 to 25	0.2
Apo α-lactalbumin	2	3	10 to 25	0.5

[a]For a single layer allowing for H_2O, we assumed that the ratio wet mass to dry mass was equal to 1.5. This assumption was based on Hook et al.'s work [2002]

However, the height of the islands also show that the proteins formed multilayers (refer to Table 11.18 and Figure 11.14). Figure 11.14 (a), it shows that the adsorption of β-casein from 0.1 g / L solution is appears to form a single layer within the islands. Lysozyme (assuming end-on orientation) appears to form a complete single layer (Figure 11.14 (b)) with perhaps a side-on layer above it or for side-on orientation form a complete bilayer (Figure 11.14 (c)). α-lactalbumin meanwhile is appears to form three complete layers (Figure 11.14 (d)). This supports our suggestion that height of the islands is useful information for multilayer determination.

Table 11.18: The estimated lateral diameter and height of islands obtained from AFM characterization in this study. Also shown are the estimated number of molecules within an average island and the expected layers formed. The data was obtained from the adsorption of proteins from 0.1 g / L solution at room temperature.

Protein	Protein dimension (nm)	Theoretical thickness for single-layer (nm)	Estimated island lateral diameter (nm)	Estimated island height (nm)	Expected layer	Estimated number of molecules clustered in island
β-casein	2.3 (radian)	6.4	100 to 200	5.74	Single-layer	424 to 1695
Lysozyme	4.5 x 3 x 3	4.5 (end on), 3 (side on)	200 to 260	6.68	Bilayer (perhaps 1 end on, 1 side on)	6722 to 9762 (side on), 4481 to 6508 (end on)
Apo α-lactalbumin	3.7 x 3.2 x 2.5	3.7	130 to 330	12.55	3 layers	5600 to 36090

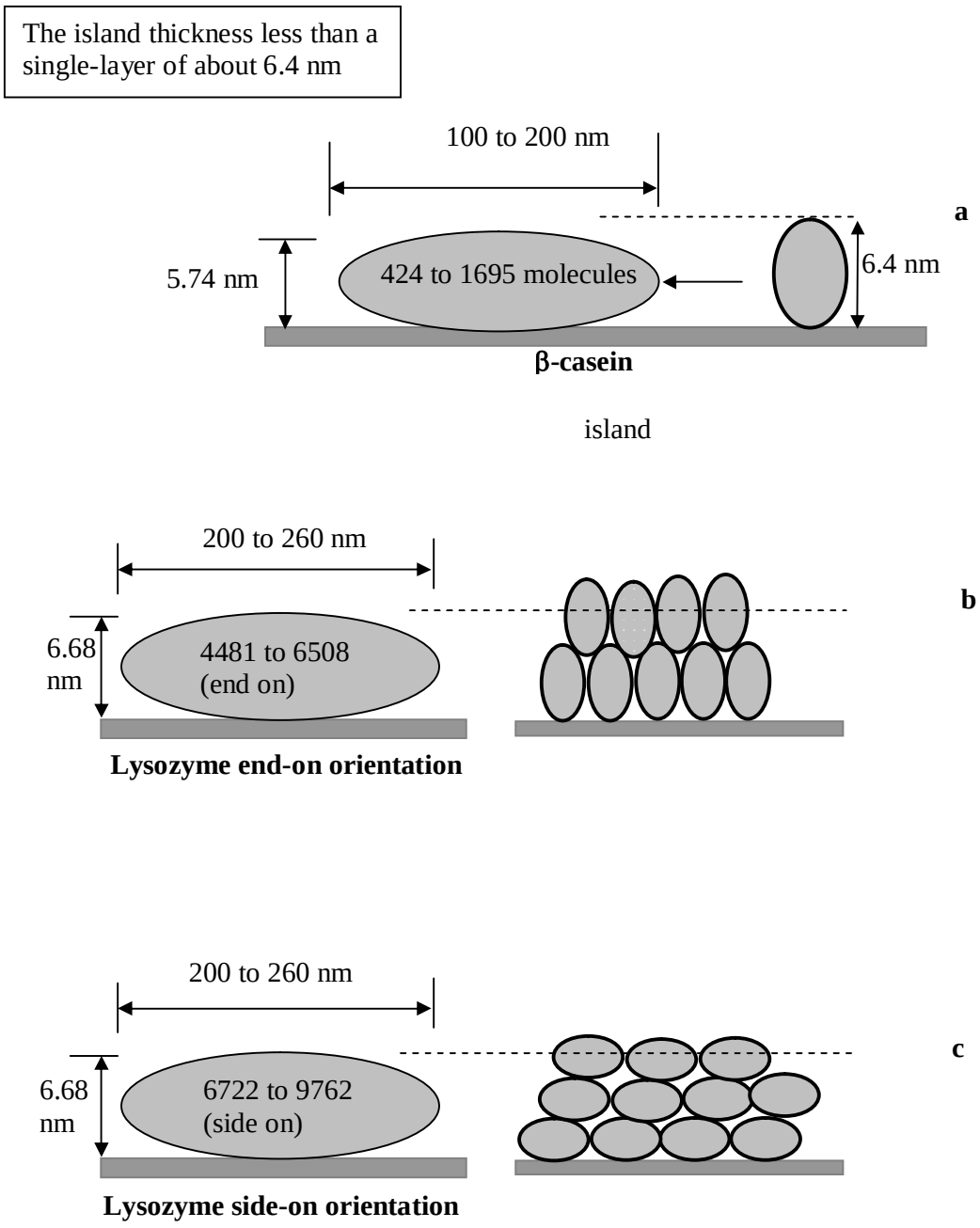

Figure 11.14: Illustration of possible conformation of protein molecules within island. (a) β-casein, (b) lysozyme with end-on orientation, (c) lysozyme with side-on orientation

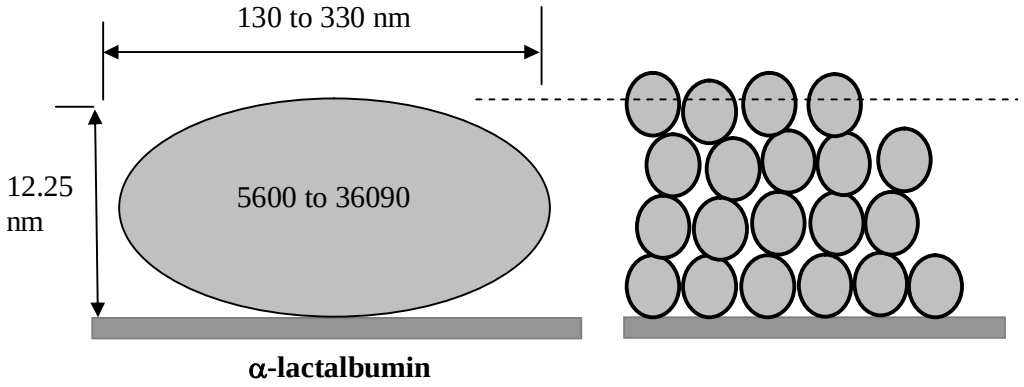

Figure 11.14: (cont.) Illustration of possible conformation of protein molecules within island (d) apo α-lactalbumin.

An AFM study done by Kim et al. [2002] on adsorption of lysozme at room temperature on a mica surface showed that adsorption from a low concentration solution (2 mg / L) formed clusters consisting of about five molecules after several minutes (refer to Figure 11.15). In contrast, at a concentration of 5 mg / L, the surface coverage increased uniformly until a complete monolayer was established after 2 hours (the time for monolayer). They also noted that bilayer formation did not start until a full monolayer was established and was build very slowly, only appearing after about a day (refer to Figure 11.16).

AFM results also showed that the molecules on the top layer tended to aggregate rather than to adsorb individually (refer to Table 11.18 and Figure 11.14). Since the QCM and AFM characterization referred to the tightly-bound molecules (after rinsing with buffer solution), we suggest that singly adsorbed molecules were desorbed during the rinsing and left the aggregated molecules remaining on the surface. The aggregated molecules bind to each other and thus have a larger collective surface area to bind with the surface and are more difficult to desorb.

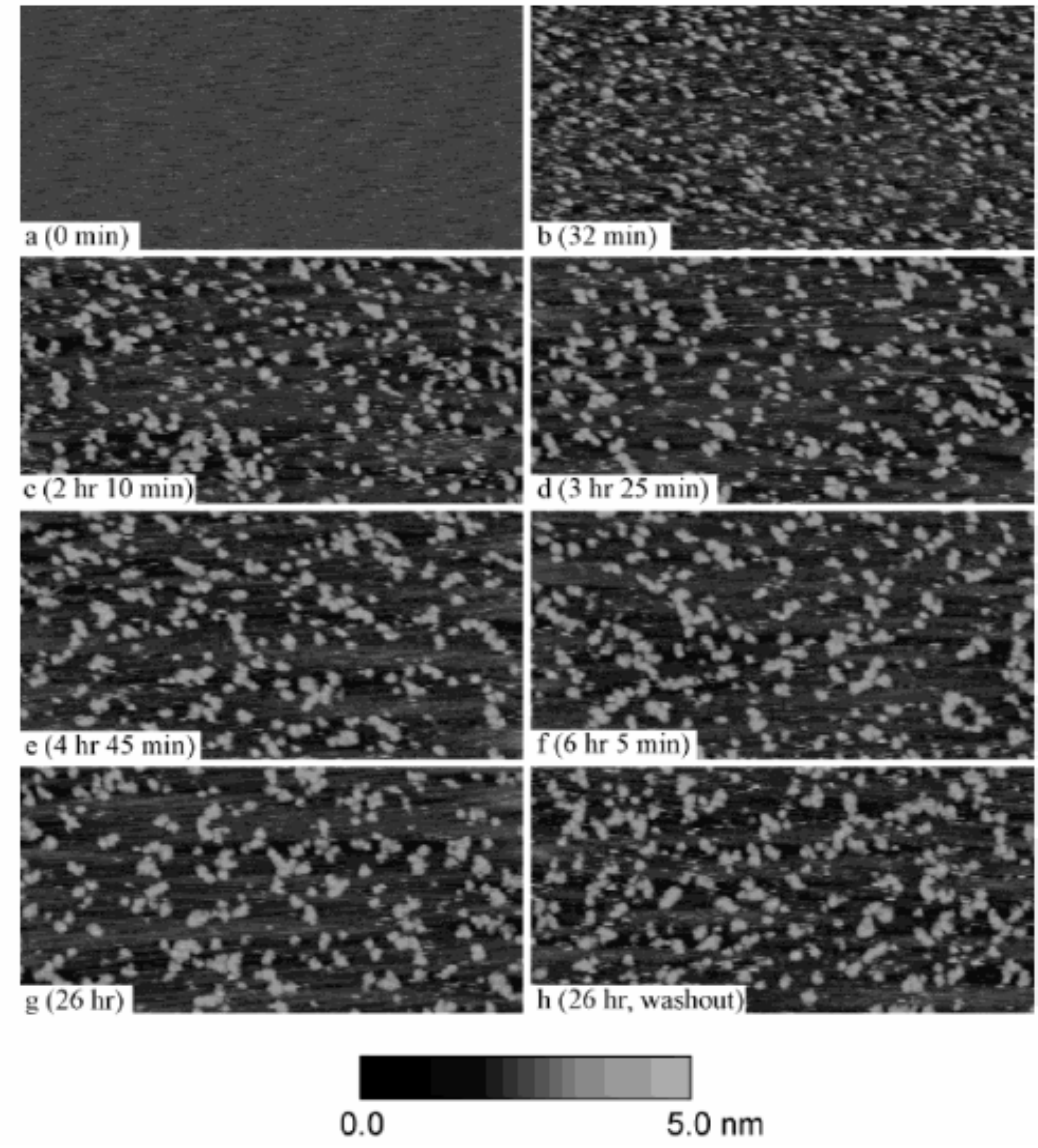

Figure 11.15: AFM images of adsorption of lysozyme on mica in 10mM acetate buffer, pH 4.0, under stopped-flow conditions. The initial bulk concentration of lysozyme is **2 mg / L**. Each image is 250 nm x 500 nm. The light areas are protein molecules, and the dark areas represent the bare mica surface. (a) Bare mica surface before contact with protein solution. (b) Adsorption after 32 min, (c) 2 h 10 min, (d) 3 h 25 min, (e) 4 h 45 min, (f) 6 h 5 min, and (g) 26 h. (h) Washout with pure buffer after 26 h. Taken from Kim et al. [2002].

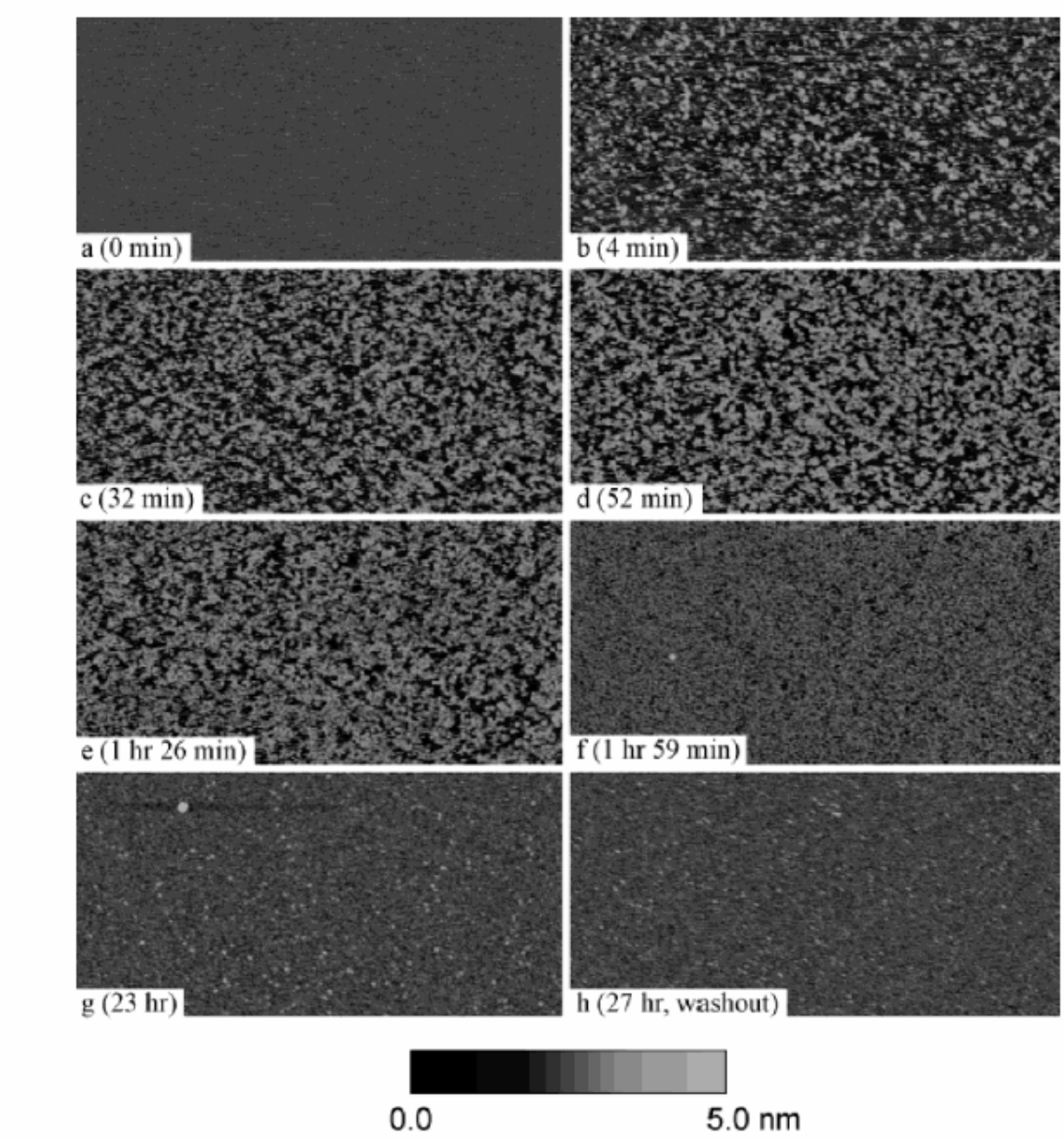

Figure 11.16: AFM images of adsorption of lysozyme on mica in 10mM acetate buffer, pH 4.0, under stopped-flow conditions. The initial bulk concentration of lysozyme is **5 mg / L**. Each image is 500 nm x 1000 nm. The light areas are protein molecules, and the dark areas represent the bare mica surface. (a) Bare mica surface before contact with protein solution. (b) Lysozyme adsorption after 4 min, (c) 32 min, (d) 52 min, (e) 1 h 26 min, (f) 1 h 59 min, and (g) 23 h. (h) Washout with buffer after 27 h. Taken from Kim et al. [2002].

11.5 Mechanisms of depositing protective layers on stainless steel

In this section of the study, we attempted to achieve a 'non-fouling' surface experimentally on a stainless steel surface. From the previous sections, it has been argued that hydrophobic interactions, electrostatic attractions and conformational entropy gain forces drove the adsorption of the studied proteins on a bare SS surface. Those forces need to be eliminated to prevent the adsorption of protein.

As explained in Chapter 2, a PEG layer can alter the surface interaction to proteins from attractive to repulsive. This is possible from PEG properties that are hydrophilic, neutral and highly water soluble; hydrophilic properties weaken the hydrophobic interactions between the proteins and the surfaces, uncharged properties (neutral) shield the electrostatic attraction between the proteins and the surfaces and high solubility properties provide a water barrier between proteins and the surface.

A range of techniques has been employed for the immobilization of PEG onto surfaces and these can be broadly classified as either physisorptive or chemisorptive. Either physisorptive or chemisorptive, both have the same aim to produce high PEG grafting density. This follows widely reported findings [Wei et al., 2003, Archambault et al., 2004, Brash, 2004, Jonsson et al., 2004, Fukai et al., 2004, Liu et al., 2007, Unsworth et al., 2008] that protein resistance is associated with high PEG grafting density.

In this study, we have decided to use a physisorptive method to modify the SS surface. The modification was done by coating the surfaces with an anchor layer; either polyethylimine (PEI) or sodium silicate layers. The poly (ethylene) glycol (PEG) molecules then were grafted onto either of these two anchor layers. There are two strategies in grafting the PEG onto such an anchor layer; first, by using single length PEG chains (monomodal) and second, by using mixed length PEG chains (bimodal).

The merits of the proposed modification methods compared to most published methods is that the process of modification is done only by passing the solution across the surfaces, does not involve any hazardous chemical substances and is cost effective. The mechanisms of depositing the protective layers on a stainless steel surface are discussed below.

11.5.1 Deposition of anchor layers on stainless steel

11.5.1.1 PEI on bare SS surface

The adsorption of PEI onto a stainless steel surface was fast and reached a steady state less than a minute. The attachment of PEI onto the stainless steel surface is expected to be based (mainly) on electrostatic interactions between positive charges on PEI and negative charges on the stainless steel surface [Wei et al., 2003, Kingshott et al., 2003]. Thierry et al [2008] also reported that the adsorption of PEI-PEG copolymers onto negatively charged silica surfaces was rapid and was expected to be driven by electrostatic attractions. Thus this method of immobilizing PEI to a SS surface is particularly attractive owing to its cost-effectiveness using the rapid and simple presumably electrostatically driven adsorption of PEI to negatively charged surfaces. Wei et al. [2003] reported that there may also be hydrogen bonding between the amine groups of PEI and the SS surface OH groups. These interaction forces were relatively weak and not strong enough to bind much PEI on the surface as shown by a huge desorption (i.e almost 85 %) into buffer observed in this study. However, there is a possibility that this removal of PEI resulted from PEI-PEI repulsion (multilayer) rather than from weak PEI-surface interactions. This will be discussed below.

It appeared that the surface mass density of tightly-bound PEI (after flushing with buffer) on a SS surface was the same (about 3 mg / m^2 (≅ 0.07 chains / nm^2)) at the two temperatures 23 and 40 °C. We expect that this is probably because the temperature used was still below the PEI melting point of 59 °C and therefore the molecules retained the same properties. Also, we expect that a PEI layer on top of a SS surface is able to transform the bare surface from a negatively charged to a positively charged surface. From the AFM characterization done in this study, the PEI molecules on the SS surface were imaged to be like islands that distributed randomly with the lateral diameter size of approximately 60 to 130 nm. The mean spacing between attached PEI molecules was about 4 nm (from QCM-D measurement). PEI with molecular weight of 23,000 g / mol, consists about 228 units (one unit of PEI is about 100 g / mol). The length of one unit PEI is about 0.45 nm (the backbone) (the length of C-C and C-N bonds are 0.15 nm [Benson, 1968]) (refer to Figure 11.17). Thus for

one molecule of PEI, the length for the backbone presumably lying down on the surface is about 100 nm (228*0.45 = 100 nm) with the width of about 0.6 nm. This indicates that 1 molecule of PEI occupies about 60 nm^2 area (100 *0.6 = 60). Thus 60 nm^2 is covered compared with 4 x 4 = 16 nm^2 of surface area per molecule of PEI. Thus there is more than a monolayer adsorbed. This also supports the possibility that the observed high removal of PEI during flushing came from multilayered PEI molecules. These further may have had weak bonding due to the electrostatic repulsion between PEI molecules.

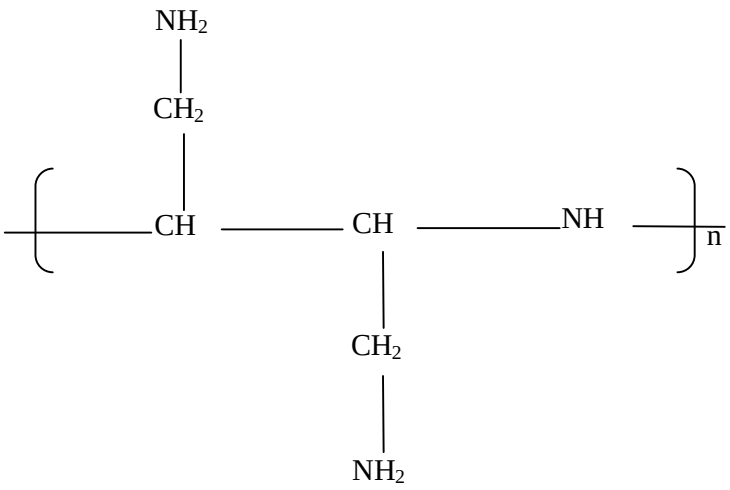

Figure 11.17: Schematic diagram of PEI structure.

11.5.1.2 Silicate on bare SS surface

The adsorption of silicate was initially fast, followed by a gradual increase before leveling off in less than 8 minutes. The attachment of silicate on a SS surface was expected to be based on physisorption interactions (hydrogen bonding and Van der Waals) [Bardina et al., 2001]. The final number density of silicate adsorbed was the same at about 2.5 chains / nm^2 for either 23 or 40 °C. The number density of silicate was higher than that of the PEI layer. A possible reason for this observation is that the size of the silicate molecule is much lower than that of PEI. The mean spacing between silicate molecules was about 0.6 nm (from

QCM-D measurements). The diameters of oxygen and silicon atom respectively are about 0.15 and 0.23 nm [Benson, 1968]. The area of one molecule of silicate is about 0.15 * 0.28 = 0.042 nm^2. Thus the fractional area coverage is (0.04 / (0.6)*(0.6) = 0.12) (i.e. 12 % covered).

The working calculation is shown below:

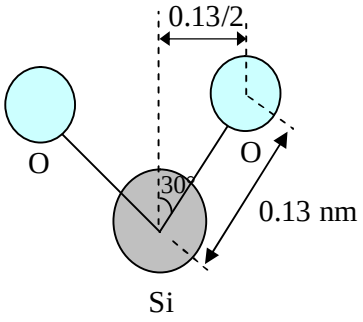

Width = 2 (0.13/2) + 0.15
= 0.28 nm

Length = 0.15 nm

Area = 0.28 * 0.15 = 0.042 nm^2

The presence of silicate solution provides a bare SS surface with silanol groups (Si-OH) [Bardina et al., 2001] and hence may transform the surface from a hydrophobic to a hydrophilic surface.

11.5.2 PEG on anchor layers on stainless steel

11.5.2.1 PEG on PEI anchor layer

PEG molecules with different MW and solution concentrations were physically grafted onto the PEI layer achieved from the previous section (as distinct from pre-reacting with the PEI and then grafting the copolymer onto the SS surface).

From the QCM-D measurements, generally adsorption of PEG350 and 550 Da on a PEI layer increased rapidly in the first few seconds followed by a steady, gradual decrease whereas for PEG2000 and 5000 Da, the adsorption suddenly increased before leveling off. There was a huge decrease in PEG number density as PEG MW was increased from 350 to 5000 Da, especially at high PEG concentration (5 and 10 g / L). This observation was consistent with others work [Archambault and Brash, 2004, Roosjen et al., 2004, Unsworth et al., 2005, Jayachandran et al., 2009]. Figure 11.18 shows an illustration comparing the forms of PEG of long MW (A) and short MW (B) and the influence on grafting density. This shows that PEG with high MW occupies a larger area than of the short PEG MW. Thus fewer PEG molecules can adsorb and as a consequence, the grafting density will be lower.

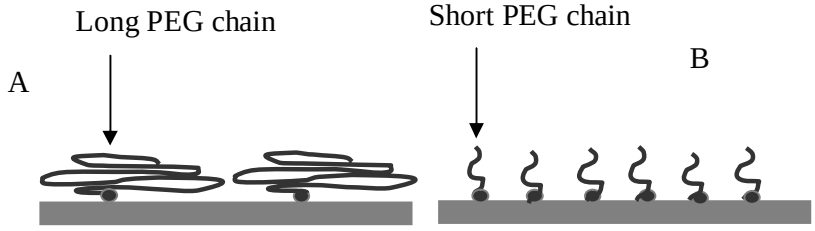

Figure 11.18: Illustration of conformation of PEG of long MW (A) and short MW (B) with influence on grafting density.

Also, for the same PEG MW, PEG grafting density was generally higher when adsorbing from a stronger solution concentration. It was reported that high PEG solution concentrations resulted in higher rates of adsorption [Veen et al., 2003] and hence increased the PEG grafting density. At PEG concentrations of

0.1 and 1 g / L, the grafting density increased if performed at a temperature of 40 instead of 23 °C. By contrast, at higher PEG concentrations (5 and 10 g / L), the grafting density *decreased* if performed at a temperature of 40 instead of 23 °C.

The same trend was observed for PEG-NHS layers; the grafting density increased as PEG-NHS concentration increased. The grafting density of PEG-NHS on SS-PEI was more than 50 % higher than that of PEG-CH_3. The grafting of PEG-NHS molecules to the SS-PEI surface is believed to be achieved through ester-amine reaction; NHS ester groups reacting with amine groups on PEI [Nnebe et al., 2004].

The tightly-bound PEG grafting density on SS-PEI surfaces achieved in this study from about 0.03 to 2.75 chains / nm^2 can be considered as high for any method even though the grafting was achieved using a physisorption method (desorption was about 30 to 40 %). With such physically adsorbed PEG containing layers, there is always a risk of displacement of adsorbed polymer layers by the protein. The ratio of PEG to PEI varied from about 4 to 40. However, it should be noted that, the grafting density achieved here is derived from the wet mass. The true chain density is likely to be about 2/3 of those given.

In an other study, the PEO dry-density of PEG600, 750 and 2000 Da achieved by chemisorption respectively ranged from 0.6 to 2.8, 0.2 to 2.3 and 0.18 to 0.98 chains / nm^2 (at room temperature) [Unsworth et al., 2008]. The small differences of PEG grafting densities between studies is suggested to be due to the different of operating conditions and method of measurement used.

11.5.2.2 PEG on silicate anchor layer

The tightly-bound PEG grafting density on SS-silicate surfaces obtained in this study ranged from 0.02 to 2.45 chains/nm^2 (wet basis). The ratio of PEG to silicate varied from about 0.01 to 1. From the calculation above, a silicate layer occupied only about 12 % of the total coverage. However, the PEG grafting density achieved on a SS-silicate surface was high (perhaps to 2.45/1.5 = 1.6 chains /nm^2 (MW for sodium silicate is 180 g mol^{-1})). Some of these PEG molecules may have attached to the SS surface directly, through its O^- and OH^- groups.

The grafting of PEG molecules to a SS-silicate surface is expected to be achieved through surface silanol groups [Bardina et al. 2001]. As a comparison, PEG grafting density generally was about 10 to 30 % lower on the SS-silicate surfaces than on the SS-PEI silicate. In another study, the grafting density of PEO (dry density) with molecular weights of 750, 2000 and 5000 Da on a silica surface was 0.4, 0.33 and 0.12 chains/nm^2, respectively [Unsworth et al., 2005]. However, it should be noted that comparison between results from different operating conditions and method of measurement may not be appropriate.

11.5.2.3 Bimodal PEG surface

In this study, it has been found that: (i) PEG grafting density generally increased as PEG concentration and temperature increased, (ii) bimodal PEG grafting density was the highest with a combination of PEG (550+350) and lowest with a combination of PEG (5k+2k), (iii) bimodal PEG grafting density was generally higher on the SS-PEI surfaces than that on the SS-silicate surfaces, (iv) bimodal PEG grafting density was about 1.5 to 5 times higher than that of the monomodal PEG.

Higher PEG chain densities on a combination of PEG (550+350) than that on PEG (5000+2000) is consistent with the expectation from literature that higher chain lengths result in lower number density. The trend results observed were consistent with Uchida et al. [2005] and Satomi et al. [2007].

Bimodal PEG grafting density was claimed to be higher than that of the monomodal density [Carignano et al., 2000, Fukai et al., 2004, Uchida et al., 2005, Satomi et al., 2007] due to the short PEG chains filling up the space close to the surface.

11.5.3 PEG conformation

PEG conformation is a very important aspect of inhibiting protein adsorption with a ‘brush’ conformation (associated with a high grafting density) widely reported (see Chapter 2) as the best conformation to inhibit adsorption of proteins. As described earlier in Chapter 2, PEG can conform either to a ‘pancake’, a ‘mushroom’ or a ‘brush’ structure. This conformation is dependent

on the grafting density or spacing between the chains, *d*, and on the length of the chain (MW) which is related to the PEG Flory radius (R_F) in solution. At low surface coverage ($d >> 2R_F$), the polymer molecules form either a 'pancake' or a 'mushroom' structure, depending whether the interaction between the polymer segments and the surface is attractive or repulsive, respectively. At $d \sim 2R_F$, the 'mushrooms' start to interact with each other until the brush transition ($d < 2R_F$), where the polymer chains stretch away from the surface resulting in a 'brush' conformation (refer to Figure 11.19). The polymer tends to collapse on the surface if there is an attractive interaction between the surface and the polymer. Also, PEG conformation has been shown to be dependent on the solvent used [refer to Figure 2.17].

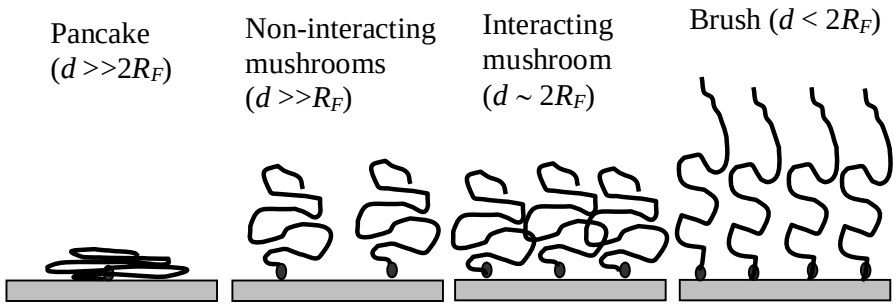

Figure 11.19: Illustration of the conformation of end-grafted PEG chains at the surface.

R_F can be calculated using Equation 2.1, $R_F = aN^v$

where *N* is a degree of polymerization (the MW for 1 unit of EG is about 44 g mol^{-1}), *a* is the characteristic monomer dimension (taken as 0.28 nm for the ethylene oxide repeat) and for high-solubility conditions, *v* can be taken as 0.6 [Unsworth et al., 2005].

Table 11.19 shows the R_F for each PEG used in this study.

Table 11.19: Comparison of R_F for each PEG studied.

PEG molecular weight (Da)	N	R_F (nm)	$2R_F$ (nm)
350	10	0.96	1.92
550	13	1.27	2.54
2000	45	2.75	5.5
5000	113	4.74	9.48

Table 11.20 shows the conformation of PEG achieved in this study. From the criteria of PEG conformation, apparently, the PEG conformed into either an interacting mushroom or a brush (dilute brush) structure under all the experimental conditions used.

Table 11.20: Expected PEG conformation achieved in this study under the overall experimental conditions (interacting brush $d/2R_F \sim 1$, molecular brush < 1).

Surface	Overall PEG grafting density	d (nm)	Criteria $d/2R_F$	Expected conformation
SS-PEI-PEG350	0.35 to 2.75	0.6 to 1.7	$d \sim 2R_F$, $d < 2R_F$	Interacting mushroom to brush (dilute brush)
SS-PEI-PEG550	0.22 to 2.56	0.63 to 2.0	$d \sim 2R_F$, $d < 2R_F$	Interacting mushroom to brush (dilute brush)
SS-PEI-PEG2k	0.10 to 0.30	1.8 to 3.2	$d \sim 2R_F$, $d < 2R_F$	Interacting mushroom to brush (dilute brush)
SS-PEI-PEG5k	0.03 to 0.15	2.6 to 5.77	$d \sim 2R_F$, $d < 2R_F$	Interacting mushroom to brush (dilute brush)
SS-silicate-PEG350	0.20 to 2.45	0.64 to 2.20	$d \sim 2R_F$, $d < 2R_F$	Interacting mushroom to brush (dilute brush)
SS-silicate-PEG550	0.30 to 1.50	0.80 to 1.80	$d \sim 2R_F$, $d < 2R_F$	Interacting mushroom to brush (dilute brush)
SS-silicate-PEG2k	0.05 to 0.20	2.24 to 4.47	$d \sim 2R_F$, $d < 2R_F$	Interacting mushroom to brush (dilute brush)
SS-silicate-PEG5k	0.02 to 0.1	3.16 to 7.0	$d \sim 2R_F$, $d < 2R_F$	Interacting mushroom to brush (dilute brush)

Note: $d = \Gamma^{-0.5}$ where Γ is a PEG grafting density [Michailidou et al., 2005].

11.6 PERFORMANCE OF PREVIOUSLY DESCRIBED PROTEIN-BLOCKING SURFACES

The effectiveness of the surfaces discussed above (i.e. SS-PEI, SS-silicate, SS-PEI-PEG, and SS-silicate-PEG surfaces) to inhibit adsorption of proteins was investigated. Here, the effectiveness and the mechanisms for each surface as a protein-blocking layer are discussed below.

11.6.1 SS-PEI surface

Table 11.21 show a summary of the QCM-D results on the performance of SS-PEI and SS-silicate surfaces as protein-blocking layers. The adsorption of protein was performed on the anchor layers (i.e. SS-PEI and SS-silicate surfaces) with the aim to distinguish the role between the anchor layers and the PEG molecules in inhibiting the adsorption of proteins.

Table 11.21: A summary of the QCM-D results on the performance of SS-PEI and SS-silicate surfaces as protein-blocking layers.

Surface	protein	Temperature (°C)	% adsorption relative to the bare SS (tightly-bound)
SS-PEI	Lysozyme	23	3
		40	2
	β-casein	23	134
		40	108
	Apo α-lactalbumin	23	129
		40	118
	Holo α-lactalbumin	23	30
SS-silicate	Lysozyme	23	48
		40	15
	β-casein	23	110
		40	60
	Apo α-lactalbumin	23	147
		40	119
	Holo α-lactalbumin	23	110

Surprisingly, the adsorption of lysozyme was down to 2 % on the surface which was covered only with a PEI layer (refer to Table 11.21). As mentioned in Section 11.4.1.1, it is expected that a PEI layer on top of a SS surface transformed the surface from a negatively charged to a positively charged surface. This may be the reason why almost no lysozyme is adsorbed on the PEI surface. The mechanism of lysozyme resistance is suggested to be due to the electrostatic repulsion between lysozyme and the PEI surface since both of them have net positive charges at pH 7.2. Since PEI molecules were formed into a multilayer in this study (fully covered the bare SS surface), these may also shield the hydrophobic interaction forces between lysozyme and the bare SS surface.

However, by contrast, the adsorption of β-casein and apo α-lactalbumin proteins (both are negatively charged) was found to be higher on a PEI layer than of the bare SS as can be seen in Table 11.21. Two possible driving forces may be considered: (i) electrostatic attraction between negatively charged proteins and positively charged PEI surface and (ii) hydrophobic attraction between the proteins and the bare SS surface. However, the latter suggestion can be discounted since a PEI layer is expected to be covered the SS surface completely. A branched PEI consists of about 25 % primary amine groups, 50 % secondary and 25 % tertiary amine groups. Only a small fraction of the groups react with the bare SS surface [Kingshott et al., 2003]; thus, a high concentration of free amino groups (positively charged) are believed available for interactions with β-casein and apo α-lactalbumin, thus, *enhancing* the adsorption.

Unexpectedly, the adsorption of holo α-lactalbumin (i.e. negatively charged) on a PEI layer was down to 30 % that on the bare SS surface. The adsorption of holo α-lactalbumin on the PEI layer should be either the same as on the bare SS surface or higher considering the above two driving forces; hydrophobic interactions and electrostatic attractions. There is no obvious explanation for this observation at this point.

A related study done by Erol et al. [2006] found a complete suppression of BSA and fibrinogen (both carry negative charges) on positive branched-PEI-coated surfaces was achieved only at NaCl concentration of 0.75 M or higher. They also conducted the experiment using a concentration of 0.15 M NaCl, but both BSA and fibrinogen were adsorbed on branched-PEI-coated surfaces. At

high salt concentration, the electrostatic interactions between the proteins and the PEI molecules are highly screened and thus limited the adsorption of proteins. In our study, the ionic strength of buffer solution used was 90 Mm, which is lower than 0.75 M, and hence screening of the electrostatic forces cannot be used as an explanation.

11.6.2 SS-silicate surface

As can be seen in Table 11.21, silicate layers apparently were overall less effective to inhibit adsorption of proteins compared to that of the PEI layers. At room temperature, a silicate layer can resist the adsorption of only lysozyme (even not as effectively as on the PEI layer) but could not resist β-casein and apo α-lactalbumin effectively (refer to Table 11.21). As mentioned earlier, presence of a silicate layer can transform the surface from a hydrophobic to a hydrophilic surface [Bardina et al., 2001]. However, a silicate layer is not expected to shield the SS surface completely (from the calculation above, the maximum fractional area coverage of silicate was only 12 %). Thus, our SS-silicate surfaces consist of hydrophilic and hydrophobic patches (hydrophobic patches are presumably more dominant than hydrophilic patches, about 90 % or more fractional coverage area). Lysozyme is a hard protein. Hard proteins are found generally to adsorb less on hydrophilic surfaces than hydrophobic surfaces (refer to Chapter 2). This may be the reason why less lysozyme than β-casein or apo α-lactalbumin was adsorbed on the silicate layers. However, some lyszoyme adsorption is still expected to occur on the hydrophobic patches. Both β-casein and apo α-lactalbumin are soft proteins. Soft proteins are found generally to adsorb even on hydrophilic surfaces (refer to Chapter 2). This supports the higher adsorption for both β-casein and apo α-lactalbumin on the silicate layers (Table 11.21).

Effect of temperature on protein resistance on anchor layers

As explained previously, the mass density of either PEI or silicate layers was the same at the two temperatures, thus, the mass density of protein adsorbed on those surfaces should be the same or higher at 40°C than at room temperature. However, unexpectedly, the adsorption of all the studied proteins was lower at 40 °C than at room temperature, about 50 % lower for β-casein and 30 % lower for lysozyme and apo α-lactalbumin. The possible reason for this observation is may be due to the high percentage of desorption at high temperature than at room temperature. β-casein for example, the percentage of desorption at 40°C was about two times higher than at room temperature.

11.6.3 SS-PEG surfaces (single chains)

As mentioned in Chapter 2, three modes of adsorption of protein onto PEG surfaces have been proposed, namely, *primary adsorption*, *secondary adsorption* and *tertiary adsorption*. Thus, protein resistance requires the exclusion of all three processes. The thickness of the grafted PEG layer must be sufficiently high to screen protein-substrate interactions, and the brush chain density must be high enough to block diffusion through this steric layer.

"Steric repulsion" and "water barrier" mechanisms are two of the most commonly described theories for protein resistance of PEG surfaces (refer to Chapter 2). It has also been suggested that protein resistance is due to blocking of the adsorption sites of proteins. A barrier to improved understanding is that many of the factors involved (PEG chain length, chain density, hydration, conformation, and distal chemistry (moiety)) are inherently correlated.

For example, protein resistance has been shown to improve as PEG grafting density and chain length (MW) are increased [Uchida et al., 2005, Yoshikawa et al., 2006, Satomi et al., 2007]. However, high chain lengths (MW) are associated with a lower PEG grafting density and vice versa. Furthermore, if the density of the layer was high enough to reach the dense-brush regime (i.e. too dense), the graft itself may become an adsorbent for protein and hence increase the adsorption of protein. Also, chains deposited in the dense-brush regime [Unsworth et al., 2005, Yeh et al., 2008] are expected to dehydrate and lose their

flexibility to sweep away the incoming proteins and thus can *enhance* the adsorption. Theoretical work done by Carignano and Szleifer [2000] revealed that very high surface coverage will modify the chemistry of the surface and it may result in an attractive surface. Herrwerth et al. [2003] suggested that the grafted chains must be sufficiently spaced to enable water to penetrate the layer, especially for methoxy-terminated surfaces (the PEG surfaces achieved in this study were methoxy-terminated). They argued that the protein resistance required both internal (to the PEG layer) and external hydrophilicity.

Table 11.22 shows a summary of the QCM-D results on the performance of PEG surfaces (single chains) as protein-blocking layers. The effectiveness and the mechanisms of SS-PEI-PEG and SS-silicate-PEG surfaces as protein-blocking layers are discussed below.

Table 11.22: A summary of the QCM-D results obtained in this study (monomodal PEG surface).

Surface	Protein	Temperature (°C)	PEG grafting density (chains / nm^2)	% adsorption relative to the bare SS (tightly-bound)	Note
Monomodal SS-PEI-PEG	β-casein	23	0.03 to 2.75	60 to 90%	• The adsorption was much more affected by PEG MW than PEG solution concentration. High PEG MW (i.e. PEG 2k and 5k Da) was better to repulse adsorption of β-casein.
		40	0.09 to 1.70	65 to 99 %	• Adsorption of β-casein slightly higher at 40 than at 23°C.
	Lysozyme	23	0.03 to 2.75	5 to 12 %	• The adsorption was much more affected by PEG solution concentration than PEG MW. Low PEG concentration (0.1 and 1 g / L) was better to repulse adsorption of lysozyme .

		40	0.09 to 1.70	4 to 6 %	• Neither PEG MW nor PEG solution concentration affect the adsorption of lysozyme significantly.
Monomodal SS-PEI-PEG	Apo α-lactalbumin	23 and 40	0.03 to 2.75	More than 100 %	• The adsorption of apo α-lactalbumin enhanced with the presence PEG molecules (at any experimental conditions used).
	Holo α-lactalbumin	23	0.03 to 2.75	11 to 15 %	• The adsorption performed on the PEG surfaces at different PEG MW. All the surfaces were prepared using PEG solution concentration of 1 g / L.
Monomodal SS-silicate-PEG	β-casein	23	0.02 to 2.45	57 to 81 %	• Adsorption was lower at high PEG MW (i.e. PEG 2k and 5k Da) and high PEG solution concentration (5 and 10 g / L).
		40	0.06 to 1.83	47 to 72 %	• No clear trend of either PEG MW or PEG solution concentration towards the adsorption of β-casein.

Monomodal SS-silicate-PEG	Lysozyme	23	0.02 to 2.45	5 to 14 %	• No clear trend of either PEG MW or PEG solution concentration towards the adsorption of lysozyme.
		40	0.06 to 1.83	4 to 5 %	• Neither PEG MW nor PEG solution concentration affect to the adsorption of lysozyme significantly.
	Apo α-lactalbumin	23 and 40	0.02 to 2.45	More than 100 %	• The adsorption of apo α-lactalbumin enhanced with the presence PEG molecules (at any experimental conditions).

11.6.3.1 Effects of PEG chain length and grafting density on protein resistance

The effectiveness of the PEG surfaces to inhibit adsorption of studied proteins in this thesis are first discussed based on the effect of PEG chain length and grafting density. From Table 11.22, generally, the studied proteins showed different behaviour towards PEG grafting densities and chain lengths (MW):

- Adsorption of β-casein generally was dependent on both the PEG chain length (MW) and grafting density. The adsorption of β-casein decreased as PEG MW was increased from 350 to 5000 Da and also decreased as the grafting density increased [Wei et al., 2003, Archambault et al., 2004, Brash, 2004, Jonsson et al., 2004, Fukai et al., 2004, Liu et al., 2007, Uchida et al., 2005, Yoshikawa et al., 2006]. A higher PEG layer (MW) implies a larger separation between the surface and the incoming proteins and hence a stronger attenuation of the long range Van der Waals interaction [Gombotz et al., 2004, Archambault et al., 2004, Roosjen et al., 2004]. Thus, it is expected that the *secondary adsorption* is minimized. Furthermore, high chain lengths are associated with large excluded volumes to sweep away more incoming proteins than short chain lengths can do. High chain lengths appear to maximize the steric repulsion mechanism.
- Neither PEG MW nor PEG grafting density affected adsorption of lysozyme significantly.
- Adsorption of apo α-lactalbumin was *enhanced* by the presence of PEG molecules (under any experimental conditions used).
- Adsorption of holo α-lactalbumin was reduced by the presence of PEG molecules.

β-casein, holo α-lactalbumin and apo α-lactalbumin are soft proteins but they behaved differently from each other with PEG molecules. Adsorption of β-casein decreased with the presence of PEG molecules but increased for apo α-lactalbumin. The results obtained in this study indicated the presence of direct apo α-lactalbumin to PEG attraction. The QCM-D results obtained were consistent with the results from AFM characterization done in this study. The "island" morphology of apo α-lactalbumin was similar on both SS-PEI-PEG and bare SS surfaces except more islands existed on the SS-PEI-PEG surface that indicated a higher mass density adsorbed.

Some studies [Wang et al., 1997, Sheth et al., 1997, Harder et al., 1998] related the interactions between PEG and proteins to whether trans or helical PEG conformers were involved. For example, Wang et al. [1997] and Harder et al. [1998] studied self-assembled monolayers (SAMs) of ethylene oxide (EO)-terminated alkane thiolates and found that when the EO moieties were in the crystalline helical or amorphous conformation, the SAMs were protein repellent. When the EOs in the SAM were in the all-*trans* form, proteins adsorbed at the SAMs. The protein resistance was explained by the structure of the water layer at the SAMs: water adsorbs much more strongly onto the helical or amorphous EO conformation than onto the all-*trans* EO conformation. Sheth et al. [1997] also explained the attraction between PEO and streptavidin with a change in conformation of the PEO (rejecting structural changes in steptavidin because the AFM measurements conducted at forces much too low to denature streptavidin). The structures and interfacial properties of PEG chains suggested that the interconversion between protein-attractive and protein-resistance PEG was due to segment rearrangements in the polymer chains with non polar segments concentrated near the solid surface and polar segments at the outer edge. The change from polar to apolar conformation may also be induced by compressing the PEO layer. Increasing the temperature or altering the polymer molecular weight [Efremova et al., 2001] could also induce an attractive-to-protein state. In this study, QCM-D measurements unable to give information of trans and helical conformation. However, apo α-lactalbumin molecule is highly hydrophobic and we expect that once it adsorbs on a PEG layer it will denature and compress the

PEG layer and hence change the PEG layer from polar to apolar conformation.

Other study claimed that the interaction between PEG and protein corresponds to a *tertiary adsorption* [Currie et al., 2003]. In this study, the adsorption of apo α-lactalbumin was higher regardless of PEG grafting density. This finding contradicted with Currie et al. [2005]. In their study, when the grafting density increased to about 0.08 chains / nm^2, the adsorption of BSA on a PEO surface start to decrease (refer to Figure 2.16). This indicates that the adsorption of apo α-lactalbumin in this study may not happen via *tertiary adsorption*. We postulate that the adsorption of apo α-lactalbumin is via *secondary adsorption*.

By contrast, the adsorption of holo α-lactalbumin on the PEI-PEG surfaces was down to less than 15 % that on the bare SS. The apo and holo forms differ only in calcium ion bindings but give significantly different behaviour towards PEG surfaces. The removal of calcium from α-lactalbumin reduced its stability and induced a conformational change (loss of calcium ions are accompanied by loss of its tertiary structure with formation of a stable molten globular state) [Wehbi et al., 2005]. Apo α-lactalbumin (calcium depleted) which is partially unfolded is more hydrophobic than the native form (holo α-lactalbumin) [Bu et al., 2000] and more prone to protein aggregation. This is because, in the apo form, hydrophobic patches are exposed thus leading to protein aggregation via hydrophobic interactions between apo-apo molecules [Kronman, 1989]. This may be the reason why less adsorption of holo than apo forms observed in this study.

The comparison between holo α-lactalbumin and β-casein is also interesting (refer to Table 11.22). Both holo α-lactalbumin and β-casein are soft proteins and are negatively charged at pH 7.2. In fact, the MW of holo α-lactalbumin is almost half that of β-casein (i.e. smaller size than of β-casein) but the findings showed that the mass adsorption of holo α-lactalbumin on PEG surfaces was about 0.25 times that of β-casein. Most probably the adsorption of β-casein on a PEG layer (thought to be *secondary adsorption*), compressed the PEG layer and induced a transformation of the PEG from polar to apolar transformation, resulting in more tendency to adsorb. Besides that, the molecule structure of β-casein may also contribute to higher adsorption compared to holo α-lactalbumin. β-casein is a flexible random coil

configuration protein whereas holo α-lactalbumin is folded with four disulfide bonds. This makes holo α-lactalbumin relatively more stable than β-casein. This may be another reason why less holo α-lactalbumin is adsorbed on PEG surfaces than of β-casein.

The presence of PEG molecules on a SS-silicate surface reduced the adsorption of lysozyme to 10 % of that SS-silicate surface (refer to Tables 11.21 and 11.22). The ability of SS-silicate-PEG surfaces to inhibit adsorption of lysozyme was almost the same regardless of PEG grafting density or chain length used (i.e. short PEG chains (350 Da) could resist lysozyme adsorption as effectively as long chains (5000 Da)). It is suggested here that the PEG grafting density was sufficient to shield the surface. Archambault et al. [2004] stated that long PEG chains (MW 5000 Da) as well as short chains (MW 2000 Da) can reject proteins provided that the chain density was sufficiently high. Experimental work done by Wu et al. [2000] also showed that a surface with a monomer containing as few as two ethylene glycol (EG) units was able to reduce bovine serum albumin (BSA) and human fibrinogen adsorption. They concluded that long chain polyethylene oxide (PEO) were not necessary requirement for non fouling properties of PEO modified surfaces. Protein resistance on the surface with short chains was attributed to the presence of stable water interfacial layers.

A slightly higher mass density of lysozyme is adsorbed on the SS-PEI-PEG surface than on the SS-PEI surface (refer to Tables 11.21 and 11.22), indicating a possibility that *secondary adsorption* occurred [Yoshikawa et al., 2006]. However, the Van der Waals interaction between lysozyme and the polymer layer is expected to be weak since PEG coated surfaces are hydrophilic and typically quite dilute (well hydrated).

From these findings, β-casein, lysozyme, holo α-lactalbumin and apo α-lactalbumin showed a different behaviour on the same PEG surfaces. We believe that the stability of proteins play a major role in the protein adsorption. Furthermore, the effectiveness of PEG surfaces to repel adsorption of proteins is dependent on the proteins used. The results found in this thesis are not in line with the results obtained by Prime and Whitesides [1993]. They found that the number of ethylene glycol (EO) chains per unit area required to eliminate adsorption was almost the same for lysozyme, ribonuclease, pyruvate kinase and fibrinogen. They suggested that the

adsorbance of each mixed self-assembled monolayer (SAM) of $SC_{11}E_6OH$ was dominated by the interfacial properties of the SAM and not the protein used.

11.6.3.2 Effects of anchor layers on protein resistance

From Table 11.22, it showed that generally the adsorption of proteins on the SS-PEI-PEG surfaces was not significantly different to that on SS-silicate-PEG surfaces. This indicates that the anchor layer does not play a significant role in the protein adsorption once the PEG molecules were sufficient to shield the anchor layer (i.e. high grafting density). This finding emphasizes the importance of PEG grafting density against protein resistance. The main function of the anchor layer is to 'functionalize' the SS since PEG hardly attached on the virgin SS surface (but the possibility of PEG molecules to attach directly to a SS surface is still there).

Addition of PEG molecules on a SS-PEI surface transformed a positicely surface (PEI surface) to a hydrophilic, uncharged surface (PEI-PEI surface) (if only the PEG grafting density covered completely the surface). If the PEG density is not cover the SS-PEI surface completely, the surface will consist some of positively charged patches. Negatively charged proteins will tend to adsorb on the patches which positively charged. Meanwhile, addition of PEG molecules on a SS-silicate surface transformed a hydrophilic and hydrophobic surface (silicate surface) to a fully hydrophilic surface (if the grafting density covered completely the surface). Tables 11.21 and 11.22 showed that the adsorption of proteins was lower on SS-silicate PEG surfaces than on SS-silicate surfaces. This indicates that some of the PEG molecules were directly attached to a bare SS surface. This is because, as described earlier, a silicate layer covered only 12 % of the surface coverage.

11.6.3.3 Effects of temperature on protein resistance

In general, the adsorption of proteins was lower at 40°C than at room temperature regardless of the surfaces used (especially on silicate-PEG based surfaces) (Refer to Table 11.22). For example, the adsorption of β-casein and lysozyme on silicate surfaces, respectively, was about 0.55 and 0.3 times lower at 40°C than at room temperature. The results obtained contradicted to other works, for example, Prime and Whiteside [1993] reported that the adsorption of pyruvate kinase on a SAM of $SC_{11}E_6OH$ surface was higher at 37°C than at room temperature. The possible reason for lower adsorption at high temperature in this study is most probably due to the percentage of desorption. The percentage of desorption of β-casein was about 1.4 to 2.3 times higher at 40°C than at room temperature. However, there was no significant different in percentage of desorption for lysozyme. There is no obvious explanation at this point for this observation. Another possibility is may be due to the PEG grafting density. Generally, the PEG grafting density on monomodal PEG surfaces was higher at 40°C than at room temperature (refer to Table 11.22).

11.6.4 SS-PEG surfaces (mixed PEG chains)

This section discusses the effectiveness of PEG bimodal surfaces (i.e. mixtures of short and long PEG chains) for inhibiting the adsorption of proteins. The mechanisms of preventing protein adsorption are discussed below. These discussions are based on the results tabulated in Table 11.23.

It has been shown that bimodal PEG surfaces are more protein resistant than monomodal PEG surfaces [Uchida et al., 2007, Satomi et al., 2007]. Uchida et al. [2007] and Satomi et al. [2007] explained that the higher protein resistance shown by bimodal PEG surfaces was due to a combined high mobility of the long chains and high density of the short chains close to the surface. Short chains provide the 'water barrier' mechanism while long chains provide the 'steric repulsion' mechanism (refer to Chapter 2).

Table 11.23: A summary of the QCM-D results obtained in this study (bimodal PEG surface).

Surface	Protein	Temperature (°C)	PEG grafting density (chains / nm^2)	% adsorption relative to the bare SS (tightly-bound)	Note
Bimodal SS-PEI-PEG	β-casein	23	0.13 to 4.27	More than 100 %	• At any combination used.
		40	0.10 to 8.54	55 to 89 %	• Adsorption was the lowest on the surfaces prepared using high PEG solution concentration (5 g / L) than using a lower PEG concentration (0.1 and 5 g / L).
	lysozyme	23	0.13 to 4.27	1 to 10 %	• The adsorption was the lowest on the surface with PEG (5k + 2k) combination than on the PEG (550+350) prepared using PEG solution concentration of 1 g / L.
		40	0.10 to 8.54	1 to 4%	• There was no significant difference in adsorption at any combination used.
	Apo α-lactalbumin	23 and 40	0.10 to 8.54	More than 100 %	• The adsorption of apo α-lactalbumin enhanced with the presence PEG molecules.

Surface	Protein	Temperature (°C)	PEG grafting density (chains / nm^2)	% adsorption relative to the bare SS (tightly-bound)	Note
Bimodal SS-silicate-PEG	β-casein	23	0.03 to 2.70	67 to 95 %	• The adsorption was lower on the surfaces prepared using PEG solution concentration of 5 g / L than with 0.1 and 1 g / L in that order.
		40	0.05 to 7.15	52 to 70 %	• The adsorption was almost the same on the surfaces regardless of concentration used.
	Lysozyme	23	0.03 to 2.70	49 to 89 %	• The adsorption was lower on the surfaces prepared using PEG solution concentration of 0.1 g / L compared to either 1 or 5 g / L.
		40	0.05 to 7.15	2 to 15 %	• The adsorption was the lowest on the surface with PEG (5k + 2k) combination compared to PEG (550 + 350).
	Apo α-lactalbumin	23 and 40	0.03 to 7.15	More than 100 %	• The adsorption of apo α-lactalbumin enhanced with the presence PEG molecules (at any experimental conditions used).

For example, Uchida et al. [2005] found that adsorption of bovine serum albumin (BSA) on mixed acetal-mercapto-PEG layers (acetal-PEG-SH) of molecular weights 5000 and 2000 Da ("PEG 5000+2000") grafted onto gold surfaces at 25°C was down to 5 % of that on the single PEG5000 surfaces. In a following work, Uchida et al. [2007] studied the adsorption of several proteins and peptides with different MW and pI on mixed PEG (5000+2000) surfaces (refer to Table 11.24). They found that mixed PEG (5000+2000) surfaces showed almost complete inhibition of non-specific adsorption regardless of the sign of charge on the protein molecule. This was not only for high molecular weight proteins but also for low molecular weight peptides.

However, by contrast, the results obtained in this study showed that each protein behaved differently towards bimodal PEG surfaces. For example, PEI-PEG bimodal surfaces were apparently resisting only the adsorption of lysozyme and not the other two proteins.

Table 11.24: Proteins and peptides used in Uchida et al. [2007].

Protein and peptides	MW (Da)	pI
Fibrinogen	340, 000	6
Bovine serum albumin (BSA)	68, 000	4.8
Myoglobin	17, 600	6.8
Lysozyme	14,600	10.9
Bradykinin	1, 060	12.5
RGDS tetrapeptide	433	6.7

From the results obtained in this study (refer to Tables 11.22 and 11.23), there are several points that can be highlighted:

(i) PEI-PEG bimodal surfaces generally better inhibited adsorption of lysozyme than PEI-PEG monomodal surfaces but not β-casein. However, silicate-PEG monomodal surfaces *better* inhibited adsorption of both lysozyme and β-casein than silicate-PEG bimodal surfaces.

(ii) The adsorption of proteins was temperature dependent. Most of the results obtained showed that the adsorption of proteins was lower at 40 °C than at room temperature.

(iii) There was no exact trend of protein resistance of PEG combinations against other properties. However, in most cases, the PEG combination between 5000 and 2000 Da apparently better inhibited the adsorption of proteins than other combinations. The PEG grafting density for PEG (5000+2000) was the lowest compared to other combinations. This indicates that well hydrated flexible surface-tethered PEG chains with packing density sufficiently low to allow chain mobility while still providing a complete surface coverage are important for better protein resistance.

11.6.4.1 Bimodal PEG surfaces versus monomodal PEG surfaces

In this study, the proteins behaved differently toward bimodal and monomodal PEG surfaces. For example, the adsorption of lysozyme was lower on bimodal PEG surfaces than on the monomodal PEG surfaces (except on bimodal silicate-PEG surfaces at room temperature). However, by contrast, the adsorption of β-casein generally was *higher* on bimodal PEG surfaces than on the monomodal PEG surfaces. Meanwhile, the adsorption behaviour of apo α-lactalbumin towards PEG surfaces was the same on the bimodal PEG surfaces as on the monomodal PEG surfaces; the adsorption was *enhanced* with the presence of PEG molecules. We believe that the adsorption mechanisms of apo α-lactalbumin on bimodal PEG surfaces were similar to those on the monomodal PEG surfaces. Thus, the discussion here is confined to β-casein and lysozyme adsorption only.

β-casein

Higher adsorption of β-casein on bimodal PEG surfaces than monomodal PEG surfaces is presumably due to the dense-brush PEG layer. Bimodal PEG grafting density achieved in this study was higher than of the monomodal PEG grafting density, by more than 50 %. As mentioned earlier in Section 11.5.3, chains that are too dense may become an adsorbent for protein and hence increase the adsorption of protein [Unsworth et al., 2008]. Also, chains organized into this dense-brush are expected [Zdyrko et al., 2003, Unsworth et al., 2005] to dehydrate and lose the flexibility to sweep the incoming proteins, thus enhancing the adsorption of protein.

Here, for the bimodal PEG surfaces, two regimes are proposed (based on Muller et al. [2005]) (refer to Figure 11.20); regime I where the deposited PEG chains are expected to be more flexible to sweep the incoming protein while in regime II, the deposited chains are dense enough to behave like a ‘solid’ at their base. Some of the protein molecules are expected to diffuse through the regime I and deposited on the “solid” of regime II via Van der Waals interactions.

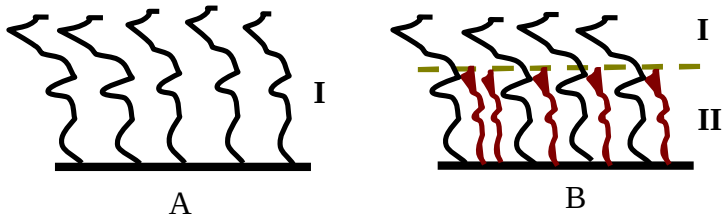

Figure 11.20: Proposed mechanism between a monomodal PEG surface (A) and a bimodal PEG surface (B). Regime 1 refers to the deposited PEG chains that are expected to be more flexible to sweep the incoming protein while regime II refer to the deposited chains that are dense enough to behave like a 'solid' at their base. Some of the protein molecules are expected to diffuse through the regime I and deposit on the base layer of regime II via Van der Waals interactions.

We expect that the chains in regime II form a dense-array of terminal methoxy groups, O-CH_3, that extend away from the surface. We suggest that β-casein adsorbed on the bimodal PEG surfaces is most likely via the *secondary adsorption* mode but not *primary* or *tertiary* adsorption modes. This is because the protein size of β-casein is larger than the distance between PEG chains. According to Halperin's model [1999], large proteins can adsorb at the outer surface of the PEO layer through Van der Waals interactions. In this study, we expect that once adsorbed on a PEG layer, β-casein is most probably denatured and compresses the PEG layer. Soft proteins have the possibility to denature upon adsorption regardless of the type of surface; either a hydrophilic surface or a hydrophobic surface (refer to Chapter 2). The compression of a PEG layer is argued by Bjorling et al. [1991] to induce changes from polar (helical) to apolar (trans) conformation thus enhancing the further adsorption of β-casein. Under a dense-brush regime, both the 'water barrier' and the 'steric repulsion' mechanisms are expected to no longer apply for PEG resistance.

Lysozyme

Interestingly, the adsorption of lysozyme on the PEG surfaces, a small protein, was lower than either β-casein or apo α-lactalbumin. The adsorption of lysozyme was almost zero on the bimodal PEG and PEGNHS surfaces with a combination of 5000 and 2000 Da. This finding is a significant achievement for surface treatments which are done simply by passing solutions through. Considering only protein size as a factor, proteins with smaller size have generally a higher adsorption. For example, the amount of lysozyme (MW 14.6kDa) adsorbed on a poly(ethylene terephthalate) (PET) surface modified with PEG was higher than that of collagen (285 kDa) on the same surface [Fukai et al., 2004]. In another study, myoglobin (16kDa) adsorbed more on PEGylated surfaces than did bovine serum albumin (BSA) (67kDa) or fibrinogen (MW 340kDa) [Michel et al., 2005].

A bare SS surface is a hydrophobic surface. Hard proteins are found generally to adsorb on hydrophobic surfaces if strong electrostatic attraction exists, as would be the case for lysozyme in our study (refer to Chapter 2). Since lysozyme is a hard protein, then less lysozyme is expected to be adsorbed on the PEG surfaces. It appears that the dense layer provided by the bimodal PEG transformed the surface from a hydrophobic surface (bare SS) to a hydrophilic surface (PEG layer). Even, if we considered that the bimodal PEG surfaces behave similarly to a hydrophobic surface (i.e. resulted from a dense-array of methoxy groups O-CH_3 that extended away from the surface), less adsorption on that surface is still reasonable. Besides that, at pH 7.2, a bare SS surface is negatively charged (refer to subsection 11.4.1). PEG molecules meanwhile are neutral. If the PEG grafting densities are sufficiently enough to cover the bare SS, it may transform the SS surface from a negatively charged to an uncharged surface (PEG layer). Thus, less adsorption of lysozyme on a neutral surface (PEG surface) is expected [Pasche et al., 2005].

However, unfortunately, the reason for a higher adsorption of lysozyme on the SS-silicate-PEG bimodal surfaces at room temperature than on the SS-silicate-PEG monomodal surfaces (*up to 10 times higher*) are still cannot be explained at this point.

The results of lysozyme adsorption on bimodal PEG surfaces obtained in this study contradicted those of Unsworth et al. [2008]. They suggested that the relatively dense arrays of methoxy groups promoted an observed increase in lysozyme

adsorption. They explained that high densities of terminal methoxy groups resulted in increased interchain association and/or adsorption-induced protein denaturation. They also suggested that the properties related to chain density (that is conformational freedom, hydration) were the main determinants of protein resistance at chain densities up to a critical value of about 0.5 chain / nm^2 and influence of the moieties (i.e. OCH_3 and OH) came into play at chain densities greater than the critical value (refer to Figure 11.21).

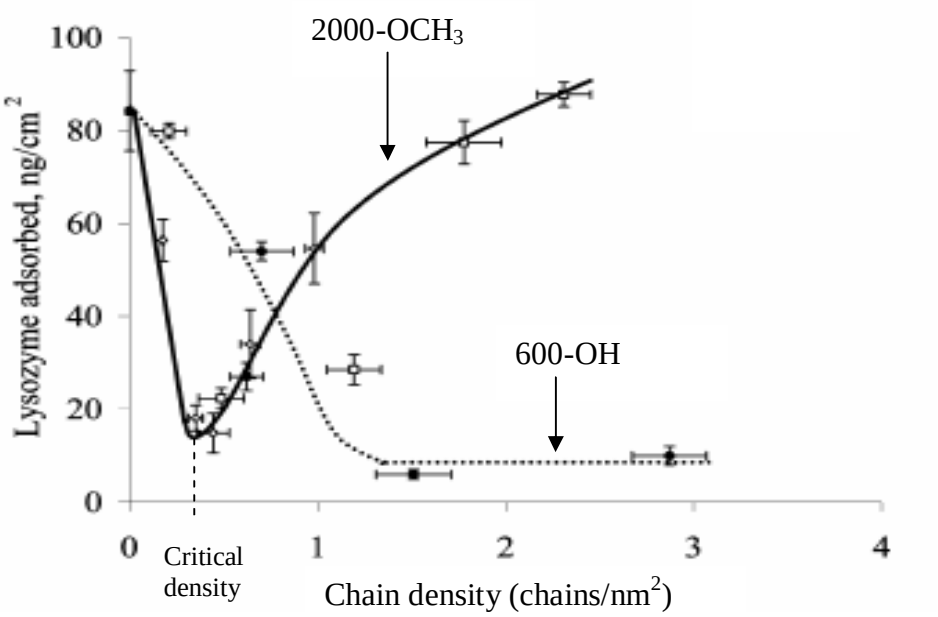

Figure 11.21: Adsorption of lysozyme on PEO-modified surfaces as a function of chain density. Taken from Unsworth et al. [2008].

However, in this study the adsorption of lysozyme was almost constant with PEG grafting density (Figure 11.22). For comparison of lysozyme adsorption achieved between this study and their study, the units of adsorption in Figure 11.21

have to be multiplied with $\frac{1g}{1x10^9 ng}\frac{1000mg}{1g}\frac{100^2 cm^2}{1m^2} = 0.01\frac{mg}{ng}\frac{cm^2}{m^2}$ to get a consistent units of $\frac{mg}{m^2}$.

Interestingly, the surface mass density of lysozyme observed in this study generally was lower than their findings (a comparison was based on $-OCH_3$ end groups).

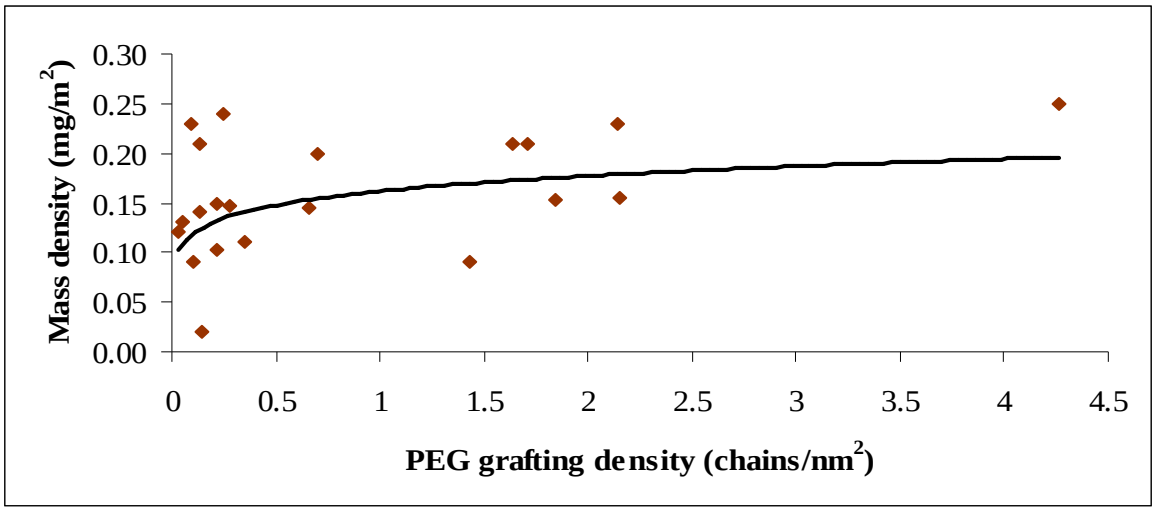

Figure 11.22: Mass density of lysozyme adsorbed on SS-PEI-PEG surfaces at a room temperature as a function of PEG grafting density (from this study).

11.6.4.2 Effect of temperature

As can be seen in Table 11.23, the adsorption of the studied proteins on the bimodal PEG surfaces was temperature dependent. The PEG bimodal surfaces were apparently more effective to inhibit the adsorption of proteins at 40 °C than at room temperature. This observation follows a similar trend to that on the monomodal PEG surfaces.

11.6.4.3 Bimodal PEI-PEG surfaces versus bimodal silicate-PEG surfaces

From Table 11.23, it shows that bimodal silicate-PEG surfaces were slightly better in inhibiting adsorption of β-casein than bimodal PEI-PEG surfaces and less so for lysozyme.

The PEG grafting densities of bimodal PEG on PEI layers were slightly higher than on silicate layers. In this study, less β-casein was adsorbed on bimodal silicate-PEG surfaces than on bimodal PEI-PEG surfaces. It may be that the increase of grafting density was sufficient to cause this better inhibition, where it was not be too dense to lose its flexibility nor too low to allow β-casein to diffuse through the layer and adsorb on the surface. On the other hand, bimodal silicate-PEG surfaces were slightly worse than bimodal PEI-PEG surfaces in inhibiting adsorption of lysozyme. In contrast, lysozyme molecules being much smaller than β-casein, may diffuse through the pores between the PEG chains on silicate-PEG surfaces and adsorb on the silica layer. As shown in subsection 11.5.2, lysozyme adsorbed more on silica surfaces than on the PEI surfaces.

Generally, the PEG coated surfaces prepared in this study were able to inhibit adsorption of β-casein and lysozyme proteins especially. The results also have shown that protein stability (i.e. a soft or a hard protein) greatly influenced the performance of PEG surfaces. It is apparently more difficult to prevent the adsorption of soft proteins than hard proteins. This is because soft proteins tend to denature regardless of the surface properties (i.e. hydrophilic or hydrophobic). The results also indicated that higher PEG grafting density is not necessarily reflected in better protein

resistance. It is also interesting to note that the protein resistance is better at high temperature than at room temperature. However, it is difficult to give a clear and concrete explanation or discussion to cover the various results of different cases.

11.7 SS-protein-PEG surface

At the end of the work (not originally planned), the surfaces were modified by coating them with a protein monolayer as an anchor layer instead of a PEI or a silicate layer. The findings obtained for the adsorption on SS-protein-PEG surfaces were more interesting and unexpected (refer to Chapter 7). Some SS-protein-PEG surfaces gave inhibition of protein far better than either SS-PEI-PEG surfaces or SS-silicate-PEG surfaces. Table 11.25 show a summary of the major findings on the adsorption of proteins on SS-protein-PEG surfaces. From the results, the SS-lysozyme (4)-PEG5k (5) surfaces appeared to be a more effective surface to inhibit proteins than SS-β casein (0.1)-PEG or SS-β lactoglobulin (0.1)-PEG surfaces (refer to Table). The adsorption of β-casein, lysozyme, holo α-lactalbumin and β-lactoglobulin on the SS-lysozyme (4)-PEG5k (5) surfaces was down to about 3, 1, 4 and 0.4 %, respectively compared to that on the bare surface. More interestingly and surprisingly also, there was almost zero adsorption of mixed protein and single protein solutions at the concentration of milk on SS-lysozyme (4)-PEG5k (5) surfaces. Therefore, the discussion has been confined to the SS-lysozyme (4)-PEG5k (5) surfaces.

Here, the possible mechanisms are discussed. The major difficulty is that the experimental findings mostly contradicted the current theory. For example, inhibition occurred even when there was thought to be an electrostatic attraction and hydrophobic interaction between holo α-lactalbumin, β-lactoglobulin and β-casein proteins and the SS-lysozyme surface.

Table 11.25: A summary of the major finding on the adsorption of proteins on the SS-protein-PEG surfaces obtained in this study.

Surface	protein	% adsorption relative to the bare SS (tightly-bound)	Note
SS-lysozyme (4)-PEG5k (5)	Lysozyme	1	PEG with different MWs (5, 20 and 40 kDa) and moieties (OH-PEG-CH_3, OH-PEG-OH, OH-PEG-NHS) also have been grafted on a SS-lysozyme (4) layer. Those surfaces also effectively suppressed the adsorption of proteins (refer to Chapter 7).
	β-casein	3	
	β-lactoglobulin	0.4	
	Holo α-lactalbumin	4	
	Single protein at the concentration of milk	Almost zero	
	Mixed protein at the concentration of milk	Almost zero	
SS-β casein (0.1)-PEG	β-casein	8	For SS-β casein (0.1)-PEG surfaces, PEG with different MW were used; 350, 2000 and 5000 Da. The PEG solution concentrations of 1 and 5 g / L were used. The adsorption was less on the surfaces that prepared using PEG concentration of 5 g / L.

Surface	protein	% adsorption relative to the bare SS (tightly-bound)	Note
SS-β lactoglobulin (0.1)-PEG5k (1)	β-casein	63	
	β-lactoglobulin	79	

11.7.1 Surface conformation

The conformation of lysozyme on a bare SS surface is clarified first followed with the conformation of the PEG layer on a lysozyme layer. Table 11.26 shows the lysozyme layer properties on a bare stainless steel surface at a temperature of 23 °C obtained from the Voigt model (strongly held adsorption)

Table 11.26: Lysozyme layer properties on a bare stainless steel surface at a temperature of 23 °C obtained from the Voigt model (strongly held adsorption) (this study).

Parameter	Lysozyme (4 g / L)
Surface density (wet basis) (mg/m^2)	8.0 ± 0.4
Surface lysozyme number density ($molecules/nm^2$)	0.33 ± 0.01
Mean layer thickness, *h* (nm)	6.75 ± 0.30
Mean spacing between molecules, *d* (nm)	1.75 ± 0.04
Dimension (nm)	3 x 3 x 4.5
Theoretical expected monolayer density (dry basis) (mg/m^2)	2 (side-on orientation), 3 (end-on orientation)
Theoretical monolayer density wet basis (assumimg that the ratio wet mass to dry mass was equal to 1.5) (mg/m^2)	3 (side-on orientation), 4.5 (end-on orientation)

The theoretical maximum surface density of lysozyme (wet basis) with end-on adsorption was about 4.5 mg / m^2. Meanwhile the experimental mass density adsorbed was about 8 mg / m^2. Thus, we expect that lysozyme formed two layers on a SS surface. It has been suggested here that lysozyme molecules (adsorbing from 4 g / L solution) covered the stainless surface with two different conformations; end on orientation in the first layer (monolayer) (I) and combination between end-on and side-on orientations in the second layer (II). Figure 1123 shows the illustration of possible lysozyme conformations on the SS surface. Noted that, all the illustration in this section was based on the QCM-D measurement (wet basis).

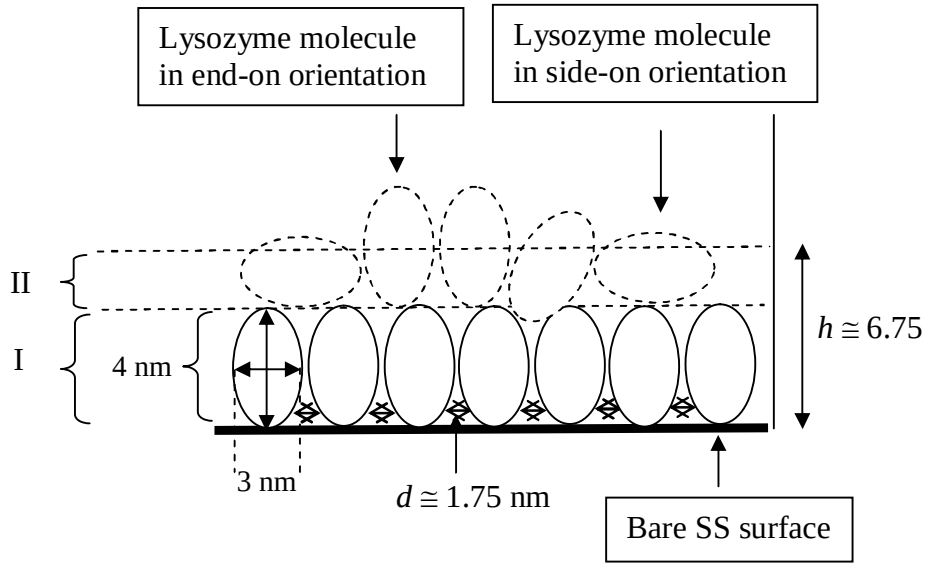

Figure 11.23: Illustration of possible lysozyme (4) conformations on the SS surface. The lysozyme molecules adsorbed in end-on orientation in the first layer (I) and a combination between side-on and end-on orientation in the second layer (II).

Now, the possible conformations of PEG 5k on the SS-lysozyme surface are discussed. It has been shown here that the number density of PEG5k (5) derived from the QCM-D measurements on the SS-lysozyme (4)-PEG5k (5) surfaces was about 0.012 molecules/ nm^2. The corresponding calculated added mean layer thickness, *h*, and the spacing between the PEG molecules, *d*, are respectively, 0.08 and 9 nm.

Thus, 1 molecule of PEG 5k occupies about 83 nm^2 surface area (i.e. 1 / 0.012). Therefore, 1 molecule of PEG 5k occupies about 9 molecules of lysozyme (in other words, there will be 1 PEG molecules for every 9 lysozyme molecules). Figure 11.24 illustrates a top view of 9 lysozyme molecules occupied by 1 PEG molecule.

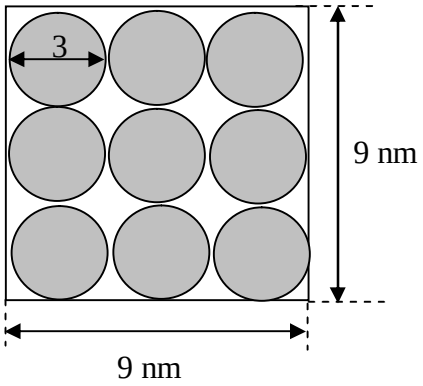

Figure 11.24: Illustration of 9 lysozyme molecules occupied by 1 PEG molecule (top view) (this study).

By referring to section 11.5.3 and Table 11.9, it appears that PEG 5k on the lysozyme layer was most likely in the interacting mushroom conformation ($d \sim 2R_F$). We expected that the PEG 5k collapsed on the lysozyme layer. The expected electrostatic attraction between the positive charges of lysozyme and negative charges of PEG from –OH groups may support our expectation that PEG molecules collapsed on the lysozyme surface. However, unfortunately, the size of collapsed PEG was unknown in this study. We are not sure whether the surface area that occupied by 1 molecule of PEG 5k (i.e.83 nm^2) can be taken as a size of the collapsed PEG.

Figure 11.25 shows the proposed illustration of possible PEG conformation on the lysozyme (4) layer. It was expected that PEG attached on the N-terminus of the proteins.

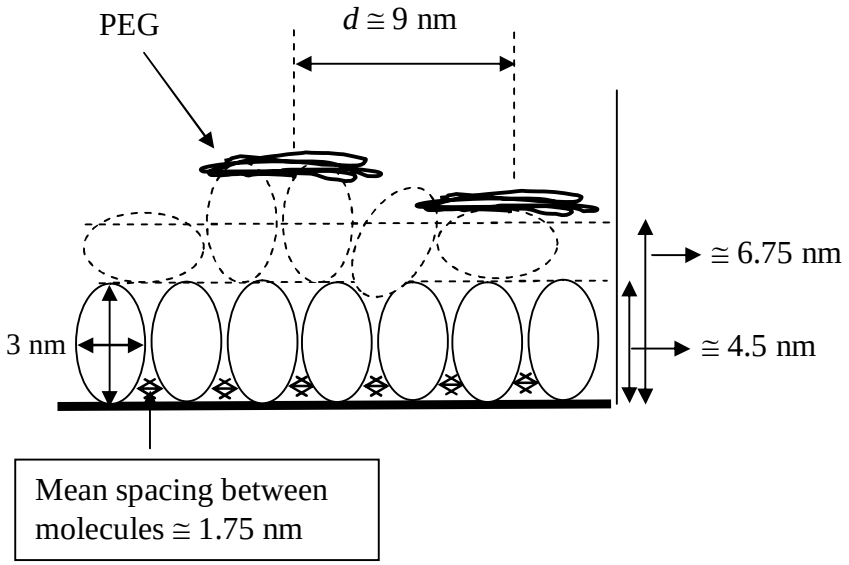

Figure 11.25: Proposed illustration of PEG conformation on the lysozyme layer.

11.7.2 Mechanism of protein adsorption on SS-lysozyme (4)-PEG5k (5) surface

From the description given above, the incoming protein to the SS-lysozyme (4)-PEG5k (5) surfaces should face both PEG and lysozyme molecules. Since the PEG molecules are presumably not extending out from the surface, therefore the water barrier mechanism is expected to be the one that plays a major contribution to the PEG to protein repulsion rather than the steric repulsion mechanism. It is believed here that the lysozyme layer itself also gives a significant contribution to the inhibition of the proteins. This is because the lyszoyme layer (without the presence of PEG) also effectively reduced the adsorption of proteins (refer to Table 11.23). Table 11.27 compares protein adsorption on the SS-lysozyme surfaces and the SS-lysozyme-PEG5k surfaces.

Table 11.27: Comparison of protein adsorption on SS-lysozyme surfaces and SS-lysozyme-PEG5k surfaces. The data refer to percentages of adsorption compared to that on bare SS.

Protein	SS-lysozyme (4) ± %	SS-lysozyme (4)-PEG5k ± %
β-casein	17 ± 7.36	2.82 ± 1.47
Lysozyme	0.22 ± 0.01	0.93 ± 0.04
Holo α-lactalbumin	0.25 ± 1.11	3.90 ± 1.65
Apo α-lactalbumin	53.95 ± 4.75	87.50 ± 5.00
β-lactoglobulin	1.52 ± 0.80	0.40 ± 0.23

In general, there was a significant difference between the percentage of protein adsorptions on the SS-lysozyme (4) surfaces and the SS-lysozyme (4)-PEG5k surfaces. The mechanisms involved for those proteins which are adsorbed less on the SS-lysozyme-PEG 5k surface than of the SS-lysozyme surface (that is, β-casein and β-lactoglobulin) support the idea of 'steric repulsion' and 'water barrier' mechanisms. Furthermore, the presence of PEG may also shield some of the exposed lysozyme area for the interactions and thus are expected to weaken the electrostatic attraction forces. The adsorption of apo α-lactalbumin increased with the presence of PEG. This observation was in line with the previous expectation (section 11.5.3) that apo α-lactalbumin interacted with PEG molecules.

Both SS-lysozyme (4) and SS-lysozyme (4)-PEG5k surfaces were much better inhibitors than surfaces trialled before. However, it is more difficult to explain why those proteins (as listed in Table 11.27) have so much lower adsorptions on the SS-lysozyme surface than either on the PEI-PEG surface or the silicate-PEG surface. Holo α-lactalbumin and β-lactoglobulin proteins for example, almost give zero adsorption on the SS-lysozyme after flushing with buffer. Both of those proteins have opposite surface charges to lysozyme but inhibition is occurring instead of attraction.

Now, come to the most crucial part, why are protein-PEG based surfaces (especially lysozyme-PEG surfaces) much better proteins inhibitors than either of the

PEI-PEG surfaces or the silicate-PEG based surfaces? The significant difference between those surfaces was the anchor layer: lysozyme, PEI or silicate layers. The contribution of PEG conformations towards protein repulsion is believed to have been not too critical in contributing towards the lysozyme-PEG5k surface as a good protein repulsion surface. The reason is that the grafting density of PEG 5k achieved on the lysozyme layer was much lower compared to those on PEI and silicate layers (refer to Table 11.28). If we consider that PEG even with a low grafting density was the reason for the inhibition of protein adsorption, then SS-PEI and SS-silicate surfaces grafted with a low PEG grafting density should be able to reduce the adsorption of protein as effectively as SS-lysozyme did. But from the experimental findings (refer to Chapter 6) they did not.

Table 11.28: Comparison of PEG5k grafting density on each surface.

Surface	PEG5k grafting density (chains / nm^2)	PEG mean spacing (nm)
SS-lysozyme	0.012	9
SS-PEI	0.097	3
SS-silicate	0.063	4

Therefore, the most probable explanation must come from the surface coverage of the anchor layer and its properties. For the lysozyme layer, it was acceptable to consider that it covered the SS surface well (i.e. the mean spacing between lysozyme molecules was about 1.75 nm). The mean spacing between PEI molecules was about 4 nm whereas that for silicate molecules was about 0.6 nm. The mean spacing between the PEI molecules was slightly larger than that for protein samples (i.e. 3 nm for lysozyme (end on-orientation), 2.3 nm for β-casein, 2.5 nm for α-lactalbumin). Thus, if the attached PEG molecules on the PEI layer were unable to sweep away the incoming proteins, the proteins will have diffused between the PEI molecules and adsorbed on the SS surface. Therefore, it is believed that, for PEI-PEG

and silicate-PEG surfaces, the PEG conformation played an important role for inhibiting protein adsorption (it can be considered as a crucial factor) meanwhile for the protein-PEG surfaces, PEG conformation apparently was not too crucial as long as the anchor layer fully covered the substrate surface. The chosen protein as an anchor layer should have less attraction to the targeted proteins than PEG molecules. However, it is unexplained why the lysozyme layer behaved so well as a protective layer for the adsorption of proteins even when incoming proteins had opposite charges to that expected on the lysozyme.

11.8 Industrial application

At first, this study was aimed to prevent or reduce biofouling formation in the dairy industry. However, the findings showed that the modified surfaces performed better only under room and body temperatures, as distinct from heat exchangers in the dairy industry which operate about 75 °C. It has been shown that the SS-lysozyme (4)-PEG5k (5) surfaces effectively inhibited adsorption of a protein mix either under a flow condition or a non-flow condition. Thus, the surfaces most probably can be applied on the inside of milk storage columns. Table 11.29 shows the operating condition so far explored for our method (protein-PEG layer) where successful inhibition was focused.

Table 11.29: Specification of the method (protein-PEG surface).

Parameter	Operating condition
Temperature	23 to 40 °C
Pressure	Atmospheric pressure
pH	Neutral pH
Surface preparation	2 hrs
Lysozyme concentration	4 g / L
Method	Pumping through

The method can be considered as a cost effective method. PEG is cheap. Lysozyme meanwhile is the cheapest amongst proteins. During the adsorption of lysozyme, the solution of lysozyme can be recycled . Furthermore, the method does not involve any harmful or hazardous usage thus is safe to be used even internally.

We believe that the method has the potential to be applied in the pharmaceutical industry, in the biosensor field and in artificial medical implants with some modifications perhaps to suit the application.

Furthermore, if the targeted protein to be repelled is a hard and basic protein, then the SS-PEI surfaces (without PEG molecules) also have the potential to be used.

CHAPTER TWELVE

CONCLUSIONS AND RECOMMENDATIONS

The conclusions of the findings obtained in this thesis are divided into three main sections:

- Adsorption of proteins on bare SS surfaces
- Adsorption of proteins on silicate-PEG and PEI-PEG surfaces
- Adsorption of proteins on protein-PEG surfaces

Adsorption of proteins on bare SS surfaces

The major experimental findings from this study in the adsorption of proteins on a bare SS surface are:

1. Adsorption of β-casein, lysozyme and apo α-lactalbumin on a bare SS surface was temperature and concentration dependent. At high temperatures and concentrations, the adsorption was governed by diffusion-reaction mechanisms whereas under lower temperature (i.e. room temperature) and low concentration conditions (i.e. 0.1 g / L) the adsorption was able to be described solely by surface-reactions.
2. β-casein demonstrated partially reversible adsorption while lysozyme and α-lactalbumin displayed irreversible adsorption on a bare SS under all the experimental conditions used.
3. The modelling results demonstrated negative free energy changes on adsorption consistent with being thermodynamically favoured to adsorb on bare SS. The adsorption of protein was an endothermic process. The proteins also showed large positive entropy change, indicating adsorption-induced denaturation mechanisms (especially apo α-lactalbumin protein).

4. Under the experimental conditions used, all the studied proteins showed a possibility to form a multilayer on the bare SS surface (especially at high concentrations and temperatures).

Adsorption of proteins on silicate-PEG and PEI-PEG surfaces

The major experimental findings from this study in the adsorption of proteins on silicate-PEG and PEI-PEG surfaces are:

1. The PEG coated surfaces prepared in this study were able to inhibit adsorption of β-casein, α-lactalbumin (calcium enriched) and lysozyme proteins especially; the lowest adsorptions relative to that on a bare SS surface were: β-casein, 45 %, holo α-lactalbumin (calcium enriched), 11 % and lysozyme, 1 %. The PEI-PEG surfaces apparently were more suitable to inhibit adsorption of lysozyme, whereas silicate-PEG surfaces appeared to be more suitable to inhibit adsorption of β-casein.
2. Protein stability (i.e. whether it is a soft or a hard protein) greatly influenced the inhibition performance of PEG surfaces. It is apparently more difficult to prevent the adsorption of soft proteins than of hard proteins. This appears to be because soft proteins tend to denature regardless of the surface properties (i.e. hydrophilic or hydrophobic) and attach more effectively in their unfolded state.
3. The adsorption of proteins was lower at 40 °C than at room temperature.
4. Unexpectedly, the adsorption of apo α-lactalbumin was *enhanced* with the presence of PEG molecules. Thus, higher PEG grafting density is not necessarily reflected in better protein resistance.
5. A PEI surface (without PEG molecules) was able to inhibit adsorption of lysozyme excellently. The adsorption of lysozyme on the PEI surface was down to 2 % relative to that on a bare SS surface.
6. Combination between PEG 5k and PEG 2k Da was superior to inhibit adsorption of proteins than other combinations trialled. Bimodal PEG surfaces (both silicate-PEG and PEI-PEG bimodal surfaces) generally better inhibited

adsorption of lysozyme but not β-casein. These results were consistent with the general conclusion that it is important for protein inhibition to have well hydrated flexible surface-tethered PEG chains with packing density sufficiently low to allow chain mobility while still providing a complete surface coverage.

Adsorption of proteins on SS-protein-PEG surfaces

The major experimental findings from the adsorption of proteins on SS-protein-PEG surfaces are:

1. The SS-lysozyme (4)-PEG5k (5) surfaces appeared to be a more effective surface to inhibit the adsorption of the studied proteins than SS-β casein (0.1)-PEG or SS-β lactoglobulin (0.1)-PEG surfaces.
2. The SS-lysozyme-PEG surfaces gave inhibition of protein adsorption far better than either SS-PEI-PEG surfaces or SS-silicate-PEG surfaces. There was almost zero adsorption on SS-lysozyme-PEG surfaces of mixed protein and single protein solutions at concentrations similar to those in milk. The adsorption of β-casein, lysozyme, holo α-lactalbumin and β-lactoglobulin meanwhile was respectively, down to about 3, 1, 4 and 0.4 %, of that on bare SS.
3. An excellent protein adsorption inhibition was achieved with SS-lysozyme-PEG surfaces at room and body temperatures, whereas at 80°C, the adsorption was *enhanced*.

RECOMMENDATIONS

There are several improvements that can be done to make this study much better in future. These improvements can be divided into two major discplines; experimental and kinetic modelling studies.

A. Modelling study

(i) Modify the fitting to allow a multilayer adsorption and a surface diffusion

In this study, it has been assumed that the adsorption is a single-layer adsorption and no surface diffusion is occurred. However, from the experimental results, it showed that the adsorption formed multilayers. Further improvements of the model, taking into account a multilayer adsorption and a surface diffusion would probably result in better interpretation.

For a model which includes a surface diffusion, aggregation and unfolding of proteins that are randomly adsorbed onto a surface, a model proposed by Pellenc et al. [2005] can be used as a first attempt (refer to Figure 12.1).

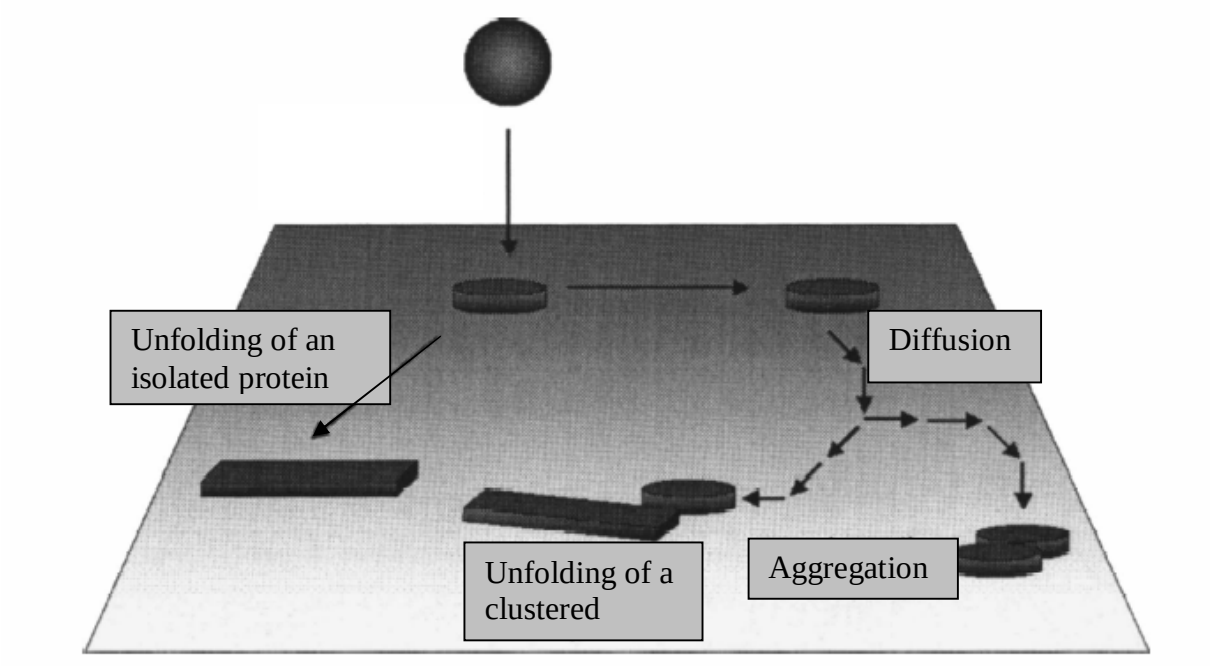

Figure 12.1: Depiction of the Pellenc surface diffusion model. At each time step, proteins adsorb at a random position. They are then allowed to diffuse on the surface unless they unfold or aggregate. Taken from [Pellenc et al., 2005].

Besides that, for diffusion-limited adsorption kinetics (i.e. diffusion-limited regime), the Leveque solution to the convective-diffusion equation can be used to predict the initial adsorption rate, $\frac{d\Gamma}{dt}$ (or flux, *J*), in terms of the free solution diffusivity, D, wall shear rate, γ, and the distance from the cell entrance to the point of observation, L (refer to Equation 12.1) [Lok et al., 1983].

$$\frac{d\Gamma}{dt} = 0.538\left(\frac{\gamma}{L}\right)^{1/3} D^{2/3}C \qquad (12.1)$$

The initial adsorption rate obtained from this study then can be compared to the initial adsorption rate predicted from the Leveque equation (Equation 12.1) and thus the diffusion coefficient can be calculated.

However, it shoud be noted that the Leveque equation is applied on a laminar liquid flow in a parallel plate geometry.

(ii) Do a modelling study on the adsorption of proteins on PEG surfaces

It is recommended that the modelling study is extended to the adsorption of proteins on PEG surfaces to explore mechanisms from thermodynamic aspects. The obtained thermodynamic parameters (ΔG, ΔS and ΔH) are believed able to give a good explanation of the mechanisms of PEG on inhibition of protein adsorption. In the study done, the mechanisms of PEG on protein adsorption inhibition was explained based only on the theories and literature. It is suggested that the equation (kinetic model) used for the adsorption of proteins on PEG surfaces is the same used for the adsorption of proteins on the bare SS surface. Thus, a comparison can be made and the role of PEG chains (from the thermodynamic aspects) can be determined.

B. Experimental study

(i) Lower critical solution temperature (LCST)

In this study, it is believed that the conformational change of PEG chains significantly affects the ability of the PEG layer to inhibit adsorption of proteins. The PEG conformational changes relate to its critical solution temperature (LCST) or clouding point. At this point, PEG undergoes a conformational reorientation to a hydrophobic state, dehydrates, collapses and is no longer mobile; hence reduces its efficiency as a protein repellent. Thus, it is worthwhile to study more on the LCST of the PEG chains. The LCST of PEG varies depending on molecular weight, ionic strength and pH of the solution. Lowering pH and increasing ionic strength will lower the LCST and the phase transisiton will occur. Thus, it is recommended that the ionic strength and pH of the solution are varied below, at and above the LCST of PEG in future study.

Additionally, the conformational change of the PEG layer can be gauged by determining its ratio of $\frac{\Delta D}{\Delta f}$ (can be obtained from the raw QCM-D data). If the $\frac{\Delta D}{\Delta f}$ is high, the layer behaves like a plastic (i.e. dehydrated).

(ii) Wettability test

In this study, it was believed that the stainless steel surface used was a hydrophobic surface (based on the literature). However, it is recommended that the hyrophobicity of the surface is checked experimentally. The hydrophobicity of the surface can be determined by using a wettability test (i.e. contact angle measurements).

(iii) AFM characterization

In this study, the AFM characterization was done ex-situ. Thus, the dynamic of protein adsorption cannot be determined. In future, it is recommended that the AFM characterization is carried out in-situ. The orientation of the adsorbed protein and the formation of multilayers are believed can be determined if the AFM characterization is done in-situ. The mechanisms of multilayers formation is also can be investigated either (i) multilayers formation is only start to form if a monolayer has completely formed or (ii) multilayers is formed even a monolayer has not completely formed (aggregation mechanism). It is suggested that the tapping mode of AFM and QCM-D is combined for simultaneous investigation and characterization of protein adsorption [Choi et al., 2003].

(iv) Flow rate

In the study done, the flow rate of the solution was kept constant. In future study, it is recommended that the flow rate is varied so that the resistance of the transport or diffusion can be determined. Besides that, the effect of shear stress on the adsorption and desorption can be investigated (i.e. shear stress or shear rate is dependent on the flow rate). Since the highest flowrate of the QCM-D used in this study is at 216 μL / min, thus , it is suggested that the flow rate is varied from 50, 100 and 200 μL / min in future study. The corresponding velocities and shear rates, respectively is about, 0.03, 0.05 and 0.12 m / s and 4, 7 and 17 s^{-1}. It has been reported that the typical employed flow velocities in the industrial equipments are in the range of 1 – 5 m / s for turbulent flow system and less than 1 m / s for laminar flow system [Danodavan and Parat, 1997]. The typical shear rates used in industrial processing are; stirring, 10^{-1} to $10^{-3}s^{-1}$; pumping, 10^{2} to 10^{3} s^{-1}; spraying,10^{3} to 10^{4} s^{-1} and rubbing, 10^{4} to $10^{5}s^{-1}$ [Fox and McSweeney, 2003].

(v) Apply these promising modified surfaces also to inhibit adhesion of bacteria

It is recommended that the proposed surfaces (especially lysozyme based surfaces such as SS-lysozyme-PEG and SS-lysozyme surfaces) are further used to prevent adhesion of bacteria (biofilm inhibition). Lysozyme molecule is able to catalyze the hydrolysis of 1,4-*β*-glycosidic linkages between *N*-acetymuramic acid and *N*-acetylglucosamine, which are components of the cell wall peptidoglycan of bacteria [Caro et al., 2009]. For the first attempt, we may use Gram (+) and Gram (-) bacterias as our samples.

REFERENCES

Abbott, N.L., Blankschtein, D and Hatton, T.A. (1993). *Interactions of globular colloids and flexible polymers-Understanding protein partitioning in 2-phase aqueous polymer systems*. ACS Symposium Series. 532. 53-69.

Abbott, N.L., Blankschtein, D. and Hatton, T.A. (1992). *Protein partitioning in 2-phase aqueous polymer systems. A neutron-scattering investigation of the polymer-solution structure and protein polymer interactions.* Macromolecules. 25. 3932-3941.

Addesso, A. and Lund, D.B. (1997). *Influence of solid surface energy on protein adsorption*. Journal of Food Processing and Preservation. 21. 319-333.

Agnes, R.D., Eileen, B.S., Amy, C.L. and Ferencz, D. (2001). *2-crown-4-ether and tri(ethylene glycol) dimethyl-ether plasma-coated stainless steel surfaces and their ability to reduce bacterial biofilm deposition*. Journal of Applied Polymer Science. 81. 3425-3438.

Al-Makhlafi,H., Mcguire. J. and Daeschel, M. (1994). *Influence of preadsorbed milk proteins on adhesion*. Applied and Environmental Microbiology. 60. 3560-3565.

Archambault, J.G., and Brash, J.L. (2004). *Protein repellent polyurethane-urea surfaces by chemical grafting of hydroxyl-terminated poly(ethylene oxide): effects of protein size and charge.* Colloids and Surfaces B: Biointerfaces.33.111-120.

Arwin, H. 2000. *Ellipsometry on thin organic layers of biological interest: characterization and applications*. Thin Solid Films.377-378. 48-56.

Bagha, A.R. and Holmberg, K. (2008). *Cationic ester-containing gemini surfactants: Adsorption at tailor-made surfaces monitored by SPR and QCM*. Langmuir. 24. 6140-6145.

Balamurugan, S., Ista, L.K., Yan, J., Lopez, G.P., Fick, J., Himmelhaus, M. and Grunze, M. (2005). *Reversible protein adsorption and bioadhesion on monolayers terminated with mixtures of oligo(ethylene glycol) and methyl groups*. Journal American Chemical Society. 127. 14548-14549.

Bansal, B. and Chen, X.D. (2006). *A Critical review of milk fouling in heat exchangers.* Comprehensive Reviews in Food Science and Food Safety. 5. 27-33.

Bansal, B. and Chen. X.D. (2006). *Fouling of heat exchangers by dairy fluids. A review*. Food and Bioproducts Processing. 84. 265-273.

Bardina, I.A., Kovaleva, N.V., S. Nikitin. (2001). *Surface properties of initial and polyethylene glycol modified silica gels*. Russian Journal of Physical Chemistry. 75. 442-445.

Benhabbour, S.R., Sheardown, H. and Adronov, A. (2008). *Protein resistance of PEG-functionalized dendronized surfaces: Effect of PEG molecular weight and dendron generation*. Macromolecules. 41. 4817-4823.

Bettoni, R. W., Dobson, C. M. and Redfield, C. (2001). *Comparison of the structural and dynamical properties of holo and apo bovine a-Lactalbumin by NMR Spectroscopy*. Journal Molecular Biology. 307. 885-898.

Bird, R.B., Stewart, W., lightfoot, E. (1962) .Jon Willey & so sic.US. Transport Phenomena.

Bjorling, M., Karlstriim, G. and Linse, P. (1991). *Conformational adaption of Poly(ethylene oxide). A ^{13}C-NMR Study*. Journal Physical Chemistry. 95.6706-6709.

Bosker, W.T.E., Iakovlev, P.A., Norde, W. and Stuart, M.A.C. (2005). *BSA adsorption on bimodal PEO brushes*. Journal of Colloid and Interface Science. 286. 496-503.

Bosker, W.T.E., Patzsch, K., Stuart, M.A.C. (2007). *Sweet brushes and dirty proteins*. Soft Matter. 3. 754-762.

Bower, C.K., Mcguire, J. and Daeschel, M.A. (1996). *The adhesion and detachment of bacteria and spores on food-contact surfaces*. Trends in Food Science & Technology. 7. 152-157.

Bre´tagnol, F., Lejeune, M., Bouraoui, A. P., Hasiwa, M. (2006). *Fouling and non-fouling surfaces produced by plasma polymerization of ethylene oxide monomer*. Acta Biomaterialia.2.165–172.

Bremmell, K.E., Kingshott, P., Ademovic, Z. (2006). *Colloid probe AFM investigation of interactions between fibrinogen and PEG-like plasma polymer surfaces*. Langmuir. 22. 313-318.

Brown, A.A., Khan, N.S., Steinbock, L. (2005). *Synthesis of oligo(ethylene glycol) methacrylate polymer brushes.* European Polymer Journal. 41. 1757-1765.

Brusatori, M.A. and Van Tassel, P.R. (1999). *A kinetic model of protein adsorption/surface-induced transition kinetics evaluated by the scaled particle theory*. Journal of Colloid and Interface Science. 219. 333–338.

Bu, Z., Cook, J., Callaway, D.J.E. (2001). *Dynamic regimes and correlated structural dynamics in native and denatured alpha-lactalbumin*. Journal of Molecular Biology. 4. 865-873.

Cabilio, N.R., Omanovic, S. and Roscoe, S.G. (2000). *Electrochemical studies of the effect of temperature and ph on the adsorption of α-lactalbumin at Pt*. Langmuir. 16. 8480-8488.

Calonder, C. and Van Tassel, P.R. (2001). *Kinetic regimes of protein adsorption.* Langmuir. 17. 4392-4395.

Can, H.K. and Gu¨ ner, A. (2006). *Thermodynamic aspects of the bovine serum albumin adsorption onto N,N_- diethylaminoethyl dextran microbeads*. Journal of Applied Polymer Science. 99. 2300–2304.

Carignano, M.A., Szleifer, I. (2000). *Prevention of protein adsorption by flexible and rigid chain molecules.* Colloids and Surfaces B: Biointerfaces.18.169-182.

Caro, A., Humblot,V., Methivier, C., Minier, M., Salmain, M. and Pradier, C.M. (2009). *Grafting of lysozyme and/or poly(ethylene glycol) to prevent biofilm growth on stainless steel surfaces*. Journal Physic Chemistry. 113. 2101-2109.

Caruso, F., Furlong, D.N. and Kingshott, P. (1997). *Characterization of ferritin adsorption onto gold*. Journal of Colloid and Interface Science. 186. 129-140.

Chalikian T.V. and Breslauer K.J. (1996). *On volume changes accompanying conformational transitions of biopolymers.* Biopolymers. 39. 619–626.

Changani, S.D., Beiny, M.T. and Fryer, P.J. (1997). *Engineering and chemical factors associated with fouling and cleaning in milk processing*. Experimental Thermal and Fluid Science. 14. 392-406.

Chen, H., Zhang, Z., Chen, Y., Brook, M.A. and Sheardown, H. (2005). *Protein repellent silicone surfaces by covalent immobilization of poly (ethylene oxide)* Biomaterials.26.2391-2399.

Chen. W.Y., Huang, H.M., Lin, C.C., Lin, F.Y. and Chan, Y.C. (2003). *Effect of temperature on hydrophobic interaction between proteins and hydrophobic adsorbents: Studies by isothermal titration calorimetry and the van't Hoff equation*. Langmuir. 19. 9395-9405.

Cho, D. and Cornec, M. A. (1999). *A kinetic study on the adsorption of compact, water-soluble proteins onto aqueous surfaces*. Bulletin Korean Chemical Society. 1999. 20. 999-1004.

Choi, E.J. and Foster, M.D. (2003). *Effect of flow on human serum albumin adsorption to self-assembled monolayers of varying packing density*. Langmuir. 19. 5464-5474.

Choi, K.H., Friedt, J.M., Laureyn, W., Frederix, F., Campitelli, A. and Borghs, G. (2003). *Investigation of protein adsorption with simultaneous measurements of atomic force microscope and quartz crystal microbalance.* Journal of Vacuum Science and Technology B. 21. 1433-1436.

Clark, A.J., Whitehead, L.A., Haynes, C.A. and Kotlicki, A. (2002). *Novel resonant-frequency sensor to detect the kinetics of protein adsorption*. Rev. Scientific Instrum. 73. 4339-4346.

Cosman, N.P., Fatih, K. and Roscoe, S.G. (2005). *Electrochemical impedance spectroscopy study of the adsorption behaviour of alpha lactalbumin and beta casein at stainless steel*. Journal of Electroanalytical Chemistry. 574. 261-271.

Cramer, C.J. and Truhlar, D.G. 1(999). *Implicit solvation models: equilibria, structure, spectra, and dynamics*. Chemical Review. 99. 2161-2220.

Currie, E.P.K., Norde, W. and Stuart, M.A.C. (2003). *Tethered polymer chains: surface chemistry and their impact on colloidal and surface properties*. Advances in Colloid and Interface Science. 100. 205-265.

Currie, E.P.K., Van der Gucht, J., Borisov, O.V. (1999). *Stuffed brushes: theory and experiment.* Pure and Applied Chemistry. 71. 1227-1241.

Dalsin, J.L. and Messersmith, P.B. (2005). *Bioinspired antifouling polymers*. Materials Today. September.

Dalsin, J.L., Lin L.J., Tosatti, S. (2005). *Protein resistance of titanium oxide surfaces modified by biologically inspired mPEG-DOPA*. Langmuir. 21. 640-646.

Daly, S.M., Przybycien, T.M., Tilton, R.D. (2003). *Coverage dependent orientation of lysozyme adsorption on silica*. Langmuir. 19. 3848-3857.

Denes, A.R., Somers, E.B., Wong, A.C.L. (2001). *12-crown-4-ether and tri(ethylene glycol) dimethyl-ether plasma-coated stainless steel surfaces and their ability to reduce bacterial biofilm deposition*. Journal of Applied Polymer Science. 81. 3425-3438.

Desroches, M. J. and Omanovic, S. (2007). *Adsorption of fibrinogen on a biomedical-grade stainless steel 316LVM surface: a PM-IRRAS study of the adsorption thermodynamics, kinetics and secondary structure changes*. Physical Chemistry Chemical Physics 10, 2502–2512.

Dong, B.Y., Manolache, S., Somers, E.B. (2005). *Generation of antifouling layers on stainless steel surfaces by plasma-enhanced crosslinking of polyethylene glycol.* Journal of Applied Polymer Science. 97. 487-497.

Du, H., Chandaroy, P. and Hui, S. W. (1997). *Grafted poly- ethylene glycol on lipid surfaces inhibits protein adsorption and cell adhesion*. Biochimica et Biophysica Acta. 1326. 236–248.

Durchschlag H. and Zipper P. (2001).*Comparative investigations of biopolymer hydration by physicochemical and modeling techniques*. Biophysic Chemistry. 93.141–157.

Edwards, D.K., Denny, V.E. and Mills, A.F. (1978). *Transfer Processes. An introduction to diffusion, convection, and radiation*. Second edition. Hemisphere Publishing Corporation. Comprehensive Reviews in Food Science and Food Safety. 5.23-33.

Ellis, J.S. and Thompson, M. (2004). *Slip and coupling phenomena at the liquid-solid interface*. Physical Chemistry Chemical Physics. 6. 4928-4938.

Engel, M.F.M., van Mierlo, C.P.M. and Visser, A.J.W.G. (2002). *Kinetic and structural characterization of adsorption-induced unfolding of bovine alpha-lactalbumin*. Journal of Biological Chemistry. 277. 10922-10930.

Englebienne, P., Hoonacker, A.V. and Verhas, M. (2003). *Surface plasmon resonance: principles, methods and applications in biomedical sciences*. Spectroscopy. 17. 255-273.

Erol, M., Du, H. and Sukhishvili, S. (2006). *Control of specific attachment of proteins by adsorption of polymer layers*. Langmuir. 22. 11329-11336.

Esquibel-King, M.A., Dias-Cabral, A.C. and Queiroz, J.A. (1999). *Study of hydrophobic interaction adsorption of bovine serum albumin under overloaded conditions using flow microcalorimetry*. Journal of Chromatography A. 865. 111–122.

Etzel, M.R. (2004). *Manufacture and use of dairy protein fractions*. Journal of Nutrition. 134. 996-1002.

Fang, F. and Szleifer. I. (2001). *Kinetics and thermodynamics of protein adsorption: A generalized molecular theoretical approach*. Biophysical Journal. 80. 2568-2589.

Fawcett, N.C., Craven, R.D., Zhang P. (1998). *QCM response to solvated, tethered macromolecules*. Analytical Chemistry. 70. 2876-2880.

Feijter, J.A.D. and A. Vrij, A. (1978). *Contact angles in thin liquid films. II. Contact angle measurements in Newton black soap films*. Journal of Colloid and Interface Science. 64. 269-277.

Feng, W., Zhu, S., Ishihara, K. and Brash, J.L. (2005). *Adsorption of fibrinogen and lysozyme on silicon grafted with poly (2-methacryloyloyloxyethyl phosphorylcholine)via surface –initiated atom transfer radical polymerization*. Langmuir. 21. 5980-5987.

Feng, W., Zhu, S., Ishihara, K. and Brash, J.L. (2005). *Adsorption of fibrinogen and lysozyme on slicon grafted with poly (2-methacryloyloxyethyl phosphorylcholine) via surface initiated atom transfer radical polymerization*. Langmuir. 21. 5980-5987.

Fernández, A. and Ramsden, J.J. (2001). *On adsorption-induced denaturation of folded proteins*. Journal of Biological Physics and Chemistry.1. 81-84.

Fogler, H.S. (1992). *Elements of chemical reaction engineering*. 2nd edition. Prentice Hall International Incorporation. New Jersey

Fox, P.F. and McSweeney, P.L.H. (2003). *Advanced dairy chemistry*. Vol. 1.Part 1. 3rd edition, Chapman and Hall London.

Fukai, R., Dakwa, P.H.R. and Chen, W. (2004). *Strategies toward biocompatible artificial implans: Grafting of functionalized poly(ethylene glycol)s to pol(ethylene terephthalate) surfaces.* Journal of Polymer Science: Part A:Polymer Chemistry.42.5389-5400.

Fuzuzaki, S., Urano, H. and Nagata, K. (199). *Adsorption of protein onto stainless steel surfaces*. Journal of Fermentation and Bioengineering. 80.6-11.

Gan, B.K., Kondyurin, A. and Bilek, M.M.M. (2007). *Comparison of protein surface attachment on untreated and plasma immersion ion implantation treated polystyrene: Protein islands and carpet*. Langmuir. 23. 2741-2746.

Garcia de la Torre, J. (2001). *Hydration from hydrodynamics. General considerations and applications of bead modeling to globular proteins*. Biophysic Chemistry. 93. 159-170.

Gulec, H. A., Lu, K. S. and Mutlu, M. (2006). *Modification of food contacting surfaces by plasma polymerisation technique. Part I: Determination of hydrophilicity, hydrophobicity and surface free energy by contact angle method*. Journal of Food Engineering. 75.187–195.

Hagel, L. (1998). *Gel filtration in protein purification*. John Wiley & Sons, New York.

Halperin, A., Fragneto, G, Schollier, A. and Sferrazza, M. (2007). *Primary versus ternary adsorption of proteins onto PEG brushes*. Langmuir. 23. 10603-10617.

Hamood al-Makulaf, Meguire, J. and Daeschel, M. (1994). *Influence of preadsorbed milk proteins on adhesion of Listeria Monocytogenes to hydrophobic and hydrophilic silica surfaces*. Applied and Environmental Microbiology.60.3560-3565.

Harder, P., Grunze, M. and Waite, J.H. (2000). *Interaction of the adhesive protein Mefp-1 and fibrinogen with methyl and oligo(ethylene glycol)-terminated self-assembled monolayers*. Journal of Adhesion. 73. 161-177.

Harding, S.E. (2001). *The hydration problem in solution biophysics: an introduction*. Biophysic Chemistry. 93.87–91.

Head-Gordon, T. and Hura, G. (2002). *Water structure from scattering experiments and simulation*. Chemical Review. 102. 2651-2670.

Helparin, A. (1999).*Polymer brushes that resist adsorption of model proteins:Design parameters*. Langmuir.15.2525-2533.

Hemmerle, J., Altmann, S.M., Maaloum, M., Horber, J.K.H., Heinrich, L., Voegel, J.C. and Scaaf, P. (1999). *Direct observation of the anchoring process during the adsorption of fibrinogen on a solid surface by force-spectroscopy mode atomic force microscopy*. Biophysics. 96. 6705-6710.

Herrwerth, S., Eck, W. , Reinhardt, S. and Grunze, M. (2003). *Factors that Determine the Protein Resistance of Oligoether Self-Assembled Monolayers - Internal Hydrophilicity, Terminal Hydrophilicity, and Lateral Packing Density*. Journal American Chemical Society. 125.9359-9366.

Heuberger, M., Drobek, T. and Voros, J. (2004). *About the role of water in surface-grafted poly(ethylene glycol) layers.* Langmuir.20.9445-9448.

Hibbert, D.B., Gooding, J.J. and Erokhin, P. (2002). *Kinetics of irreversible adsorption with diffusion: Application to biomolecule immobilization*. Langmuir. 18. 1770-1776.

Hook, F., and Kasemo, B. (2001).*Variations in coupled water, viscoelastic properties, and film thickness of a Mefp-1 protein film during adsorption and cross-linking: a quartz crystal microbalance with dissipation monitoring, ellipsometry, and surface plasmon resonance study*. Analytical Chemistry. 73. 5796-5804.

Hook, F., Rodahl, M., Brzezinski, P. and Kasemo, B. (1998). *Energy dissipation kinetics for protein and antibody-antigen adsorption under shear oscillation on a quartz crystal microbalance*. Langmuir. 14.729-734.

Hook, F., Rodahl, M., Kasemo, B. and Brzezinski. P. (1998). *Structural changes in hemoglobin during adsorption to solid surfaces: Effects of pH, ionic strength and ligand binding*. Biophysics. 95. 12271-12276.

Hook, F., Voros, J., Rodahl, M., Kurrat, R., Boni, P., Ramsden, J.J., Textor, M., Spencer, N.D., Tengvall, P., Gold, J. and Kasemo, B. (2002). *A comparative study of protein adsorption on titanium oxide surfaces using in situ ellipsometry, optical waveguide lightmode spectroscopy and quartz crystal microbalance/dissipation*. Colloids and Surfaces B:Biointerfaces. 24. 155-170.

Houssein, A., Gilles, C. and Maurice, B. (2005). *Quantitative determination of surface energy using atomic force microscopy: the case of hydrophobic/hydrophobic contact and hydrophilic/hydrophilic contact*. Surface and Interface Analysis.37. 755–764.

Imamura, K., Kawasaki, Y., Awadzu, T., Sakiyama, T. and Nakanishi, K. (2003). *Contribution of acidic amino resides to the adsorption op peptides onto a stainless steel surface*. Journal of Colloid and Interface Science. 267. 294-301.

Irwin, E.F., Ho, J.E., Kane, S.R., and Healy, K.E. (2005). *Analysis of interpenetrating polymer networks via quartz crystal microbalance with dissipation monitoring*. Langmuir. 21.5529-5536.

Jackler, G., Steitz, R. and Czeslik. C. (2002). *Effect of temperature on the adsorption of lysozyme at the silica/water interface studied by optical and neutron reflectometry*. Langmuir.18. 6565-6570.

Janocha, B., Hegemann, D., Oehr, C., Brunner, H., Rupp, F. and Geis-Gerstorfer, J. (2001). *Adsorption of protein on plasma-polysiloxane layers of different surface energies. Surface & Coatings Technology*. 142-144. 1051-1055.

Jennissen, H.P., Sanders, A., Schnittler, H.J. and Hlady, V. (1999). *TIRF-rheometer for measuring protein adsorption under high shear rates: Constructional and fluid dynamic aspects*. Mat.-wiss. u. Werkstofftech. 30.850-861.

Jonsson, M. and Johansson, H.O. (2004). *Effect of surface grafted polymers on the adsorption of different model proteins*. Colloids and Surfaces B: Biointerfaces. 37. 71-81.

Kaplan, H. and Giiner, A. (2006). *Thermodynamic aspects of the bovine serum albumin adsorption onto N,N'-Diethylaminoethyl dextran microbeads*. Journal of Applied Polymer Science. 99. 2300-2304.

Karlsson, C.A., Wahlgren, M.C. and Tragardh, A.C. (1998). *Some surface-related aspects of the cleaning of new and reused stainless-steel surfaces fouled by protein.*

International Dairy Journal. 8. 925-933.

Karlsson, M., Ekeroth, Elwing, H. and Carlsson, U. (2005). *Reduction of irreversible protein adsorption on solid surfaces by protein engineering for increased stability*. The Journal of Biologal Chemistry. 280, 25558-25564.

Kim, D.T., Blanch, H.W. and Radke, C.J. (2002). *Direct imaging of lysozyme adsorption onto mica by atomic force microscopy*. Langmuir. 18.5841-5850.

Kingshott, P., Jiang, W., Nikolaj, G. B., and Lone, G. (2003). *Covalent attachment of Poly(ethylene glycol) to surfaces, critical for reducing bacterial adhesion*. Langmuir. 19. 6912-6921.

Koutsopoulos, S., John van der Oost, J.V.D. and Norde, W. (2005). *Structural features of a hyperthermostable endo-b-1,3-glucanase in solution and adsorbed on ‘‘invisible’’ particles*. Biophysical Journal. 88. 467–474.

Kronman, M.J. (1989). *Metal-ion binding and the molecular conformational properties of alpha-lactalbumin*. Critical Reviews in Biochemistry and Molecular Biology. 24. 565-667.

Kumar, C.G. and Anand, S.K. (1998). *Significant of microbial biofilm in food industry: A review.* International Journal of Food Microbiology.42.9-27.

Lamotte, L.B., Nonville, S., Goubard, F., Marque, P. and Pauthe, E. (2008). *Kinetics of conformational changes of fibrinogen adsorbed onto model surfaces*. Colloids and Surfaces B: Biointerfaces. 63. 129-137.

Latour, R.A. (2006). *Thermodynamic perspectives on the molecular mechanisms providing protein adsorption resistance that include protein-surface interactions*. Journal of Biomedical Materials Research Part A. 843-854.

Lee, M., Park, S.K., Chung, C. and Kim, H. (2004). *QCM study of beta-casein adsorption on the hydrophobic surface: Effect of ionic strength and cations*. Bulletin of the Korean Chemical Society.25. 1031-1035.

Lee, W.K., Ko, J.S., and Kim, H.M. (2001). *Effect of electrostatic interaction on the adsorption of globular proteins on octacalcium phosphate crystal film*. Journal of Colloid and Interface Science. 246. 70–77.

Li, H.B. Zhang, W.K. Zhang, X. (1998). Single molecule force spectroscopy on poly(vinyl alcohol) by atomic force microscopy. Macromolecular Rapid Communications. 19. 609-611.

Liu, G., Chen, Y., Zhang, G. and Yang, S. (2007). *Protein resistance of (ethylene oxide)$_n$ monolayers at the air/water interface: effects of packing density and chain length*. Physical Chemistry Chemical Physics. 9. 6073-6082.

Liu, G., Cheng, H., Yan, L. and Zhang, G. (2005). *Study of the kinetics of the pancake-to-brush transtition of poly(N-isopropylacrylamide) chains*. Journal Physic Chemistry. 109. 22603-22607.

Liu, G.M., Chen, Y.J., Zhang, G.Z. (2007). *Protein resistance of (ethylene oxide)(n) monolayers at the air/water interface: effects of packing density and chain length*. Physical Chemistry Chemical Physics. 9. 6073-6082.

Liu, X.Q. and Sano, Y. (1998). *Kinetic studies on the initial crystallization process of lysozyme in the presence of D_2O and H_2O*. Journal of Protein Chemistry. 17. 9-14.

Lok, B.K., Cheng, Y. and Robertson, C.R. (1983). *Protein adsorption on crosslinked polydimethylsiloxane using total internal-reflection fluorescence*. Journal Colloid Interface Science. 91. 104 – 116.

Luthgens, E. and Janshoff, A. (2005). *Equalibrium coverage fluctuations: A new approach to quantify reversible adsorption of proteins*. Chemical Physic Chemistry. 6. 444-448.

Ma, H., Hyun, J., Stiller, P. and Chilkoti, A. (2004). *"Non-fouling" oligo (ethylene glycol)-functionalized polymer brushes synthesized by surface-initiated atom transfer radical polymerization*. Advanced Materials. 16. 338-341.

Malmsten, M., Emoto, K. and Alstine, J.M.V. (1998). *Effect of chain density on inhibition of protein adsorption by Poly(ethylene glycol) based coatings*. Journal of Colloidal and Interface Science. 202. 507-517.

Malmstrom, J., Agheli, H., Kingshott, P. and Sutherland, D.S. (2007). *Viscoelastic modeling of highly hydrated laminin layers at homogeneous and nanostructured surfaces: Quantification of protein layer properties using QCM-D and SPR*. Langmuir. 23.9760-9768.

Mensah, J.A., Yeap, K.Y. and McFarlane, A.J. (2007). *The influential role of pulp chemistry, flocculant structure on dewaterability of kaolinite and smectite clay dispersions couette Taylor flow conditions*. Powder Technology. 179.79–83.

Marple, V.A. and Liu, B.Y.H. (1774). *Characteristics of laminar jet impactors*. Environement Science Technology. 8. 648-654.

Marple, V.A. and Willeke, K. (1976). *Impactor design*. Atmospheric Environment. 10. 891-896.

Martin, S.J., Granstaff, V.E. and Frye, G.C. (1991). *Characterization of a quartz microbalance with simultaneous mass and liquid loading*. Analytical Chemistry. 63. 2272-2281.

Masel, R.I. (1996). *Principles of adsorption and reaction on solid surfaces*. Wiley Series in Chemical Engineering 1st edition.

Matulis, D. (2001). *Thermodynamics of the hydrophobic effect. III. Condensation and aggregation of alkanes, alcohols, and alkylamines*. Biophysical Chemistry. 67-82.

Matyjaszewski, K. and Xia, J. (2001). *Atom transfer radical polymerization*. Chemical Review.101. 2921-2990.

McColl, J., Yakubov, G. E. and Ramsden, J.J. (2008). *Temperature dependence of mucin adsorption*. Langmuir. 24. 902-905.

McHale, G. and Newton, M.I. (2004). *Surface roughness and interfacial slip boundary condition for quartz crystal microbalances*. Journal of Applied Physics. 95. 373-380.

Mcpherson, T., Kidane, A., Szleifer, I. and Park, K. (1998). *Prevention of protein adsorption by tethered poly (ethylene oxide) layers:Experiment and single chain mean field analysis*. Langmuir. 14. 176-186.

Mensah, J.A., Yeap, K.Y. and McFarlane, A.J. (2007). *The influential role of pulp chemistry, flocculant structure type and shear rate on dewaterability of kaolinite and smectite clay dispersions under couette Taylor flow conditions*. Powder Technology. 179. 79-83.

Menz, B., Knerr, R., Gopferich, A. and Steinem, C. (2005). *Impedance and QCM analysis of the protein resistance of self-assembled PEGylated alkanethiol layers on gold*. Biomaterials. 26. 4237-4243.

Michael, R., Fredrik, H., Claes, F., Craig, A.K., Anatol, K., Peter, B., Marina, V. and Bengt, K. (1997). *Simultaneous frequency and dissipation factor QCM measurements of biomolecular adsorption and cell adhesion*. Faraday Discuss. 107. 229-246.

Michailidou, V.N., Loppinet, B., Prucker, O. (2005). *Cooperative diffusion of end-grafted polymer brushes in good solvents*. Macromolecules. 38, 8960-8962.

Mikhaylova, Y., Dutschk, V., Muller, M., Grundke, K. and Eichhorn, K.J. (2007). *Study of the solid-liquid interface of hydroxyl-terminated hyperbranched aromatic polyesters (HBP-OH) in aqueous media II. Adsorption of model proteins*. Colloids and Surfaces A: Physicochem.Eng.Aspects. 297. 19-29.

Miller, R., Fainerman,V.B., Aksenenko, E.V. (2004). *Dynamic surface tension and adsorption kinetics of beta-casein at the solution air interface*. Langmuir. 20. 771-777.

Morison, K.R. and Tie, S.H. (2002). *The development and investigation of a model milk mineral fouling solution.* Trans IChemE. 80. 326 – 331.

Moya, S.E., Brown, A.A., Azzaroni, O. (2005). *Following polymer brush growth using the quartz crystal microbalance technique*. Macromolecular Rapid Communications. 26. 1117-1121.

Murray, B.S. and Cros, L. (1998). *Adsorption of beta-lactoglobulin and beta-casein to metal surfaces and their removal by a non-ionic surfactant, as monitored via a quartz crystal microbalance*. Colloids and Surfaces B:Biointerfaces.10. 227-241.

Murray, B.S. and Deshaires, C. (2000). *Monitoring Protein Fouling of Metal Surfaces via a Quartz Crystal Microbalance*. Journal of Colloid and Interface Science. 227. 32–41.

Nakanishi, K., Sakiyama, T. and Imamura, K. (2001). *Review on the adsorption of proteins on solid surfaces, a common but very complicated phenomenon.* Journal of Bioscience and Engineering. 3. 233-244.

Nath, N., Hyun, J., Ma, H. and Chilkoti, A. (2004). *Surface Engineering for Control of Protein and Cell Interactions*. Surface Science. 570. 98-110.

Nnebe, I.M., Tilton, R.D. and Schneider, J.W. (2004). *Direct force measurement of the stability of poly(ethylene glycol)-polyethylenimine graft films.* Journal of Colloid and Interface Science. 276. 306-316.

Nomura, T. and Okuhara, M. (1982). *Frequency shifts of piezoelectric quartz crystals immersed in organic liquids.* Analytica Chimica Acta. 142. 281-284.

Norde, W. and Gage, D. (2004). *Interaction of BSA and human blood plasma with PEO-tethered surfaces: influence of PEO chain length, grafting density and temperature*. Langmuir. 20.4162-4167.

Norman, A.I., Alessi, M.L., Knowlton, S.E. (2005). *Helical and coil conformations of poly(ethylene glycol) in iso-butyric acid and water.* Abstract of Papers of the American Chemical Society. 230. 3572-3573.

Ostuni, E., Robert, G., Chapman, R., Holmlin,E.,Takayama,S. and Whitesides, G.M. (2001). *A Survey of structure-property relationships of surfaces that resist the adsorption of protein.* Langmuir. 17. 5605-5620.

Ostuni, E., Grzybowski, B.A., Mrksich, M. (2003). *Adsorption of proteins to hydrophobic sites on mixed self-assembled monolayers*. Langmuir. 19. 1861-1872.

Otsuka, H., Nagasaki, Y. and Kataoka, K. (2001). *Self-assembly of poly(ethylene glycol)-based block copolymers for biomedical applications*. Current Opinion in Colloid & Interface Science. 6. 3-10.

Otsuka, H., Satomi, T., Itadani, J.H., Nagasaki, Y., Okano, T., Horiike, Y. and Kataoka, K. (2001). *Functionilized PEG-brush layer for controlling protein and cell interactions*. European Cells & Materials. 6. Suppl. 1, 102.

Ozkaya, B. (2006). *Adsorption and desorption of phenol on activated carbon and a comparison of isotherm models*. Journal of Hazadours Materials. 129. 158-163.

Paeng, K., Choi, J., Park, Y. and Sohn, D. (2003). *Temperature effect of hydrophobically modified polyethylene oxide at the air-water interface*. Colloids and Surfaces A. 220. 1-7.

Pasche, S., Voros, J., Griesser, H. J., Spencer, N. D. and Textor, M. (2005). *Effects of ionic strength and surface charge on protein adsorption at PEGylated surfaces*. Journal Physic Chemistry B. 109. 17545-17552.

Paul, S., Paul, D., Basova, T. and Ray, A. K. (2008). *Studies of adsorption and viscoelastic properties of proteins onto liquid crystal phthalocyanine surface using Quartz Crystal Microbalance with Dissipation technique.* Journal Physical Chemistry C. 112. 11822-11830.

Pelenc, D., Gallet, O. and Berry, H. (2005). *Adsorption-induces conformational changes in protein diffusion-aggregation surface assemblies*. Physical Review E: 72. 051904.

Pereira, P, Kelly, S.M., Gellert, P.R. and van der Walle, C.F. (2008). *Interdomain mobility and conformational stability of type III fibronectin domain pairs control surface adsorption, desorption and unfolding*. Colloids and Surfaces B: Biointerfaces. 64. 1-9.

Poulsen, L.V. (1999). *Microbial biofilm in food processing*. Lebensm.-Wiss.u-Technology. 32. 321-326.

Prime, K.L. and Whitesides, G.M. (1993). *Adsorption of proteins onto surfaces containing end-attached oligo(ethylene oxide): A model system using self-assembled monolayers*. Journal American Chemistry Society. 115. 10714-10721.

Pyun, J., Kowalewski, T. and Matyjaszewski, K. (2003). *Synthesis of polymer brushes using atom transfer radical polymerization*. Macromolecular Rapid Communication. 24. 1043–1059.

Haverkamp, R.G., Marshall, A. T. and Williams, M. A. K. (2007). *Model for stretching elastic biopolymers which exhibit conformational transformations*. Physical Review. 75.

Raghavan, D., VanLandingham, M., Gu, X. and Nguyen, T. (2000). *Characterization of heterogeneous regions in polymer systems using tapping mode and force mode Atomic Force Microscopy*. Langmuir. 16.9448-9459.

Reimhult, E., Larsson, C., Kasemo, B. (2004). *Simultaneous surface plasmon resonance and quartz crystal microbalance with dissipation monitoring measurements of biomolecular adsorption events involving structural transformations and variations in coupled water*. Analytical Chemistry. 76. 7211-7220.

Regan, L. (2003). *Molten globules move into action*. Proceeding of the National Academy of Sciences of the United States of America. 100. 3553-3554.

Roach, P., Farrar, D. and Perry, C.C. (2005). *Interpretation of protein adsorption:surface-induced conformational changes*. Journal American Chemical Society. 127. 8168-8173.

Roosjen, A., Mei, H.C., Busscher, H.J. and Norde, W. (2004). *Microbial adhesiaon to poly(ethylene oxide) brushes: Influence of polymer chain length and temperature*. Langmuir. 20. 10949-10955.

Rosmaninho, R., Santos, O., Nylander, T., Paulsson, M., Beuf, M., Benezech, T., Yiantsios, S., Andritsos, N., Karabelas, A., Rizzo, G., Steinhagen, H. M. and Melo, L. F. (2007). *Modified stainless steel surfaces targeted to reduce fouling –Evaluation of fouling by milk components*. Journal of Food Engineering. 80. 1176–1187.

Rundqvist, J., Hoh, J.H. and Haviland, D.B. (2005). *Poly(ethylene glycol) self-assembled monolayer island growth*. Langmuir. 21. 2981-2987.

Sakiyama, T., Tomura, J., Imamura, K. and Nakanishi, K. (2004). *Adsorption characteristics of bovine serum albumin and its peptide fragments on a stainless steel surface*. Colloids and Surfaces B: Biointerfaces. 33. 77-84.

Santos, O., Nylander, T., Rosmaninho, R. (2004). *Modified stainless steel surfaces targeted to reduce fouling - surface characterization*. Journal of Food Engineering. 64. 63-79.

Santos, O., Nylander, T., Rosmaninho, R., Rizzo, G., Yiantsios, S., N.Andritsos, Karabelas, A., M.Steinhagen, H., Melo, L., Petermann, L.B., Gabet, C., Braem, A., Tragardh, C. and Paulsson, M. (2006). *Modified stainless steel surfaces targeted to reduce fouling-surface characterization*. Journal of Food Enginering. 64. 63-79.

Satomi, T., Nagasaki, Y., Kobayashi, H., Tateishi, T., Kataoka, K. and Otsuka, H. (2007). *Physicochemical characterization of densely packed poly (ethylene glycol) layer for minimizing nonspecific protein adsorption*. Journal of Nanoscience and Nanotechnology. 7. 2394-2399.

Satulovsky, J., Carignano, M.A. and Szleifer, I. (2000). *Kinetic and thermodynamic control of protein adsorption*. Biophysics. 97. 9037-9041.

Schroen, C. G. P. H., Stuart, M. A. C., Maarschalk, K. V., Padt, T A. and Riet, K. (1995). *Influence of Preadsorbed Block Copolymers on Protein Adsorption: Surface Properties, Layer Thickness, and Surface Coverage*. Langmuir. 11. 3068-3074.

Seitz, R., Brings, R. and Gieger, R. (2005). *Protein adsorption on solid-liquid interfaces monitored by laser-ellipsometry*. Applied Surface Science. 252.154-157.

Sharma, S., Johnson, R.W., Desai, T.A. (2004). *XPS and AFM analysis of antifouling PEG interfaces for microfabricated silicon biosensors*. Biosensors and Bioelectronics. 20. 227-239.

Sharma, R., Johnson, W., and Desai, T.A. (2004). *Evaluation of the stability of nonfouling ultrathin poly(ethylene glycol) films for silicon-based microdevices.* Langmuir. 20. 348-356.

Shen, D., Huang, M., Chow, L. M. and Yang, M. (2001). *Kinetic profile of the adsorption and conformational change of lysozyme on self-assembled monolayers as revealed by quartz crystal resonator*. Sensors and Actuators B. 77. 664-670.

Shen, D.Z., Huang, M.H., Chow, L.M. (2001). *Kinetic profile of the adsorption and conformational change of lysozyme on self-assembled monolayers as revealed by quartz crystal resonator*. Sensors and Actuators B: Chemical. 77. 664-670.

Sheth, S.R. and Leckband, D. (1997). *Measuremnet of attractive forces between proteins and end-grafted poly (ethylene glycol) chains*. Applied Biological Sciences. 94. 8399-8404.

Silva, L.P. (2002). *Atomic force microscopy and proteins*. Protein and Peptide Letters. 9. 117-125.

Smith, J.M. and Van Ness, H.C. (1987). *Introduction to chemical engineering thermodynamics*. 4th edition. McGraw-Hill Book Company.

Snopok, B.A. and Kostyukevich, E.V. (2006). *Kinetic studies of protein–surface interactions: A two-stage model of surface-induced protein transitions in adsorbed biofilms*. Analytical Biochemistry. 348. 222–231.

Stalgren, J.J.R., Eriksson, J. and Boschkova, K. (2002). *A comparative study of surfaces using the quartz crystal microbalance and the ellipsometer*. Journal of colloid and interface science. 253.190-195.

Su, X.D., Wu, Y.J. and Knoll, W. (2005). *Comparison of surface plasmon resonance spectroscopy and quartz crystal microbalance techniques for studying DNA assembly and hybridization*. Biosensors and Bioelectronics. 21. 719-726.

Teixeiraa, P., Lopesb, Z., Azeredoa, J., Oliveiraa, R. and Vieira, M. J. (2005). *Physico-chemical surface characterization of a bacterial population isolated from a milking machine*. Food Microbiology .22.247–251.

Tiberg, F., Nylander, T., Su, T. J., Lu, J. R. and Thomas. R. K. (2001). *α-Casein Adsorption at the silicon oxide-aqueous solution interface*. Biomacromolecular. 844-850.

Uchida, K., Hoshino, Y., Tamura, A., Yoshimoto, K., Kojima, S., Yamashita, K., Yamanaka, I., Otsuka, H., Kataoka, K., and Nagasaki, Y. (2007). *Creation of a mixed poly(ethylene glycol) tethered-chain surface for preventing the nonspecific adsorption of proteins and peptides.* Biointerphases.2. 126-130.

Uchida, K., Otsuka, H., Kaneko, M., Kataoka, K. and Nagasaki, Y. (2005). *A reactive poly (ethylene glycol) layer to achieve specific surface plasmon resonance sensing with a high S/N: The substantial role of a short underbrushed PEG layer in minimizing nonspecific adsorption*. Analytical Chemistry. 77. 1075-1080.

Unsworth, L.D., Sheardown, H. and Brash, J.L. (2005). *Protein resistance of surfaces prepared by sorption of end-thiolated poly(ethylene glycol) to gold:Effect of surface chain density*. Langmuir. 21. 1036-1041.

Unsworth, L.D., Tun, Z., Sheardown, H. and Brash, J.L. (2008). *In situ neutron relectrometry investigation of gold-chemisorbed PEO layers of varying chain density: Relationship of layer structure to protein resistance.* Journal of Colloid and Interface Science. 296. 520-526.

Van Tassel, P. R. (2003). *Statistical mechanical modeling of protein adsorption*. Mat.wiss. u. Werkstofftech. 34. 1129-1132.

Van Tassel, P.R., Guemouri, L., Ramsden, J.J., Tarjus, G., Viot, P. and Talbot, J. (1998). *A particle-level model of irreversible protein adsorption with a postadsorption transition*. Journal of Colloid and Interface Science. 207. 317-323.

Vanderah, D. J., Walker, M. L., Rocco, M. A. and Rubinson, K. A. (2008). *Self-assembled monolayers of an oligo(ethylene oxide) disulfide and its corresponding thiol assembled from water: Characterization and protein resistance*. Langmuir. 24. 826-829.

Vasquez, M., Nemethyt, G. and Scheraga H.A. (1994). *Conformational energy calculations on polypeptides and proteins*. Chemical Review. 94. 2183–2239.

Veen, M. V. D., Cohen Stuart, M. and Norde, W. (2007). *Spreading of proteins and its effect on adsorption and desorption kinetics*. Colloids and Surfaces B: Biointerfaces. 54,136–142.

Visser, J. and Jeurnink, T.J.M. 1(997). *Fouling of heat exchangers in the dairy industry*. Experimental Thermal and Fluid Science. 14. 407-424.

Vogler E.A, Martin D.A, Montgomery D.B, Graper J, and Sugg H.W. (1993). *A graphical method for predicting protein and surfactant adsorption properties*. Langmuir. 9. 497-507.

Vogler E.A. (1992a). *Practical use of concentration-dependent contact angles as a measure of solid–liquid adsorption. I. Theoretical aspects*. Langmuir. 8. 2005-2012.

Vogler E.A. (1992b). *Practical use of concentration-dependent contact angles as a measure of solid–liquid adsorption. II. Experimental aspects*. Langmuir. 8. 2013-2020.

Vogler E.A. (1993). *Interfacial chemistry in biomaterials science*. Surfactant Science Series. 49. 184–250.

Vogler E.A. (1998). *Structure and reactivity of water at biomaterial surfaces*. Advanced Colloid Interface Science. 74. 69-117.

Vogler E.A. (2001). *How water wets biomaterials*. In: Morra M, editor. Water in biomaterials surface science. Wiley; New York: 269–290.

Voros, J. (2004). *The density and reflective index of adsorbing protein layers*. Biophysical society. 87. 553-561.

Wang, M.S., Palmer, L.B., Schwartz, J.D. (2004). *Evaluating protein attraction and adhesion to biomaterials with the atomic force microscope*. Langmuir. 20. 7753-7759.

Wang, R.L.C., Kreuzer , H.J. and Grunze, M. (1997). *Molecular conformation and solvation of oligo(ethylene glycol)-terminated self-assembled monolayers and their resistance to protein adsorption*. Journal of Physical Chemistry B. 101. 9767-9773.

Wang, Y., Somers, E.B., Manolache, S. (2003). *Cold plasma synthesis of poly(ethylene glycol)-like layers on stainless-steel surfaces to reduce attachment and biofilm formation by Listeria monocytogenes*. Journal of Food Science. 68. 2772-2779.

Wegener, J., Janshoff, A. and Steinem, C. (2001). *The quartz crystal microbalance as a novel means to study cell-substrate interactions in situ*. Cell Biochemistry and Biophysics. 34. 121-151.

Wei, J., Ravn, D.B., Gram, L. and Kingshott, P. (2003). *Stainless Steel modified with PEG can prevent protein adsorption but not bacterial adhesion*. Colloids and Surfaces B:Biointerfaces 32. 275-291.

Wertz, C.F. and Santore, M.M. (2002). *Adsorption and reorientation kinetics of lysozyme on hydrophobic surfaces.* Langmuir. 18. 1190-1199.

Wu, Y.J., Timmons, R.B.,.Jen, J.S and Molock, F.E. (2000). *Non-fouling surfaces produced by gas phase pulsed plasma polymerization of an ultra low molecular weight ethylene oxide containing monomer*. Colloids and surfaces B: Biointerfaces. 18.235-248.

Yang, L.M.C., Diaz, J.E., McIntire,T.M., Weiss, G.A., and Penner, R.M. (2008). *Covalent virus layer for mass-based biosensing*. Analytical Chemistry. 80. 933-943.

Yang. Z., Galloway, J.A. and Yu, H. (1999). *Protein interactions with poly(ethylene glycol) self-assembled monolayers on glass substrates: diffusion and adsorption*. Langmuir. 15. 8405-8411.

Yoshikawa, C., Goto, A., Tsujii, Y., Fukuda, T., Kimura, T., Yamamoto, K. and Kishida, A. (2006). *Protein repellency of well-defined, concentrated poly(2-hydroxyethyl methacrylate) brushes by the size exclusion effect*. Macromolecules. 2284-2290.

Yeh, P.Y.J., Kizhakkedathu, J.N., Madden, J.D. and Chiao, M. (2007). *Electric field and vibration-assisted nanomolecule desorption and anti-biofouling for biosensor applications*. Colloids and Surface B: Biointerfaces. 59. 67-73.

Yeh, P.Y.J., Kizhakkedathu, J.N., Madden, J.D. and Chiao, M. (2008). *An investigation of vibration-induced protein desotpion mechanism using a micromachined membrane and PZT plate*. Biomedical Microdevices. 10. 701-708.

Zhang, D. and Ortiz, C. (2004). *Synthesis and single molecule force spectroscopy of graft copolymers of poly(2-hydroxyethyl methacrylate-g-ethylene glycol).* Macromolecules. 37.4271-4282.

Zhang, F., Kang, E.T., Neoh, K.G., Wang, P. and Tan, K.L. (2001). *Surface modification of stainless steel by grafting of PEG for reduction in protein adsorption*. Biomaterials. 22. 1541-1548.

Zhao, Q. and Muller-Steinhagen, H. (2001). *Intermolecular and adhesion forces of deposits on modified heat transfer surfaces*. In Proceedings of the heat exchanger fouling, fundamental approaches and technical solutions conference, Davos, Switzerland.

Zhao, Y.L., Chen, Y.M., Chen, C.F. (2005). *Synthesis of well-defined star polymers and star block copolymers from dendrimer initiators by atom transfer radical polymerization*. Polymer. 26. 5808-5819.

Zhdanov, V.P. and Kasemo, B. (1998). *Monte Carlo simulation of the kinetics of protein adsorption.* PROTEINS: Structure, Function and Genetics. 30. 177-182.

Zheng, J., Lingyan, L., Tsao, H.K., Sheng, Y.J., Chen, S. and Jiang, S. (2005). *Strong repulsive forces between protein and oligo(ethylene glycol) self-assembled monolayers. A molecular simulation study*. Biophysical Journal. 89.158-166.

Zhou, C., Friedt, J.M., Angelova, A. (2004). *Human immunoglobulin adsorption investigated by means of quartz crystal microbalance dissipation, atomic force microscopy, surface acoustic wave, and surface plasmon resonance techniques.* Langmuir. 20. 5870-5878.

Zhou, Y., Liedberg, B., Gorochovceva, N., Makuska, R., Dedinaite, A., Claesson, P.M. (2007). *Chitosan-N-poly(ethylene oxide) brush polymers for reduced nonspecific protein adsorption*. Journal of Colloid and Interface Science. 305. 62-71.

Zhu, B., Eurell, T., Gunawan, R. and Leckband, D. (2001). *Chain length dependence of the protein and cell resistance of oligo(ethylene glycol)-terminated self-assembled monolayers on gold*. Journal of Biomedical Material Research. 56.406-416.

Zhuang, H., Lu, P., Lim, S.P. (2008). *Effects of interface slip and viscoelasticity on the dynamic response of droplet quartz crystal microbalances.* Analytical Chemistry. 80. 7347-7353.

Zong, Y., Xu, F., Su, X.D. (2008). *Quartz crystal microbalance with integrated surface plasmon grating coupler*. Analytical Chemistry. 80. 5246-5250.

Zdyrko,B.,Varshney, K. and Luzinov, I. (2004). *Effect of molecular weight on synthesis and surface morphology of high-density poly(ethylene glycol) grafted layers*. Langmuir. 20. 6727-6735.

APPENDIX A

QCM-D EXPERIMENT

Initial adsorption rate of proteins on bare SS surfaces

Table A.1: Initial adsorption rate (within *10 seconds* of adsorption) and r^2 for the slope of β-casein, α- lactalbumin and lysozyme on bare stainless steel surfaces under all the experimental conditions. Based on [O.Santos et al, 2006 and S.Mutlu et al, 2007].

		β-casein		α-lactalbumin		lysozyme	
Concentration (mg/ml)	temperature	initial rate ($mg/m^2.s$)	r^2	initial rate ($mg/m^2.s$)	r^2	initial rate ($mg/m^2.s$)	r^2
0.1	23°C	0.1765	0.9969	0.0839	0.9706	0.0200	0.8966
	30°C	0.2807	0.9997	0.0884	0.9642	0.0495	0.9331
	35°C	0.3311	0.9956	0.0995	0.9918	0.0582	0.9598
	40°C	0.3777	0.9738	0.1706	0.9961	0.1028	0.9783
0.5	23°C	0.5070	0.9773	0.0992	0.9992	0.1631	0.8978
	30°C	0.6295	0.9702	0.1567	0.9471	0.1814	0.9935
	35°C	0.9291	0.8385	0.2686	0.9684	0.2657	0.9914
	40°C	0.9701	0.6310	0.2836	0.9619	0.3657	0.9065
1.0	23°C	0.7035	0.9929	0.9875	0.9916	0.2433	0.9941
	30°C	1.8296	0.9656	1.1422	0.9911	0.2794	0.9275
	35°C	2.4776	0.9561	1.3248	0.9962	0.3604	0.9885
	40°C	3.0819	0.9697	1.3615	0.9481	0.4073	0.9757

Time to reach saturation on a bare SS

Table A.2: Approximate time of β-casein, lysozyme and α-lactalbumin to reach a saturation on a bare SS surface under extreme experimental conditions.

Sample	Temperature (°C)	Concentration (g / L)	Time to reach plateau (min)
β-casein	23 40	0.1 1.0	≅ 5 ≅ <1
Lysozyme	23 40	0.1 1.0	≅ 180 ≅ 130
α-lactalbumin	23 40	0.1 1.0	≅ 30 ≅ 2

Effects of temperature and concentration on fitted shear viscosity of proteins (β-casein, lysozyme and α-lactalbumin) layer on a bare SS surface

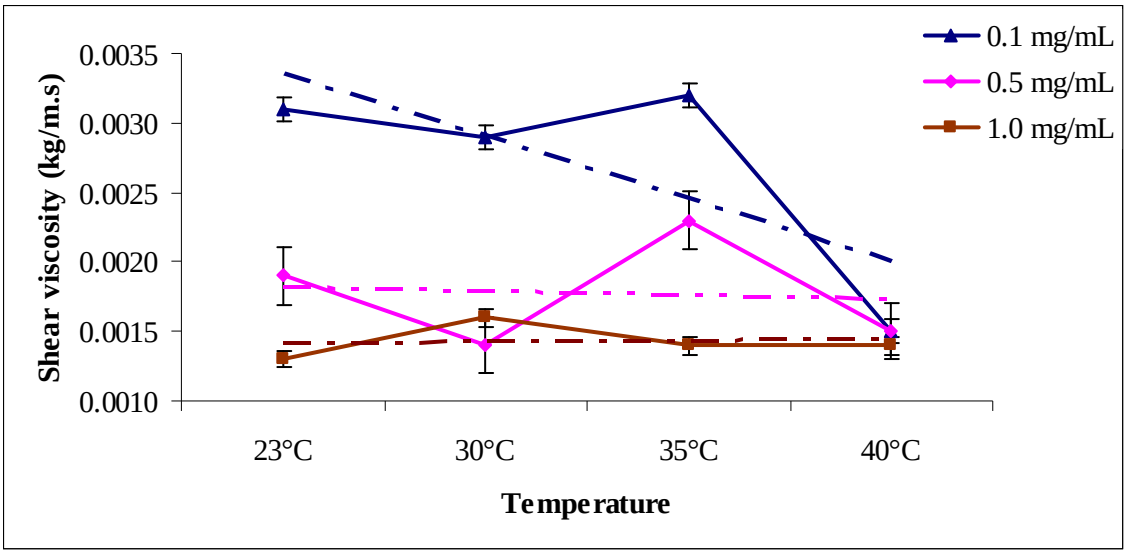

Figure A.1: Fitted shear viscosity of β-casein layer at a plateau desorption (tightly-bound) under all the experimental conditions modeled using the Voigt model. The lines were drawn as a guide for the eyes.

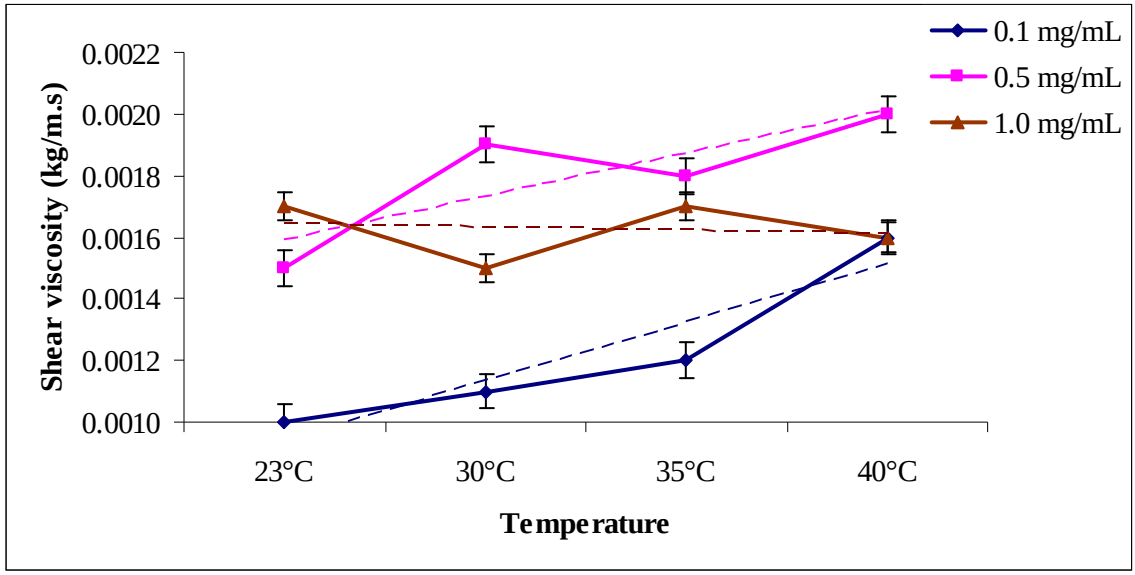

Figure A.2: Fitted shear viscosity of lysozyme layer at a plateau desorption (tightly-bound) under all the experimental conditions modelled using the Voigt model. The lines were drawn as a guide for the eyes.

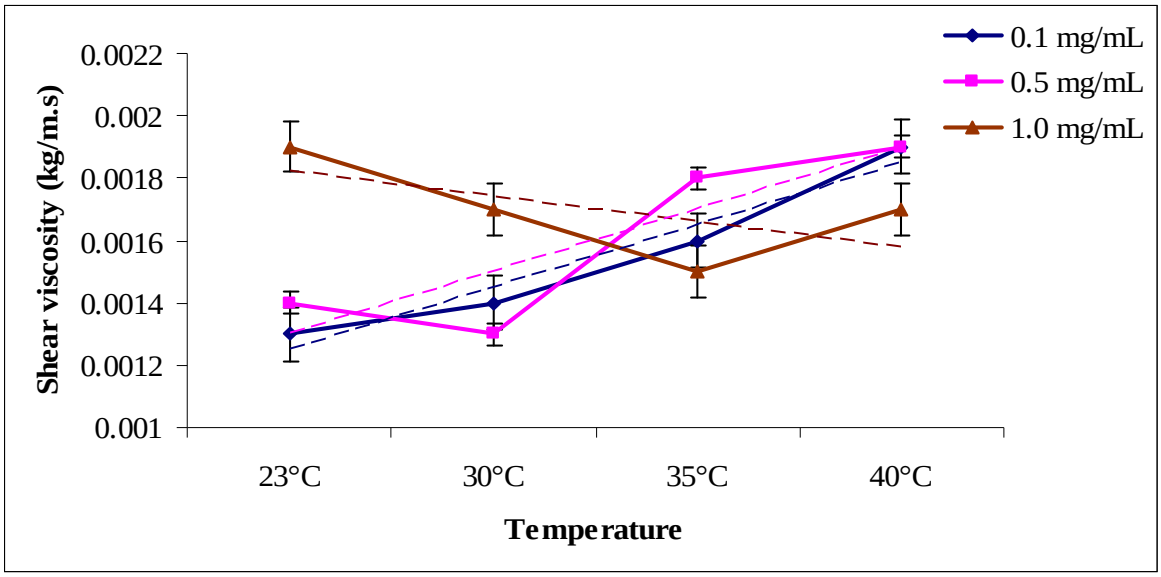

Figure A.3: Fitted shear viscosity of α-lactalbumin layer at a plateau desorption (tightly-bound) under all the experimental conditions modelled using the Voigt model. The lines were drawn as a guide for the eyes.

SAUERBREY MODEL

Mass surface density of proteins ((β-casein, lysozyme and α-lactalbumin) on a bare SS surface calculated using the Sauerbrey model.

It has been show in this study that the Voigt model was more accurate to interpret the data than the Sauerbrey model. Figures A.4 to A.12 show the mass surface density, number molecules density and mean layer thickness of β-casein, lysozyme and apo α-lactalbumin adsorbed on a bare SS surface calculated using the Sauerbrey model.

β-casein

The comparison of the two models (the Voigt and Sauerbrey models) revealed that the Sauerbrey model underestimated the Voigt model by 30 to 60 % of mass density, 22 to 52 % of layer thickness and 55 to 75 % of number molecules adsorbed (refer to Figures A.4 to A.6 for the Sauerbrey model and Chapter 6 for the Voigt model) .

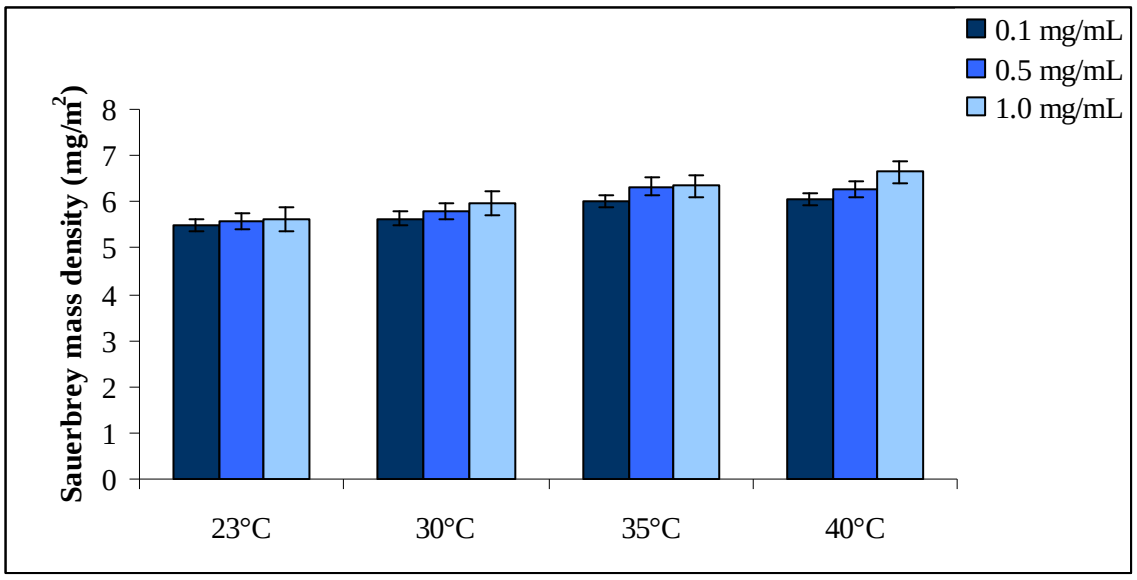

Figure A.4: Mass density of tightly-bound β-casein adsorbed on a stainless steel surface as a function of temperature an concentration calculated using the Sauerbrey model.

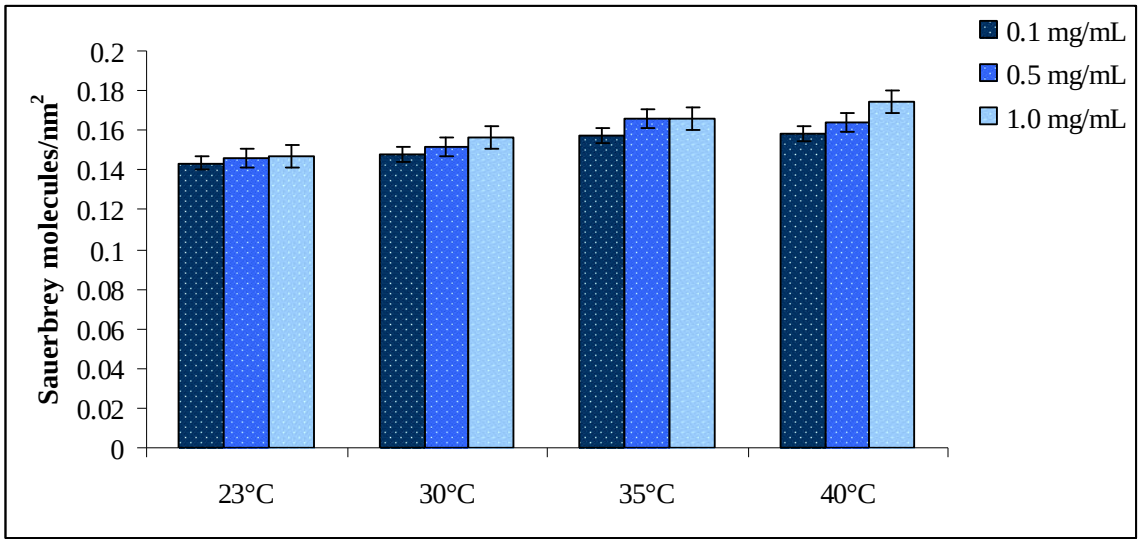

Figure A.5: Number density of tightly–bound β-casein molecules adsorbed on a stainless steel surface calculated using the Sauerbrey model.

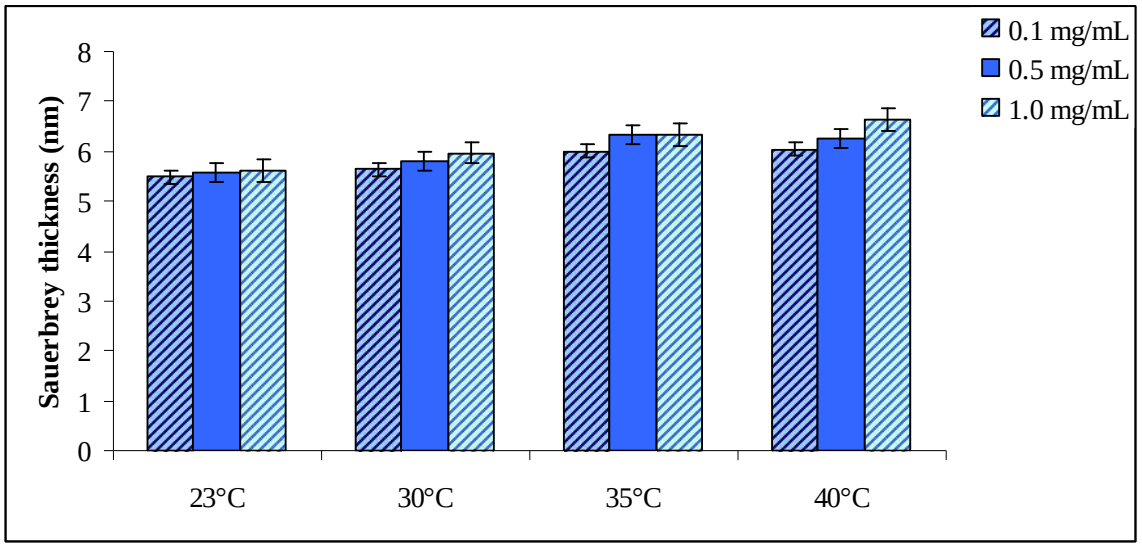

Figure A.6: Mean layer thickness of tightly–bound β-casein on a stainless steel surface calculated using the Sauerbrey model.

Lysozyme

The comparison of the two models (the Voigt and Sauerbrey models) revealed that the Sauerbrey model underestimated the Voigt model by 50 to 70 % of mass density, 70 to 74 % of mean layer thickness and 40 to 50 % of number molecules adsorbed (refer to Figures A.7 to A.9 for the Sauerbrey model and Chapter 6 for the Voigt model) .

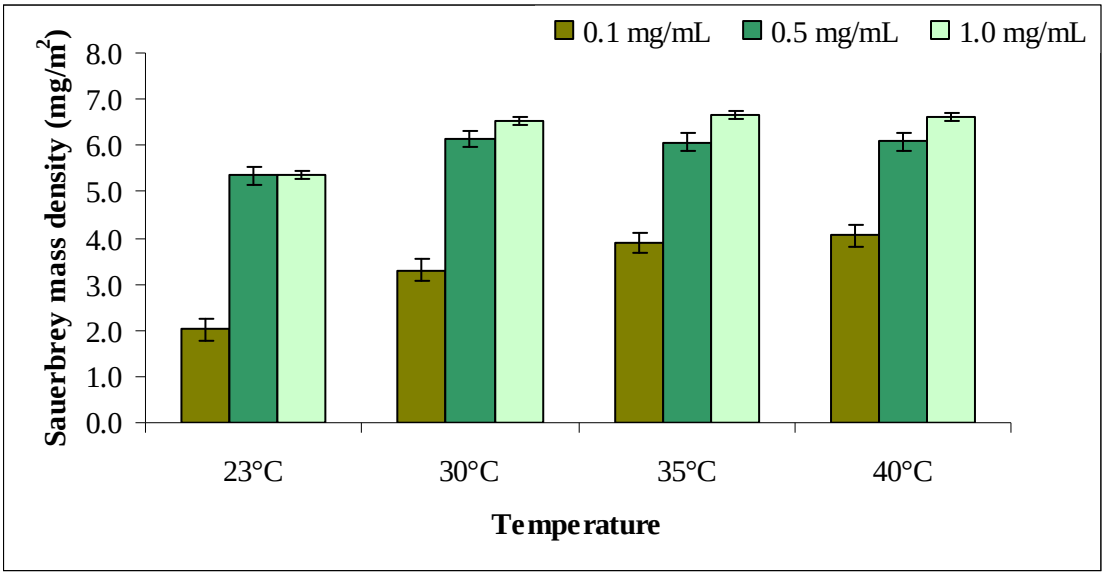

Figure A.7: Mass density of tightly-bound lysozyme adsorbed on a stainless steel surface as a function of temperature an concentration calculated using the Sauerbrey model.

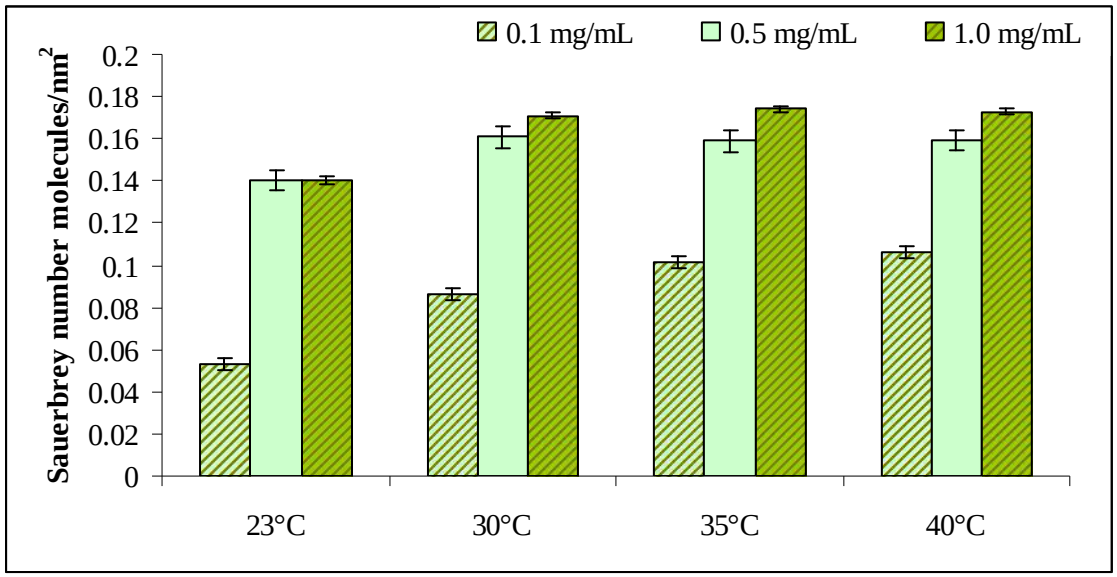

Figure A.8: Number density of tightly–bound lysozyme molecules adsorbed on a stainless steel surface calculated using the Sauerbrey model.

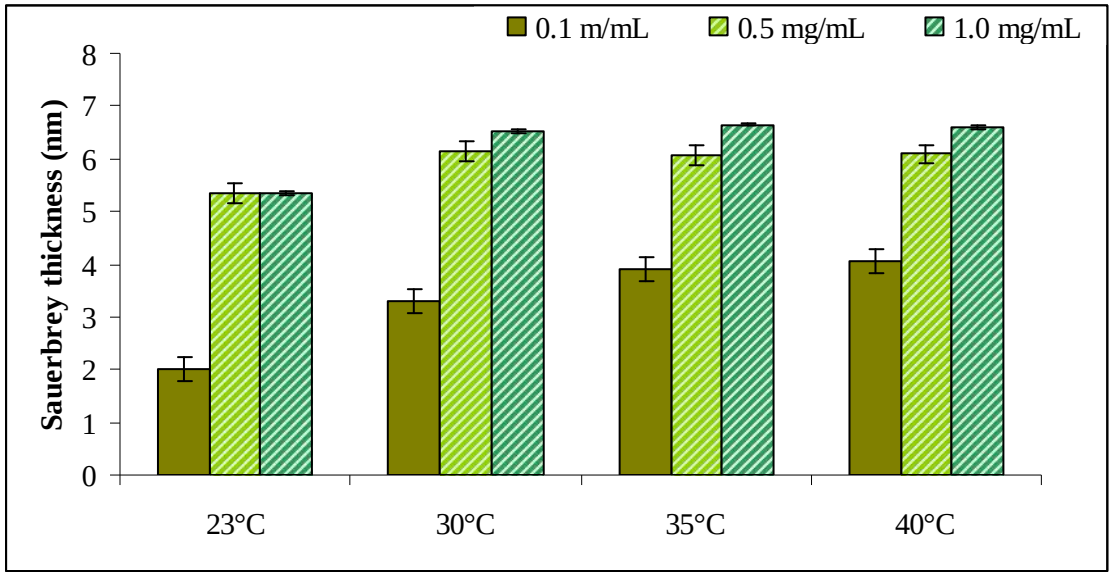

Figure A.9: Mean layer thickness of tightly–bound lysozyme on a stainless steel surface calculated using the Sauerbrey model.

α-lactalbumin

The comparison of the two models (the Voigt and Sauerbrey models) revealed that Sauerbrey equation underestimated the Voigt model by 30 to 60 % of mass density, 22 to 52 % of mean layer thickness and 55 to 75 % of number molecules adsorbed (refer to Figures A.10 to A.12 for the Sauerbrey model and Chapter 6 for the Voigt model).

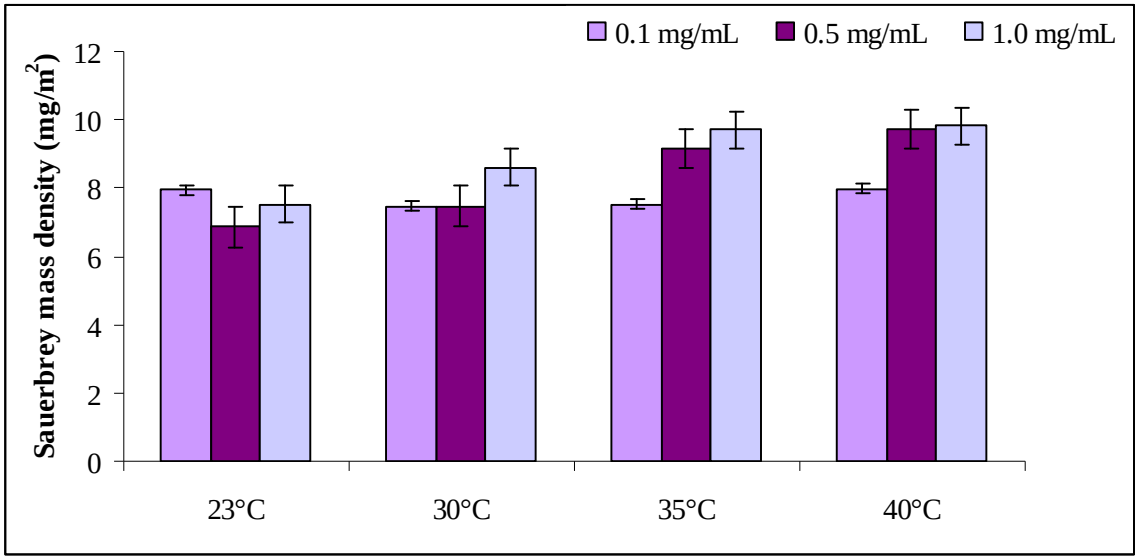

Figure A.10: Mass density of tightly-bound α-lactalbumin adsorbed on a stainless steel surface as a function of temperature and concentration calculated using the Sauerbrey model.

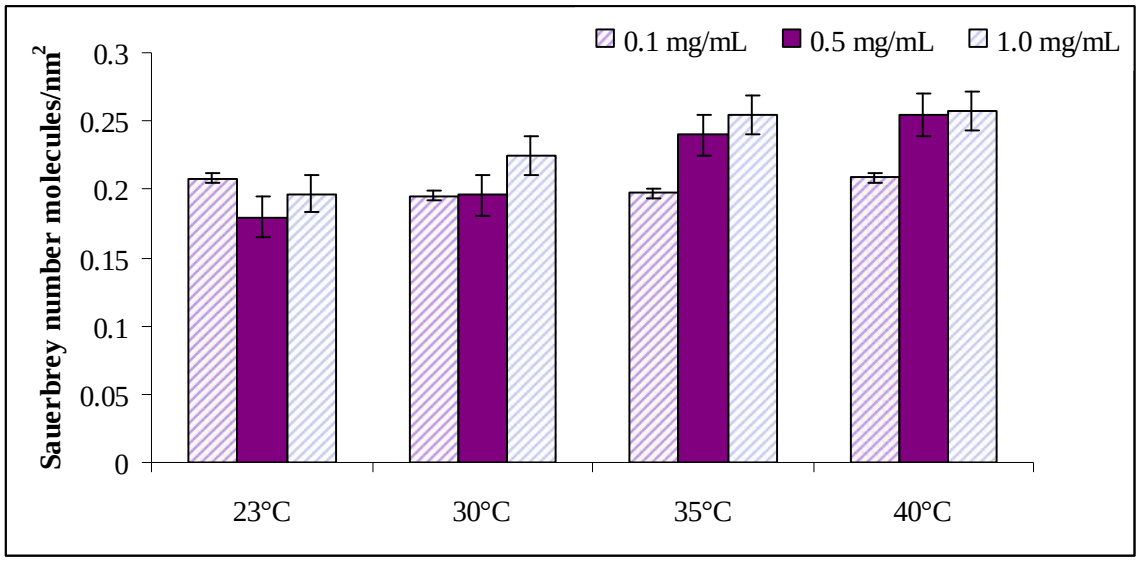

Figure A.11: Number density of tightly–bound α-lactalbumin molecules adsorbed on a stainless steel surface calculated using the Sauerbrey model.

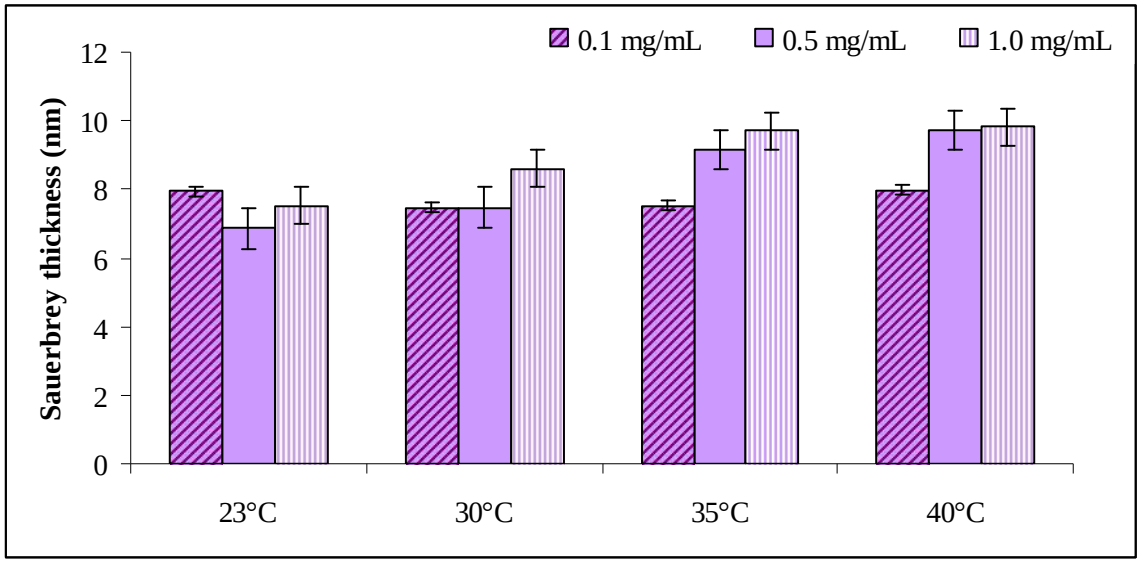

Figure A.12: Mean layer thickness of tightly–bound α-lactalbumin on a stainless steel surface calculated using the Sauerbrey model.

PEG number density on SS-PEI surfaces interpreted using the Sauerbrey model

Figure A.13 shows the tightly-bound PEG molecules on the stainless steel surface coated with a PEI layer calculated using the Sauerbrey model. Generally, there was no much difference in the trend of PEG number density with the respect of PEG molecular weights and bulk concentrations; the number density increased as concentration increased and vice versa with PEG molecular weight. The comparison of the two models (the Voigt and Sauerbrey models) revealed that the Sauerbrey model underestimated the Voigt model more than 90 % (refer to chapter 6 for the data interpreted using the Voigt model).

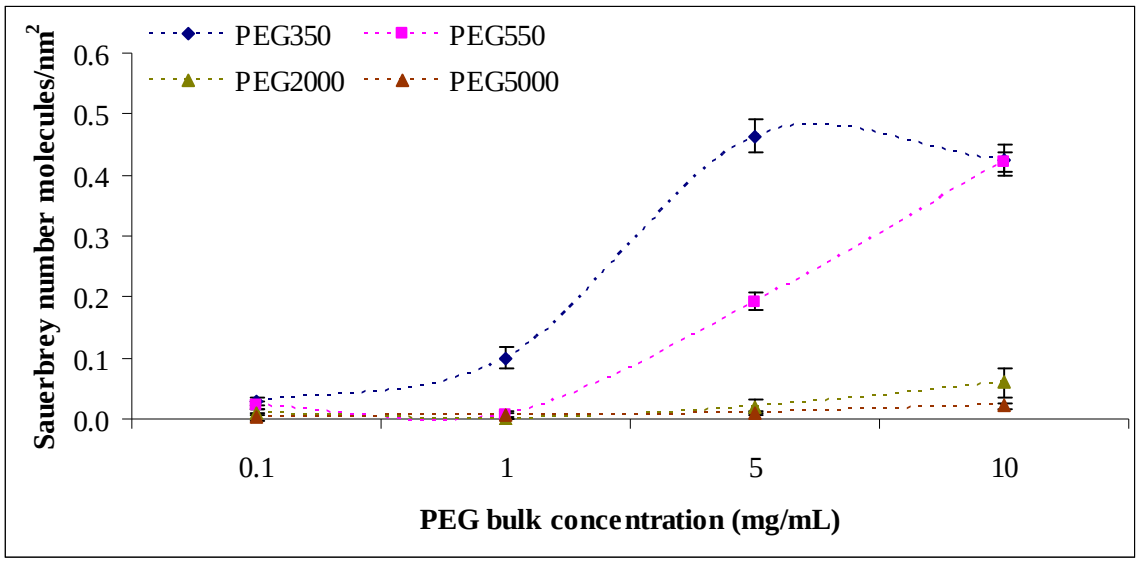

Figure A.13: Number density of tightly–bound PEG molecules on PEI coated stainless steel surfaces as a function of PEG molecular weight and concentration. The experiment was conducted at temperature of 23 °C. The data was obtained using the Sauerbrey model.

APPENDIX B

SURFACE REACTION MODEL

SURFACE REACTION MODEL

Shown below is all the fitting results obtained for each surface reaction model proposed in this study.

Extended Langmuir model (partly irreversible adsorption)

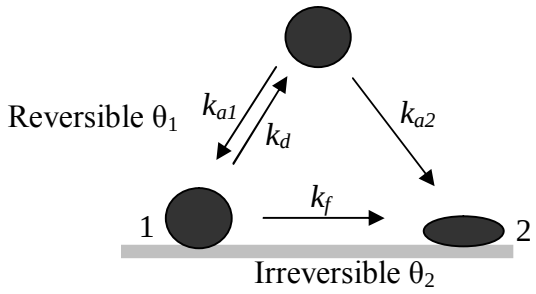

Figure B.1: Schematic diagram of the extended Langmuir model (partly irreversible adsorption)

$$\frac{d\theta_1}{dt} = k_{a1}C_0\left(1-\theta_1-\theta_2\right)-\left(k_d+k_f\right)\theta_1 \qquad \text{(B.1)}$$

$$\frac{d\theta_2}{dt} = k_{a2}C_0\left(1-\theta_1-\theta_2\right)+k_f\theta_1 \qquad \text{(B.2)}$$

k_{a1}, k_d, k_f, k_{a2} were taken as parameters to be fitted.

β-casein

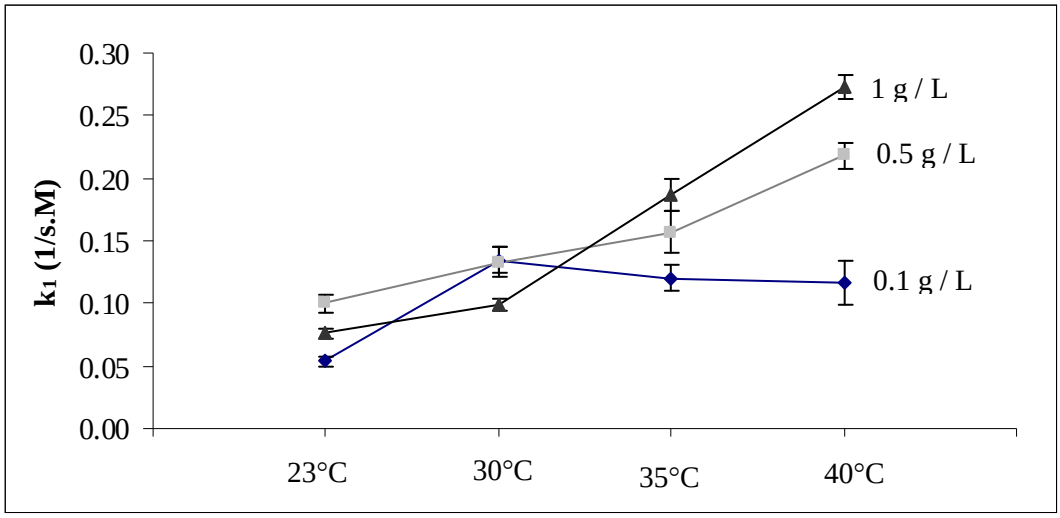

Figure B.2: Fitted k_1 as a function of temperature and concentration of β-casein in the solution modeled using an extended Langmuir model (partly irreversible adsorption).

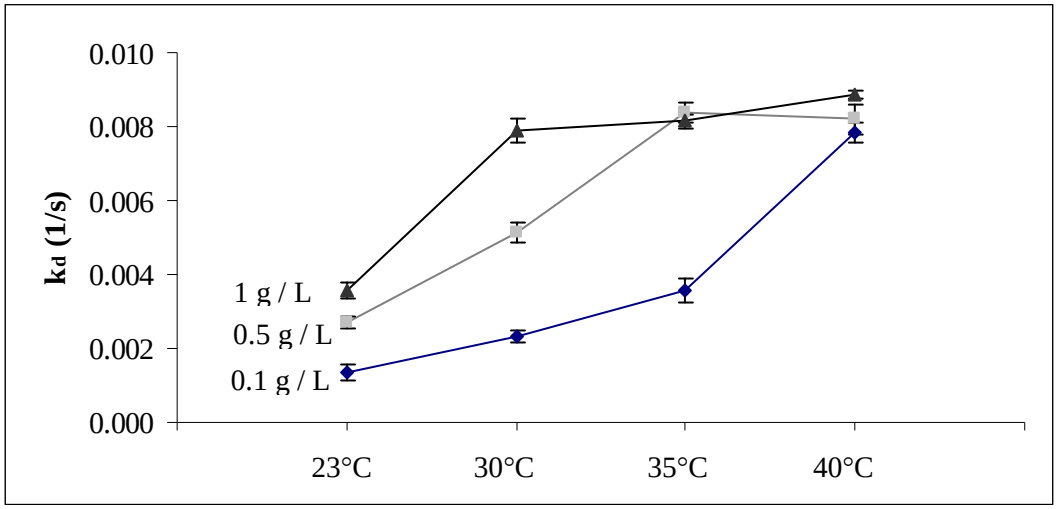

Figure B.3: Fitted k_d, as a function of temperature and concentration of β-casein in the solution modeled using an extended Langmuir model (partly irreversible adsorption).

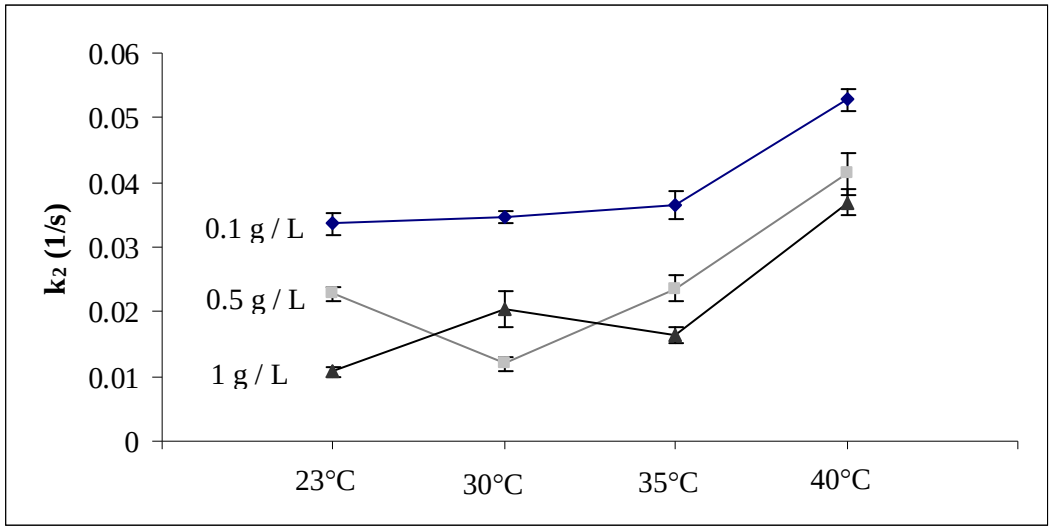

Figure B.4: Fitted k_2 as a function of temperature and concentration of β-casein in the solution modeled using an extended Langmuir model (partly irreversible adsorption).

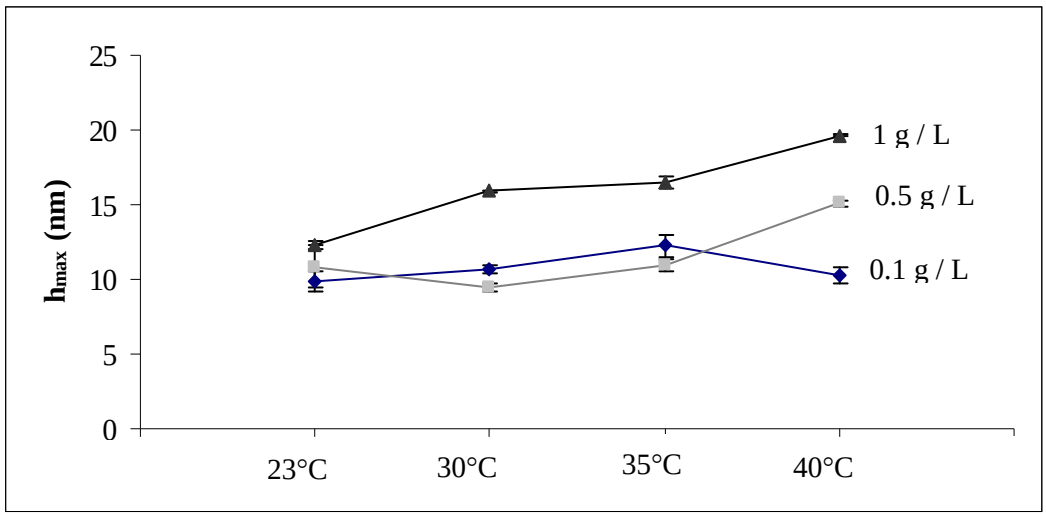

Figure B.5: Fitted h_{max} as a function of temperature and concentration of β-casein in the solution modeled using an extended Langmuir model (partly irreversible adsorption).

Lysozyme

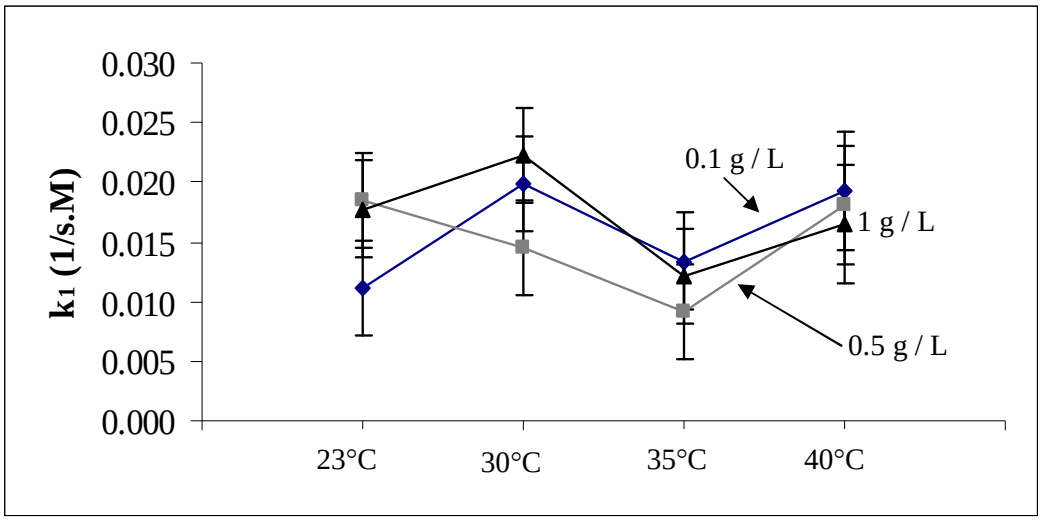

Figure B.6: Fitted k_1 as a function of temperature and concentration of lysozyme in the solution modeled using an extended Langmuir model (partly irreversible adsorption).

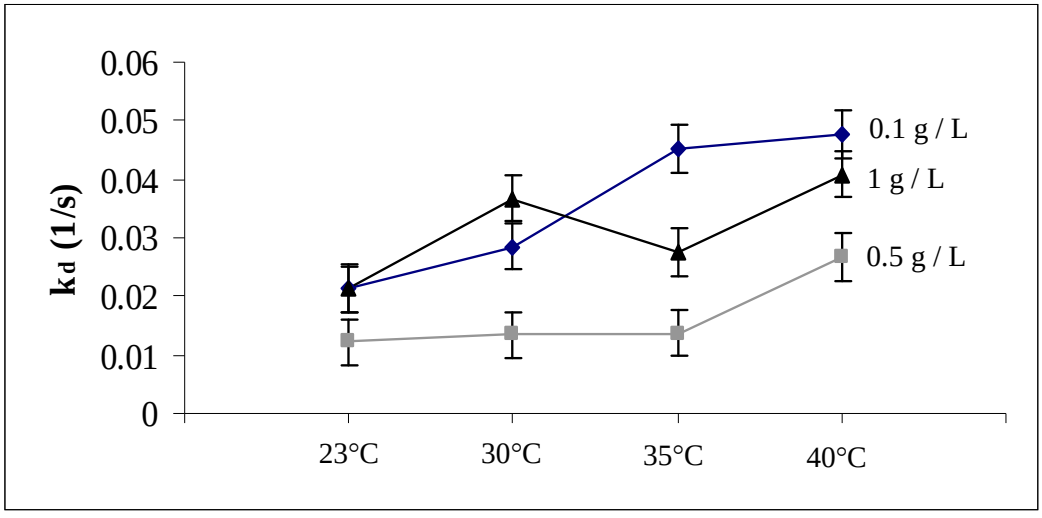

Figure B.7: Fitted k_d, as a function of temperature and concentration of lysozyme in the solution modeled using an extended Langmuir model (partly irreversible adsorption).

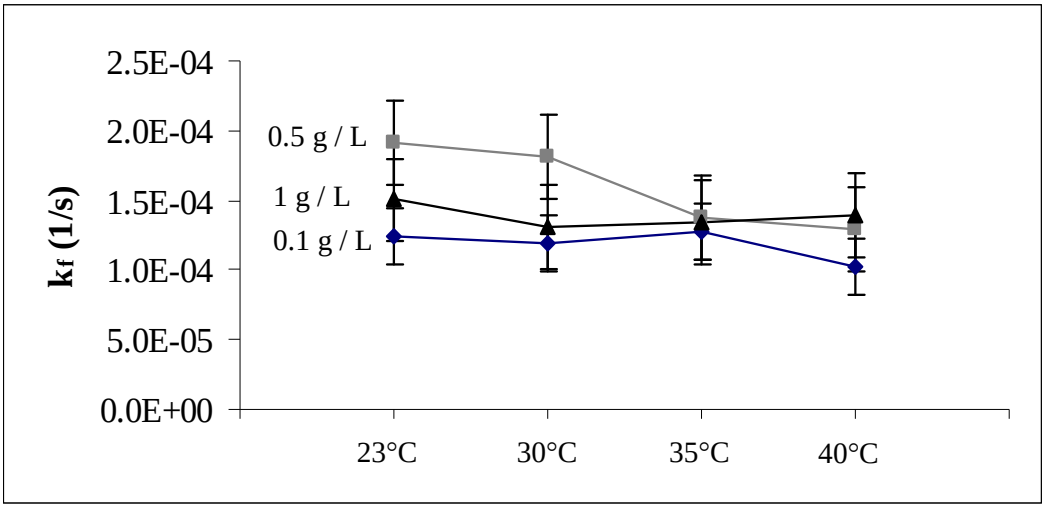

Figure B.8: Fitted k_f as a function of temperature and concentration of lysozyme in the solution modeled using an extended Langmuir model (partly irreversible adsorption).

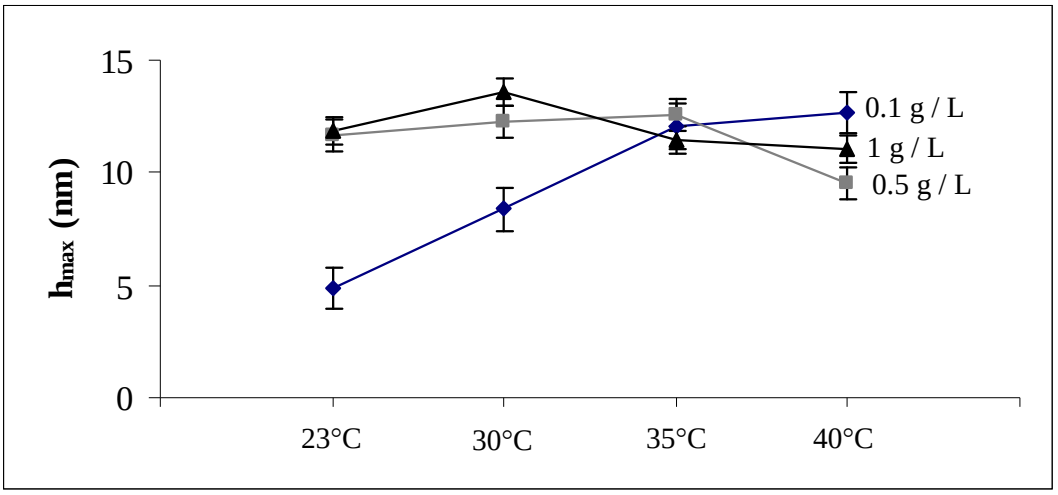

Figure B.9: Fitted h_{max} as a function of temperature and concentration of lysozyme in the solution modeled using an extended Langmuir model (partly irreversible adsorption).

α-lactalbumin

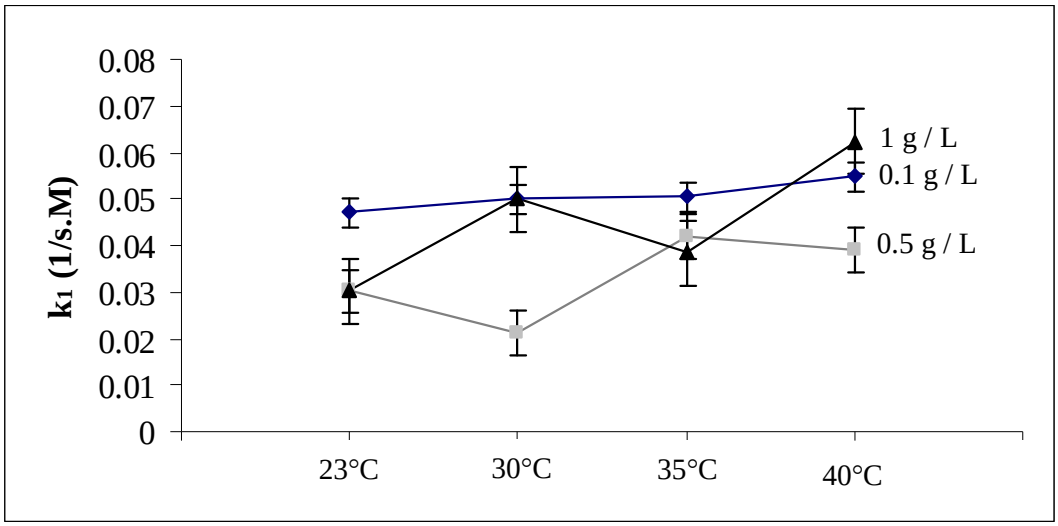

Figure B.10: Fitted k_1 as a function of temperature and concentration of α-lactalbumin in the solution modeled using an extended Langmuir model (partly irreversible adsorption).

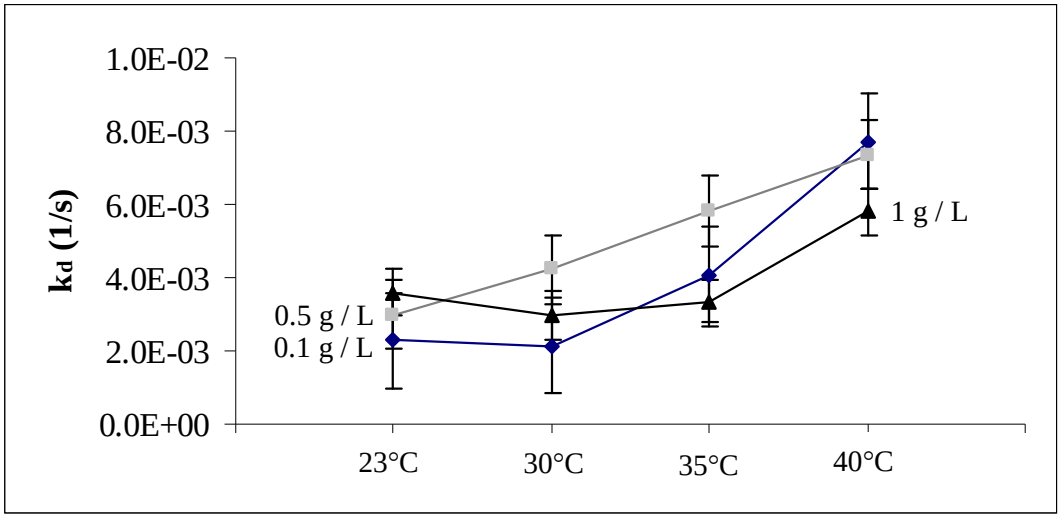

Figure B.11: Fitted k_d as a function of temperature and concentration of α-lactalbumin in the solution modeled using an extended Langmuir model (partly irreversible adsorption).

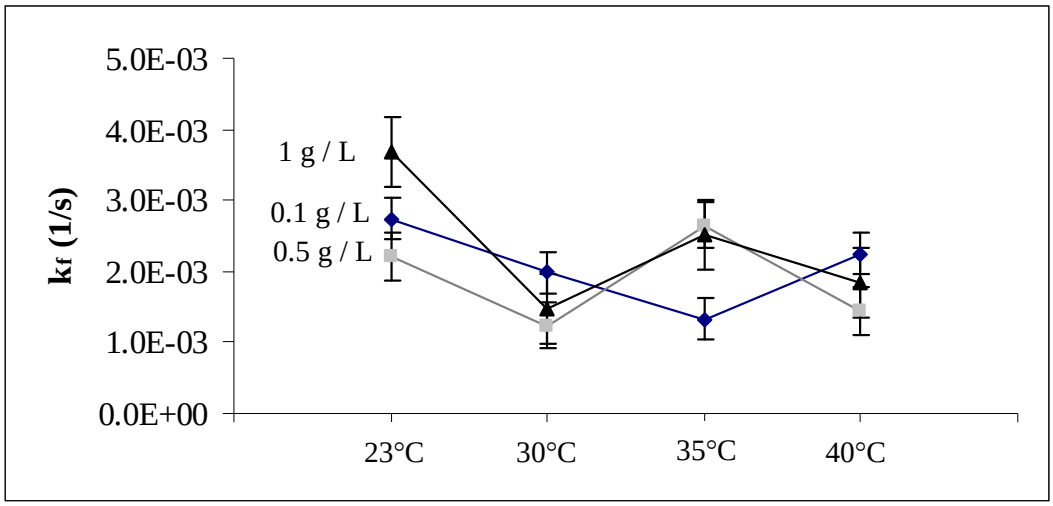

Figure B.12: Fitted k_f as a function of temperature and concentration of α-lactalbumin in the solution modeled using an extended Langmuir model (partly irreversible adsorption).

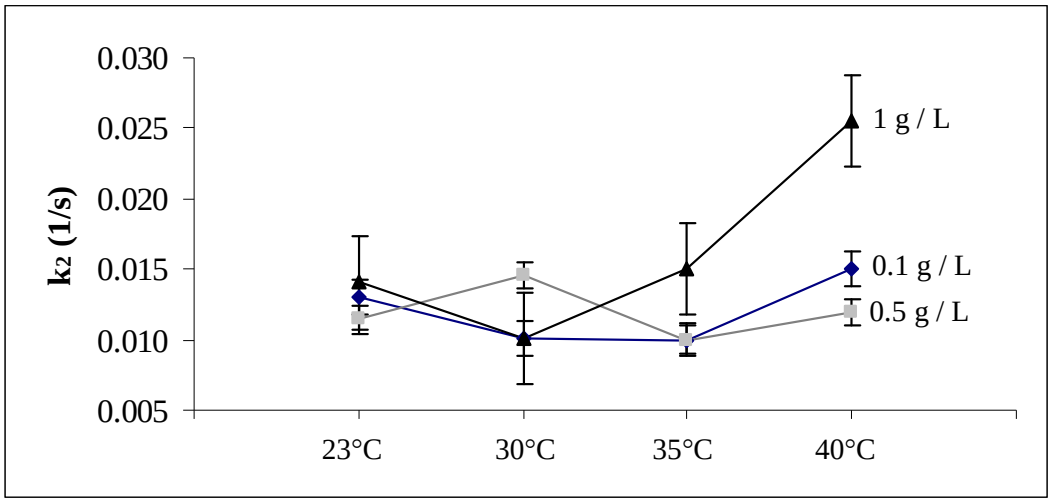

Figure B.13: Fitted k_2 as a function of temperature and concentration of α-lactalbumin in the solution modeled using an extended Langmuir model (partly irreversible adsorption).

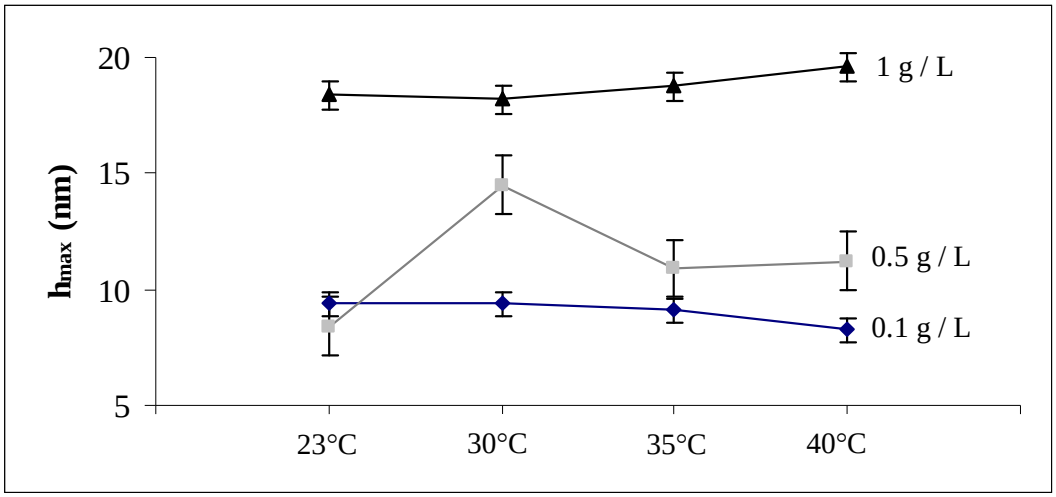

Figure B.14: Fitted h_{max} as a function of temperature and concentration of α-lactalbumin in the solution modeled using an extended Langmuir model (partly irreversible adsorption).

Extended Langmuir model with free reversibility

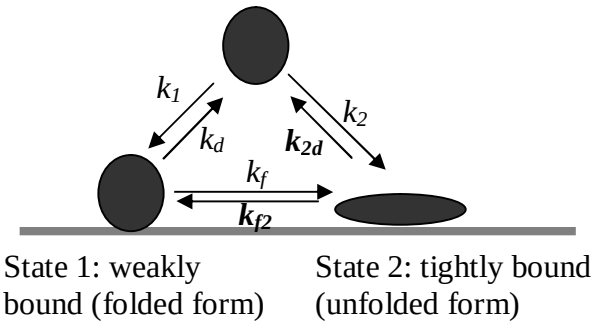

Figure B.15: Schematic diagram of the extended Langmuir model with free reversibility

$$\frac{\Delta\theta_1}{\Delta t} = k_1 C_O\left(1-\theta_1-a\theta_2\right)-\left(k_d\right)\theta_1 - k_f\theta_1\left(1-\theta_1-a\theta_2\right)/a + k_{f_2}\theta_2\left(1-\theta_1-a\theta_2\right) \qquad \text{(B.3)}$$

$$\frac{\Delta\theta_1}{\Delta t} = k_1 C_O\left(1-\theta_1-a\theta_2\right)-\left(k_d\right)\theta_1 - k_f\theta_1\left(1-\theta_1-a\theta_2\right)/a + k_{f_2}\theta_2\left(1-\theta_1-a\theta_2\right) \qquad \text{(B.4)}$$

k_1, k_d, k_f, k_{f2}, k_2, k_{2d}, and a were taken as parameters to be fitted.

β-casein

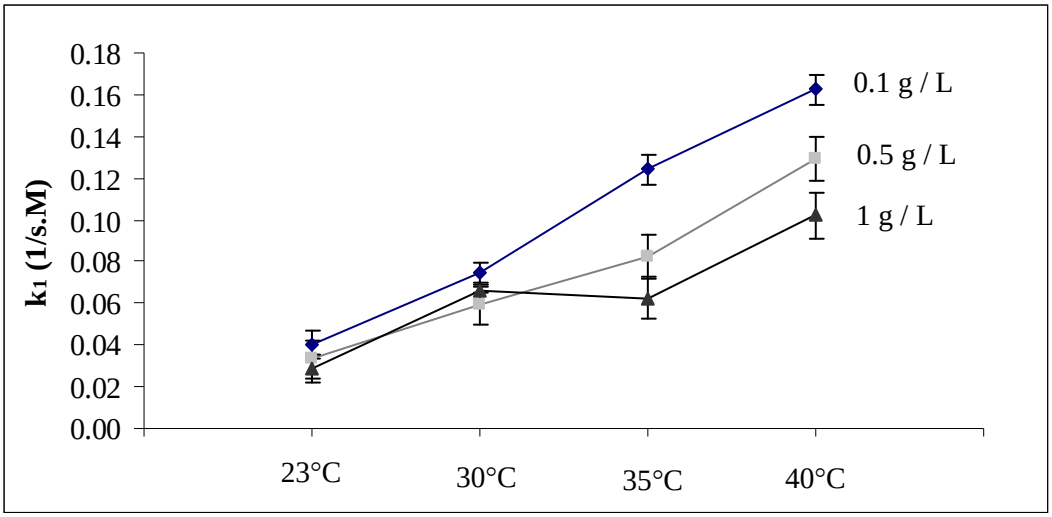

Figure B.16: Fitted k_1 as a function of temperature and concentration of β-casein in the solution modeled using an extended Langmuir model with free reversibility.

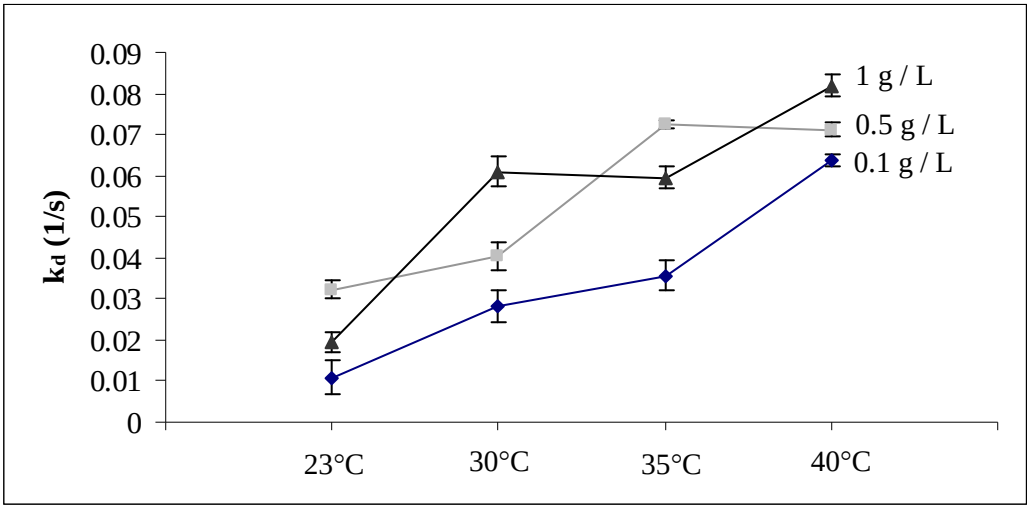

Figure B.17: Fitted k_d as a function of temperature and concentration of β-casein in the solution modeled using an extended Langmuir model with free reversibility.

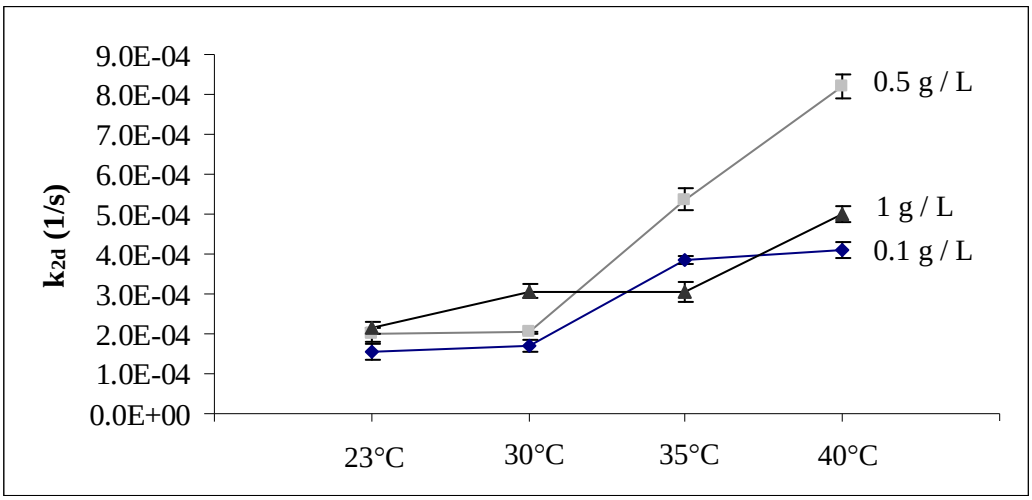

Figure B.18: Fitted k_{2d} as a function of temperature and concentration of β-casein in the solution modeled using an extended Langmuir model with free reversibility.

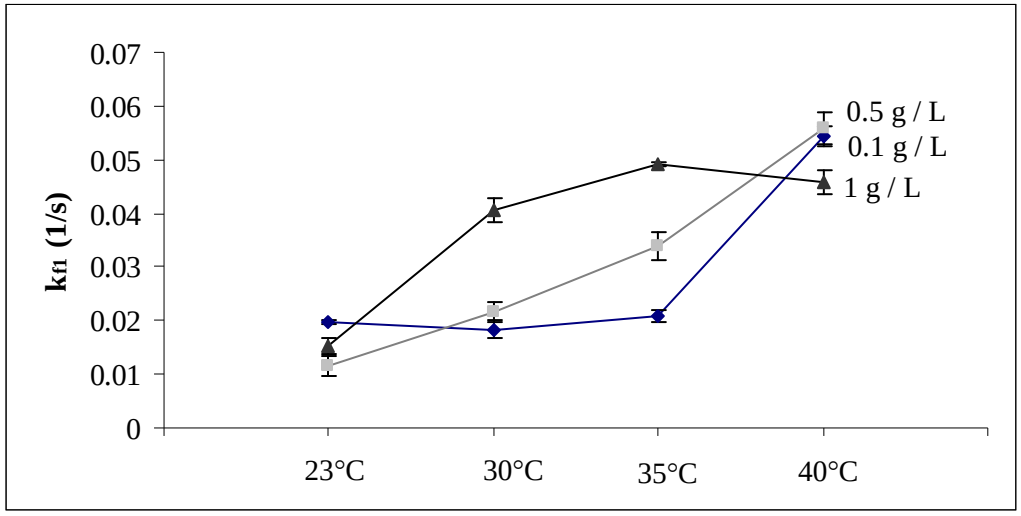

Figure B.19: Fitted k_{fl} as a function of temperature and concentration of β-casein in the solution modelled using an extended Langmuir model with free reversibility.

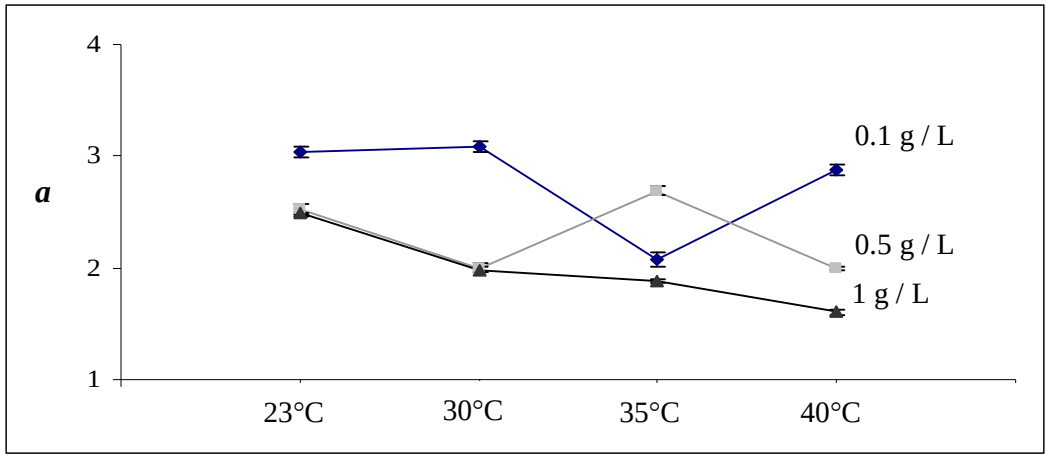

Figure B.20: Fitted *a* as a function of temperature and concentration of β-casein in the solution modeled using an extended Langmuir model with free reversibility.

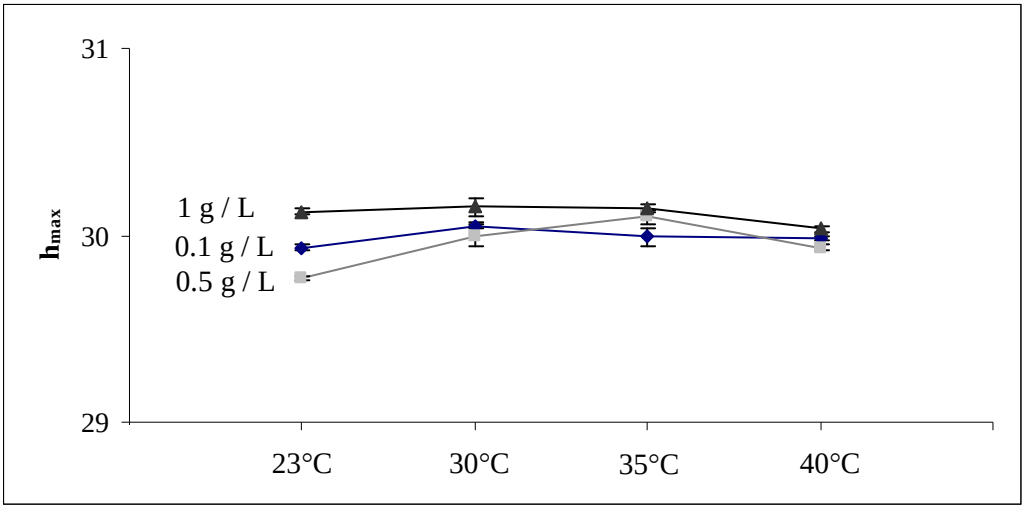

Figure B.21: Fitted h_{max} as a function of temperature and concentration of β-casein in the solution modeled using an extended Langmuir model with free reversibility.

Lysozyme

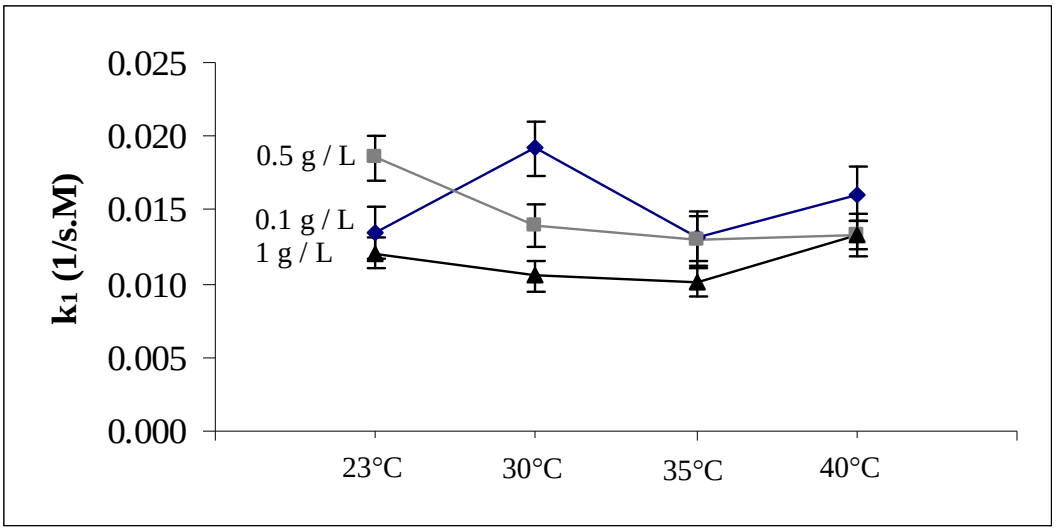

Figure B.22: Fitted k_1 as a function of temperature and concentration of lysozyme in the solution modeled using an extended Langmuir model with free reversibility.

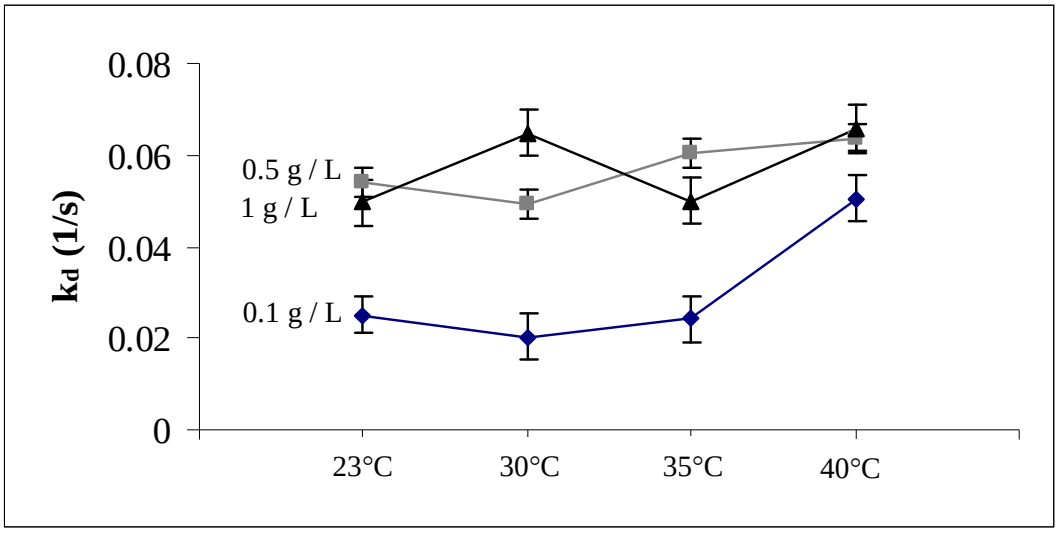

Figure B.23: Fitted k_d as a function of temperature and concentration of lysozyme in the solution modeled using an extended Langmuir model with free reversibility.

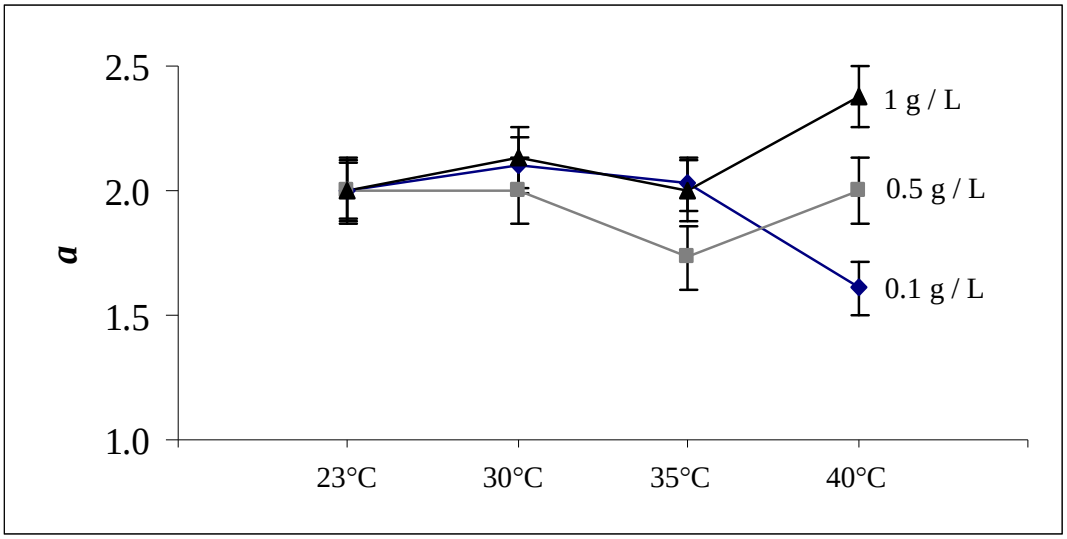

Figure B.24: Fitted a as a function of temperature and concentration of lysozyme in the solution modeled using an extended Langmuir model with free reversibility.

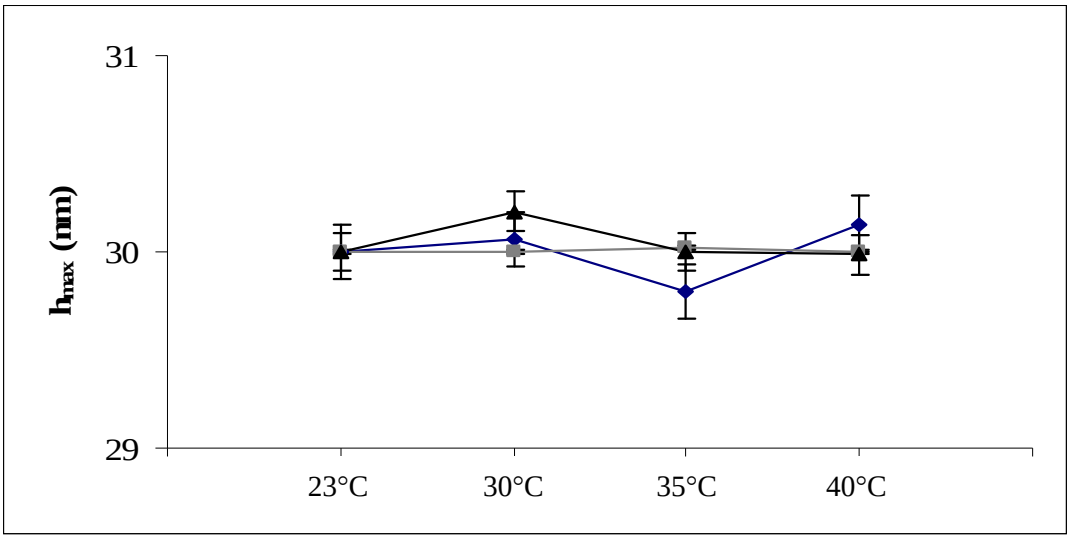

Figure B.25: Fitted h_{max} as a function of temperature and concentration of lysozyme in the solution modeled using an extended Langmuir model with free reversibility.

α-lactalbumin

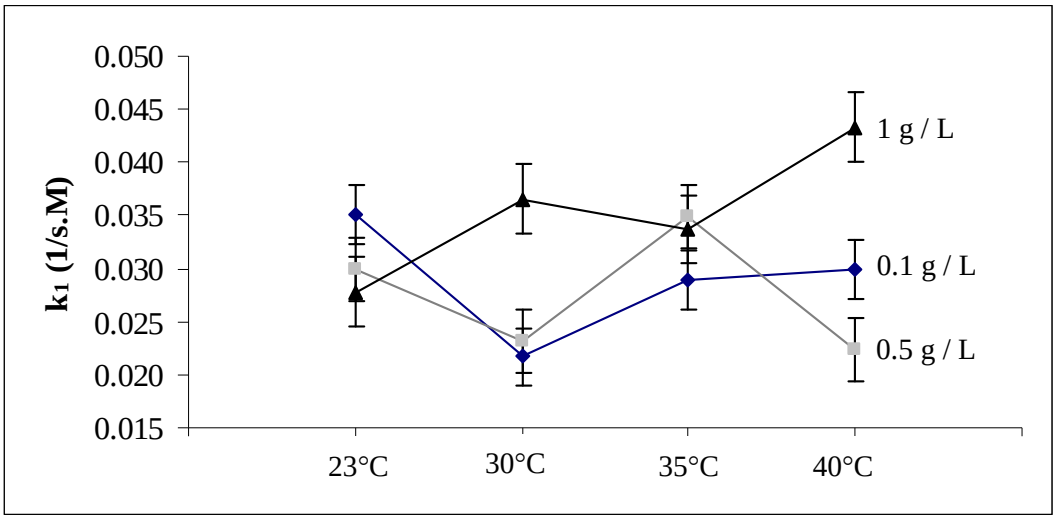

Figure B.26: Fitted k_1 as a function of temperature and concentration of α-lactalbumin in the solution modeled using an extended Langmuir model with free reversibility.

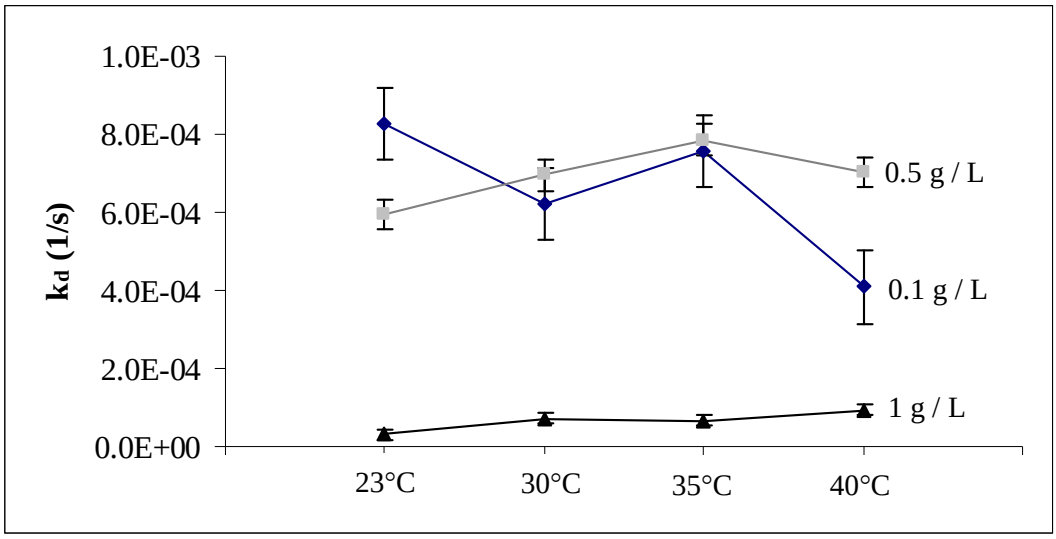

Figure B.27: Fitted k_d as a function of temperature and concentration of α-lactalbumin in the solution modeled using an extended Langmuir model with free reversibility.

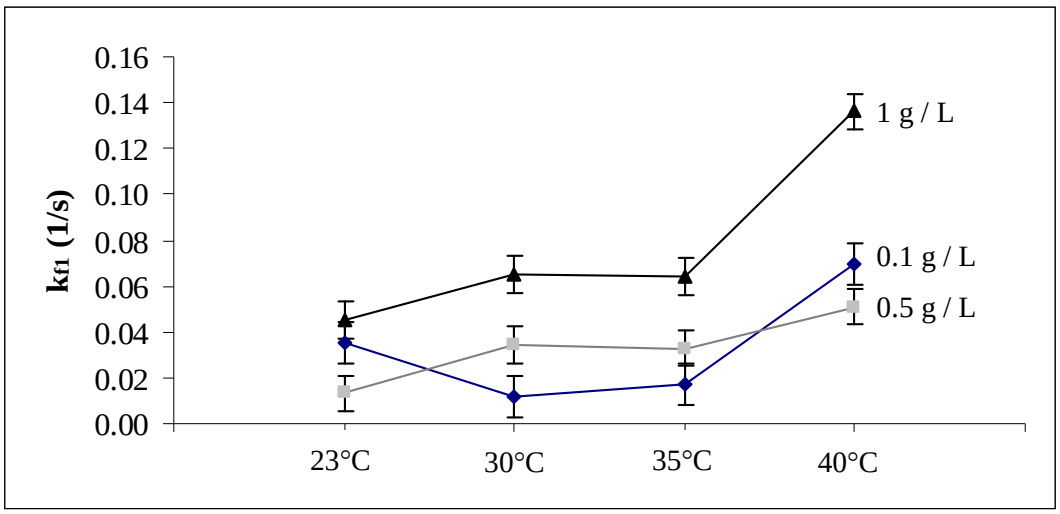

Figure B.28: Fitted k_{f1} as a function of temperature and concentration of α-lactalbumin in the solution modeled using an extended Langmuir model with free reversibility.

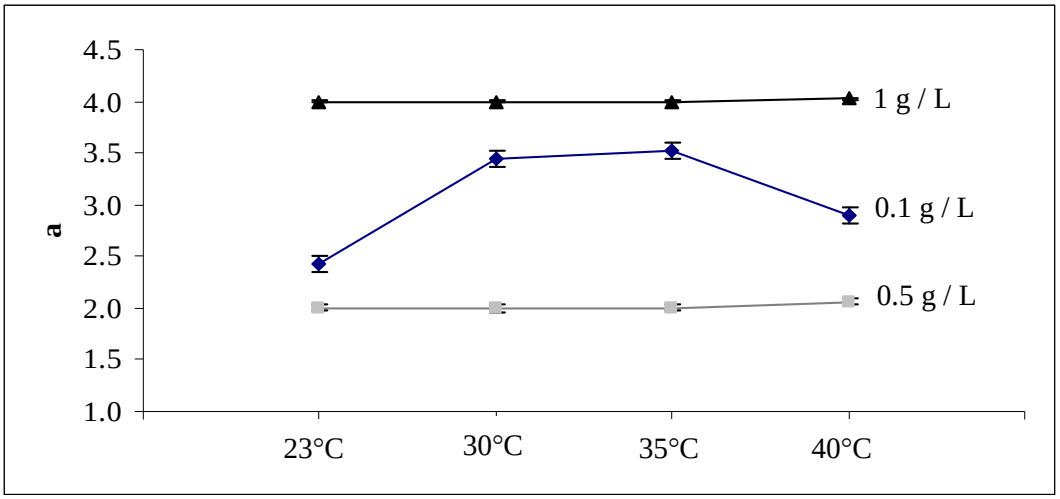

Figure B.29: Fitted *a* as a function of temperature and concentration of α-lactalbumin in the solution modeled using an extended Langmuir model with free reversibility.

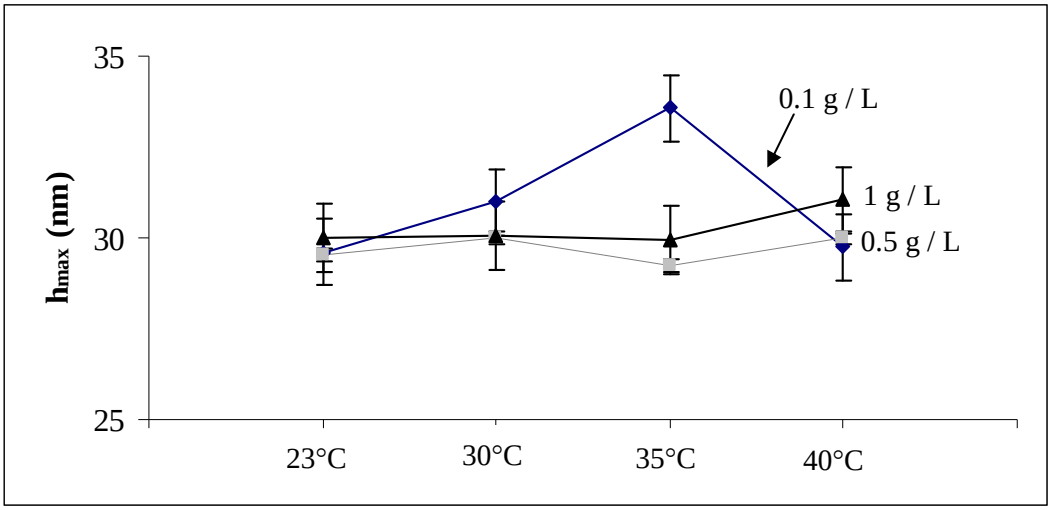

Figure B.30: Fitted h_{max} as a function of temperature and concentration of β-casein in the solution modeled using an extended Langmuir model with free reversibility.

Extended Langmuir model with diffusion hindrance through very small pores

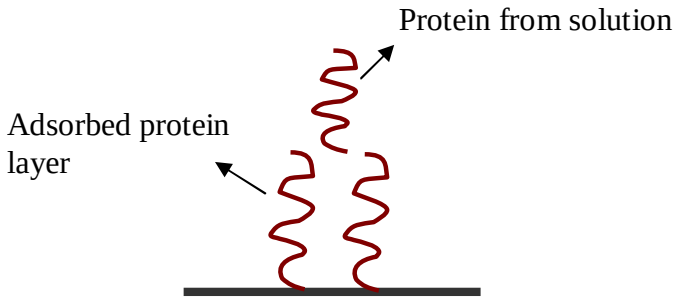

Figure B.31: Schematic diagram of the proposed kinetic model (extended Langmuir model with diffusion hindrance through very small pores)

$$\frac{\Delta\theta_1}{\Delta t} = k_1 C_O (1 - \theta_1 - a\theta_2)^n - (k_d)\theta_1 - k_f \theta_1 (1 - \theta_1 - a\theta_2)^n / a + k_{f2}\theta_2 \qquad \text{(B.5)}$$

$$\frac{\Delta\theta_2}{\Delta t} = k_2 C_o (1 - \theta_1 - a\theta_2)^n / a + k_f \theta_1 (1 - \theta_1 - a\theta_2)^n / a - k_{f2}\theta_2 - k_{2d}\theta_2 \qquad \text{(B.6)}$$

k_1, k_d, k_f, k_{f2}, k_2, k_{2d}, a and n were taken as parameters to be fitted.

β-casein

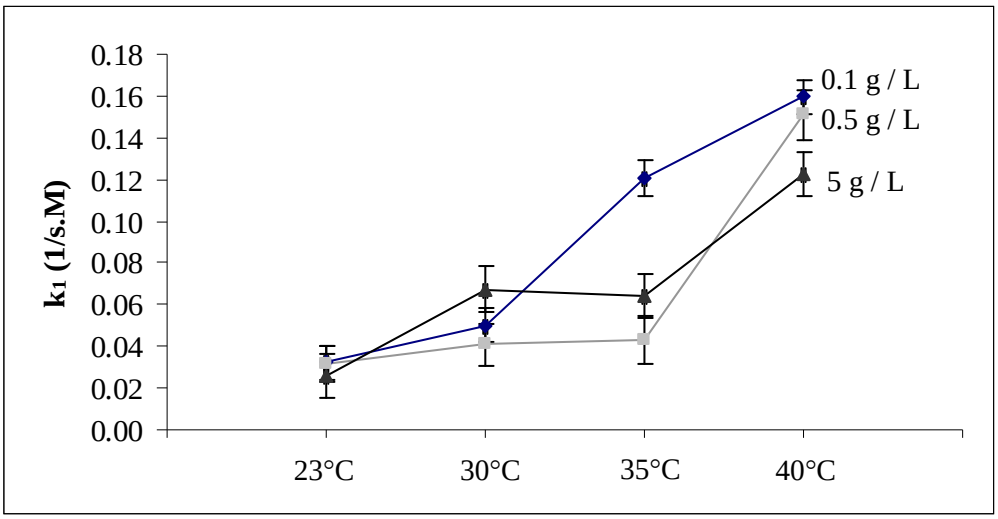

Figure B.32: Fitted k_1 as a function of temperature and concentration of β-casein in the solution modeled using an extended Langmuir model with diffusion hindrance through very small pores.

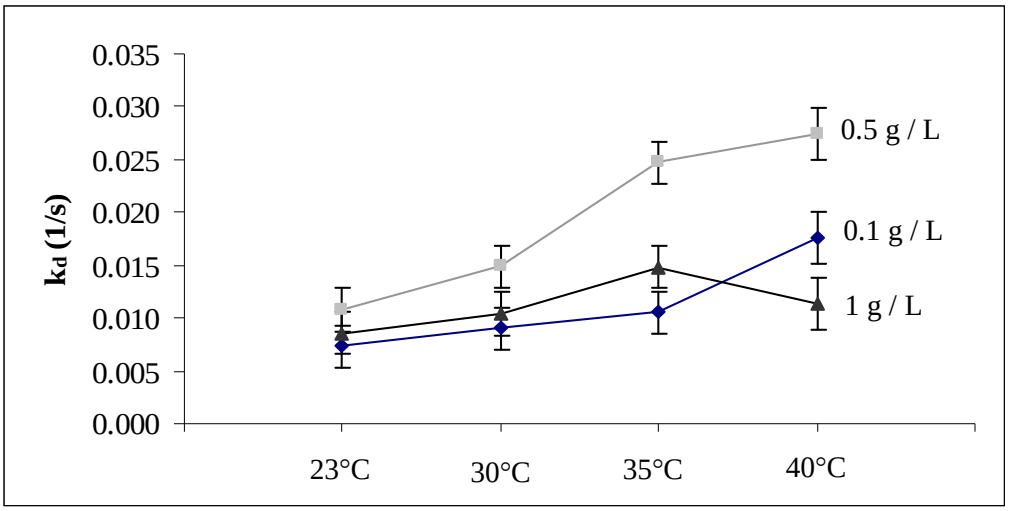

Figure B.33: Fitted k_d as a function of temperature and concentration of β-casein in the solution modeled using an extended Langmuir model with diffusion hindrance through very small pores.

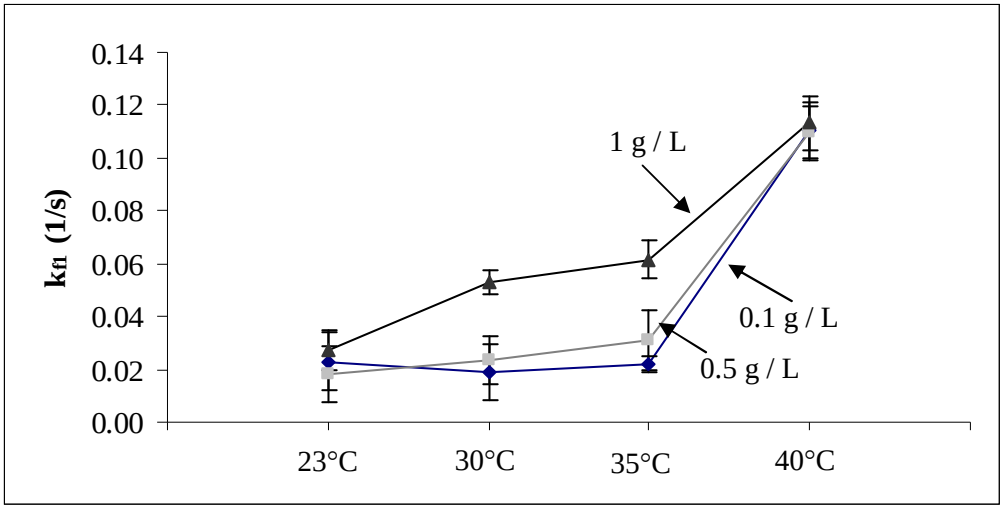

Figure B.34: Fitted k_{f1} as a function of temperature and concentration of β-casein in the solution modeled using an extended Langmuir model with diffusion hindrance through very small pores.

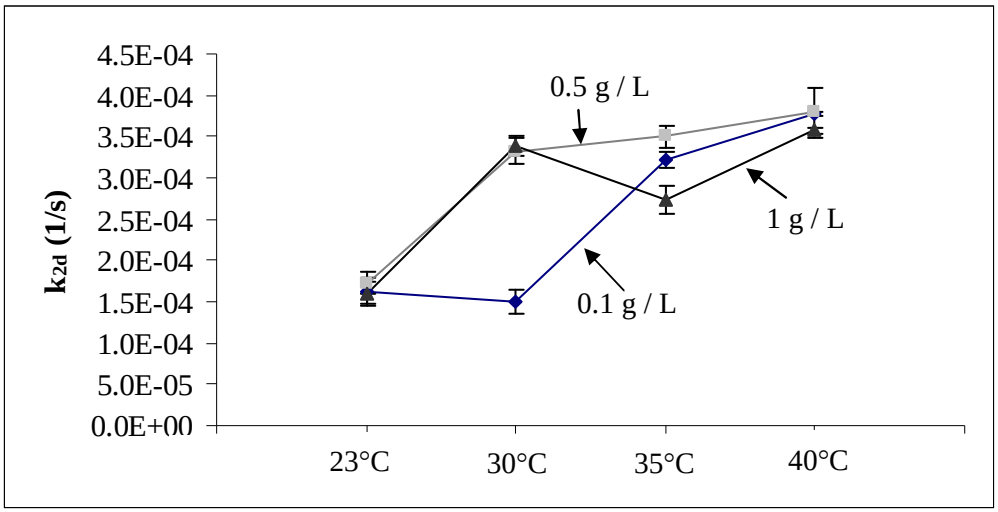

Figure B.35: Fitted k_{2d} as a function of temperature and concentration of β-casein in the solution modeled using an extended Langmuir model with diffusion hindrance through very small pores.

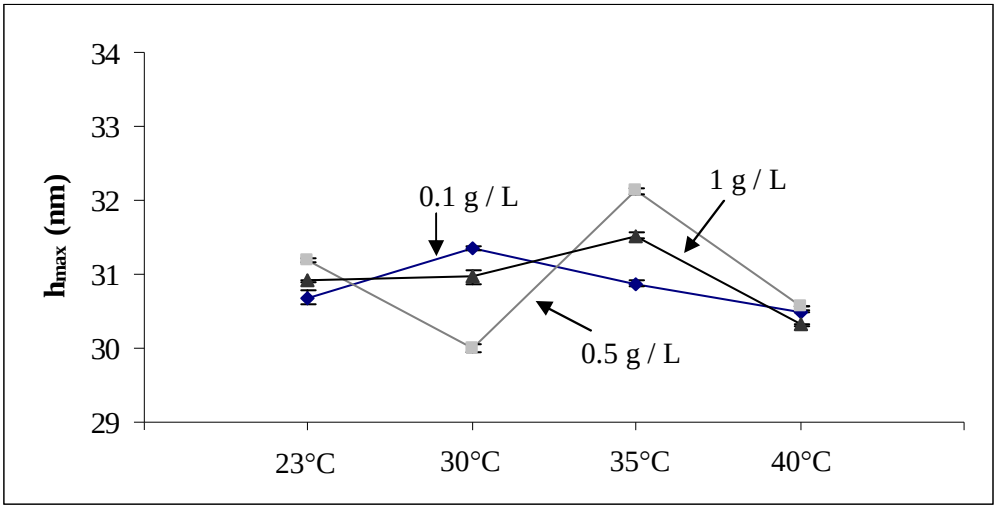

Figure B.36: Fitted h_{max} as a function of temperature and concentration of β-casein in the solution) modeled using an extended Langmuir model with diffusion hindrance through very small pores.

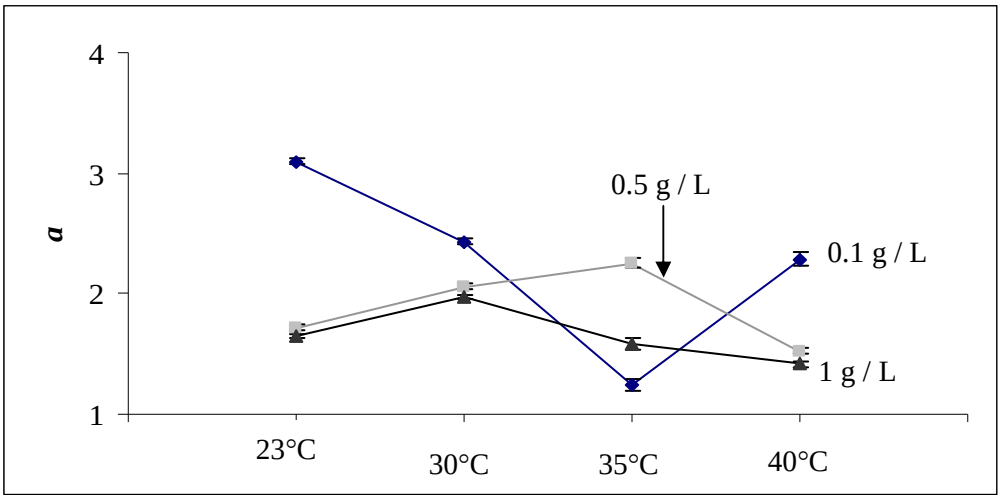

Figure B.37: Fitted *a* as a function of temperature and concentration of β-casein in the solution modeled using an extended Langmuir model with diffusion hindrance through very small pores.

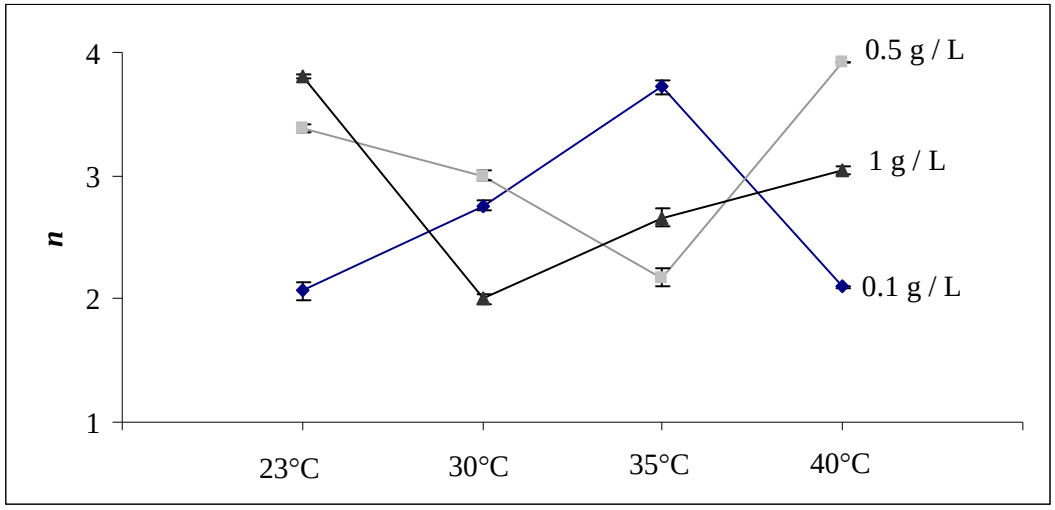

Figure B.38: Fitted *n* as a function of temperature and concentration of β-casein in the solution modeled using an extended Langmuir model with diffusion hindrance through very small pores.

Lysozyme

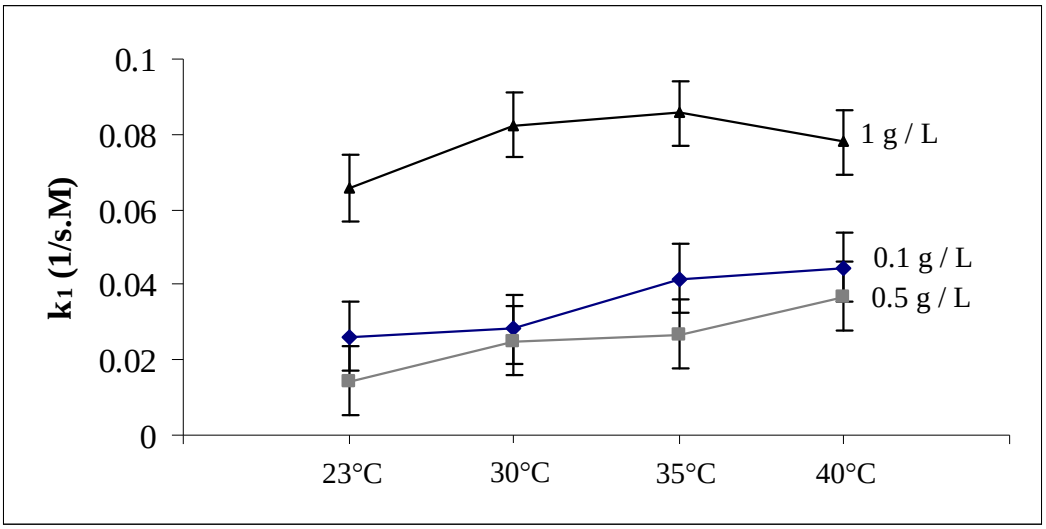

Figure B.39: Fitted k_1 as a function of temperature and concentration of lysozyme in the solution modeled using an extended Langmuir model with diffusion hindrance through very small pores.

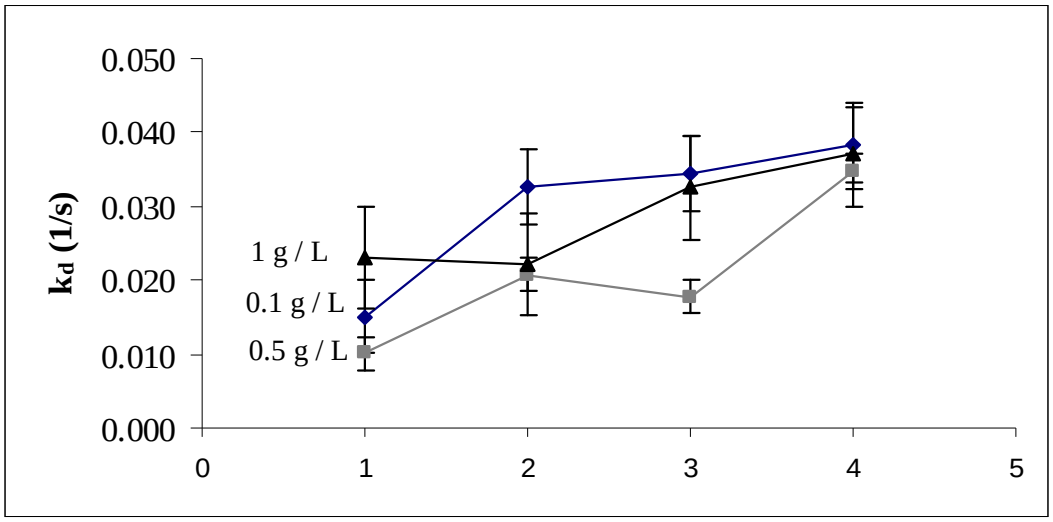

Figure B.40: Fitted k_d as a function of temperature and concentration of lysozyme in the solution modeled using an extended Langmuir model with diffusion hindrance through very small pores.

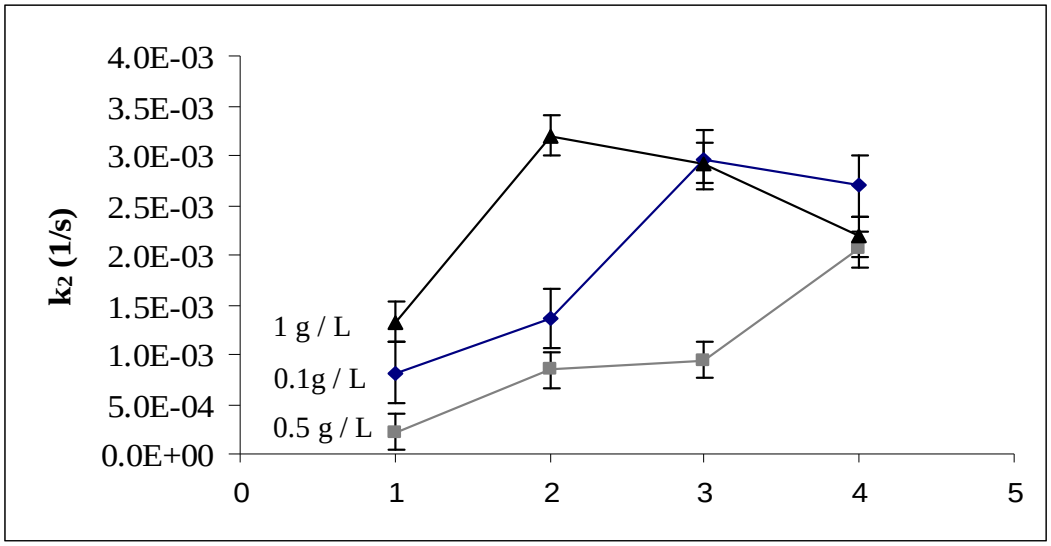

Figure B.41: Fitted k_2 as a function of temperature and concentration of lysozyme in the solution modeled using an extended Langmuir model with diffusion hindrance through very small pores.

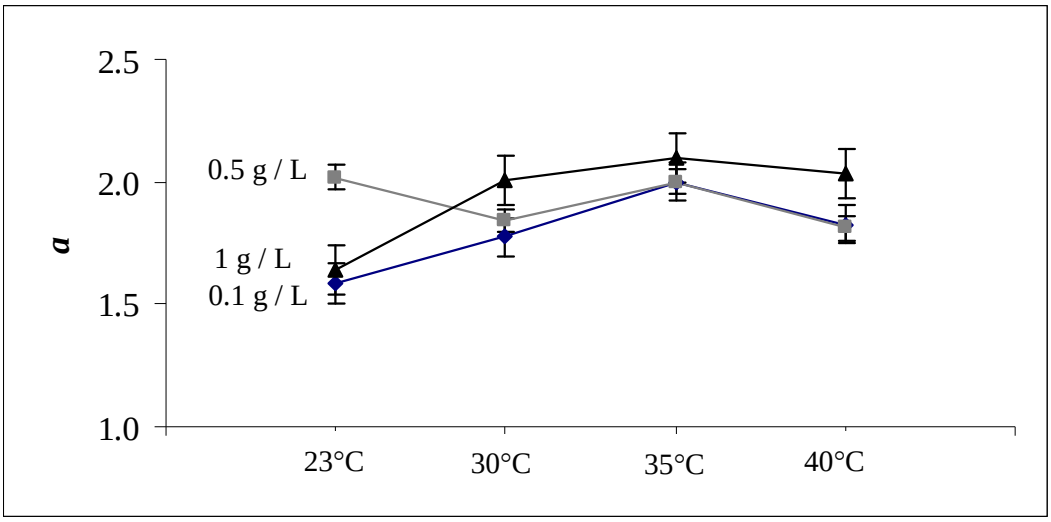

Figure B.42: Fitted *a* as a function of temperature and concentration of lysozyme in the solution modeled using an extended Langmuir model with diffusion hindrance through very small pores.

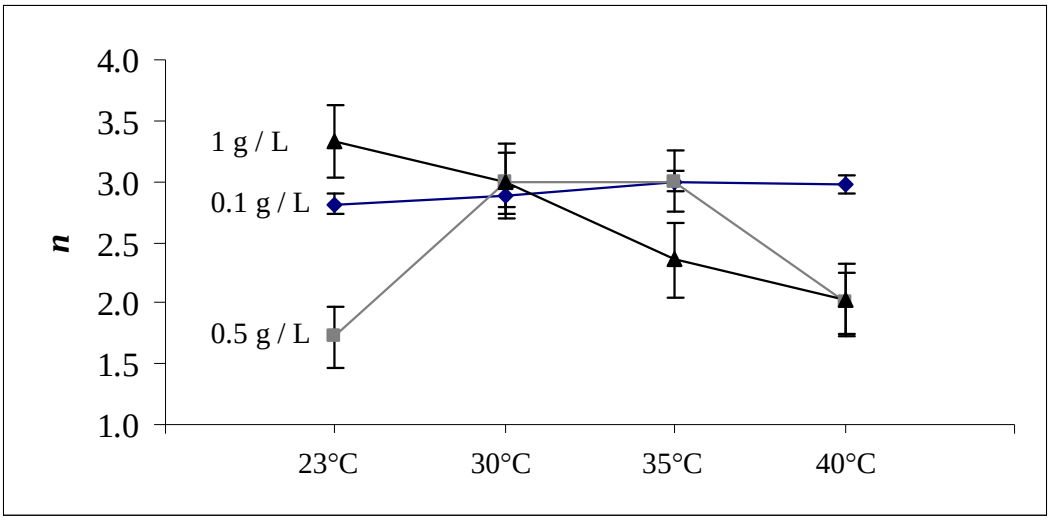

Figure B.43: Fitted *n* as a function of temperature and concentration of lysozyme in the solution modeled using an extended Langmuir model with diffusion hindrance through very small pores.

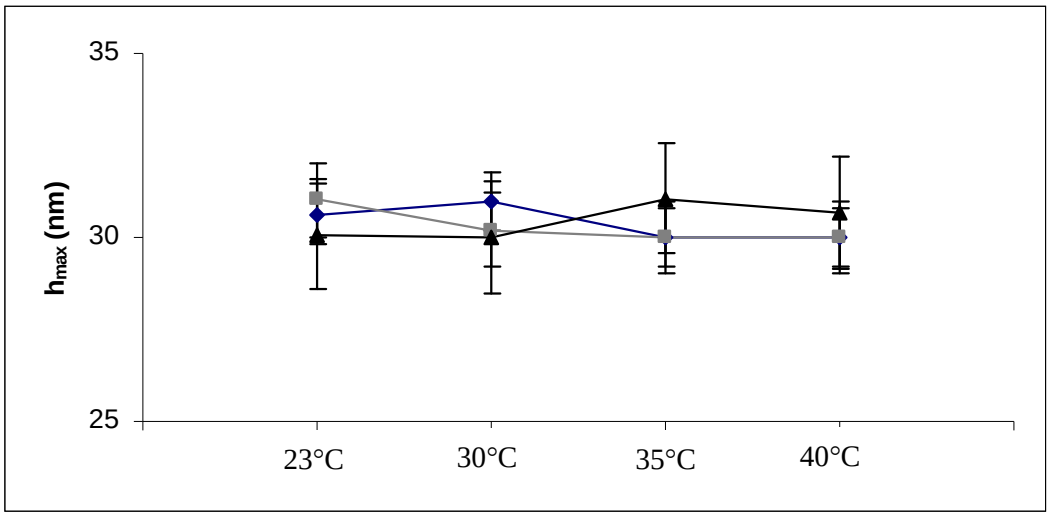

Figure B.44: Fitted h_{max} as a function of temperature and concentration of lysozyme in the solution modeled using an extended Langmuir model with diffusion hindrance through very small pores.

α-lactalbumin

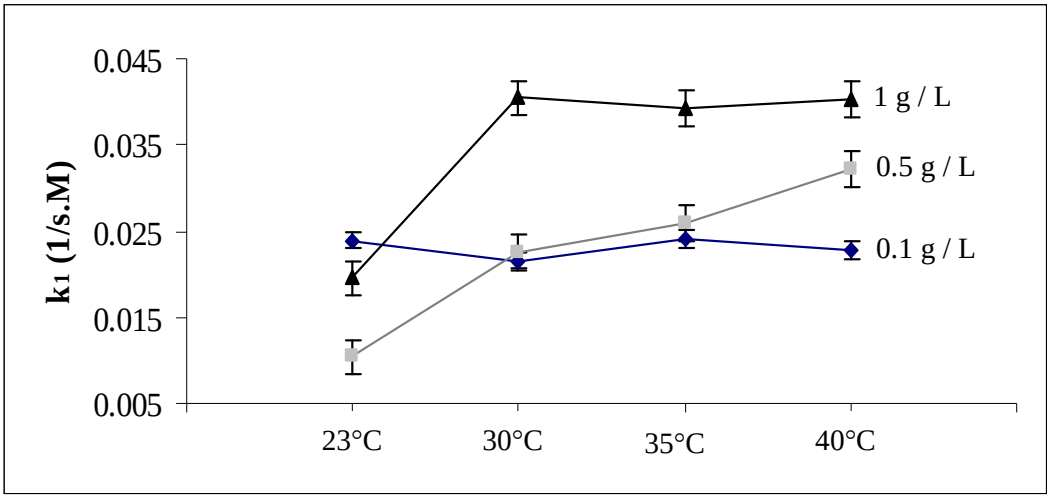

Figure B.45: Fitted k_1 as a function of temperature and concentration of α-lactalbumin in the solution) modeled using an extended Langmuir model with diffusion hindrance through very small pores.

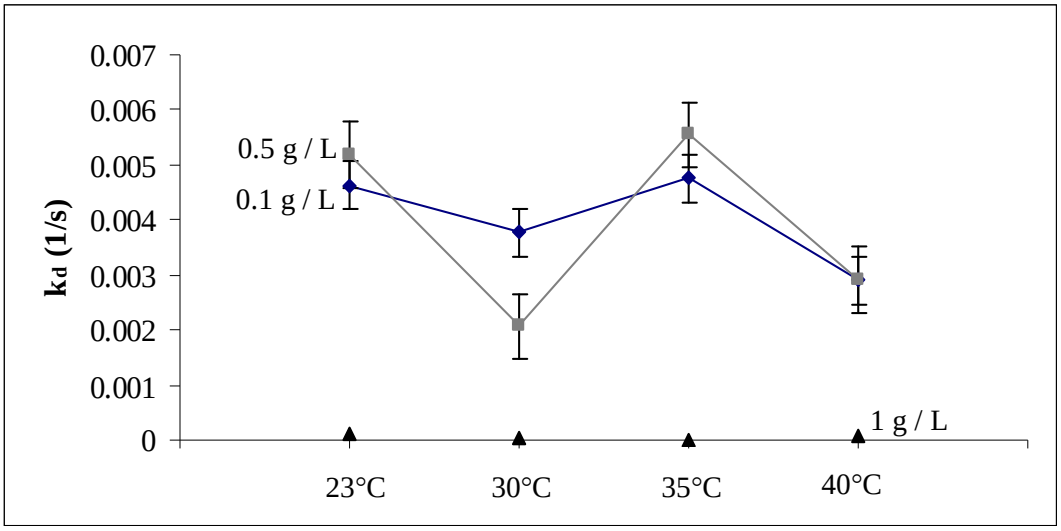

Figure B.46: Fitted k_d as a function of temperature and concentration of α-lactalbumin in the solution modeled using an extended Langmuir model with diffusion hindrance through very small pores.

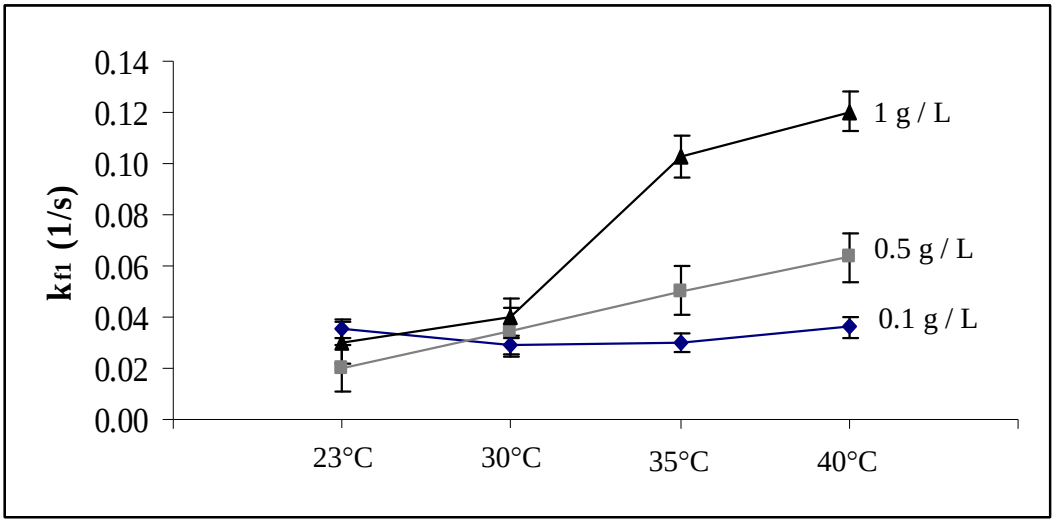

Figure B.47: Fitted k_{f1} as a function of temperature and concentration of α-lactalbumin in the solution modeled using an extended Langmuir model with diffusion hindrance through very small pores.

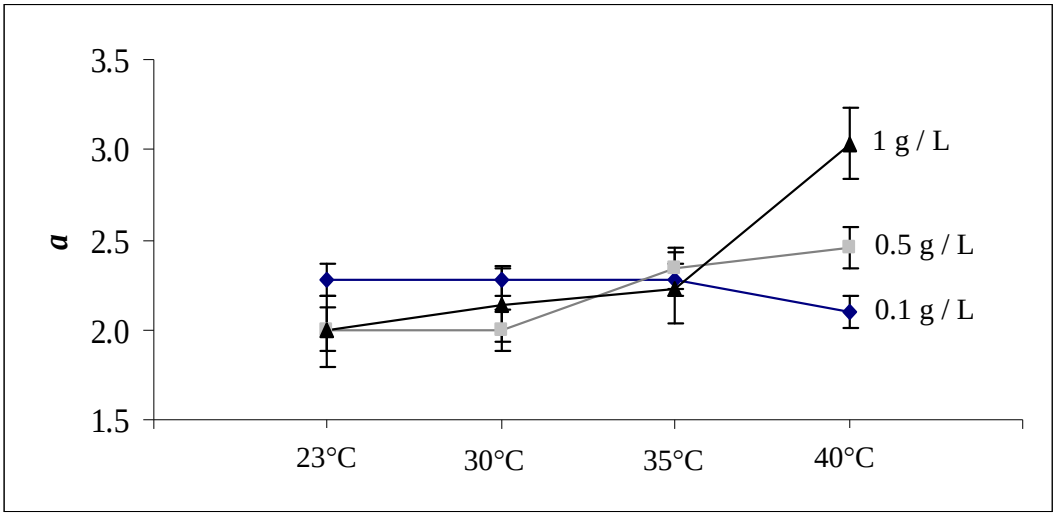

Figure B.48: Fitted *a* as a function of temperature and concentration of α-lactalbumin in the solution modeled using an extended Langmuir model with diffusion hindrance through very small pores.

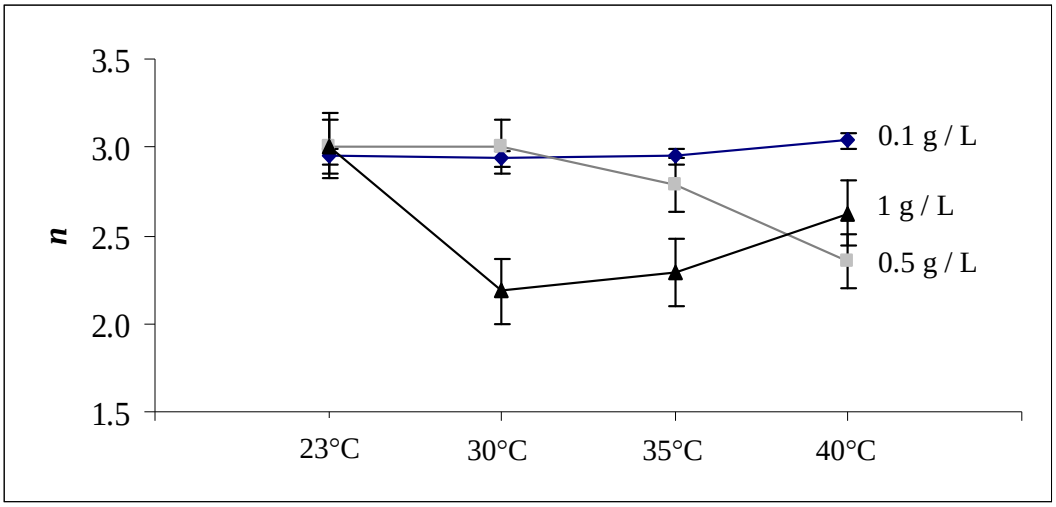

Figure B.49: Fitted *n* as a function of temperature and concentration of α-lactalbumin in the solution modeled using an extended Langmuir model with diffusion hindrance through very small pores.

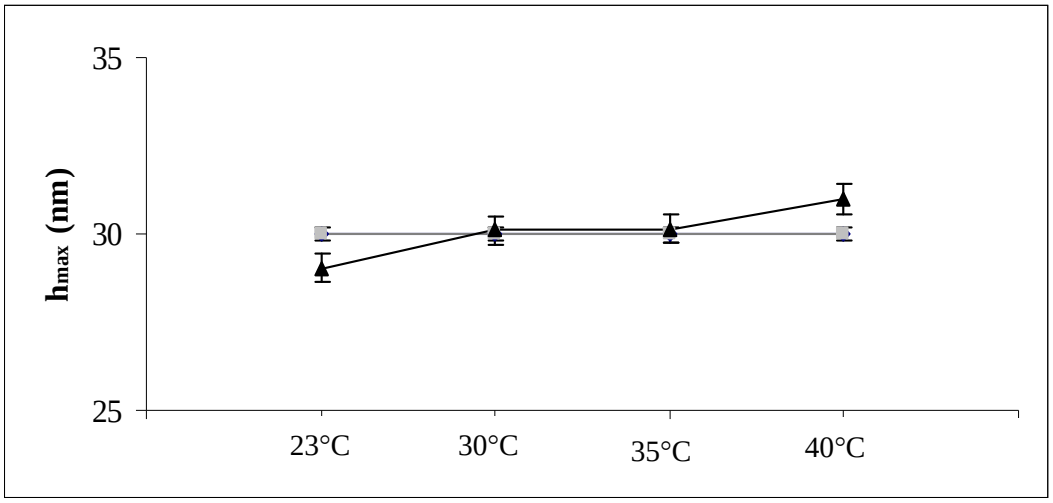

Figure B.50: Fitted h_{max} as a function of temperature and concentration of α-lactalbumin in the solution modeled using an extended Langmuir model with diffusion hindrance through very small pores.

APPENDIX C

ADSORPTION OF MILK SOLUTION ON A COMMERCIAL SS 316 SURFACE

Figure C.1 shows the image of the SS 316 commercial surface after adsorption of milk solution for about 1 hr (refer to Chapter 5, section 5.4). Half of the disk has been modified with lysozyme (4)-PEG5k (5) solution (region B). Region A refers to the unmodified surface (control). As can be seen, there was no significant difference between modified and unmodified regions. This indicates that the proposed method (lysozyme (4)-PEG5k (5)) unable to inhibit adsorption of protein at high temperature (95 °C). This finding is consistent with the result obtained from QCM-D measurement (refer to Chapter 7).

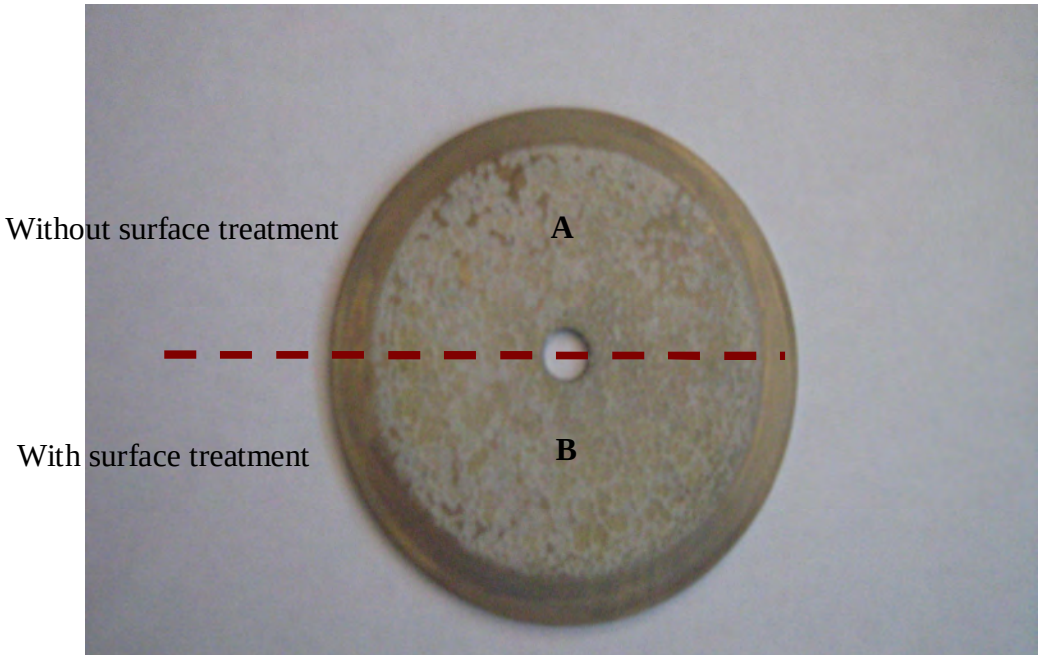

Figure C.1: Image of the SS 316 commercial surface after adsorption of milk solution for 1 hr. Region A refers to the unmodified surface whereas region B refers to the modified surface with lysozyme (4)-PEG5k (5).

APPENDIX D

SIZE EXCLUSION CHROMATOGRAPHY (SEC) RESULT

The SEC experiment was carried out after the QCM-D experimental results obtained showed that PEG molecules enhanced the adsorption of apo α-lactalbumin. This experiment has been performed to see whether apo α-lactalbumin associated with PEG in solution. 4 samples were tested (see Chapter 5, section 5.9):

A1: apo α-lactalbumin solution (2 g / L)

A2: holo α-lactalbumin solution (2 g / L)

C1: mixture of PEG5000 (2 g / L) and apo α-lactalbumin solution (2 g / L)

C2: mixture of PEG5000 (2 g / L) and holo α-lactalbumin solution (2 g / L)

Figure D.1 shows the SEC chromatogram of the run with 4 samples (A1, A2, C1 and C2). As can be seen, there was only one peak at the native protein position for all samples. This indicates that there was no association between apo α-lactalbumin and PEG in solution. However, apo α-lactalbumin associated with grafted PEG molecules as observed from QCM-D measurements.

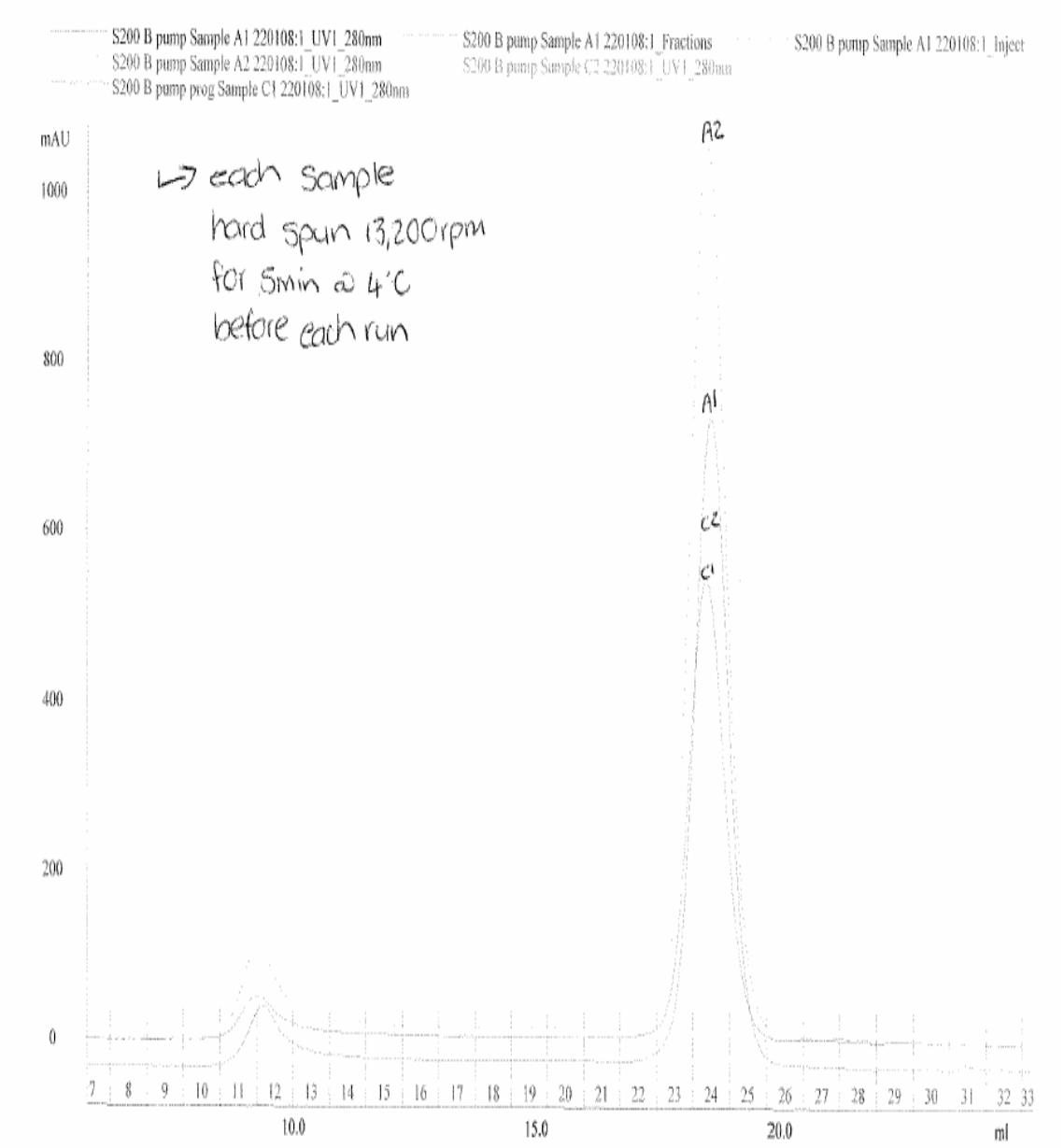

Figure D.1: SEC chromatogram of the run with 4 samples; apo α-lactalbumin solution (2 g / L) (A1), holo α-lactalbumin solution (2 g / L) (A2), mixture of PEG5000 (2 g / L) (C1) and mixture of PEG5000 (2 g / L) (C2).

APPENDIX E

PUBLICATION

JOURNAL

N. Ngadi, J. Abrahamson, C. Fee, and K. Morison, 'QCM-D Study on Relationship of PEG Coated Stainless Steel Surfaces to Protein Resistance', International Journal of Chemical and Biomolecular Engineering 1;3 www.waset.org Summer 2008,pp. 126-130.

N. Ngadi, J. Abrahamson, C.Fee and K. Morison, 'Are PEG Molecules a Universal Protein Repellent?', International Journal of Biological and Life Sciences 1:3 2009, pp. 116-120.

N. Ngadi, J. Abrahamson, C. Fee and K. Morison, 'QCM-D Study of β-casein Adsorption on Bimodal PEG Brushes', International Journal of Biological and Life Sciences 1:3 2009, pp. 145-150.

CONFERENCE

N. Ngadi, J. Abrahamson, C. Fee, and K. Morison, 'QCM-D Study on Relationship of PEG Coated Stainless Steel Surfaces to Protein Resistance', WASET International Conference, 2008, July, France.

N. Ngadi, J. Abrahamson, C.Fee and K. Morison, 'Are PEG Molecules a Universal Protein Repellent?' International Conference on Chemical Engineering, 2009, Jan, Dubai.

N. Ngadi, J. Abrahamson, C. Fee and K. Morison, 'QCM-D Study of β-casein Adsorption on Bimodal PEG Brushes', International Conference on Bioinformatics and Biotechnology, 2009, April, Rome.

N. Ngadi, J. Abrahamson, C. Fee and K. Morison, 'Study of Adsorption Kinetics and Voscoelastic Properties of Protein with QCM-D', 15th Regional Symposium on Chemical Engineering (RSCE), 2008, December, Kuala Lumpur.

N. Ngadi, J. Abrahamson, C. Fee and K. Morison, 'Inhibition of Protein Adsorption onto Stainless Steel by a PEG Layer', CHEMECA, 2007, Oct, Melbourne.